

LOUGHBOROUGH
UNIVERSITY OF TECHNOLOGY
LIBRARY

AUTHOR

FISHENDEN C R

COPY NO.

062057 / 01

VOL NO.

CLASS MARK

ARCHIVE
COPY

FOR REFERENCE ONLY

THE PERFORMANCE OF A BRANCHED

ANNULAR DIFFUSER SYSTEM

by

COLIN RICHARD FISHENDEN

A DOCTORAL THESIS

Submitted for the award of Doctor of Philosophy
of the Loughborough University of Technology

April 1974

Supervisor: Dr S.J. Stevens,

Department of Transport Technology.

© by Colin Richard Fishenden, 1974

Loughborough University of Technology Library	
Date	July 74
Class	
Acc. No.	062057/01

SUMMARY

Low speed tests have been carried out on a branched annular diffuser system having a geometry similar to that employed in some gas turbine engine combustion systems. The system comprised a straight walled pre-diffuser followed by a sudden area expansion in which the flow was divided between two concentric annuli separated by a bluff body simulating a combustion chamber. The overall geometric area ratio was maintained at 2.0 and all tests were carried out with fully developed flow at inlet. The design flow split between the outer and inner annuli was 2.15:1. The system was tested with five different pre-diffuser geometries to show the effect of increasing the area ratio, increasing the included angle and canting the pre-diffuser. For each pre-diffuser geometry the influence of varying the flow split and the axial distance between pre-diffuser outlet and combustion chamber head (dump gap) were investigated. In addition to determining the overall performance characteristics, the pressure losses for the inner and outer flow fields were calculated and the losses further sub-divided in order to identify regions of high loss.

When operating at the design flow split there was an asymmetric growth of the boundary layers along the inner and outer walls of the symmetrical pre-diffusers. This resulted in separation occurring on the inner wall when the pre-diffuser area ratio was increased beyond 1.6. An initial attempt at optimising the geometry was made by canting the pre-diffuser. This resulted in improvements in both the pre-diffuser flow stability and the overall system performance.

The effect of increasing the pre-diffuser area ratio for a constant included angle of 12° was to improve the overall performance at the expense of increasing the system length and decreasing the pre-diffuser outlet flow stability. Increasing the included angle from 12° to 18° for a constant pre-diffuser area ratio of 1.8 resulted in a significant

(ii)

decrease in overall performance and pre-diffuser flow stability.

The optimum dump gaps for the various pre-diffuser geometries have been established and these are in reasonable agreement with the non-dimensional value (D/h_2) of 1.1 often used in practice. The results indicate that decreasing the dump gap leads to an improvement in pre-diffuser flow stability, however, it is not possible to reduce the dump gap much below the optimum value because of the rapid decrease in overall performance.

Analysis of the pressure losses in the system showed that the majority of the overall loss occurred in the region downstream of the plane of maximum velocity over the combustion chamber head. This was attributed to the strong local acceleration and subsequent diffusion of the flow as it passed over the head.

ACKNOWLEDGEMENTS

The work reported in this thesis was carried out in the Department of Transport Technology under the financial support of the Ministry of Defence.

The author wishes to thank Dr. S.J. Stevens for the interest and encouragement shown in the work and for the many useful discussions held in relation to it. The invaluable assistance given by Mr. W.H. Brooks in connection with the experimental facility is gratefully acknowledged.

Thanks are also due to the staff of the Loughborough University Computer Centre for their advice on the use of the graph plotting facilities and to Mrs. E. Churney for making such a magnificent job of the typing.

LIST OF CONTENTS

<u>Chapter</u>	<u>Title</u>	<u>Page</u>
	Summary	(i)
	Acknowledgements	(iii)
	List of Contents	(iv)
	List of Figures	(vii)
	List of Tables	(xi)
	List of Symbols	(xii)
1	<u>INTRODUCTION</u>	
	1-1 Diffusers and Diffuser Systems	1
	1-2 Characteristics of Combustion Chamber Diffuser Systems	2
	1-3 Performance Parameters	5
	1-4 Boundary Layer and Velocity Profile Parameters	12
	1-5 Factors Influencing Diffuser System Performance	15
	1-6 Review of Previous Work Relating to Combustion Chamber Diffuser Performance	22
	1-7 Choice of Diffuser System to be Investigated	25
	1-8 Objectives and Scope of Investigation	26
2	<u>EXPERIMENTAL FACILITY</u>	
	2-1 Design of Basic Facility	36
	2-2 Method of Controlling "Design" Variables	36
	2-3 Choice of Pre-diffuser Geometries	37
	2-4 Instrumentation	38
3	<u>EXPERIMENTAL WORK</u>	
	3-1 Scope of Tests	50
	3-2 Experimental Technique	52
	3-3 Reduction of Data and Computational Methods	54
	3-4 Accuracy	55
	3-5 Calibration Tests	57

	3-6 Inlet Conditions	58
4	<u>PRESENTATION AND DISCUSSION OF RESULTS</u>	
	4-1 Performance Characteristics	63
	4-2 Pre-diffuser Outlet Conditions	67
	4-3 Settling Length Flow Conditions	82
	4-4 Static Pressure Distributions	83
	4-5 Summary of Overall Performance	87
5	<u>FURTHER ANALYSIS OF LOSSES</u>	
	5-1 Method and Scope of Analysis	131
	5-2 Presentation of Data	133
	5-3 Discussion of Results	135
6	<u>CONCLUSIONS AND RECOMMENDATIONS</u>	
	6-1 Conclusions	158
	6-2 Topics for Future Research	160
7	<u>REFERENCES</u>	162

APPENDICES

<u>Appendix</u>	<u>Title</u>	<u>Page</u>
1	<u>SYSTEM AND PRE-DIFFUSER GEOMETRIES</u>	165
2	<u>CALIBRATIONS</u>	167
	A2-1 Inlet Conditions	167
	A2-2 Pressure Probe Calibrations	167
	A2-3 Pre-diffuser Outlet Conditions	169
	A2-4 Settling Length Conditions	169
3	<u>SAMPLE READINGS AND REDUCTION OF DATA</u>	175
	A3-1 Pre-diffuser Outlet Profiles	175
	A3-2 Head Rake Data	175
	A3-3 Settling Length Velocity Profiles	176
	A3-4 Static Pressures	176
	A3-5 Preparation of Data for Computer Analysis	176
4	<u>ANALYSIS OF DATA BY COMPUTER PROGRAM</u>	184
	A4-1 Main Performance Analysis Program (P1)	184
	A4-2 Head Rake Data Analysis Program (P4)	185
	A4-3 Performance Contour Map Analysis Program (P3)	186
5	<u>PRE-DIFFUSER OUTLET PROFILES</u>	204
6	<u>HEAD STATIC PRESSURE AND VELOCITY PROFILES</u>	219
7	<u>SETTLING LENGTH VELOCITY PROFILES</u>	229
8	<u>COMBUSTION CHAMBER STATIC PRESSURE DISTRIBUTION PLOTS</u>	241
9	<u>SUMMARY OF BOUNDARY LAYER AND VELOCITY PROFILE PARAMETERS</u>	247
10	<u>SUMMARY OF PERFORMANCE PARAMETERS</u>	252

LIST OF TABLES

<u>Table No.</u>	<u>Title</u>	<u>Page</u>
1-4	Boundary Layer and Velocity Profile Parameter Definitions	35
2-3-1	Pre-Diffuser Geometries	37
2-4-1	Pressure Probe Measurements	40
3-1	Summary of Tests Carried Out	62
4-2	Influence of Test Variables on Outlet Velocity Profile	73
4-5	Comparison of Optimum Overall Performance	89

APPENDICES

<u>Table No.</u>	<u>Title</u>	<u>Page</u>
A3-1	Pre-diffuser Outlet Traverse Data for Test 3-0718/A	179
A3-2	Pre-diffuser Outlet Static Pressure Traverse Data for Test 3-0718/A	180
A3-3	Head Rake Data for Test 3-0718/A	180
A3-4	Settling Length Traverse Data for Test 3-0718/A	181
A3-5	Key Static Pressures at Stations 2 & 4 for Test 3-0718/A	181
A4-1	List of Principal Variables in Main Performance Analysis Program	189
A4-2	Listing of Main Performance Analysis Program	190
A4-3	Sample Calculations for Test 3-0718/A	196
A4-4	Main Performance Analysis Program Output Listing for Test 3-0718/A	198
A4-5	Program P4 Output Listing for Test 3-0718/A	202
A9-1/5	Summary of Boundary Layer and Velocity Profile Parameters	247/251
A10-1/5	Summary of Performance Parameters	252/256

LIST OF PRINCIPAL SYMBOLS

A	area of cross-section
A_B	blocked area
AR	area ratio
AR_e	effective area ratio for a branched system (defined in the text)
B	blocked area fraction, A_B/A
\tilde{C}_p	pressure recovery coefficient based on $\alpha_1 \frac{1}{2} \rho \bar{u}_1^2$
C'_p	ideal pressure recovery coefficient (defined in the text)
C^*_p	locus of maximum pressure recovery for a given non-dimensional length
D	dump gap; diameter
E	effective area fraction, $(1 - B)$
h	annulus height
H	width of combustion chamber; boundary layer shape parameter, δ^*/θ
\bar{L}	length of a simple diffuser (e.g. a pre-diffuser)
L_v	variable length of dump diffuser system, $(\bar{L} + D)/h_1$
m	mass flow, $\rho \bar{u} A$
p	static pressure
P	total pressure
$\Delta \tilde{P}$	mass weighted mean total pressure loss
q	dynamic pressure
\bar{q}	mean dynamic pressure based on mass derived velocity, $\frac{1}{2} \rho \bar{u}^2$
\tilde{q}	mass weighted mean dynamic pressure, $\alpha \frac{1}{2} \rho \bar{u}^2$
Q	volume flow
R	radius
RD	velocity profile radial distortion factor (defined in the text)
R_m	radius at which the axial velocity is at a maximum
R_s	radius of stagnation streamline
S	flow split ratio for branched system, $(m_o/m_i)_4$
S_g	flow split giving maximum effectiveness
S_{C_p}	flow split giving maximum pressure recovery

S_λ	flow split giving minimum loss coefficient
S^*	design flow split
u	velocity
\bar{u}	mass derived mean velocity, $m/\rho A$
U	maximum velocity in cross-section
$\sqrt{\langle u'^2 \rangle}$	r.m.s. velocity fluctuation in axial direction
y	distance out from wall
α	velocity profile kinetic energy flux coefficient, $\frac{1}{A} \int^A \left(\frac{u}{U}\right)^3 dA$
γ	aerodynamic stability parameter (defined in the text)
δ^*	boundary layer displacement thickness
ϵ	cant angle of a diffuser
ξ	diffuser effectiveness, C_p/C_p'
θ	boundary layer momentum thickness
$\tilde{\lambda}$	loss coefficient
ν	kinematic viscosity
ρ	fluid density
ϕ	diffuser wall angle

Superscripts

-	area mean or mass derived quantity (e.g. velocity, $\bar{u} = \frac{1}{A} \int^A u \cdot dA$)
~	mass weighted mean quantity (e.g. total pressure, $\tilde{P} = \frac{1}{m} \int^A P \cdot dm$)

Subscripts

i	inner wall or inner annulus
o	outer wall or outer annulus
w	value at wall
H	value on combustion chamber head
II	quantities based on two-dimensional definitions

- 1 diffuser or diffuser system inlet station
 - 2 diffuser or pre-diffuser outlet station
 - 3 station in plane of maximum velocity over combustion chamber head
 - 4 branched diffuser system outlet station
-

LIST OF FIGURES

<u>Figure No.</u>	<u>Title</u>	<u>Page</u>
1-2-1	Typical Modern Gas Turbine with "Faired" Combustion Chamber Diffuser System	28
1-2-2	Geometric Characteristics of a Rectilinear Annular Diffuser	28
1-2-3	Types of Annular Diffuser	29
1-2-4	Typical Dump Diffuser System	29
1-2-5	Simple Annular Dump Diffuser System	29
1-5-1	Influence of Inlet Blockage on Diffuser Performance after Sovran & Klomp ⁽¹⁾	30
1-5-2	Variation of Diffuser Effectiveness with Inlet Blockage Fraction	30
1-5-3	Influence of Entry Swirl on Loss Coefficient for Constant Inner Core Annular Diffusers after Gurevich ⁽⁵⁾	31
1-5-4	Total Pressure Contours in Annular Diffusers - Data of Hoadley reported by Horlock ⁽¹¹⁾	31
1-5-5	Annular Diffuser Performance Chart after Sovran & Klomp ⁽¹⁾	32
1-5-6	Influence of Flow Split on Branched Diffuser Performance	32
1-6-1	Performance of a Wide Angle Annular Diffuser after Stevens & Fry ⁽¹⁴⁾	33
1-6-2	Performance of a Wide Angle Annular Diffuser with Free Surface Expansion after Fishenden ⁽¹⁵⁾	33
1-6-3	Performance of a Wide Angle Annular Diffuser with Internal Struts - Data of Fishenden and Brown reported by Stevens ⁽²⁰⁾	34
1-6-4	Static Pressure Recovery Characteristic of a Branched Diffuser after Ehrich ⁽¹⁶⁾	34
2-1-1	Layout of Test Facility	43
2-1-2	Experimental Facility	44
2-2-1	Settling Length Throttle and Traverse Mechanism	45
2-3-1	Pre-diffuser Geometries in Relation to Performance Chart of Sovran & Klomp ⁽¹⁾	45

2-4-1	Stations and Location of Instrumentation	46
2-4-2	Combustion Chamber Head Rakes	46
2-4-3	Location of Static Pressure Tappings	47
2-4-4	Settling Length Traverse Probe	48
2-4-5	Traverse Mechanism and Pitot Probe	48
2-4-6	Wedge Static Probe	49
2-4-7	Pitot-Wedge Static Combination Probe	49
<hr/>		
3-1-1	Range of Tests for each Pre-diffuser	59
3-6-1	Comparison of Original and Modified Intakes	59
3-6-2	Inlet Velocity Profile	60
3-6-3	Influence of Pipe Roughness on Fully Developed Velocity Profile after Bradley & Cockrell ⁽⁸⁾	61
3-6-4	Experimental Axial Turbulence Intensity Distribution at Inlet	61
<hr/>		
4-1-1	Variation of Ideal Overall Pressure Recovery with Flow Split	93
4-1-2	Variation of Effective Overall Area Ratio with Flow Split	93
4-1-3/7	Pre-Diffuser and Overall Performance Curves	94/98
4-1-8	Combined Dump Region and Settling Length Losses	99
4-1-9	Typical Variation of Pressure Recovery with Dump Gap	99
4-2-1	Symmetry of Pre-Diffuser Outlet Velocity Profiles	100
4-2-2	Example of Detailed Measurements near Wall	100
4-2-3/5	Pre-Diffuser Outlet Profiles (Diffuser 3)	101/103
4-2-6/8	Pre-Diffuser Outlet Boundary Layer Shape Factors	104/106
4-2-9	Pre-Diffuser Outlet Velocity Profile Radial Distortion Factors	107
4-2-10	Pre-Diffuser Outlet Profile Energy Coefficients	108
4-2-11	Variation of Pre-Diffuser Outlet Effective Area Fraction with Geometry for Optimum Flow Split	109
4-2-12	Relationship between Energy Coefficient and Blockage Fraction for Pre-Diffuser Outlet Flows	109

4-2-13	Flow Regimes after Carlson & Johnston ⁽¹⁷⁾	110
4-2-14	Pre-Diffuser Outlet Flow Separation Limits	111
4-3-1/3	Settling Length Velocity Profiles (Diffuser 3)	112/114
4-3-4	Settling Length Energy Coefficients	115
4-4-1/8	Static Pressure Distributions (various tests)	116/123
4-5-1/5	Overall Performance Contour Maps	124/128
4-5-6	Variation of Overall Effectiveness with Variable Length at Overall Design Flow Split	129
4-5-7	Optimum Geometry for a Given Length	130
<hr/>		
5-1-1	Division of Losses	144
5-1-2	Analysis of Head Rake Data	145
5-1-3	Typical Flow Pattern in Dump Region	145
5-2-1	Head Static Pressure and Velocity Profiles for Test Series 3-12	146
5-2-2/4	Overall Flow Field Loss versus Flow	147/149
5-2-5	Comparison of Net Diffusion in each Flow Field	150
5-2-6/8	Local Flow Field Loss versus Flow	151/153
5-3-1	Comparison of Flow Conditions in Dump Region for Small and Large Dump Gaps	154
5-3-2	Division of Local Losses in the Outer Settling Length Annulus	154
5-3-3	Settling Length Velocity Profiles and Division of Losses (Tests 3-1223 & 3-1208)	155
5-3-4	Settling Length Losses versus Flow, in terms of Local Entry Dynamic Pressure	156
5-3-5	Typical Overall Pressure Recovery versus Flow Characteristics (Diffuser 3)	157
5-3-6	Typical Variation in Overall Stability Margin with Dump Gap (Diffuser 3)	157

(x)

APPENDICES

<u>Figure No.</u>	<u>Title</u>	<u>Page</u>
A1-1	Diffuser System Geometry	165
A1-2	Pre-diffuser Geometries	166
<hr/>		
A2-1	Comparison of Inlet Dynamic Pressure Fluctuations	171
A2-2	Effect of Flow Split on Inlet Velocity Profile	171
A2-3	Wedge Static Probe Calibrations	172
A2-4	Comparison of Head Rake Measurements with Traverse Data	172
A2-5	Comparison of Pre-diffuser Outlet Profiles using Various Methods	173
A2-6	Symmetry of Settling Length Velocity Profiles	174
<hr/>		
A3-1	Pre-diffuser Outlet Profiles for Test 3-0718/A	182
A3-2	Settling Length Velocity Profiles for Test 3-0718/A	183
<hr/>		
A4-1	Main Functions of Computer Programs used for Data Analysis	187
A4-2	Flow Diagram for Main Performance Analysis Program	188
A4-3	Flow Diagram for Head Rake Data Analysis Program	201
A4-4	Method of Analysing Performance Contour Maps	203
<hr/>		
A5-1/3	Pre-diffuser Outlet Velocity Profiles for "CT" Tests	204/206
A5-4/15	Pre-diffuser Outlet Profiles	207/218
<hr/>		
A6-1/10	Head Static Pressure and Velocity Profiles	219/228
<hr/>		
A7-1/12	Settling Length Velocity Profiles	229/240
<hr/>		
A8-1	Key to Static Pressure Distribution Plots	241
A8-2/6	Combustion Chamber Static Pressure Distributions	242/246
<hr/>		

CHAPTER 1. INTRODUCTION.

1-1 DIFFUSERS AND DIFFUSER SYSTEMS

In many internal fluid flow systems it is desirable to reduce the velocity level or to increase the static pressure of the flow at some stage. In either case the conversion of kinetic energy into pressure energy is involved and this can be achieved by allowing the fluid to pass through a duct of increasing cross-sectional area, referred to as a diffuser.

The diffuser is however, limited in its ability to produce the required conversion of energy. The adverse pressure gradient causes the boundary layers to thicken, and if the pressure gradient is too severe, separation occurs allowing some of the fluid to flow back in the direction of decreasing pressure. In this case the main flow does not fill the whole of the diffuser and further useful conversion of energy may be inhibited. In addition, the formation of eddies in the separated region results in some kinetic energy being converted into random energy, thus reducing the amount of energy available for conversion. In order to avoid separation the rate of velocity decrease and consequent pressure rise must be carefully controlled.

In many applications a diffuser is employed to reduce the velocity of the fluid entering a component in order to avoid excessive losses. One such application is in the design of closed circuit wind tunnels where a diffuser is placed upstream of the return circuit. Another similar example is in gas turbine engine design where a diffuser is interposed between the compressor and combustion chamber. In this case the object is to reduce the pressure loss occurring in the combustion chamber.

In addition to the performance characteristics, the diffuser exit velocity distribution and flow stability can be equally important in cases where the component immediately downstream is sensitive to inlet flow conditions. Typical examples are the subsonic intake diffuser prior to

a gas turbine compressor, and the diffuser prior to the combustion chamber. In both cases serious loss in performance may arise due to flow instability.

In many applications diffusion may not be confined to a simple duct, but may be distributed between a number of ducts arranged in parallel or in series. An example of such a case is the type of compressor exit or combustion chamber diffuser system in which the diffusing flow is divided into three streams which feed the combustion chamber. This type of system is discussed in more detail in the next section.

1-2 CHARACTERISTICS OF COMBUSTION CHAMBER DIFFUSER SYSTEMS

A typical modern gas turbine engine combustion system is shown in Fig. 1-2-1. The combustion chamber is annular and has a discrete number of fuel injectors which are linked to an external fuel supply manifold. The compressor supplies high pressure air at an axial velocity corresponding to a Mach No. of typically 0.30. This air passes through an initial diffuser (A) and is then distributed between the diffusers (B), (C) and (D). The flow passing through (B) is a relatively small proportion (15 to 20%) of the total and is used to achieve approximately stoichiometric conditions in the primary zone of the combustion chamber. The remainder of the flow is divided into two streams passing through diffusers (C) and (D), the proportions of which will depend upon the combustion chamber design. The flow then passes into the chamber via several rows of dilution holes, where it mixes with the gases from the primary zone, thus reducing the exit temperature to an acceptable level.

It will be seen that diffusers (A) and (B) are parallel to the engine axis, whereas (C) and (D) are inclined to the axis. However, all four diffusers have straight walls and may be classed as rectilinear annular diffusers.

1-2-1 Rectilinear Annular Diffusers

The geometric characteristics of a typical rectilinear annular diffuser are shown in Fig. 1-2-2. The line a-a represents the centre-line of the diffuser cross-section. The geometry can be described by four non-dimensional parameters;

- (i) the ratio of inlet annulus height to mean radius h_1/\bar{R}_1
 - (ii) the ratio of mean length to inlet annulus height \bar{L}/h_1
 - (iii) the inclination of the diffuser to the axis ϵ
- and (iv) the wall angle relative to the diffuser cross-section
centre-line (a-a) ϕ

It may be noted that the above parameters differ from those commonly found in the literature. They were chosen partly for convenience, but also because they can be used to describe diffusers ranging from axial to radial flow with no loss of generality. As an example, \bar{L}/h_1 is considered a more appropriate form of non-dimensional length than the ratio $\bar{L}/\Delta R_1$ used by Sovran & Klomp⁽¹⁾ since the latter parameter tends to infinity as ϵ approaches 90° .

Annular diffusers may be classified in terms of their inclination to the axis as shown in Fig. 1-2-3. Referring to Fig. 1-2-1 it is seen that (C) and (D) are wide angle diffusers having $|\epsilon| > \phi$, whereas (A) and (B) are symmetrical ($\epsilon = 0$). Under certain circumstances it may be necessary to offset the cross-section centre-line of (A) or (B) thus giving a canted diffuser. It is convenient to identify canted diffusers as being those for which $|\epsilon| \leq \phi$.

Two important factors in diffuser design are the amount of diffusion and the rate of diffusion which are to be attempted. The area ratio, $AR = A_2/A_1$, is a measure of the amount of diffusion and can be expressed as,

$$AR = \left[1 + 2 \left(\frac{\bar{L}}{h_1} \right) \tan \phi \right] \cdot \left[1 + \left(\frac{\bar{L}}{h_1} \right) \left(\frac{h_1}{\bar{R}_1} \right) \sin \epsilon \right] \quad 1-2-1$$

Symmetrical diffusers are a special case for which the above expression reduces to,

$$AR = 1 + 2 \left(\frac{\bar{L}}{h_1} \right) \tan \phi \quad 1-2-2$$

The rate of diffusion is generally assessed in terms of the area ratio and non-dimensional length (\bar{L}/h_1) of the diffuser. One parameter which offers a measure of the rate of diffusion is the ratio, $\left(\frac{AR - 1}{\bar{L}/h_1} \right)$. It will be seen from Eqn. 1-2-2 that this is equal to $(2 \tan \phi)$ for symmetrical diffusers and it may be noted that ϕ (or 2ϕ , the included angle) is often used as a measure of the rate of diffusion for this class of diffuser.

In general, however, the rate of diffusion can be expressed as,

$$\left(\frac{AR-1}{\bar{L}/h_1} \right) = 2 \tan \phi + \left(\frac{h_1}{R_1} \right) \sin \epsilon + 2 \left(\frac{\bar{L}}{h_1} \right) \left(\frac{h_1}{R_1} \right) \tan \phi \sin \epsilon \quad 1-2-3$$

It is interesting to note that canting a diffuser (i.e. increasing $|\epsilon|$) whilst maintaining the same area ratio necessitates changing the included angle, 2ϕ .

1-2-2 Linking of Diffusers in Combustion Chamber Systems

Although it is important to investigate the characteristics of single diffusers, it is equally important to investigate the characteristics of the diffuser system and the interactions between the various components.

The two wide angle diffusers shown in Fig. 1-2-1 are linked to the axial diffuser by smooth bends. These are necessary in order to avoid severe distortion of the flow since this would have an adverse effect upon performance. The performance of the system can also be affected by the proportion of flow passing through each diffuser. Furthermore, the manner in which the flow divides prior to the branch can influence local conditions at entry to diffusers (B), (C) and (D). For example, if the flow in one branch is in excess of the design value this may cause the splitters to operate at incidence, with the attendant possibility of separation.

Attempts have been made to develop an alternative system which has a simple geometry as well as being less sensitive to the division of flow. Such a system is described in the following section.

1-2-3 The Dump Diffuser System

A typical dump-type combustion chamber diffuser system is shown in Fig. 1-2-4. It is so called because the compressor exit flow is "dumped" into what appears as a duct of very much larger cross-section area. The system has four components in which diffusion takes place. These are labelled (A), (B), (C) and (D) and can be compared directly with those in Fig. 1-2-1. The flow is forced to separate at exit from the initial diffuser and follows the streamline, s-s. This boundary of the flow is often referred to as a "free surface". The remaining volume of the dump region is filled by two standing vortices.

It may be noted that the sharp edged splitters shown in Fig. 1-2-1 have been replaced by the blunt hemitroidal head of the combustion chamber. This arrangement is thought to render the system less sensitive to variations in the division of flow. In addition it can be appreciated that the dump system is geometrically more simple and has fewer critical dimensions which would be subject to close manufacturing tolerances.

The present work represents an initial investigation of the performance characteristics of a simple dump diffuser system as shown in Fig. 1-2-5. It may be noted that no provision is made for flow into the combustion chamber and this considerably simplifies the discussion contained in the following sections.

1-3 PERFORMANCE PARAMETERS

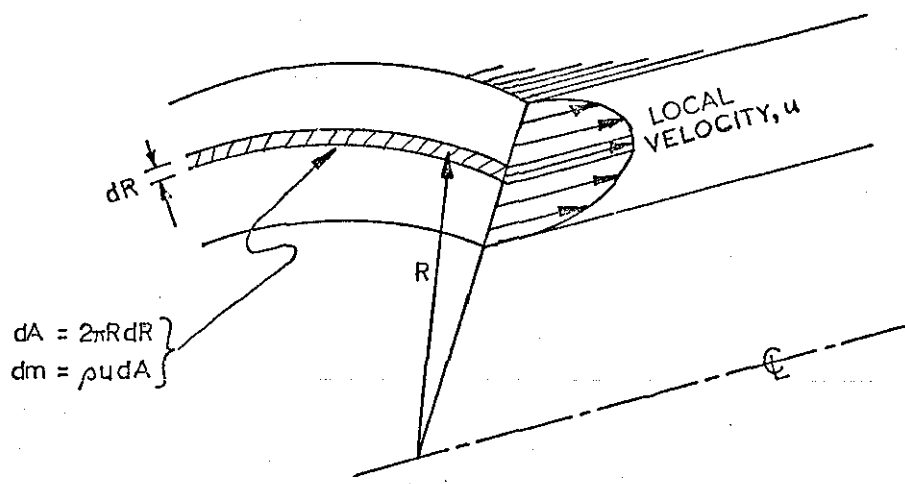
In general the performance of a diffuser can be assessed using three quantitative parameters, the relative importance of which will depend upon the application being considered. These parameters are:

- (i) the static pressure rise achieved by the diffuser,
- (ii) the effectiveness of the diffuser in achieving the above rise in static pressure,
- and (iii) the total pressure loss occurring in the diffuser.

Each parameter is normally represented by a non-dimensional coefficient. Before considering the definition of these coefficients it is important to note that the flow in a diffuser will generally have a non-uniform velocity distribution, and possibly a non-uniform static pressure distribution resulting from streamline curvature. With non-uniform inlet flow the kinetic energy flux entering the diffuser is greater than it would be for the same mass flow entering under uniform conditions. The kinetic energy flux contained in a non-uniform flow is considered in the following section and this leads to the definition of equivalent mean flow quantities. Throughout the present work the flow is assumed to be incompressible.

1-3-1 Equivalent Mean Flow Quantities

The kinetic energy flux of a non-uniform incompressible flow is obtained by integrating the velocity profile as shown below.



The kinetic energy entering the elemental area, dA , in unit time is $(u^2 dm/2)$ and the total flux is therefore,

$$\frac{1}{2} \int^A u^2 dm = \frac{1}{2} \int^A (u^2) \rho u dA$$

1-3-1

It is often convenient to express the kinetic energy flux for a non-uniform flow in terms of that which would be obtained for the equivalent uniform flow (i.e. having the same integrated mass flow). Under uniform conditions the velocity would be, $\bar{u} = m/\rho A$ (termed the mass-derived velocity) and the kinetic energy flux,

$$\frac{1}{2} m \bar{u}^2 = \frac{1}{2} \rho A \bar{u}^3 \quad 1-3-2$$

Comparing Eqns. 1-3-1/2 leads to the definition of the kinetic energy flux coefficient[†], α given as,

$$\alpha = \frac{\frac{1}{2} \int^A (u^2) \rho u \, dA}{\frac{1}{2} \rho A \bar{u}^3} = \frac{1}{A} \int^A \left(\frac{u}{\bar{u}}\right)^3 dA \quad 1-3-3$$

This definition may also be written in terms of dynamic pressures as,

$$\alpha = \frac{1}{m} \int^A \frac{q}{\bar{q}} \, dm = \frac{\tilde{q}}{\bar{q}} \quad 1-3-4$$

where $\bar{q} = \rho \bar{u}^2/2$, and \tilde{q} is the mass-weighted mean dynamic pressure defined,

$$\tilde{q} = \frac{1}{m} \int^A q \, dm = \alpha \bar{q} \quad 1-3-5$$

The energy coefficient, α has a value of 1.0 for uniform flow and rises above unity as the flow distortion or non-uniformity increases. The flux in kinetic energy for a non-uniform flow may now be written as,

$$\frac{1}{2} \int^A u^2 \, dm = \alpha \frac{1}{2} \rho \bar{u}^2 \left(\frac{m}{\rho}\right) = \tilde{q} \left(\frac{m}{\rho}\right) \quad 1-3-6$$

The flux in potential energy (i.e. static pressure energy) is similarly obtained as,

$$\frac{1}{\rho} \int^A p \, dm = \tilde{p} \frac{m}{\rho} \quad 1-3-7$$

where \tilde{p} is the mass-mean static pressure defined,

[†]Henceforward referred to simply as the "energy coefficient".

$$\tilde{p} = \frac{1}{m} \int^A p \, dm \quad 1-3-8$$

Finally, the total flux in energy is obtained from Eqns. 1-3-6/7 as,

$$\frac{m}{\rho} (\tilde{p} + \alpha \frac{1}{2} \rho \bar{u}^2) = \frac{m}{\rho} (\tilde{p} + \tilde{q}) = \frac{m}{\rho} \tilde{P} \quad 1-3-9$$

It may be noted that the mass-mean pressures, \tilde{P} , \tilde{p} and \tilde{q} are the equivalent mean flow quantities for a non-uniform flow, derived on an energy basis.

1-3-2 Performance Parameters for Simple Diffusers

The pressure recovery coefficient, \tilde{C}_{P_2} relates the actual static pressure rise to the maximum attainable with an infinite area ratio.

With non-uniform inlet flow the maximum energy which can be converted into pressure energy is $(\alpha_1 \frac{1}{2} \rho \bar{u}_1^2)$ per unit volume flow (see Eqn. 1-3-6). The pressure recovery coefficient is therefore defined,

$$\tilde{C}_{P_2} = \frac{\tilde{P}_2 - \tilde{P}_1}{\alpha_1 \frac{1}{2} \rho \bar{u}_1^2} \quad 1-3-10$$

Since a diffuser has a finite area ratio the pressure recovery coefficient will always be less than unity. Diffuser effectiveness relates the actual static pressure rise to the maximum achievable in the diffuser with ideal flow (i.e. with no pressure losses). The maximum conversion of kinetic energy is achieved with uniform outlet flow ($\alpha_2 = 1.0$) thus,

$$(p_2' - \tilde{p}_1) = \frac{1}{2} \rho (\alpha_1 \bar{u}_1^2 - \bar{u}_2^2) = \alpha_1 \frac{1}{2} \rho \bar{u}_1^2 \left(1 - \frac{1}{\alpha_1 AR^2} \right)$$

$$\text{and, } C'_{P_2} = \frac{p_2' - \tilde{p}_1}{\alpha_1 \frac{1}{2} \rho \bar{u}_1^2} = \left(1 - \frac{1}{\alpha_1 AR^2} \right) \quad 1-3-11$$

The effectiveness, \tilde{E}_2 is therefore defined,

$$\tilde{E}_2 = \frac{\tilde{C}_{P_2}}{C'_{P_2}} = \frac{\tilde{P}_2 - \tilde{P}_1}{\alpha_1 \frac{1}{2} \rho \bar{u}_1^2 \left(1 - \frac{1}{\alpha_1 AR^2} \right)} \quad 1-3-12$$

The maximum value for effectiveness is, by definition, unity. It may be noted that this is not true of the form of effectiveness often encountered in the literature. This is because the pressure recovery is commonly defined in terms of a two-dimensional reference process (i.e. one with uniform flow at inlet and outlet). The resulting definitions for pressure recovery and effectiveness are,

$$C_{P2_{II}} = \frac{P_2 - P_1}{\frac{1}{2}\rho \bar{u}_1^2} \quad \text{and} \quad \epsilon_{2_{II}} = \frac{P_2 - P_1}{\frac{1}{2}\rho \bar{u}_1^2 \left(1 - \frac{1}{AR^2}\right)}$$

Commenting on this approach, Sovran & Klomp⁽¹⁾ state that "A more convenient, though possibly less meaningful reference process can be defined on the basis of uniform flow conditions". Livesey⁽²⁾, however, has reported a consistent set of definitions that are not subject to qualification and the present definitions are in line with these.

For a diffuser flow in which pressure losses occur the energy equation may be written as,

$$\tilde{P}_1 + \alpha_1 \frac{1}{2}\rho \bar{u}_1^2 = \tilde{P}_2 + \alpha_2 \frac{1}{2}\rho \bar{u}_2^2 + \Delta\tilde{P}_{1-2} \quad 1-3-13$$

where $\Delta\tilde{P}_{1-2}$ is the mass-mean total pressure loss.

The loss coefficient, $\tilde{\lambda}_{1-2}$ is defined as,

$$\tilde{\lambda}_{1-2} = \frac{\Delta\tilde{P}_{1-2}}{\alpha_1 \frac{1}{2}\rho \bar{u}_1^2} \quad 1-3-14$$

Re-arranging Eqn. 1-3-13 and dividing by $(\alpha_1 \frac{1}{2}\rho \bar{u}_1^2)$ we obtain

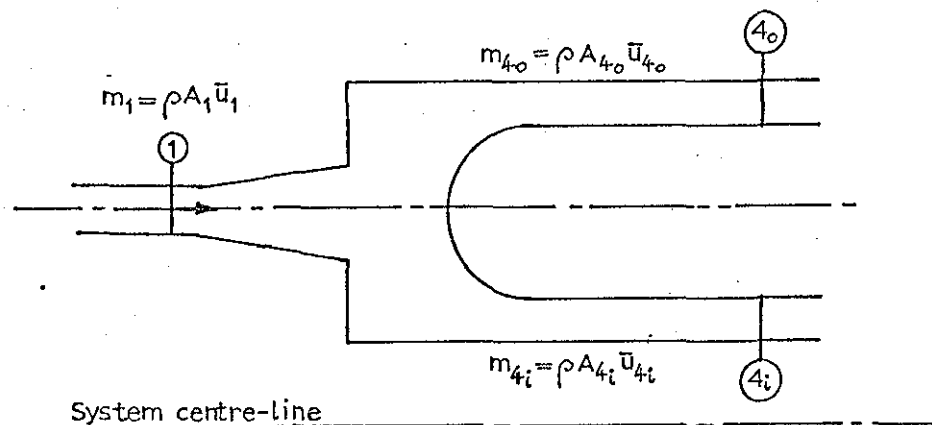
$$\begin{aligned} \tilde{C}_{P2} &= 1 - \frac{\alpha_2}{\alpha_1 AR^2} - \tilde{\lambda}_{1-2} \\ \text{or, } \tilde{C}_{P2} &= \left(1 - \frac{1}{\alpha_1 AR^2}\right) - \left(\frac{\alpha_2 - 1}{\alpha_1 AR^2}\right) - \tilde{\lambda}_{1-2} \quad 1-3-15 \end{aligned}$$

The first term on the left hand side of Eqn. 1-3-15 represents the ideal pressure recovery (Eqn. 1-3-11). The value of $(\alpha_2 - 1)$ is a measure

of the distortion of the outlet flow and the second term therefore represents the reduction in pressure recovery due to excess kinetic energy at the outlet plane. The pressure recovery may therefore be reduced by insufficient diffusion as represented by the second term, or by inefficient diffusion as represented by the loss coefficient.

1-3-3 Performance Parameters for Branched Systems

In essence the performance parameters for branched systems are defined in the same way as for simple diffusers. The defining equations are, however, complicated because of the need to allow for variations in the division of flow. The present work is restricted to consideration of the simple branched system shown below.



For this system it is necessary to write the energy equation in terms of total energy flux rather than energy flux per unit volume flow as in Eqn. 1-3-13.

$$\text{i.e. } \frac{m_1}{\rho} (\tilde{p}_1 + \tilde{q}_1) = \frac{m_{4i}}{\rho} (\tilde{p}_{4i} + \tilde{q}_{4i}) + \frac{m_{4o}}{\rho} (\tilde{p}_{4o} + \tilde{q}_{4o}) + \frac{m_1}{\rho} \Delta \tilde{P}_{1-4} \quad 1-3-16$$

Dividing by $(m_1 \tilde{q}_1 / \rho)$, re-arranging and substituting $\tilde{q} = \alpha \frac{1}{2} \rho \bar{u}^2$, we

have

$$\tilde{C}_{p4} = 1 - \left(\frac{m_{4i} \alpha_{4i} \bar{u}_{4i}^2 + m_{4o} \alpha_{4o} \bar{u}_{4o}^2}{m_1 \alpha_1 \bar{u}_1^2} \right) - \tilde{\lambda}_{1-4} \quad 1-3-17$$

where,
$$\tilde{C}_{p4} = \left(\frac{m_{4i} \tilde{p}_{4i} + m_{4o} \tilde{p}_{4o} - m_1 \tilde{p}_1}{m_1 \alpha_1 \frac{1}{2} \rho \bar{u}_1^2} \right) = \frac{\tilde{P}_4 - \tilde{P}_1}{\alpha_1 \frac{1}{2} \rho \bar{u}_1^2} \quad 1-3-18$$

$$\text{and } \tilde{\lambda}_{1-4} = \frac{\Delta \tilde{P}_{1-4}}{\alpha_1 \frac{1}{2} \rho \bar{u}_1^2} \quad 1-3-19$$

In order to define effectiveness for the branched system we require the ideal pressure recovery, \tilde{C}'_{p4} and this is given by Eqn. 1-3-17 with $\tilde{\lambda}_{1-4} = 0$ and $\alpha_{4_i} = \alpha_{4_o} = 1.0$,

$$\text{i.e. } \tilde{C}'_{p4} = 1 - \frac{(m_{4_i} \bar{u}_{4_i}^2 + m_{4_o} \bar{u}_{4_o}^2)}{m_1 \alpha_1 \bar{u}_1^2} \quad 1-3-20$$

The effectiveness, $\tilde{\xi}_4$ is defined as $(\tilde{C}_{p4} / \tilde{C}'_{p4})$ and from Eqns. 1-3-18 and 1-3-20 it can be seen that this is a complicated expression. In particular it may be noted that it is difficult to simplify Eqn. 1-3-20 by introducing an area ratio as was done in Eqn. 1-3-11 of the previous section. The following approach is therefore adopted. Firstly, we define the flow split ratio, S as

$$S = (m_o/m_i)_4 = \left(\frac{\bar{u}_o A_o}{\bar{u}_i A_i} \right)_4 \quad 1-3-21$$

Since $m_1 = m_{4_i} + m_{4_o}$ by continuity, the mass flow and velocity ratios in Eqn. 1-3-20 may be expressed:

$$m_{4_i}/m_1 = \left(\frac{1}{1+S} \right); \quad m_{4_o}/m_1 = \left(\frac{S}{1+S} \right) \quad 1-3-22$$

$$\text{and } \bar{u}_{4_i}/\bar{u}_1 = \left(\frac{1}{1+S} \right) \left(\frac{A_1}{A_{4_i}} \right); \quad \bar{u}_{4_o}/\bar{u}_1 = \left(\frac{S}{1+S} \right) \left(\frac{A_1}{A_{4_o}} \right) \quad 1-3-23$$

Substituting the above identities in Eqn. 1-3-20 and simplifying gives,

$$\tilde{C}'_{p4} = 1 - \frac{1}{\alpha_1} \left(\frac{1}{1+S} \right)^3 \left(\frac{1}{AR_i^2} + \frac{S^3}{AR_o^2} \right) \quad 1-3-24$$

$$\text{where, } AR_i = (A_{4_i}/A_1) \quad \text{and} \quad AR_o = (A_{4_o}/A_1) \quad 1-3-25$$

It is now convenient to define an effective area ratio, AR_e for the branched system such that,

$$\tilde{C}'_{p4} = 1 - \frac{1}{\alpha_1 AR_e^2} \quad 1-3-26$$

Comparing Eqns. 1-3-24 and 1-3-26 shows that,

$$\frac{1}{AR_e^2} = \left(\frac{1}{1+S} \right)^3 \left(\frac{1}{AR_i^2} + \frac{S^3}{AR_o^2} \right) \quad 1-3-27$$

The effectiveness of a branched diffuser system may now be expressed in the simplified form,

$$\tilde{C}'_{p4} = \frac{\tilde{C}'_{p4}}{\left(1 - \frac{1}{\alpha_1 AR_e^2} \right)} \quad 1-3-28$$

It may be noted that the effective area ratio and ideal pressure recovery are functions of both the system geometry and the flow split ratio. The division of flow therefore has a direct influence on system performance and this may be assessed by considering the changes in effective area ratio with varying flow split. The influence of flow split is discussed in Sect. 1-5-3.

1-4 BOUNDARY LAYER AND VELOCITY PROFILE PARAMETERS

1-4-1 Boundary Layer Parameters

In the present work boundary layer parameters are used to describe the state of development of a boundary layer and the characteristics of the corresponding velocity profile. The generally accepted axi-symmetric definitions have been adopted and these are given in Table 1-4.

The definition of displacement thickness, δ^* arises from considering the mass flow deficit in the boundary layer as compared with a uniform flow of velocity U ,

$$\text{thus, } \rho U 2\pi R_w \delta^* = \rho \int_{R_w}^{R_m} (U - u) 2\pi R dR$$

$$\text{and, } \delta^* = \int_{R_w}^{R_m} \left(1 - \frac{u}{U} \right) \frac{R}{R_w} dR \quad 1-4-1$$

where R_w is the wall radius and R_m the radius at the edge of the

boundary layer. Comparison of Eqn. 1-4-1 with the two-dimensional definition,

$$\delta_{II}^* = \int_0^{y=\delta} \left(1 - \frac{u}{U}\right) dy$$

shows that $\delta^* \rightarrow \delta_{II}^*$ as $R_w \rightarrow \infty$. However, it should be noted that the concept of wall displacement valid for two-dimensional boundary layers (implicit in the definition of δ_{II}^*) is not applicable for axi-symmetric flows,

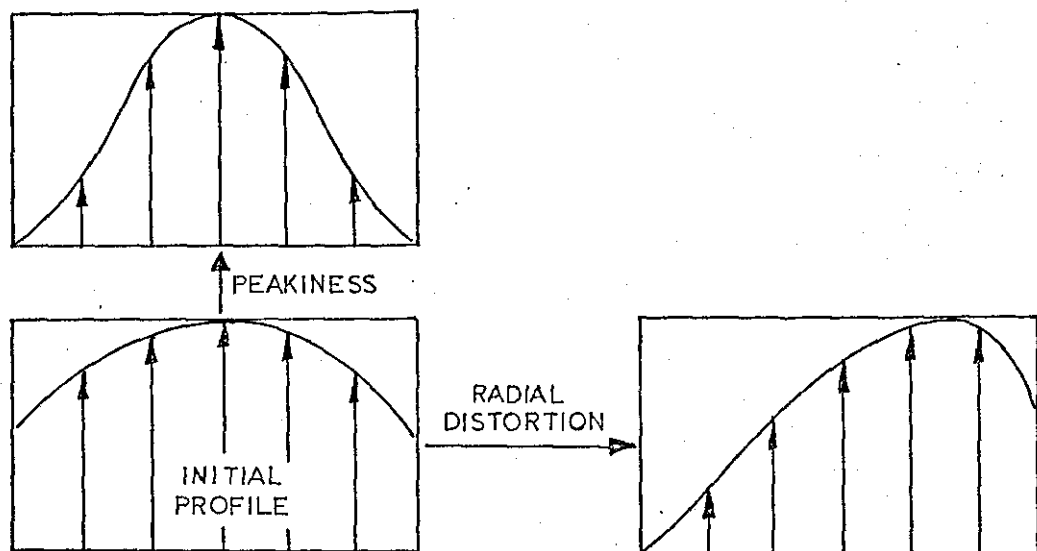
$$\text{i.e. } 2\pi \int_{R_w}^{R_m} u R dR \neq U\pi \left[R_m^2 - (R_w + \delta^*)^2 \right]$$

The shape parameter, $H = \delta^*/\theta$ is of particular interest from the point of view of describing boundary layer velocity profiles since it may be used to indicate how close a particular profile is to separation. Separation criteria are by no means accurate, however values of H between 2.4 and 2.6 are commonly found to correspond with the onset of separation.

1-4-2 Velocity Profile Parameters

In most diffuser applications the flow can be characterised as having a non-uniform velocity profile with a single point of maximum velocity in any one cross-section. The location of this point of maximum velocity and the magnitude of the velocity depend largely upon the pressure gradients to which the two wall boundary layers are subjected. In the context of the present work it is important to distinguish between two characteristics relating to the shape of velocity profiles, namely peakiness and radial distortion. These are illustrated in the diagram over.

If the adverse pressure gradients are appreciable (as in a diffuser) but equal in magnitude for both boundary layers, a symmetrical peaked profile is formed. If, however, one boundary layer is subjected to a higher pressure gradient than the other, the boundary layer growth is unequal and the peak position is displaced from the centre of the duct. The resulting velocity profile is said to be radially distorted.



Whereas peakiness and radial distortion are related to each other, they are dealt with separately here.

(i) Profile Peakiness

Most of the commonly used profile peakiness parameters derive from the blocked area concept suggested by Sovran & Klomp⁽¹⁾ for evaluating inlet profile effects on various diffuser geometries. The blocked area, A_B is given by

$$A_B = \int_0^A \left(1 - \frac{u}{U}\right) dA = A \left(1 - \frac{\bar{u}}{U}\right)$$

The blocked area fraction, B and the effective area fraction, E are then obtained as,

$$B = \left(1 - \frac{\bar{u}}{U}\right) = (1 - E) = 2 \frac{(R_{w_i} \delta_i^* + R_{w_o} \delta_o^*)}{(R_{w_o}^2 - R_{w_i}^2)} \quad 1-4-2$$

These parameters are particularly convenient since, knowing the mass flow and cross-section area, they may be calculated from a single measurement of the maximum velocity. The blocked area fraction has been widely adopted for use in correlating the effects of inlet profile variations on diffuser performance.

The energy coefficient, α (see Sect. 1-3-1) is a further parameter

which relates to the peakiness of a velocity profile. In view of its importance in determining diffuser performance the energy coefficient is a logical choice of parameter for representing profile peakiness. It is however, necessary to have detailed velocity profile data in order to evaluate α .

(ii) Radial Distortion

One obvious choice of parameter for describing radial distortion is the distance of the profile peak from the centre of the duct (expressed as a fraction of the annulus height). However, this is not very satisfactory for making quantitative comparisons of velocity profiles since the peak position cannot always be determined accurately. Radial distortion is therefore usually assessed by comparing δ^* , θ and H for the inner and outer wall boundary layers. Taking this approach one step further it is possible to define specific parameters which relate directly to radial distortion. As an example, the difference in displacement thickness ($\delta_i^* - \delta_o^*$) between the inner and outer boundary layers may be used in formulating a radial distortion factor, RD, of the form

$$RD = \left(\frac{\delta_i^* - \delta_o^*}{\delta_i^* + \delta_o^*} \right) \quad 1-4-3$$

Although arbitrarily defined, such a factor can be expected to provide a good quantitative measure of radial distortion. It may be noted that non-dimensionalising with respect to $(\delta_i^* + \delta_o^*)$ has the effect of making RD essentially independent of profile peakiness.

1-5 FACTORS INFLUENCING DIFFUSER SYSTEM PERFORMANCE

The factors which influence the performance of branched diffuser systems can be considered under three headings; inlet conditions, system geometry, and division of flow. The influences of inlet conditions and geometry on the performance of simple diffusers have been dealt with at length in the literature. Compared with simple diffusers the geometric and flow variables

for branched systems are much larger in number. The influence of each variable will not therefore be discussed in detail, except in the case of variables which are peculiar to branched systems.

1-5-1 Inlet Conditions

(i) Mach Number and Reynolds Number

Tests carried out by Little & Wilbur⁽³⁾ on conical diffusers indicate that pressure recovery is essentially independent of Mach number below a critical value at which local sonic conditions are obtained near the inlet corner. McDonald & Fox⁽⁴⁾, again working with conical diffusers, have shown that performance is not sensitive to Reynolds numbers above 7×10^4 . In relation to annular diffusers, Gurevich⁽⁵⁾ has shown that the loss coefficient is insensitive to Mach numbers between 0.25 and 0.7 for diffusers operating with low entry swirl. It is assumed that these results will also apply in the case of branched systems.

(ii) The Inlet Velocity Profile and its Characteristics

A large amount of work has been reported on the effects of inlet velocity profile variation upon diffuser performance. Whereas profile shape and turbulent mixing are generally regarded as the main factors influencing performance, it has remained difficult to isolate the effects of each. For this reason much of the literature relates to experiments in which the inlet profile distortion was varied without controlling the turbulent mixing.

In correlating the effects of inlet profile variation on diffuser performance Sovran & Klomp⁽¹⁾ have used the inlet blockage fraction, B_1 as a measure of profile distortion. In their investigation they were able to show that the outlet effective area fraction, E_2 correlated with the inlet blockage fraction and area ratio as shown in Fig. 1-5-1. Using this correlation the appropriate value of E_2 may be substituted in the indicated equation to obtain the effectiveness, ξ_{II} of a given diffuser.

$$\text{i.e. } \xi_{II} = \frac{1}{E_1^2} \left[\frac{1 - \frac{(E_1/E_2)^2}{AR^2}}{1 - \frac{1}{AR^2}} \right] \quad 1-5-1$$

where $E_1 = 1 - B_1$.

A representative variation of ξ_{II} with B_1 has been deduced from Fig. 1-5-1 together with additional data due to Wolf & Johnston⁽⁶⁾ and Tyler & Williamson⁽⁷⁾ (see Fig. 1-5-2). It can be seen that ξ_{II} falls significantly as B_1 is increased. It may be noted that the two-dimensional definition of ξ_{II} takes no account of the increase in available energy as B_1 is increased (i.e. the increase in α_1 is not accounted for). Therefore, in terms of the present definition (Eqn. 1-3-12), the effectiveness, ξ would decrease more rapidly with increased inlet distortion than is indicated in Fig. 1-5-2.

Although the importance of inlet turbulence has long been appreciated, it is only recently that experiments have been conducted to show its independent influence on diffuser performance. By using an artificial velocity profile generator Bradley & Cockrell⁽⁸⁾ were able to generate a high turbulence flow at entry to a conical diffuser whilst maintaining the same velocity profile as that given by a long smooth entry pipe. The axial turbulence intensity produced by the profile generator was approximately twice that obtained with fully developed pipe flow. This increase in turbulence intensity was shown to produce an improvement in pressure recovery of between 10 and 12%. Williams⁽¹⁰⁾ also observed similar improvements in the pressure recovery of three annular diffusers when the inlet turbulence was raised by placing a coarse grid upstream of the inlet plane. In this case it is interesting to note that the loss coefficients were not significantly altered and that the improvements in performance were solely attributable to reductions in outlet profile distortion.

It is thus apparent that turbulent mixing and inlet profile distortion

have opposing influences on diffuser performance. Since most methods of producing distorted velocity profiles also produce high turbulence levels it is reasonable to suggest that the independent influence of profile distortion is more severe than that indicated in Fig. 1-5-2. The effect of radial distortion of the inlet profile has not been dealt with specifically, however on physical grounds it can be argued that inlet radial distortion will be accentuated by the diffuser, thus rendering the flow on one wall more prone to separation than would have been the case with "symmetrical" inlet flow.

(iii) Entry Swirl

A good symptomatic assessment of the influence of entry swirl on the performance of annular diffusers may be obtained by reference to the work of Gurevich⁽⁵⁾. As an example, the influence of swirl angle on loss coefficient for constant inner core diffusers is shown in Fig. 1-5-3. Data has been selected to cover a range of wall angles. Under zero swirl conditions, the loss coefficient increases with increasing wall angle as would be expected. The influence of swirl is generally to increase the loss coefficient, however, small amounts of swirl are seen to have a beneficial effect, particularly for the higher wall angles. This effect can be explained by reference to the total pressure contours reported by Horlock⁽¹¹⁾ for a constant inner core annular diffuser operating with and without swirl (see Fig. 1-5-4). For zero swirl the flow is distorted and separation occurs on the outer wall near the exit plane. When swirl is introduced, the situation is reversed and separation occurs on the inner wall. At some intermediate stage, separation will be eliminated and this is thought to correspond with the minimum loss conditions shown in Fig. 1-5-3.

1-5-2 Diffuser System Geometry

(i) Pre-diffuser

One major variable of the diffuser system (see Fig. 1-2-5) is the

amount of diffusion attempted in the pre-diffuser. As the area ratio of the pre-diffuser is increased the mean velocity at exit is reduced, thus implying a lower loss in the remainder of the system. At the same time, however, the pre-diffuser outlet velocity profile becomes more distorted and this may be accompanied by flow separation. The problem is illustrated in Fig. 1-5-5 which shows the main features of the annular diffuser performance chart due to Sovran & Klomp⁽¹⁾. Three lines have been added to the performance chart:

- (a) A line denoted C_p^* which defines the area ratio producing maximum pressure recovery for a given non-dimensional length.
- (b) A line denoted C_p^{**} which defines the non-dimensional length producing maximum pressure recovery for a given area ratio.
- (c) A line of first stall due to Howard, Henseler & Thornton-Trump⁽¹²⁾.

For practical purposes, the C_p^* line is the more important of the two optimum lines and is often used in determining minimum length geometries for low area ratio diffusers. However, for area ratios above approximately 1.7 it becomes necessary to increase the non-dimensional length beyond that specified by the C_p^* line, in order to avoid flow separation (stall).

In the case of the arrangement being considered, the above effects will be modified by the downstream geometry, in particular the proximity of the combustion chamber head[†]. In connection with this, Henderson⁽¹³⁾ found that target plates placed downstream of a conical diffuser had the effect of improving the performance and flow stability. It was, however, found that losses around the plate far outweighed the improvement in performance of the diffuser.

(ii) Downstream Section

Four important geometric variables may be identified for the downstream section of the dump diffuser system. These are the area ratio, the ratio of outer to inner annulus areas, the distance of the head from the pre-diffuser

[†] Hereafter referred to as "the head"

exit plane (dump gap) and the width of the combustion chamber in relation to the pre-diffuser outlet annulus height. For a given application the overall area ratio will be fixed, therefore the area ratio of the downstream section is determined by that chosen for the pre-diffuser. The outer to inner annulus area ratio does not have a direct influence on performance, however it is important when considering the division of flow between the annuli surrounding the combustion chamber. This is discussed in the next section.

The width and axial location of the combustion chamber can be expressed in terms of the non-dimensional parameters, H/h_2 and D/h_2 (see Fig. 1-2-5). The value of H/h_2 specifies the amount by which the flow must be displaced radially, and the dump gap (D/h_2) specifies the distance over which the flow can turn in order to negotiate the combustion chamber. By analogy with flow conditions around bluff bodies in a free stream, it can be appreciated that there will be a local acceleration and subsequent diffusion of the flow as it passes around the head and into the parallel walled annuli. For a decrease in D/h_2 and/or an increase in H/h_2 , it can be argued that the local acceleration will increase with attendant penalties in performance. In a similar way, the shape of the head can also be expected to have an influence on the performance.

1-5-3 Division of Flow

Branched combustion chamber diffuser systems are usually designed such that the mean velocities are equal in the two annuli surrounding the combustion chamber. It is, however, important to consider flow split ratios other than the design value implied by $\bar{u}_{4_o} = \bar{u}_{4_i}$. Qualitatively it can be appreciated that the division of flow determines the pressure recovery achieved in each annulus. If energy losses are neglected, the pressure recovery will be proportional to the net reduction of velocity in each annulus. Thus, for annulus flows greater than design, the pressure recovery will be low, and vice-versa for flows which are higher than design. The

effect on overall performance will now be demonstrated by reference to the equations of Sect. 1-3.

Let us consider a simple two-dimensional branched system of area ratio 2.0, for which the downstream annulus areas are equal and the inlet flow is uniform (see Fig. 1-5-6). The inner and outer area ratios, AR_i and AR_o (see Eqn. 1-3-25) are both equal to 1.0 and the expression for the overall pressure recovery (Eqn. 1-3-24) therefore reduces to,

$$\tilde{C}'_{p_4} = 1 - \left(\frac{1}{1+S} \right)^3 (1+S^3) \quad 1-5-2$$

where \tilde{C}'_{p_4} is the ideal mass-mean pressure recovery and S is the flow split ratio. The design flow split, S_4^* is defined as the flow split for which the inner and outer annulus velocities are equal. Thus, for the system being considered, $S_4^* = (A_o/A_i)_4 = 1.0$. The variation of ideal pressure recovery with flow split, given by Eqn. 1-5-2, is shown in Fig. 1-5-6(a). It can be seen that the pressure recovery is reduced when the flow split departs from the design value, S_4^* . It is interesting to consider this in terms of the effective area ratio, AR_e as defined by Eqn. 1-3-27. In this case, Eqn. 1-3-27 reduces to

$$\frac{1}{AR_e^2} = \left(\frac{1}{1+S} \right)^3 (1+S^3) \quad 1-5-3$$

For the design flow split, $S = S_4^*$, we find that $AR_e = 2.0$ (i.e. the effective area ratio is equal to the geometric area ratio, $(A_{4_i} + A_{4_o})/A_1$). For other flow splits the effective area ratio is lower than the geometric area ratio (see Fig. 1-5-6(b)). It may be noted that $AR_e = AR_i$ for $S = 0$ and $AR_e = AR_o$ for $S = \infty$.

To summarise, three points are to be noted;

- (i) The ideal pressure recovery of a branched system depends upon the flow split at which it operates.
- (ii) The maximum ideal pressure recovery is only obtained at the flow split for which the mean velocities are equal in the two branches (i.e. the design flow split).

- (iii) The effective area ratio is only equal to the geometric area ratio when the system operates at the design flow split.

In addition to its influence on overall performance, the flow split will also influence conditions at exit from the pre-diffuser. The static pressures associated with a disproportionate amount of flow passing down one annulus are such as to imply changes in boundary layer development in the pre-diffuser. It is therefore apparent that the flow split will influence the performance of the pre-diffuser.

1-6 REVIEW OF PREVIOUS WORK RELATING TO COMBUSTION CHAMBER DIFFUSERS

Whereas a large amount of work has been reported on the performance of simple diffusers, little attention has been paid to more complicated geometries. In particular, there is little published information available on combustion chamber diffuser systems, even though a considerable amount of knowledge must have been gained in the development of modern gas turbine engines. Considerable design problems arise due to difficulties concerning the flow characteristics of the compressor exit environment and the necessarily complex geometry of the ducts themselves. Experimental evidence of the influence of flow characteristics on the performance of simple diffusers has been dealt with in the foregoing sections. The limited information available on more complex diffuser system geometries is now briefly reviewed.

1-6-1 Investigations of the Performance of a Wide Angle

Annular Diffuser

A variety of tests have been carried out at Loughborough⁽²⁰⁾ on a wide angle diffuser having a geometry typical of that employed in the "faired" type of combustion chamber diffuser system shown in Fig. 1-2-1. In addition to investigating the basic performance and flow behaviour, the penalties associated with the addition of internal struts and the effect of replacing the outlet bend by a free surface expansion were studied.

(i) Basic Performance after Stevens & Fry⁽¹⁴⁾

The basic geometry comprised a wide angle annular diffuser ($AR = 2.0$, $L/h_2 = 6.2$, $\epsilon = 40^\circ$) interposed between two constant area bends connecting it with the parallel inlet and outlet annuli. The geometry and corresponding performance are given in Fig. 1-6-1. Comparing the results with those for a constant inner core diffuser ($AR = 2.0$, $L/h_1 = 5.0$) showed that the loss coefficient for the wide angle diffuser was very much higher (0.163 compared with 0.055). This increase in loss was considered to be due to the higher turbulence level of the flow from the inlet bend increasing the energy dissipation. The high turbulent mixing was, however, confined to the flow adjacent to the inner wall and the initial radial distortion of the flow in the inlet bend was accentuated by the adverse pressure gradient in the diffuser to the extent that intermittent transitory stalling occurred on the outer wall just upstream of the outlet bend. In the outlet bend, radial momentum transfer reduced the velocity profile distortion and a significant recovery of static pressure was achieved.

(ii) Effect of Replacing Outlet Bend by Free Surface Expansion

In an attempt to stabilise the point of separation in the diffuser, tests were carried out by the author⁽¹⁵⁾ on a modified geometry in which the outlet bend was replaced by a free surface expansion (see Fig. 1-6-2). The amounts of diffusion attempted in the diffuser and the free surface expansion region were varied (by "cutting back" the diffuser) whilst the overall area ratio was maintained at 2.0. The results indicate that the performance penalty was small for a free surface expansion ratio, AR_{fs} of 1.0, but that the penalty increased as the length of the diffuser was decreased. The loss occurring in the diffuser was not significantly affected by the change in downstream geometry, therefore the increased energy loss was attributed to the energy required to sustain the vortex system, and that dissipated by turbulent mixing as the highly sheared velocity profile at

diffuser exit was transformed to almost uniform conditions in the settling length.

(iii) Influence of Internal Struts

Two preliminary tests were carried out to assess the influence of internal struts on the performance of the wide angle diffuser. The struts ran the entire length of the diffuser, with the position of maximum thickness situated in the diffuser exit plane (see Fig. 1-6-3). In the first test, struts were incorporated in the existing rig (Fig. 1-6-1) and this effectively reduced the diffuser area ratio to 1.7. The results indicated an increase in loss coefficient of 0.03 without any serious separation on the outer wall of the diffuser. In the second test the diffuser was modified to restore the area ratio to 2.0 and the increase in loss coefficient due to the struts was found to be approximately 0.05. Due to the increased pressure gradient in the modified diffuser, separation took place on the outer wall at diffuser exit. It is interesting to note that the increases in loss coefficient were of the same order as those measured by Gurevich⁽⁵⁾ in a constant inner core annular diffuser (AR = 2.0) having struts whose chord was approximately half the length of the diffuser.

1-6-2 Aerodynamic Stability of Branched Diffuser Systems

Although no experimental work has been published on the performance of branched diffuser systems, Ehrich⁽¹⁶⁾ has carried out a theoretical investigation of the aerodynamic stability of such systems and suggests that stability will be maintained provided that,

$$\gamma = \left[\frac{\partial C_{p_a}}{\partial B_a} + \frac{\partial C_{p_b}}{\partial B_b} \right] < 0 \quad 1-6-1$$

where the subscripts 'a' and 'b' refer to the two branches and B_a and B_b are the flow fractions in each branch (see Fig. 1-6-4). With ideal, one-dimensional flow the pressure recovery in each branch would increase with decreasing flow (i.e. $\partial C_p / \partial B$ always negative), however these ideal

considerations are modified by the occurrence of pressure losses and separated flow. At low flow fractions separation is likely to occur and $\partial C_p / \partial B$ will then be positive as indicated in Fig. 1-6-4. Under certain conditions the stability parameter, γ can therefore become positive and the system become unstable with oscillations in flow between the two branches.

1-7 CHOICE OF DIFFUSER SYSTEM TO BE INVESTIGATED

In view of the lack of data on dump diffuser systems, the primary objective of the present investigation was to obtain a fundamental understanding of their operation and to assess the influence of some of the main variables. From the outset it was considered important to limit the number of variables studied and to maintain an independent control over each one. In view of this it was decided that no attempt should be made to simulate the flow into the combustion chamber. Instead, the system was designed with two constant area ducts, or settling lengths, surrounding the combustion chamber (as shown in Fig. 1-2-5).

Current thinking suggested that two-dimensional and annular segment rigs were to be avoided because of the uncertainty associated with the three-dimensional effects inevitably encountered when using end walls. Despite the manufacturing complexity, it was decided that the test rig should be fully annular.

The choice of geometry represented a compromise between two objectives, namely, that the system should be representative of current designs and that the annulus heights should be sufficient to carry out detailed measurements. The geometric details are summarised in the following table.

Geometry chosen for the present investigation

	Current Design Values	Chosen Value
Inlet Radius Ratio, $(R_i/R_o)_1$	0.84 - 0.90	0.85
Overall Area Ratio, $(A_{4_i} + A_{4_o})/A_1$	1.8 - 2.5	2.0
Combustion Chamber "Size", H/h_1	3.3 - 3.9	3.5
Design Flow Split	Various	2.15

Design flow splits for combustion systems vary considerably depending upon the design philosophy employed. For convenience, it was decided to make the settling length annulus heights equal, and this, in conjunction with a typical combustion chamber size, gave a design flow split of 2.15.

The test rig was manufactured entirely from perspex to facilitate flow visualisation, and provisions were made for:

- (i) varying the pre-diffuser geometry,
- (ii) varying the axial location of the combustion chamber (i.e. the dump gap),
- and (iii) varying the division of flow between the two annuli (i.e. the flow split ratio, S).

Fully developed flow was chosen as the pre-diffuser inlet condition, since this was considered to be more representative of compressor exit flow than the thin inlet boundary layer condition frequently used in diffuser research.

1-8 OBJECTIVES AND SCOPE OF INVESTIGATION

The general objective of the work was to obtain a fundamental

understanding of the fluid mechanic behaviour of a simple dump diffuser system. The specific objectives are summarised as follows.

(i) To investigate the influence of flow split and dump gap on the overall performance for each of five pre-diffuser geometries. The pre-diffuser geometries were to be consistent with demonstrating,

(a) the influence of increasing the area ratio for a constant included angle,

(b) the influence of increasing the included angle for a constant area ratio,

and (c) the effect of canting the pre-diffuser.

(ii) For each set of test conditions, to measure:

(a) the velocity profiles at pre-diffuser outlet and in the settling length annuli, paying particular attention to flow stability,

(b) the static pressure profile at pre-diffuser exit and the wall static pressure distribution throughout the system,

and (c) the velocity and static pressure variation in planes perpendicular to the head surface, this to be carried out in the region of maximum velocity over the head.

(iii) To estimate the energy losses occurring in each component of the system and thereby to identify regions of high loss.

Chapters 2 and 3 describe the experimental facility, the choice of test geometries and flow conditions, and the experimental techniques employed. Chapter 4 gives details of the experimental results. A further analysis of the energy losses is presented in Chapter 5 and conclusions relevant to the whole investigation are given in Chapter 6.

Fig.1-2-1 TYPICAL MODERN GAS TURBINE WITH "FAIRED" COMBUSTION
CHAMBER DIFFUSER SYSTEM.

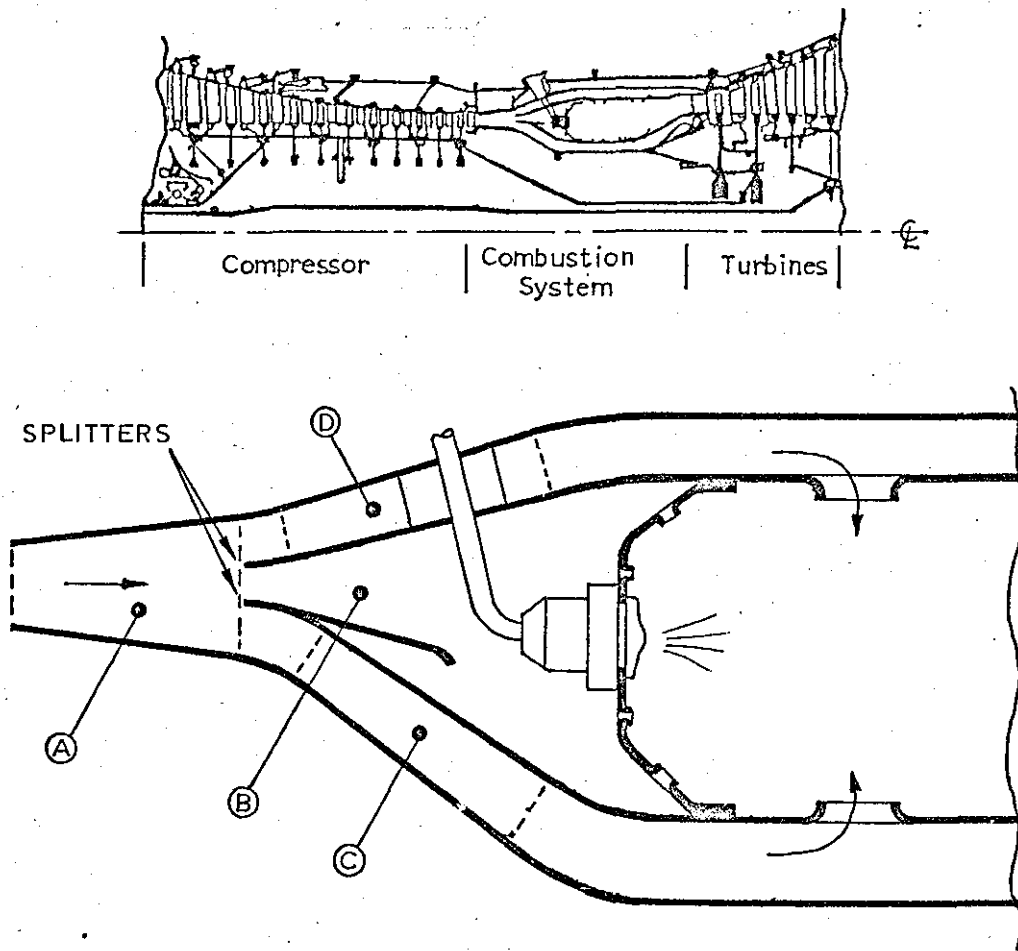


Fig.1-2-2 GEOMETRIC CHARACTERISTICS OF A RECTILINEAR
ANNULAR DIFFUSER

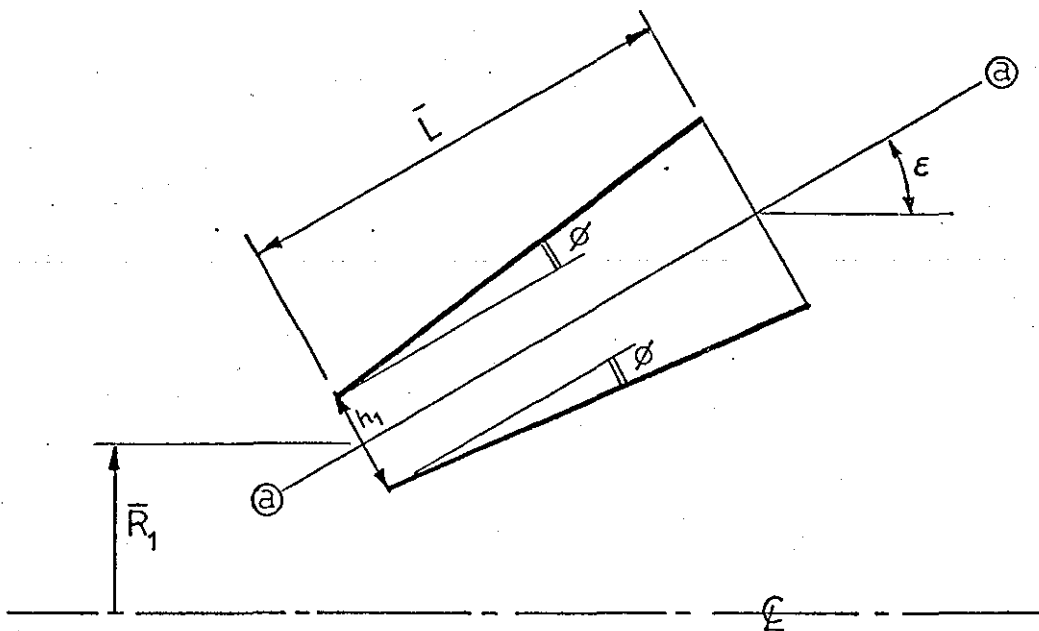


Fig.1-2-3 TYPES OF ANNULAR DIFFUSER.

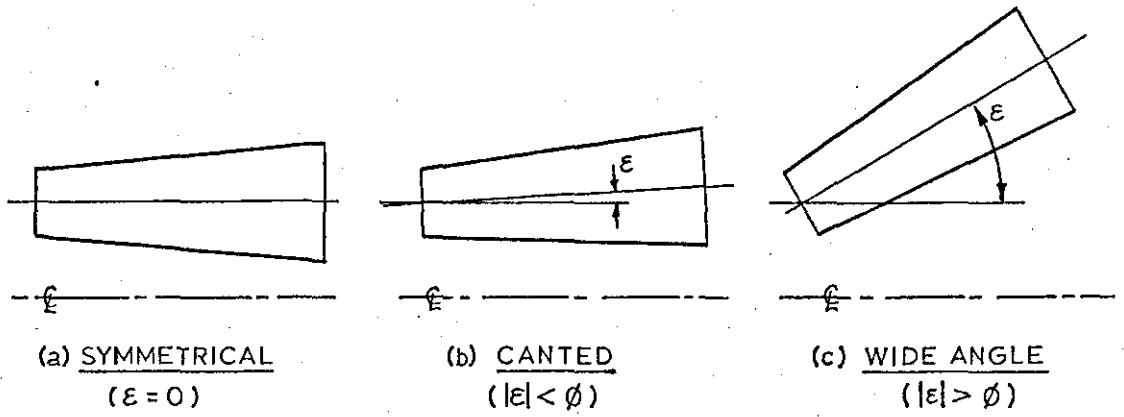


Fig.1-2-4 TYPICAL DUMP DIFFUSER SYSTEM.

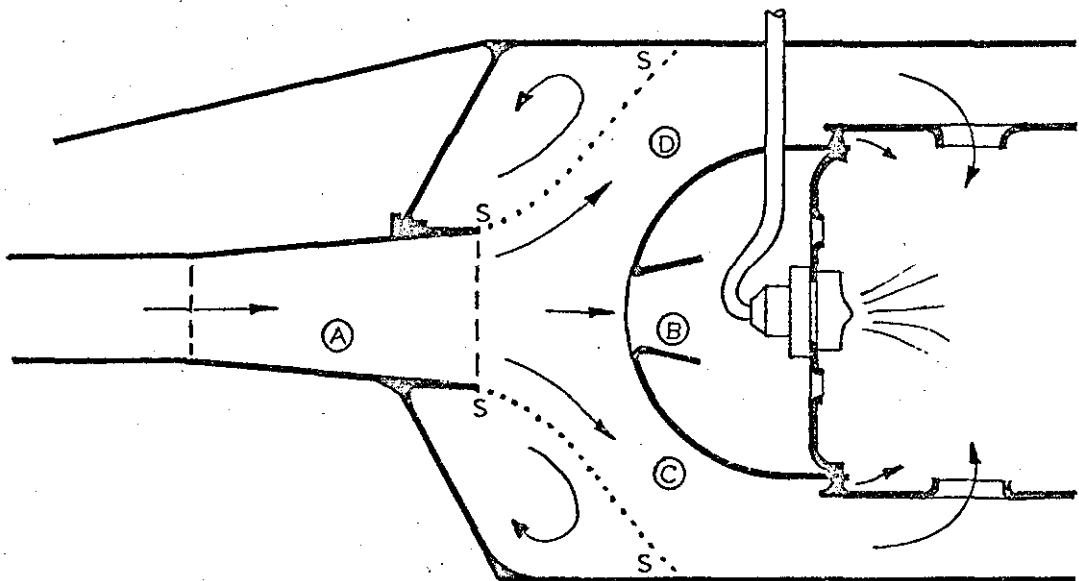


Fig.1-2-5 SIMPLE ANNULAR DUMP DIFFUSER SYSTEM.

(As used for present investigation)

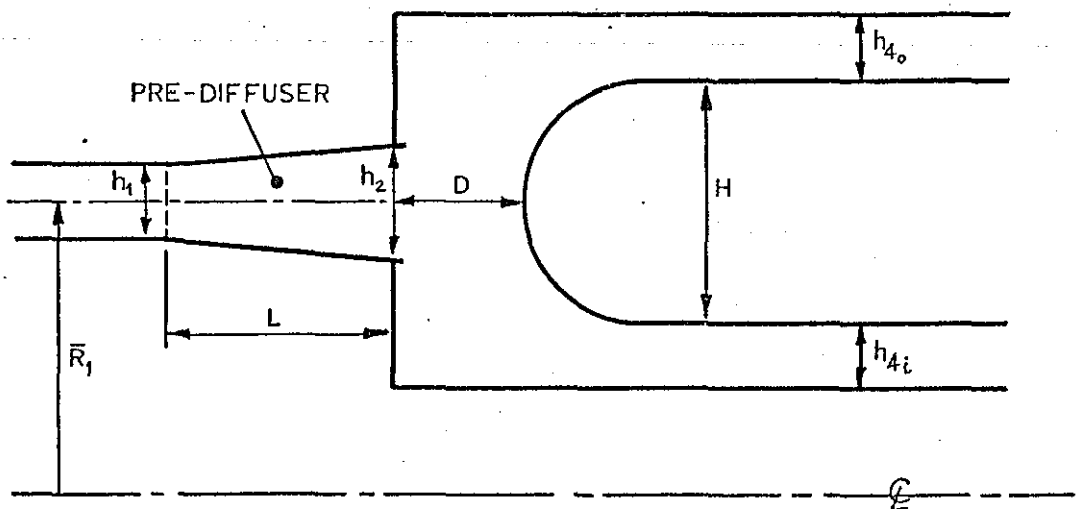


Fig.1-5-1 INFLUENCE OF INLET BLOCKAGE ON DIFFUSER PERFORMANCE AFTER SOVRAN & KLOMP⁽¹⁾

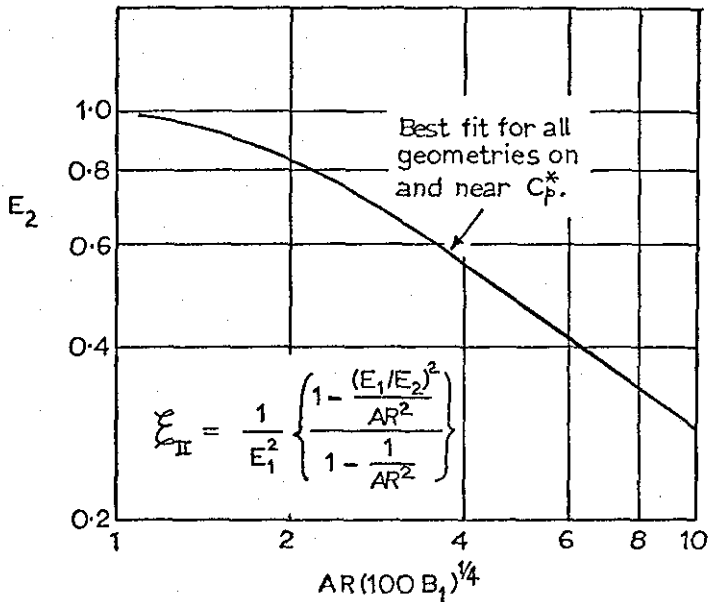


Fig.1-5-2 VARIATION OF DIFFUSER EFFECTIVENESS WITH INLET BLOCKAGE FRACTION.

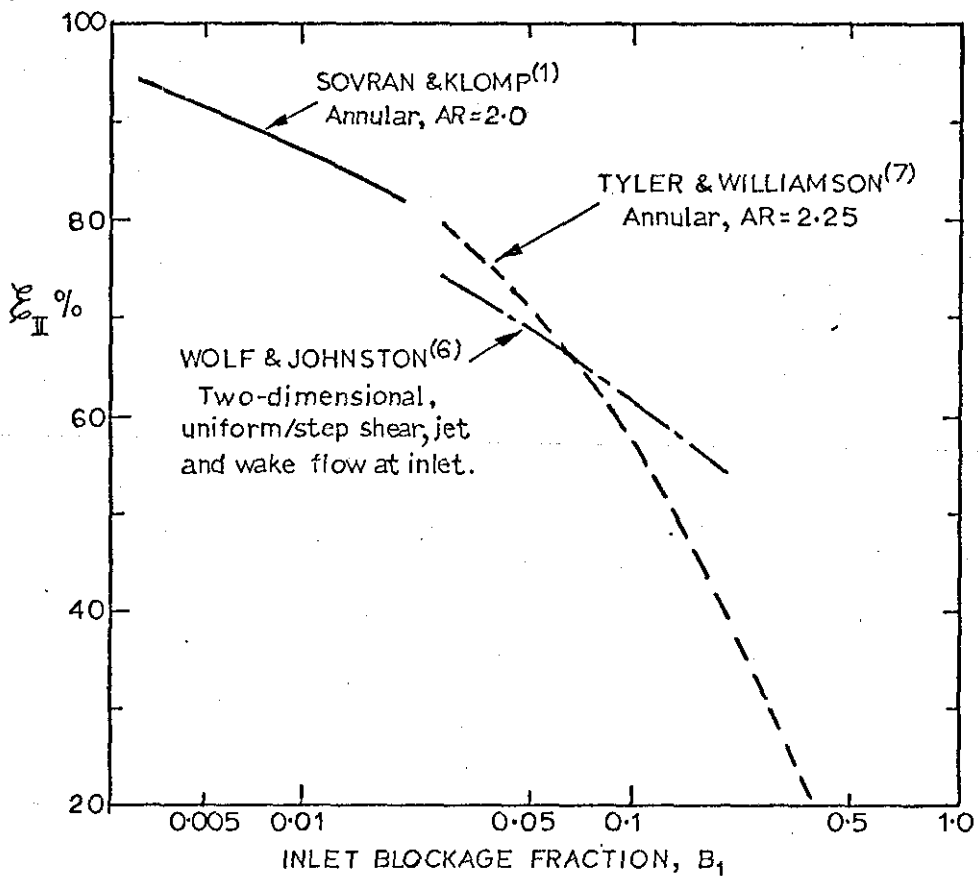


Fig.1-5-3 INFLUENCE OF ENTRY SWIRL ON LOSS COEFFICIENT FOR CONSTANT INNER CORE ANNULAR DIFFUSERS AFTER GUREVICH⁽⁵⁾

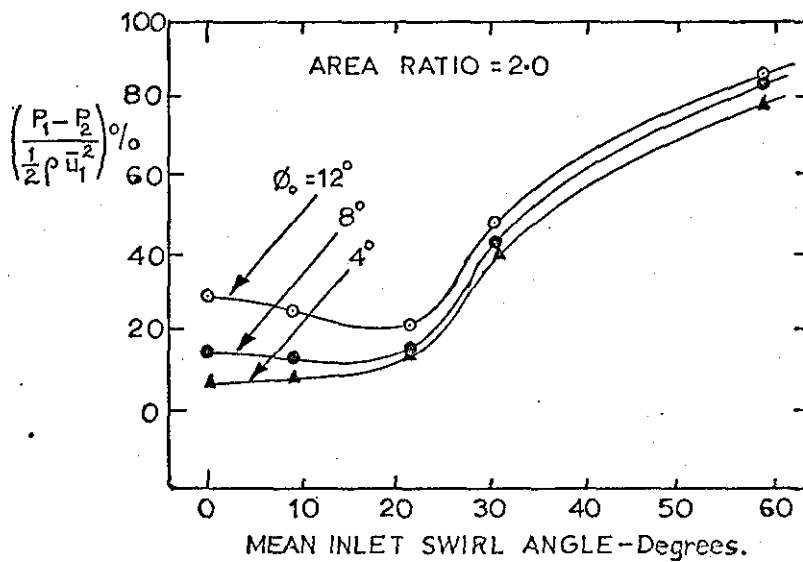
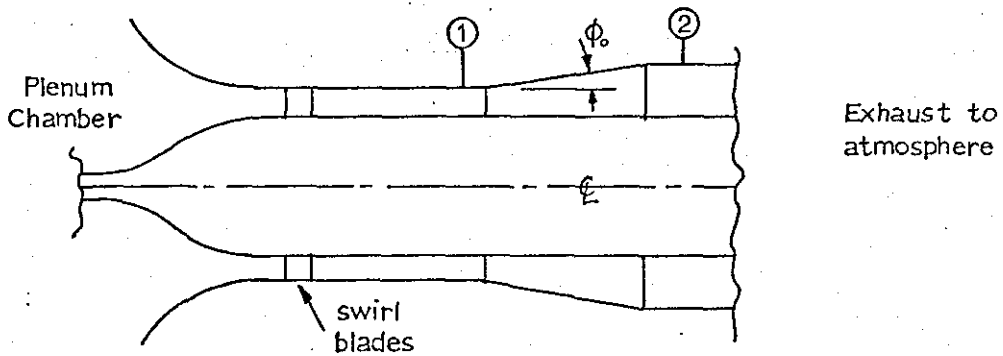
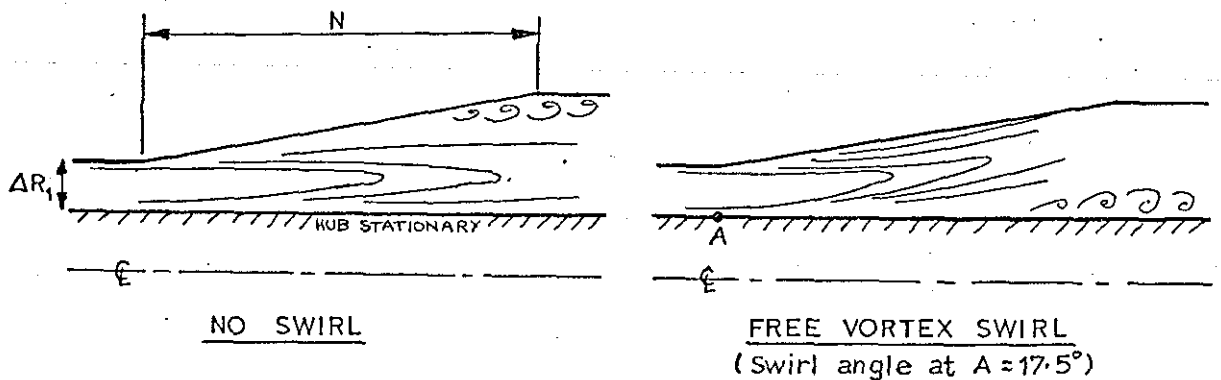


Fig.1-5-4 TOTAL PRESSURE CONTOURS IN ANNULAR DIFFUSERS.

DATA OF HOADLEY REPORTED BY HORLOCK⁽¹¹⁾



DIFFUSER GEOMETRY: $N/\Delta R_1 = 19.1, AR = 4.57$

~~~~~ indicates SEPARATION



Fig. 1-5-5 ANNULAR DIFFUSER PERFORMANCE CHART  
AFTER SOVRAN & KLOMP<sup>(1)</sup>

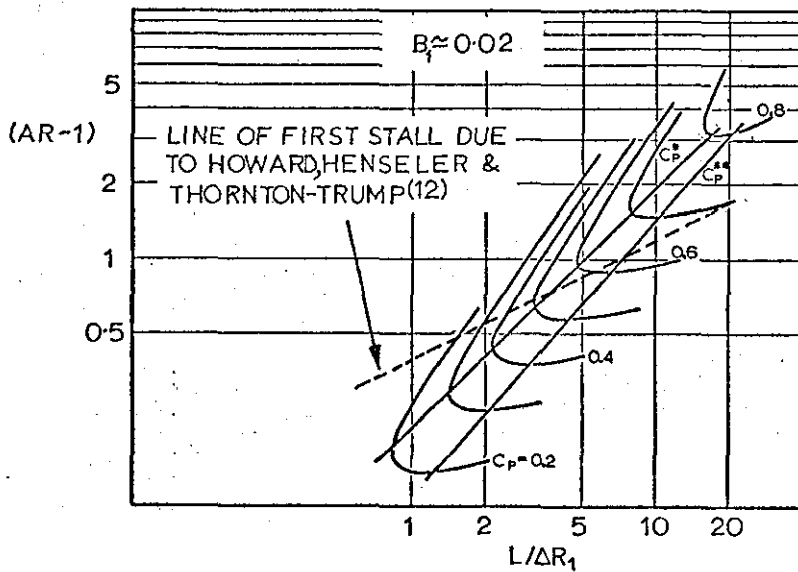


Fig. 1-5-6 INFLUENCE OF FLOW SPLIT ON BRANCHED DIFFUSER PERFORMANCE

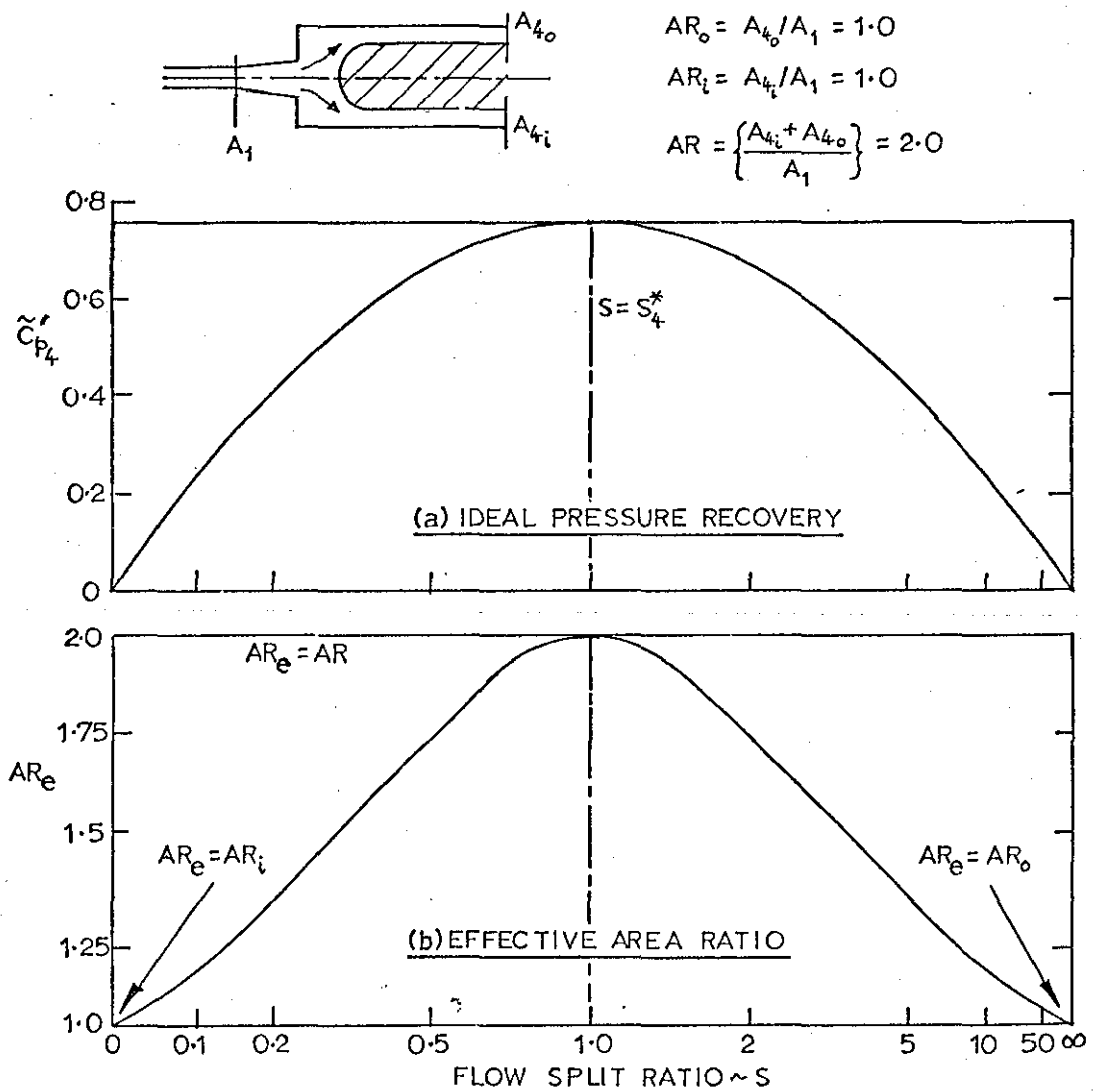
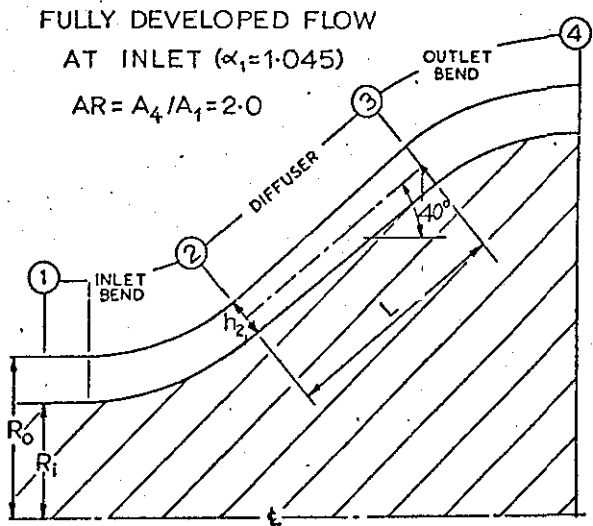


Fig.1-6-1 PERFORMANCE OF A WIDE ANGLE ANNULAR DIFFUSER AFTER STEVENS & FRY<sup>(14)</sup>.



| COMPONENT PERFORMANCE     | $\tilde{\lambda}$ | $\tilde{C}_p$ |
|---------------------------|-------------------|---------------|
| INLET BEND & ENTRY LENGTH | 0.043             | -0.053        |
| DIFFUSER                  | 0.163             | 0.492         |
| OUTLET BEND               | 0.140             | 0.086         |
| OVERALL                   | 0.220             | 0.525         |

NOTE: Parameters are referred to  $\alpha_{12} \frac{1}{2} \rho \bar{u}_1^2$

Fig.1-6-2 PERFORMANCE OF WIDE ANGLE DIFFUSER WITH FREE SURFACE EXPANSION AFTER FISHENDEN<sup>(15)</sup>.

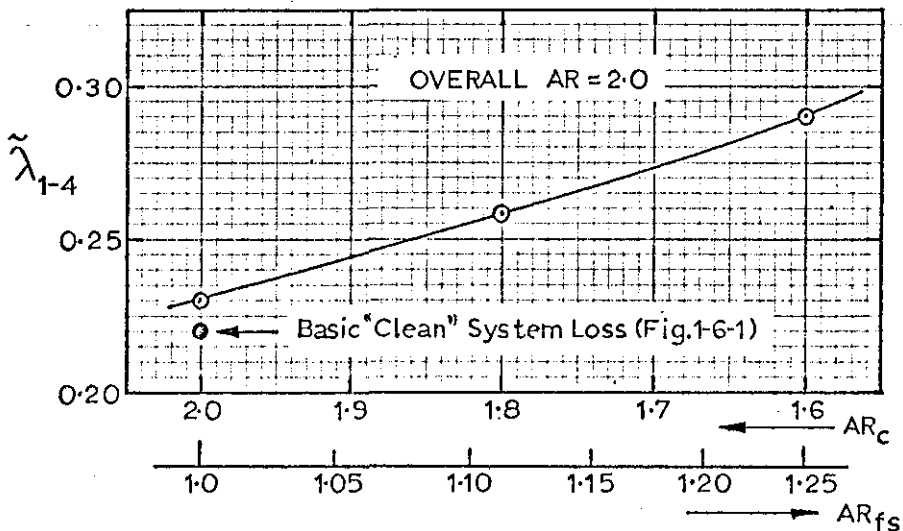
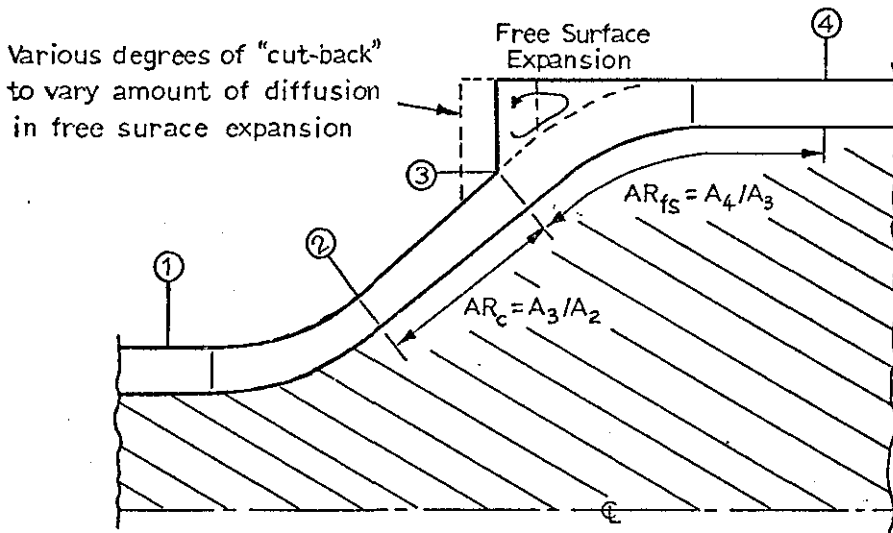
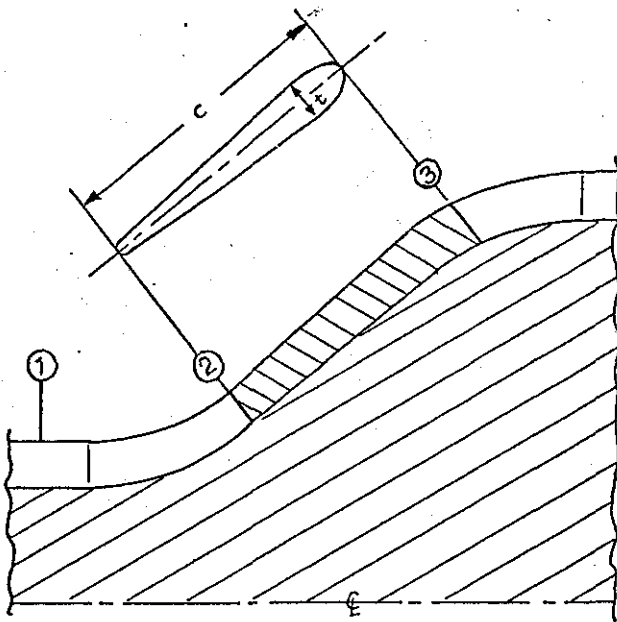


Fig.1-6-3 PERFORMANCE OF WIDE ANGLE DIFFUSER WITH STRUTS.

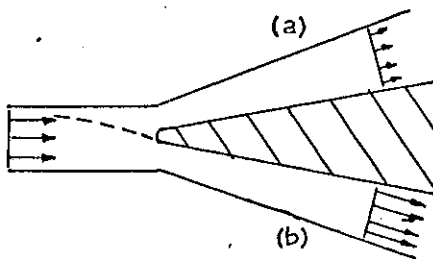
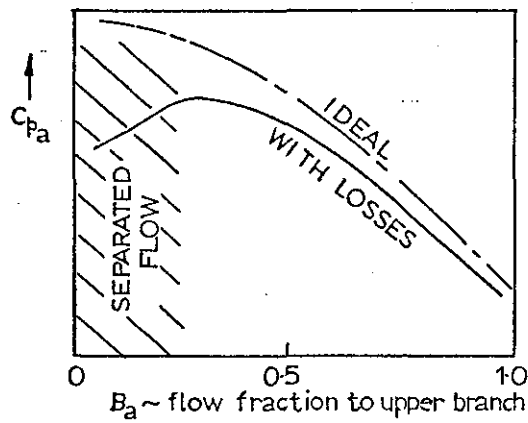
DATA OF FISHENDEN AND BROWN REPORTED BY STEVENS<sup>(20)</sup>



| GEOMETRY   |      |       | LOSS DUE TO STRUTS    |
|------------|------|-------|-----------------------|
| $AR_{1-3}$ | s/c  | t/c % | $\Delta\lambda_{1-3}$ |
| 1.7        | 2.5  | 17    | 0.03                  |
| 2.0        | 1.25 | 8.5   | 0.05                  |

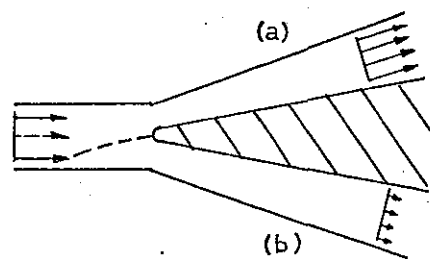
s/c = Pitch/chord Ratio.

Fig.1-6-4 STATIC PRESSURE RECOVERY CHARACTERISTIC OF A BRANCHED DIFFUSER AFTER EHRICH<sup>(16)</sup>.



LOW FLOW TO UPPER BRANCH

$B_a \rightarrow 0$



HIGH FLOW TO UPPER BRANCH

$B_a \rightarrow 1.0$

Table 1-4 BOUNDARY LAYER AND VELOCITY PROFILE  
PARAMETER DEFINITIONS.

| PARAMETER                  | SYMBOL                           | GENERALISED <sup>†</sup> AXI-SYMMETRIC DEFINITION                                          |                             |
|----------------------------|----------------------------------|--------------------------------------------------------------------------------------------|-----------------------------|
| DISPLACEMENT THICKNESS     | $\delta^*$                       | $\int_{R_w}^{R_m} \left(1 - \frac{u}{U}\right) \frac{R}{R_w} dR$                           | BOUNDARY LAYER PARAMETERS   |
| MOMENTUM THICKNESS         | $\theta$                         | $\int_{R_w}^{R_m} \left(1 - \frac{u}{U}\right) \frac{u}{U} \frac{R}{R_w} dR$               |                             |
| SHAPE FACTOR               | H                                | $\delta^*/\theta$                                                                          |                             |
| MASS-DERIVED MEAN VELOCITY | $\left(\frac{\bar{u}}{U}\right)$ | $\frac{2}{(R_o^2 - R_i^2)} \int_{R_i}^{R_o} \left(\frac{u}{U}\right) R dR$                 | VELOCITY PROFILE PARAMETERS |
| ENERGY COEFFICIENT         | $\alpha$                         | $\frac{2}{(R_o^2 - R_i^2) (\bar{u}/U)^3} \int_{R_i}^{R_o} \left(\frac{u}{U}\right)^3 R dR$ |                             |
| RADIAL DISTORTION FACTOR   | RD                               | $\left(\frac{\delta_i^* - \delta_o^*}{\delta_i^* + \delta_o^*}\right)$                     |                             |

<sup>†</sup>  $R_m$  is radius at point of maximum velocity

$R_w$  is appropriate wall radius (inner or outer)

## CHAPTER 2. EXPERIMENTAL FACILITY

### 2-1 DESIGN OF BASIC FACILITY

As stated in Chapter 1, it was decided that the test rig was to be fully annular. The layout of the test facility is shown in Figs. 2-1-1 and 2-1-2. A suction system was chosen in order to avoid uncertainty regarding the inlet turbulence structure and flow asymmetry presented by a "blown" system. The choice of a vertical layout reduced the number of inlet support struts required and thus ensured that strut wake effects were minimised. Concentricity of the tubes was ensured by a flanged and spigotted method of construction; the manufacturing tolerances were typically  $500.00 \pm 0.07$  mm. The majority of the rig components were fabricated from perspex allowing ease of flow visualisation and "setting up" of instrumentation.

The air intake was designed with an internal contraction of 8:1 in order to minimise the effects of large scale atmospheric turbulence. A Dufaylite honeycomb screen was also incorporated. The inner core of the inlet length was positioned by means of three aerofoil struts in the intake throat. Stable transition to turbulent flow was ensured by trip wires on the inner and outer walls just downstream of the intake throat. An entry length of approximately 24 hydraulic diameters was provided in order to give conditions substantially consistent with fully developed flow at inlet to the diffuser system.

After passing through the working section the flow was discharged into a plenum chamber, from which it was extracted by a Keith Blackman 2513S centrifugal fan. The drive was provided by an electric motor with a resistive speed control. To avoid recirculation problems, waste air was discharged to atmosphere via a duct terminating outside the laboratory.

### 2-2 METHOD OF CONTROLLING "DESIGN" VARIABLES

#### 2-2-1 Dump Gap

The inner core of the test rig was supported by a hollow wooden pillar

secured to the base of the plenum chamber (see Fig. 2-1-1). The combustion chamber assembly was mounted on four struts joined to a central boss located on a lead screw passing down the centre of the pillar. Adjustment of the axial position of the combustion chamber was achieved by rotating a graduated wheel fixed to the lower end of the lead screw. In this way the dump gap (D) could be set to any desired value within the range 0 to 200 mm, with an accuracy of  $\pm 0.10$  mm. Concentricity of the combustion chamber with the inner and outer tubes was maintained at the lower end by six struts spaced at  $60^\circ$  intervals around each of the annuli, and at the upper end by three equi-spaced aerofoil struts fixed to the outer wall of the combustion chamber.

2-2-2 Flow Split

The quantity of flow passing down the outer annulus was controlled by means of a ring throttle (see Fig. 2-2-1). To extend the range of flow split ratios obtainable, a perforated blockage ring was provided for the inner annulus. This gave an area blockage of 55% and was only fitted when a high flow in the outer annulus was required.

2-3 CHOICE OF PRE-DIFFUSER GEOMETRIES

The geometric details of the five pre-diffusers used in the investigation are given in Table 2-3-1. (Further details are given in Appendix 1).

Table 2-3-1 Pre-diffuser Geometries

| Diffuser Reference Number | $h_1/\bar{R}_1$ | AR    | $\bar{L}/h_1$ | $\epsilon$ (deg) | $2\phi$ (deg) |
|---------------------------|-----------------|-------|---------------|------------------|---------------|
| 1                         | 0.1622          | 1.4   | 1.900         | 0                | 12.0          |
| 2                         | "               | 1.6   | 2.850         | 0                | 12.0          |
| 3                         | "               | 1.8   | 3.805         | 0                | 12.0          |
| 4                         | "               | 1.8   | 2.525         | 0                | 18.0          |
| 5                         | "               | 1.608 | 2.850         | 3.333            | 11.33         |

It is to be noted that more than one geometric parameter is required to identify a particular diffuser. For this reason the diffusers are referred to by their reference numbers throughout. The geometry of the pre-diffusers is shown in relation to the performance chart of Sovran & Klomp<sup>(1)</sup> in Fig. 2-3-1. Diffusers 1, 2 and 3 were "symmetrical", having area ratios of 1.4, 1.6 and 1.8 respectively, and constant included angle ( $2\phi$ ). An included angle of  $12^\circ$  was chosen as this placed all three diffusers close to the optimum  $C_p^*$  line of Sovran & Klomp.

In view of the stabilising effect of the combustion chamber head, it was considered that a higher rate of diffusion could be accepted in the pre-diffuser without a serious loss in performance. To test this hypothesis, Diffuser 4 was designed with the same area ratio as Diffuser 3 (1.8), but with an included angle of  $18^\circ$ .

Diffuser 5 represented an initial optimisation of the geometry, the design being based upon data obtained from tests with the first four diffusers. The main feature was a change in inclination angle ( $\epsilon$ ), thus giving a "canted" diffuser. In order to assess any change in performance and/or flow stability the diffuser was designed with the same area ratio and non-dimensional length ( $\bar{L}/h_1$ ) as Diffuser 2. In this way the same rate of diffusion was maintained. The included angle was reduced from  $12^\circ$  to  $11.33^\circ$  in accordance with Equation 1-2-1 (Section 1-2-1).

#### 2-4 INSTRUMENTATION

The test programme called for measurement of the velocity profiles and static pressures at six stations as shown in Fig. 2-4-1. These were:

Station 1 Pre-diffuser "Inlet" - two annulus heights upstream of the actual inlet plane.

Station 2 Pre-diffuser "Outlet" - 2.5 mm upstream of the actual outlet plane.

Stations  $3_i, 3_o$       Combustion chamber head - two planes  $120^\circ$  apart, in the region of maximum velocity over the head.

Stations  $4_i, 4_o$       Settling Length - two planes six annulus heights downstream of the beginning of the parallel walled annuli.

In addition, the static pressure distribution was required for all surfaces of the working section. The pressure variation around the head was considered particularly important. Static pressure tappings and traverse locations were provided in three radial planes spaced circumferentially  $120^\circ$  apart (denoted Red, Blue and Green as shown in Fig. 2-4-1). Special items of instrumentation were provided at other circumferential locations, the majority being in the  $120^\circ$  segment between "Blue" and "Red".

Three static pressure tappings 0.7 mm in diameter were provided at each of the six stations described above and at intermediate positions along the internal surfaces as shown in Fig. 2-4-3. Additional tappings were provided along the walls of Diffusers 2, 3, 4 and 5 in one radial plane (Blue). In order to prevent contamination by ingested dust all tappings were blanked off when not in use.

#### 2-4-1 Measurement of Static Pressure and Velocity Profiles

The test rig geometry and flow conditions were such that different methods had to be employed for measuring static pressure and velocity profiles at each station. These are described in Table 2-4-1 over.



Table 2-4-1 Pressure Probe Measurements

| Station                         | Method of Measurement                                                                                         |
|---------------------------------|---------------------------------------------------------------------------------------------------------------|
| 1                               | Pitot probe traverse + wall static pressure measurement.                                                      |
| 2                               | (i) Separate pitot and wedge static probe traverses<br>or (ii) Pitot/wedge static combination probe traverse. |
| 3 <sub>i</sub> , 3 <sub>o</sub> | Fixed Rakes: 4 pitot + 1 wedge static probe each.                                                             |
| 4 <sub>i</sub> , 4 <sub>o</sub> | Pitot probe traverse using special probe and<br>traverse gear + wall static pressure measurement.             |

Traverses at stations 1 and 2 were carried out using the traverse mechanism shown in Fig. 2-4-5. The radial position of each probe could be set to within  $\pm 0.05$  mm. The pitot probes had flattened heads which were angled slightly to ensure contact with the wall when "setting up". At station 1 the static pressure was constant across the annulus and equal to the adjacent wall value. At station 2, however, the static pressure was non-uniform and traverses had to be carried out in order to determine the radial distribution. Previous experience<sup>(15)</sup> indicated that wedge static probes were well suited to this purpose because of their insensitivity to flow direction in the plane of the wedge. Two probes were constructed as follows.

- (i) A miniature wedge static probe (see Fig. 2-4-6), the measurements from which could be used, together with those from separate pitot probes, for determining dynamic pressure.
- (ii) A pitot/wedge static combination probe which could be used directly to measure static pressure and dynamic pressure to a reasonable accuracy (see Fig. 2-4-7).

The length of the test programme dictated that pitot and static traverses could not be carried out at each of the three circumferential positions for every test. In the majority of tests a single traverse of the combination probe was therefore used to measure the velocity and static pressure profiles.

In view of the variable head position and inaccessibility of the inner annulus, it was not possible to carry out traverses at stations  $3_i$  and  $3_o$ . A fixed rake was therefore mounted on each of the inner and outer surfaces of the head as shown in Fig. 2-4-2.

At stations  $4_i$  and  $4_o$ , in the settling lengths, the flow was in equilibrium and the static pressures were assumed equal to the adjacent wall values in each annulus. A special pitot probe and traverse mechanism were provided in order to overcome the difficulty in traversing the inner annulus (see Figs. 2-2-1 and 2-4-4). This instrumentation was used to traverse from the inner and outer walls of both annuli at one circumferential position. In addition two rakes, each comprising three pitot tubes, were mounted in the inner annulus approximately  $120^\circ$  from the traverse plane.

All pressure measurements were taken on a D.I.S.A. Digital Voltmeter (Type 55D 30) connected to a Furness Controls Micromanometer. Details of pressure probe calibrations are given in Appendix 2.

#### 2-4-2 Additional Measurements

##### (i) Approximate Flow Split Ratio

A simple method was devised for "setting up" the required flow split for each test. Two transverse cylinder probes, each having three forward facing interconnected tappings were used to obtain the "mean" total pressure,  $P_m$ , in each settling length annulus. The approximate flow split was obtained from two measurements of "mean" dynamic pressure ( $q_m = P_m - P_w$ ) as,

$$S \approx \left( \frac{A_o}{A_i} \right)_3 \left( \frac{q_{m_o}}{q_{m_i}} \right)_3^{\frac{1}{2}} = 2.15 \left( \frac{q_{m_o}}{q_{m_i}} \right)_3^{\frac{1}{2}} \quad 2-4-1$$

(ii) Inlet Turbulence Intensity

For comparison purposes the axial turbulence intensity was measured at inlet (station 1), using D.I.S.A. constant temperature hot wire anemometer equipment.

(iii) Flow Visualisation

Wool tufts (mounted on lengths of hypodermic tubing) were employed for determining the position of local stagnation points (as for example on the combustion chamber head) and for investigating possible regions of separation.

Fig.2-1-1 LAYOUT OF TEST FACILITY.

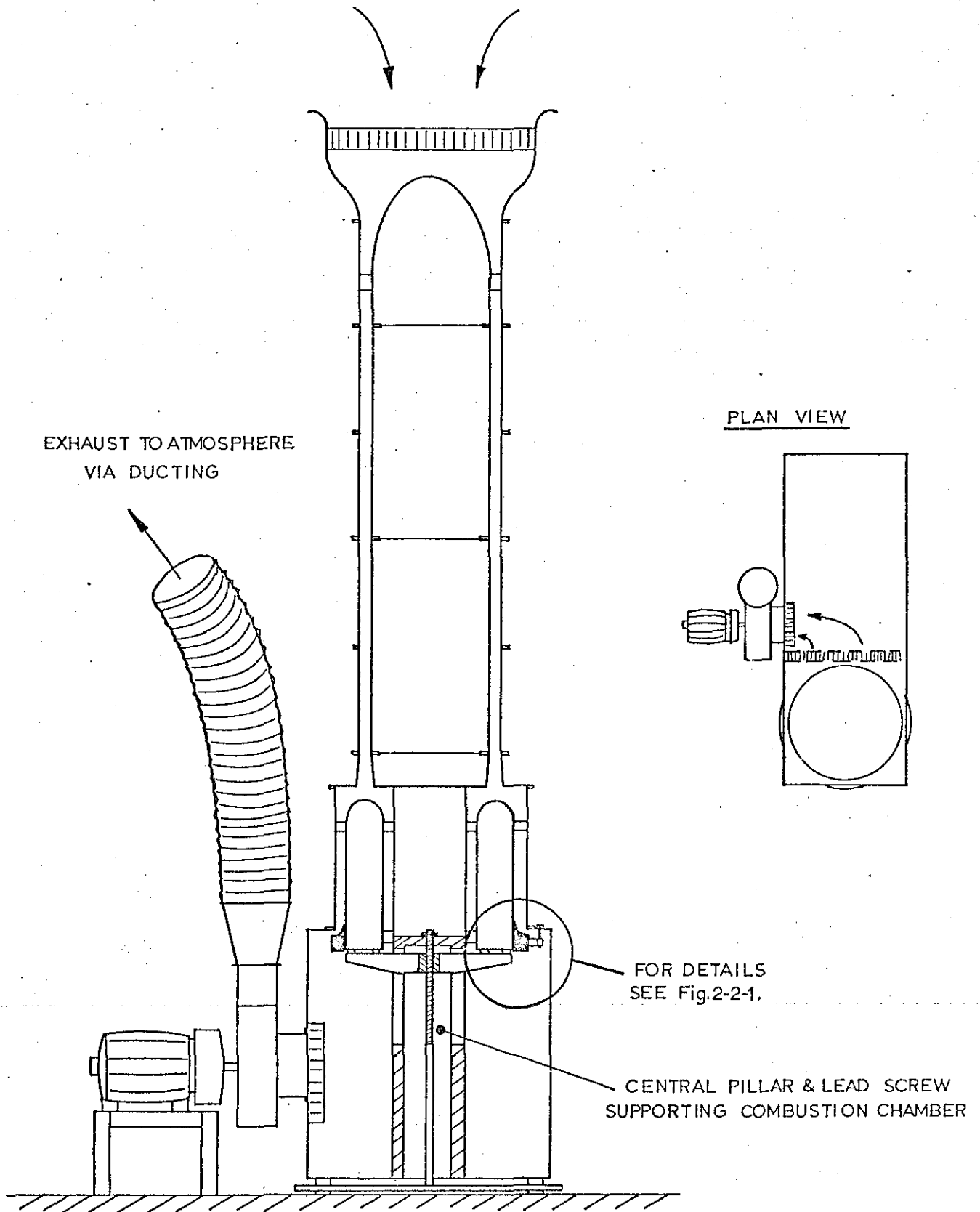
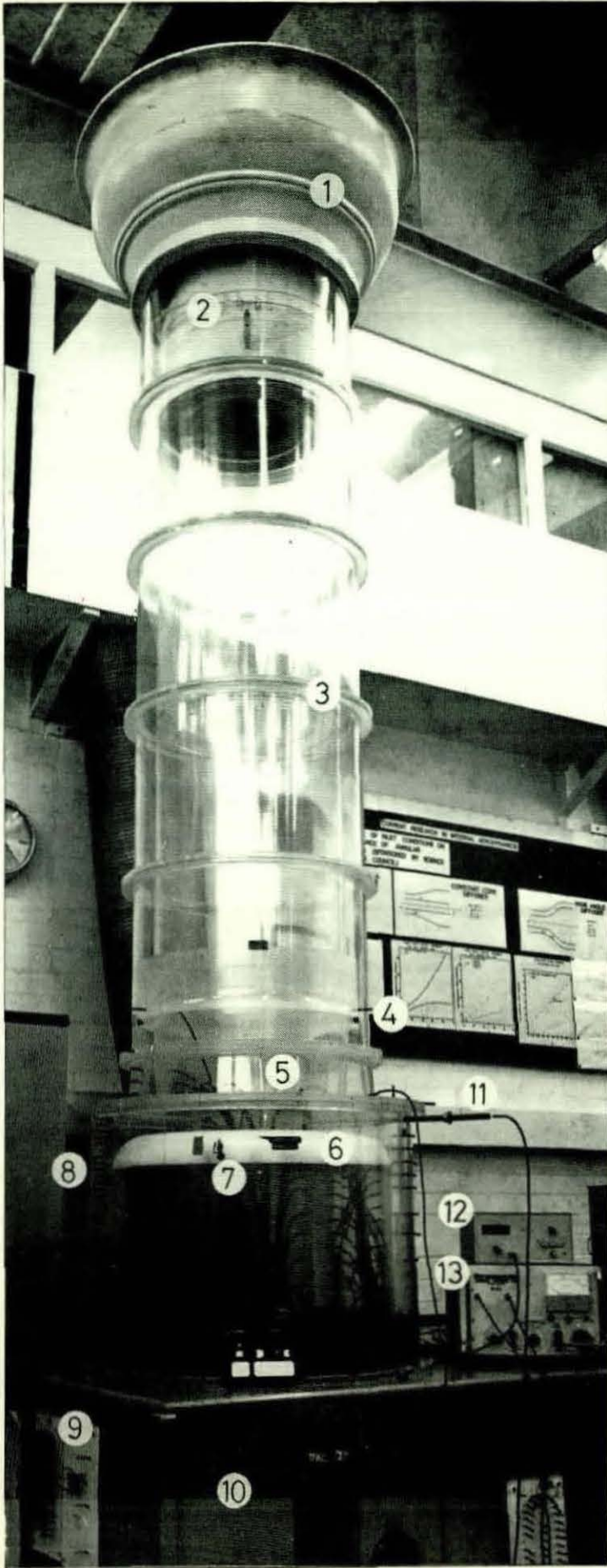


Fig 2-1-2 EXPERIMENTAL FACILITY.



KEY

- (1) Intake Flare
- (2) Intake Bullet
- (3) Inlet Length
- (4) Inlet Station(1)
- (5) Pre-diffuser
- (6) Combustion Chamber Head
- (7) Head Rake
- (8) External Static Pressure Tappings
- (9) Internal Static Pressure Tappings
- (10) Plenum Chamber
- (11) Traverse Gear
- (12) DISA Digital Voltmeter
- (13) Furness Controls Micromanometer

APPROXIMATE SCALE

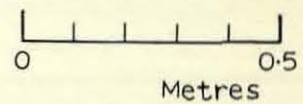




Fig.2-2-1 SETTLING LENGTH THROTTLE & TRAVERSE MECHANISM.

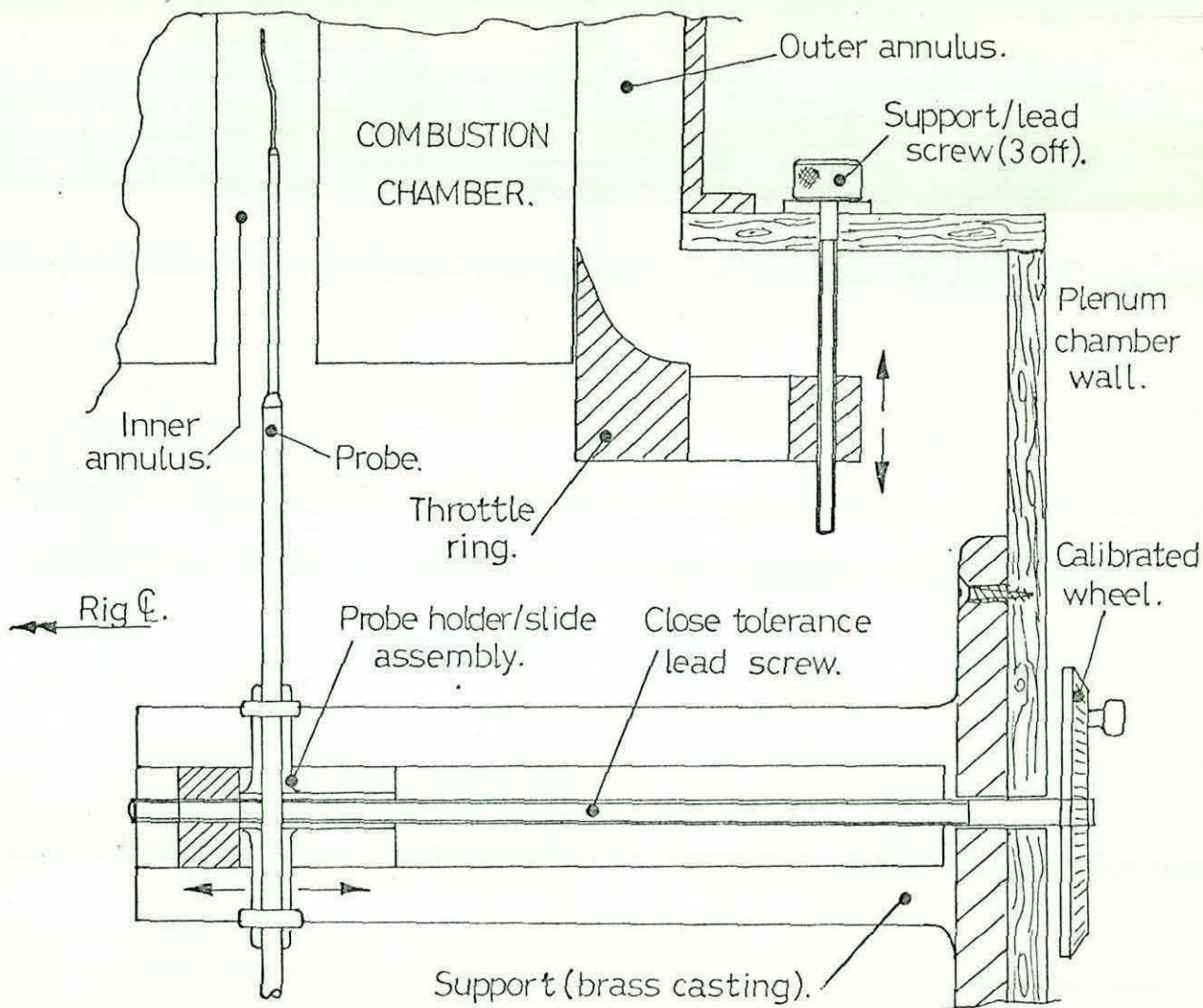


Fig.2-3-1 PRE-DIFFUSER GEOMETRIES IN RELATION TO PERFORMANCE CHART OF SOVRAN & KLUMP<sup>(1)</sup>

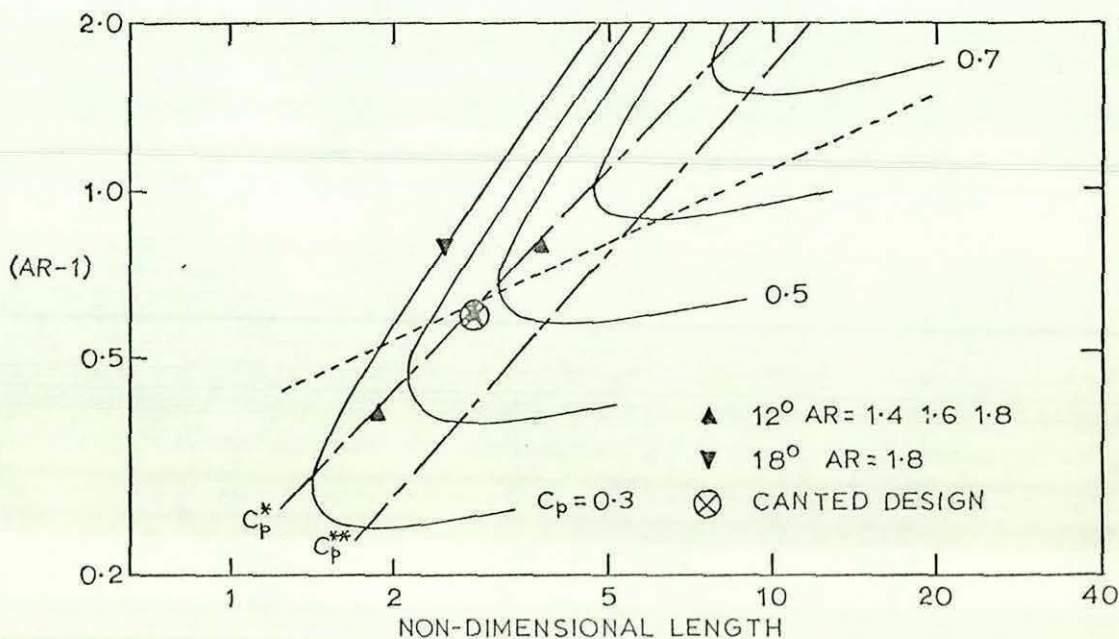


Fig.2-4-1 STATIONS AND LOCATION OF INSTRUMENTATION.

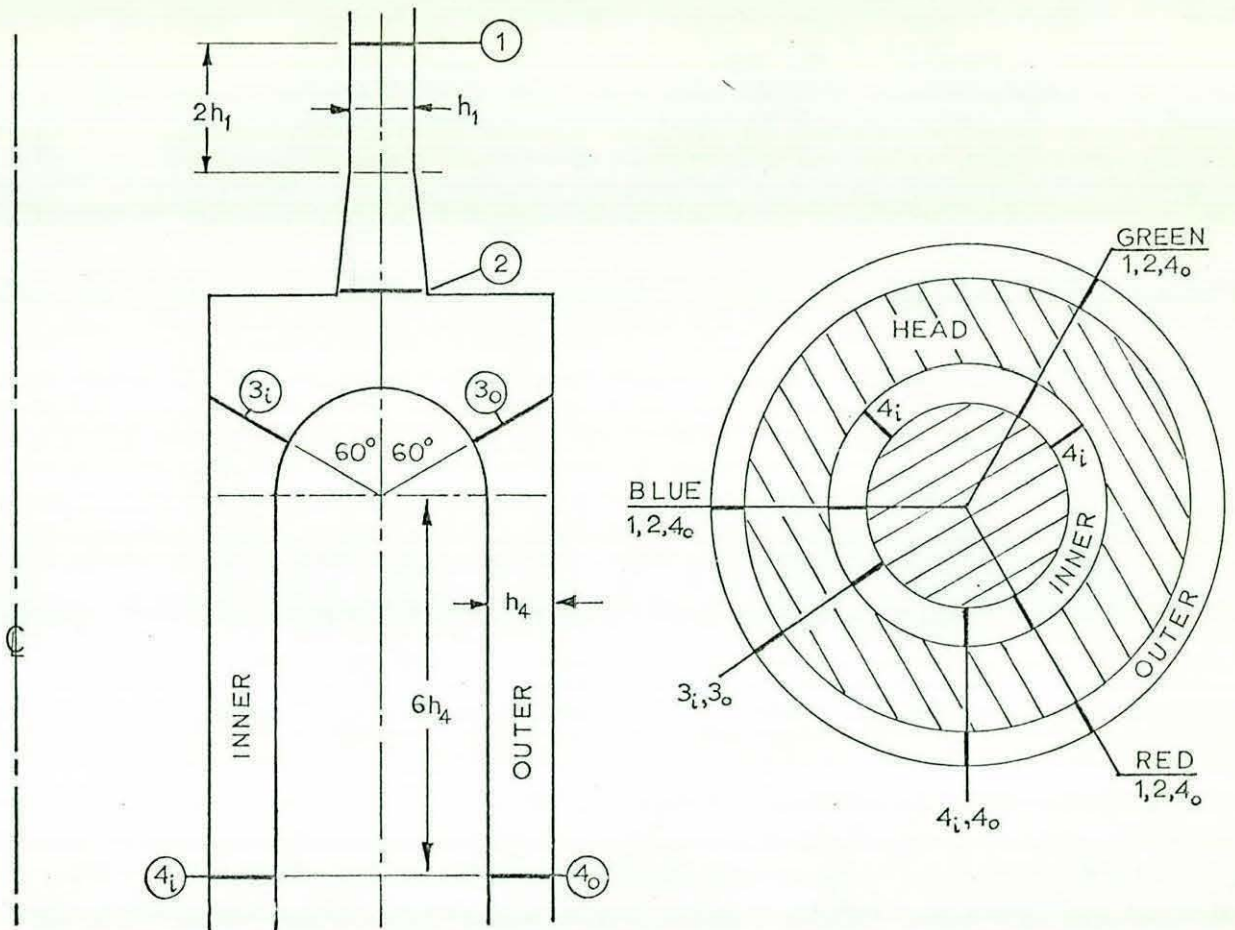


Fig.2-4-2 COMBUSTION CHAMBER HEAD RAKES.

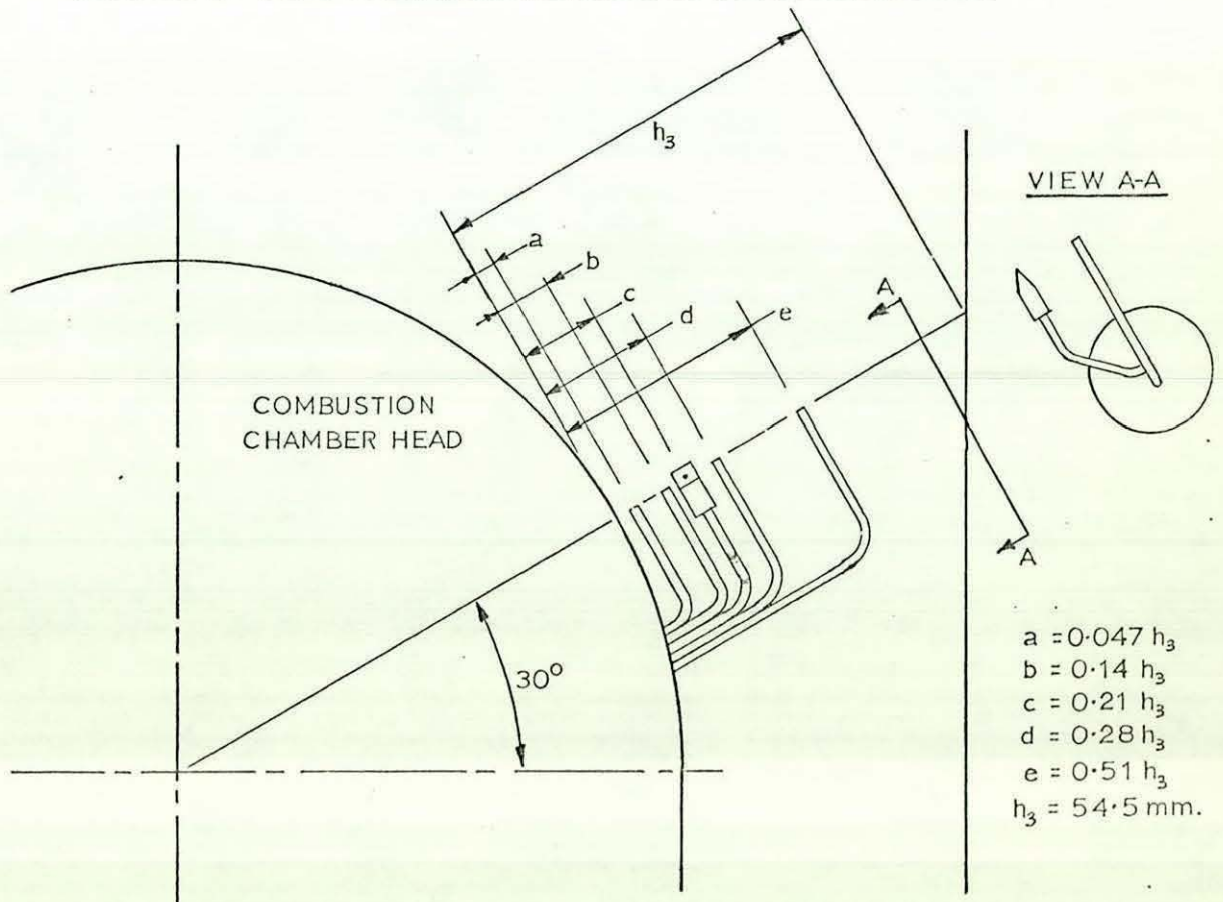
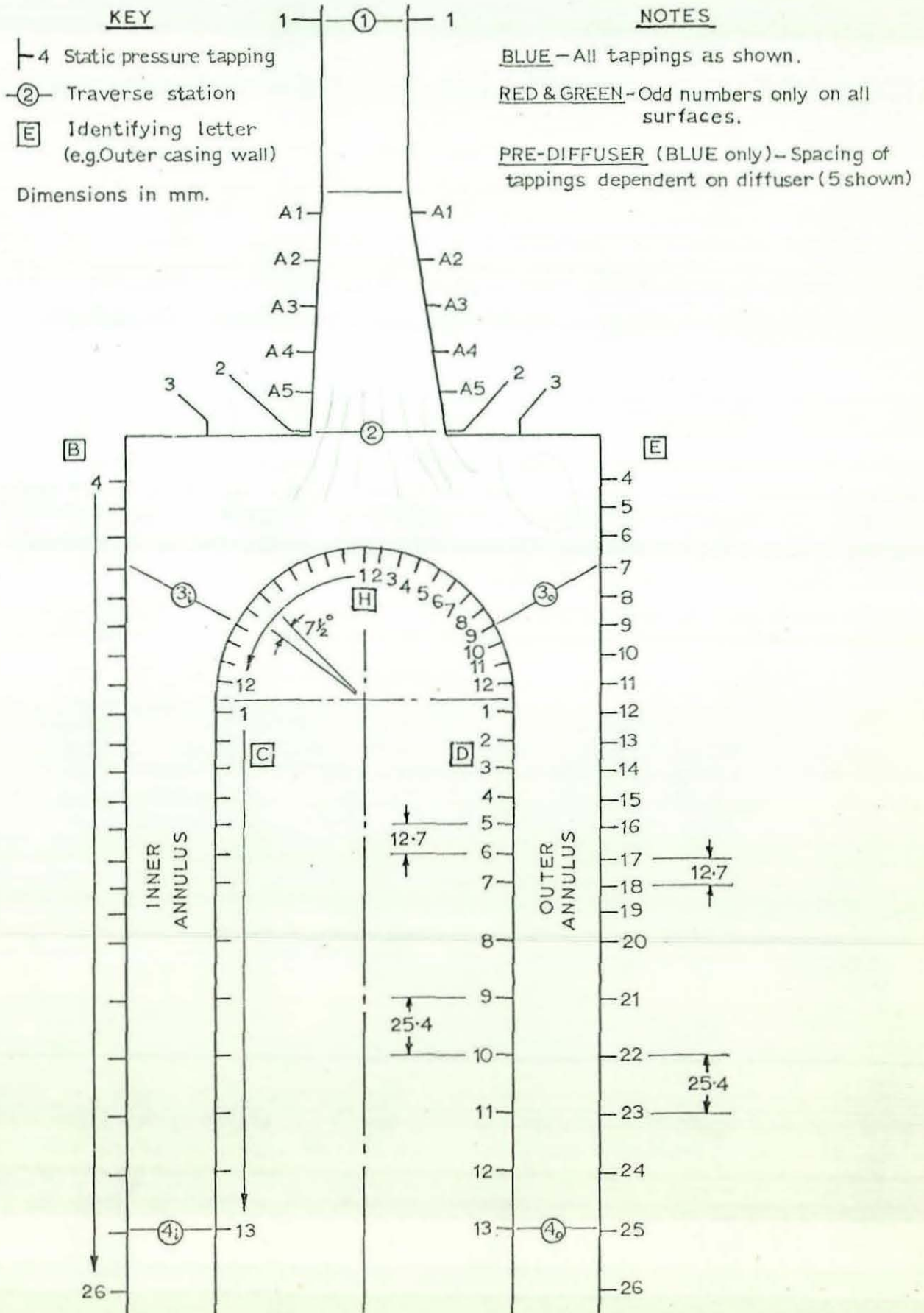




Fig. 2-4-3 LOCATION OF STATIC PRESSURE TAPPINGS.





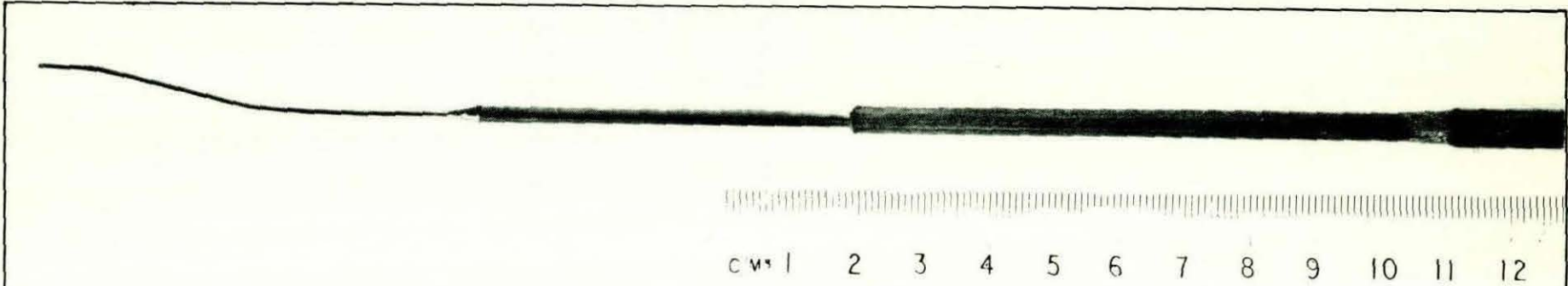


Fig. 2-4-4 Settling Length Traverse Probe.

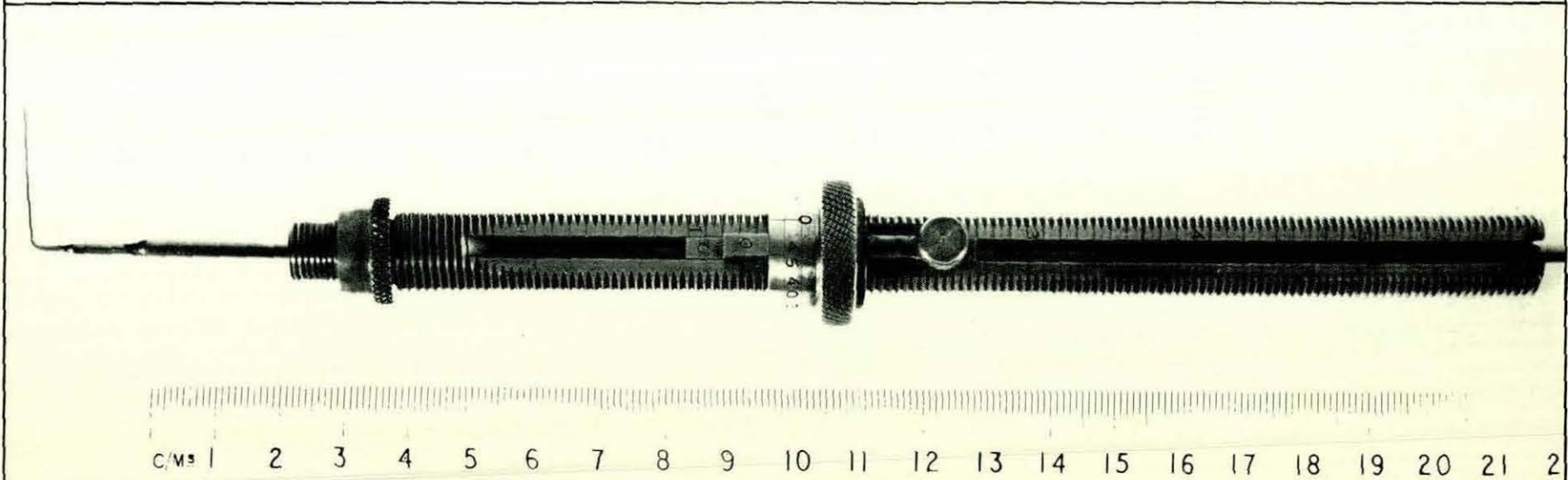


Fig. 2-4-5 Traverse Mechanism and Pitot Probe.

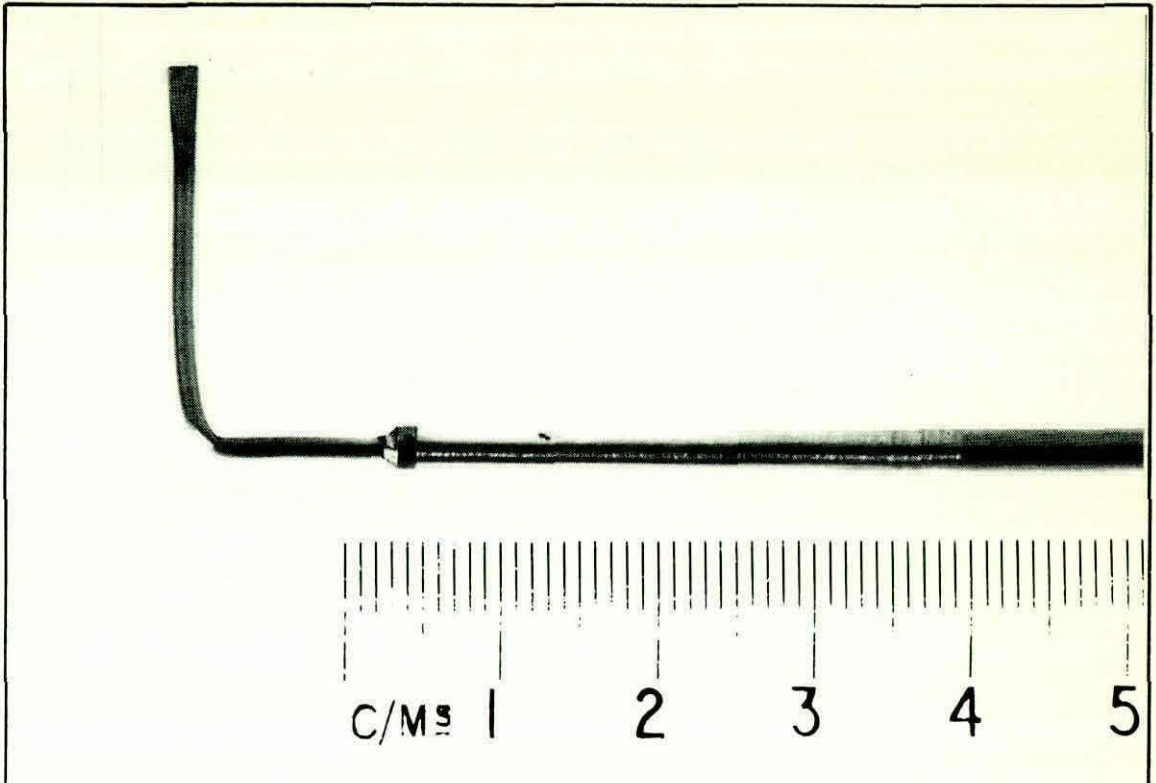


Fig 2-4-6 Wedge Static Probe.

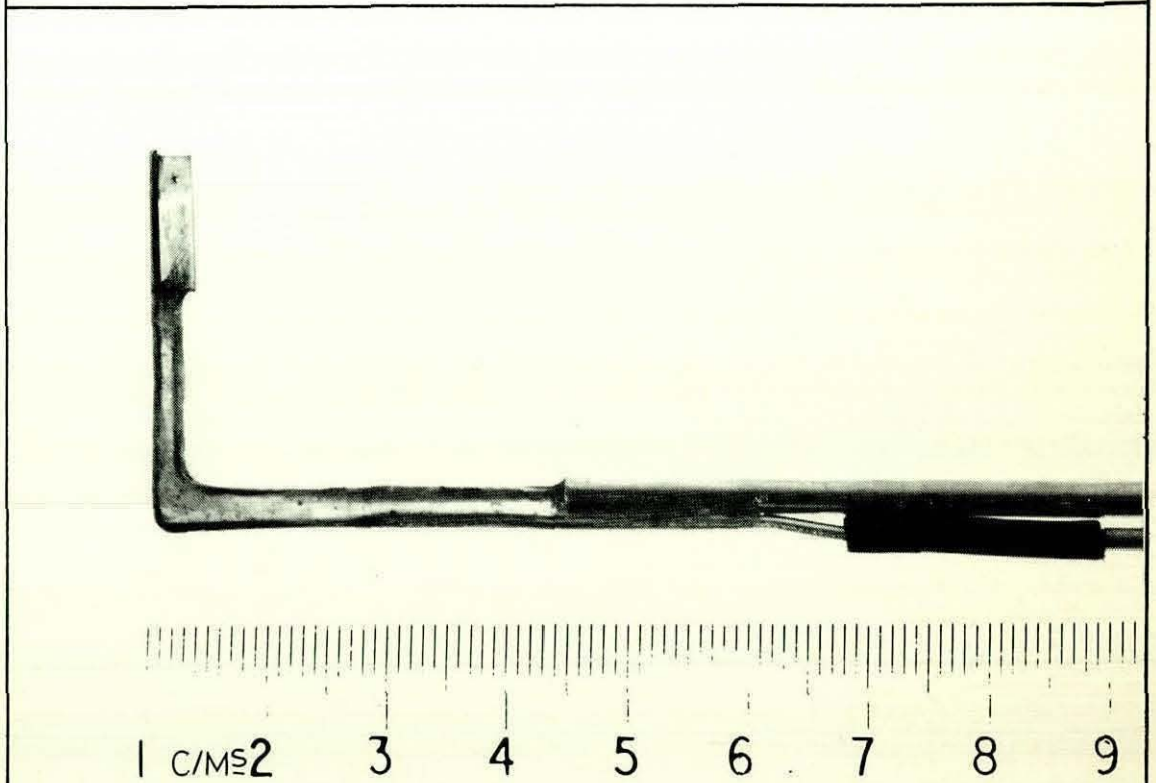


Fig 2-4-7 Pitot-Wedge Static Combination Probe.

CHAPTER 3. EXPERIMENTAL WORK

3-1 SCOPE OF TESTS

In carrying out the experimental programme it was considered essential that the effects of each variable should be isolated. The geometric and flow parameters were therefore varied independently. The five pre-diffusers were chosen so that the following parameters could be varied in a systematic manner.

- (i) Increasing the area ratio for a constant included angle
- (ii) Increasing the included angle for a constant area ratio
- (iii) Canting the pre-diffuser whilst retaining the same area ratio and non-dimensional length.

The range of tests carried out with each pre-diffuser is summarised in Fig. 3-1-1. Three values of dump gap were chosen and for each of these a minimum of three tests were carried out at varying flow split ratios. On average 11 tests were carried out with each pre-diffuser. The following convention has been adopted to indicate the scope and nature of each test.

CT - "Complete Test"

Measurement of the following items:-

- (i) The velocity and static pressure profiles at pre-diffuser outlet (Stn. 2) by means of three total pressure traverses and at least one static pressure traverse.
- (ii) The velocity profiles in the settling lengths (Stns. 4<sub>i</sub> and 4<sub>o</sub>) at one circumferential position and confirmatory checks at other positions.
- (iii) The complete static pressure distribution at one circumferential position (Blue).
- (iv) The velocity and static pressure profiles in the plane of each head rake (Stns. 3<sub>i</sub> and 3<sub>o</sub>).

- (v) "Key" static pressures on the inner and outer walls (Stns. 2, 4<sub>i</sub> and 4<sub>o</sub>) for each circumferential position.

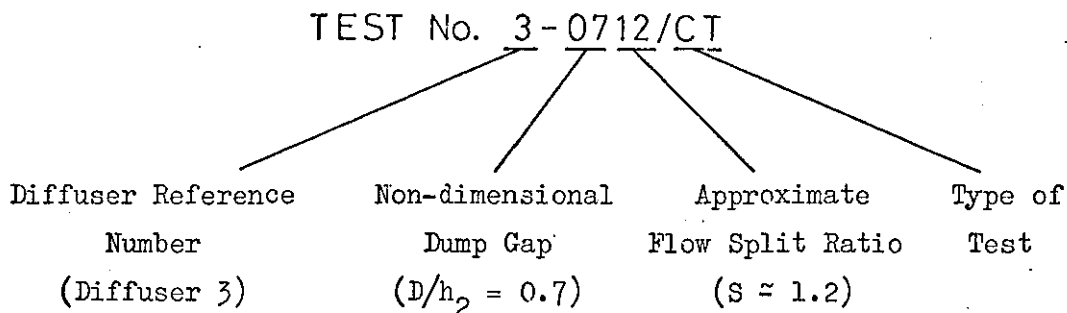
A - "Auxiliary Test"

Measurement of the following items:-

- (i) The velocity and static pressure profiles at pre-diffuser outlet by means of a combination probe traverse (Blue only).
- (ii) The settling length velocity profiles at one circumferential position.
- (iii) The static pressure distribution, at least over the combustion chamber head.

Items (iv) and (v) above..

For convenience each test is identified by a Test Number and this provides information on the geometry and flow conditions employed. The numbers are used extensively in the text where it is necessary to refer to a particular test. The numbering system is explained by means of the example below.



In addition it is often useful to refer to a particular series of tests carried out with a certain pre-diffuser and dump gap. In this case the first part of the test number is used. As an example, "Test Series 3-07" would refer to the series of tests at various flow splits, carried out with Diffuser 3 (AR = 1.8, 2  $\phi$  = 12°) and a non-dimensional dump gap of 0.7.

A summary of the configurations tested is given in Table 3-1. The choice of flow split for the first few tests was somewhat arbitrary. The

results of these tests indicated that the optimum performance was likely to be achieved for a flow split ratio lower than the design value of 2.15 (i.e. with more flow passing down the inner annulus). In order to confirm this the majority of tests were carried out at flow split ratios in the range 0.8 to 2.3. The optimum position for the combustion chamber was found to vary depending upon the pre-diffuser area ratio. Values of dump gap were therefore chosen to cover the most useful range of combustion chamber positions for each diffuser. In the case of diffusers having the same area ratio (2 and 5; 3 and 4), tests were carried out for the same three positions of the combustion chamber. This meant that the values of  $D/h_2$  for tests with Diffuser 5 were slightly different to those for Diffuser 2. For the sake of clarity the values will be quoted as 0.5, 0.8 and 1.5.

Throughout the test programme the inlet conditions were maintained approximately constant. Typical conditions were as follows:-

|                                                                       |       |                   |
|-----------------------------------------------------------------------|-------|-------------------|
| Mean inlet velocity ( $\bar{u}_1$ )                                   | ..... | 26 m/sec          |
| Inlet Reynolds No. $\left( \frac{\bar{u}_1 (D_o - D_i)}{\nu} \right)$ | ..... | $1.6 \times 10^5$ |

### 3-2 EXPERIMENTAL TECHNIQUE

#### 3-2-1 "Setting up"

The Micromanometer and Digital Voltmeter were switched on and allowed to warm up for a minimum period of 1 hour. During this time the combustion chamber was set to the required position and the ring throttle adjusted to approximately the correct opening (as dictated by experience). If necessary the inner annulus blockage ring was fitted.

Towards the end of the warm up period the fan was started and its speed adjusted to give a maximum inlet dynamic pressure ( $\rho U_1^2/2$ ) of between 45 and 55 mm w.g. This was measured by a pitot probe located midway across the annulus. The flow split was set to the required value by means of

successive measurements from the transverse cylinder probes and adjustments of the ring throttle (see Sect. 2-4-2). At this point the inlet conditions were checked and the fan speed adjusted as necessary.

### 3-2-2 Velocity and Static Pressure Profile Traverses

The inlet velocity profile was assumed constant throughout the tests and equal to that obtained during calibration. The inlet reference dynamic pressure ( $\rho U_1^2/2$ ) was recorded before and after each traverse or series of measurements.

In the case of "CT" Tests, three pitot probes were traversed simultaneously at pre-diffuser outlet. The technique adopted was to traverse out from the inner wall for approximately 80% of the annulus height and then to traverse from the outer wall for sufficient distance to obtain an overlap in the total pressure readings. All the total pressures were recorded relative to the outer wall static pressure. A similar technique was employed with the combination probe ("A" Tests) but in this case the local dynamic pressure was recorded. A pitot probe was traversed from the outer wall in order to provide additional measurements close to the wall. The static pressure profiles were obtained by traversing either of the available wedge probes; the readings were also referenced to the outer wall static pressure.

Traverses from the inner and outer walls of each settling length were carried out using the special probe and traverse mechanism. The total pressures were referenced to the adjacent wall static tapping.

### 3-2-3 Static Pressure Distribution and other Measurements

The static pressure at each point was measured as a differential relative to the inlet plane static pressure. Any significant fluctuation in the static pressure readings was noted. An independent check was made of the key static pressures at pre-diffuser outlet and in the settling length for each of the three circumferential positions.

The head rake total and static pressures were recorded relative to the adjacent static pressure tapings on the surface of the head.

Investigations with wool tufts were used to determine the following:-

- (i) the extent of separation in the pre-diffuser (where appropriate)
- (ii) the stagnation point on the head
- and (iii) the stagnation points on the hub and casing walls, as between the main flow and the re-circulating vortex flow.

### 3-3 REDUCTION OF DATA AND COMPUTATIONAL METHODS

#### 3-3-1 Velocity and Static Pressure Profile Data

The velocity profile data was non-dimensionalised in terms of the maximum velocity to give values of  $(u/U)$ . These values were then plotted versus non-dimensional distance from the inner wall  $(y_1/h)$ . In the case of pre-diffuser outlet profile data, dynamic pressure (and hence velocity) was obtained as the difference between the measured total and static pressures at successive radial positions. Mean curves were drawn for the static pressure and velocity profiles and from these data was tabulated ready for analysis by computer program. A sample set of readings and calculations is given in Appendix 3.

#### 3-3-2 Analysis by Computer Program

Extensive use was made of the University I.C.T. 1905 digital computer facilities. One main program was used for initial analysis of the majority of the data. Embodied in the program were calculation procedures for the following:-

- (i) boundary layer and velocity profile parameters
- (ii) overall performance parameters
- (iii) pre-diffuser performance parameters
- (iv) volume flow rates at each station
- and (v) detailed performance data suitable for subsequent analysis of local pressure losses.

A separate program was used for analysis of the head rake data. Curve fitting techniques were employed to make the best use of the data available. In addition to printed results the velocity and static pressure profiles were output in graphical form. Other programs were used in the correlation of performance parameters, the analysis of static pressure distributions, and the plotting of graphs. Relevant details of the programs and calculation procedures are given in Appendix 4.

### 3-4 ACCURACY

#### 3-4-1 Experimental Accuracy

Measurements were made with pitot and wedge static pressure probes under conditions ranging from steady fully developed flow to separated flow. The accuracy of these measurements depended largely upon local flow conditions. A general assessment of the experimental accuracy is afforded by considering the integrated volume flows at each station. The results are summarised in terms of the inlet volume flow,  $Q_1$ , as follows.

##### Pre-diffuser Outlet:

$$Q_2 = Q_1 \begin{matrix} +6\% \\ -1\% \end{matrix} \text{ (mean for all tests, } Q_1 + 3.3\%)$$

##### Settling Lengths:

$$Q_4 = (Q_{4_i} + Q_{4_o}) = Q_1 \begin{matrix} +4\% \\ 0\% \end{matrix} \text{ (mean for all tests, } Q_1 + 2.1\%)$$

In view of the complexity of the measurements these results are very good. It may be noted that the error in pre-diffuser outlet flow is consistent with the higher level of turbulence at that plane. Pressure probe calibration details are given in Appendix 2.

Wall static pressures could be read to an accuracy of  $\pm 0.2$  mm w.g. On average this represented  $\pm 0.5\%$  of the inlet mass weighted dynamic pressure ( $\alpha_1 \rho \bar{u}_1^2 / 2$ ).

#### 3-4-2 Accuracy of Calculated Parameters

In common with most work based on large numbers of experimental



measurements, it is difficult to make an accurate assessment of the maximum possible errors involved. This is particularly true in relation to the integral parameters upon which most of the present work is based. Realistic estimates of the maximum likely errors in the more important performance parameters are given in the table below.

| Parameter                          | Pre-diffuser  |                               | Overall       |                               |
|------------------------------------|---------------|-------------------------------|---------------|-------------------------------|
|                                    | Typical Value | Error                         | Typical Value | Error                         |
| Pressure Recovery $\tilde{c}_p$    | 0.500         | $\pm 0.025$<br>( $\pm 5\%$ )  | 0.500         | $\pm 0.015$<br>( $\pm 3\%$ )  |
| Effectiveness $\tilde{\epsilon}$   | 0.850*        | $\pm 0.050$<br>( $\pm 6\%$ )  | 0.700         | $\pm 0.020$<br>( $\pm 3\%$ )  |
| Loss Coefficient $\tilde{\lambda}$ | 0.080*        | $\pm 0.030$<br>( $\pm 40\%$ ) | 0.250         | $\pm 0.025$<br>( $\pm 10\%$ ) |

\*Note: Absolute values are quoted here to avoid confusion with percentage errors; elsewhere in the text values of Effectiveness and Loss Coefficient are quoted as percentages.

It may be noted that the errors quoted for the pre-diffuser parameters are larger than for the overall parameters, this being because of the non-uniformity of static pressure in the outlet plane. The comparatively large errors associated with the loss coefficients arise because each loss coefficient is calculated as the difference between two large quantities. It should also be noted that the percentage errors in loss coefficient increase as the loss decreases towards zero. Generally speaking, scatter and inconsistencies in the results are small and tend to suggest that the errors listed above are, if anything, pessimistic.

### 3-5 CALIBRATION TESTS

Initial calibration tests were carried out using Diffuser 1, since the flow in this diffuser was expected to be free from separation. The results of these tests are given in Appendix 2 and the main conclusions summarised below.

- (i) Excellent symmetry of flow was observed at the pre-diffuser inlet station.
- (ii) Within experimental error, the inlet velocity profile was shown to be independent of downstream conditions (notably flow split).
- (iii) Good symmetry of flow was observed at pre-diffuser outlet and in the settling lengths.
- (iv) The circumferential variation in wall static pressures was within experimental error.

### 3-6 INLET CONDITIONS

Preliminary running of the test rig was carried out with a simple bell-mouth intake flare fitted as shown in Fig. 3-6-1(a). During initial tests, low frequency fluctuations (0.2 to 1 Hz) in flow were observed throughout the rig. These were eventually traced to the effects of large scale turbulence within the laboratory. In order to eliminate the undesired fluctuations the intake was modified to include a Dufaylite honeycomb screen followed by an 8:1 area contraction as shown in Fig. 3-6-1(b). This reduced the velocity fluctuations from  $\pm 2\%$  to  $\pm \frac{1}{2}\%$  with a circumferential asymmetry of  $\pm 1\%$  in velocity. All subsequent testing was carried out using the modified intake.

The inlet velocity profile is shown in Fig. 3-6-2. It is peakier than that measured by Stevens<sup>(9)</sup> (for a similar Reynolds number and inlet radius ratio) and has a value of  $\alpha_1 = 1.062$  compared with 1.045 for that due to Stevens. The original intake gave an inlet profile very similar to that of Stevens. It is therefore thought that the increased turbulence presented

by the honeycomb screen was responsible for the change in profile when the modified intake was fitted. It may be noted that the change in profile is similar to that observed by Bradley & Cockrell<sup>(8)</sup> when using smooth and rough pipes to generate fully-developed flow (see Fig. 3-6-3).

The inlet turbulence intensity distribution is shown in Fig. 3-6-4. It can be seen that the results are in good agreement with those of Stevens. It is concluded that the inlet conditions were consistent with fully-developed flow.

Fig.3-1-1 RANGE OF TESTS FOR EACH PRE-DIFFUSER.

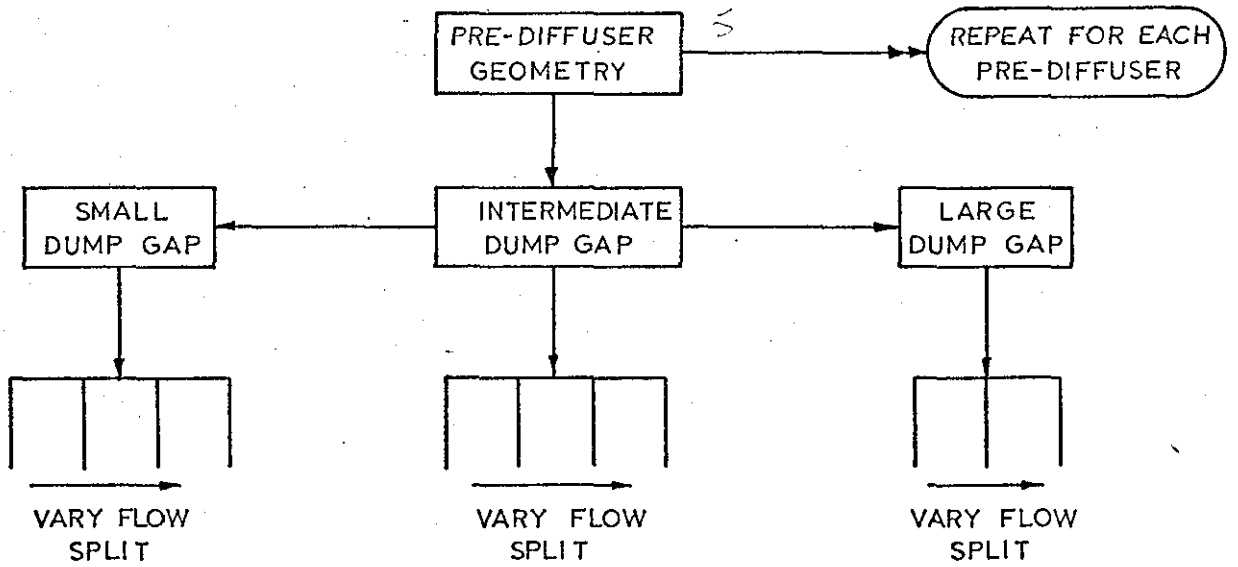


Fig.3-6-1 COMPARISON OF ORIGINAL AND MODIFIED INTAKES.

(a) BELL-MOUTH INTAKE  
(NOT USED IN EXPERIMENTAL PROGRAMME)

(b) MODIFIED INTAKE

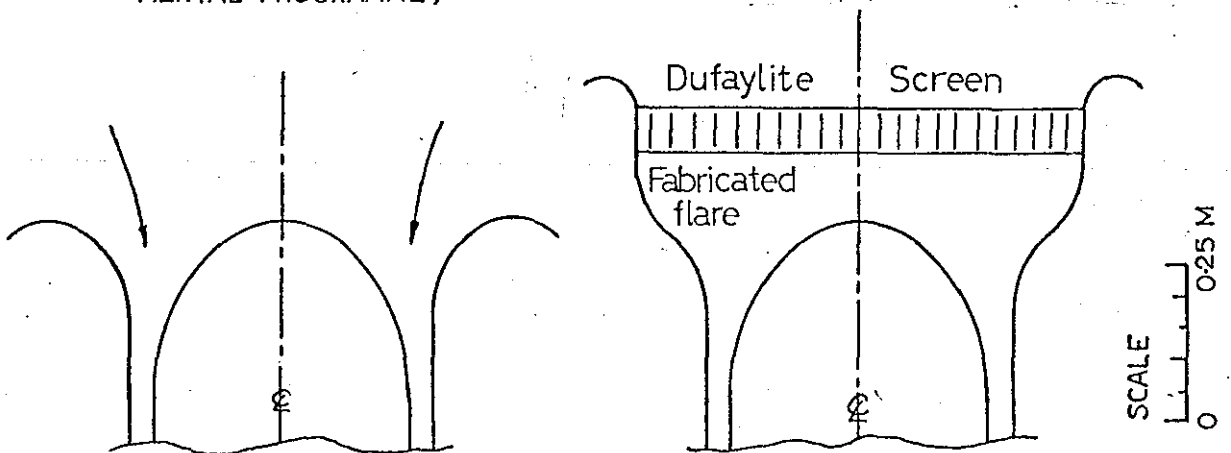


Fig.3-6-2 INLET VELOCITY PROFILE.

$H_0 = 1.366$ ,  $H_i = 1.356$   
 $U/U_0 = 0.8744$ ,  $B_1 = 0.1256$ ,  $\alpha_1 = 1.062$

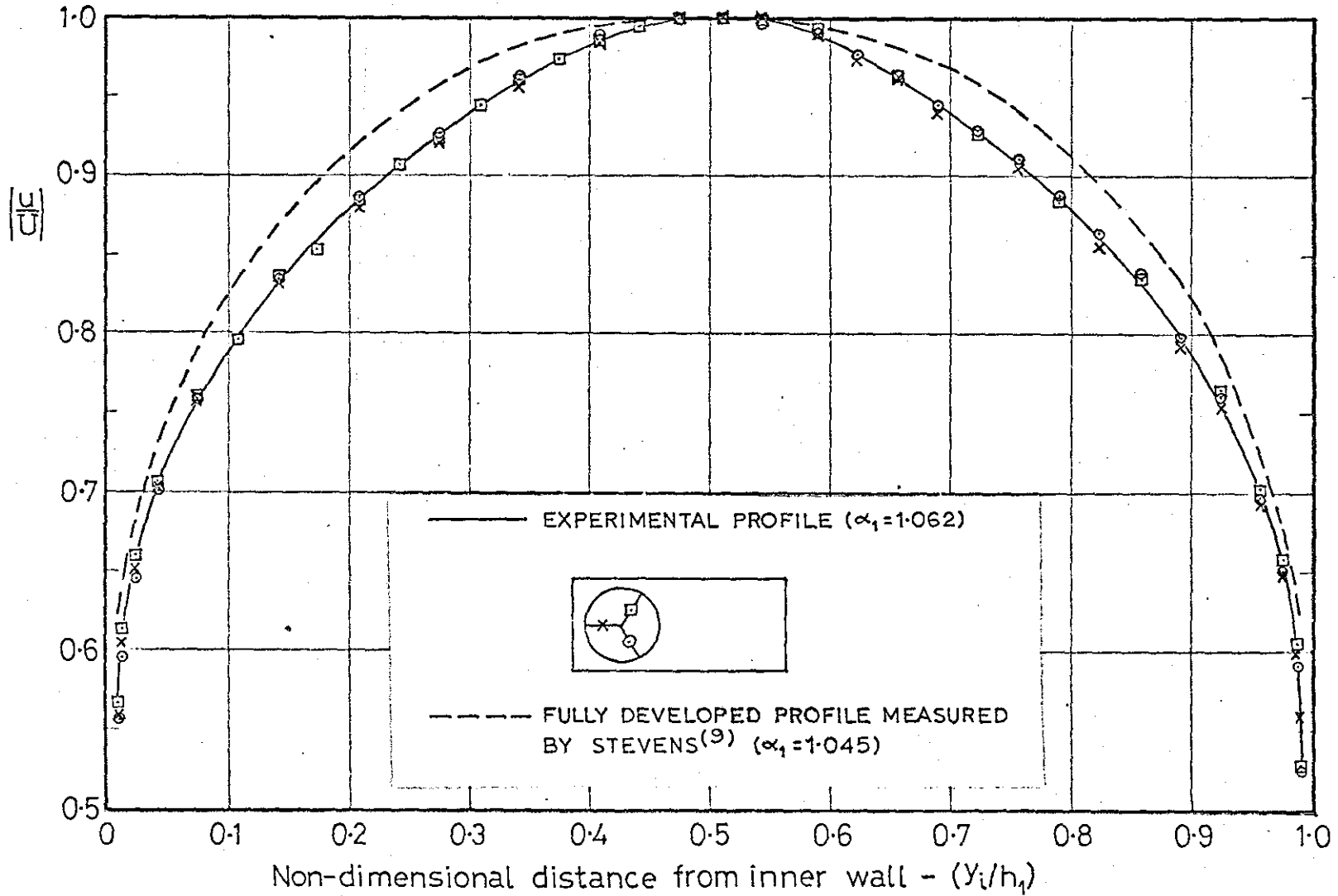


Fig. 3-6-3 INFLUENCE OF PIPE ROUGHNESS ON FULLY-DEVELOPED VELOCITY PROFILE AFTER BRADLEY & COCKRELL<sup>(8)</sup>

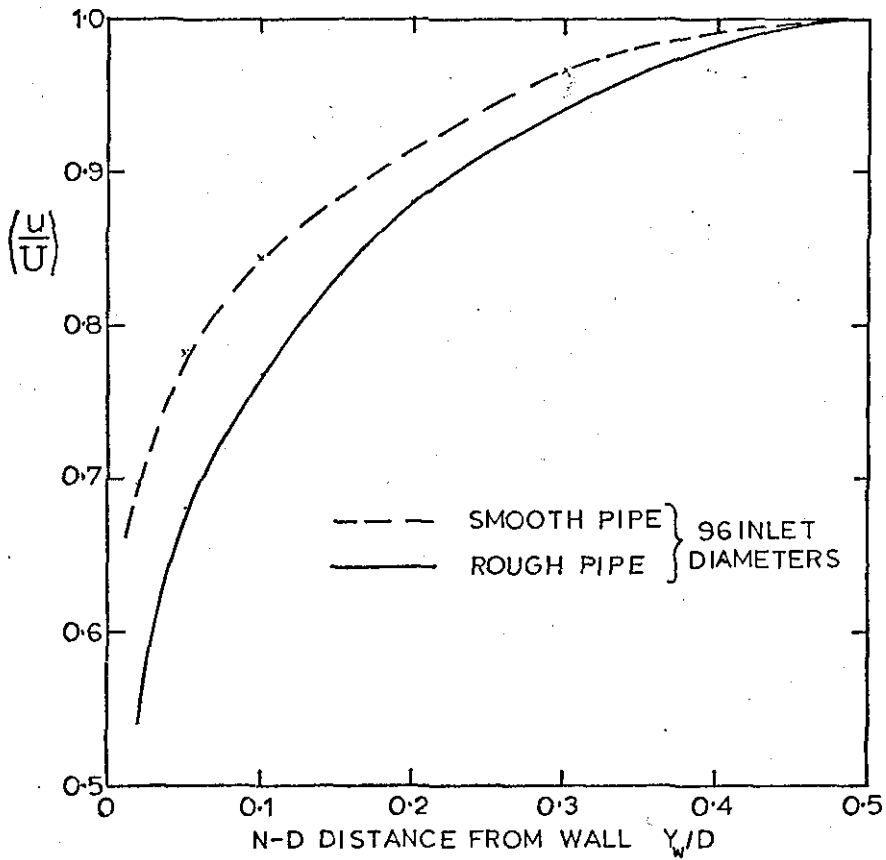
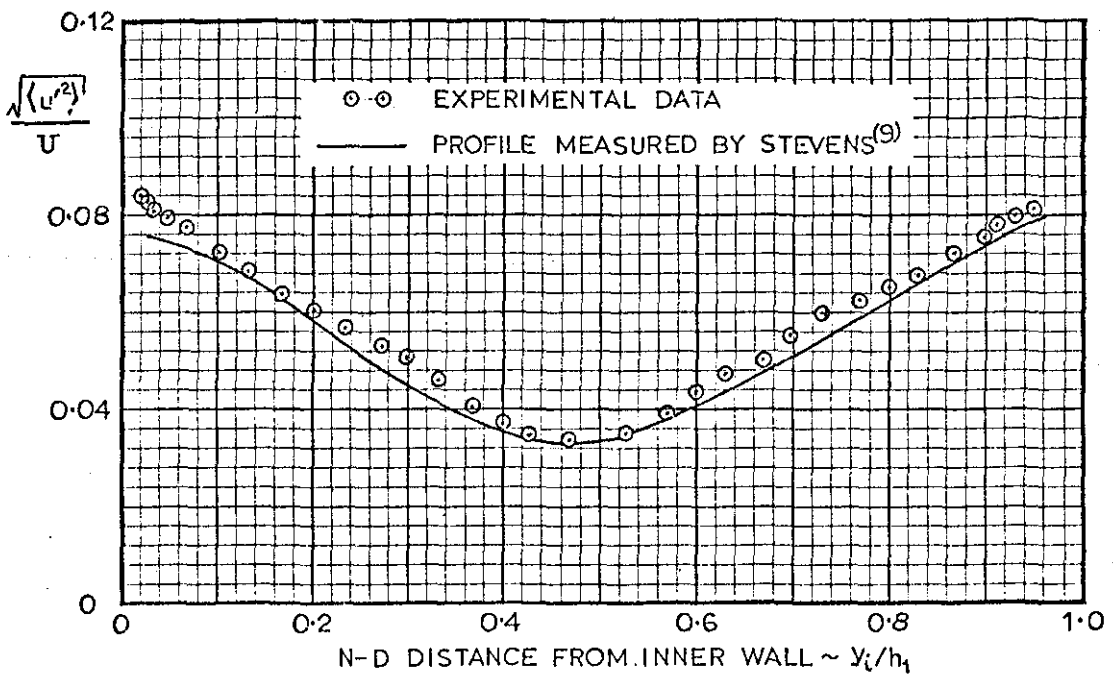


Fig. 3-6-4 EXPERIMENTAL AXIAL TURBULENCE INTENSITY DISTRIBUTION AT INLET.



| D <small>IFFUSER</small><br>No. | PRE-DIFFUSER<br>GEOMETRY |               |               |                  | NON-DIMENSIONAL DUMP GAP ( $D/h_2$ ) and FLOW SPLIT RATIO (S) |                                  |                          |
|---------------------------------|--------------------------|---------------|---------------|------------------|---------------------------------------------------------------|----------------------------------|--------------------------|
|                                 | $AR_{1-2}$               | $2\phi^\circ$ | $\bar{L}/h_1$ | $\epsilon^\circ$ | SMALL $D/h_2$                                                 | INTERMEDIATE $D/h_2$             | LARGE $D/h_2$            |
| 1                               | 1.4                      | 12            | 1.900         | 0                | $D/h_2 = 0.5$                                                 | 1.0                              | 2.0                      |
|                                 |                          |               |               |                  | $S = 0.71, 1.42^*, 1.75^*, 2.20^*, 3.23$                      | $S = 1.30^*, 1.72^*, 2.57^*$     | $S = 0.79, 1.64, 3.40^*$ |
| 2                               | 1.6                      | 12            | 2.850         | 0                | $D/h_2 = 0.5$                                                 | 0.8                              | 1.5                      |
|                                 |                          |               |               |                  | $S = 0.82, 1.20^*, 1.71, 2.48$                                | $S = 0.81, 1.21^*, 1.54, 2.12^*$ | $S = 0.88, 1.47, 2.30$   |
| 3                               | 1.8                      | 12            | 3.805         | 0                | $D/h_2 = 0.4$                                                 | 0.7                              | 1.2                      |
|                                 |                          |               |               |                  | $S = 0.83, 1.26^*, 1.67, 2.36$                                | $S = 0.78, 1.17^*, 1.82, 2.30$   | $S = 0.84, 1.37, 2.32$   |
| 4                               | 1.8                      | 12            | 2.525         | 0                | $D/h_2 = 0.4$                                                 | 0.7                              | 1.2                      |
|                                 |                          |               |               |                  | $S = 0.83, 1.19, 1.77, 2.25^*$                                | $S = 0.78, 1.13^*, 1.77, 2.27$   | $S = 0.85, 1.27, 2.16$   |
| 5                               | 1.6                      | 11.3          | 2.850         | 3.33             | $D/h_2 = 0.5$                                                 | 0.8                              | 1.5                      |
|                                 |                          |               |               |                  | $S = 1.31, 1.79, 2.22, 3.21^*$                                | $S = 1.20, 1.70, 2.24, 3.24$     | $S = 1.10, 1.77, 2.94$   |

\* "CT" TESTS

Table 3-1 SUMMARY OF TESTS CARRIED OUT.

## CHAPTER 4. PRESENTATION AND DISCUSSION OF RESULTS

In this chapter the fluid dynamic behaviour and performance characteristics of each system are presented. The influence of the major variables, namely flow split, dump gap and pre-diffuser geometry, is discussed. The fluid dynamic characteristics are illustrated by means of typical examples; the majority of the velocity profiles and static pressure distributions are given in Appendices 5, 6, 7 and 8. The data is summarised graphically by means of suitable parameters whose physical significance is discussed in the text where appropriate.

### 4-1 PERFORMANCE CHARACTERISTICS

The variation of ideal pressure recovery,  $\tilde{C}_{p4}$  and effective area ratio,  $AR_e$  (see Sect. 1-3-3) with flow split ratio,  $S$  are shown in Figs. 4-1-1/2. The ideal pressure recovery is that which would be achieved with zero losses and uniform outlet flow;  $AR_e$  is the equivalent area ratio of a simple diffuser having the same ideal pressure recovery as the branched system operating at a given flow split. These are basic characteristics of the system and form a basis for the discussion of results. The performance characteristics of each system and its corresponding pre-diffuser are shown in Figs. 4-1-3 to 4-1-7. The graphs show the variation in loss coefficient,  $\tilde{\lambda}$ , pressure recovery,  $\tilde{C}_p$ , and effectiveness,  $\tilde{\xi}$  with flow split for each non-dimensional dump gap,  $D/h_2$ . The overall design flow split,  $S_4^* = 2.15$  is indicated on each figure and dotted lines have been added to indicate the range of optimum flow splits.

#### 4-1-1 Influence of Flow Split

The curves for  $\tilde{C}_{p4}$  and  $AR_e$  (Figs. 4-1-1/2) show that the net diffusion is reduced as the flow split is moved away from the overall design value. In such cases the system is said to be operating "off-design". Much of the discussion in this section centres upon the relationship of optimum flow



split to design flow split. In order to avoid unnecessary repetition the optimum flow splits are referred to using the following convention.

- $S_{\lambda}$  . . . . flow split giving minimum loss
- $S_{C_p}$  . . . . flow split giving maximum pressure recovery
- $S_{\xi}$  . . . . flow split giving maximum effectiveness.

The suffices (2) and (4) are used to denote values for the pre-diffuser and overall system respectively.

It can be seen that the performance curves (Figs. 4-1-3/7) are adequately defined by the experimental data. There is a striking similarity between each family of curves, thus indicating that the characteristics of each system are fundamentally the same.

The overall loss coefficient,  $\tilde{\lambda}_{1-4}$  is seen to depend upon flow split and dump gap. The value of  $S_{\lambda_4}$  is generally lower than design,  $S_4^*$ , and decreases as the dump gap is decreased. Taking Diffuser 1 as an example, it is seen that  $S_{\lambda_4}$  drops from approximately 1.7 to 1.0 as  $D/h_2$  is decreased from 2.0 to 0.5. In addition, the sensitivity to flow split increases as  $D/h_2$  is reduced; at the large dump gap the variation in loss is barely significant. It may be noted that the overall loss curves bear little relationship to that for effective area ratio (Fig. 4-1-2), i.e. as the amount of diffusion decreases the loss does not decrease as might have been expected.

On comparing the pre-diffuser and overall losses it is apparent that the pre-diffuser has a strong influence on the variation of  $\tilde{\lambda}_{1-4}$  with flow split. Although  $\tilde{\lambda}_{1-2}$  is generally low (a typical value being 7%), the variation is significant. The influence of the pre-diffuser can be demonstrated by considering the dump plus settling length loss,

$\tilde{\lambda}_{2-4} = \tilde{\lambda}_{1-4} - \tilde{\lambda}_{1-2}$  (see Fig. 4-1-8). It can be seen that  $\tilde{\lambda}_{2-4}$  is essentially independent of flow split except in the case of small dump gaps. It may therefore be said that the pre-diffuser characteristics are of major importance in determining  $S_{\lambda_4}$ . In all cases except Diffuser 1,  $D/h_2 = 0.5$ ,

it can be seen that values of  $S_{\lambda_2}$  correspond closely with those of  $S_{\lambda_4}$ .

The curves of overall pressure recovery,  $\tilde{C}_{p_4}$  are of similar form to that for  $\tilde{C}'_{p_4}$  (Fig. 4-1-1), however the optimum flow split,  $S_{c_{p_4}}$  is seen to drop from  $S_4^*$  as  $D/h_2$  is reduced. To assist in explaining this, the overall pressure recovery may be written (see Eqns. 1-3-17/25) in the form,

$$\tilde{C}_{p_4} = 1 - \frac{1}{\alpha_1} \left( \frac{1}{1+S} \right)^3 \left[ \frac{\alpha_{4i}}{AR_i^2} + \frac{\alpha_{4o} S^3}{AR_o^2} \right] - \tilde{\lambda}_{1-4}$$

It was found that the velocity profile distortion in the settling lengths did not vary significantly with  $S$ , values of  $\alpha_4$  (inner and outer) being between 1.025 and 1.040. Thus, neglecting any losses,  $\tilde{C}_{p_4}$  would be very nearly equal to  $\tilde{C}'_{p_4}$  (see Eqn. 1-3-24). The shift in  $S_{c_{p_4}}$  from design is therefore due mainly to energy losses, i.e. due to inefficient rather than insufficient diffusion at design conditions.

Whereas  $S_{\lambda_4}$  and  $S_{c_{p_4}}$  are both "off-design", the values do not correspond and it is difficult to identify a single optimum flow split. The overall effectiveness,  $\tilde{E}_4$  has been defined in such a way that it shows the reduction in pressure recovery arising from outlet flow distortion and pressure loss, relative to a fixed datum, namely 100% (for uniform outlet flow and zero loss). By definition,  $S_{E_4}$  represents the most "effective" operating condition for the system. It may be noted that  $S_{E_4}$  is generally between  $S_{\lambda_4}$  and  $S_{c_{p_4}}$ . Taking Diffuser 2,  $D/h_2 = 0.5$  as an example,

$$S_{\lambda_4} = 1.25, S_{E_4} = 1.5 \text{ and } S_{c_{p_4}} = 1.7.$$

It is suggested that  $S_{E_4}$  represents a suitable compromise between conditions giving minimum loss and maximum pressure recovery.  $S_{E_4}$  is therefore taken to be the optimum flow split for the system. It should be emphasised that this is, in general, an "off-design" flow split for which the effective area ratio is somewhat less than the maximum.

The characteristics of the pre-diffusers are considerably easier to analyse since the ideal pressure recovery does not vary with flow split.

The optimum flow splits,  $S_{\lambda_2}$ ,  $S_{C_{p2}}$  and  $S_{E_2}$  are essentially equal. The error associated with  $\tilde{\lambda}_{1-2}$  is relatively large (see Sect. 3-4-2) and values of  $S_{\lambda_2}$  are considered less reliable than  $S_{C_{p2}}$  and  $S_{E_2}$ . The optimum flow split,  $S_{E_2}$  varies between 1.2 and 1.4 for the symmetric pre-diffusers (Nos. 1, 2, 3 & 4) whereas the values are between 1.5 and 2.0 for the canted pre-diffuser (No. 5). The latter pre-diffuser was in fact, designed with the objective of achieving just such a change in  $S_{E_2}$ . It can be seen that this also had the effect of shifting the overall optimum flow split,  $S_{E_4}$  towards the design value. It can be appreciated that the large displacement of  $S_{E_4}$  from design for the symmetric pre-diffusers has resulted from a mis-match between the pre-diffuser and downstream section geometries. The importance of careful component matching was not fully realised at the beginning of the research programme. Therefore, the introduction of the canted pre-diffuser (5) should be regarded as a development based on experience gained in testing with the first four pre-diffusers.

#### 4-1-2 Influence of Dump Gap

The performance curves (Figs. 4-1-3/7) show that initial increases in dump gap have a beneficial effect upon performance, but that beyond a certain value the effect is minimal. In the case of Diffuser 4 (Fig. 4-1-6), the results indicate that an increase in  $D/h_2$  from 0.7 to 1.2 resulted in a decrease in performance for  $S \approx 1.3$ . This trend is indicated by the results for the other diffusers, however it is not specifically shown. The trend is more readily demonstrated by plotting the performance parameters versus  $D/h_2$  for constant flow split. An example of the variation in  $\tilde{C}_{p4}$  with dump gap is given in Fig. 4-1-9 for Diffuser 3. It is seen that  $\tilde{C}_{p4}$  increases rapidly as  $D/h_2$  is increased from 0.4 to 1.0 and reaches a maximum in the region of  $D/h_2 \approx 1.0$ . Further increase in  $D/h_2$  results in a slow decrease in  $\tilde{C}_{p4}$ . Similar results were obtained with the other diffusers and it was shown that  $\tilde{\lambda}_{1-4}$  and  $\tilde{E}_4$  exhibit the same characteristics.

Careful examination of the performance curves shows that the optimum dump gap varies with flow split. The optimum dump gap and flow split for each system are fully established and discussed in Sect. 4-5. Before discussing the overall performance in more detail it is necessary to consider the fluid dynamic behaviour of the system.

#### 4-2 PRE-DIFFUSER OUTLET CONDITIONS

In the previous section it has been shown that the variation in pre-diffuser performance is an important factor in determining the optimum flow split for each system. In this section it will be shown that changes in pre-diffuser performance are associated with changes in both the outlet velocity and static pressure profiles. The characteristic variations of these profiles with flow split and dump gap are illustrated using typical examples for one pre-diffuser. In this connection, the results for Diffuser 3 have been chosen since they provide good examples of flow separation.

##### 4-2-1 Outlet Flow Axi-symmetry

Generally speaking, the velocity profiles measured at pre-diffuser outlet exhibited excellent symmetry of flow at the three circumferentially spaced measuring planes. Two sample sets of profiles are shown in Fig. 4-2-1. The profiles for Diffuser 1 (Test 1-1026/CT)<sup>†</sup> exhibit excellent symmetry of flow whereas agreement between those for Diffuser 4 (Test 4-0422/CT) can only be considered as "fair". These results illustrate the range of symmetry obtained with the five pre-diffusers; results for Diffusers 2, 3 & 5 lay between the two extremes indicated in Fig. 4-2-1. Data for other CT Tests<sup>†</sup> is given in Appendix 5.

For CT Tests the mean velocity profiles were used in obtaining pre-diffuser performance parameters, whereas profiles measured at the BLUE

---

<sup>†</sup> See Sect. 3-1 for description of the test numbering system.

position only were used in the case of A Tests. As far as consistency of results is concerned, it is not considered that any serious error was introduced by using this approach.

#### 4-2-2 Presentation of Data

The outlet conditions for Diffuser 3 are shown in Figs. 4-2-3/5. Each figure shows the velocity and static pressure profiles measured at constant dump gap for various flow splits (i.e. for each "Test Series"). Similar profiles for Diffusers 1, 2, 4 & 5 are given in Appendix 5. The graphs were drawn by computer and the following comments relate to the method of presentation.

(i) The curves were drawn using the mean profile data supplied to the main performance analysis program (see Appendices 3 & 4); the experimental data was specified separately. The graphs therefore provided a convenient method of checking that no errors were present in the main program input data.

(ii) In some cases (e.g. Test 3-0708/A, outer boundary layer) it can be seen that the velocity profile curves do not pass through the experimental data close to the wall. In such cases the curves were defined using additional data as illustrated in Fig. 4-2-2. The additional data is that deduced from total pressures recorded with low instrument damping (i.e. from fluctuating readings).

(iii) In the case of CT Tests, only the mean profiles are shown. The experimental data has been omitted for the sake of clarity, but it is given in Appendix 5.

The influence of the test variables on the outlet velocity profile is summarised in Figs. 4-2-6/10. The first three figures show the variations in  $H_{2_i}$  and  $H_{2_o}$  with flow split for each category of dump gap. Whereas the shape factors provide useful information on the boundary layer growth in the pre-diffuser, it is also interesting to consider the changes in peakiness and radial distortion of the velocity profile that are implied.

The outlet profile peakiness is described by means of the energy coefficient,  $\alpha_2$  (see Fig. 4-2-9). Radial distortion is described by means of the arbitrarily defined radial distortion factor,  $RD_2$  (see Sect. 1-4-2) where,

$$RD_2 = \left( \frac{\delta_i^* - \delta_o^*}{\delta_i^* + \delta_o^*} \right)_2$$

It may be noted that this factor is essentially independent of profile peakiness. The variations in  $RD_2$  with the test variables are shown in Fig. 4-2-10. The values of  $RD_2$  are to be interpreted as follows.

- $RD_2 < 0$       Profile distorted toward the inner wall
- $RD_2 \approx 0$       "Symmetrical" profile
- $RD_2 > 0$       Profile distorted toward the outer wall

A complete summary of the boundary layer parameter data is given in Appendix 9.

#### 4-2-3 Discussion of Outlet Velocity Profiles

Taking the outlet velocity profiles for Diffuser 3 (Figs. 4-2-3/5) as typical examples, it is seen that variations in flow split give rise to consistent changes in profile shape. As  $S$  is increased at constant dump gap the point of maximum velocity moves toward the outer wall and the inner boundary layer moves nearer to separation (i.e. the momentum near the wall is decreased). Conversely, the outer wall boundary layer moves further away from separation as  $S$  is increased. At all three dump gaps separation is clearly indicated on the inner wall for flow splits close to the overall design value,  $S_4^* = 2.15$ . It may further be noted that the velocity profiles are almost "symmetrical" for flow splits close to the pre-diffuser optimum value ( $S_{E_2} \approx 1.2$  as shown in Fig. 4-1-5).

Comparison of velocity profiles for approximately the same flow split shows that increasing the dump gap gives rise to an increase in profile peakiness. This is typified by the reduction in momentum near the walls and is due to the decreasing influence of the downstream blockage presented

by the head.

The overall trends for all the pre-diffusers are more conveniently discussed in terms of the boundary layer and velocity profile parameters shown in Figs. 4-2-6/10. The discussion centres upon comparison of the parameters at the two flow splits,  $S_{\epsilon_2}$  and  $S_4^*$  (as indicated on each group of curves).

#### Influence of Flow Split

Referring first to the outlet shape factor curves (Figs. 4-2-6/8) it can be seen that  $H_{2_i} \approx H_{2_o}$  (indicating a nearly symmetrical profile) at  $S_{\epsilon_2}$ . As the flow split is increased toward  $S_4^*$ ,  $H_{2_i}$  increases and  $H_{2_o}$  decreases. The radial distortion of the velocity profiles (as represented by the difference in the inner and outer shape factors) is appreciable at  $S_4^*$ . The variations in radial distortion are demonstrated in a more quantitative manner by the curves of  $RD_2$  (Fig. 4-2-9). It can be seen that  $RD_2 \approx 0$  at  $S_{\epsilon_2}$  and that values increase (in most cases linearly) toward  $S_4^*$ . The changes in outlet profile radial distortion are brought about by changes in the pressure gradients to which the inner and outer wall boundary layers are subjected. It is via this mechanism that the flow split exerts such a strong influence on boundary layer development in the pre-diffuser.

The curves of  $\alpha_2$  (Fig. 4-2-10) show that increases in radial distortion are accompanied by increases in peakiness of the outlet profile. The minimum peakiness is obtained at  $S_{\epsilon_2}$  where it can be noted that the profiles are essentially symmetrical ( $RD_2 \approx 0$ ). The combination of increasing radial distortion and peakiness represents a strong trend toward separation on the inner wall for  $S > S_{\epsilon_2}$ , and on the outer wall for  $S < S_{\epsilon_2}$ . Pre-diffuser flow separation is discussed in detail in Sect. 4-2-5, however it is worth noting that separation was observed on the inner wall at  $S_4^*$  for Diffusers 2, 3 and 4.

### Influence of Dump Gap

Referring to Fig. 4-2-10 it can be seen that  $\alpha_2$  generally increases with dump gap at constant flow splits. This is due to a decreasing tendency for the presence of the head to inhibit boundary layer growth in the pre-diffuser. At small dump gaps the downstream blockage presented by the head causes the flow to decelerate more evenly across the annulus, thus producing a less peaky profile.

The variation in  $\alpha_2$  over the range of flow split (for a fixed  $D/h_2$ ) decreases with increasing dump gap. In a similar way the rate of change in  $RD_2$  with flow split also decreases with increasing  $D/h_2$ . These trends indicate that the influence of flow split on boundary layer development in the pre-diffuser decreases as  $D/h_2$  is increased. This can be explained by considering the dump region as a fluid "accumulator" which tends to isolate the pre-diffuser from downstream influences when its volume becomes large (i.e. when the dump gap is large). On physical grounds it can be argued that the influence of flow split on the pre-diffuser becomes negligible as  $D/h_2$  tends to infinity.

### Influence of Pre-diffuser Geometry

The influence of pre-diffuser geometry on the outlet velocity profile was as expected in that the profile peakiness increased with both increasing area ratio and included angle. This can be seen by comparing values of  $\alpha_2$  for similar dump gaps (Fig. 4-2-10). A more direct comparison of outlet profile peakiness for the five pre-diffusers is shown in Fig. 4-2-11, in which peakiness is presented in terms of the outlet effective area fraction,  $E_2$ . For comparison purposes the correlation due to Sovran & Klomp<sup>(1)</sup> has been added and it may be noted that this represents the case of  $D/h_2 = \infty$ . The comparison is made in terms of values of  $E_2$  obtained at the optimum flow split,  $S_{E_2}$ . The experimental data has been interpolated to give curves of  $E_2$  for constant values of  $D/h_2$ .



It can be seen that the  $D/h_2 = 1.5$  curve (Diffusers 1, 2 & 3) is parallel to that of Sovran & Klomp, but that values of  $E_2$  are approximately 0.05 higher. The closeness of the  $D/h_2 = 1.5$  and 1.0 curves suggests that little increase in peakiness results from further increase in dump gap. It can be seen that the variation in  $E_2$  with area ratio is similar to that for simple diffusers (as represented by the correlation) but that values of  $E_2$  rise as  $D/h_2$  is decreased. Furthermore, increasing the included angle (and thereby the mean rate of diffusion) whilst maintaining the same area ratio results in a decrease in  $E_2$ , representing an increase in profile peakiness.

The comparison of outlet profiles for Diffusers 2 & 5 is of particular interest. It can be seen from Figs. 4-2-6/10 that the profiles obtained at  $S_4^*$  have been much improved by canting the pre-diffuser. At  $D/h_2 = 0.8$ , for example,  $H_{2i}$  has been reduced from 2.5 to 2.12 with a corresponding decrease in  $RD_2$  from 0.52 to 0.3. Similarly,  $\alpha_2$  has decreased from 1.335 to 1.295 and it may be noted that separation on the inner wall has been eliminated by canting the pre-diffuser. The main reason for the improvement is the relative displacement of the head from the diffuser exit centre-line. The decreased gap between the head and the inner wall at exit gives rise to a reduction in static pressure. The momentum of the flow adjacent to the inner wall is therefore maintained at a higher level than that in the symmetrical pre-diffuser and separation is avoided.

The independent influence of each test variable on the outlet velocity profile is summarised in Table 4-2 over. The length of the diffusing system is represented by the total "variable length",  $(\bar{L} + D)/h_1$ .

In the context of correlations of profile parameters with diffuser geometry and performance, it may be noted that the present results provide a good basis for comparing the blockage fraction,  $B$  with  $\alpha$  (see Fig. 4-2-12). The significance of  $\alpha$  is demonstrated by the performance equations of Sect. 1-3, however  $B$  has been used almost universally in correlation work. The

results shown in Fig. 4-2-12 cover a wide range of flow conditions (including separation) and it can be seen that there is a strong relationship between the two parameters. This tends to substantiate the case for using B in performance correlation work, particularly since it may be measured with relative ease.

Table 4-2 Influence of Test Variables on Outlet Velocity Profile

| Action               | Effect(s)                                                                                                                                 | System Length<br>( $\bar{L} + D$ )/ $h_1$ |
|----------------------|-------------------------------------------------------------------------------------------------------------------------------------------|-------------------------------------------|
| Increase<br>AR       | Decrease mean outlet velocity.<br>Increase profile peakiness.                                                                             | Increase                                  |
| Increase<br>$2\phi$  | Increase profile peakiness.<br>Increase max. outlet velocity.                                                                             | Decrease                                  |
| Cant<br>Pre-diffuser | Shift optimum flow split.<br>Minimal change in outlet velocity<br>profile at optimum flow split, $S_{\mathcal{E}_2}$                      | Negligible<br>change                      |
| Increase<br>$D/h_2$  | Increase profile peakiness.<br>Increase max. outlet velocity.                                                                             | Increase                                  |
| Vary Flow<br>Split   | Radial distortion of profile for<br>$S \neq S_{\mathcal{E}_2}$ accompanied by increase<br>in peakiness.<br>Increase max. outlet velocity. | No change                                 |

4-2-4 Discussion of Static Pressure Profiles

The following discussion relates mainly to the outlet static pressure profiles for Diffuser 3 (Figs. 4-2-3/5), these being typical of the changes that occur in all the pre-diffusers. A striking feature of these profiles is the large variation in pressure across the annulus. This is a feature not usually encountered in diffuser research and resulted in the necessity for integrating the static pressure on a mass-weighted basis in order to obtain meaningful pressure recovery coefficients. As with the outlet velocity profiles, the influences of dump gap and flow split are

inter-related; the influence of flow split decreasing as the dump gap is increased.

#### Influence of Flow Split

It may be seen that the pressure difference between the inner and outer walls is small at the optimum flow split,  $S_{\epsilon_2}$ , of approximately 1.2. At other flow splits the wall pressures are unequal; the inner wall pressure increases and the outer wall pressure decreases as  $S$  is increased. The increased adverse pressure gradient along the inner wall causes more rapid growth of the boundary layer and vice-versa for the outer wall.

#### Influence of Dump Gap

Comparing Figs. 4-2-3/5 it can be seen that close proximity of the head to the outlet plane gives rise to a "hump" in the static pressure profiles. This can be attributed to the influence of the high pressure associated with the stagnation region close to the head. The radial pressure gradients provide the forces required to turn each stream of flow around the head. Since the outlet static pressure also dictates the axial pressure gradient (at least in the latter part of the pre-diffuser), the outlet velocity profile is the result of a complicated balance between the momentum and pressure forces in each flow field. At small dump gaps the rapid deceleration associated with flow stagnation extends into the pre-diffuser with the effect of reducing the velocity profile peakiness.

#### 4-2-5 Pre-Diffuser Separation Limits

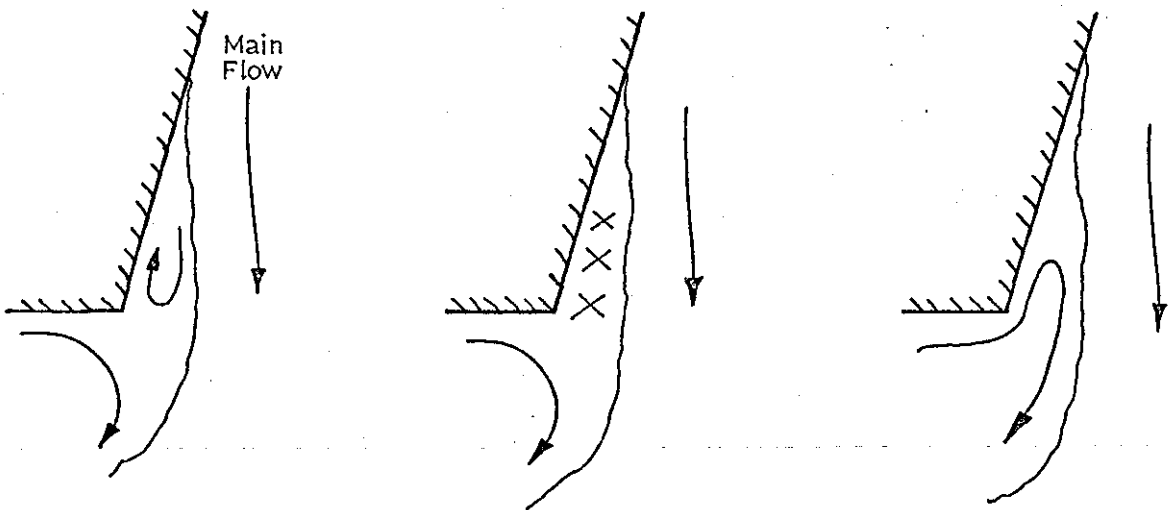
Several examples of pre-diffuser outlet flow separation are shown for Diffuser 3 in Figs. 4-2-3/5 and these are now discussed along with the results for the other pre-diffusers. Wool tufts were used to investigate the flow in cases where dynamic pressure measurements indicated that separation was likely. The flow regimes of Carlson & Johnston<sup>(17)</sup> (see Fig. 4-2-13) were used as a basis for interpreting the tuft behaviour. It was found that the "Intermittent Transitory Stall" regime of Carlson &

Johnston corresponded closely with conditions at which the indicated wall velocity became sensibly zero. A typical example of this is shown in Fig. 4-2-4 for  $S = 1.82$  (inner boundary layer). "Incipient Transitory Stall" and "Unsteady Flow" were found to be associated with indicated values of  $u/U$  near the wall of up to approximately 0.1 (e.g. Fig. 4-2-4,  $S = 0.77$ , outer boundary layer). It is interesting to note that tuft behaviour indicating "Fixed Stall" was not observed although zero values of  $u/U$  were obtained at distances from the wall of up to 9 mm or  $y_1/h_2 = 0.13$ , for Diffuser 4 (see Appendix 5). In such situations the proximity of the vortex in the dump region is considered to have had some influence upon the nature of flow in the separated region. The diagrams below show three possible flow patterns and the information available would tend to suggest that (b) is the most appropriate.

(a) Opposing Vortices

(b) "Dead Air" Region

(c) Extension of Standing Vortex



For the purpose of defining separation limits it was found convenient to use the criterion of zero indicated wall velocity, corresponding with intermittent transitory stall. This approach had the advantage that results could be interpolated (in respect of flow split) to give reasonably well defined limits beyond which separation could be said to occur.

Separation limits (based on the above criteria) are shown in Fig. 4-2-14. It can be seen that separation occurred on the inner wall at  $S_4^*$  for Diffusers 2, 3 & 4. The range of flow splits over which relatively steady flow was obtained decreased with increasing area ratio (Diffusers 1, 2 & 3) and also with increasing included angle (Diffuser 4). As would be expected, the most steady flow was obtained at  $S \approx 1.2$  for the symmetrical pre-diffusers. Comparing Diffusers 2 and 5 shows that canting had the effect of eliminating separation at  $S_4^*$  and shifting the optimum flow split to approximately 1.7. The objectives and results of canting the pre-diffuser are discussed in more detail in Sect. 4-2-7.

Values of shape factor,  $H$ , of approximately 2.6 are generally associated with the onset of separation and it is interesting to note that the intermittent transitory stall limits of Fig. 4-2-14 correspond with values between 2.4 and 2.8 (see Figs. 4-2-6/8). It can be appreciated that the widening of the limits at small dump gaps is due to the decreased profile peakiness as discussed in Sect. 4-2-3.

Referring back to Fig. 4-2-1, it is interesting to note that the velocity profiles for Test 4-0422/CT indicate that the separation was not asymmetric as is often the case in annular diffuser flows (see Appendix 5 for other CT-Test results). It is therefore considered that the presence of the head had a stabilising influence in so far that no serious three-dimensionality in the flow was observed.

#### 4-2-6 Discussion of Outlet Conditions in Relation to Pre-Diffuser

##### Performance

In this section the relationship between outlet conditions and pre-diffuser performance is discussed. Reference is made to the performance curves (Figs. 4-1-3/8) and the corresponding outlet profile data (Figs. 4-2-6/10). For a given pre-diffuser, operating at a particular dump gap, it has been shown that the maximum pressure recovery and minimum energy loss is obtained at a flow split giving an essentially symmetrical outlet

velocity profile. The pressure recovery coefficient for a simple diffuser (Eqn. 1-3-15) may be written,

$$\tilde{C}_{P_2} = 1 - \frac{\alpha_2}{\alpha_1 AR^2} - \tilde{\lambda}_{1-2} \quad 4-2-1$$

Comparison of the terms  $\left(\frac{\alpha_2}{\alpha_1 AR^2}\right)$  and  $\tilde{\lambda}_{1-2}$  over the range of flow splits covered by the tests shows that changes in the outlet energy coefficient,  $\alpha_2$  are responsible for approximately 70% of any given change in pressure recovery with changing flow split. The majority of the reduction in pressure recovery at flow splits other than  $S_{E_2}$  is therefore due to the increase in outlet kinetic energy flux associated with distortion of the flow (i.e. due to insufficient diffusion). Similar remarks also apply in respect of changes in pressure recovery for varying dump gap and constant flow split.

Whereas variations in  $\tilde{C}_{P_2}$  are mainly related to changes in  $\alpha_2$ , no clear correlation between energy loss and outlet profile distortion is evident. This is illustrated by the examples for Diffuser 2 given in the table below.

Comparison of Performance for Various Outlet Conditions  
(Diffuser 2)

| D/h <sub>2</sub> | S    | α <sub>2</sub> | RD <sub>2</sub> | $\tilde{\lambda}_{1-2}$ % | $\tilde{C}_{P_2}$ |
|------------------|------|----------------|-----------------|---------------------------|-------------------|
| 1.5              | 1.20 | 1.34           | 0.10            | 7.3                       | 0.420             |
| 0.8              | "    | 1.26           | 0               | 5.3                       | 0.470             |
| 0.5              | "    | 1.12           | 0.10            | 6.5                       | 0.514             |
| 0.5              | 2.48 | 1.32           | 0.77            | 10.3                      | 0.399             |

It may be noted that no significant change in loss coefficient has resulted from the increase in  $\alpha_2$  from 1.12 to 1.34 for increasing dump gap at constant flow split. However, the combination of increasing radial distortion and peakiness (as represented by RD<sub>2</sub> and α<sub>2</sub>) gave an increase in loss coefficient from 6.5 to 10.3% at constant dump gap. The independent

influence of radial distortion may be assessed by comparing the performance at conditions giving the same outlet profile peakiness ( $\alpha_2$ ). Three typical examples are given in the table below.

Influence of Radial Distortion on Pre-diffuser Performance

| DIFFUSER No. | D/h <sub>2</sub> | S    | $\alpha_2$ | RD <sub>2</sub> | $\tilde{\lambda}_{1-2}$ % | $\tilde{\xi}_2$ % |
|--------------|------------------|------|------------|-----------------|---------------------------|-------------------|
| 2            | 0.8              | 1.2  | 1.265      | 0               | 5.3                       | 75.5              |
|              | 0.5              | 2.3  | "          | 0.74            | 9.4                       | 68.0              |
| 4            | 0.7              | 1.1  | 1.521      | -0.14           | 7.8                       | 66.9              |
|              | 0.4              | 2.35 | "          | 0.82            | 11.5                      | 62.5              |
| 5            | 0.8              | 1.7  | 1.285      | 0.11            | 7.4                       | 71.2              |
|              | 0.5              | 3.5  | "          | 0.72            | 12.0                      | 63.0              |

It may be seen that radial distortion ( $RD_2 > 0$ ) causes the loss coefficient to rise by approximately 4% with a corresponding drop in effectiveness for the same value of  $\alpha_2$  (i.e. for the same net reduction in kinetic energy, diffusion becomes less efficient when the flow is radially distorted). This implies that the increased loss associated with the near separated boundary layer outweighs any decrease in loss associated with the other boundary layer. The results suggest that some form of radial distortion parameter could be used to advantage in correlating diffuser performance with flow conditions and geometry.

Generally speaking the loss coefficient does not vary significantly with dump gap even though the outlet profile peakiness increases rapidly with increasing dump gap over most of the flow split range (see Fig. 4-2-10). Thus, for the particular case of constant pre-diffuser geometry, it appears that energy losses are not directly related with profile peakiness. This is a somewhat surprising result since losses are generally considered to arise from high turbulent mixing such as occurs in regions of near separated

flow (i.e. with high peakiness profiles). A more detailed investigation of the turbulence structure of the flow within the pre-diffuser would no doubt give some insight into this apparent anomaly. In the absence of more detailed information, it is suggested that the higher reduction in kinetic energy achieved at small dump gaps causes proportionately more loss to be generated in the core region of the flow and that this is equivalent to the loss generated in the near-separated regions at large dump gaps (i.e. the losses are substantially the same but generated in different regions of the flow).

#### 4-2-7 Pre-diffuser Design Flow Split Ratios

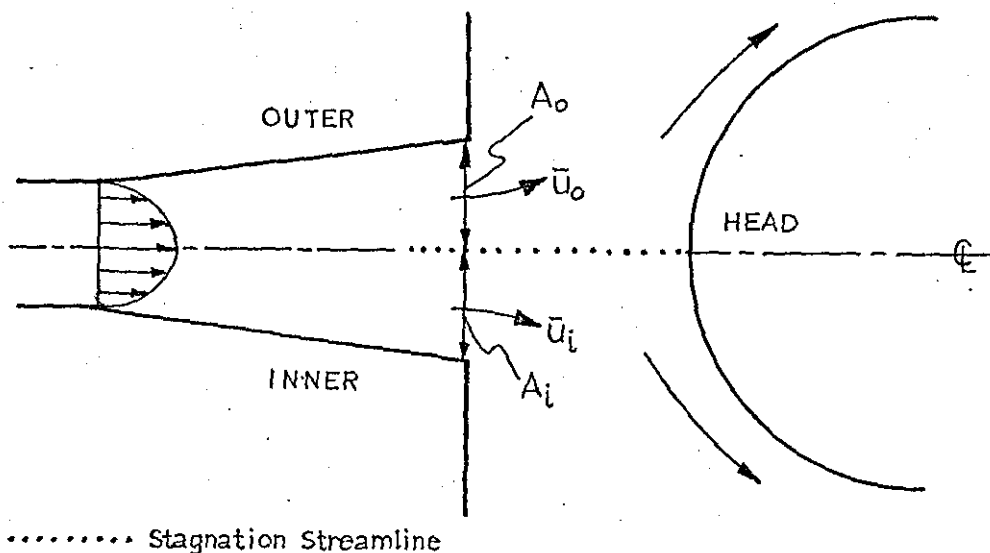
It has been noted in the foregoing sections that the optimum pre-diffuser performance is not generally obtained at the overall design flow split,  $S_4^* = 2.15$ . The symmetrical pre-diffusers were not in fact designed to satisfy any particular objective as regards giving optimum performance at  $S_4^*$ . The appropriate "design" flow split for these pre-diffusers is considered in the light of the experimental results and the criterion used in designing the canted diffuser is discussed. In view of the need to minimise system length, attention is focused on results for small and intermediate dump gaps.

In the case of Diffusers 2, 3 & 4 the optimum flow split is approximately 1.2 whereas it is nearer 1.4 for Diffuser 1. Having regard to the outlet velocity profile parameters and separation limits it is reasonable to define a pre-diffuser "design" flow split,  $S_2^*$  equal to 1.2 as being applicable for the symmetrical diffusers operating at small to intermediate dump gaps. At this flow split the following design objectives are, in the main achieved:

- (i) optimum performance in terms of  $\tilde{C}_{p2}$  and  $\tilde{\lambda}_{1-2}$ ,
  - (ii) maximum net reduction in velocity giving minimum kinetic energy at entry to the dump section
- and (iii) operating point midway between the inner and outer boundary layer separation limits (i.e. optimum outlet flow stability).



The design objective can therefore be expressed in terms of a requirement to obtain a "symmetrical" outlet velocity profile at the design flow split chosen for the system as a whole. Some insight into ways of satisfying this objective can be gained by considering the pre-diffuser and dump region geometry shown below.



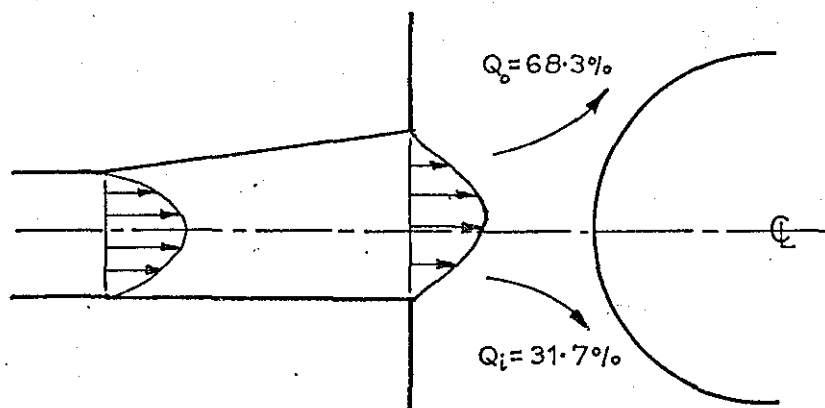
The pre-diffuser and combustion chamber head are on the same local centre-line and it is assumed that the stagnation streamline is coincident with this centre-line in the dump region. The design flow split is given by,

$$S_2^* = \left( \frac{\bar{u}_o}{\bar{u}_i} \cdot \frac{A_o}{A_i} \right)_2 \quad 4-2-2$$

Substituting typical values of  $(\bar{u}_o/\bar{u}_i)_2 \approx 0.97$  for a symmetrical outlet profile and  $(A_o/A_i)_2 \approx 1.14$  in Eqn. 4-2-2 gives an estimated design flow split of  $S_2^* = 1.1$ . The discrepancy between this and the value of 1.2 quoted above is due to the assumption that the flow divides along the centre-line. Experimental results show that the stagnation streamline is typically 48% of the annulus height from the inner wall.

In the absence of any suitable theory the above approach was used as a basis for designing the canted diffuser. The objective was to obtain a pre-diffuser giving a symmetrical outlet profile for  $S = S_4^*$  and  $D/h_2 = 0.8$ . An iterative process was used to obtain the combination of wall angles

giving  $S_2^* \approx 2.15$  by Eqn. 4-2-2. The area ratio and non-dimensional length were to be the same as for Diffuser 2. Values of  $(\bar{u}_o/\bar{u}_i)_2$  were obtained by integrating a typical symmetrical profile using the assumption that the flow would divide along the head centre-line.



CANTED PRE-DIFFUSER,  $S = S_4^* = 2.15$

The final choice of geometry corresponded to:

$$(A_o/A_i)_2 = 1.75, (\bar{u}_o/\bar{u}_i)_2 = 1.25 \text{ and } S_2^* = 2.18$$

The experimental results indicate that a realistic value of  $S_2^*$  is 1.7 ( $D/h_2 = 0.8$ , Fig. 4-1-7). The discrepancy between this and the estimated value is again due to the assumption concerning the stagnation streamline. This was approximately 44% of the annulus height from the inner wall as against the 38% initially assumed. However, it may be noted that a flow split of approximately 2.0 was required to induce symmetrical flow at  $D/h_2 = 1.5$ , this being in reasonable agreement with the estimated value. It is therefore apparent that the optimum inclination or "cant" angle,  $\epsilon$  (defined in Fig. 1-2-2) depends upon the dump gap chosen (i.e. higher  $\epsilon$  for small dump gaps, lower  $\epsilon$  for large dump gaps). This is due to the decreased influence of flow split at the larger dump gaps. It is therefore difficult to arrive at a general rule for determining  $S_2^*$  and hence to predict optimum pre-diffuser geometries. The simple method described above was partially successful, however a more rigorous approach is clearly required. The present results form a basis for further testing of canted

pre-diffusers and this would no doubt lead to the establishment of better criteria for matching pre-diffuser geometry with downstream geometry.

In order to simplify the discussion in the following sections, "design" flow splits will be used for reference purposes instead of the optimum flow splits used earlier. Appropriate values are:

Symmetrical Diffusers (Nos. 1, 2, 3 & 4) . . . . .  $S_2^* = 1.2$

Canted Diffuser (No. 5) . . . . .  $S_2^* = 1.7$

Whereas these values are only strictly applicable for intermediate dump gaps, it is not considered that any serious error will be incurred by their use for other dump gaps.

#### 4-3 SETTLING LENGTH FLOW CONDITIONS

The velocity profiles measured at Station 4 (six annulus heights downstream of the beginning of the parallel walled settling length annuli) are given in Figs. 4-3-1/3 for Diffuser 3. Profiles for the other tests are given in Appendix 7. The experimental data has been omitted for the sake of clarity but sample data is given in Appendix 2. The static pressure difference between the inner and outer walls of each annulus was in all cases negligible.

It can be seen that the velocity profiles are close to uniform with  $u/U > 0.9$  over approximately 80% of each annulus. There is no significant change in profile with varying dump gap for a fixed flow split, however a definite trend is shown with varying flow split. This is best considered in terms of the flow passing down each annulus; at high flow fractions the profile peak is biased toward the combustion chamber wall and vice-versa at low flow fractions. The profiles tend to be symmetrical for the pre-diffuser design flow split,  $S_2^*$  (1.2 for Diffuser 3). These trends are repeated for all five diffusers (see Appendix 7). Changes in radial distortion of the settling length profiles are related to changes in flow pattern in the dump region. Due to the complexity of flow conditions in the dump

region, discussion of these changes in profile is deferred to a later section (see Chapter 5).

The inner and outer annulus energy coefficients (all tests) are plotted in Fig. 4-3-4. It can be seen that the values of  $\alpha_{4_i}$  and  $\alpha_{4_o}$  vary very little with pre-diffuser geometry, dump gap and flow split. A typical value is 1.03. The equation for overall pressure recovery (Eqn. 1-3-17) may be written in the form,

$$\tilde{C}_{p_4} = 1 - \frac{1}{\alpha_1 (1+S)^3} \left( \frac{\alpha_{4_i}}{AR_i^2} + \frac{S^3 \alpha_{4_o}}{AR_o^2} \right) - \tilde{\lambda}_{1-4}$$

and from this it is clear that the small changes in the energy coefficients are not responsible for any significant variation in overall pressure recovery. Reductions in  $\tilde{C}_{p_4}$  relative to the ideal value,  $\tilde{C}_{p_4}^i$  (see Fig. 4-1-1) are therefore due mainly to inefficient diffusion (i.e. pressure loss) rather than to excess kinetic energy flux at Station 4.

#### 4-4 STATIC PRESSURE DISTRIBUTIONS

##### 4-4-1 Examples of the Complete Static Pressure Distribution

For each test the wall static pressures were measured throughout the diffuser system (see Fig. 2-4-3). Typical examples of the static pressure distributions are given in Figs. 4-4-1/8. The following points should be noted.

(i) Each figure represents a cross-section of the diffuser system in diagrammatic form. The vertical (i.e. axial) dimensions are scaled from the appropriate test geometry, however the horizontal dimensions are arbitrary. The inner and outer walls of the system are represented by straight lines and the pre-diffuser inlet and outlet planes are identified by chain dotted lines.

(ii) The two upper scales ( $C_{p_w}$ ) relate to the static pressure coefficients for the inner and outer walls whereas the two lower scales ( $C_{p_H}$ ) relate to the static pressure coefficients for the

combustion chamber. The distribution on the head is plotted in polar co-ordinates. Negative values of  $C_{pH}$  appear inside the semi-circle representing the head.

The figures have been chose to illustrate particular features of the static pressure distribution and these are now discussed in turn.

(i) TEST 1-0522 (Fig. 4-4-1)

This demonstrates the features of a particularly bad pressure distribution obtained at the overall design flow split and a small dump gap. At pre-diffuser outlet the pressure on the inner wall is higher than that on the outer wall. This pressure differential persists throughout the system and the final pressure recovery in the outer annulus is 0.207 compared with 0.436 in the inner annulus. The mean velocities in each annulus are equal ( $\bar{u}_{4_o} / \bar{u}_{4_i} = 1.023$ ) and without losses the pressure recovery would be similar in each annulus. The lower pressure recovery achieved in the outer annulus is therefore due to a high total pressure loss and this is confirmed by the further analysis of losses presented in Chapter 5.

The pressure distribution on the head shows that the flow accelerates from the stagnation point to about two thirds of the way round the head before diffusing into the surrounding annuli. The minimum value of  $C_{pH}$  on the outer surface of the head is -1.09 compared with 0.06 on the inner surface. The severe adverse pressure gradient on the outer surface did not cause local separation, however, a large pressure loss was undoubtedly generated in the adjacent region of rapidly diffusing flow. Although the pressure gradients around the head are high and indicate rapid changes in flow velocity, the wall pressures in the outer annulus quickly equalise and little change in static pressure occurs in the last two thirds of the settling length. In the inner annulus the wall pressures are nearly constant throughout the settling length.

(ii) TEST 2-0812 (Fig. 4-4-2)

This demonstrates the features of a relatively good distribution obtained at the pre-diffuser "design" flow split (1.2) and an intermediate dump gap. Compared with Test 1-0522 the pressure gradients throughout the system are less severe. The pressure recovery is similar along both walls of the pre-diffuser and there is no rapid change in pressure at entry to the dump region. The pressure recovery in the outer annulus is higher than in the inner, mainly because of the difference in mean flow velocities ( $\bar{u}_{4_o} / \bar{u}_{4_i} = 0.562$ ). It is of interest to note that the pressure difference between the inner and outer flow fields does not become significant until the flow enters the parallel walled settling length annuli. This suggests that conditions near the head are influenced more by the pre-diffuser geometry and outlet conditions than by the downstream geometry.

(iii) TESTS 3-0408 and 3-0423 (Figs. 4-4-3/4)

These show the effects of varying the flow split at constant dump gap. A rapid acceleration and diffusion of flow occurs in the inner annulus near the head for  $S = 0.8$  and in the outer annulus for  $S = 2.3$ . In the first case both the pre-diffuser and the downstream section operate off-design and the pressure distribution is completely asymmetric. In the second case the downstream section operates close to design ( $S = S_4^*$ ) and the settling length annulus pressure recoveries are similar. The pressure distribution in the pre-diffuser and dump region is, however, asymmetric since the pre-diffuser operates off-design. It is interesting to note that the change in flow split from 0.8 to 2.3 does not significantly affect the pressure recovery in the first half of the pre-diffuser and that large differences in pressure are confined to a region near the outlet plane.

Comparing the distributions for Tests 1-0522 and 3-0423 indicates that increasing the pre-diffuser area ratio from 1.4 to 1.8 has the effect of reducing the amount of local diffusion downstream of the minimum pressure points on the head. This is associated with the lower mean velocity at

entry to the dump region and is considered an important factor leading to the reduction in overall loss coefficient from 47.8 to 32.1%.

(iv) TESTS 3-0412 and 3-1214 (Figs. 4-4-5 and 4-4-6)

These show the effects of increasing the dump gap at flow splits close to pre-diffuser design. It can be seen that the local diffusion near the head is lower for  $D/h_2 = 1.2$  and that the final pressure recovery in each annulus is higher. The increase in dump gap therefore produces an improvement in overall performance ( $\tilde{\Sigma}_4$  rises from 62.4 to 70.7%), even though the pre-diffuser outlet flow kinetic energy is increased by reason of the increased outlet profile peakiness. This is considered to be due to the overriding influence of the decrease in flow turning angle in the dump region.

(v) TESTS 2-0822 and 5-0822 (Fig. 4-4-7)

The distribution around the head for Test 5-0822 has been added to the plot for Test 2-0822 to show the effect of canting the pre-diffuser. The point of maximum pressure on the head has been shifted outwards and the minimum pressures are both higher than for Test 2-0822. Performance parameters for the two tests are compared in the table below.

Comparison of Performance for Tests 2-0822 and 5-0822

| Test No. | S    | $C_{P4_i}$ | $C_{P4_o}$ | $\tilde{\lambda}_{1-4} \%$ | $\tilde{\Sigma}_4 \%$ |
|----------|------|------------|------------|----------------------------|-----------------------|
| 2-0821   | 2.12 | 0.435      | 0.553      | 24.3                       | 67.4                  |
| 5-0822   | 2.24 | 0.450      | 0.577      | 21.9                       | 70.4                  |

The improvement in overall performance is considered to be due to the reduction in local diffusion near the head, this being linked with the reduction in pre-diffuser outlet profile distortion. In addition, the increase in pre-diffuser outer wall angle from  $6^\circ$  to  $9^\circ$  (relative to the rig axis) tends to reduce the turning angle of the outer flow field in the

dump region.

(vi) TEST 5-0817 (Fig. 4-4-8)

This shows the complete distribution obtained with the canted pre-diffuser operating close to design ( $S_2^* = 1.7$ ). The pre-diffuser and head static pressure distribution compares favourably with that obtained for Diffuser 2 operating near design (Test 2-0812, Fig. 4-4-2). It may be noted that the pressure recovery in the outer annulus is similar in both cases, whereas that achieved in the inner annulus is higher with the canted pre-diffuser. It can therefore be stated that canting the pre-diffuser facilitated running at a higher flow split without adversely affecting the pressure distribution on the head or the ultimate pressure recovery achieved in the outer settling length annulus.

4-4-2 Combustion Chamber Static Pressure Distributions

It has not been possible to present the complete static pressure distributions for all the tests carried out. However, for completeness, the static pressure distributions around the combustion chamber have been plotted by computer and these are given in Appendix 8. The changes in distribution are consistent between the five diffusers and the trends illustrated by the examples of the previous section are confirmed.

4-5 SUMMARY OF OVERALL PERFORMANCE

This section is intended to provide a summary of important results relating to overall system performance and to indicate the relative merits of each pre-diffuser. The results of Sect. 4-1 are presented in a more general way by means of performance contour maps and each system is assessed in terms of its overall performance, length and flow stability.

4-5-1 Overall Performance Contour Maps

The overall performance of each system is summarised by the contour maps shown in Figs. 4-5-1/5. Two maps are given for each system, one of overall loss coefficient,  $\tilde{\lambda}_{1-4}$  and one of overall effectiveness,  $\tilde{\epsilon}_4$ .



Contours of constant performance are plotted against flow split and dump gap and the following lines have been added.

- (i) A chain dotted line showing the overall design flow split,  $S_4^*$ .
- (ii) An optimum dump gap line (labelled  $\square$ ), this being the locus of points defining the optimum dump gap for any given flow split.
- (iii) An optimum flow split line (labelled  $\circ$ ), this being the locus of points defining the optimum flow split for any given dump gap.
- (iv) Dotted lines showing the pre-diffuser separation limits as in Fig. 4-2-14.

The maps were derived from the results given in Figs. 4-1-3/7 using an analytical method based on curve fitting techniques. This approach was chosen in order to avoid inconsistencies which would have arisen from curve fitting "by eye". Whilst the contour maps are the result of a considerable amount of interpolation, the performance figures indicated are considered to be within the limits of experimental error. A more detailed description of the method used in constructing the contour maps is given in Appendix 4.

The contour maps serve to illustrate the sensitivity of each system to changes in flow split and dump gap and the following points may be noted (see Figs. 4-5-1/5).

- (i) The optimum performance is not achieved at the design flow split except in the case of Diffuser 5.
- (ii) The optimum flow split decreases toward the pre-diffuser design flow split,  $S_2^*$  as the dump gap is decreased. The difference between optimum and design flow split performance increases as the dump gap is decreased.
- (iii) The minimum loss coefficient is obtained at a flow split somewhat lower than that for maximum effectiveness except in the case of Diffuser 5 where both are achieved close to design.
- (iv) There is a limited range of conditions for which the performance of each system is insensitive to changes in flow split and dump

gap. Outside this range the performance drops rapidly with changing flow split and decreasing dump gap.

- (v) Whereas the flow split range giving stable pre-diffuser flow increases with decreasing dump gap, this beneficial influence on flow stability is offset by the deterioration in overall performance.

4-5-2 Comparison of Optimum Performance for each System

It was suggested in Section 4-1-1 that  $S_{\epsilon_4}$  (the flow split giving maximum effectiveness) represents a suitable compromise between conditions giving maximum pressure recovery and minimum loss. In terms of performance the optimum operating conditions are taken to be those for which the maximum overall effectiveness is achieved. The performance achieved by each system under these conditions is compared in Table 4-5.

Table 4-5 Comparison of Optimum Overall Performance

| DIFFUSER No. | $AR_2$ | $2\phi^\circ$ | $D/h_2$ | S    | $\tilde{\lambda}_{1-4}$ | $\tilde{\epsilon}_4$ | $\tilde{c}_{p4}$ | Pre-diffuser Flow Stability |
|--------------|--------|---------------|---------|------|-------------------------|----------------------|------------------|-----------------------------|
| 1            | 1.4    | 12            | 1.74    | 2.02 | 22.7                    | 69.6                 | 0.531            | Good                        |
| 2            | 1.6    | 12            | 1.20    | 1.76 | 21.2                    | 71.4                 | 0.540            | Close to separation         |
| 3            | 1.8    | 12            | 1.06    | 1.82 | 19.9                    | 73.3                 | 0.556            | Just separated              |
| 4            | 1.8    | 18            | 0.85    | 1.70 | 23.0                    | 69.2                 | 0.523            | Separated                   |
| 5 (CANTED)   | 1.6    | 11.3          | 1.22    | 2.22 | 20.6                    | 72.1                 | 0.551            | Good                        |

The effects of varying the pre-diffuser geometry on the overall performance can be summarised as follows.

- (i) Increasing the area ratio produced a gain in performance but this was accompanied by an increased tendency toward separation in the pre-diffuser. The optimum dump gap decreased with increasing

pre-diffuser area ratio.

- (ii) Increasing the included angle,  $2\phi$  (and thus reducing the non-dimensional length) produced a decrease in performance as well as an increased tendency toward pre-diffuser separation. The optimum dump gap decreased with increasing included angle.
- (iii) Canting the pre-diffuser produced a marginal gain in performance and a large improvement in pre-diffuser flow stability at flow splits close to design. The optimum flow split was shifted to the design value but the optimum dump gap was not significantly altered.

On the basis of performance alone, Diffuser 3 would appear to give the best results, however the pre-diffuser operated with separated flow at the optimum performance point and also at the overall design flow split. Since separation did not appear to produce any general instability in the flow it is difficult to judge how serious the effects might be in an engine environment. It is nevertheless recommended that separation should be avoided.

The results obtained for the canted pre-diffuser are very encouraging and suggest that gains in performance and flow stability could be obtained by re-designing all the symmetrical pre-diffusers. Whereas canting the pre-diffuser is clearly desirable for systems having high overall design flow splits, the choice of pre-diffuser area ratio and length depends very much upon the trade-off between system length and performance. This aspect of system design is discussed in the following section.

#### 4-5-3 Comparison of Performance on the Basis of Length

In the cases under consideration there are two independent variables which influence the system length, namely, the pre-diffuser length and the dump gap. It is therefore appropriate to compare the performance of each system on the basis of "variable length",  $L_v$ , defined,

$$L_v = (\bar{L} + D)/h_1$$

The overall effectiveness obtained at the design flow split is plotted versus  $L_v$  for each system in Fig. 4-5-6.

(i) Increasing Area Ratio

It can be seen in Fig. 4-5-6 that the improvement in performance obtained by increasing the pre-diffuser area ratio from 1.4 to 1.8 is associated with an increase in  $L_v$  of nearly 50%. This represents an increase in system length of approximately 1.7 inlet annulus heights for an increase in overall effectiveness of 3.7% (equivalent to a decrease in loss coefficient of 2.8%). It may be noted that a straight line can be drawn which is tangent to the three curves for Diffusers 1 to 3. This line defines the limit of performance for systems with symmetrical pre-diffusers of  $12^\circ$  included angle. Following this approach it is possible to define the optimum dump gap and pre-diffuser area ratio for a given length as shown in Fig. 4-5-7. The curves are necessarily approximate because of the method of derivation however they do provide a good guide to optimum design. It is of some interest to note that values on the optimum dump gap ( $D/h_2$ ) curve compare favourably with the value of 1.1 often used in practice. So far as pre-diffuser flow stability is concerned, the results indicate that separation is likely for values of  $L_v$  greater than 4.5.

(ii) Canting

It can be seen that the canted pre-diffuser gave a significant improvement in performance compared with Diffuser 2 over the whole range of  $L_v$ . It would be reasonable to suppose that a similar improvement in performance could be achieved for other area ratios but this would need to be confirmed by further tests. In the case studied (1.6 area ratio), canting gave an improvement in effectiveness of 1.8% for the same length or a reduction in length of 0.4 inlet annulus heights for the same performance. Pre-diffuser flow stability was much improved and results suggest that the separation limit could be extended beyond  $L_v = 6.0$  for higher area ratio canted pre-diffusers of the same included angle.

(iii) Increasing Included Angle

Comparing Diffusers 3 and 4 on Fig. 4-5-6 shows that increasing the included angle (constant area ratio) significantly reduced the system length and performance. An important point is that the performance and pre-diffuser flow stability was inferior to that attainable with a 12° symmetrical pre-diffuser for a particular length (e.g.  $L_v = 4.0$ ). The optimum included angle would need to be established by further experimental work (preferably using canted pre-diffusers) but it is clearly lower than 18°.

Fig.4-1-1 VARIATION OF IDEAL OVERALL PRESSURE RECOVERY WITH FLOW SPLIT.

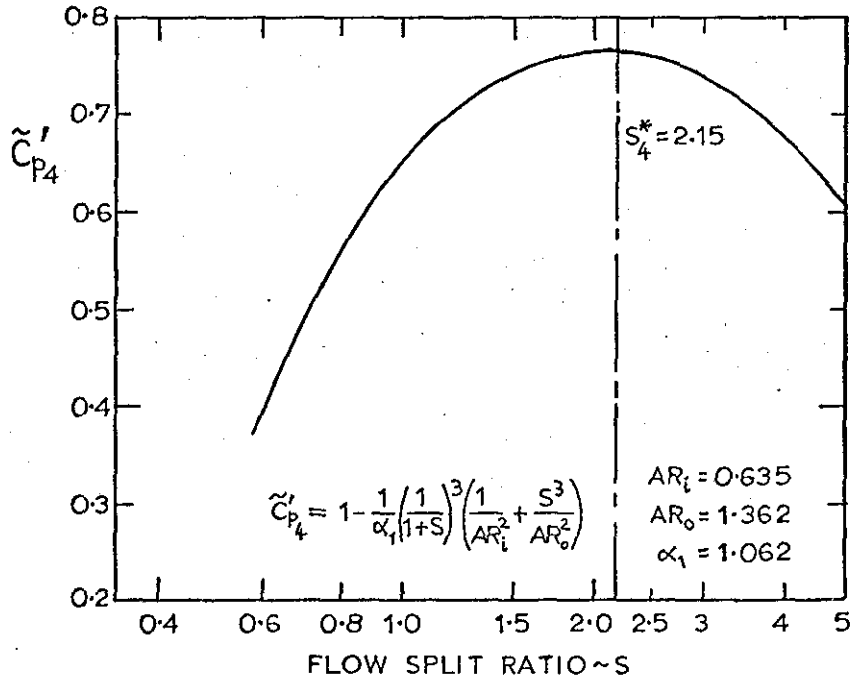


Fig.4-1-2 VARIATION OF EFFECTIVE OVERALL AREA RATIO WITH FLOW SPLIT.

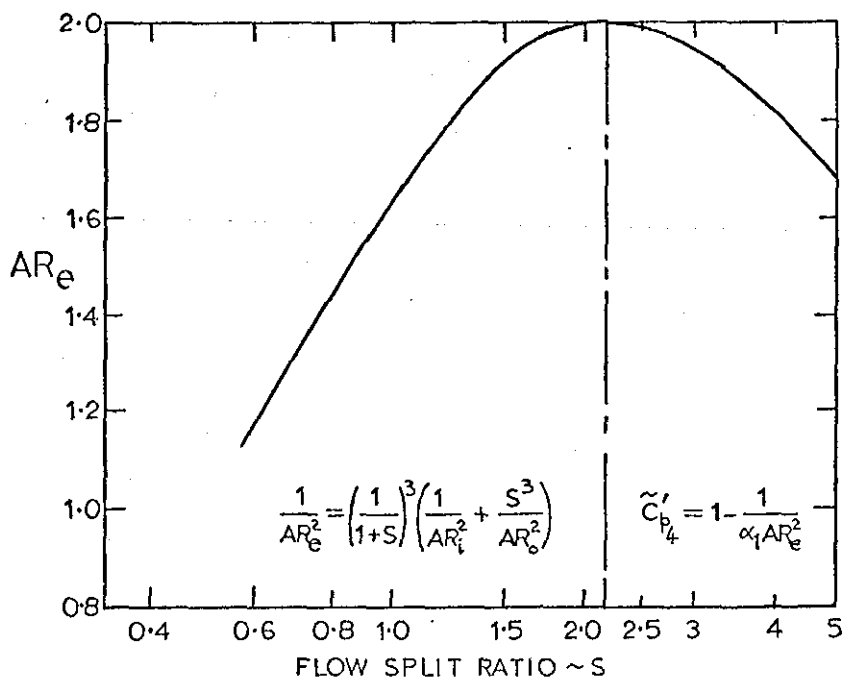


Fig.4-1-3 PRE-DIFFUSER AND OVERALL PERFORMANCE CURVES.

DIFFUSER 1, AR=1.4, 2φ=12°

- △—  $D/h_2 = 0.5$
- $D/h_2 = 1.0$
- $D/h_2 = 2.0$
- — — Overall Design Flow Split -  $S_4^*$
- ..... Locus of optimum flow split for each parameter

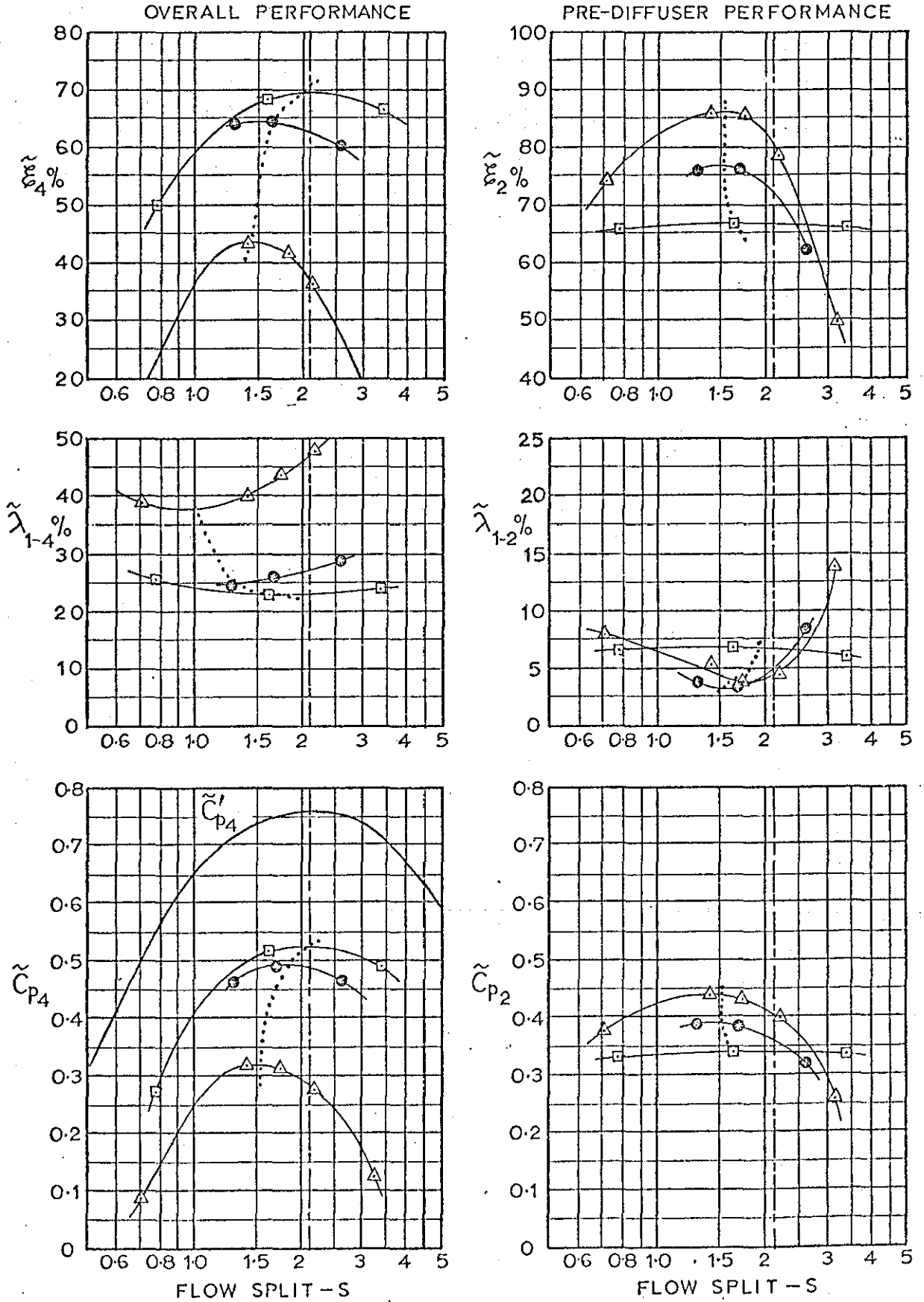


Fig. 4-1-4 PRE-DIFFUSER AND OVERALL PERFORMANCE CURVES.

DIFFUSER 2, AR=1.6,  $2\phi=12^\circ$

- $\triangle$   $D/h_2 = 0.5$
- $\circ$   $D/h_2 = 0.8$
- $\square$   $D/h_2 = 1.5$
- Overall Design Flow Split -  $S_4^*$
- ..... Locus of optimum flow split for each parameter

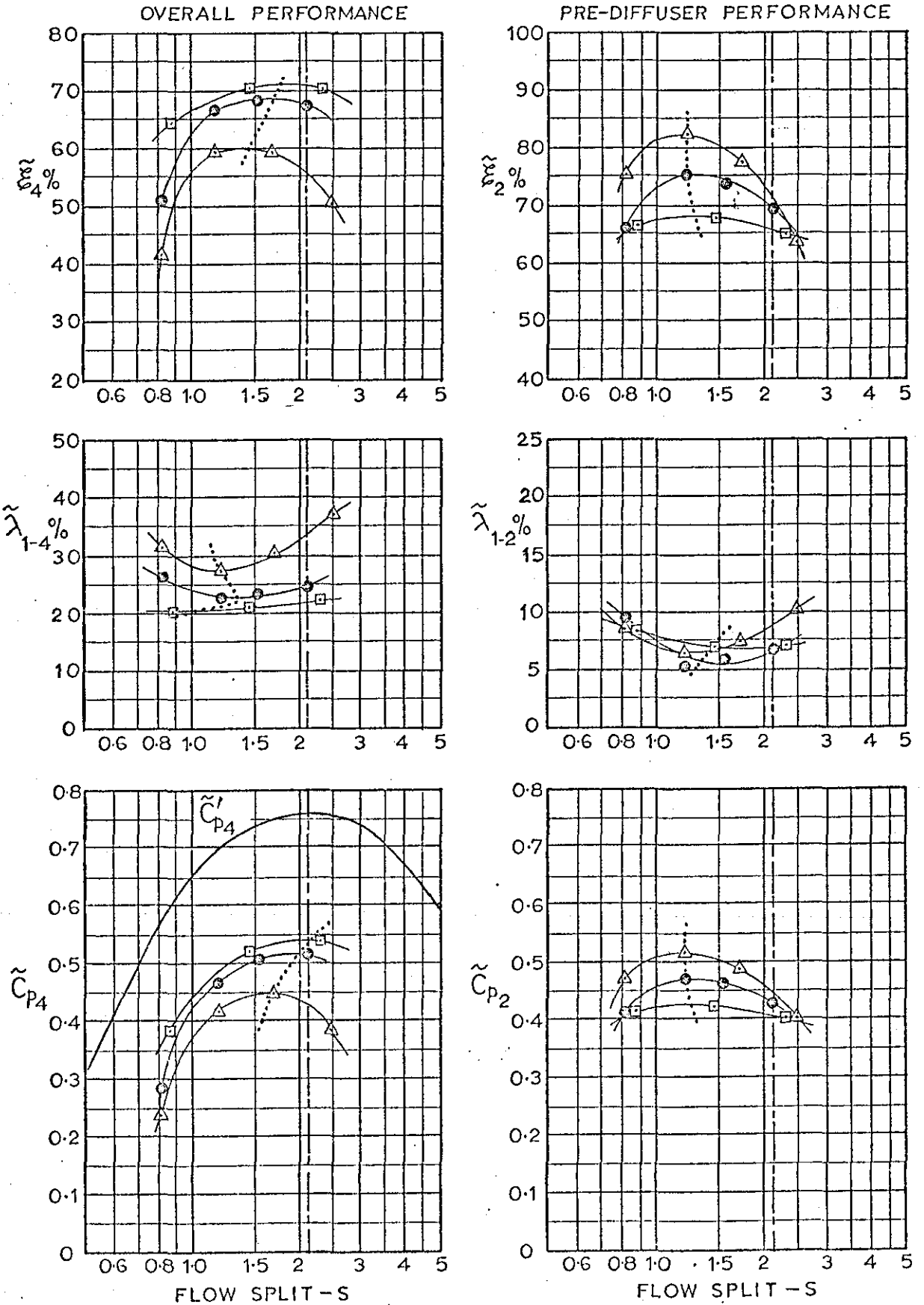




Fig.4-1-5 PRE-DIFFUSER AND OVERALL PERFORMANCE CURVES.

DIFFUSER 3, AR=18,  $2\phi=12^\circ$

- $\triangle$   $D/h_2=0.4$
- $\bullet$   $D/h_2=0.7$
- $\square$   $D/h_2=1.2$
- Overall Design Flow Split -  $S_4^*$
- ..... Locus of optimum flow split for each parameter

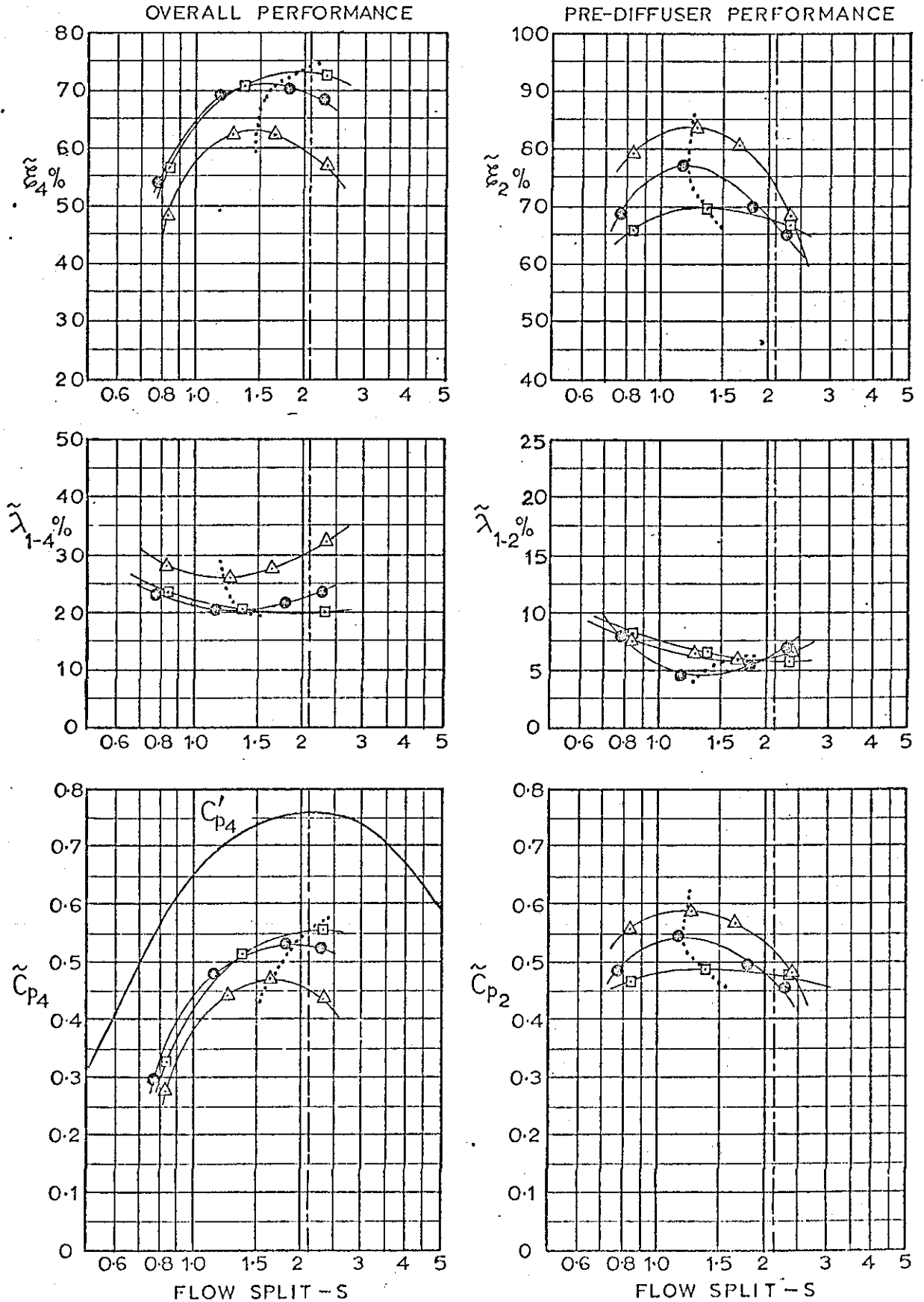


Fig. 4-1-6: PRE-DIFFUSER AND OVERALL PERFORMANCE CURVES.

DIFFUSER 4, AR=18,  $2\phi=18^\circ$

- $\triangle$   $D/h_2 = 0.4$
- $\circ$   $D/h_2 = 0.7$
- $\square$   $D/h_2 = 1.2$
- — — Overall Design Flow Split -  $S_4^*$
- ..... Locus of optimum flow split for each parameter

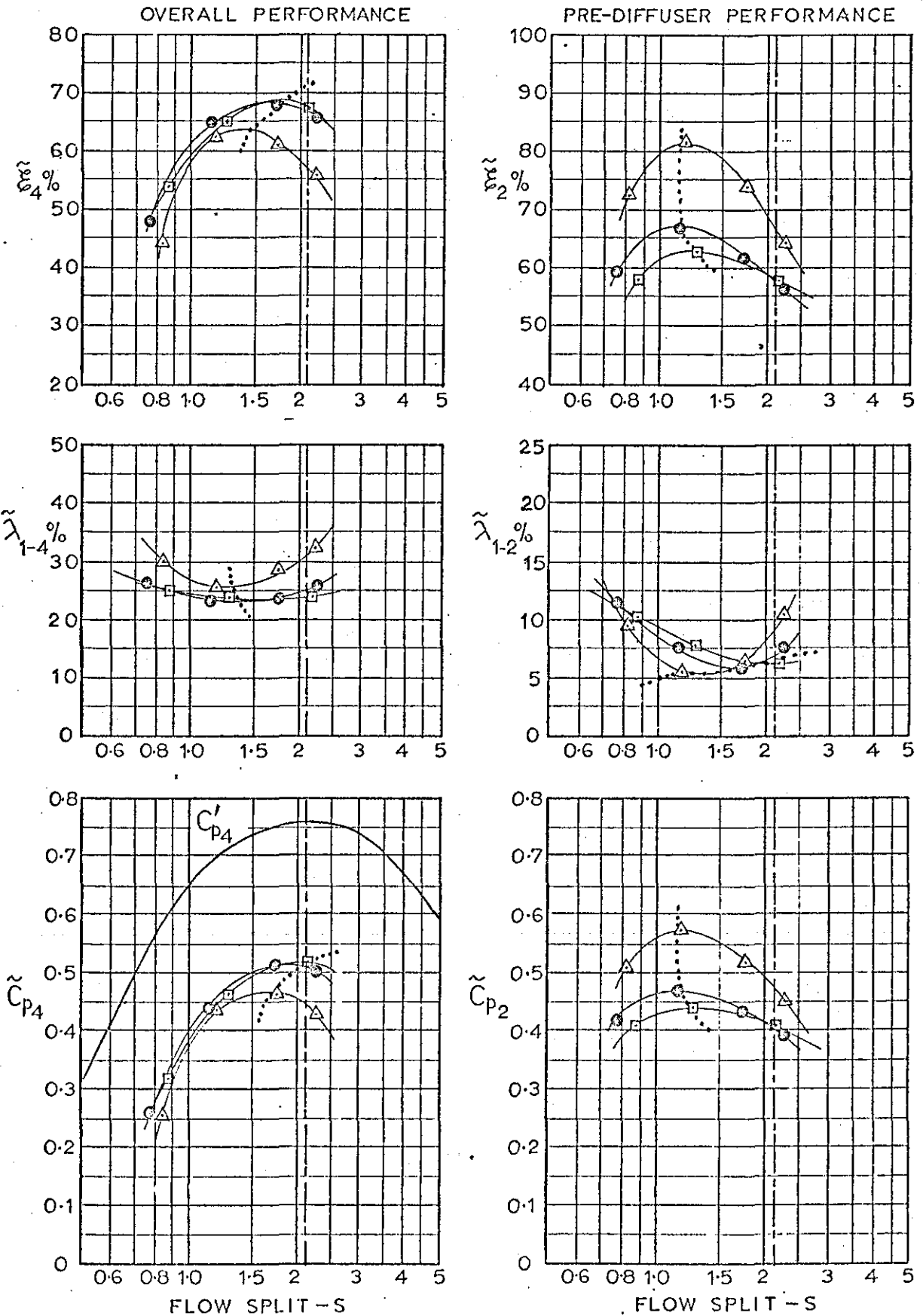


Fig. 4-1-7 PRE-DIFFUSER AND OVERALL PERFORMANCE CURVES.

DIFFUSER 5, AR=1.6,  $2\phi=11.3^\circ$  (Canted)

- $\triangle$  —  $D/h_2 = 0.5$
- $\circ$  —  $D/h_2 = 0.8$
- $\square$  —  $D/h_2 = 1.5$
- Overall Design Flow Split -  $S_4^*$
- ..... Locus of optimum flow split for each parameter

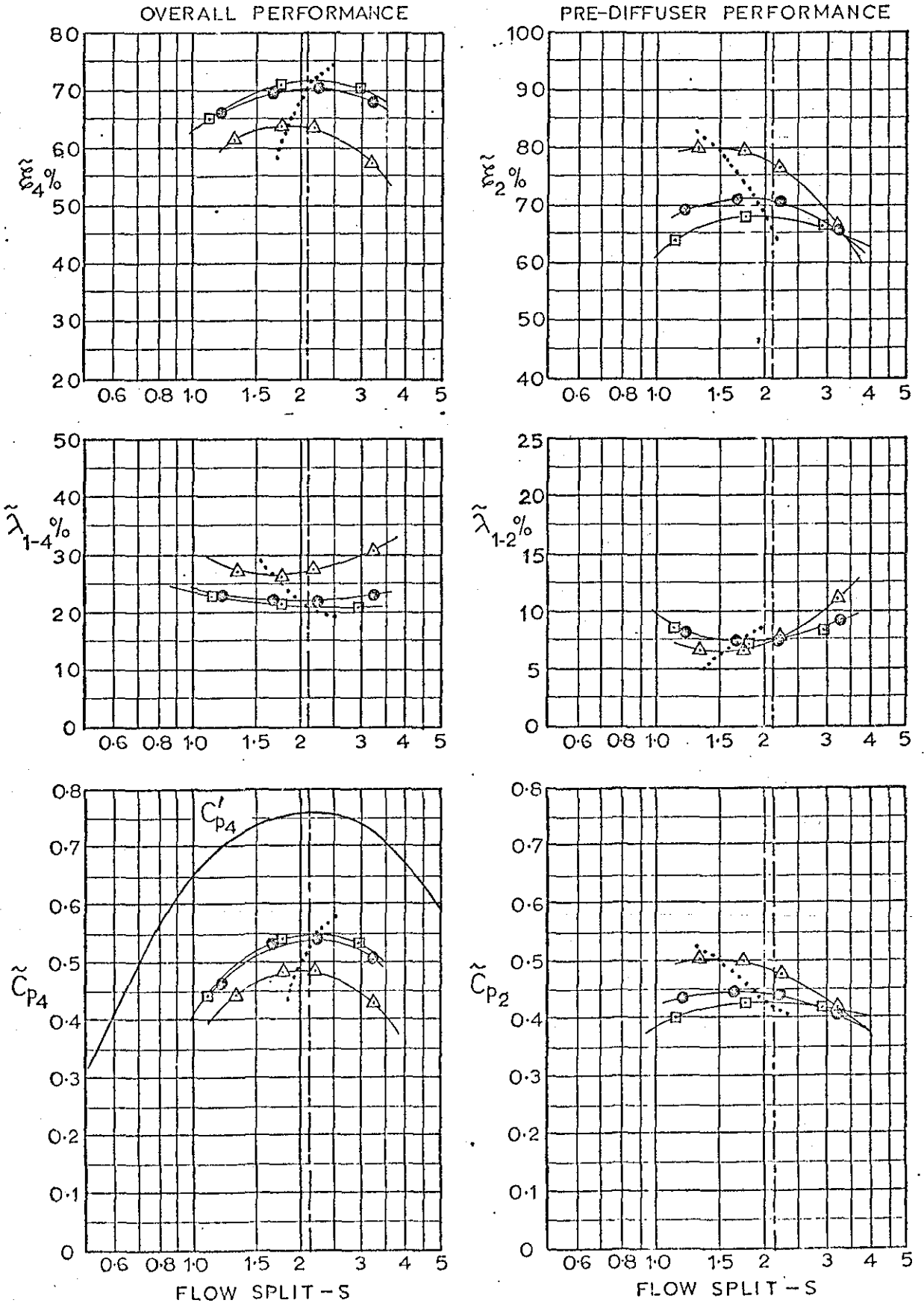


Fig.4-1-8 COMBINED DUMP REGION AND SETTLING LENGTH LOSSES.

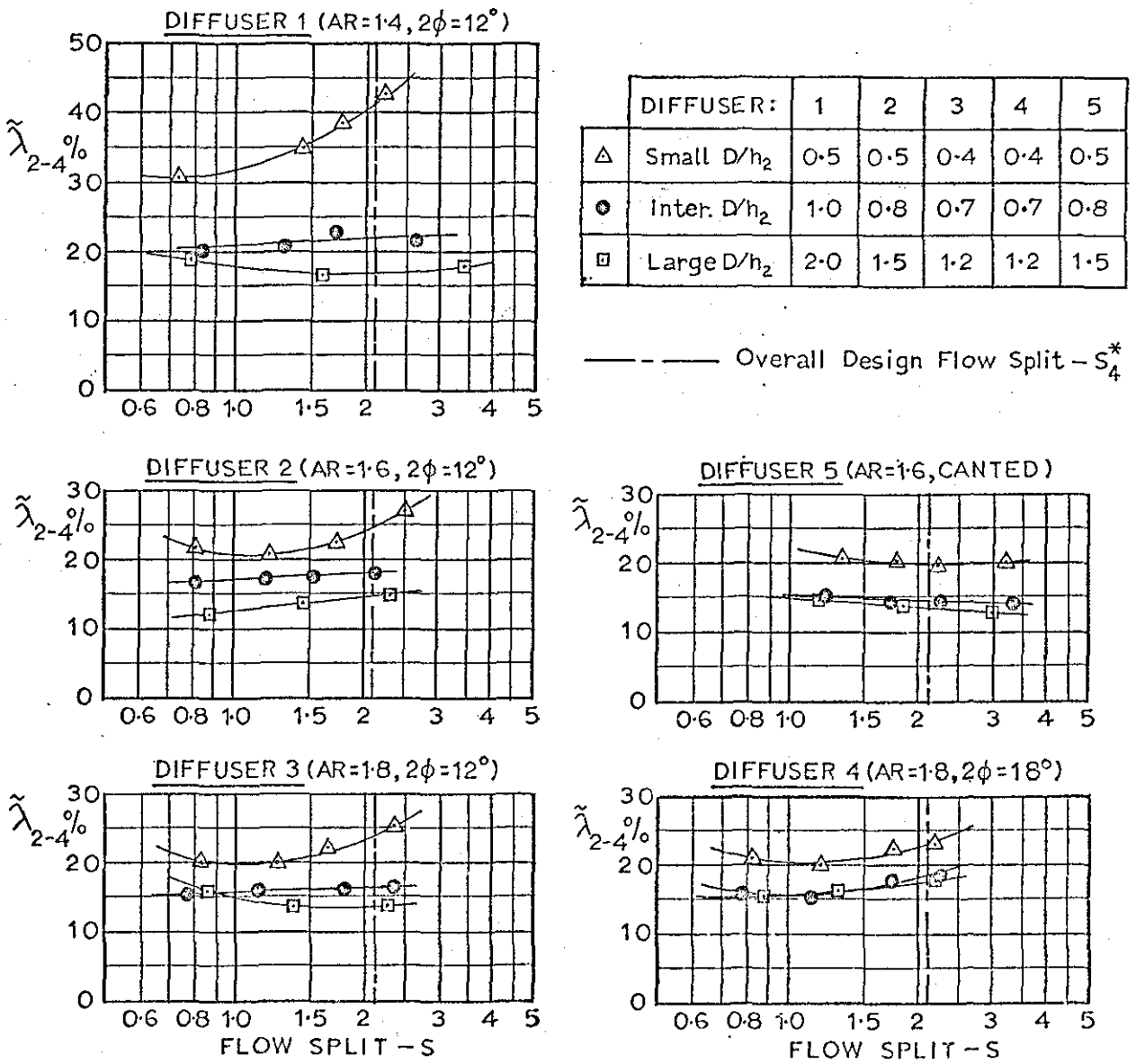


Fig.4-1-9 TYPICAL VARIATION OF PRESSURE RECOVERY WITH DUMP GAP.

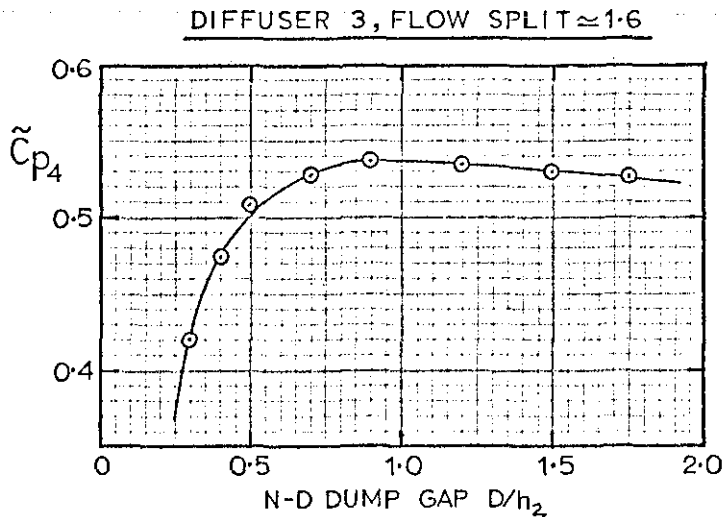


Fig.4-2-1 SYMMETRY OF PRE-DIFFUSER OUTLET VELOCITY PROFILES.

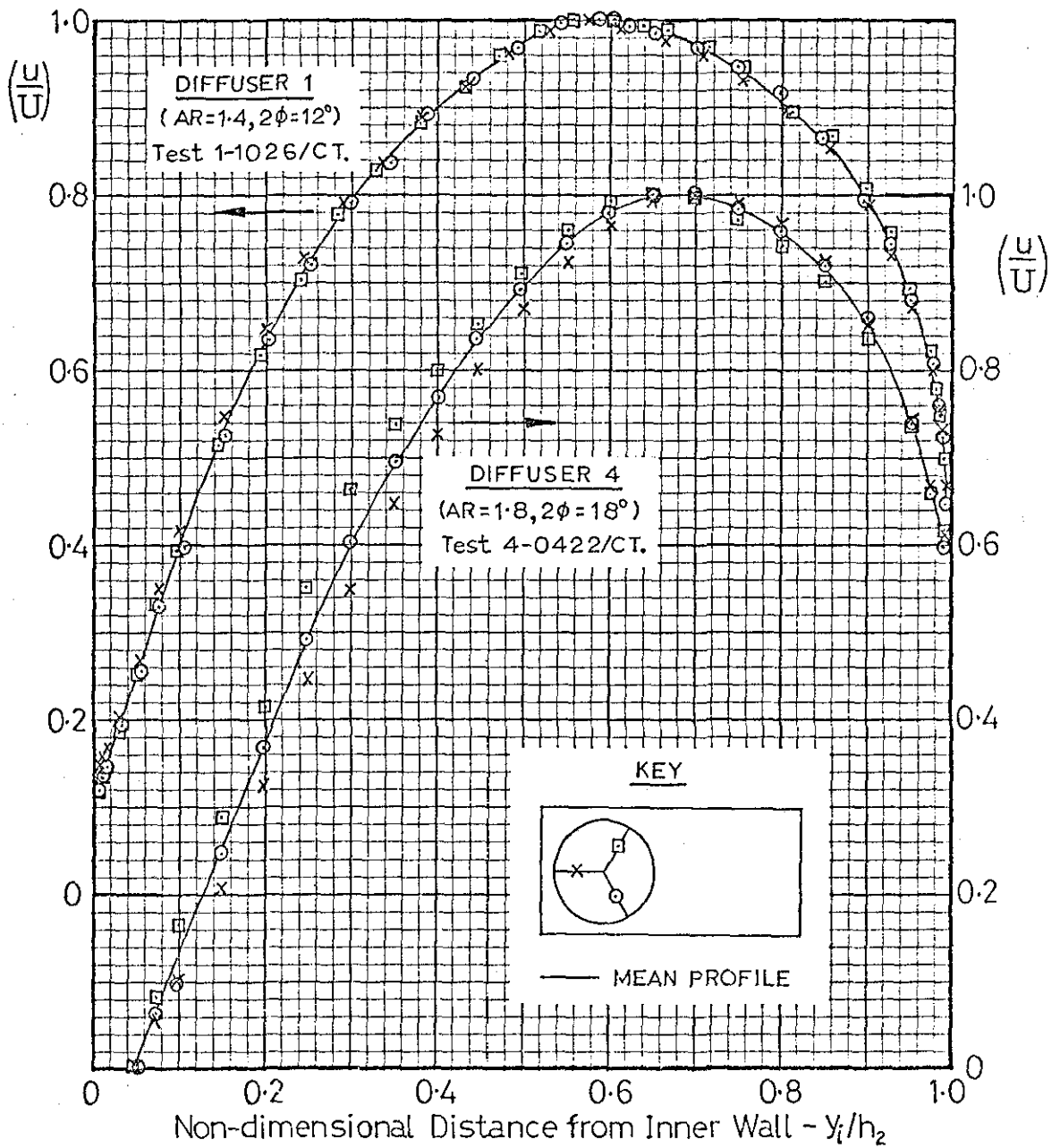


Fig.4-2-2 EXAMPLE OF DETAILED MEASUREMENTS NEAR WALL.  
(Test 3-0708, Outer Boundary Layer-Fig.4-2-4)

NOTE: Significant fluctuations were only observed for separated and near-separated boundary layers.

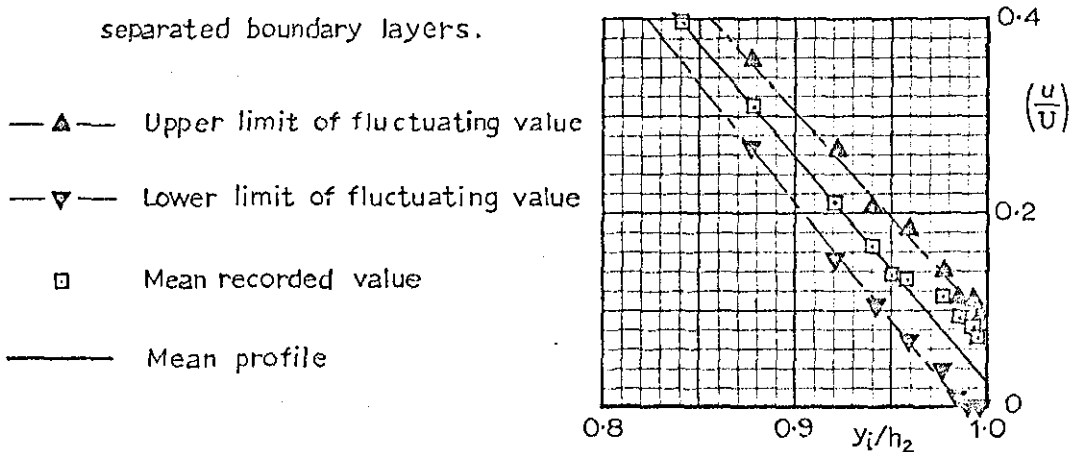


Fig. 4-23 PRE-DIFFUSER OUTLET PROFILES  
FOR TEST SERIES 3-04.

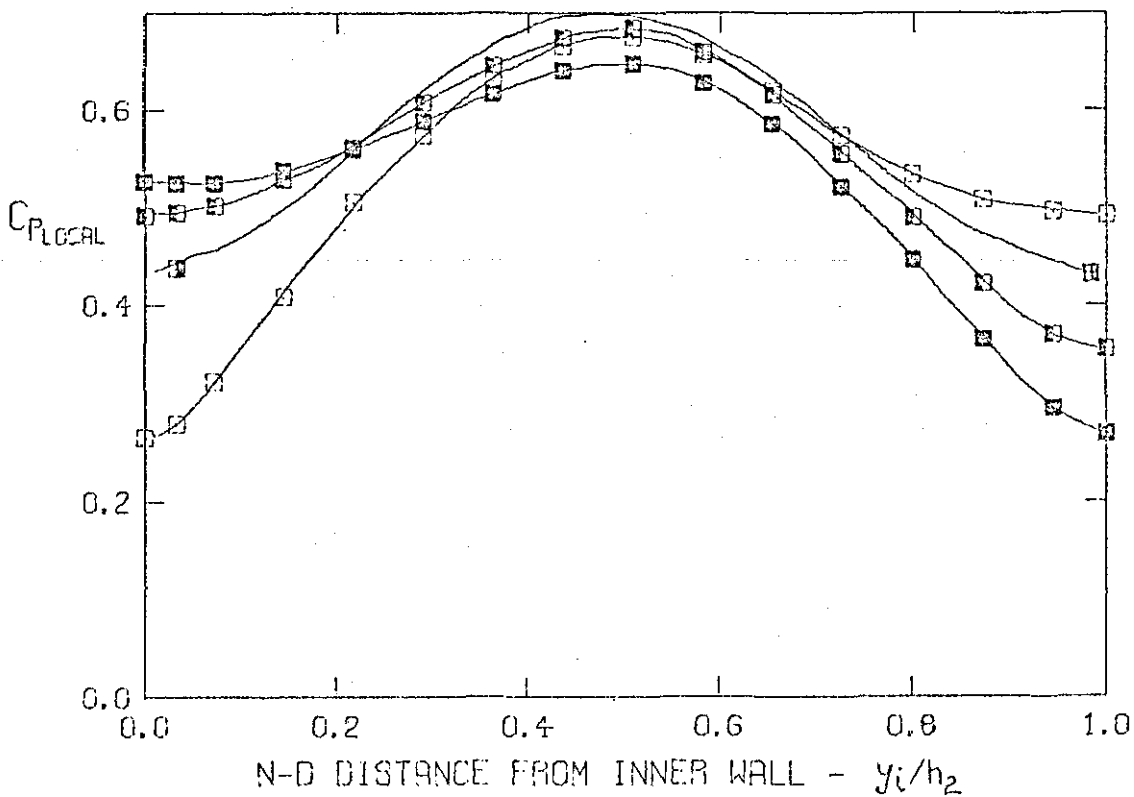
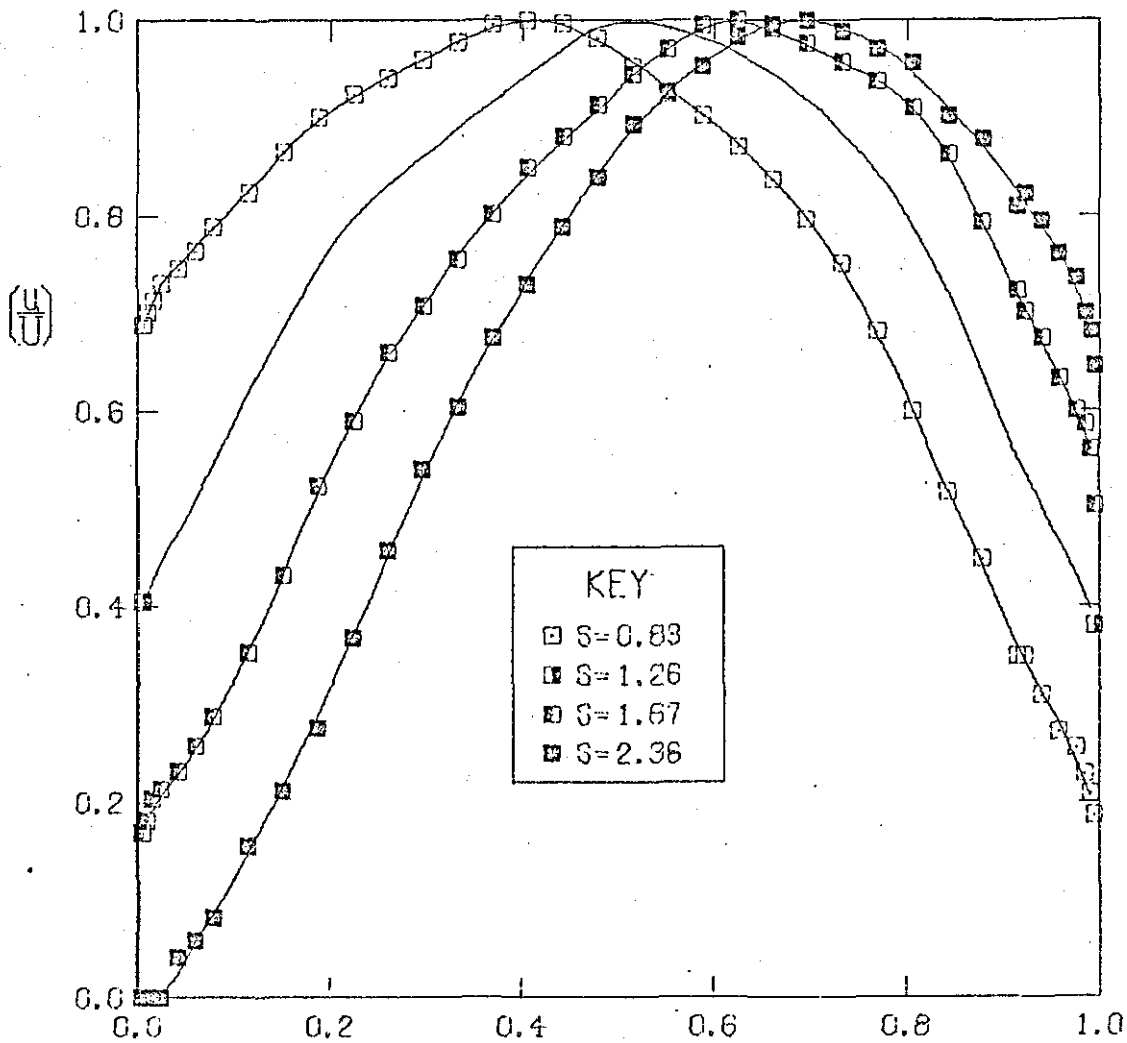


Fig. 4-2-4 PRE-DIFFUSER OUTLET PROFILES  
FOR TEST SERIES 3-0%

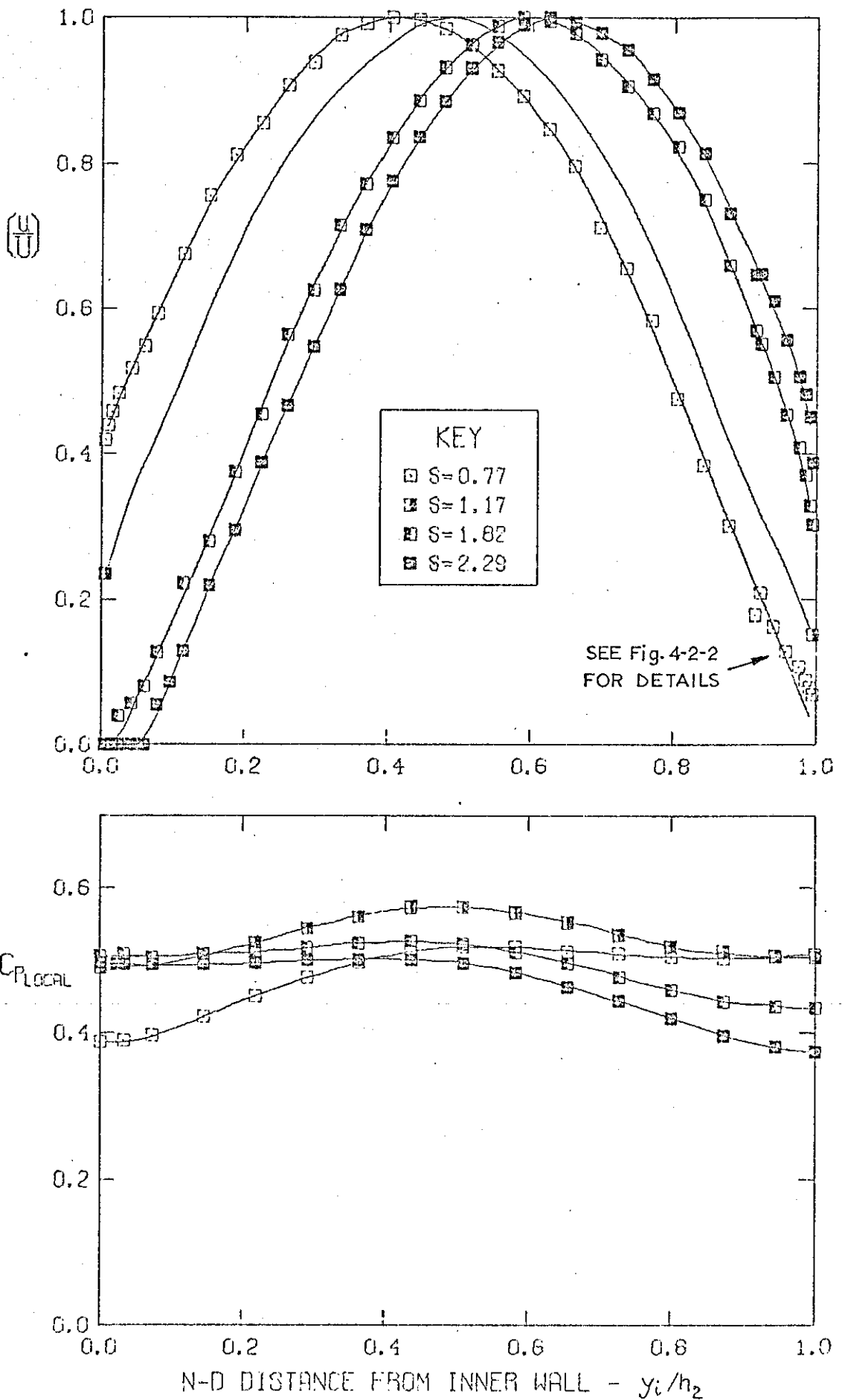


Fig. 4-2-5 PRE-DIFFUSER OUTLET PROFILES  
FOR TEST SERIES 3-12.

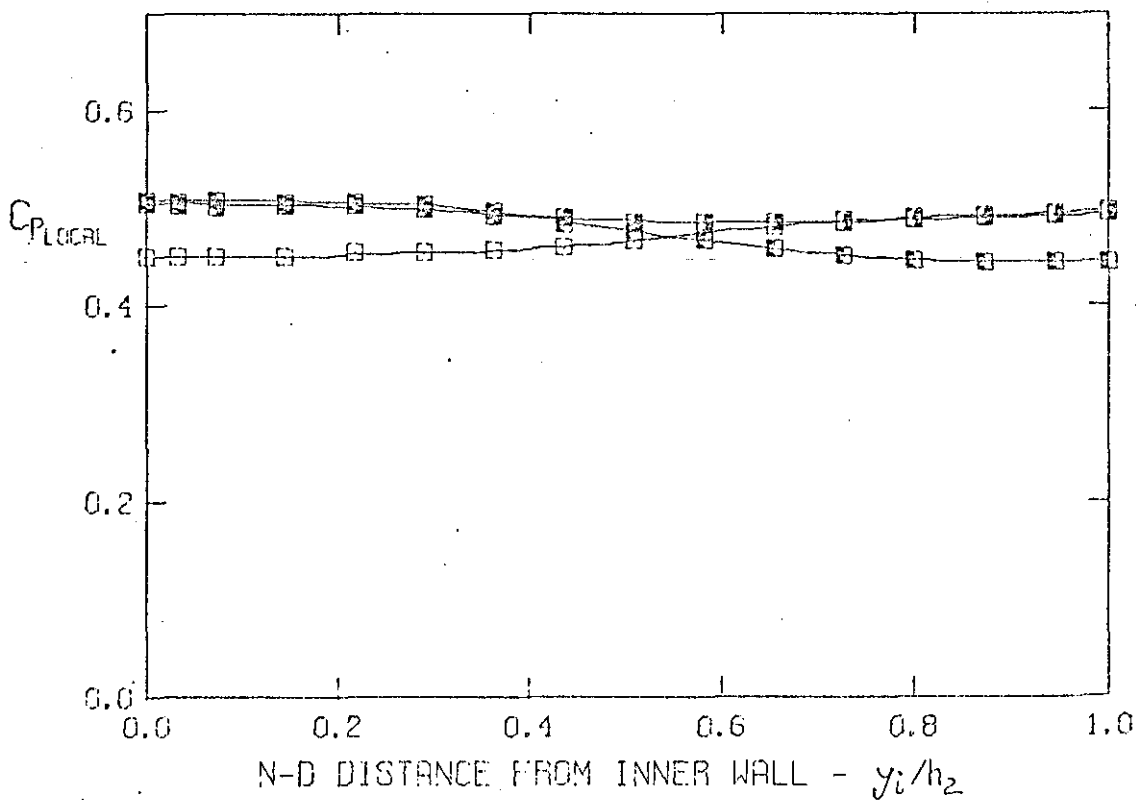
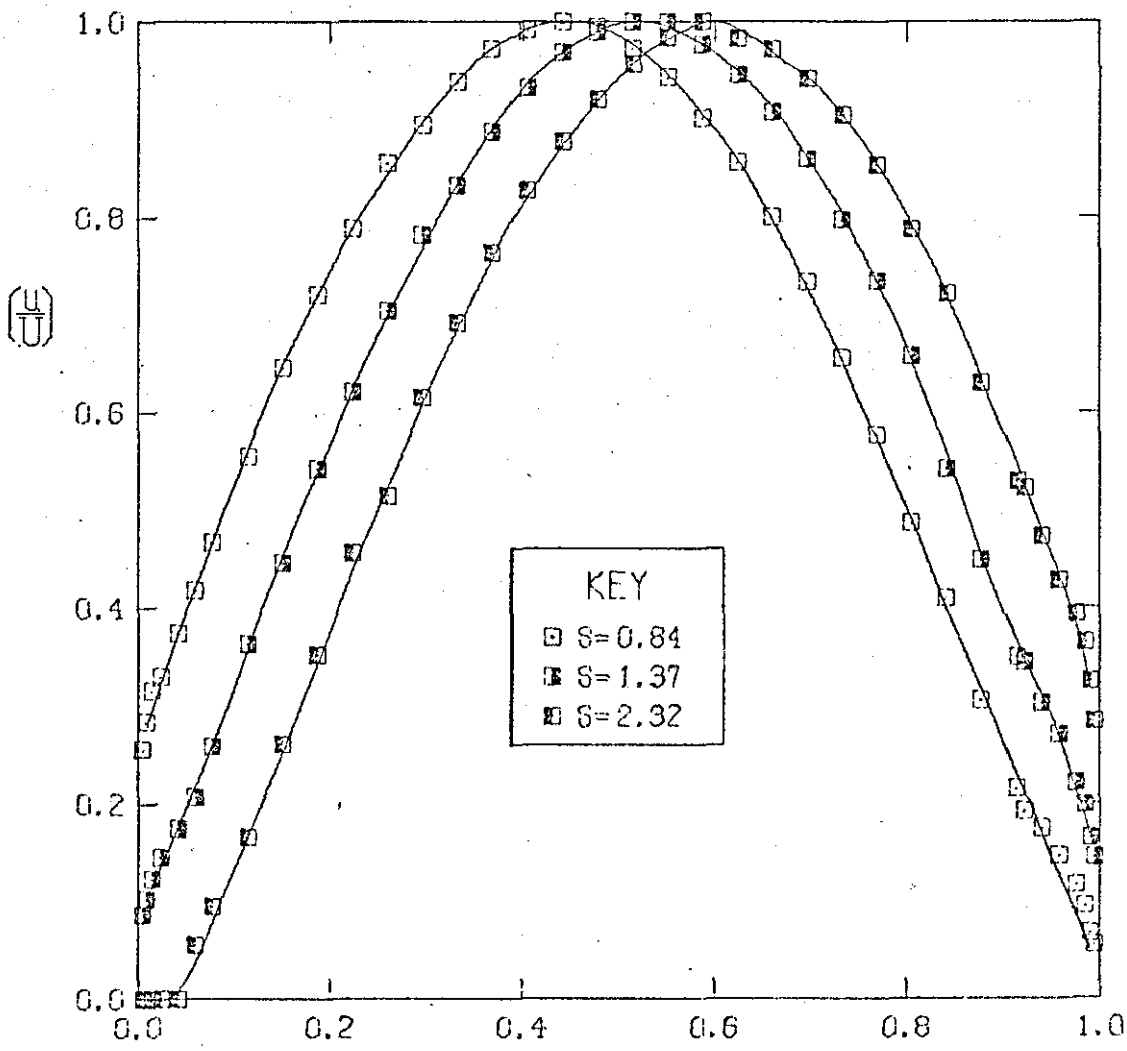
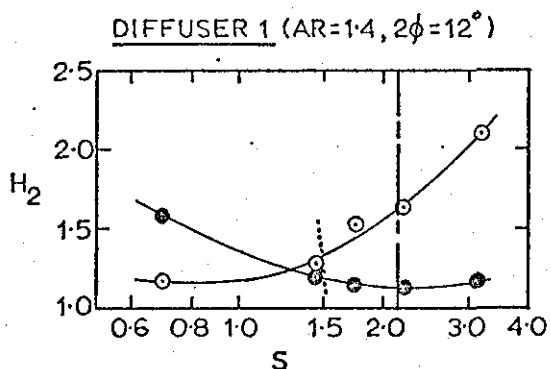




Fig.4-2-6 PRE-DIFFUSER OUTLET BOUNDARY LAYER SHAPE FACTORS.

SMALL DUMP GAPS

| DIFFUSER:          | 1   | 2   | 3   | 4   | 5   |
|--------------------|-----|-----|-----|-----|-----|
| D/h <sub>2</sub> : | 0.5 | 0.5 | 0.4 | 0.4 | 0.5 |



- Inner Boundary Layer
- Outer Boundary Layer
- - - Overall Design Flow Split - S<sub>4</sub>\*
- ..... Optimum Flow Split - S<sub>ξ<sub>2</sub></sub>
- ⊗ Intermittent Transitory Stall (ψ/U ≈ 0 at wall)

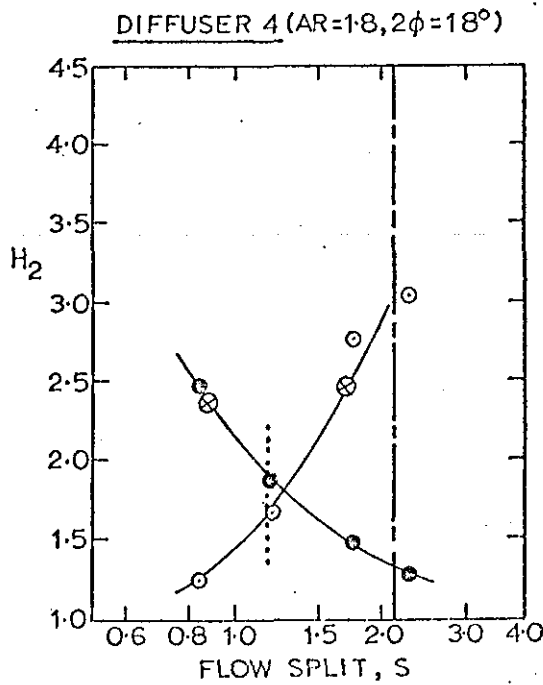
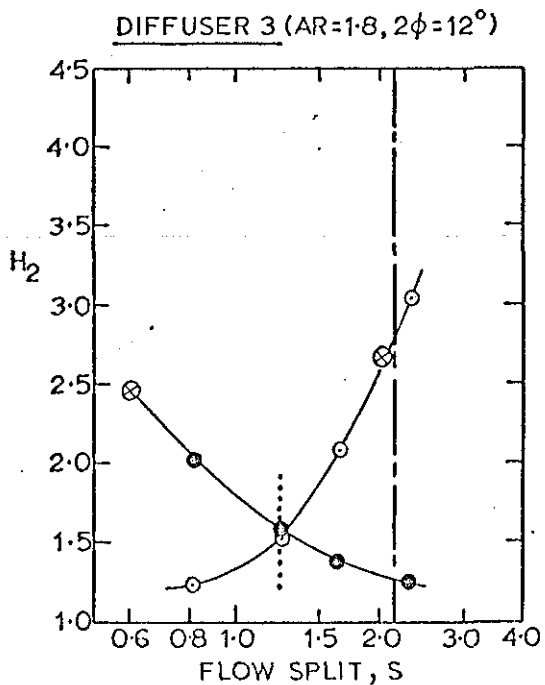
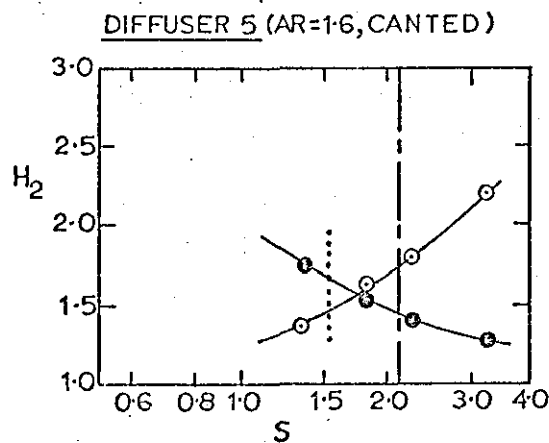
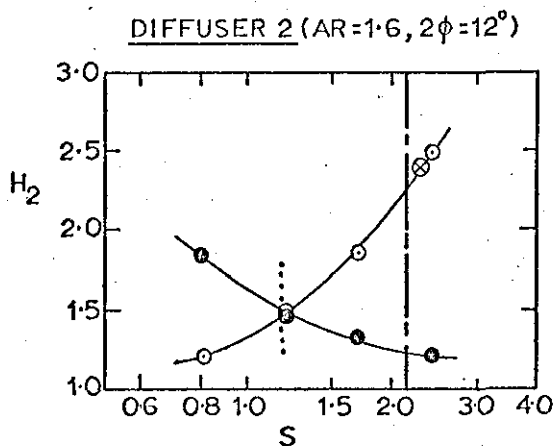
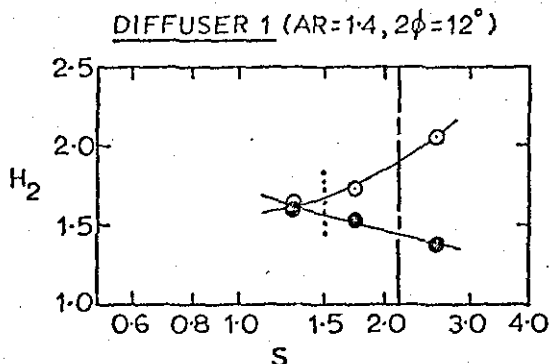


Fig.4-2-7 PRE-DIFFUSER OUTLET BOUNDARY LAYER SHAPE FACTORS.  
INTERMEDIATE DUMP GAPS

| DIFFUSER: | 1   | 2   | 3   | 4   | 5   |
|-----------|-----|-----|-----|-----|-----|
| $D/h_2$ : | 1.0 | 0.8 | 0.7 | 0.7 | 0.8 |



- Inner Boundary Layer
- Outer Boundary Layer
- - — Overall Design Flow Split -  $S_4^*$
- ..... Optimum Flow Split -  $S_{E_2}$
- ⊗ Intermittent Transitory Stall ( $\psi/U \approx 0$  at wall)

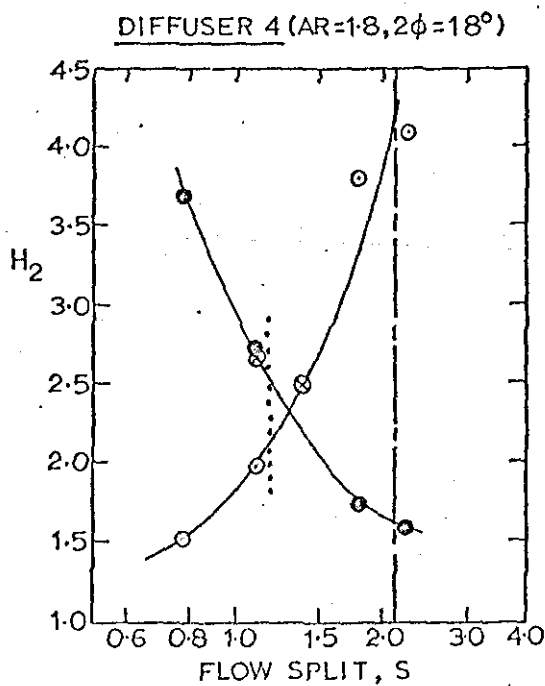
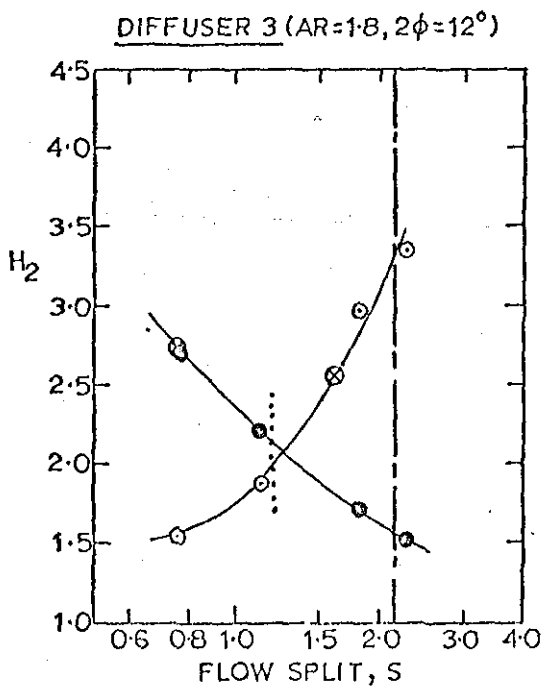
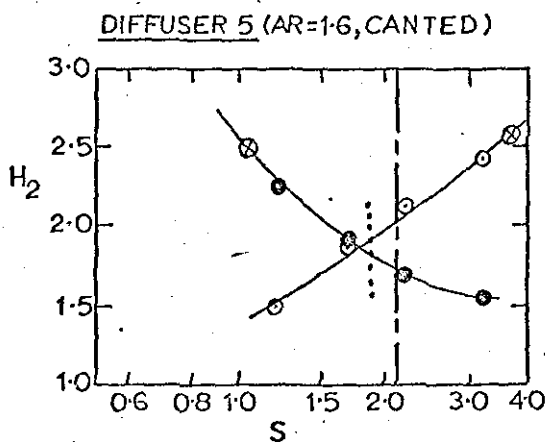
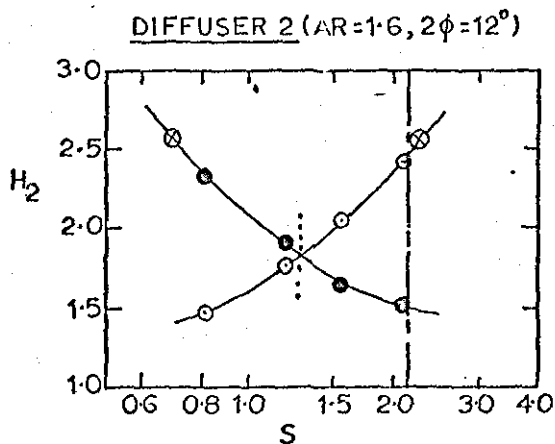
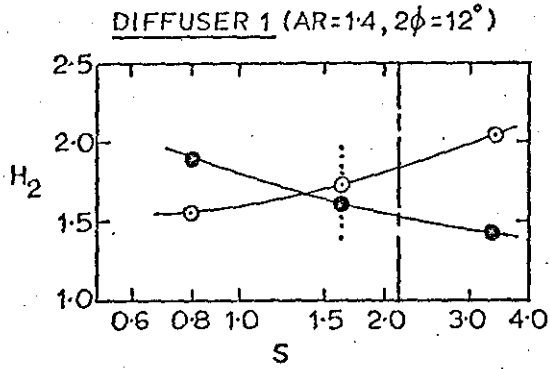


Fig 4-2-8 PRE-DIFFUSER OUTLET BOUNDARY LAYER SHAPE FACTORS.  
LARGE DUMP GAPS

| DIFFUSER: | 1   | 2   | 3   | 4   | 5   |
|-----------|-----|-----|-----|-----|-----|
| $D/h_2$ : | 2.0 | 1.5 | 1.2 | 1.2 | 1.5 |



- Inner Boundary Layer
- Outer Boundary Layer
- Overall Design Flow Split -  $S_4^*$
- ..... Optimum Flow Split -  $S_{E2}$
- ⊗ Intermittent Transitory Stall ( $\psi/U=0$  at wall.)

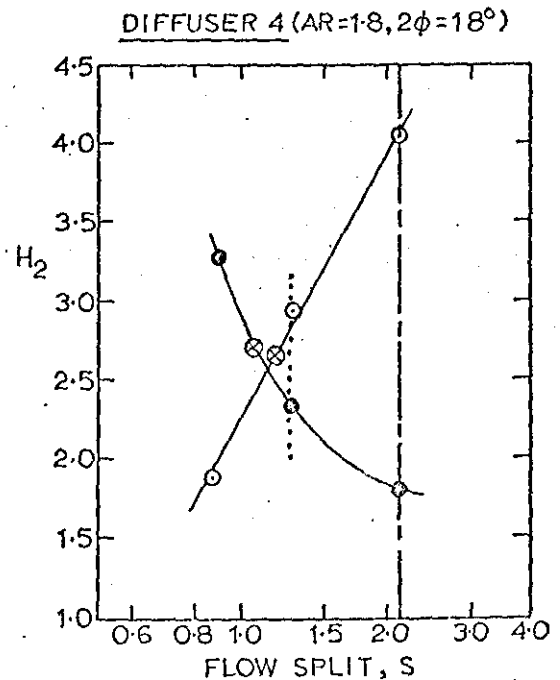
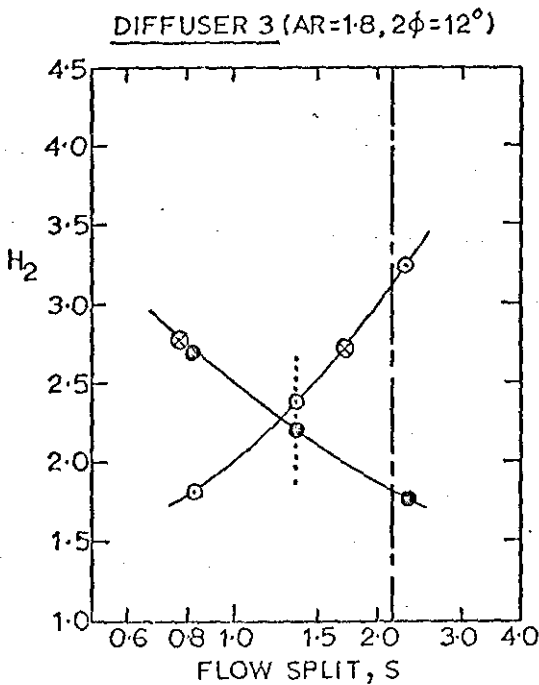
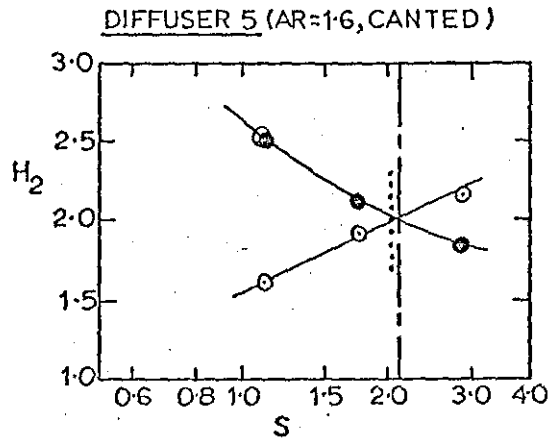
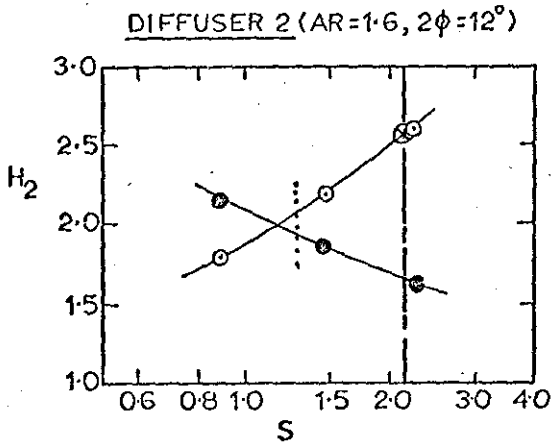
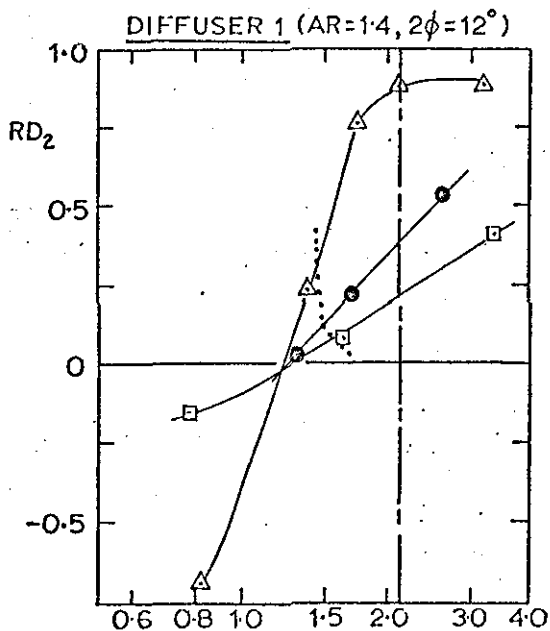


Fig. 4-2-9 PRE-DIFFUSER OUTLET VELOCITY PROFILE RADIAL

DISTORTION FACTORS.



| DIFFUSER:        | 1   | 2   | 3   | 4   | 5   |
|------------------|-----|-----|-----|-----|-----|
| △ Small $D/h_2$  | 0.5 | 0.5 | 0.4 | 0.4 | 0.5 |
| ● Inter. $D/h_2$ | 1.0 | 0.8 | 0.7 | 0.7 | 0.8 |
| □ Large $D/h_2$  | 2.0 | 1.5 | 1.2 | 1.2 | 1.5 |

— Overall Design Flow Split -  $S_4^*$   
 ..... Optimum Flow Split -  $S_{\epsilon_2}$

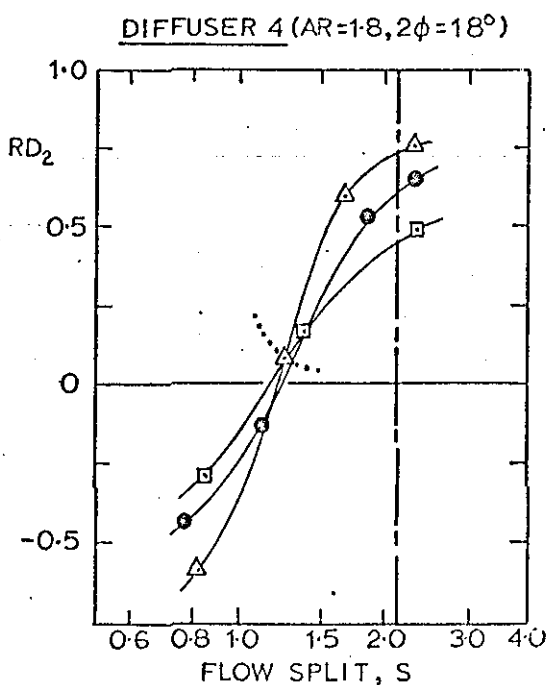
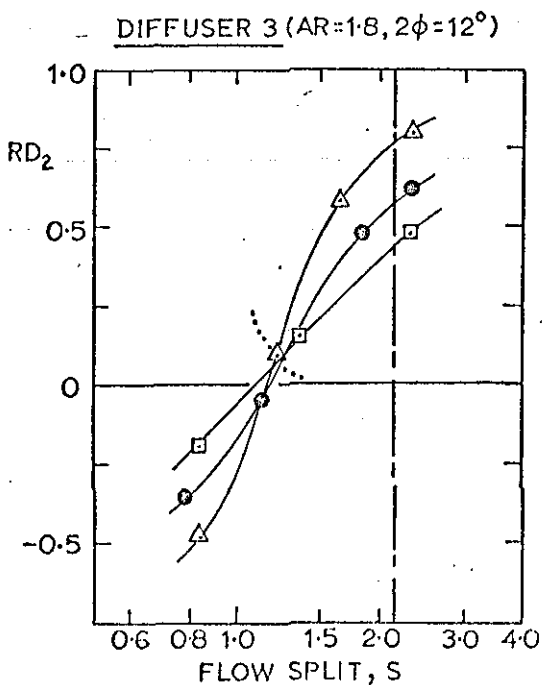
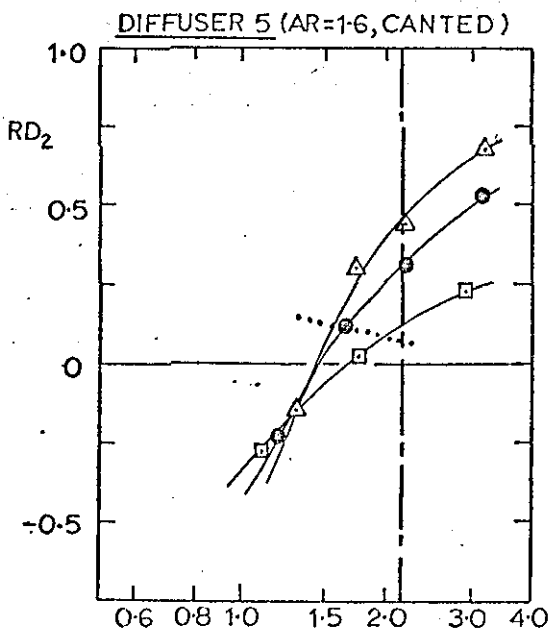
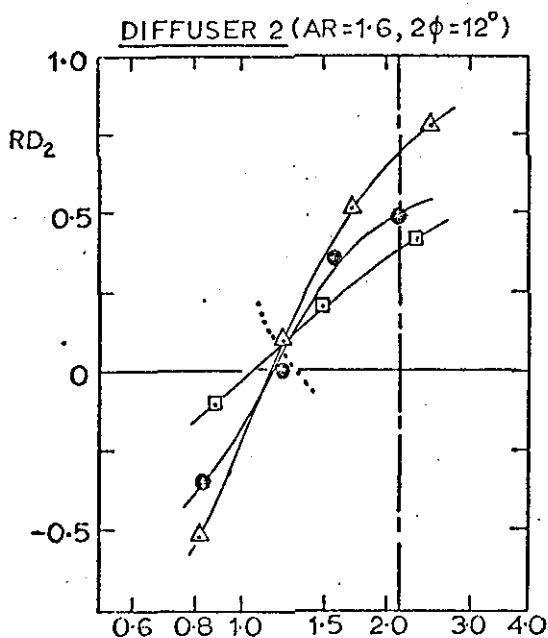


Fig. 4-2-10 PRE-DIFFUSER OUTLET PROFILE ENERGY COEFFICIENTS.

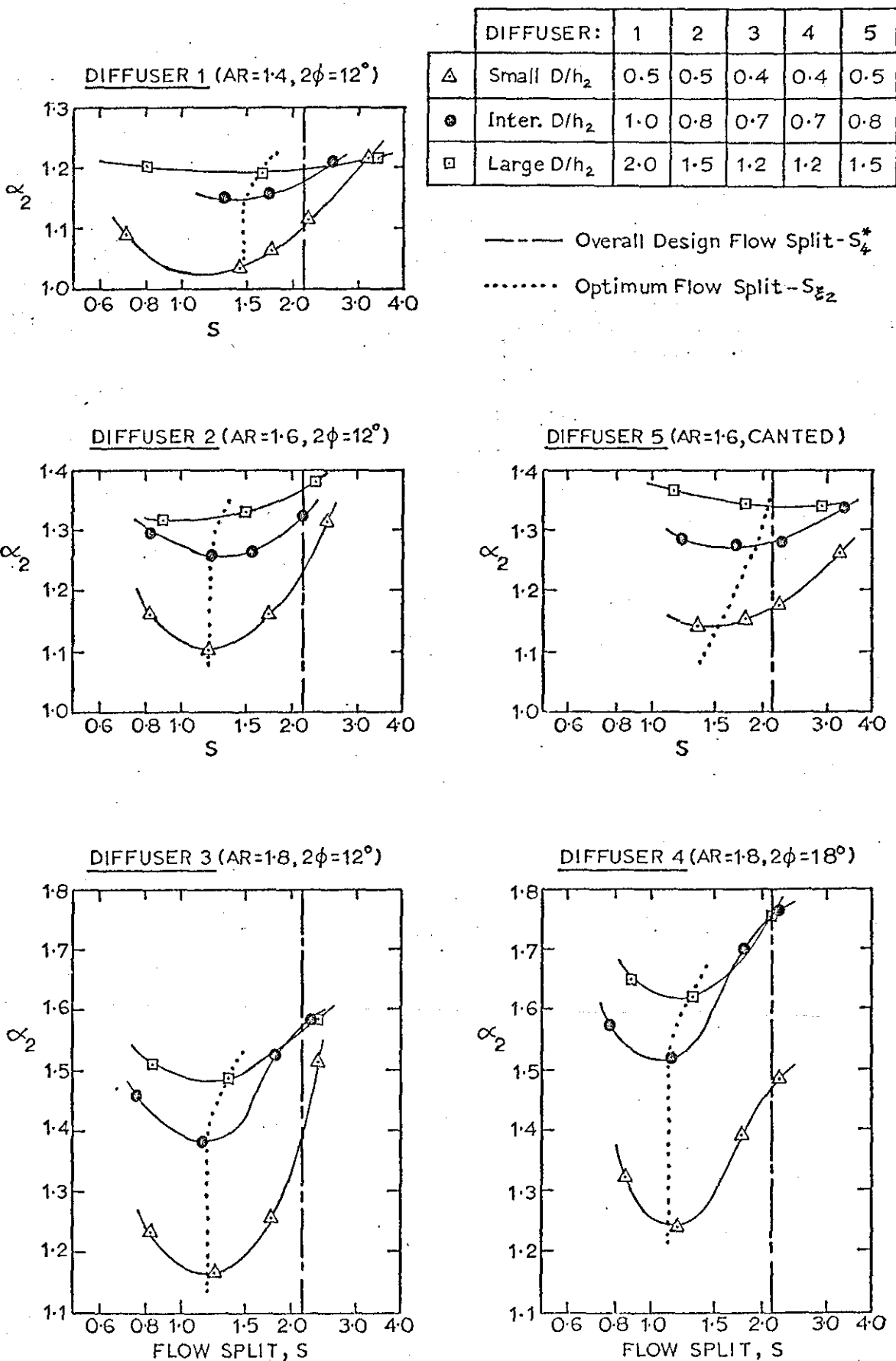


Fig.4-2-11 VARIATION OF PRE-DIFFUSER OUTLET EFFECTIVE AREA FRACTION WITH GEOMETRY FOR OPTIMUM FLOW SPLIT.

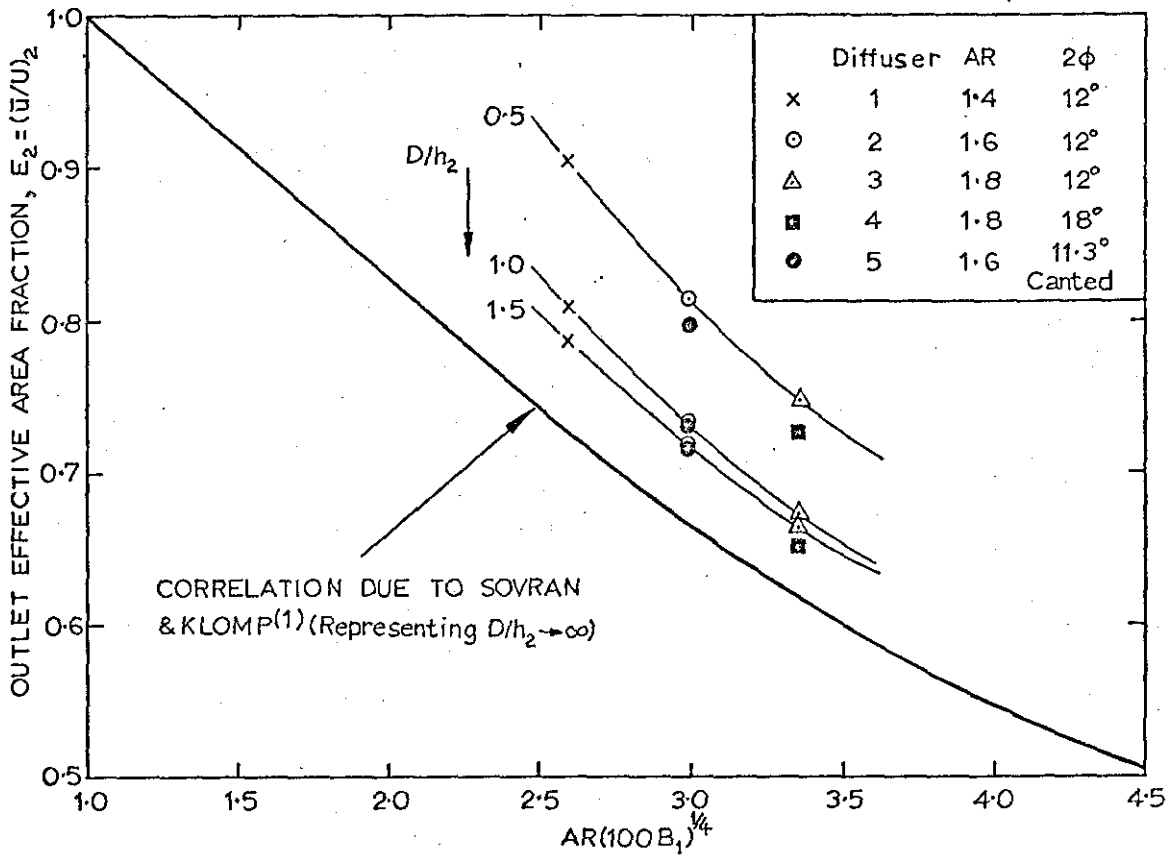


Fig.4-2-12 RELATIONSHIP BETWEEN ENERGY COEFFICIENT AND BLOCKAGE FRACTION FOR PRE-DIFFUSER OUTLET FLOWS.

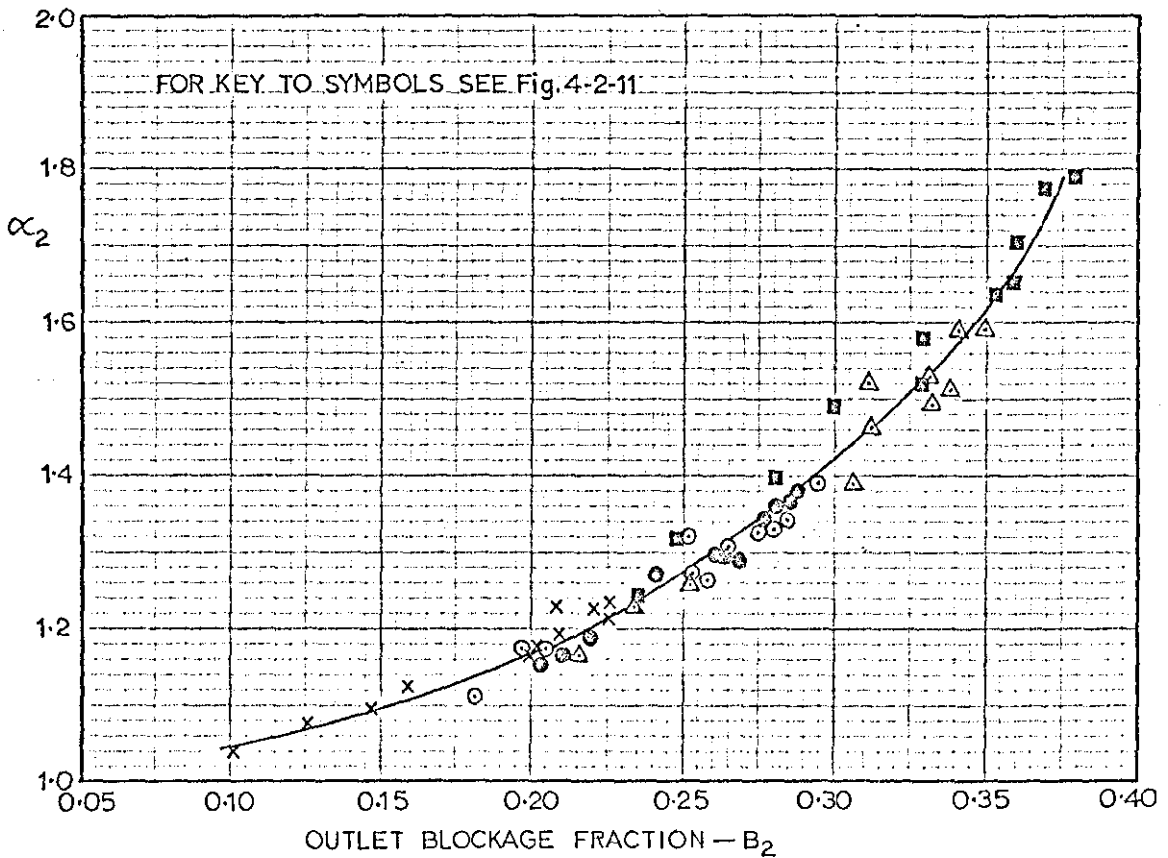


Fig. 4-2-13 FLOW REGIMES AFTER CARLSON & JOHNSTON<sup>(17)</sup>

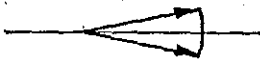
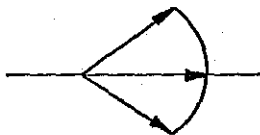
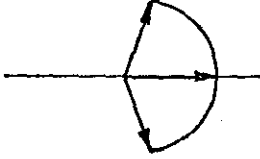
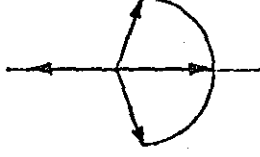


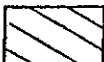
| <u>Tuft Pattern</u>                                                                 | <u>Symbol</u> | <u>Description</u>                                                                                                               |
|-------------------------------------------------------------------------------------|---------------|----------------------------------------------------------------------------------------------------------------------------------|
|    | S             | Steady flow - small or no oscillations of tufts.                                                                                 |
|    | U             | Unsteady flow - medium amplitude oscillations of tufts with no back flow observed.                                               |
|   | TI            | Incipient transitory stall - large amplitude oscillations of tufts on the verge of the tuft pointing upstream.                   |
|  | IT            | Intermittent transitory stall - large amplitude oscillations of tufts with the tuft pointing upstream for short periods of time. |
|  | T             | Transitory stall - tuft points upstream for approximately the same period of time as it points downstream.                       |
|  | F             | Fixed stall - tuft points upstream for long periods of time.                                                                     |

Fig.4-2-14 PRE-DIFFUSER OUTLET FLOW SEPARATION LIMITS.

NO SEPARATION  
OBSERVED FOR  
DIFFUSER 1 (AR=1.4,  $2\phi=12^\circ$ )

- $\blacktriangle$   $\bullet$   $\blacksquare$  Inner Boundary Layer I.T.
- $\triangle$   $\circ$   $\square$  Outer Boundary Layer I.T.
- Overall Design Flow Split -  $S_4^*$
- ..... Optimum Flow Split For Steady Flow
- - - Intermittent Transitory Stall ( $\psi/U \approx 0$  at wall)
-  SEPARATION

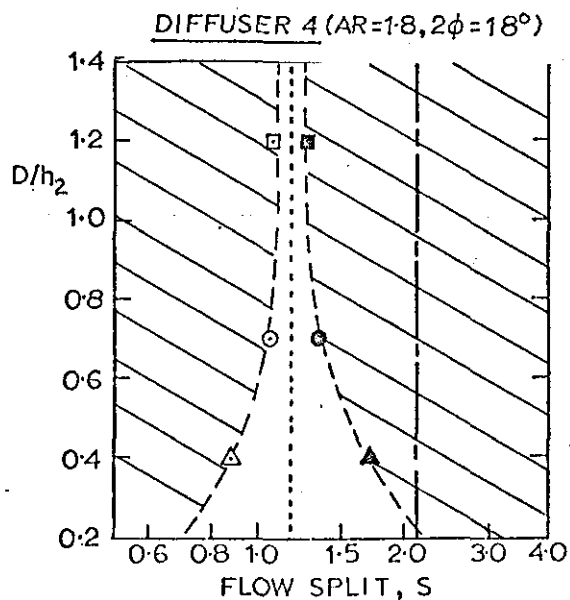
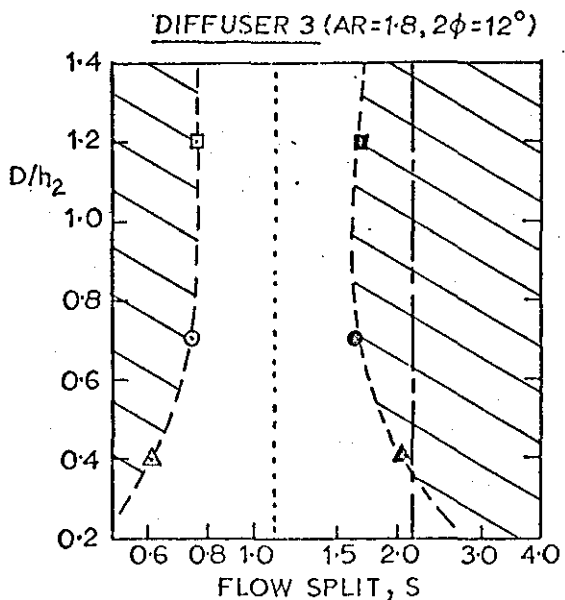
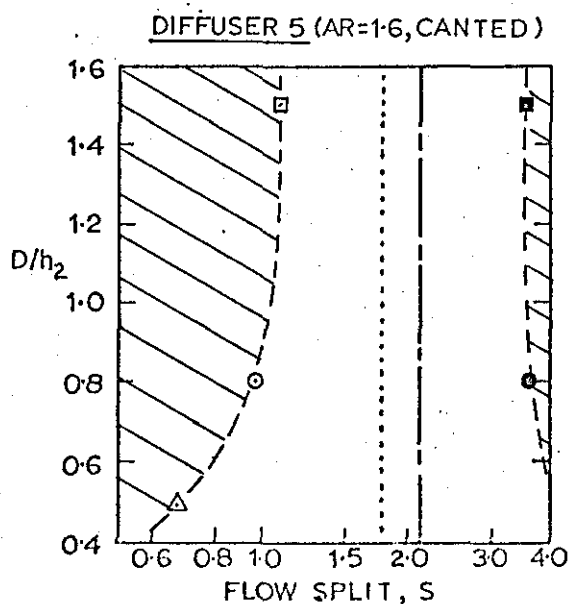
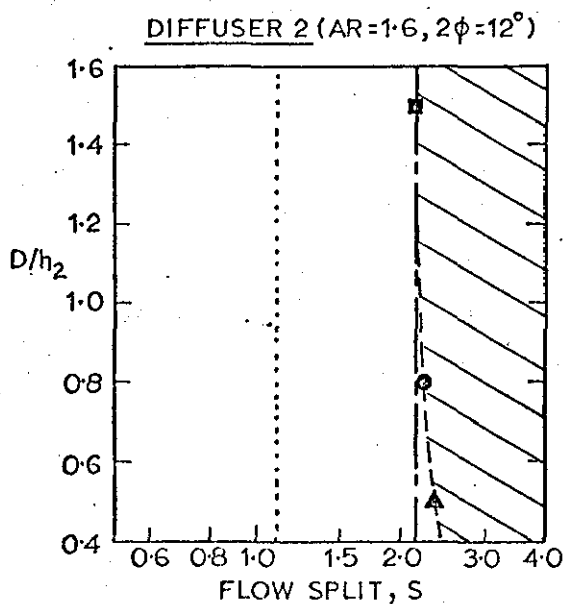




Fig.4-3-1 SETTLING LENGTH VELOCITY PROFILES  
FOR TEST SERIES 3-04.

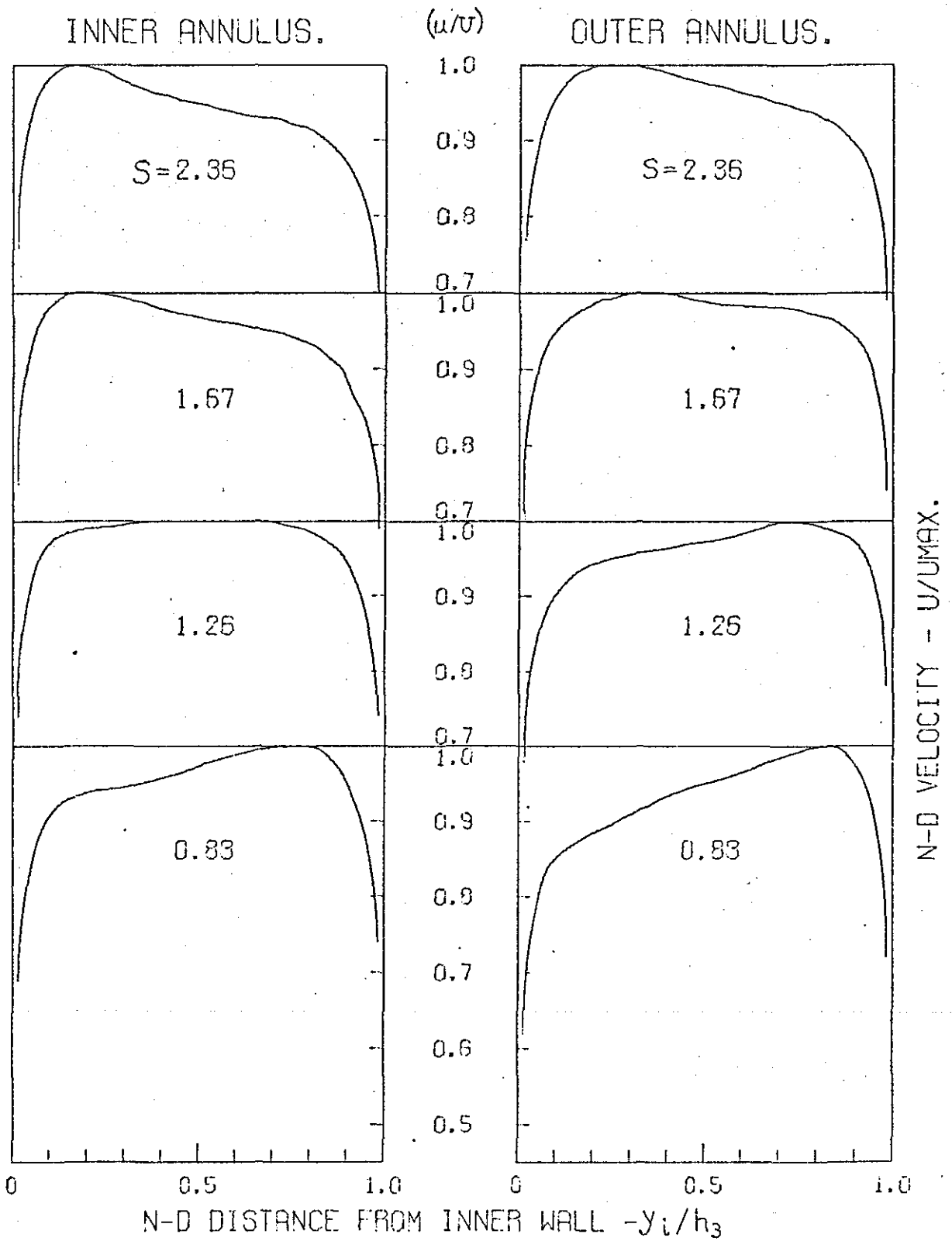


Fig.4-3-2 SETTLING LENGTH VELOCITY PROFILES  
FOR TEST SERIES 3-07.

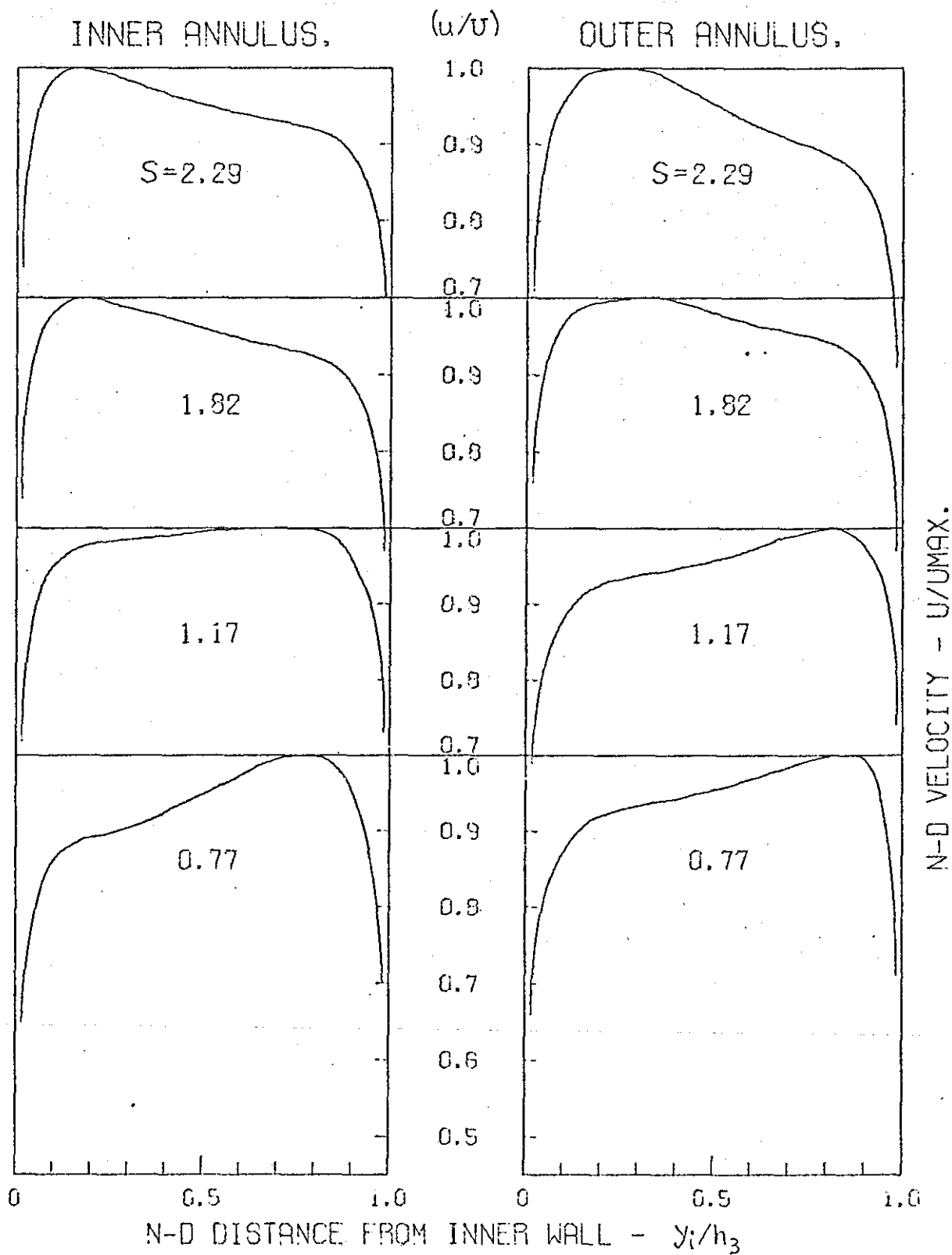


Fig.4-3-3 SETTLING LENGTH VELOCITY PROFILES  
FOR TEST SERIES 3-12.

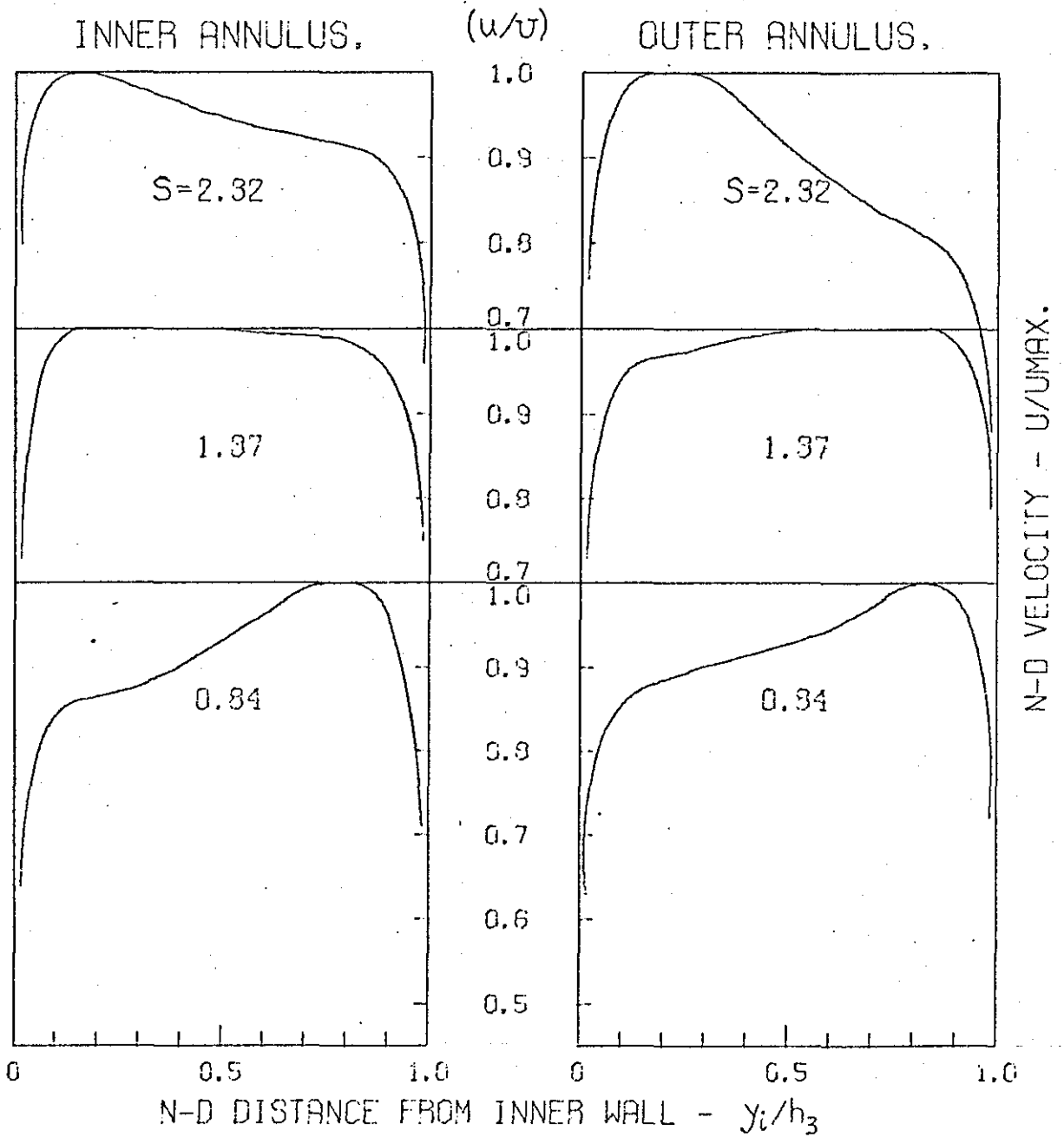
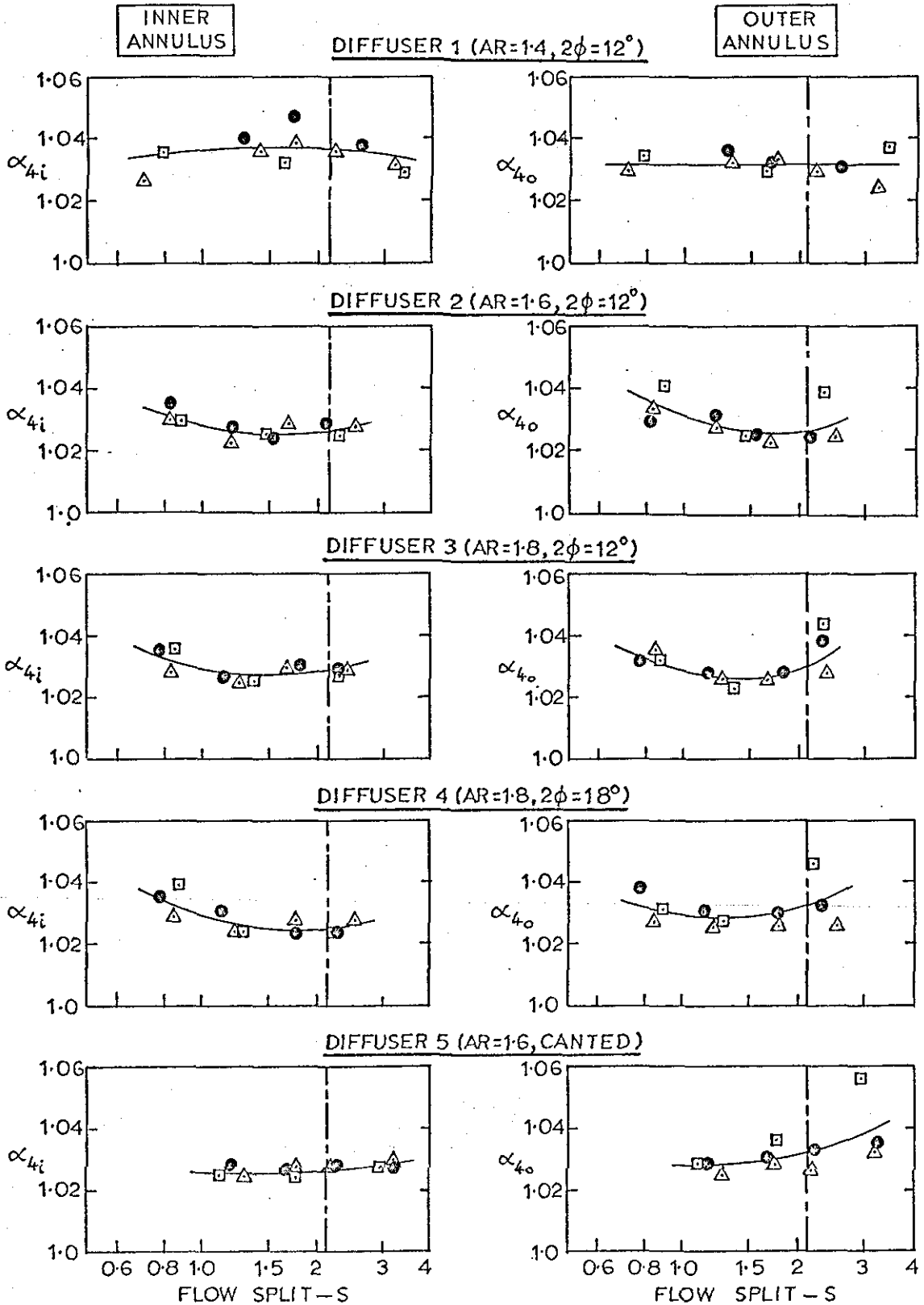


Fig.4-3-4 SETTLING LENGTH ENERGY COEFFICIENTS.

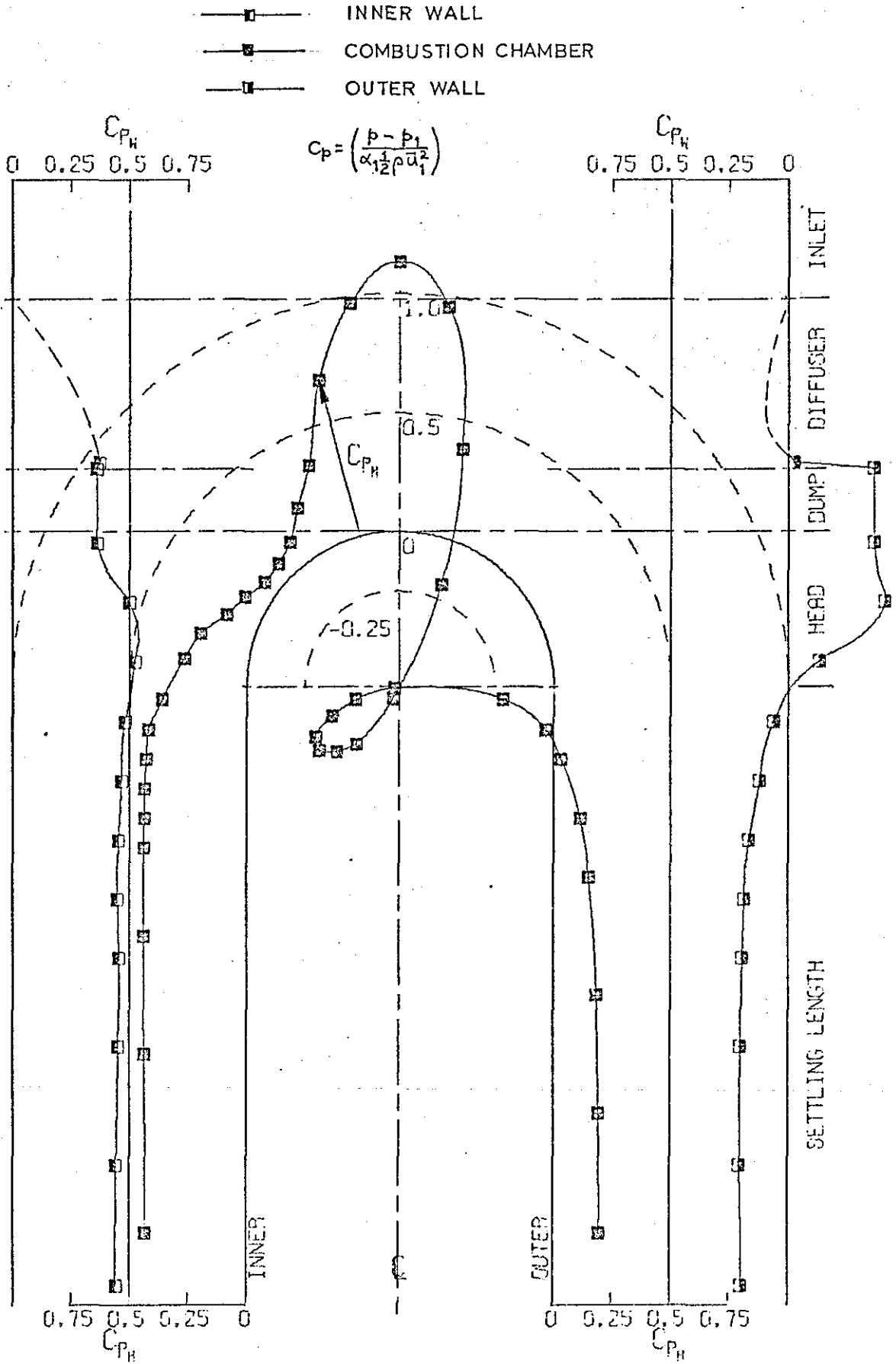
| DIFFUSER: |                         | 1   | 2   | 3   | 4   | 5   |
|-----------|-------------------------|-----|-----|-----|-----|-----|
| △         | Small D/h <sub>2</sub>  | 0.5 | 0.5 | 0.4 | 0.4 | 0.5 |
| ●         | Inter. D/h <sub>2</sub> | 1.0 | 0.8 | 0.7 | 0.7 | 0.8 |
| □         | Large D/h <sub>2</sub>  | 2.0 | 1.5 | 1.2 | 1.2 | 1.5 |

----- Overall Design  
Flow Split - S<sub>4</sub>\*



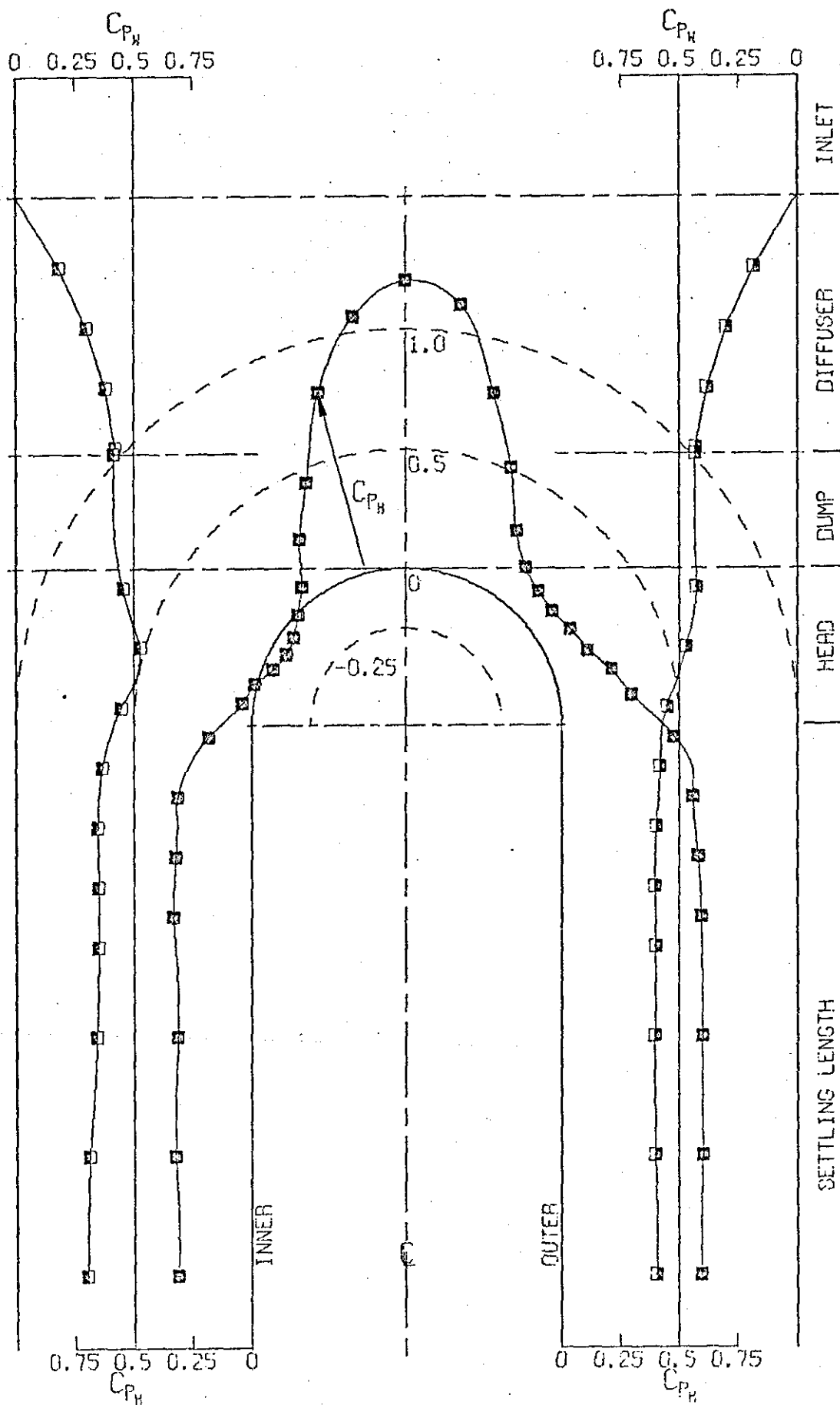
STATIC PRESSURE DISTRIBUTION  
FOR TEST 1-0522

Fig.4-4-1



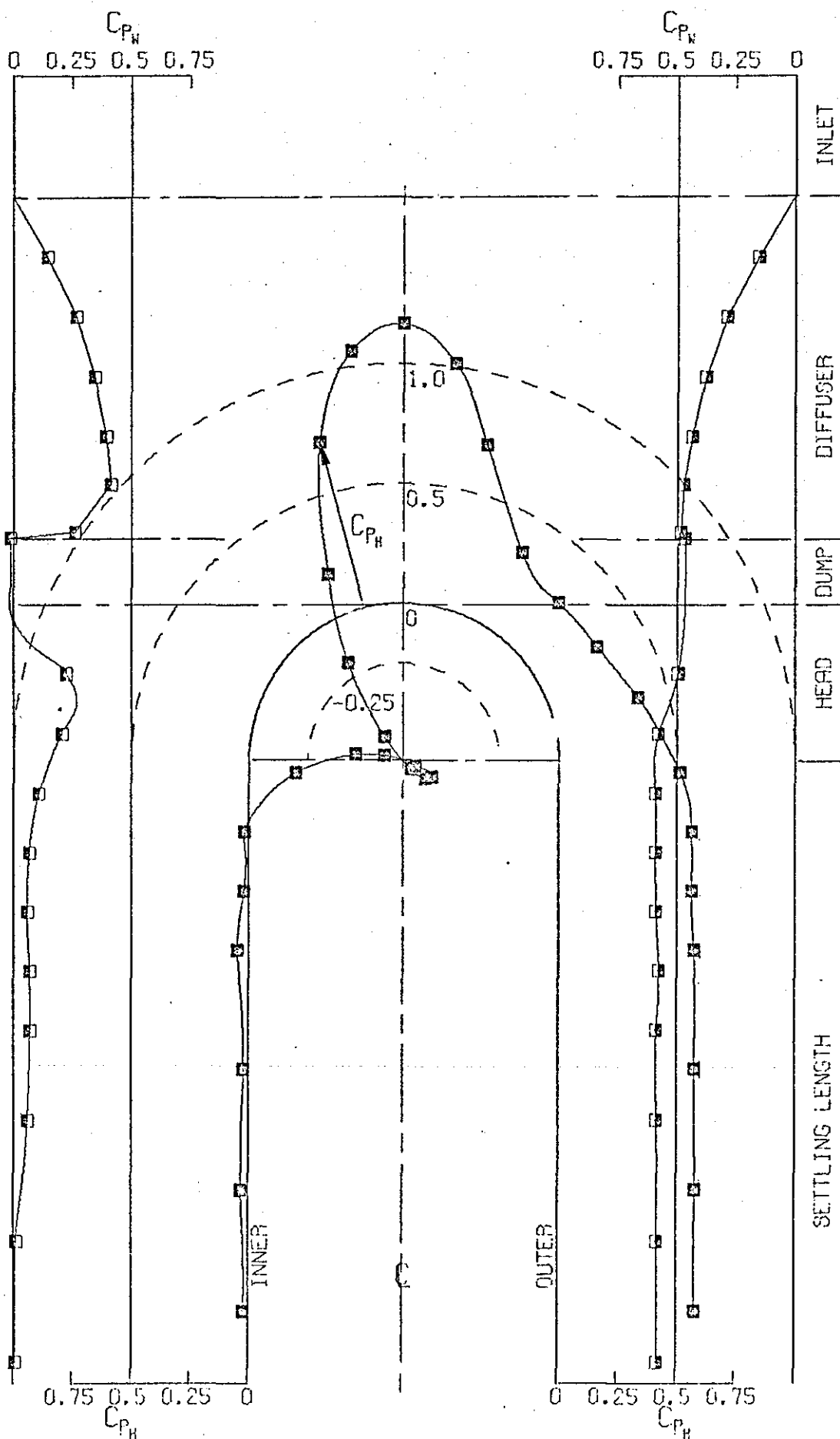
STATIC PRESSURE DISTRIBUTION  
FOR TEST 2-0812

Fig.4-4-2



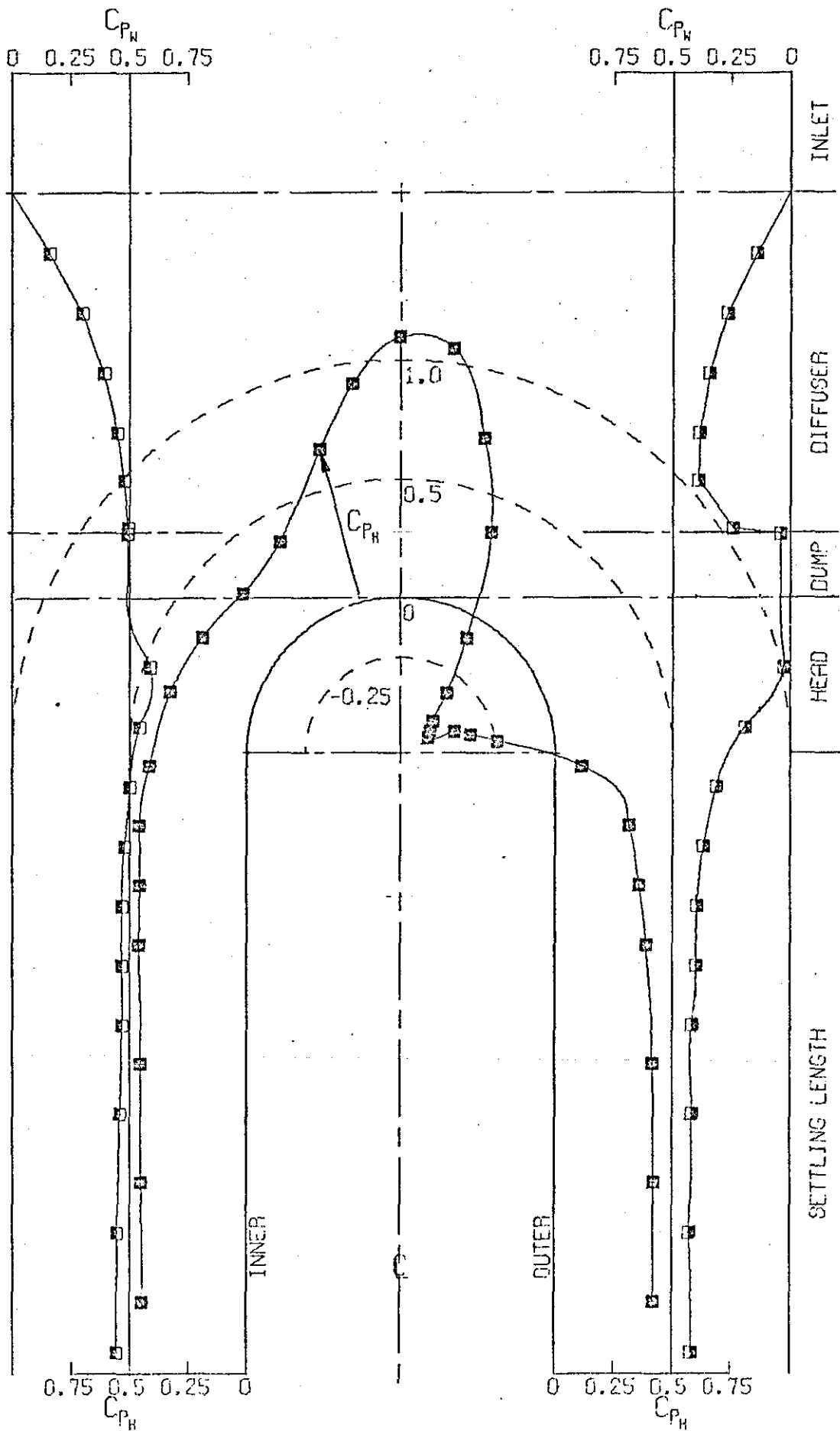
STATIC PRESSURE DISTRIBUTION  
FOR TEST 3-0408

Fig. 4-4-3



STATIC PRESSURE DISTRIBUTION  
FOR TEST 3-0423

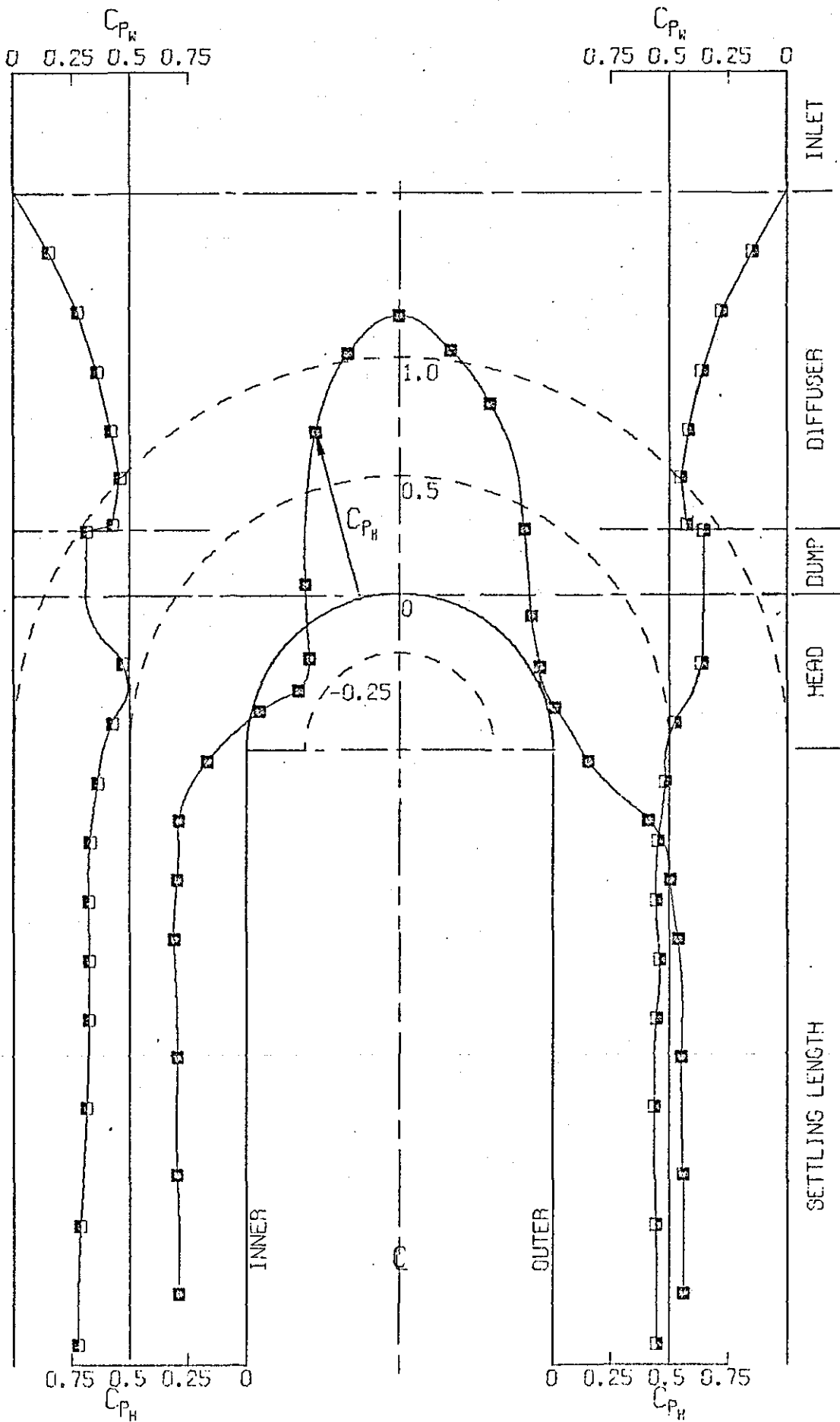
Fig. 4-4-4





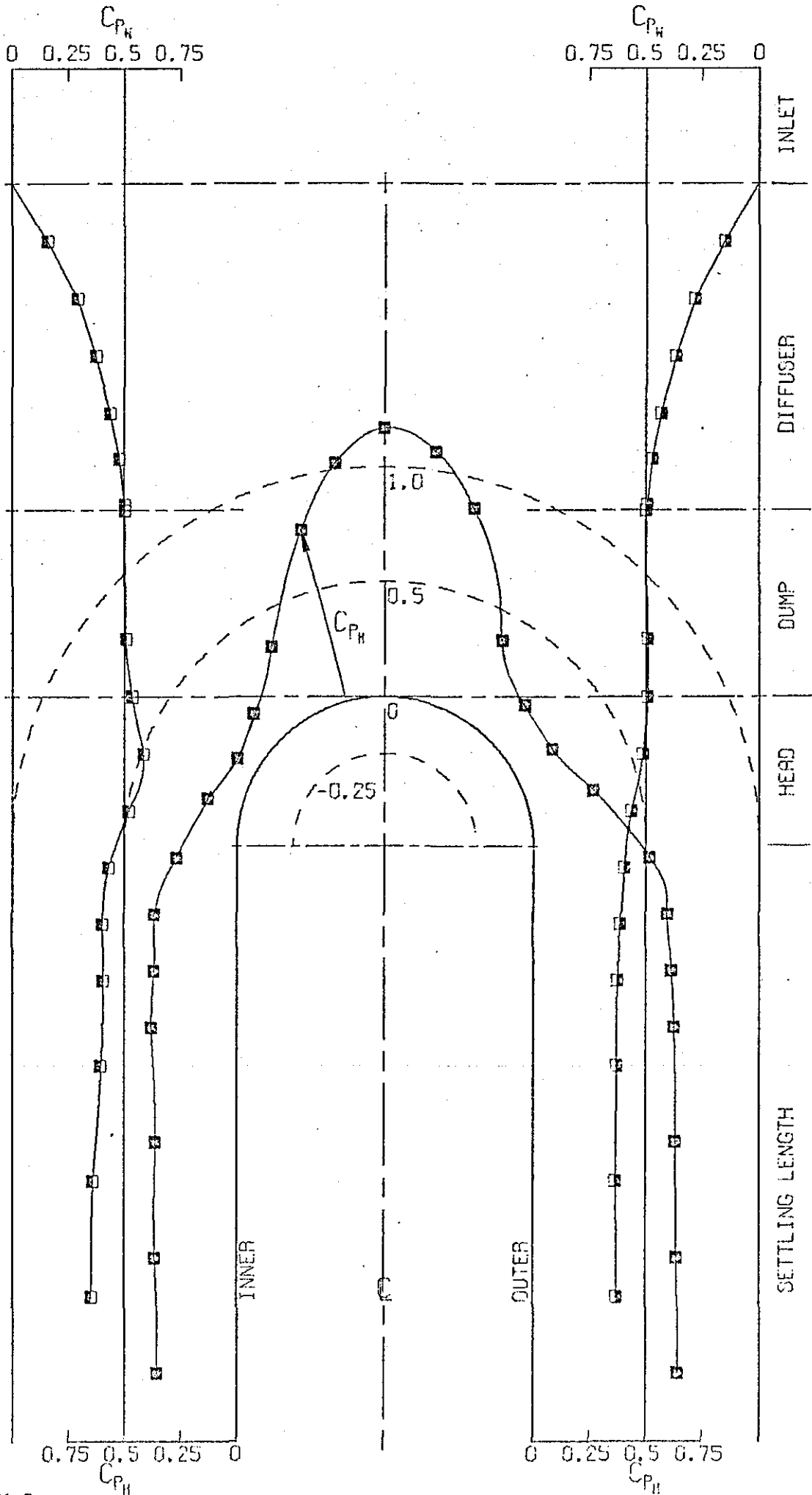
STATIC PRESSURE DISTRIBUTION  
FOR TEST 3-0412

Fig.4-4-5



STATIC PRESSURE DISTRIBUTION  
FOR TEST 3-1214

Fig.4-4-6

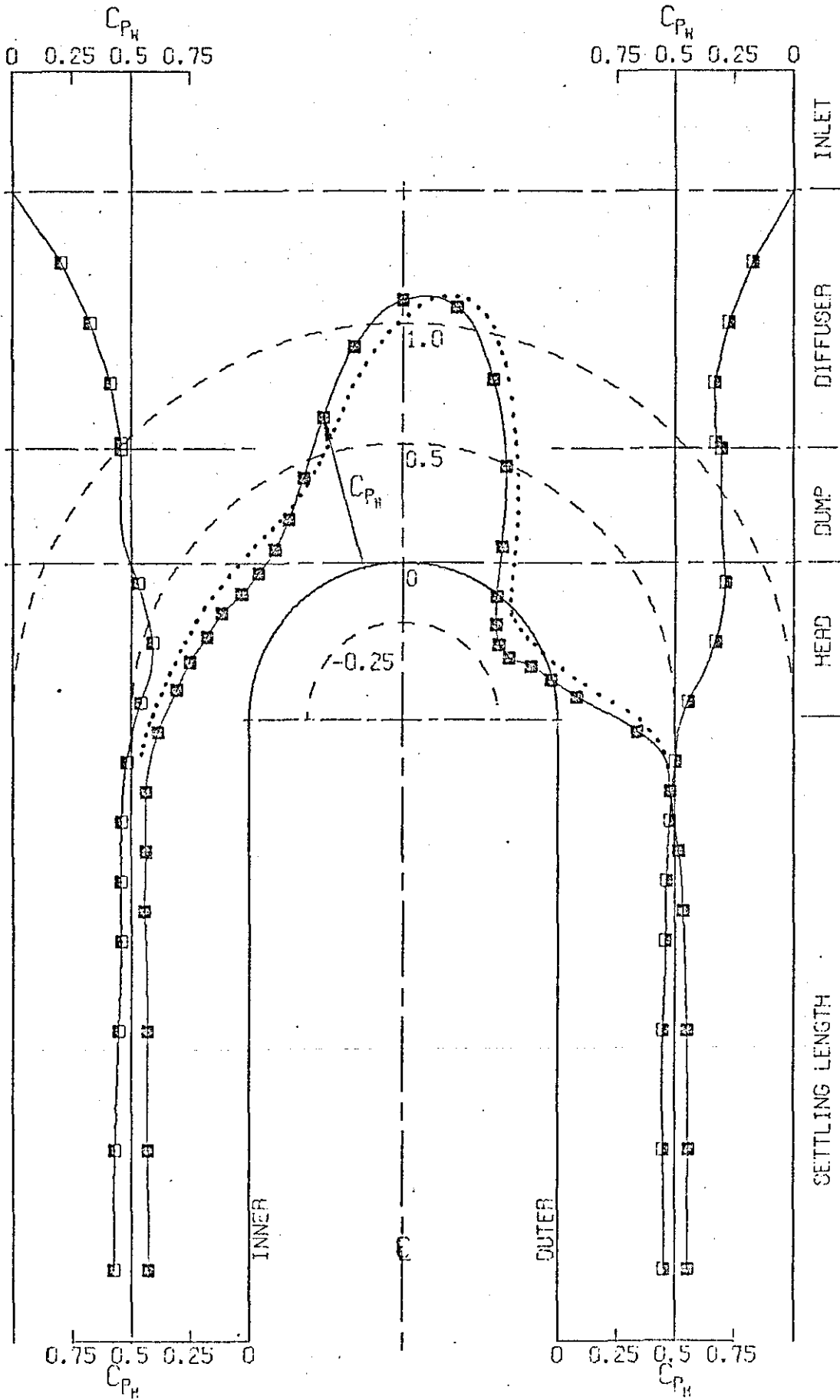


STATIC PRESSURE DISTRIBUTION

Fig.4-4-7

FOR TEST 2-0822(—■—)

AND TEST 5-0822(.....)



STATIC PRESSURE DISTRIBUTION  
FOR TEST 5-0817

Fig.4-4-8

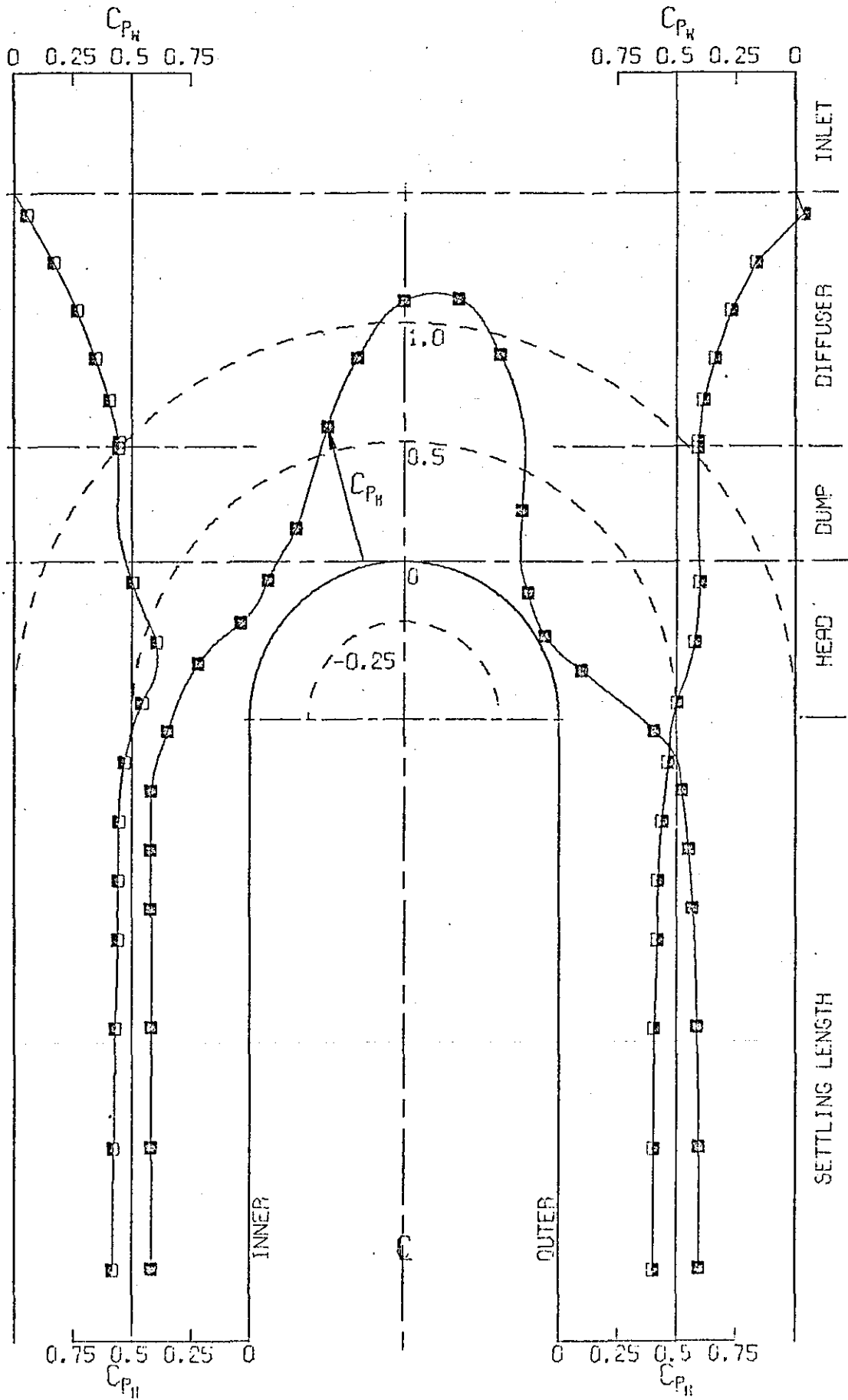


Fig.4-5-1 OVERALL PERFORMANCE CONTOUR MAPS

DIFFUSER 1, AR=1.4, 2 $\phi$  = 12°

NO PRE-DIFFUSER SEPARATION.

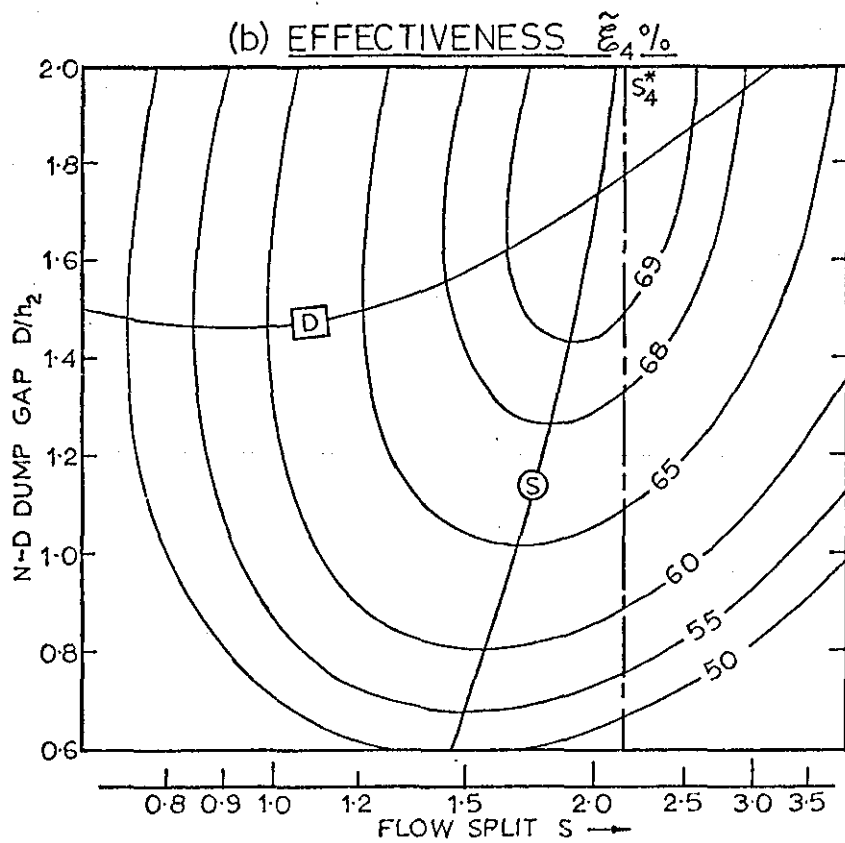
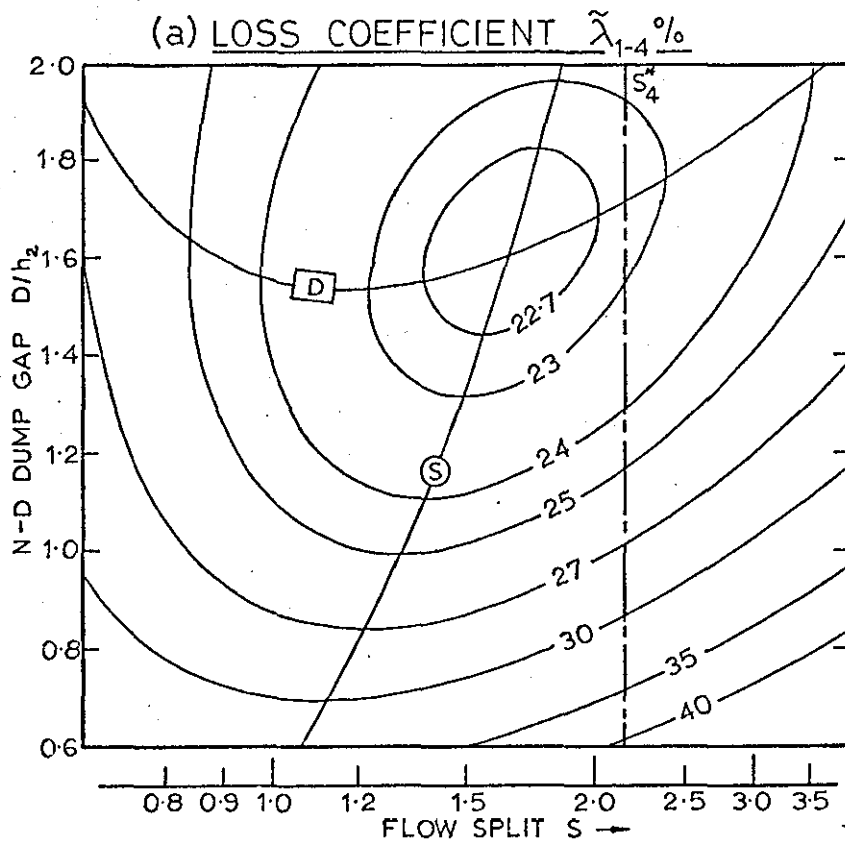
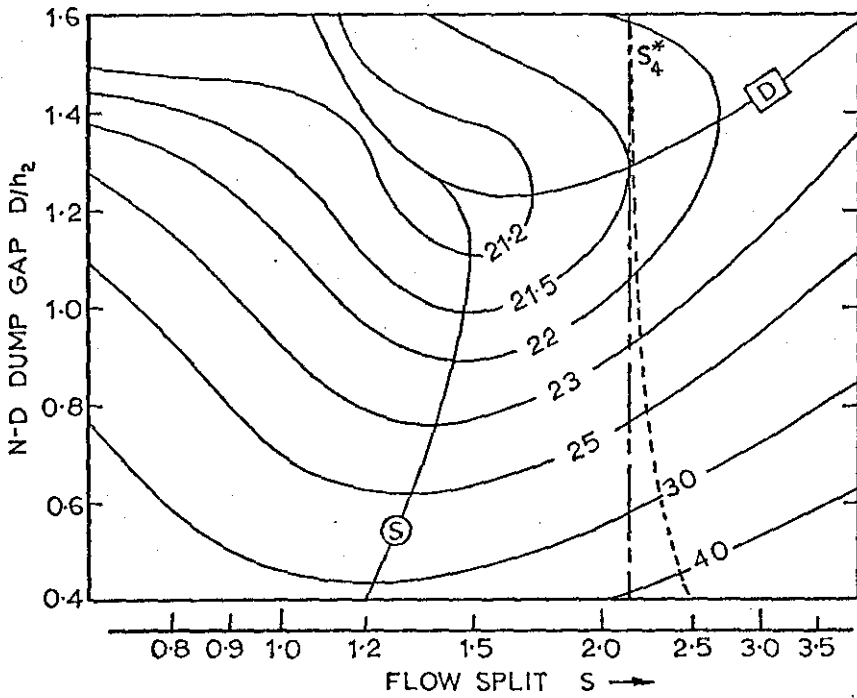


Fig.4-5-2 OVERALL PERFORMANCE CONTOUR MAPS

DIFFUSER 2, AR=1.6, 2 $\phi$ =12 $^{\circ}$

----- PRE-DIFFUSER SEPARATION LIMITS.

(a) LOSS COEFFICIENT  $\tilde{\lambda}_{1-4}$  %



(b) EFFECTIVENESS  $\frac{\Delta T}{T_4}$  %

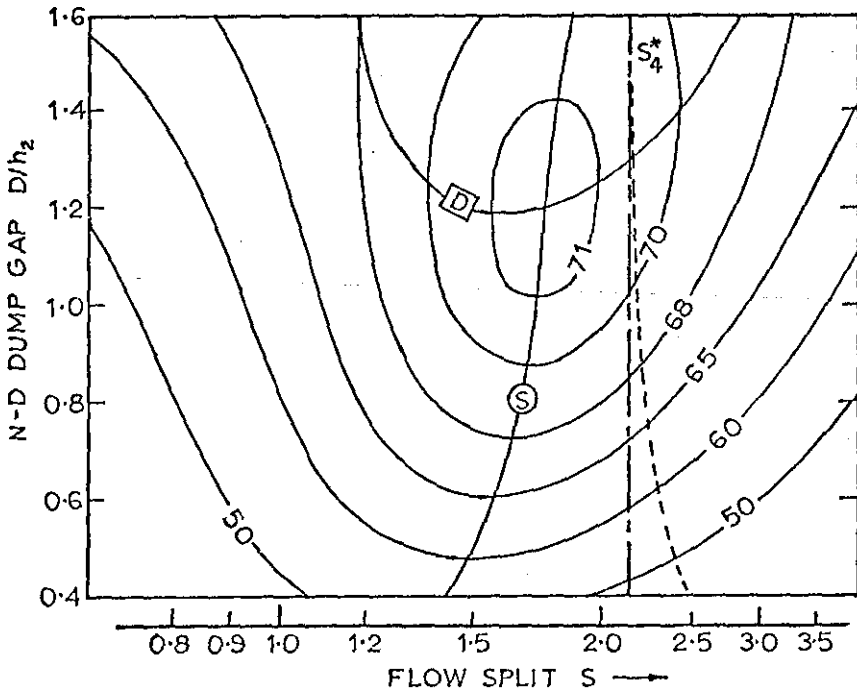
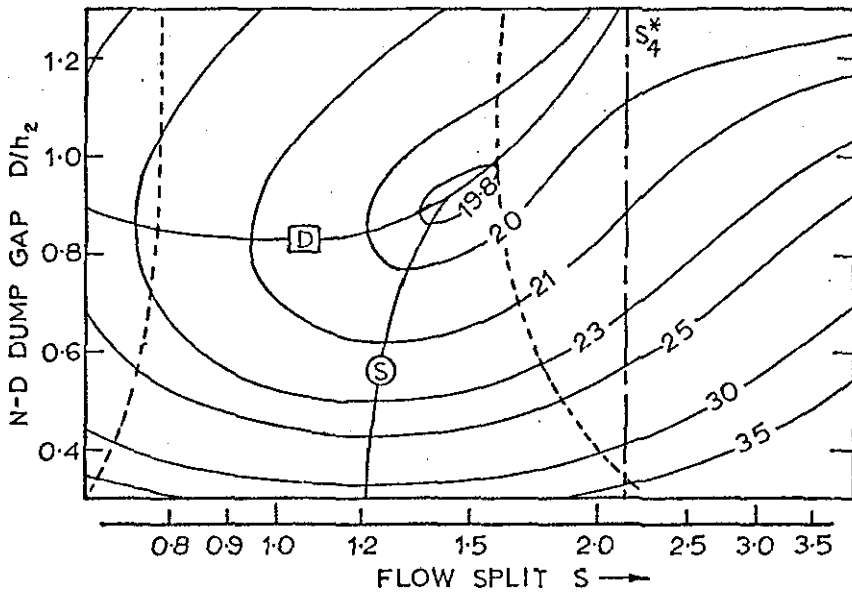


Fig.4-5-3 OVERALL PERFORMANCE CONTOUR MAPS  
DIFFUSER 3, AR=1.8, 2 $\phi$ =12 $^{\circ}$

----- PRE-DIFFUSER SEPARATION LIMITS.

(a) LOSS COEFFICIENT  $\tilde{\lambda}_{1-4} \%$



(b) EFFECTIVENESS  $\tilde{\epsilon}_4 \%$

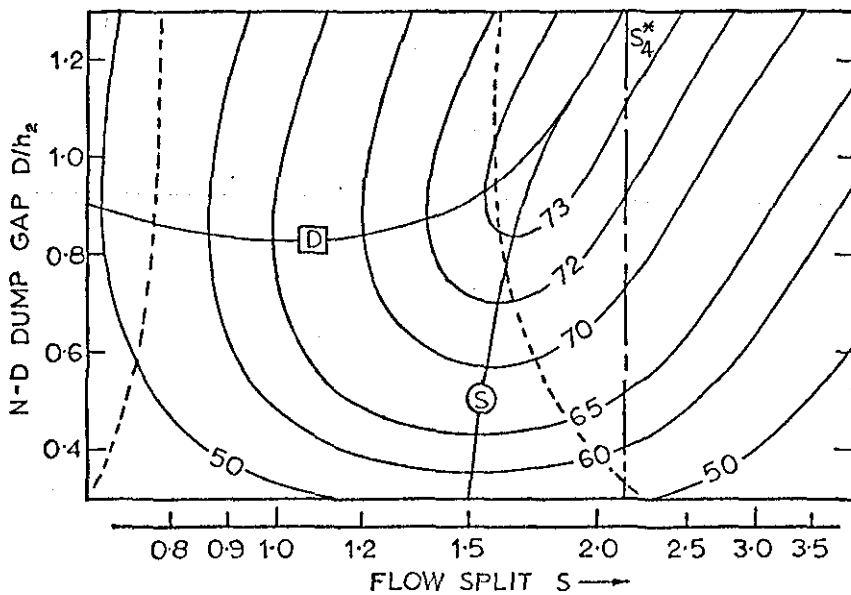
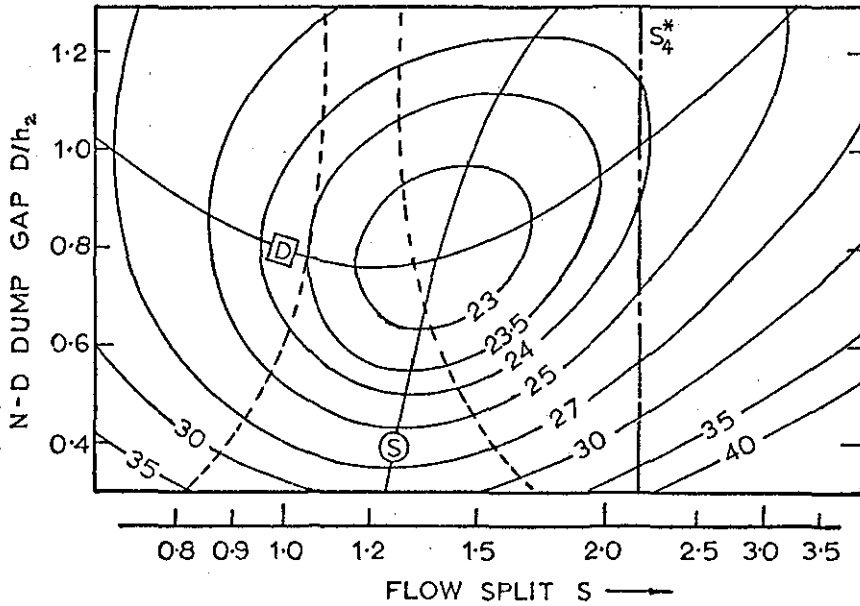


Fig.4-5-4 OVERALL PERFORMANCE CONTOUR MAPS  
DIFFUSER 4, AR=1.8, 2 $\phi$ =18 $^\circ$

----- PRE-DIFFUSER SEPARATION LIMITS.

(a) LOSS COEFFICIENT  $\tilde{\lambda}_{1-4} \%$



(b) EFFECTIVENESS  $\frac{200}{4} \%$

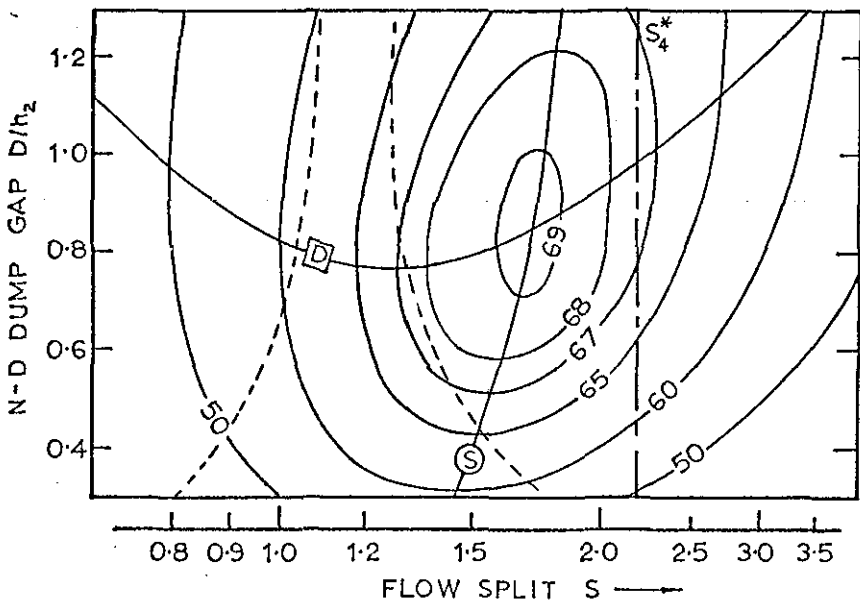


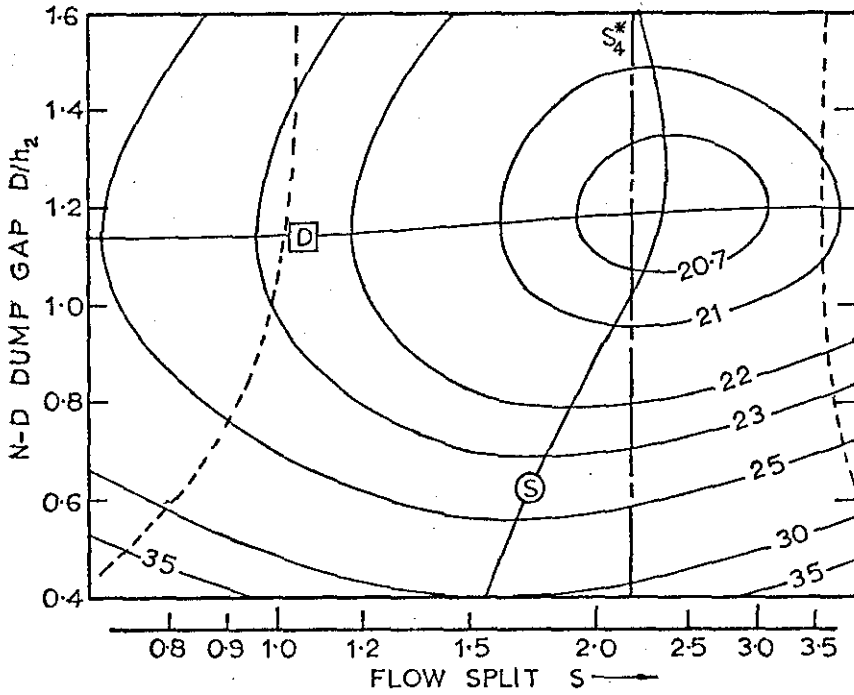


Fig.4-5-5 OVERALL PERFORMANCE CONTOUR MAPS

DIFFUSER 5, AR=1.6, 2 $\phi$  = 11.3 $^{\circ}$ (Canted)

----- PRE-DIFFUSER SEPARATION LIMITS.

(a) LOSS COEFFICIENT  $\tilde{\lambda}_{1.4}$  %



(b) EFFECTIVENESS  $\tilde{\epsilon}_{1.4}$  %

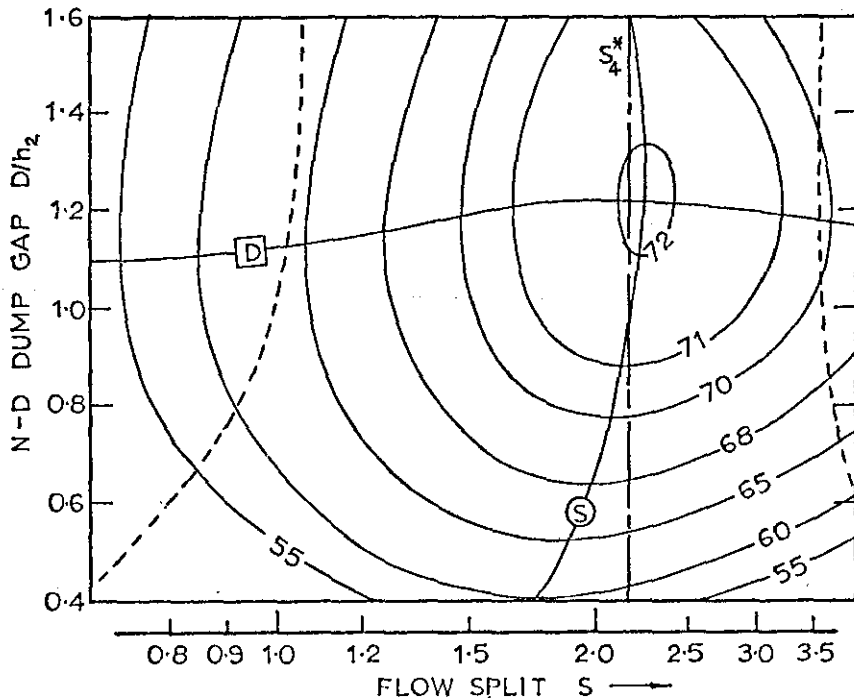
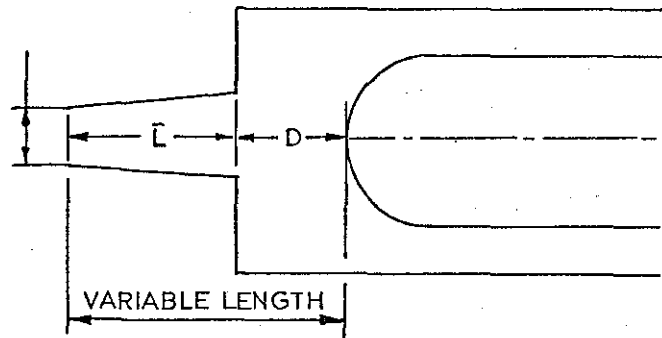


Fig.4-5-6 VARIATION OF OVERALL EFFECTIVENESS WITH VARIABLE LENGTH AT OVERALL DESIGN FLOW SPLIT.



|   | Pre-diffuser Geometry |             |
|---|-----------------------|-------------|
|   | AR                    | 2φ°         |
| 1 | 1.4                   | 12          |
| 2 | 1.6                   | 12          |
| 3 | 1.8                   | 12          |
| 4 | 1.8                   | 18          |
| 5 | 1.6                   | 11.3 Canted |

----- LIMIT OF PERFORMANCE WITH SYMMETRICAL PRE-DIFFUSERS OF 12° INCLUDED WALL ANGLE

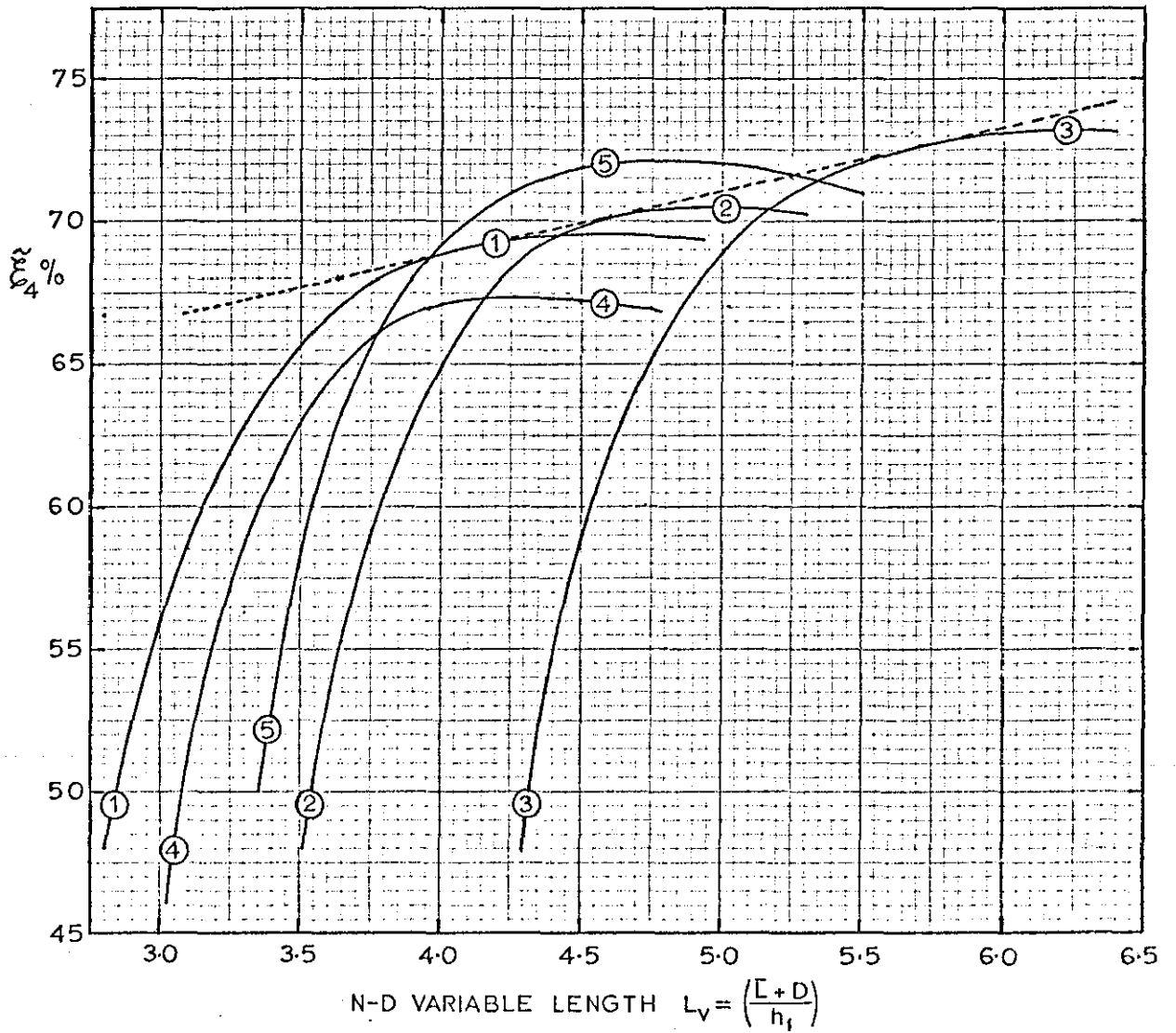
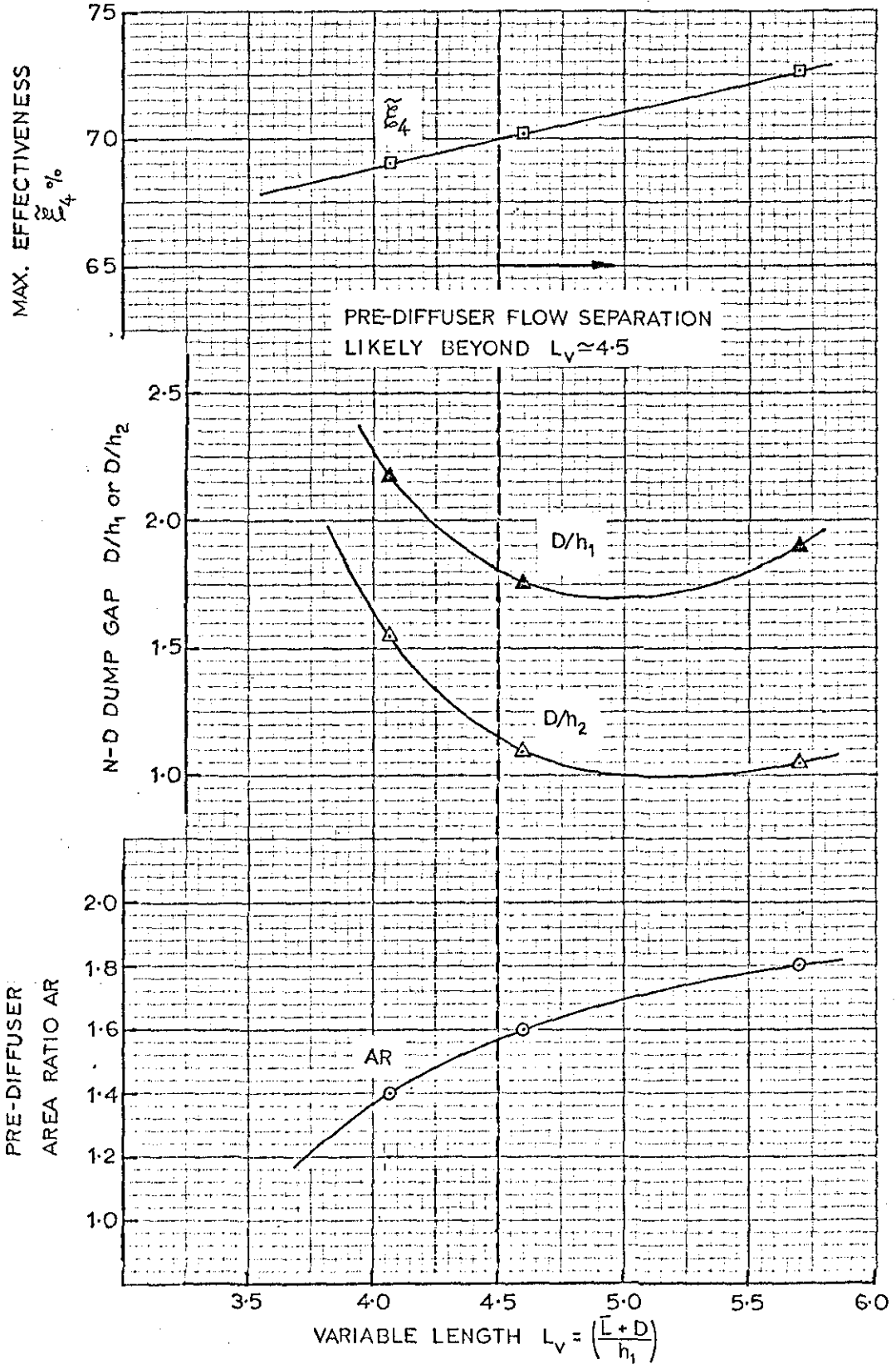


Fig.4-5-7 OPTIMUM GEOMETRY FOR A GIVEN LENGTH

(Symmetrical pre-diffusers,  $2\phi=12^\circ$ , Overall design flow split)

NOTE: CANTING THE PRE-DIFFUSER CAN PRODUCE A RISE IN  $\frac{\eta}{\xi_4}$  OF 1.8% AND MOVE THE SEPARATION LIMIT BEYOND  $L_v \approx 6.0$



## CHAPTER 5. FURTHER ANALYSIS OF LOSSES

This chapter is intended to provide more detailed analysis of the energy losses that occur in the diffuser system. The overall energy loss is sub-divided in order to assist in identifying regions of high loss. The influence of each "design" variable on the generation of local losses is discussed and conclusions are drawn which provide the basis for a better understanding of the fluid mechanic behaviour of the branched diffuser system.

### 5-1 METHOD AND SCOPE OF ANALYSIS

#### 5-1-1 Division of Losses

The first step in calculating the local losses was to divide the flow into two fields separated by the stagnation streamline in the pre-diffuser as shown in Fig. 5-1-1. The proportions of flow passing down the inner and outer annuli at Station 4 were used to locate the position of the stagnation streamline within the pre-diffuser, such that

$$\frac{\int_{R_s}^{R_o} (u/U) R \, dR}{\int_{R_i}^{R_s} (u/U) R \, dR} = S = \left( \frac{Q_o}{Q_i} \right)_4 \quad 5-1-1$$

where  $R_s$  is the stagnation streamline radius. An iterative process was used to solve for  $R_s$  in Eqn. 5-1-1 for the pre-diffuser inlet and outlet flows. From this point on, the stagnation streamline was treated as a solid boundary and the inner and outer flow fields considered separately. Each flow field was divided into sections (see Fig. 5-1-1) and the local energy loss calculated for each. The sections are as follows:

- (i) Pre-diffuser (stations 1 to 2)
- (ii) "Dump" Region (stations 2 to 3)
- (iii) Settling Length (stations 3 to 4)

The flow in each settling length was further sub-divided into two

regions, each comprising 50% of the annulus flow. Energy losses were then calculated for each region to indicate whether the majority of loss was generated near the combustion chamber wall or the casing wall. A crude attempt was also made to estimate the energy dissipated in the vortex region of the dump section. A comprehensive knowledge of the flow conditions at Stations 1, 2 and 4 enabled the pre-diffuser and overall losses for each flow field to be calculated with reasonable confidence (to an accuracy of better than  $\pm 0.03$  on loss coefficient). Analysis of the flow conditions in the plane of the head rakes (Stn. 3) was rendered difficult by the complexity of the flow in the dump region. Also, the measurements afforded by the rakes were very limited. The method used in analysing the head rake data is dealt with in the following section.

#### 5-1-2 Analysis of Head Rake Data

Each head rake provided one static and four total pressure measurements which were supplemented by two measurements from wall pressure tappings. A typical set of data is shown in Fig. 5-1-2(a). The static pressure profile was obtained from the three measured values using a curve fit based on more detailed calibration data (see Appendix 2). Local values of dynamic pressure were calculated using interpolated static pressures and the measured totals. Parabolic curve fitting techniques were then used to obtain the maximum dynamic pressure and hence values of  $u/U$ . These values were extrapolated to zero to complete the non-dimensional velocity profile (Fig. 5-1-2(b)).

A typical example of the flow pattern in the dump region is illustrated in Fig. 5-1-3. The streamline indicates the boundary separating the main flow to the settling length from the re-circulating flow in the vortex region. Energy is transported to the vortex region by the turbulent motion of the fluid, such that at Stn. 3 there is a discrete volume flow whose kinetic energy has been drawn from the main stream. The boundary of the vortex region at Stn. 3 was calculated using an iterative method to obtain

the distance from the head up to which the integrated main flow was equal to that in the settling length. The static pressure and velocity of the flow in the main stream were then integrated and the loss coefficient,  $\tilde{\lambda}_{2-3}$  calculated. A crude estimate of the energy loss in the vortex region was made on the assumption that the kinetic energy contained in the vortex flow at Stn. 3 was totally dissipated. It should be noted that  $\tilde{\lambda}_{2-3}$  includes the loss attributable to the vortex region since most of the energy required to sustain the vortex is transferred upstream of Stn. 3.

It may be noted that no continuity check could be made at Stn. 3. In the majority of cases the total indicated flow (discounting the reverse flow near the casing wall) was in excess of that in the settling length, thus indicating a positive vortex flow adjacent to the main stream. In the remaining cases the total flow was less than that in the settling length, thus indicating an error in the measurements. These cases are commented on later.

## 5-2 PRESENTATION OF DATA

### 5-2-1 Head Rake Data

A typical set of velocity and static pressure profiles for Stn. 3 are shown in Fig. 5-2-1. The remainder of the curves are given in Appendix 6. The head rakes were not fitted until tests with Diffuser 2 were under way, therefore no data is available for tests with Diffuser 1 or for Test Sers. 2-08. The following general comments apply in relation to the results.

(i) The velocity profiles do not vary significantly with pre-diffuser geometry or dump gap for a particular flow split.

(ii) There is a consistent change in velocity profile with flow split. The profiles become more peaky (i.e. concave in shape) as the annulus flow is decreased.

(iii) The static pressure difference across the annulus increases with flow as does the peak velocity near the head.

(iv) The static pressure difference and peak velocity tend to decrease with increasing dump gap and pre-diffuser area ratio.

The integrated flows in the outer annulus were consistent with there being a significant vortex flow (equivalent to typically 10% of the main stream flow in the annulus). In the inner annulus the flows were, in a number of cases, lower than those measured in the settling length (indicating zero vortex flow) even though significant vortex flows were confirmed by wool tuft observations. In these cases it is considered that the appropriate values of  $\tilde{\lambda}_{2-3}$  have been over-estimated and those of  $\tilde{\lambda}_{3-4}$  under-estimated. Results for the inner annulus must therefore be treated with caution. For this reason attention is focused on the analysis of local losses for the outer annulus (see Sect. 5-3-2 onward).

#### 5-2-2 Flow Field and Local Losses

The experimental flow field loss coefficients are given in graphical form as follows.

- Figs. 5-2-2/4 Overall flow field loss versus flow for small, intermediate and large dump gaps.
- Fig. 5-2-6 Pre-diffuser local loss versus flow.
- Fig. 5-2-7 Dump region local loss versus flow.
- Fig. 5-2-8 Settling length local loss versus flow.

The above curves are plotted versus annulus flow (as a percentage of the total inlet flow) since this is more meaningful than flow split ratio when considering individual flow fields. The annulus flows equivalent to the overall design flow split of 2.15 are,

$$\text{Outer annulus flow, } Q_o = 68.3\%$$

$$\text{Inner annulus flow, } Q_i = 31.7\%$$

All the local losses are presented in terms of the same reference pressure, namely the mass-mean inlet dynamic pressure.

$$\text{i.e. } \tilde{\lambda}_{\text{Local}} = \frac{\Delta \tilde{P}_{\text{Local}}}{\alpha_1 \frac{1}{2} \rho \bar{u}_1^2}$$

This method of presentation was chosen since it facilitates direct comparison of the energy losses occurring in different regions of the flow. Taking a more specific example, the inner flow field pre-diffuser loss coefficient has been defined,

$$\left(\tilde{\lambda}_{1-2}\right)_i = \frac{\left(\Delta\tilde{P}_{1-2}\right)_i}{\alpha_1 \frac{1}{2} \rho \bar{u}_1^2} = \frac{\alpha_{1i} \left(\bar{u}_{1i}\right)^2}{\alpha_1 \left(\bar{u}_1\right)^2} \left[ 1 - \frac{\alpha_{2i} \left(\bar{u}_{2i}\right)^2}{\alpha_{1i} \left(\bar{u}_{1i}\right)^2} \right] - \tilde{C}_{p_{2i}} \quad 5-2-2$$

It should be noted that the local losses can be added to obtain the overall flow field loss (i.e.  $\tilde{\lambda}_{1-4} = \tilde{\lambda}_{1-2} + \tilde{\lambda}_{2-3} + \tilde{\lambda}_{3-4}$  for either flow field) and that the mean loss for any given section is the mass-mean of the two flow field losses,

e.g. for the pre-diffuser, 
$$\tilde{\lambda}_{1-2} = \frac{Q_i \left(\tilde{\lambda}_{1-2}\right)_i + Q_o \left(\tilde{\lambda}_{1-2}\right)_o}{\left(Q_i + Q_o\right)} \quad 5-2-3$$

### 5-3 DISCUSSION OF RESULTS

#### 5-3-1 Overall Flow Field Losses (Figs. 5-2-2/4)

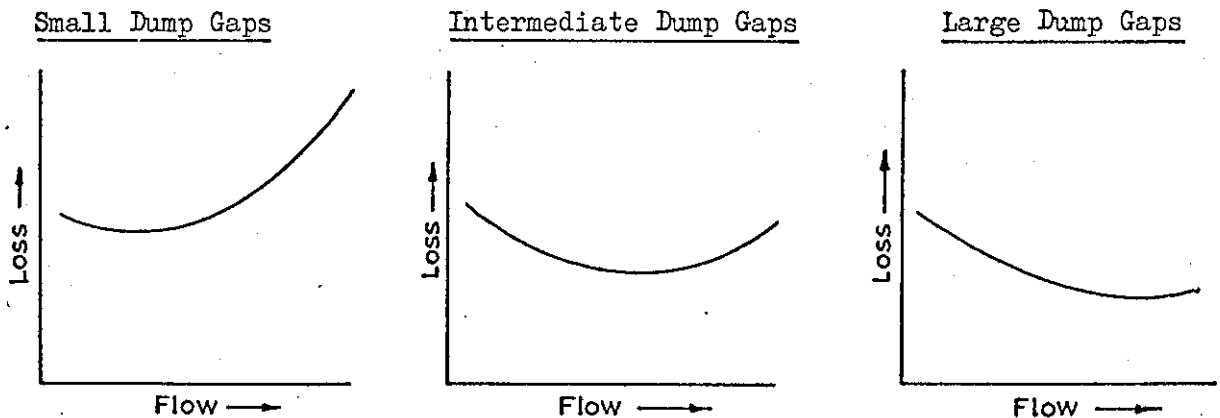
The overall flow field losses tend to decrease with increasing pre-diffuser area ratio and increase with increasing angle (i.e. the trends are substantially the same as for the mean overall losses as discussed in Chapter 4). The results for Diffusers 2 and 5 are particularly interesting since they show that canting the pre-diffuser leads to a re-distribution of loss between the two flow fields. This is most pronounced at the small dump gap ( $D/h_2 = 0.5$ , Fig. 5-2-2) for which it can be seen that the outer flow field loss has decreased for a particular flow fraction whilst that for the inner has increased. The decrease in outer flow field loss is mainly due to two factors; the decrease in turning angle in the dump region and the decrease in dynamic pressure at exit from the pre-diffuser (associated with the reduced outlet profile distortion). It may be noted that both these factors lead to a lower velocity near the head at Stn. 3. As stated in Chapter 4, the net effect of canting the pre-diffuser is to reduce the mean overall loss. This is because the decrease in outer flow



field loss outweighs the increase in loss in the inner flow field.

Due to the dominant influence of dump gap and flow split any deeper understanding of the system performance must start from a consideration of these factors. Taking each category of dump gap in turn (Figs. 5-2-2/4) it can be seen that the loss versus flow curves are similar in form for all pre-diffuser geometries and that the characteristics for the inner and outer flow fields are essentially the same. The most striking feature of the curves is that the gradients change significantly with dump gap. The loss generally increases with flow at small dump gaps whereas it decreases with flow at large dump gaps. The characteristic for intermediate dump gaps can be seen as a cross between these two extremes as indicated in the diagrams below.

Typical variations in overall flow field loss with flow



In view of the reversal in trend with increasing dump gap it is difficult to isolate any one common factor as being responsible for the change in loss with flow. The net reduction in kinetic energy (i.e. the amount of diffusion) occurring in each flow field decreases with increasing annulus flow as shown in Fig. 5-2-5. Since the loss also decreases with flow for large dump gaps one might postulate that the loss is dependent upon the amount of diffusion. This may well be true for large dump gaps, however it is clear that such a relationship does not apply for small dump gaps since the loss increases with decreasing diffusion. Similar

difficulties are encountered when considering the possible influence of other variables (e.g. the dynamic pressure levels in the dump region) and this leads to the conclusion that different factors influence the generation of losses at different dump gaps. The analysis of local losses is intended to assist in explaining these trends.

### 5-3-2 General Features relating to Local Losses

The local losses for the pre-diffuser, dump, and settling length regions of each flow field are given in Figs. 5-2-6/8. In view of the large number of results, no attempt is made in this section to distinguish between those for each diffuser. Observations are restricted to the following considerations; firstly the level of loss as a percentage of the overall flow field loss, and secondly the variation in loss with flow.

#### (i) Pre-diffuser Loss (Fig. 5-2-6)

The energy loss occurring in the pre-diffuser is relatively small in relation to the amount of diffusion achieved. It represents typically 25% (i.e. one quarter) of the overall flow field loss, however the proportion does vary somewhat with dump gap and annulus flow. The level of loss and its variation with flow are substantially the same for each flow field. Initially the loss decreases to a minimum in the mid-flow range and then increases with increasing flow. The variation is more pronounced for small dump gaps and in this respect the characteristics are similar to those for the mean pre-diffuser loss given in Chapter 4.

#### (ii) Dump Region Loss (Fig. 5-2-7)

There is a relatively high degree of scatter in the loss coefficients quoted for the dump region and furthermore there appears to be little similarity between the curves for the inner and outer flow fields. The outer flow field loss is relatively low as would be expected for a region of predominantly accelerating flow (see Fig. 5-1-3). Some results for the inner flow field also support this supposition (i.e. those for the higher flows), however others are unexpectedly high. Analysis of the integrated

volume flows indicates that the "high loss" results are of dubious accuracy and should be discounted. It can therefore be stated that in general the dump region only accounts for a small proportion of the overall loss.

Concentrating attention on the results for the outer flow field, it can be seen that there is a tendency for the loss to decrease with flow for large dump gaps and to increase with flow for small dump gaps. At the design flow (68.3%) the trend is for the loss to decrease with increasing dump gap.

(iii) Settling Length Loss (Fig. 5-2-8)

The most significant feature of the results is that they show the settling length loss to account for the majority (typically 60%) of the overall flow field loss. As with the dump region losses, some results are of dubious accuracy and are to be discounted (i.e. those showing low losses in the inner flow field). The trends with flow are not very clearly defined but for small dump gaps the loss does appear to increase with flow.

5-3-3 Discussion of Pre-diffuser Losses

The variations in mass-mean pre-diffuser loss and outlet flow conditions have been discussed fully in Sect. 4-2. It is however, of interest to discuss the variation of the flow field losses with flow (Fig. 5-2-6). Since the boundary layer contained in each flow field moves toward separation as the flow is reduced (see Figs. 4-2-6/8) it is reasonable to expect the loss to increase with decreasing flow. The results indicate that this indeed is the case for the lower half of the flow range, but that the loss increases again at higher flows where the boundary layer on the opposing wall moves toward separation. In most cases the loss in the flow field containing a "near-separated" boundary layer is somewhat higher than that for the other flow field but both flow field losses are higher than those for which neither boundary layer is close to separation (i.e.

when the outlet profile is "symmetrical"). This confirms that losses are associated with radial distortion of flow in the pre-diffuser. Integration of the boundary layer flows at inlet and outlet shows that under extreme conditions (e.g. a high flow split combined with a small dump gap) up to 20% of the outer boundary layer flow is transferred to the inner boundary layer. The situation is reversed at low flow splits and in both cases it is the near-separated boundary layer that accumulates flow. There is therefore a considerable interchange of turbulent energy under these conditions and it is this that leads to the high loss throughout the flow. It would appear that the relatively localised effect of separation does not, in itself, strongly influence the loss.

Comparison of the curves in Figs. 5-2-6 and 5-2-2/4 indicates that the pre-diffuser loss has only a small influence on the behaviour of the overall loss with changing flow. The reversal in slope of the overall loss curves with changing dump gap (noted in Sect. 5-3-1) is therefore not directly attributable to variations in pre-diffuser loss.

#### 5-3-4 Discussion of Dump Region Losses

In so far as the trends of dump region loss with flow can be established (Fig. 5-2-7), they do appear to follow those for the overall loss (i.e. a decrease with flow for large dump gaps and vice-versa for small dump gaps). Some appreciation of the loss characteristics can be obtained by considering the flow conditions in the dump region. For small dump gaps there is a strong acceleration over the head and the experimental results indicate that at the design flow, the mean velocity in the outer flow field at Stn. 3 rises to a value approximately equal to that at pre-diffuser inlet. Under these conditions there is a high radial velocity gradient near the wall at pre-diffuser outlet and this implies a high energy transfer to the vortex region (see Fig. 5-3-1(a)). Estimates of the energy dissipated in the vortex indicate that up to half the dump

region loss (3 to 4%) can be attributed to the energy required in sustaining the vortex and that this increases as the annulus flow increases. This factor, combined with the increased dynamic pressure at the higher flows, accounts for the increase in loss with flow for small dump gaps.

For large dump gaps the flow conditions are modified due to the increased volume of the dump region (see Fig. 5-3-1(b)). The flow continues to diffuse downstream of the pre-diffuser and only subsequently accelerates over the head. It is reasonable to assume that the amount of diffusion increases as the flow decreases. The associated increase in turbulent mixing is considered to account for the increase in loss with decreasing flow. When expressed as a function of local entry conditions (i.e. as  $(\Delta \bar{P}_{2-3})_0 / \alpha_{2_0} \frac{1}{2} \rho \bar{u}_{2_0}^2$ ) the outer flow field loss coefficients are increased by a factor varying between 2.5 at low flows and 1.5 at high flows. Expressed in this way the loss coefficients show a predominant trend of decreasing with increasing flow. Thus, at low flows, the increase in diffusion coupled with the inferior outlet conditions from the pre-diffuser combine to produce an increase in dump region losses.

#### 5-3-5 Discussion of Settling Length Losses

The experimental results (Fig. 5-2-8) indicate that a large proportion of the overall flow field loss occurs in the settling length. In broad terms this can be attributed to the high dynamic pressures at Stn. 3 and the large amount of diffusion and associated mixing that occurs as the flow turns into the parallel walled section. The increase in loss with flow for small dump gaps can be attributed to these effects. There are no marked trends with flow for the intermediate and large dump gaps and it is therefore concluded that variations in overall loss are related more to the changes in dump region and pre-diffuser loss at the larger dump gaps.

Typical results for the further division of losses in the settling length are given in Fig. 5-3-2. There is clear evidence to show that the

majority of loss is attributable to the 50% of flow adjacent to the combustion chamber wall. Some results show gains in total pressure for the casing wall flow of up to 9%, thus indicating that energy is transferred to this region from the flow adjacent to the combustion chamber wall. The velocity profiles at Stns. 3 and 4 (see Figs. 4-3-1/3 & 5-2-1 for examples) indicated that the amount of diffusion is far greater near the combustion chamber wall than the casing wall. This is supported by the static pressure distributions given in Figs. 4-4-1/8. The rapid local diffusion and radial energy transfer therefore combine to produce a high loss in the flow adjacent to the combustion chamber.

#### 5-3-6 Stability of Settling Length Flows

##### (i) Local Instability

In certain cases where the annulus flow was low, significant fluctuations in total pressure were observed in the flow at Stn. 3. To assist in assessing the significance of this, the velocity profile was measured during two tests (3-1223 and 3-1208) at a plane approximately midway between Stns. 3 & 4. This permitted a further breakdown of losses and the results are given in Fig. 5-3-3. It can be seen that the bulk of loss occurs in the initial region of rapid diffusion and that little loss occurs in the downstream section where the change in velocity profile is small. In the two low flow cases (3-1223 inner annulus, 3-1208 outer annulus) the peak velocity shifts from the combustion chamber wall to near the casing wall, whereas in the other two cases all three profiles show a steady progression toward more uniform flow. This suggests that the flow near the head becomes unstable under certain conditions and a rapid re-distribution of flow occurs. In assessing this, a suitable criterion for the stability of a velocity profile in a radial field is that due to Wattendorf<sup>(18)</sup>. This states that unstable flow is likely to occur if  $d(uR)/dR < 0$ . Applying this criterion to the profiles measured at Stn. 3

indicates that they are potentially unstable under all conditions.

However, the profiles obtained at low flows are more prone to instability as demonstrated by the following examples.

$$\text{Test 3-1208, outer (low flow): } d\left(\frac{u}{U} R\right)/dR = -1.95$$

$$\text{Test 3-1223, outer (high flow): } d\left(\frac{u}{U} R\right)/dR = -0.7$$

The profiles shown in Fig. 5-3-3 suggest that the effect of such instability only becomes significant at low flows where the corresponding pre-diffuser outlet boundary layer is separated. The observed fluctuations in total pressure at Stn. 3 indicate that the instability manifests itself as an increase in large scale turbulent mixing. It may be noted that the flow at Stn. 4 is not affected except in that the profile peak is shifted towards the casing wall. In view of the trends in radial distortion of the settling length velocity profiles (see Sect. 4-3 and Appendix 7) it can reasonably be assumed that the local instability described above also occurs at low flows for the smaller dump gaps.

Having established the manner in which conditions change with flow, it is now appropriate to consider the settling length losses as a function of the dynamic pressure at Stn. 3. Results for the outer flow field are given in Fig. 5-3-4, where the loss coefficient is defined,

$$(\tilde{\lambda}_{3-4})_0 = \left( \frac{\Delta \tilde{P}_{3-4}}{\alpha_3 \frac{1}{2} \rho \bar{u}_3^2} \right)_0 = \frac{\Delta \tilde{P}_{3-4}_0}{\tilde{q}_3}_0 \quad 5-3-2$$

It can be seen that there is a predominant trend of decreasing loss coefficient with increasing flow. Calculations show that the mean velocity reduction (and hence by continuity the area ratio,  $A_4/A_3$ ) does not change significantly with flow for a particular dump gap. Thus, the increase in loss coefficient (Eqn. 5-3-2) at low flows can be attributed to the increase in profile deformation (i.e. radial transfer of momentum) and the increased turbulent mixing associated with local instability of the flow near the head.

(ii) General Instability

No general instability of the system (e.g. oscillations of high and low flow in the settling lengths) was observed during any of the tests carried out. It is, however, of interest to consider the "margin" of stability for the system. In order to obtain a symptomatic assessment of this, the stability parameter put forward by Ehrich<sup>(16)</sup> (see Sect. 1-6) may be used in the form,

$$\gamma = \left[ \frac{\partial C_{p4_i}}{\partial (Q_{4_i}/Q_1)} + \frac{\partial C_{p4_o}}{\partial (Q_{4_o}/Q_1)} \right]$$

where  $\gamma$  is negative for a stable system and positive for an unstable system. Typical curves of pressure recovery versus flow are given in Fig. 5-3-5. It may be noted that the slopes of the curves for the inner and outer annuli are both negative over most of the flow range. The pressure recovery versus flow characteristics have been analysed and values of  $\gamma$  determined for a variety of cases. The most significant result of this analysis is that the stability margin decreases with increasing dump gap. An example of the variation in  $\gamma$  with dump gap is given in Fig. 5-3-6. The decrease in margin at large dump gaps is considered to be due to the change in the loss versus flow characteristics noted in Sect. 5-3-1. For small dump gaps the flow field loss increases with flow thus giving relatively high negative values of  $\partial C_{p4}/\partial Q$ . However, for large dump gaps the loss decreases with flow and values of  $\partial C_{p4}/\partial Q$  are therefore less negative. In order to gain the maximum margin of stability, systems should therefore be designed with the minimum dump gap consistent with achieving the required performance.



Fig.5-1-1 DIVISION OF LOSSES.

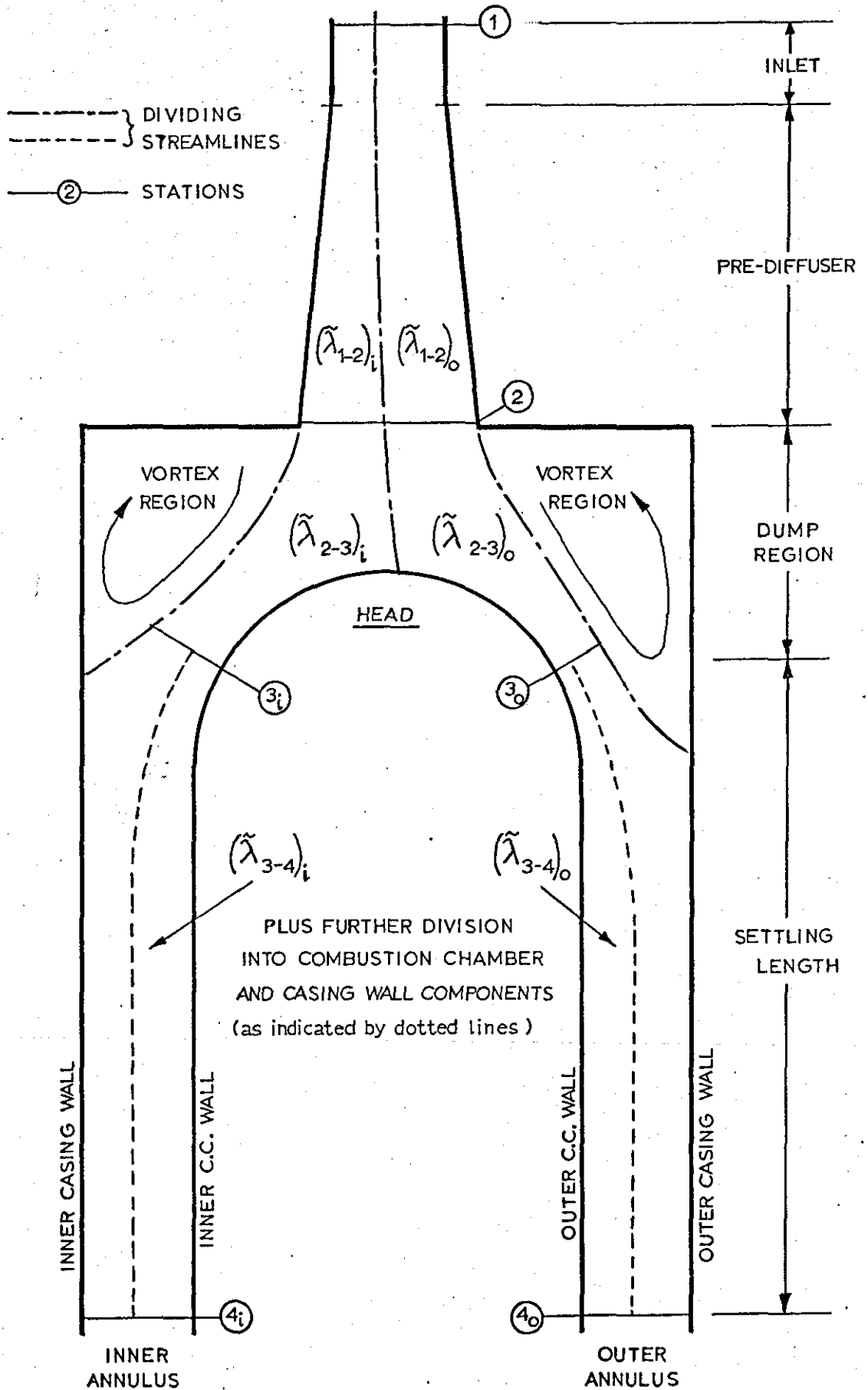
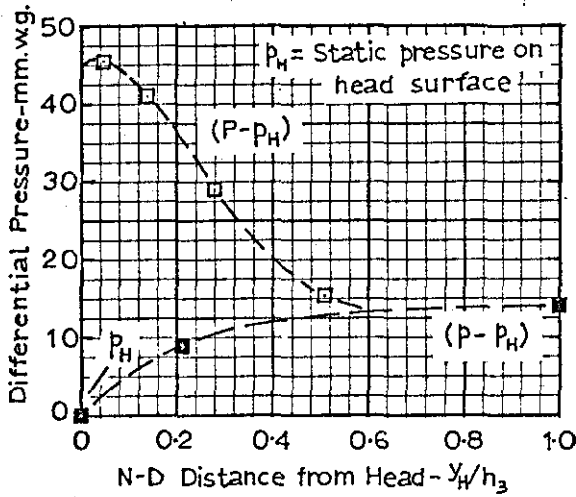
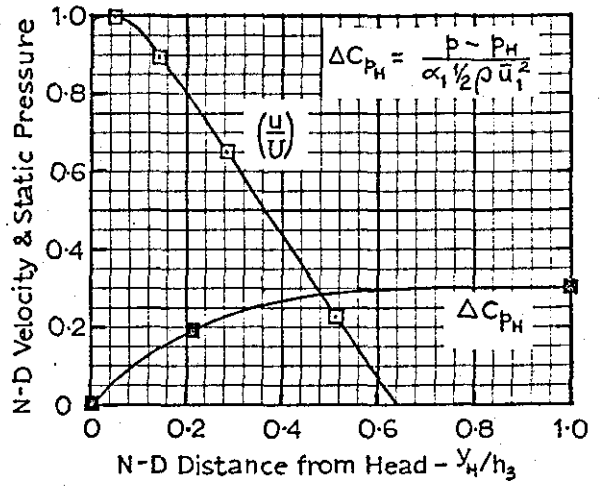


Fig 5-1-2 ANALYSIS OF HEAD RAKE DATA.



(a) MEASURED PRESSURES



(b) NON-DIMENSIONAL PROFILES

Fig 5-1-3 TYPICAL FLOW PATTERN IN DUMP REGION.

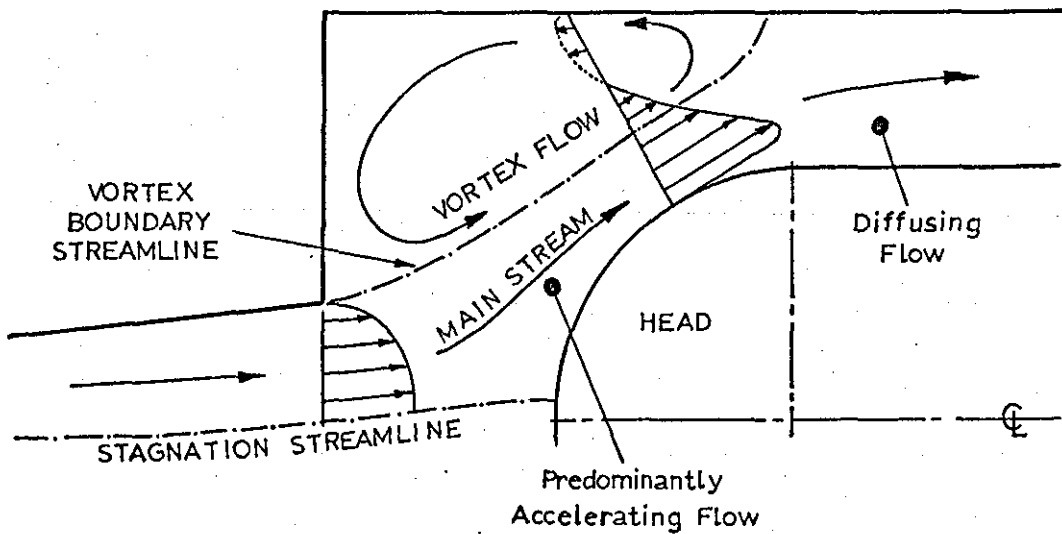


Fig.5-2-1 HEAD STATIC PRESSURE AND VELOCITY PROFILES  
FOR TEST SERIES 4-12.

DIFFUSER 4 (AR=1.8, 2φ=18°, D/h<sub>2</sub>=1.2 .

S/S = Vortex boundary streamline position.

UH/U1 = (U<sub>3</sub>/U<sub>1</sub>) = Ratio of max. velocity over head to max. inlet velocity.

$\Delta\text{CPH} = \frac{P - P_H}{\alpha_{1/2} \rho \bar{u}_1^2}$  = Change in pressure recovery across annulus.

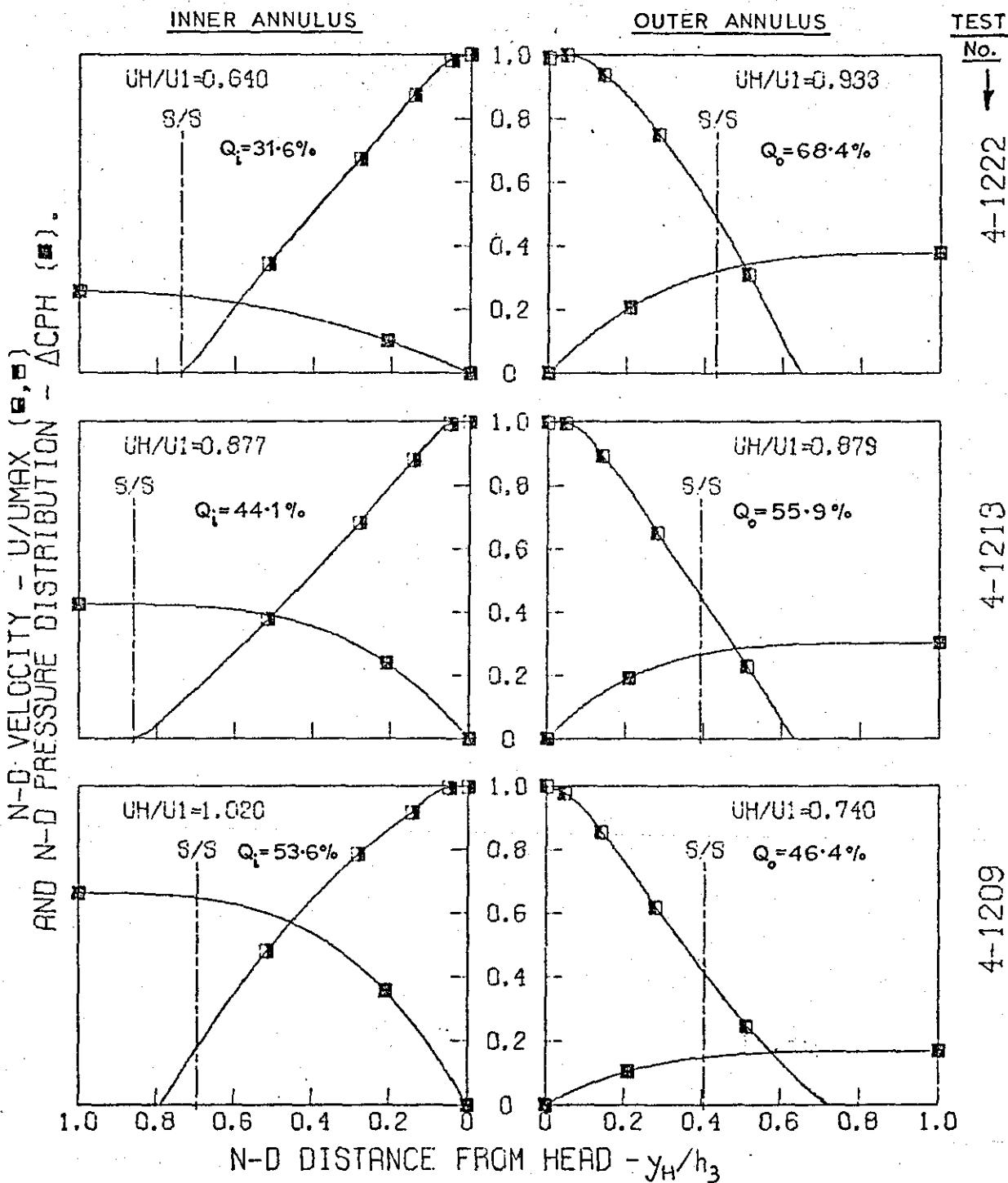


Fig.5-2-2 OVERALL FLOW FIELD LOSS versus FLOW

SMALL DUMP GAPS

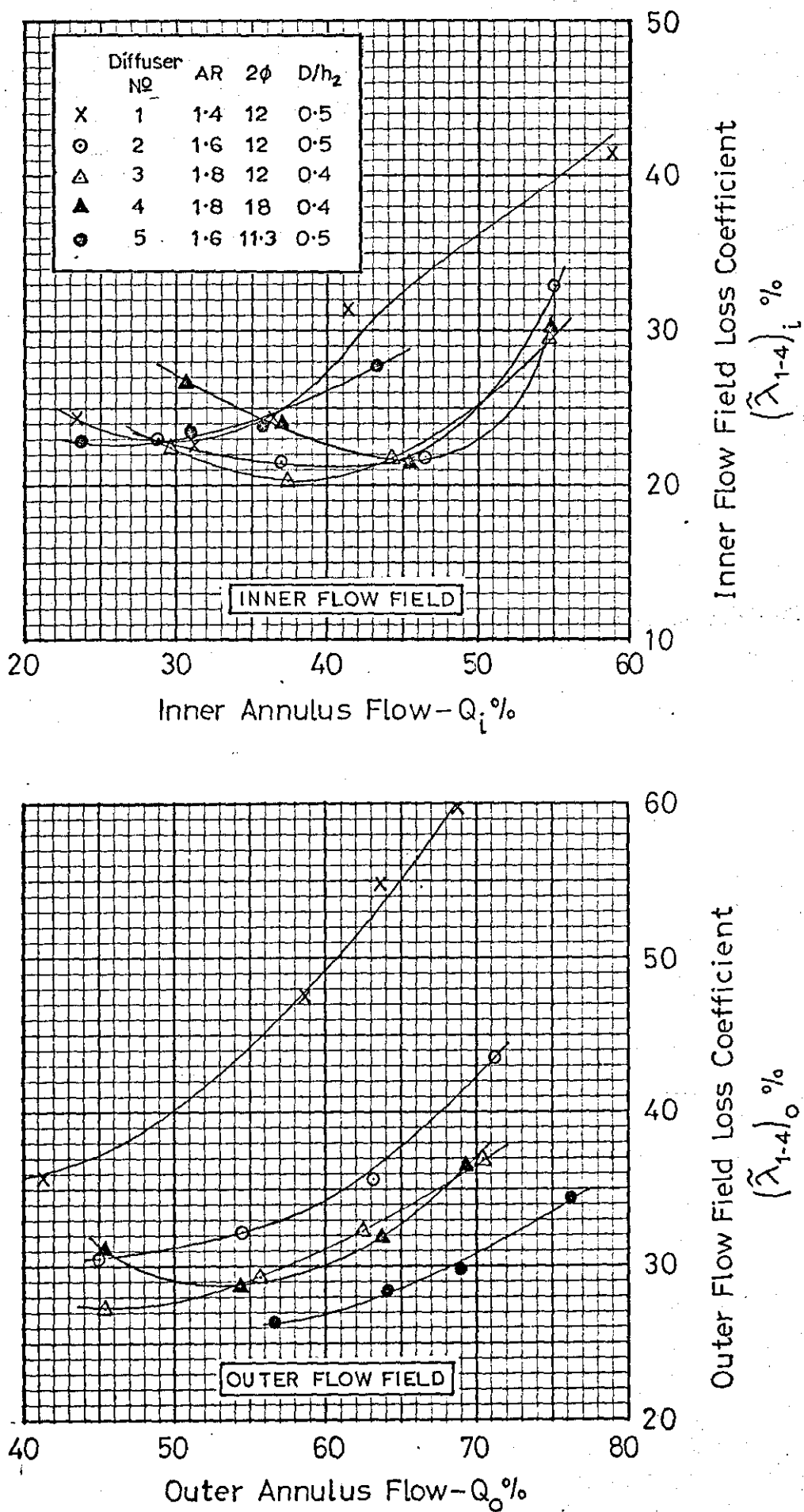


Fig.5-2-3 OVERALL FLOW FIELD LOSS versus FLOW

INTERMEDIATE DUMP GAPS

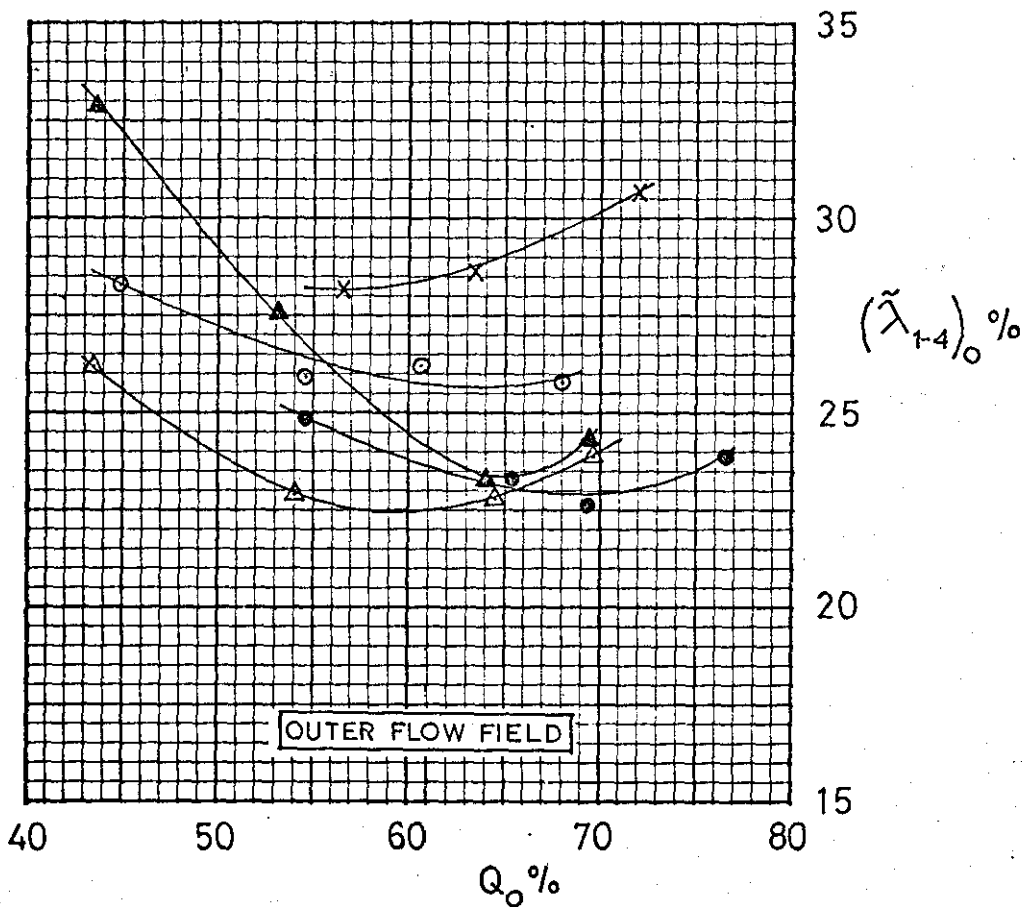
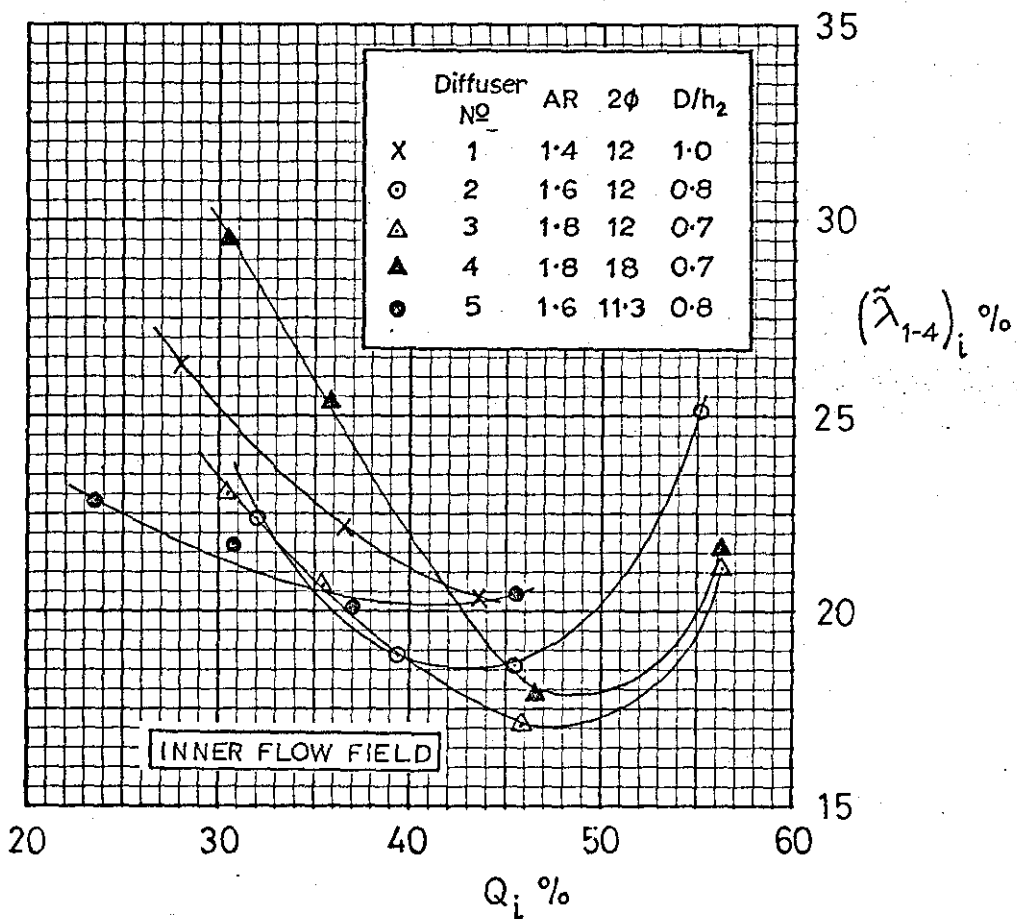


Fig.5-2-4 OVERALL FLOW FIELD LOSS versus FLOW  
LARGE DUMP GAPS

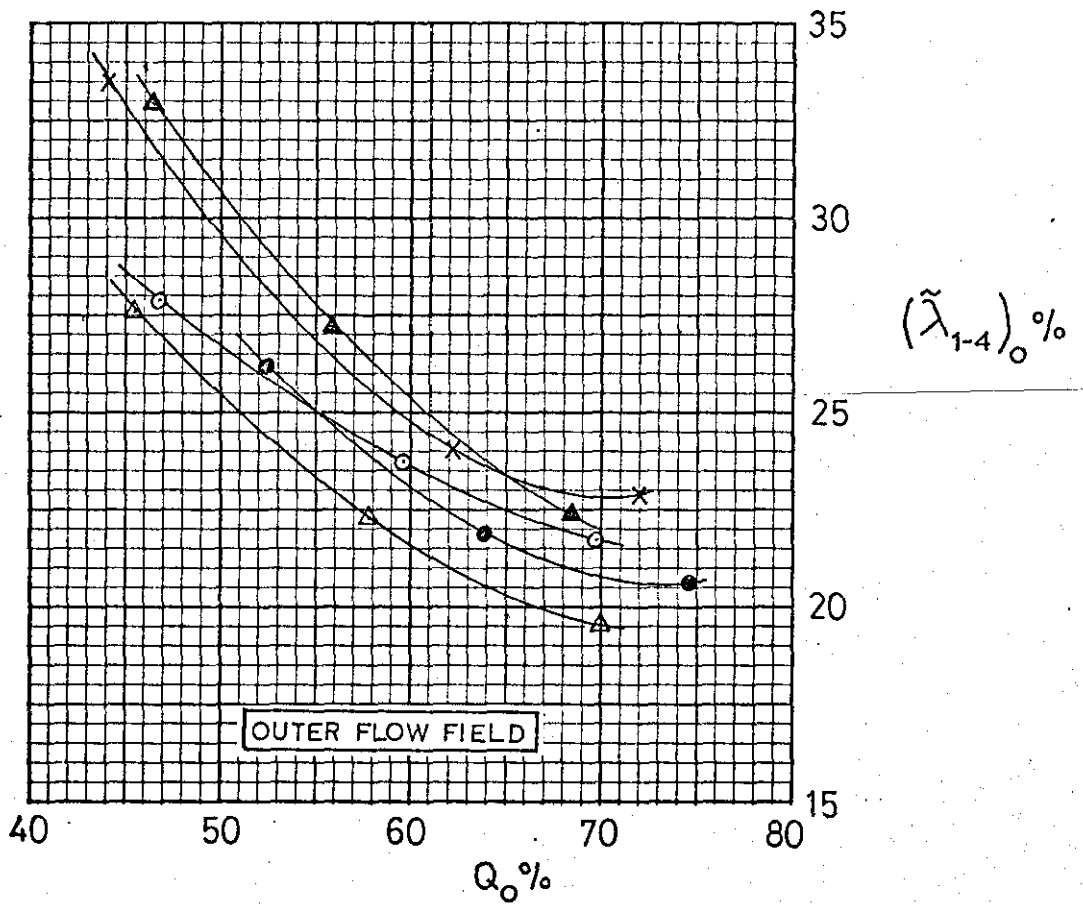
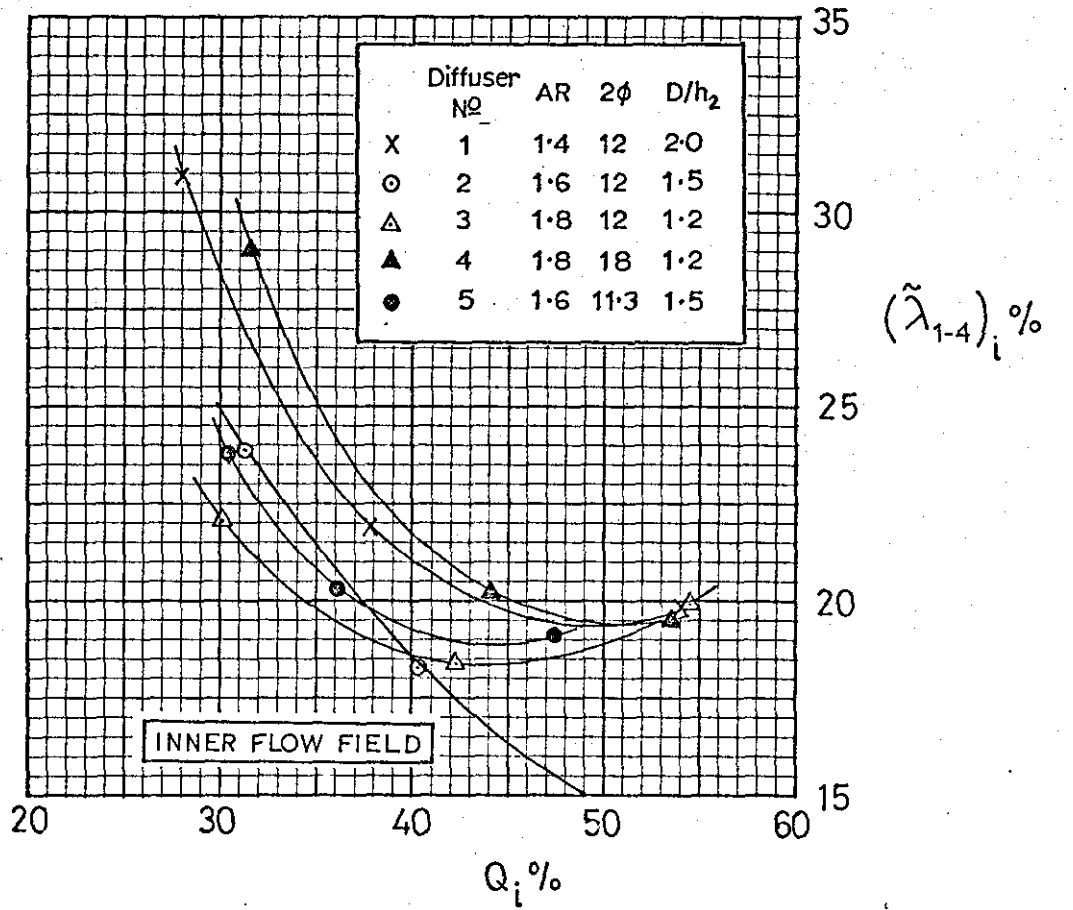


Fig.5-2-5 COMPARISON OF NET DIFFUSION IN EACH FLOW FIELD.

TYPICAL VARIATION FOR ALL PRE-DIFFUSER GEOMETRIES AND DUMP GAPS.

$$\text{REDUCTION IN KINETIC ENERGY IN INNER FLOW FIELD} = \left( \frac{\alpha_{1i} \bar{u}_{1i}^2 - \alpha_{4i} \bar{u}_{4i}^2}{\alpha_{1i} \bar{u}_{1i}^2} \right) \times 100\%$$

AND SIMILARLY FOR OUTER FLOW FIELD.

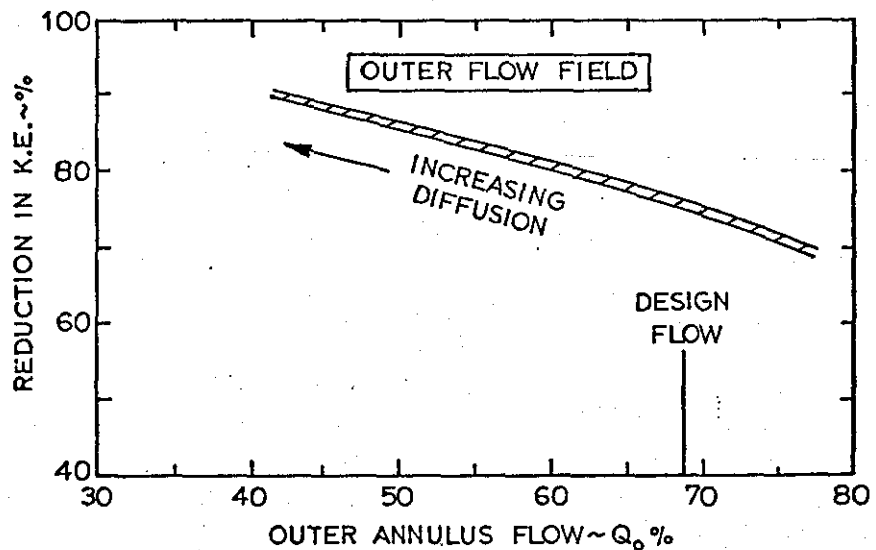
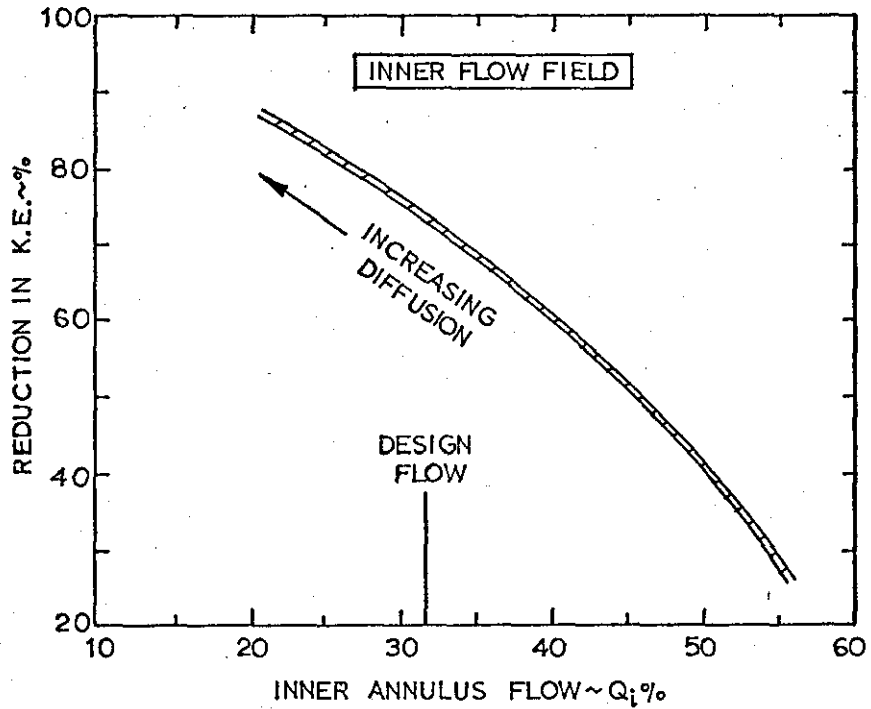
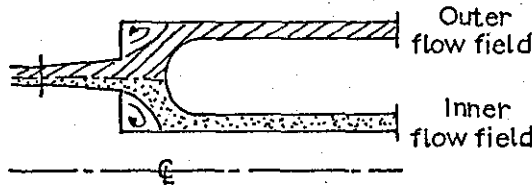


Fig. 5-2-6

LOCAL FLOW FIELD LOSS versus FLOW

(PRE-DIFFUSER)

|   | Diffuser No | AR  | 2φ   |
|---|-------------|-----|------|
| X | 1           | 1.4 | 12   |
| ○ | 2           | 1.6 | 12   |
| △ | 3           | 1.8 | 12   |
| ▲ | 4           | 1.8 | 18   |
| ● | 5           | 1.6 | 11.3 |

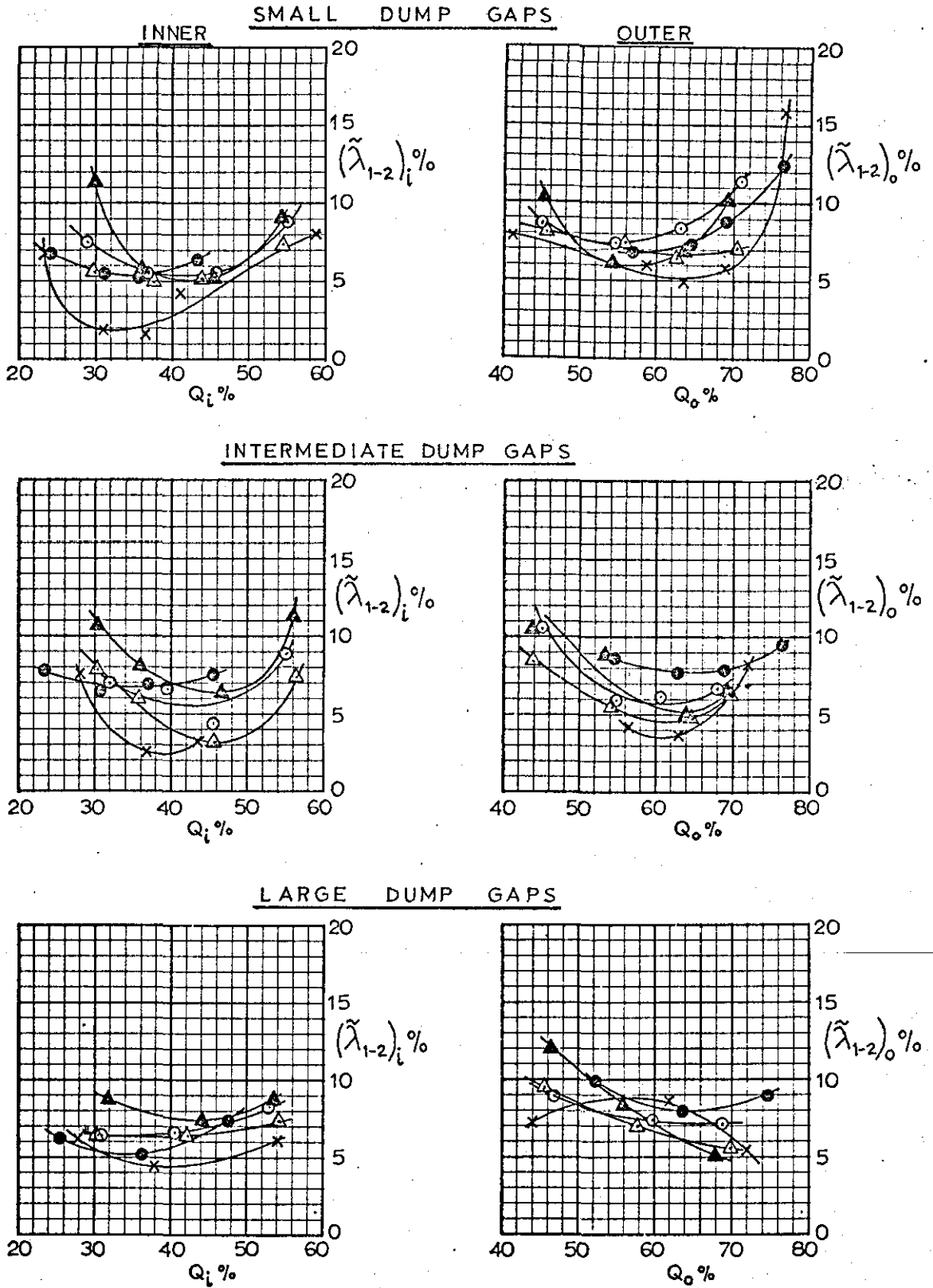




Fig. 5-2-7

LOCAL FLOW FIELD LOSS versus FLOW

(DUMP REGION)

|   | Diffuser No. | AR  | 2φ   |
|---|--------------|-----|------|
| X | 1            | 1.4 | 12   |
| ○ | 2            | 1.6 | 12   |
| △ | 3            | 1.8 | 12   |
| ▲ | 4            | 1.8 | 18   |
| ● | 5            | 1.6 | 11.3 |

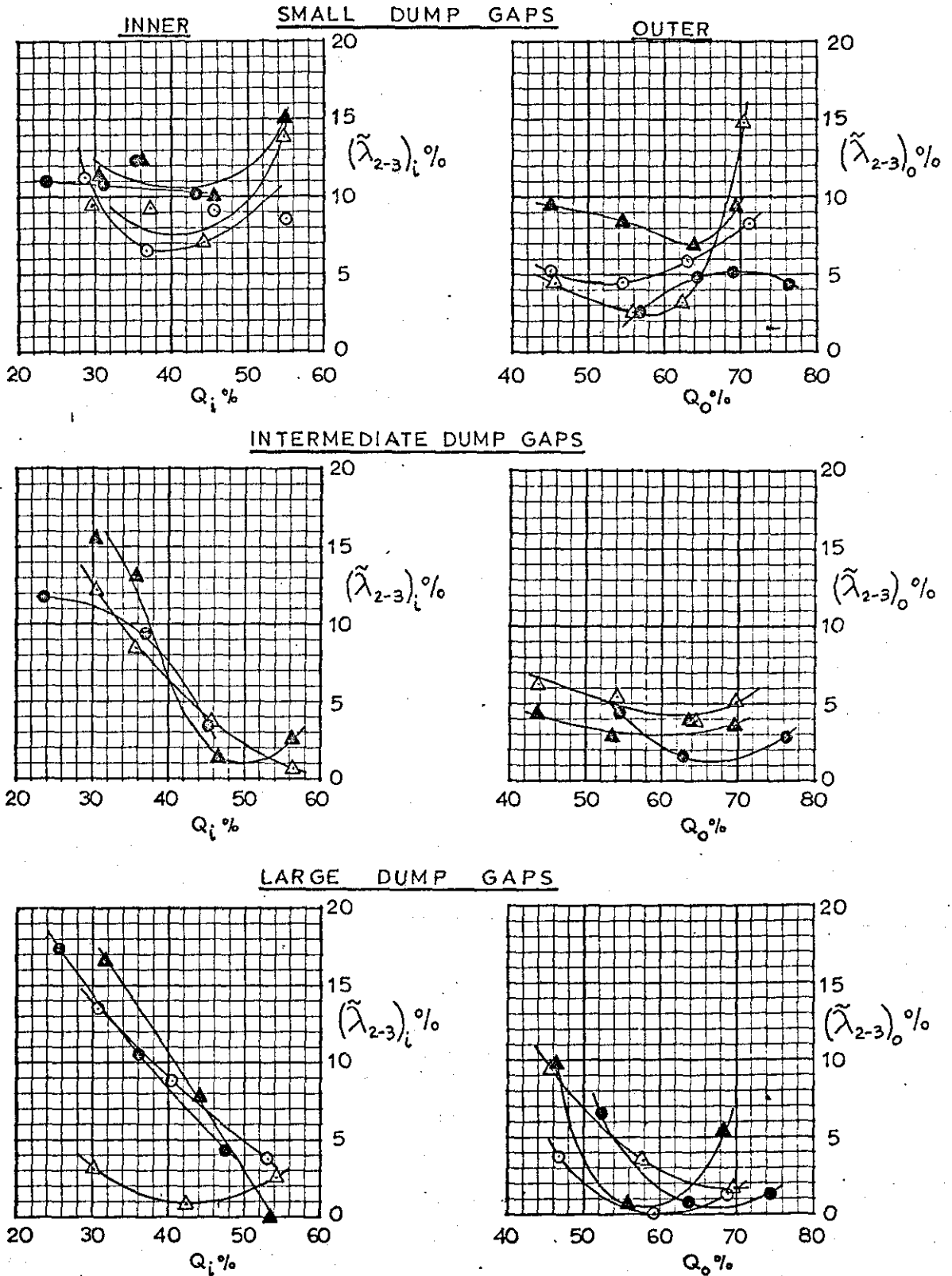


Fig. 5-2-8

LOCAL FLOW FIELD LOSS versus FLOW

(SETTLING LENGTH)

|   | Diffuser No | AR  | 2φ   |
|---|-------------|-----|------|
| X | 1           | 1.4 | 12   |
| ○ | 2           | 1.6 | 12   |
| △ | 3           | 1.8 | 12   |
| ▲ | 4           | 1.8 | 18   |
| ● | 5           | 1.6 | 11.3 |

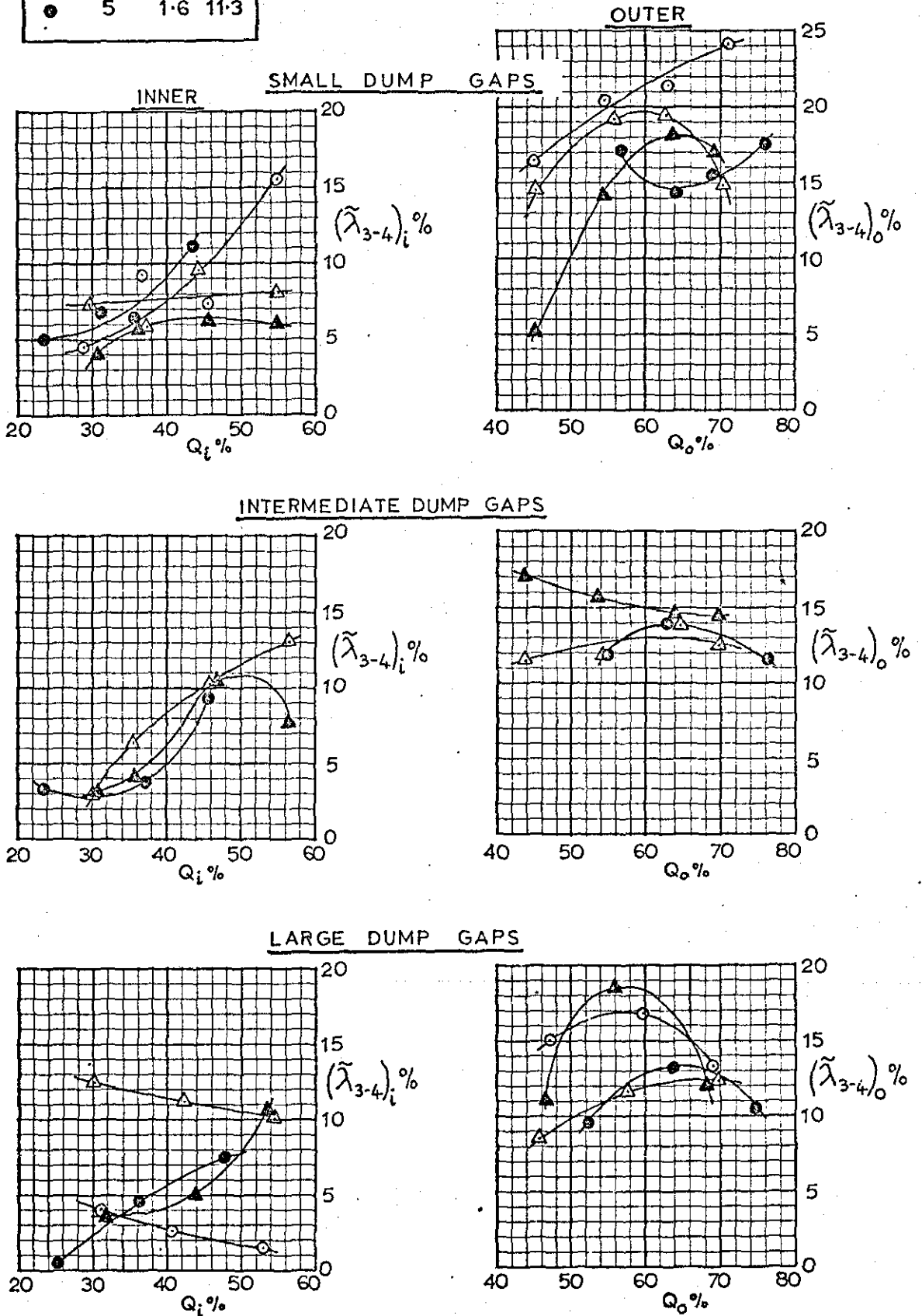
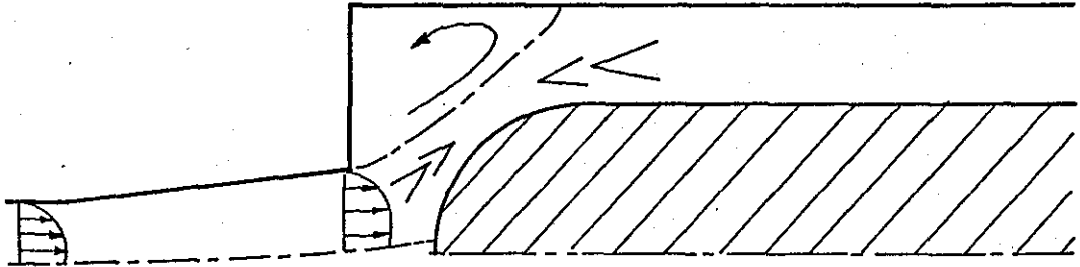


Fig.5-3-1 COMPARISON OF FLOW CONDITIONS IN DUMP REGION FOR SMALL AND LARGE DUMP GAPS.

- > Indicates local acceleration
- < Indicates local diffusion

(a) SMALL DUMP GAP (High loss case: high annulus flow)



(b) LARGE DUMP GAP (High loss case: low annulus flow)

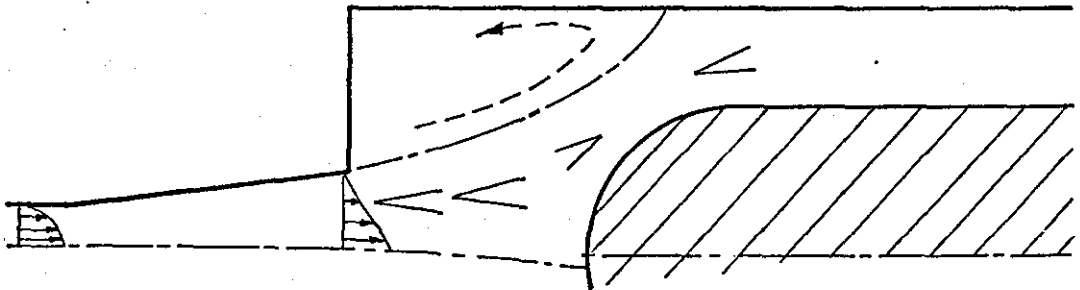


Fig.5-3-2 DIVISION OF LOCAL LOSSES IN THE OUTER ANNULUS SETTLING LENGTH (Diffusers 3,4&5)

- Small dump gaps
- ⊙ Inter. dump gaps
- Large dump gaps

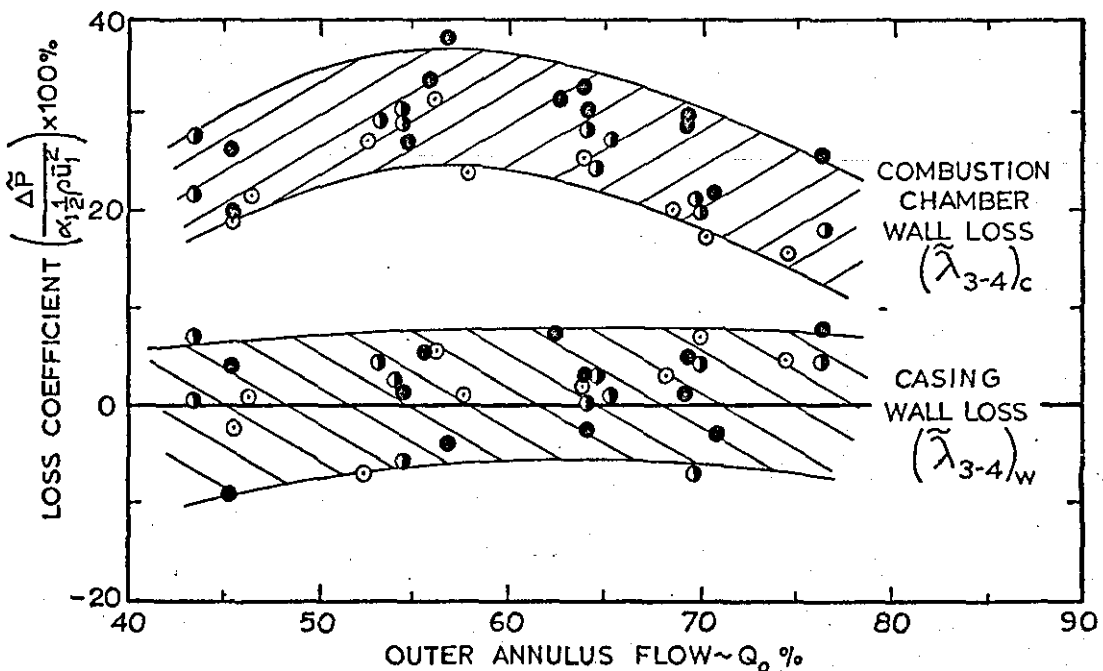
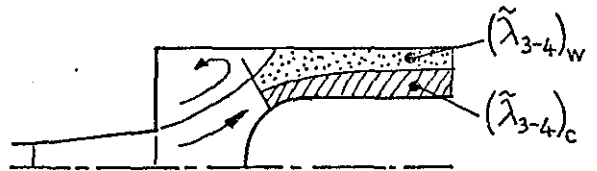


Fig. 5-3-3 SETTLING LENGTH VELOCITY PROFILES AND DIVISION OF LOSSES (Tests 3-1223 & 3-1208)

NOTE: LOCAL LOSS COEFFICIENT DEFINED AS  $\left(\frac{\Delta\tilde{P}}{\alpha_1 \frac{1}{2} \rho u_1^2}\right)$

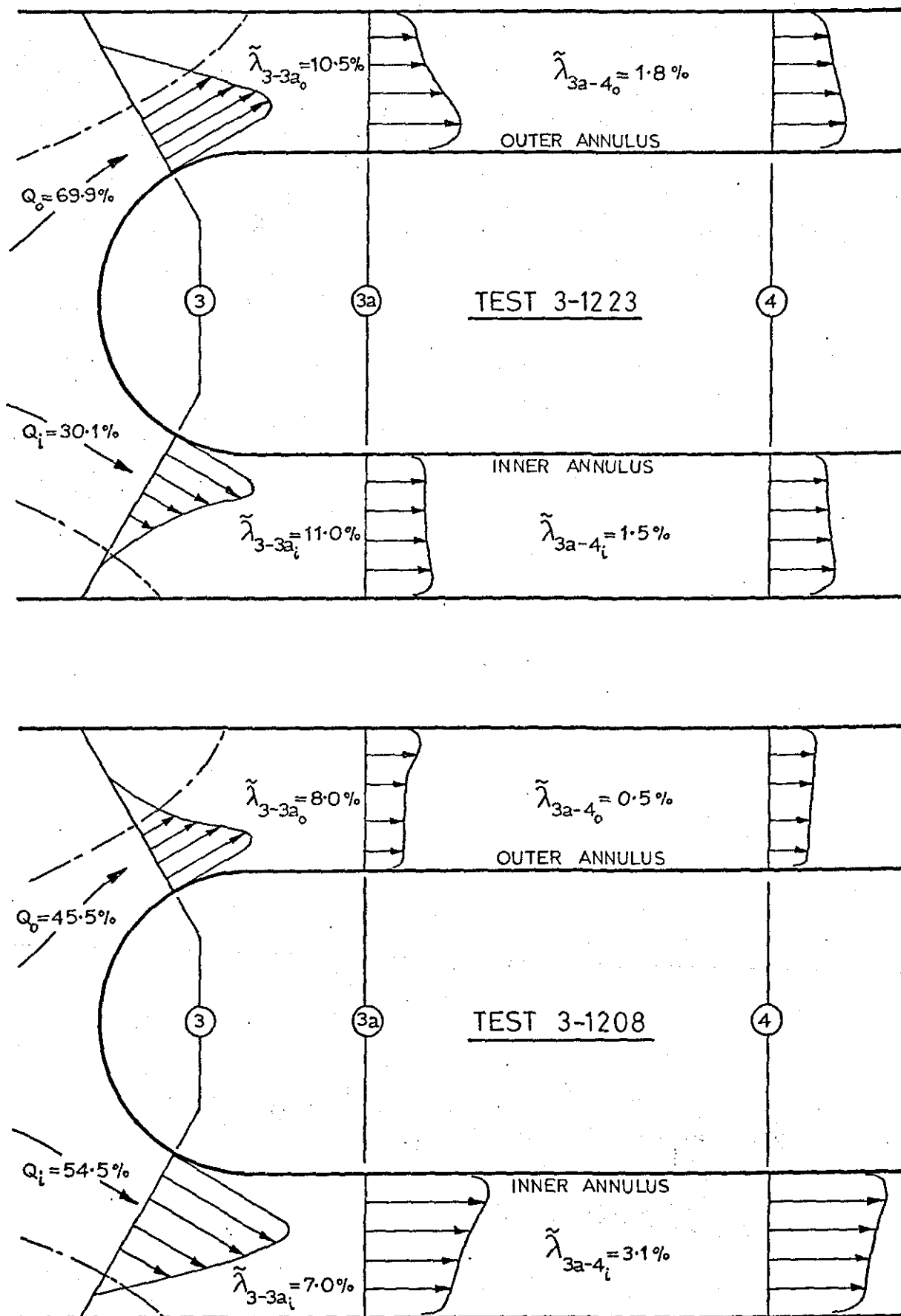


Fig.5-3-4 SETTLING LENGTH LOSSES VERSUS FLOW IN TERMS OF LOCAL ENTRY DYNAMIC PRESSURE.

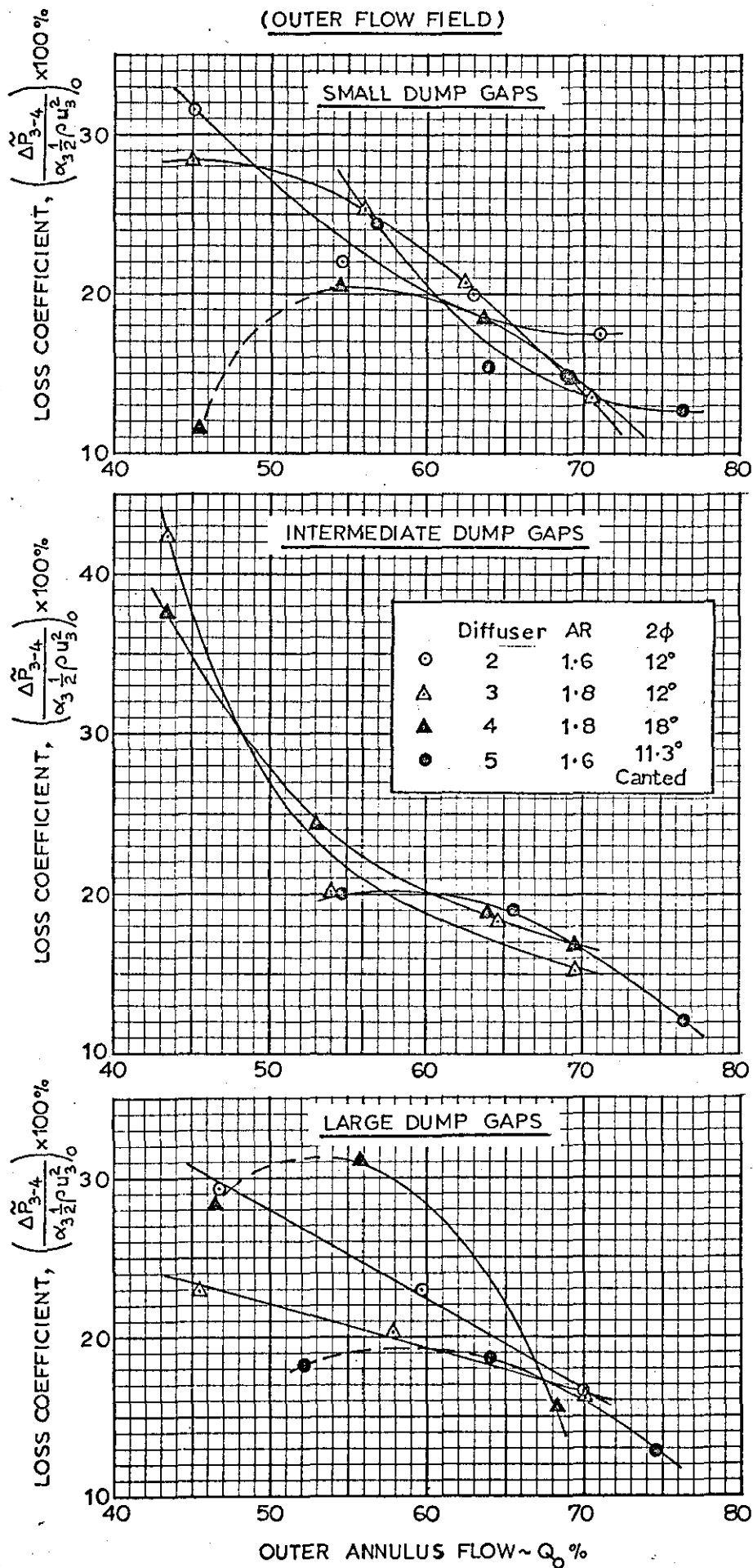


Fig.5-3-5 TYPICAL OVERALL PRESSURE RECOVERY VERSUS FLOW CHARACTERISTICS (Diffuser 3).

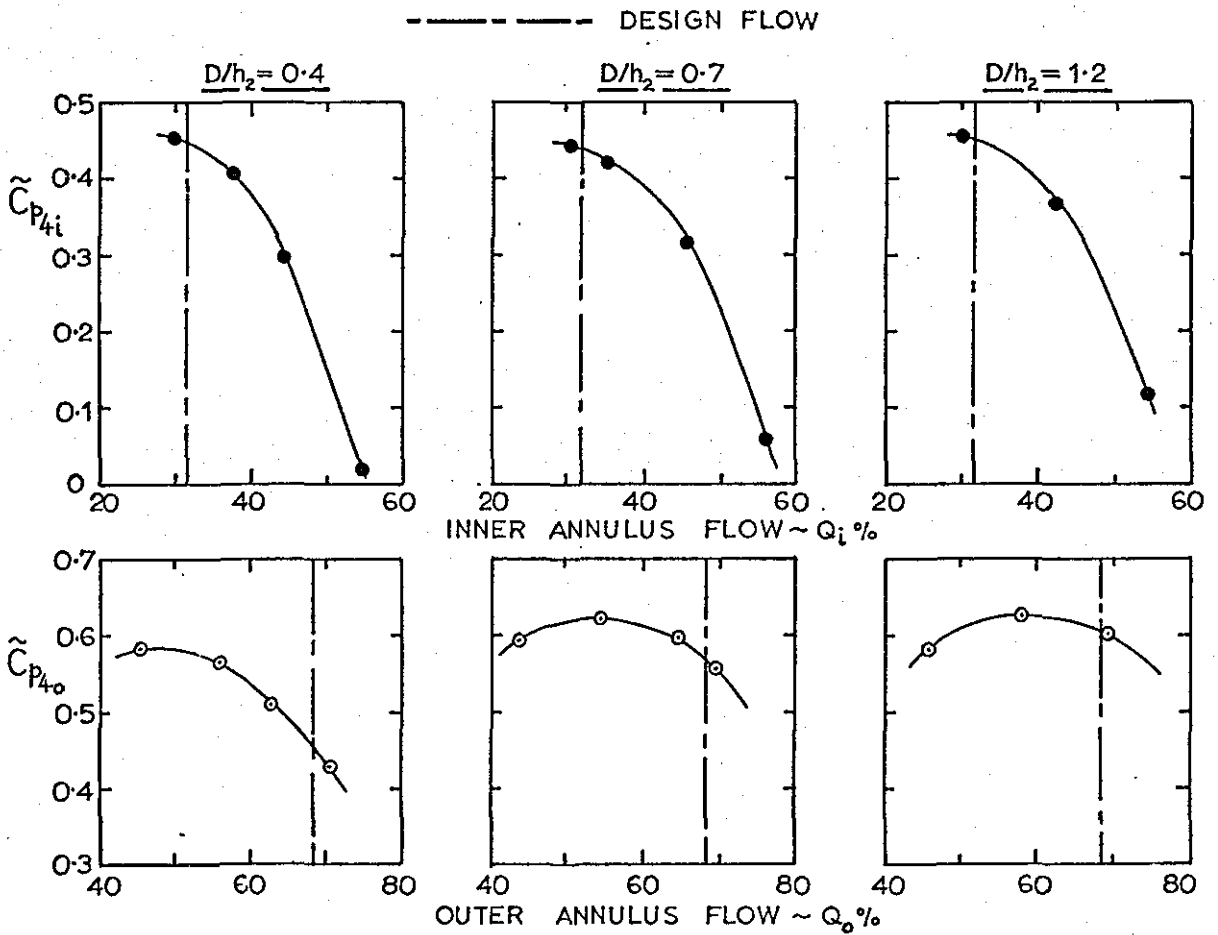
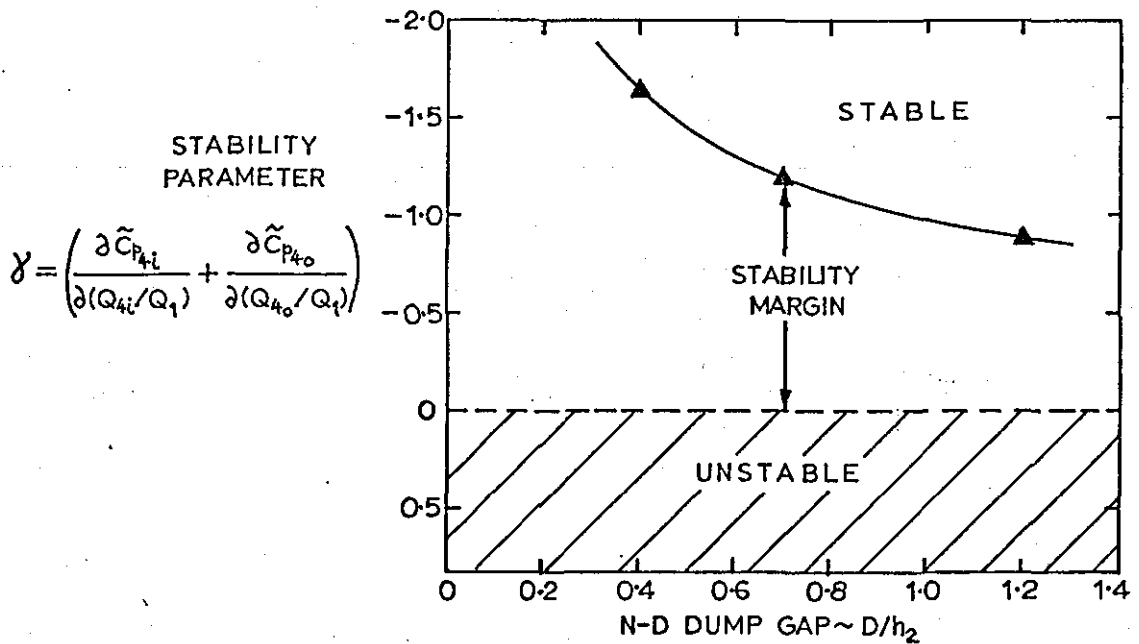


Fig.5-3-6 TYPICAL VARIATION IN OVERALL STABILITY MARGIN WITH DUMP GAP.

(Diffuser 3; Overall design flow split)



## CHAPTER 6 CONCLUSIONS AND RECOMMENDATIONS

### 6-1 CONCLUSIONS

Low speed tests have been carried out to investigate the performance of a dump diffuser system of overall geometric area ratio 2.0, having fully developed flow at inlet. The system was tested with five different pre-diffuser geometries to show the effect of increasing the area ratio, increasing the included angle and canting the pre-diffuser. For each pre-diffuser geometry the influences of varying the flow split and dump gap were investigated. In addition to considering the overall performance characteristics, the pressure losses for the inner and outer flow fields have been determined and the losses further sub-divided in order to identify regions of high loss.

#### 6-1-1 Overall Performance

The influences of flow split and dump gap on the overall performance of the system have been established and the optimum operating conditions for each of the pre-diffuser geometries have been defined. It was found that the symmetrical pre-diffusers produced severely distorted outlet velocity profiles when the system was operated at the design flow split and this was accompanied by separation on the inner wall for the 1.6 and 1.8 area ratio pre-diffusers. This was attributed to bad matching of the pre-diffuser and downstream section geometries. The overall performance and pre-diffuser flow stability were improved by canting the pre-diffuser and these results have highlighted the need for careful component matching.

The main conclusions relating to the influence of pre-diffuser geometry are summarised as follows.

- (i) Increasing the area ratio for a constant included angle of  $12^\circ$  produced improvements in the overall performance at the expense of increasing the system length and decreasing the pre-diffuser outlet flow stability.
- (ii) Increasing the included angle for a fixed area ratio of 1.8 resulted

in a significant decrease in overall performance and pre-diffuser flow stability. For the same overall system length the performance and flow stability was, under all conditions, inferior to that obtained with the 1.4 area ratio, 12° included angle pre-diffuser.

(iii) Canting the pre-diffuser resulted in a significant improvement in flow stability for flow splits close to design and a modest improvement in overall performance. It should be noted here that canting the pre-diffuser is only advantageous in cases where the overall design flow split of the system is significantly different from unity.

The upper limit of performance for systems having 12° symmetrical pre-diffusers has been established and data has been provided which enables the optimum dump gap and pre-diffuser area ratio to be obtained for any given length of system. The improvement in overall performance obtained by increasing the system length is relatively small and may in practice be offset by the tendency toward separation in the pre-diffuser. It has been shown that the pre-diffuser flow stability can be improved by decreasing the dump gap, however this is not felt to be of very great practical importance since it involves a serious penalty in overall performance.

6-1-2 Division of Losses

It has been demonstrated that the majority of the overall pressure loss can be attributed to the region of local diffusion downstream of the plane of maximum velocity over the combustion chamber head. Generally speaking the overall loss can be divided between the components of the system on a percentage basis as follows.

|                                             |     |
|---------------------------------------------|-----|
| Pre-diffuser .....                          | 25% |
| Dump region .....                           | 15% |
| Annuli surrounding combustion chamber ..... | 60% |

The analysis of losses further showed that the variation in flow field loss with flow fraction was dependent upon dump gap. For small dump gaps the loss in each flow field increased with increasing flow fraction and



vice-versa for large dump gaps. Using the stability criterion of Ehrich<sup>(16)</sup> it was shown that the stability margin for the system decreases as the dump gap is increased. This is directly attributable to the change in loss versus flow characteristics with increasing dump gap.

In broad terms the results have shown that the critical part of the system is the dump region. It is in this region that the flow accelerates over the head, thus causing a subsequent local diffusion and the generation of a large proportion of the overall loss. Any attempt to design a low loss system must therefore begin with an investigation into methods of reducing the acceleration of flow over the combustion chamber head.

#### 6-2 TOPICS FOR FUTURE RESEARCH

The present work represents a detailed investigation of the performance characteristics of a simple dump diffuser system geometry. However, there are many factors influencing performance that have not been dealt with in the present investigation. The main topics for future research are listed below.

- (i) The influence of compressor exit conditions on performance.
- (ii) The influence of head porosity on performance and flow stability.
- (iii) Further investigation of canted pre-diffusers for the present high design flow split system.
- (iv) Determination of the optimum included angle for pre-diffusers.
- (v) The effect of using curved rather than straight walled pre-diffusers.

Items (iii), (iv) and (v) would be extensions of the present work. Although these are important, it is recommended that further testing of different pre-diffuser geometries should be delayed until a better understanding of the influence of inlet conditions and head porosity has been established. Initially, therefore, the majority of future research should be concentrated on items (i) and (ii).

There are three aspects of compressor exit conditions which need to be investigated in relation to diffuser system performance, namely, radial distortion of the velocity profile, turbulence intensity and stator blade wake effects. Of these, radial distortion is likely to have the most critical effect upon performance and flow stability. An investigation into these effects is already under way at Loughborough.

The bleeding off of primary air into the combustion chamber will effectively reduce the blockage effect of the head and this should make it possible to reduce the dump gap below the optimum values determined by the present investigation. However, primary air holes are usually spaced at intervals around the combustion chamber head and this will lead to some three-dimensionality in the flow and the possibility of pockets of separated flow forming in the pre-diffuser. In view of the common occurrence of stability problems in engine combustion systems it is recommended that a detailed investigation be made of the flow conditions in the vicinity of a porous head.

---

CHAPTER 7    REFERENCES

- 1    Sovran, G. and Klomp, E.D., "Experimentally Determined Optimum Geometries for Rectilinear Diffusers with Rectangular, Conical, or Annular Cross-Section" - Fluid Mechanics of Internal Flow, Elsevier, 1967.
- 2    Livesey, J.L., "Duct Performance Parameters Considering Spacially Non-Uniform Flow" - A.I.A.A. Paper No. 72-85, 1972.
- 3    Little, B.H. and Wilbur, S.W., "Performance and Boundary Layer Data from 12-degree and 23-degree Conical Diffusers of Area Ratio 2.0 at Mach Numbers up to Choking and Reynolds Numbers up to  $7.5 \times 10^6$ " - N.A.C.A. Report 1201, 1954.
- 4    McDonald, A.T. and Fox, R.W., "An Experimental Investigation of Incompressible Flow in Conical Diffusers" - A.S.M.E. Preprint 65-FE-25, 1965.
- 5    Gurevich, D.V., "An Experimental Study of Diffusing Exit Channels in Helicopter Gas Turbines" - Helicopter Power Plant II, Oberongiz, 1959 (M.O.D. Joint Intelligence Bureau, D.S.I. Translation No. 680, 1961).
- 6    Wolf, S. and Johnston, J.P., "Effects of Non-Uniform Inlet Velocity Profiles on Flow Regimes and Performance in Two-Dimensional Diffusers" - Report PD-12, Mech. Eng. Dept., Stanford University, 1966.
- 7    Tyler, R.A. and Williamson, R.G., "Diffuser Performance with Distorted Inflow" - Proceedings of Symposium on Subsonic Fluid Flow Losses in Complex Passages and Ducts, I. Mech. E. Proceedings Vol. 182, Part 3D, 1967-68.
- 8    Bradley, C.I. and Cockrell, D.J., "The Response of Diffusers to Flow Conditions at their Inlet" - Symposium on Internal Flows, University of Salford, Paper 5, 1971.
- 9    Stevens, S.J., "Turbulent Incompressible Flow in Annular Diffusers" - Ph.D. Thesis, Loughborough University of Technology, 1970.
- 10    Williams, G.J., "The Influence of Inlet Conditions on the Boundary Layer Growth and Overall Performance of Annular Diffusers" - Ph.D. Thesis, Loughborough University of Technology, 1971.
- 11    Horlock, J.H., "Boundary Layer Problems in Axial Turbomachines" - Flow Research on Blading, Elsevier, 1970.

- 12 Howard, J.G.H., Henseler, H.J. and Thornton-Trump, A.B., "Performance and Flow Regimes for Annular Diffusers" - A.S.M.E. Preprint 67-WA/FE-21, 1967.
- 13 Henderson, F.D., "The Effect of Profile and Length on the Efficiency of Pump Diffusers" - R.P.E. Tech. Note 181, 1959.
- 14 Stevens, S.J. and Fry, P., "Measurements of the Boundary Layer Growth in Annular Diffusers" - Jnl. of Aircraft, Feb. 1973.
- 15 Fishenden, C.R., "An Investigation into Two Methods of Reducing Losses Incurred by Transverse Pipes in a Wide Angle Annular Diffuser" - B. Tech. Final Year Project, Loughborough University of Technology, 1970.
- 16 Ehrich, F.F., "Aerodynamic Stability of Branched Diffusers" - A.S.M.E. Paper No. 70-GT-27, 1970.
- 17 Carlson, J.J. and Johnston, J.P., "Effects of Wall Shape on Flow Regimes and Performance in Straight Two-Dimensional Diffusers" - Stanford University, Mech. Eng. Dept., Thermoscience Division, Report PD-11, 1965.
- 18 Wattendorf, F., "Study of the Effect of Curvature on Fully Developed Turbulent Flow" - Proceedings of the Royal Society, Vol. A148, 1935.
- 19 Girerd, H. and Guienne, P., "Nouvelles Sondes de Pression pour Mesures Aérodynamiques" - Compte rendu Académie Scientifique, Vol. 288, pp. 651-653, July 1949.
- 20 Stevens, S.J., "The Performance of Annular Diffusers" - Report No. TT 71 R 03, Dept. of Transport Technology, Loughborough University, 1971.
- 21 Morris, R.E., "Multiple Head Instrument for Aerodynamic Measurements" - Engineer, 1961.

APPENDICES

APPENDIX 1.  
SYSTEM AND PRE-DIFFUSER GEOMETRIES

Fig. A1-1 DIFFUSER SYSTEM GEOMETRY.

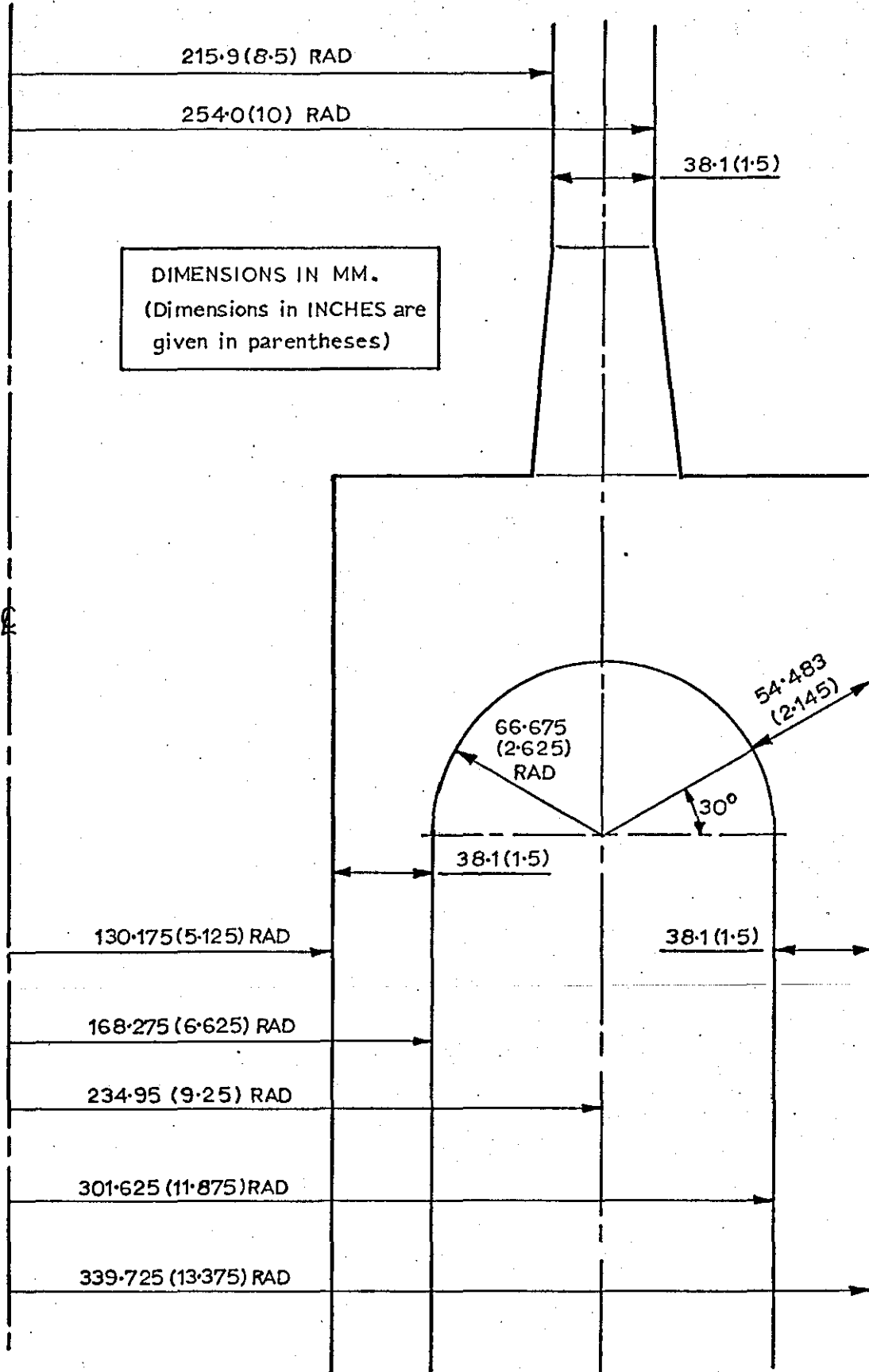
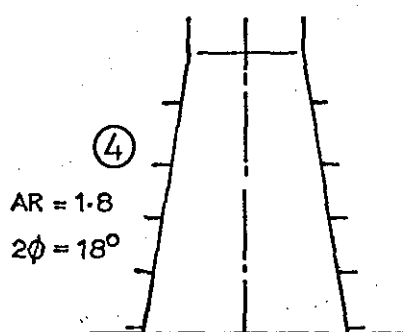
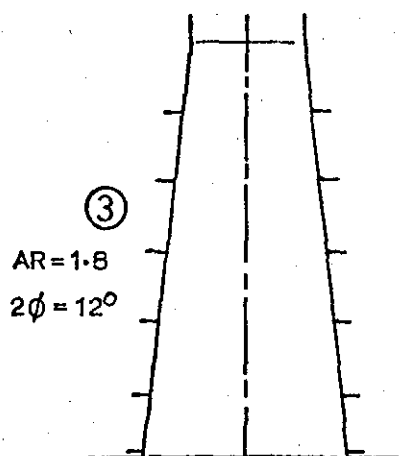
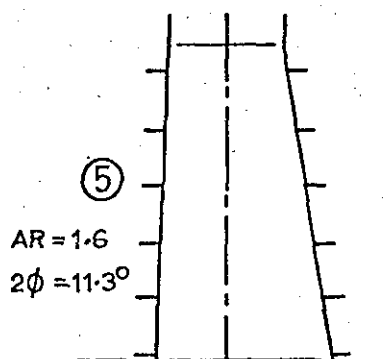
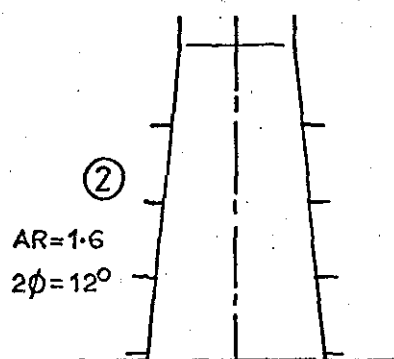
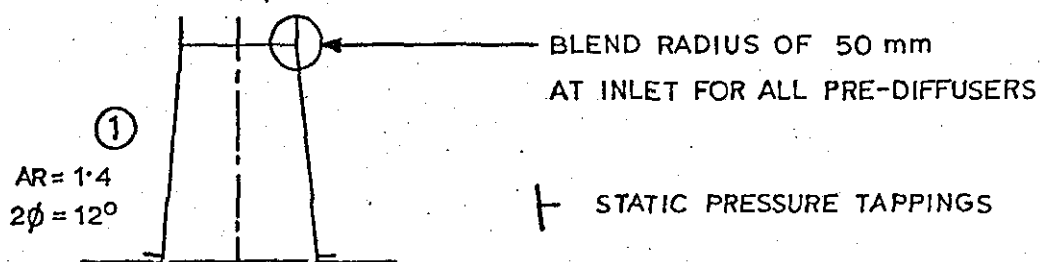


Fig. A1-2 PRE-DIFFUSER GEOMETRIES.



NOTE: Stn. 2 located 2.5 mm upstream of pre-diffuser outlet plane.

TABLE OF DIMENSIONS (MM)

| Diffuser No. | L      | $h_{\text{outlet}}$ | $R_{i,\text{outlet}}$ | $R_{o,\text{outlet}}$ | $\phi_i^\circ$ | $\phi_o^\circ$ | $\epsilon^\circ$ |
|--------------|--------|---------------------|-----------------------|-----------------------|----------------|----------------|------------------|
| 1            | 72.49  | 53.34               | 208.28                | 261.62                | 6.00           | 6.00           | 0                |
| 2            | 108.76 | 60.96               | 204.47                | 265.43                | 6.00           | 6.00           | 0                |
| 3            | 145.01 | 68.58               | 200.66                | 269.24                | 6.00           | 6.00           | 0                |
| 4            | 96.22  | 68.58               | 200.66                | 269.24                | 9.00           | 9.00           | 0                |
| 5            | 108.56 | 59.72               | 211.48                | 271.20                | 2.33           | 9.00           | 3.33             |

APPENDIX 2 CALIBRATIONS

A2-1 INLET CONDITIONS

(i) Velocity Fluctuations

During preliminary running of the test rig low frequency fluctuations in flow were observed at the inlet station. The fluctuations were reduced to an acceptable level by modifying the intake flare. Typical dynamic pressure traces obtained with the original and modified intakes are shown in Fig. A2-1. The velocity fluctuations were reduced from approximately  $\pm 2\%$  to  $\pm \frac{1}{2}\%$  and the circumferential symmetry improved from  $\pm 3\%$  to  $\pm 1\%$ .

(ii) Influence of Downstream Conditions

Two tests were carried out to assess the influence of flow split on the inlet velocity profile under extreme conditions (see Fig. A2-2). The variation in profile was considered to be within experimental error. No detectable difference in static pressure between the inner and outer wall tappings was observed under either condition and it was concluded that the inlet conditions were effectively independent of downstream conditions.

A2-2 PRESSURE PROBE CALIBRATIONS

(i) Pitot Probes

The pitot probes were calibrated against an N.P.L. standard pitot-static probe in a low speed wind tunnel. The probes were found to be accurate to within 1% of free stream dynamic pressure at zero incidence and to within 3% at an incidence of  $10^\circ$  (considered to be the maximum which would be encountered at pre-diffuser exit).

(ii) Wedge Static Probes

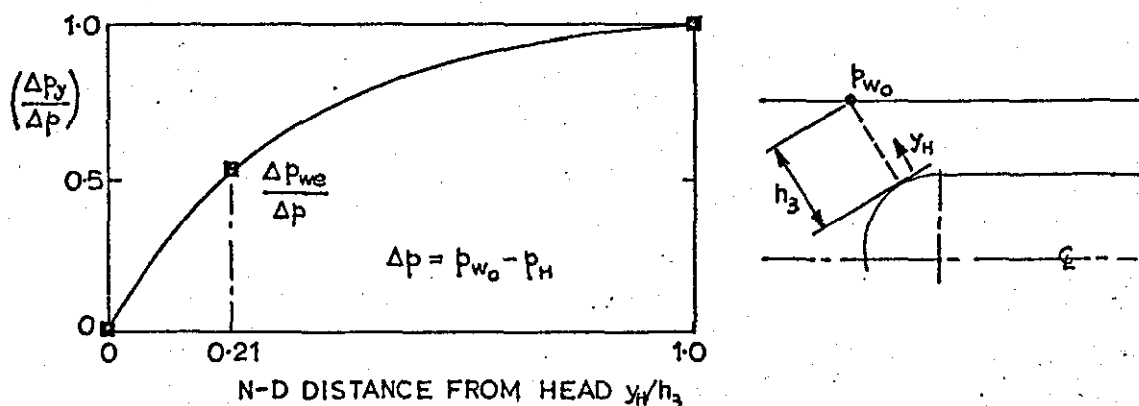
The miniature wedge static and pitot/wedge static combination probes were constructed according to designs developed by Girerd & Guienne<sup>(19)</sup> and Morris<sup>(21)</sup> respectively. The wedge statics were assumed insensitive to changes in flow direction in the plane of the wedge but were calibrated for changes in incidence perpendicular to the wedge (see Fig. A2-3).



It was considered that the probes could be aligned with the flow to within  $\pm 3^\circ$  and over this range the maximum error was  $\pm \frac{0}{3}\%$ . In view of the small errors and the likelihood that high turbulence in the pre-diffuser exit plane would produce higher readings, no corrections were applied to the experimental measurements.

(iii) Head Rakes

The accuracy of the outer annulus head rake probes was checked by comparing readings with those taken from pitot and wedge static probes traversed in the same plane. A sample set of data is given in Fig. A2-4 from which it can be seen that the measurements are in good agreement. The static pressure traverse measurements were used as a basis for determining a suitable curve fit for obtaining the static pressure profile from the three static pressures normally measured.



A suitable equation for non-dimensional static pressure difference (see diagram above) was found to be,

$$\frac{\Delta p_y}{\Delta p} = 1 - (1 - y_H/h_3)^n \quad \text{A2-1}$$

where the index,  $n$  is determined from the wedge static pressure reading,  $\Delta p_{we}$  such that,

$$n = \log \left( 1 - \frac{\Delta p_{we}}{\Delta p} \right) / \log (a) \quad \text{A2-2}$$

where  $a = (1 - y_{we}/h_3) = 0.79$

The static pressure profile calculated from Eqns. A2-1/2 is shown in Fig. A2-4 and it can be seen that it agrees closely with the traverse data.

### A2-3 PRE-DIFFUSER OUTLET CONDITIONS

Comparative measurements of the outlet velocity profile were carried out for Test 1-1026/CT using three different methods:

- (i) separate pitot and wedge static probe traverses
- (ii) pitot/wedge static combination probe traverse
- and (iii) D.I.S.A. constant temperature hot wire anemometer traverse.

The results are compared in Fig. A2-5 and it can be seen that there is good agreement between the data. The circumferential symmetry of the velocity profiles (see Fig. 4-2-1) and the static pressure profiles (see Fig. A2-5) was considered excellent. The circumferential variation in static pressure was  $\pm \frac{1}{2}\% \tilde{q}_1$  for the inner wall and  $\pm \frac{3}{4}\% \tilde{q}_1$  for the outer wall. Integration of the mean velocity profile indicated an excess in volume flow relative to that calculated at inlet of + 2.6%, this being consistent with the higher level of turbulence in the pre-diffuser outlet plane. On the strength of these results it was considered sufficient to take traverses at only one circumferential position for the majority of tests, but to check the circumferential symmetry for each new pre-diffuser geometry.

### A2-4 SETTLING LENGTH CONDITIONS

The velocity profiles in the inner and outer annuli were measured at various circumferential positions as shown in Fig. A2-6. It was only possible to traverse in the inner annulus by means of the special traverse gear (see Fig. 2-2-1), however two three-probe rakes were provided in order to check the symmetry of flow. In view of the good symmetry, and the near-uniformity of flow (see Fig. A2-6), it was considered sufficient to measure the velocity profile at one circumferential position for each test.

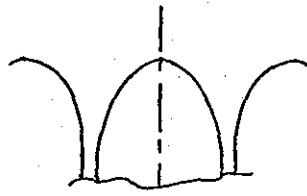
The circumferential variation in static pressure was  $\pm 1\% \tilde{q}_1$  in the inner annulus and  $\pm 1\frac{1}{2}\% \tilde{q}_1$  in the outer annulus. It was therefore decided that the inner and outer annulus static pressures at the three circumferential positions should be measured in order to obtain mean values for each test.

---

Fig.A2-1 COMPARISON OF INLET DYNAMIC PRESSURE FLUCTUATIONS.

Traces taken on Sanbourn recorder with same instrument damping to show low frequency fluctuations.

(a) ORIGINAL INTAKE



(b) MODIFIED INTAKE

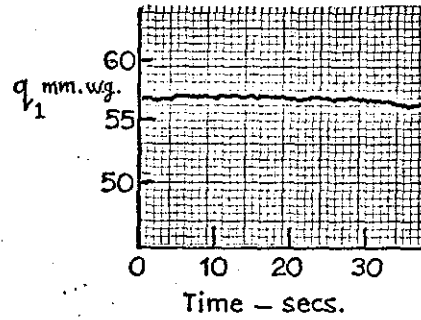
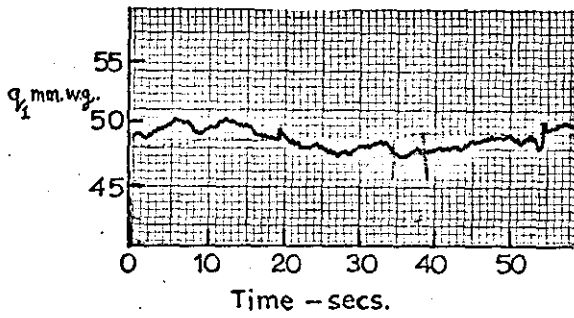
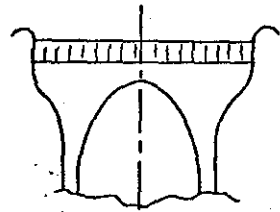


Fig.A2-2 EFFECT OF FLOW SPLIT ON INLET VELOCITY PROFILE.

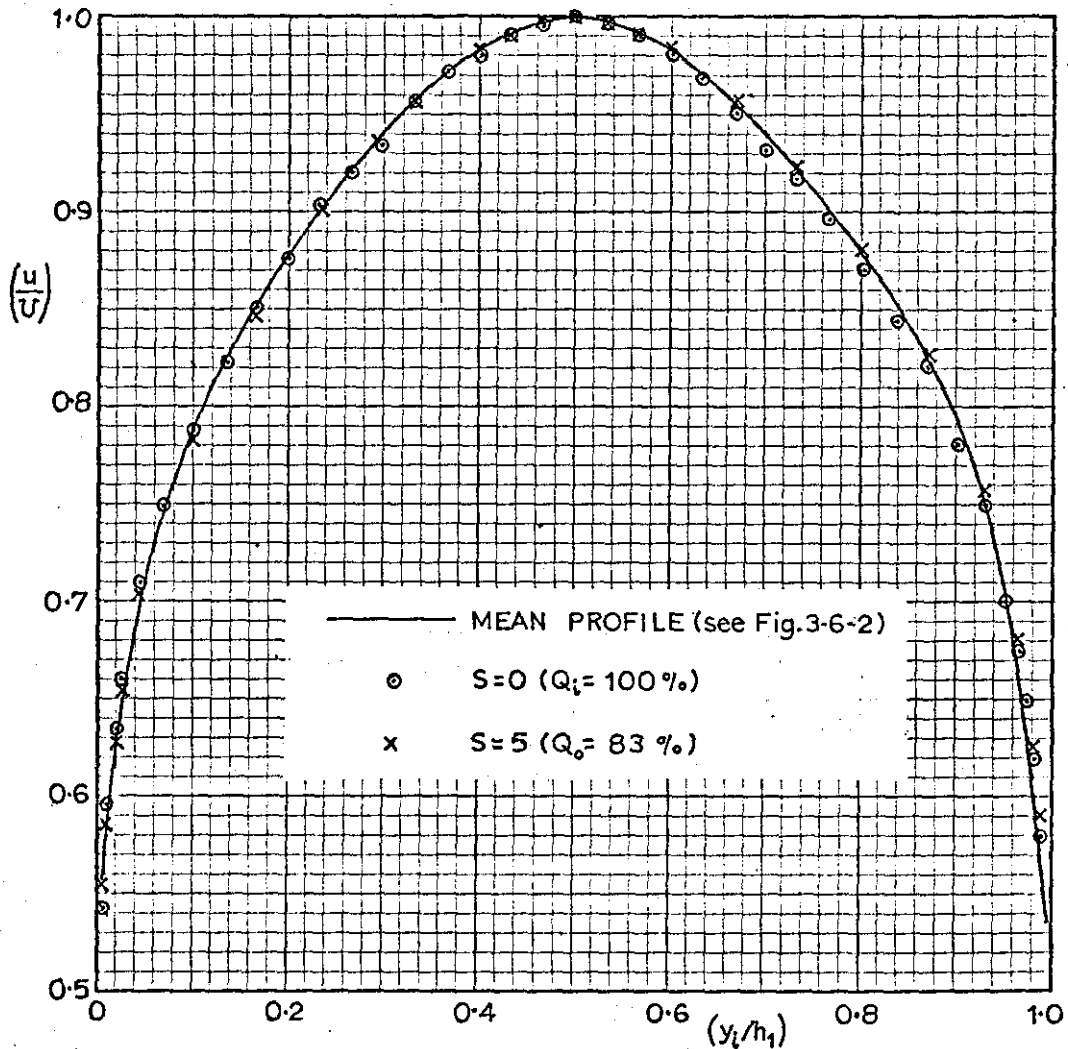


Fig.A2-3 WEDGE PROBE CALIBRATIONS.

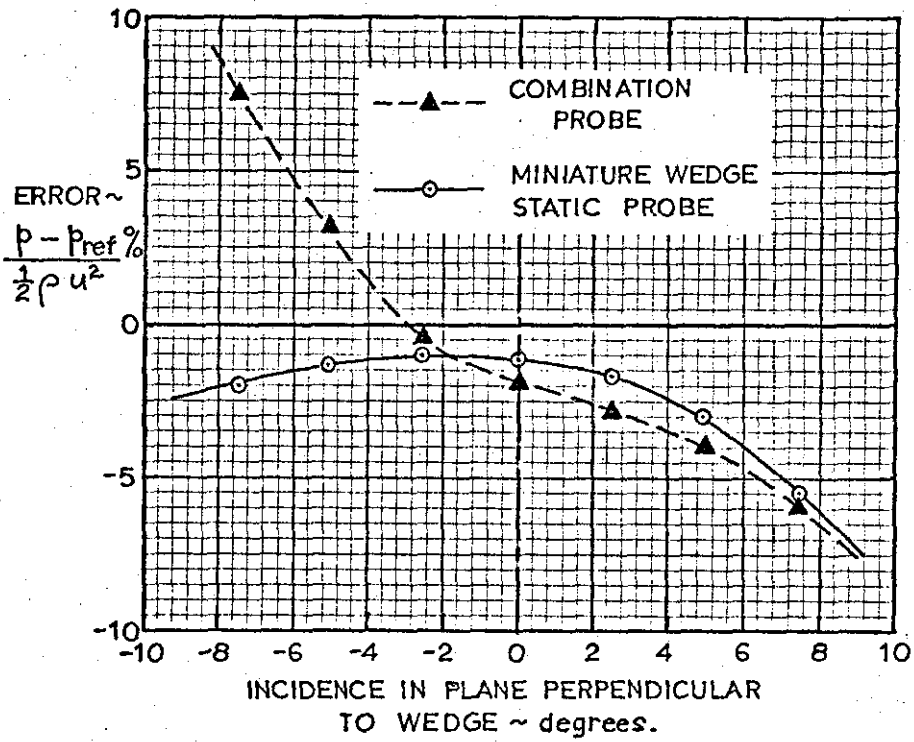


Fig.A2-4 COMPARISON OF HEAD RAKE MEASUREMENTS WITH TRAVERSE DATA.

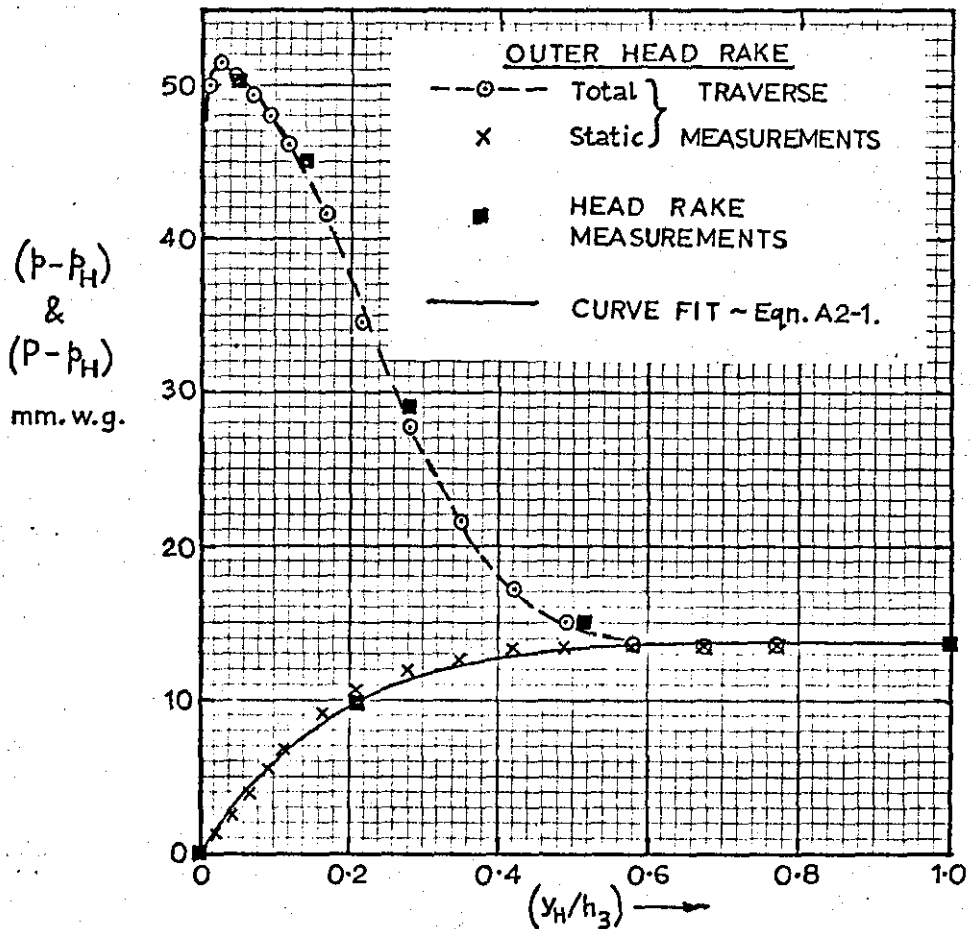


Fig. A2-5. COMPARISON OF PRE-DIFFUSER OUTLET PROFILES USING VARIOUS METHODS (Test 1-1026/CT).

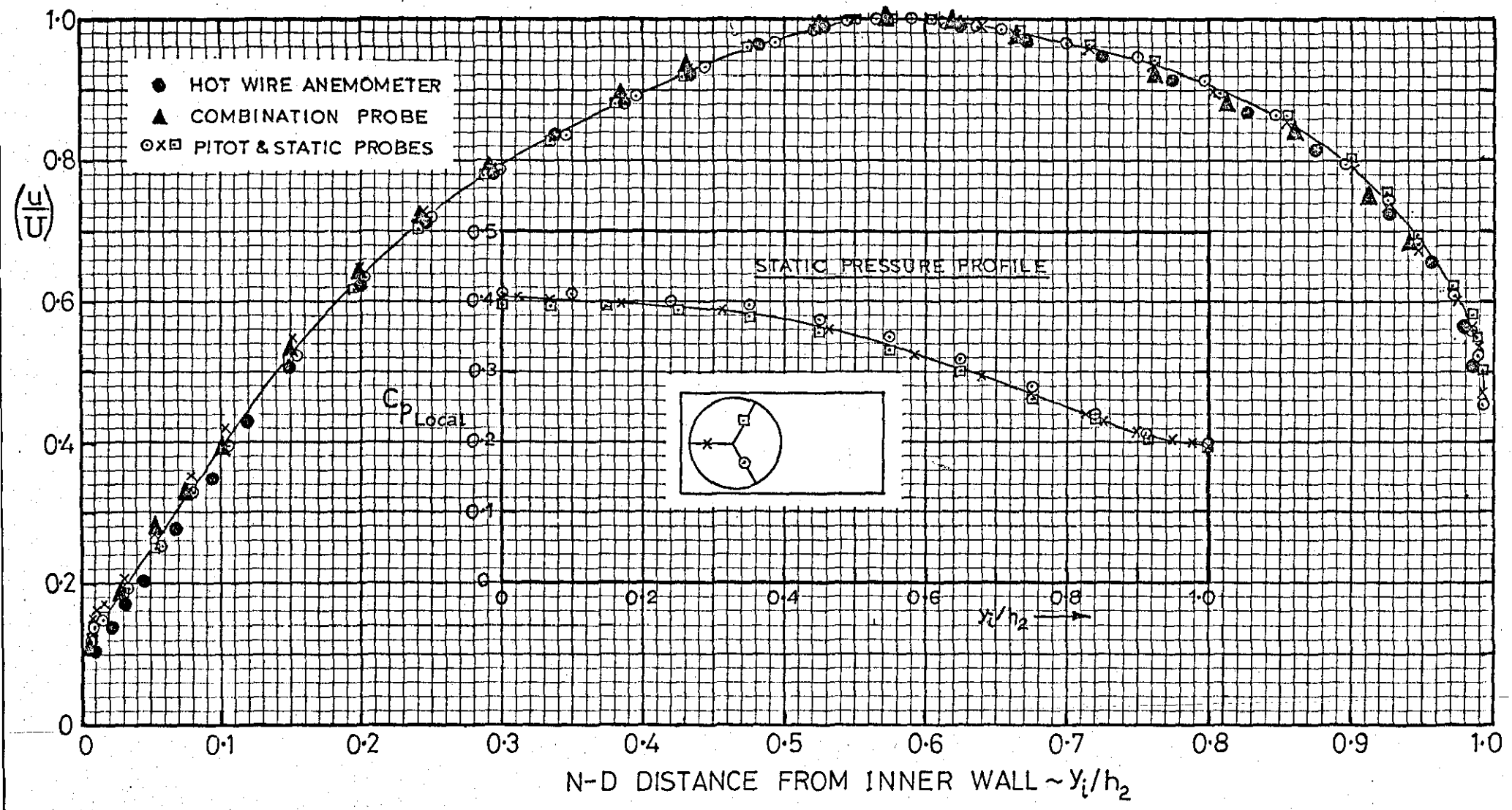
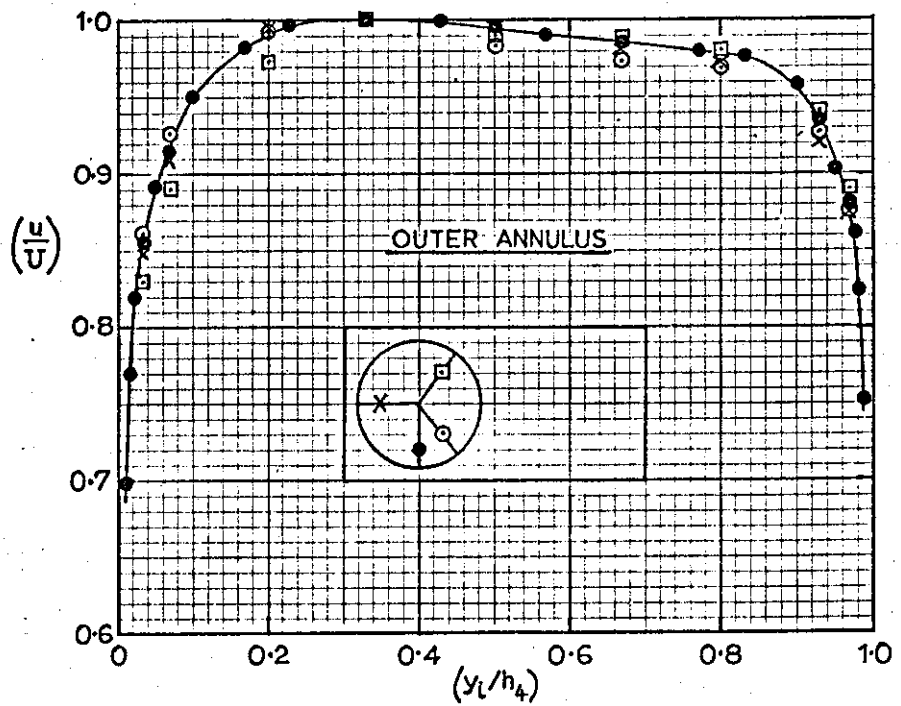
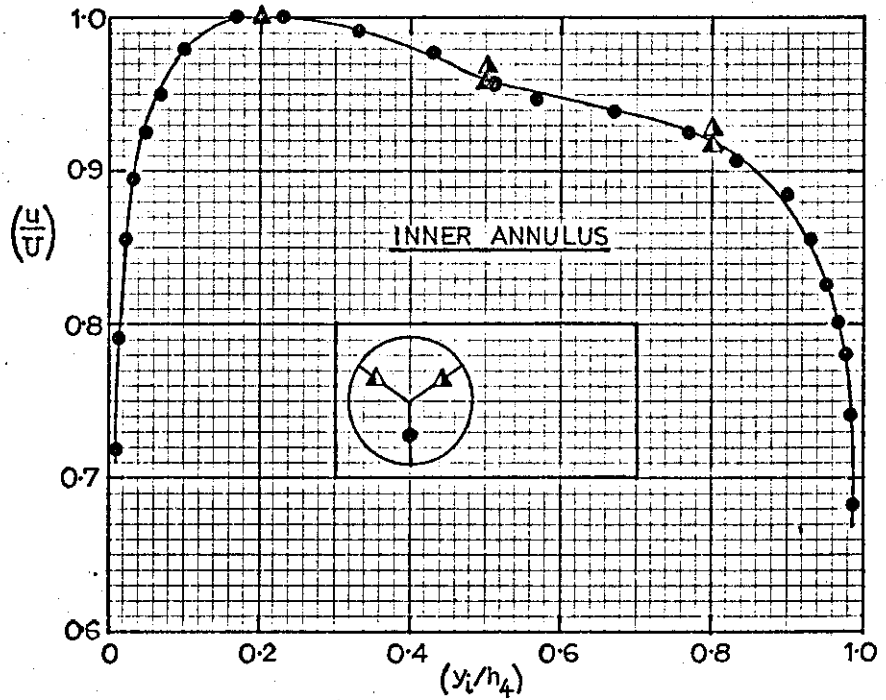


Fig.A2-6 SYMMETRY OF SETTLING LENGTH  
VELOCITY PROFILES.

(NOTE LARGE  $u/U$  SCALE)



APPENDIX 3    SAMPLE READINGS AND REDUCTION OF DATA

A sample set of readings for Test 3-0718/A is reproduced in Tables A3-1/5. The measurements of the static pressure distribution have been omitted since they are not used in analysing the performance of the system. Analysis of the velocity profiles and other data required for input to the analysis programs is dealt with in this appendix and a description of the computer programs and calculation procedures is given in Appendix 4.

A3-1    PRE-DIFFUSER OUTLET PROFILES

For the test being considered the pre-diffuser outlet velocity and static pressure profiles were measured using the pitot-wedge static combination probe. The dynamic pressure measurements were made using the wedge static pressure as a reference and supplementary measurements were made near the outer wall using a pitot probe, the readings from which were referenced to the outer wall static pressure (see Table A3-1). The static pressure profile was measured by making a second traverse of the combination probe, the readings from the wedge static being referred to the outer wall static pressure (see Table A3-2).

The first step in analysing the data was to plot the static pressure profile as shown in Fig. A3-1(a). A correction was then applied to the measured dynamic pressures for the error in static pressure due to the radial displacement of the wedge static and pitot probe measuring planes. As an example, a correction of -0.4 mm w.g. was made for  $y_1/h_2 = 0.697$  as illustrated in Fig. A3-1. A similar correction was applied to the readings taken with the pitot probe. Values of  $(u/U)$  were then calculated as  $u/U = \sqrt{q/q_{\max}}$  where  $q_{\max} = 30.5$  mm w.g., and plotted as shown in Fig. A3-1(b).

A3-2    HEAD RAKE DATA

The data obtained from the inner and outer head rakes is given in Table A3-3. All pressures were measured relative to the static pressure



on the surface of the head,  $p_H$ . The value of  $(p_H - p_1)$  was also measured for each case. The data was plotted before continuing the test (see figures accompanying Table A3-3) in order to check that the measurements were mutually consistent (i.e. that the data lay on smooth curves). A value of  $(P - p_H)$  for  $y_H/h_3 = 0$  was estimated for each profile. It was found that such values were required in order to obtain realistic curve fits for the velocity profiles. Whereas the wall velocity must be zero, it is not considered that any significant error was introduced by assuming it to be non-zero since the velocity gradient near the wall was extremely high (see, for example, the more detailed data of Fig. A2-4).

### A3-3 SETTling LENGTH VELOCITY PROFILES

The traverse data for the settling lengths is given in Table A3-4. All total pressures were referenced to the wall static pressure in the traverse plane. Since there were no static pressure gradients across the annuli, values of  $u/U$  were calculated directly from the measured dynamic pressures and the non-dimensional velocity profiles plotted as shown in Fig. A3-2.

### A3-4 STATIC PRESSURES

The wall static pressures at the three circumferential positions were measured at pre-diffuser outlet and in the settling lengths as shown in Table A3-5. Mean values of  $(p - p_1)/\frac{1}{2}\rho \bar{u}_1^2$  were calculated ready for input to the performance analysis program. It may be noted that the mean static pressure difference across the pre-diffuser outlet plane of  $(22.5 - 19.3) = 3.2$  mm w.g. agrees with the value shown in Fig. A3-1.

### A3-5 PREPARATION OF DATA FOR COMPUTER ANALYSIS

#### (i) Velocity Profiles

The velocity profiles were prepared for analysis by tabulating values of  $u/U$  at equal intervals of  $y_1/h$  across the velocity profile. Each boundary layer was treated separately, the number of values of  $u/U$  depending upon the boundary layer thickness. The number of points taken for each complete

profile are given in the table below.

Number of Points used for Computer Analysis of Velocity Profiles

|                             | Number of Points | Step Distance $\Delta y_i/h$ | Step Distance mm (ins)        |
|-----------------------------|------------------|------------------------------|-------------------------------|
| Inlet Profile               | 75               | 0.0133                       | 0.508 (0.02)                  |
| Pre-diffuser Outlet Profile | 50               | 0.020                        | Dependent upon annulus height |
| Settling Length Profiles    | 30               | 0.033                        | 1.270 (0.05)                  |

A sample table of data taken from Fig. A3-1 for the inner boundary layer is given below. It may be noted that the first tabulated value is for  $y_i/h_2 = 0.01$  (i.e: half the step distance from the wall).

Tabulated Data for Inner Boundary Layer at Pre-Diffuser Outlet

|           |     |      |      |      |      |       |      |      |      |
|-----------|-----|------|------|------|------|-------|------|------|------|
| $y_i/h_2$ | .01 | .03  | .05  | .07  | .09  | ..... | .55  | .57  | .59  |
| $u/U$     | 0   | .020 | .065 | .105 | .150 | ..... | .987 | .997 | 1.00 |

(ii) Pre-diffuser Outlet Static Pressure Profile

The pre-diffuser outlet static pressure profile was treated in the same manner as the velocity profile. The data was supplied as a table of 50 values of  $(p - p_{w_0})_2$  in mm w.g. together with a value of  $\frac{1}{2}\rho U_1^2$  for reference purposes.

(iii) Additional Data

Apart from specifying the geometry, there were two additional groups of parameters required for analysis of the system performance. These were:

- (a) The velocity ratios,  $U_2/U_1$ ,  $U_{4_i}/U_1$  and  $U_{4_o}/U_1$  as given in Tables A3-1/5. These parameters were required in order to calculate the volume flow at each station from the non-dimensional velocity profiles.
- (b) The mean static pressures for the outer wall at Stn. 2 and in the settling lengths (Stns.  $4_i$  &  $4_o$ ). These were input as the values of  $(p - p_1)/\frac{1}{2}\rho \bar{u}_1^2$  given in Table A3-5.
- (iv) Head Rake Data

The head rake data was analysed by a separate computer program, the input data being the measured pressures as listed in Table A3-3.

---

Table A3-1 PRE-DIFFUSER OUTLET TRAVERSE DATA: TEST 3-0718/A

DATE: 2/5/72     $T_0 = 299^\circ\text{K}$      $p_0 = 757 \text{ mm. Hg.}$      $\frac{1}{2}\rho U_1^2 = 54.8 \text{ mm.w.g.}$

| $y_i/h_2$ | $q_{\text{obs}}$<br>mm. w.g. | Displacement<br>correction<br>mm. w.g. | $q_{\text{corr}}$<br>mm. w.g. | $(\frac{U}{U})_2$ | COMMENTS                                                                           |
|-----------|------------------------------|----------------------------------------|-------------------------------|-------------------|------------------------------------------------------------------------------------|
| .005      | 0                            | -                                      | 0                             | 0                 | } Separation confirmed by wool tuft observations                                   |
| .009      | 0                            | -                                      | 0                             | 0                 |                                                                                    |
| .015      | 0                            | -                                      | 0                             | 0                 |                                                                                    |
| .024      | 0.05                         | -                                      | 0.05                          | .040              |                                                                                    |
| .042      | 0.1                          | -                                      | 0.1                           | .057              |                                                                                    |
| .060      | 0.2                          | -                                      | 0.2                           | .081              |                                                                                    |
| .078      | 0.5                          | -                                      | 0.5                           | .128              |                                                                                    |
| .115      | 1.5                          | -                                      | 1.5                           | .222              |                                                                                    |
| .151      | 2.4                          | -                                      | 2.4                           | .280              |                                                                                    |
| .187      | 4.3                          | -                                      | 4.3                           | .375              |                                                                                    |
| .224      | 6.2                          | +0.1                                   | 6.3                           | .454              | <u>PITOT-WEDGE</u><br><u>STATIC</u><br><u>COMBINATION</u><br><u>PROBE</u>          |
| .260      | 9.6                          | +0.1                                   | 9.7                           | .564              |                                                                                    |
| .296      | 11.8                         | +0.1                                   | 11.9                          | .625              |                                                                                    |
| .333      | 15.5                         | +0.1                                   | 15.6                          | .715              |                                                                                    |
| .369      | 18.2                         | -                                      | 18.2                          | .772              |                                                                                    |
| .406      | 21.3                         | -                                      | 21.3                          | .836              |                                                                                    |
| .442      | 24.0                         | -                                      | 24.0                          | .887              |                                                                                    |
| .478      | 26.6                         | -0.1                                   | 26.5                          | .932              |                                                                                    |
| .515      | 28.5                         | -0.2                                   | 28.3                          | .963              |                                                                                    |
| .552      | 30.0                         | -0.2                                   | 29.8                          | .988              |                                                                                    |
| .588      | 30.8                         | -0.3                                   | 30.5                          | 1.000             | $\left(\frac{U_2}{U_1}\right) = \sqrt{\frac{30.5}{54.8}}$<br>$= \underline{0.746}$ |
| .624      | 30.5                         | -0.3                                   | 30.2                          | .995              |                                                                                    |
| .660      | 29.5                         | -0.3                                   | 29.2                          | .978              |                                                                                    |
| .697      | 27.5                         | -0.4                                   | 27.1                          | .943              |                                                                                    |
| .733      | 25.5                         | -0.4                                   | 25.1                          | .907              |                                                                                    |
| .768      | 23.5                         | -0.4                                   | 23.1                          | .870              |                                                                                    |
| .806      | 21.0                         | -0.3                                   | 20.7                          | .824              |                                                                                    |
| .842      | 17.4                         | -0.2                                   | 17.2                          | .751              |                                                                                    |
| .878      | 13.5                         | -0.2                                   | 13.3                          | .660              |                                                                                    |
| .914      | 10.0                         | -0.1                                   | 9.9                           | .570              |                                                                                    |

|      |     |      |     |      |                              |
|------|-----|------|-----|------|------------------------------|
| .922 | 9.5 | -0.2 | 9.3 | .552 | <u>PITOT</u><br><u>PROBE</u> |
| .940 | 7.9 | -0.1 | 7.8 | .506 |                              |
| .958 | 6.3 | -    | 6.3 | .454 |                              |
| .976 | 5.1 | -    | 5.1 | .409 |                              |
| .985 | 4.2 | -    | 4.2 | .371 |                              |
| .991 | 3.3 | -    | 3.3 | .329 |                              |
| .995 | 2.8 | -    | 2.8 | .303 |                              |

Table A3-2 PRE-DIFFUSER OUTLET STATIC PRESSURE TRAVERSE  
DATA FOR Test 3-0718/A.

| $y_i/h_2$ | $(p-p_{w_0})/2$<br>mm.w.g. |
|-----------|----------------------------|
| 0.033     | 3.3                        |
| 0.073     | 3.1                        |
| 0.145     | 3.3                        |
| 0.218     | 3.5                        |
| 0.291     | 3.7                        |
| 0.364     | 4.0                        |
| 0.437     | 4.1                        |
| 0.509     | 3.95                       |
| 0.582     | 3.4                        |
| 0.655     | 2.75                       |
| 0.728     | 1.9                        |
| 0.800     | 1.1                        |
| 0.873     | 0.4                        |
| 0.945     | 0.1                        |

DATE: 2/5/72

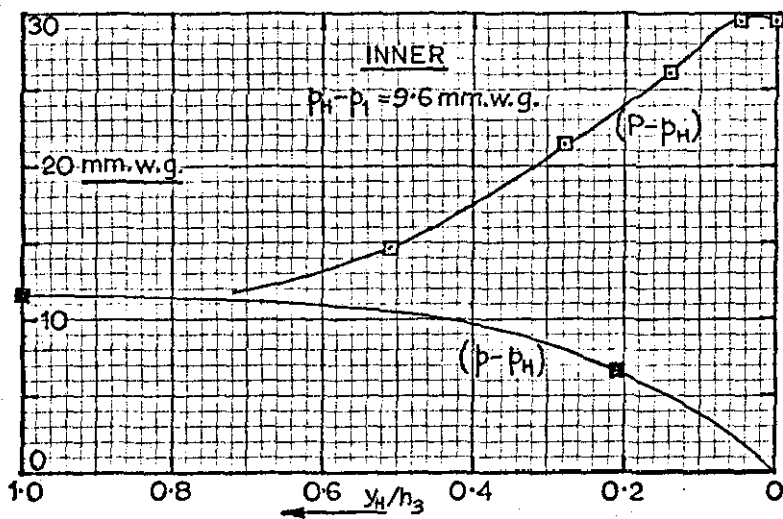
$\frac{1}{2}\rho U_1^2 = 54.8$  mm.w.g.

$(P_{w_i} - P_{w_0}) = 3.2$  mm.w.g.

$(P_{w_0} - P_1) = 19.3$  mm.w.g.

TRAVERSE DATA FROM WEDGE  
STATIC ELEMENT OF  
COMBINATION PROBE

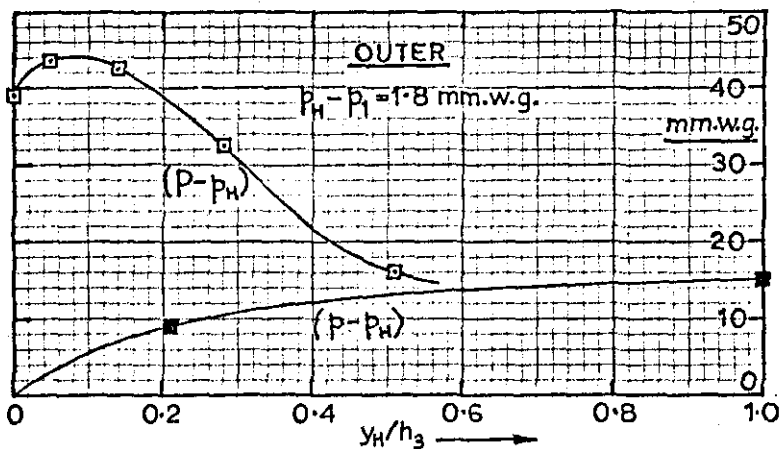
Table A3-3 HEAD RAKE DATA FOR Test 3-0718/A.



$\frac{1}{2}\rho U_1^2 = 49.5$  mm.w.g.

INNER

| $y_H/h_3$ | COMMENT      | $(P - P_H)$<br>mm.w.g. |
|-----------|--------------|------------------------|
| 0.0       | Estimated    | 29.5                   |
| 0.047     | Pitot        | 29.5                   |
| 0.140     | "            | 26.0                   |
| 0.280     | "            | 21.3                   |
| 0.510     | "            | 14.7                   |
| 0.210     | Wedge static | 6.6                    |
| 1.000     | Static       | 11.5                   |



OUTER

| $y_H/h_3$ | COMMENT      | $(P - P_H)$<br>mm.w.g. |
|-----------|--------------|------------------------|
| 0.0       | Estimated    | 39.0                   |
| 0.047     | Pitot        | 43.6                   |
| 0.140     | "            | 42.5                   |
| 0.280     | "            | 32.4                   |
| 0.510     | "            | 16.0                   |
| 0.210     | Wedge static | 9.0                    |
| 1.000     | Static       | 14.9                   |

Table A3-4 SETTLING LENGTH TRAVERSE DATA FOR  
TEST 3-0718/A.

$$\frac{1}{2}\rho U_1^2 = 54.8 \text{ mm.w.g.}$$

| $y_i/h_4$ | INNER ANNULUS                 |                            | OUTER ANNULUS                 |                            | COMMENTS                                                                               |
|-----------|-------------------------------|----------------------------|-------------------------------|----------------------------|----------------------------------------------------------------------------------------|
|           | P - p <sub>w</sub><br>mm.w.g. | $\left(\frac{u}{U}\right)$ | P - p <sub>w</sub><br>mm.w.g. | $\left(\frac{u}{U}\right)$ |                                                                                        |
| 0.013     | 8.3                           | 0.707                      | 6.0                           | 0.722                      | $\left(\frac{U_{4i}}{U_1}\right) = 0.550$<br>$\left(\frac{U_{4o}}{U_1}\right) = 0.458$ |
| 0.027     | 11.6                          | 0.836                      | 8.0                           | 0.834                      |                                                                                        |
| 0.047     | 14.0                          | 0.918                      | 9.4                           | 0.904                      |                                                                                        |
| 0.067     | 15.3                          | 0.960                      | 10.1                          | 0.937                      |                                                                                        |
| 0.100     | 16.0                          | 0.982                      | 10.9                          | 0.974                      |                                                                                        |
| 0.167     | 16.6                          | 1.000                      | 11.2                          | 0.987                      |                                                                                        |
| 0.267     | 16.3                          | 0.991                      | 11.5                          | 1.000                      |                                                                                        |
| 0.367     | 15.9                          | 0.979                      | 11.5                          | 1.000                      |                                                                                        |
| 0.467     | 15.5                          | 0.966                      | 11.2                          | 0.987                      |                                                                                        |
| 0.987     | 6.2                           | 0.611                      | 4.0                           | 0.590                      |                                                                                        |
| 0.973     | 9.4                           | 0.752                      | 6.7                           | 0.763                      |                                                                                        |
| 0.953     | 11.1                          | 0.818                      | 8.2                           | 0.844                      |                                                                                        |
| 0.933     | 12.0                          | 0.850                      | 8.8                           | 0.875                      |                                                                                        |
| 0.900     | 13.0                          | 0.885                      | 9.5                           | 0.909                      |                                                                                        |
| 0.833     | 13.9                          | 0.915                      | 10.1                          | 0.937                      |                                                                                        |
| 0.733     | 14.4                          | 0.931                      | 10.4                          | 0.951                      |                                                                                        |
| 0.633     | 14.8                          | 0.944                      | 10.6                          | 0.960                      |                                                                                        |
| 0.533     | 15.1                          | 0.954                      | 10.9                          | 0.974                      |                                                                                        |
| 0.433     | —                             | —                          | 11.3                          | 0.991                      |                                                                                        |

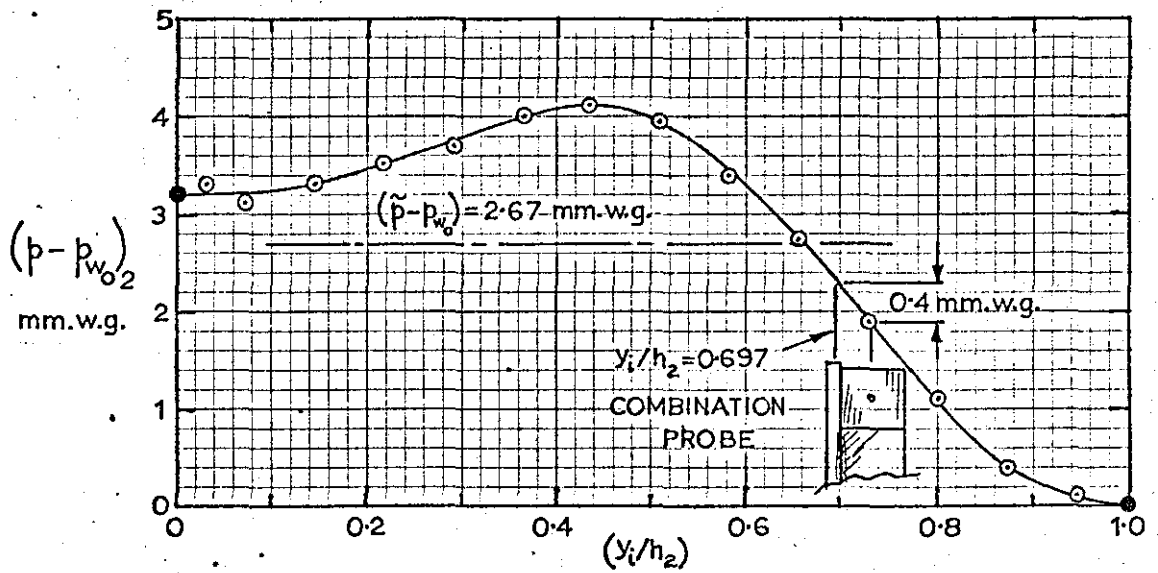
Table A3-5 KEY STATIC PRESSURES AT STATIONS 2 & 4  
FOR Test 3-0718/A.

$$\frac{1}{2}\rho U_1^2 = 54.8 \text{ mm.w.g.}$$

|                | RED  | BLUE | GREEN | MEAN  | $\Delta P / \frac{1}{2}\rho \bar{u}_1^2$ |
|----------------|------|------|-------|-------|------------------------------------------|
| $P_{2i} - P_1$ | 22.1 | 22.4 | 23.0  | 22.5  | 0.5367                                   |
| $P_{2o} - P_1$ | 18.7 | 19.3 | 19.9  | 19.3  | 0.4603                                   |
| $P_{4i} - P_1$ | 17.9 | 18.9 | 19.4  | 18.73 | 0.4467                                   |
| $P_{4o} - P_1$ | 26.1 | 26.7 | 27.0  | 26.6  | 0.6345                                   |

Fig A3-1 PRE-DIFFUSER OUTLET PROFILES FOR Test 3-0718/A.

(a) STATIC PRESSURE PROFILE.



(b) NON-DIMENSIONAL VELOCITY PROFILE.

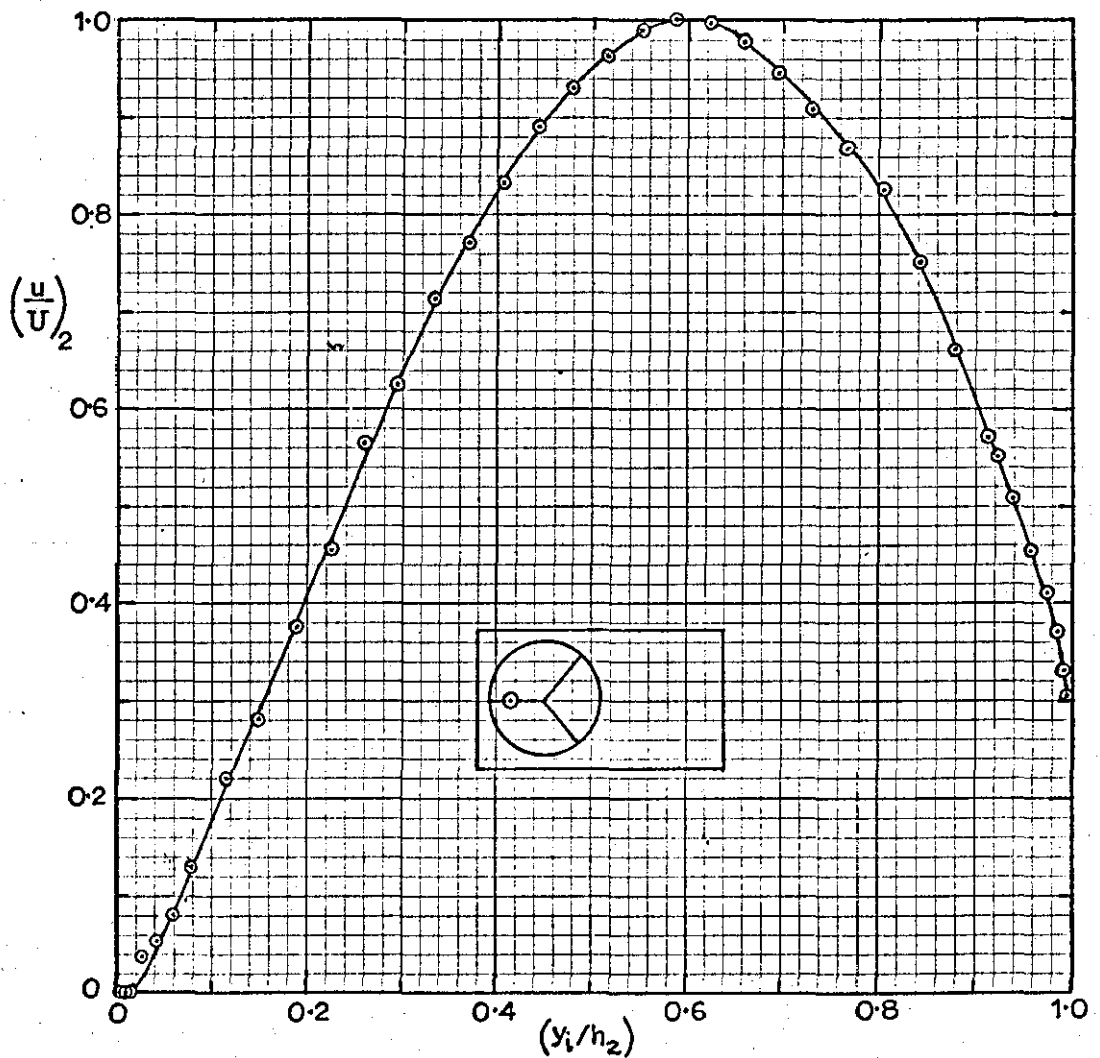
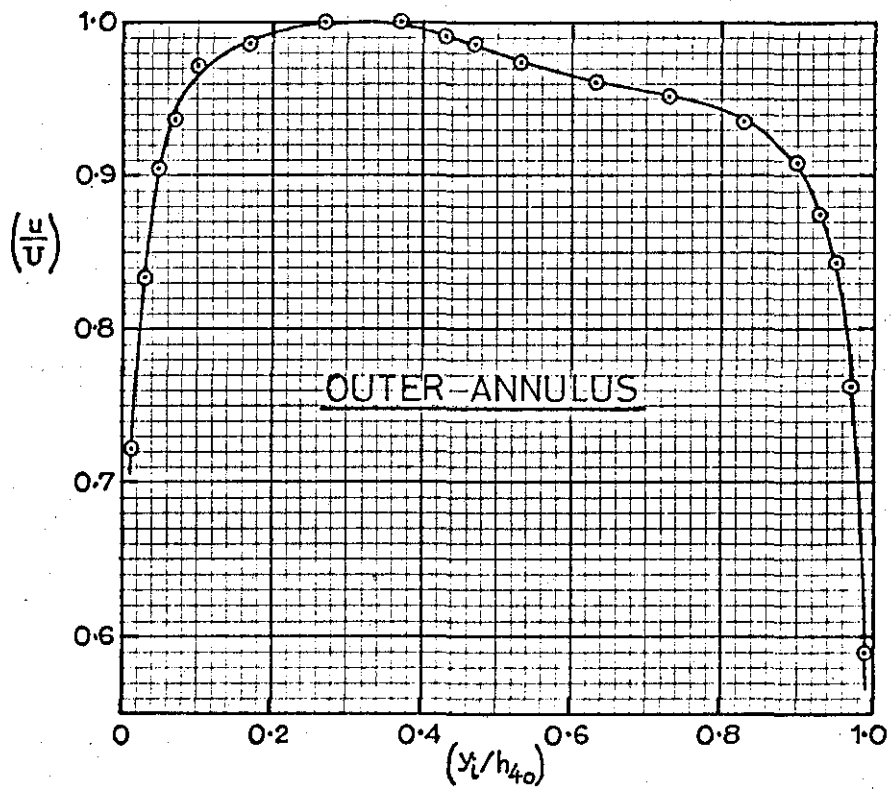
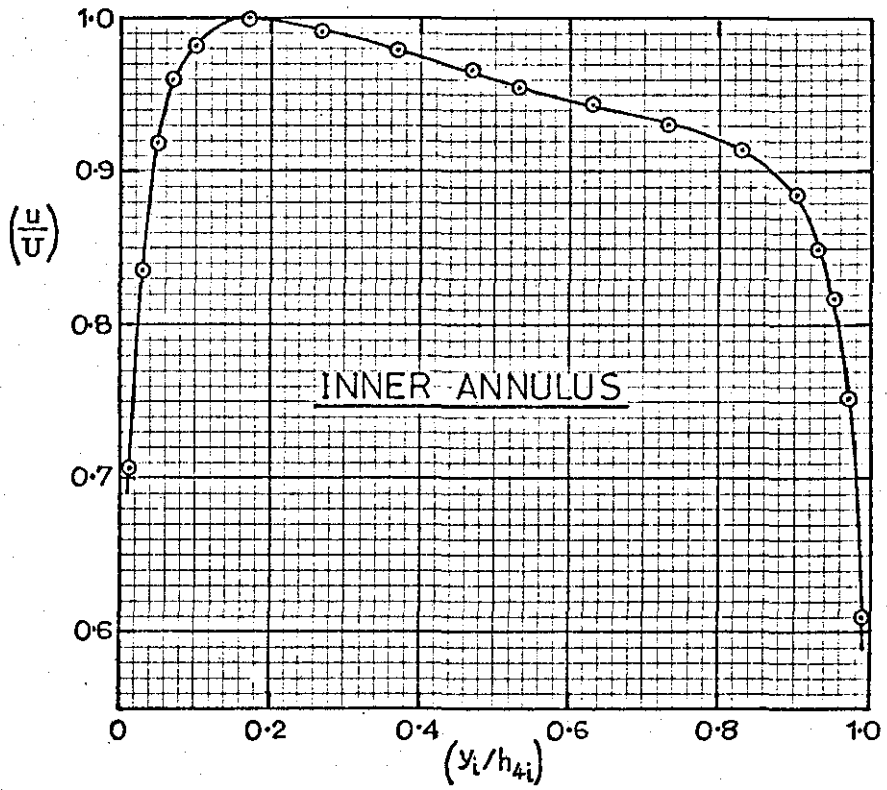


Fig.A3-2 SETTLING LENGTH VELOCITY PROFILES  
FOR Test 3-0718/A.





APPENDIX 4 ANALYSIS OF DATA BY COMPUTER PROGRAM

Six computer programs were used for the analysis and plotting of data, the main functions of which are shown in Fig. A4-1. For convenience the programs are numbered P1 to P6. The two analysis programs (P1 and P4) provided all of the data on the flow and performance characteristics for each test. Apart from printed output, data was also output from the main analysis program (P1) on punched cards to provide a convenient method of obtaining data in summary form (via the selective print program, P2) and to provide the necessary input data for Program P4 to calculate the losses between Stns. 2 & 3 and 3 & 4 from the head rake data. The remaining programs were used mainly for graph plotting and it is not considered necessary to describe them in detail. The only point of interest is the method of curve fitting employed in Program P3 for deriving the performance contour maps and this is described in Sect. A4-3.

All the programs were written by the author in FORTRAN IV language. The programs were run on the Loughborough University I.C.T. 1905 computer.

A4-1 MAIN PERFORMANCE ANALYSIS PROGRAM (P1)

A flow diagram for the main performance analysis program is given in Fig. A4-2 and a listing of the program is reproduced in Table A4-2. A list of the principal variables used in the program is given in Table A4-1. The "WRITE" statements have been edited from the program listing in order to save space. It should be noted that several parameters have been re-named since the program was written (see Table A4-1) and that the present Stn. 4 is denoted Stn. 3 in the program.

The boundary layer, velocity profile and performance parameters were calculated according to the definitions of Table 1-4 and Sect. 1-3. Integration of the velocity and static pressure profiles was carried out using subroutine "INTEGRAL". This subroutine calculates the integral of the desired quantity (e.g.  $\int_{R_1}^{R_m} (u/U)^3 R dR$ ) in a series of steps across the

annulus. A parabola is fitted through each successive group of three values (using subroutine "FIT 3") and the analytic integral is obtained for the curve between the first two points. This is repeated for successive steps until the required integral is obtained. This method was chosen since it facilitated easy determination of integrals between any specified radii (i.e. radii not necessarily corresponding with the tabulated data representing the profile to be integrated). This was necessary in order to accurately determine the stagnation streamline radii in the pre-diffuser (using subroutine "SPLIT MK 2") and hence the flow field velocity profile and performance parameters. Subroutine "FIT 3" is a general purpose curve fitting routine which calculates the coefficients  $C_1$ ,  $C_2$  and  $C_3$  in the equations for curves of the form,

$$Y = C_1 X^{E1} + C_2 X^{E2} + C_3 X^{E3}$$

In the case of calls to "FIT 3" from "INTEGRAL",  $E1 = 0$ ,  $E2 = 1$  and  $E3 = 2$  (i.e. a parabolic curve fit is used).

It is not possible to give a complete set of calculations as carried out by Program P1, however some of the more important calculations are given in Table A4-3 to demonstrate the use of the equations of Sect. 1-3. Reference is made to the appropriate parts of the program by means of the line numbers (see Table A4-2). The sample calculations are relevant to Test 3-0718/A and a complete set of results is given in Table A4-4.

#### A4-2 HEAD RAKE DATA ANALYSIS PROGRAM (P4)

This program was used for initial analysis of the head rake data and further division of the losses between Stns. 2 & 3 and 3 & 4. There were also two optional routines available to the program, the first for further sub-dividing the losses in the settling length and the second for plotting the velocity and static pressure profiles calculated by the program from the head rake data. A flow diagram for the program is given in Fig. A4-3. The method of analysing the head rake data has been dealt with in Sect. 5-1-2.

part (iii) and Sect. A2-2. The curve fit used for the static pressure profile is given by Eqns. A2-1/2.

Further analysis of the system losses was facilitated by inputting data on cards output by Program P1. The local losses were calculated as,

$$(\tilde{\lambda}_{a-b})_{\text{Local}} = \left( \frac{\Delta \tilde{P}_a - b}{\alpha_1 \frac{1}{2} \rho \bar{u}_1^2} \right) = \frac{\alpha_a \left( \frac{\bar{u}_a}{\bar{u}_1} \right)^2}{\alpha_1} \left\{ 1 - \frac{\alpha_b \left( \frac{\bar{u}_b}{\bar{u}_a} \right)^2}{\alpha_a} \right\} - \left( \frac{\tilde{p}_b - \tilde{p}_a}{\alpha_1 \frac{1}{2} \rho \bar{u}_1^2} \right)$$

where the suffices 'a' and 'b' refer to parameters for the planes between which the loss was calculated. The method of calculation was substantially the same as that used in Program P1 and the same subroutines were used for the necessary integrations. A sample set of output data from the basic program is given in Table A4-5 for Test 3-0718/A.

#### A4-3 PERFORMANCE CONTOUR MAP ANALYSIS PROGRAM (P3)

The operation of Program P3 is illustrated in Fig. A4-4. The input data consisted of values of  $\tilde{\lambda}_{1-4}$  and  $\tilde{\xi}_4$  obtained from tests with each pre-diffuser geometry. A least squares parabolic curve fit was used to interpolate along each constant  $D/h_2$  curve to obtain the performance figures at small intervals of  $Q_0$ . Interpolated values along each constant  $Q_0$  curve were then obtained using a curve fit of the form,

$$P = \frac{C_1}{(D/h_2)} + C_2 (D/h_2) + C_3$$

where  $P = \tilde{\lambda}_{1-4}$  or  $(1 - \tilde{\xi}_4)$  as appropriate, and  $C_1$ ,  $C_2$  and  $C_3$  are constants. This curve fit was found to correspond closely with the observed variation in performance with dump gap (see for example Fig. 4-1-9). The remainder of the program consisted of the necessary logic and plotting instructions required to obtain the performance contour maps in a suitable form.

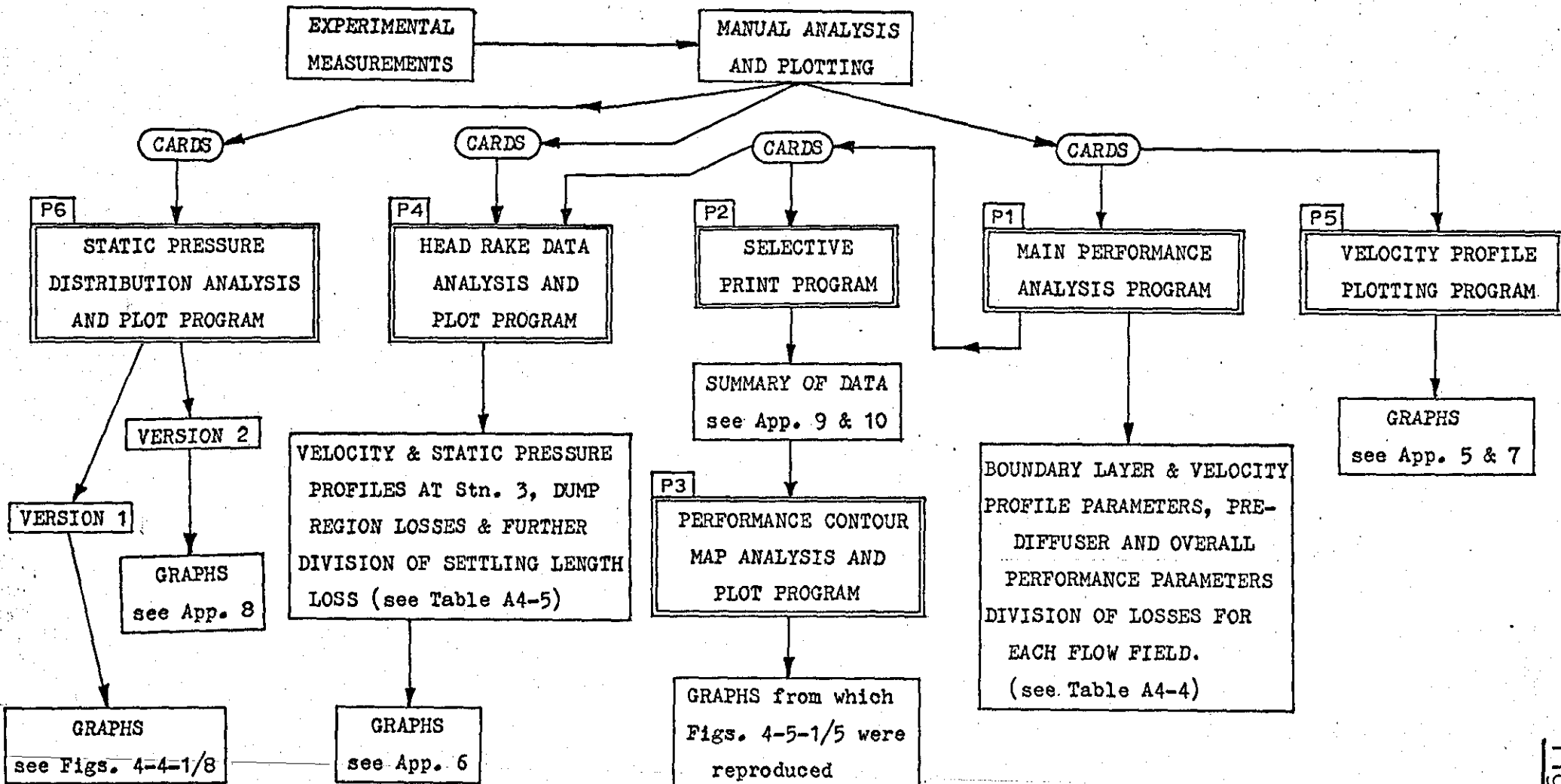


Fig.A4-1 MAIN FUNCTIONS OF COMPUTER PROGRAMS USED FOR DATA ANALYSIS.

Fig.A4-1.

Fig. A4-2 FLOW DIAGRAM FOR MAIN PERFORMANCE ANALYSIS PROGRAM (P1).

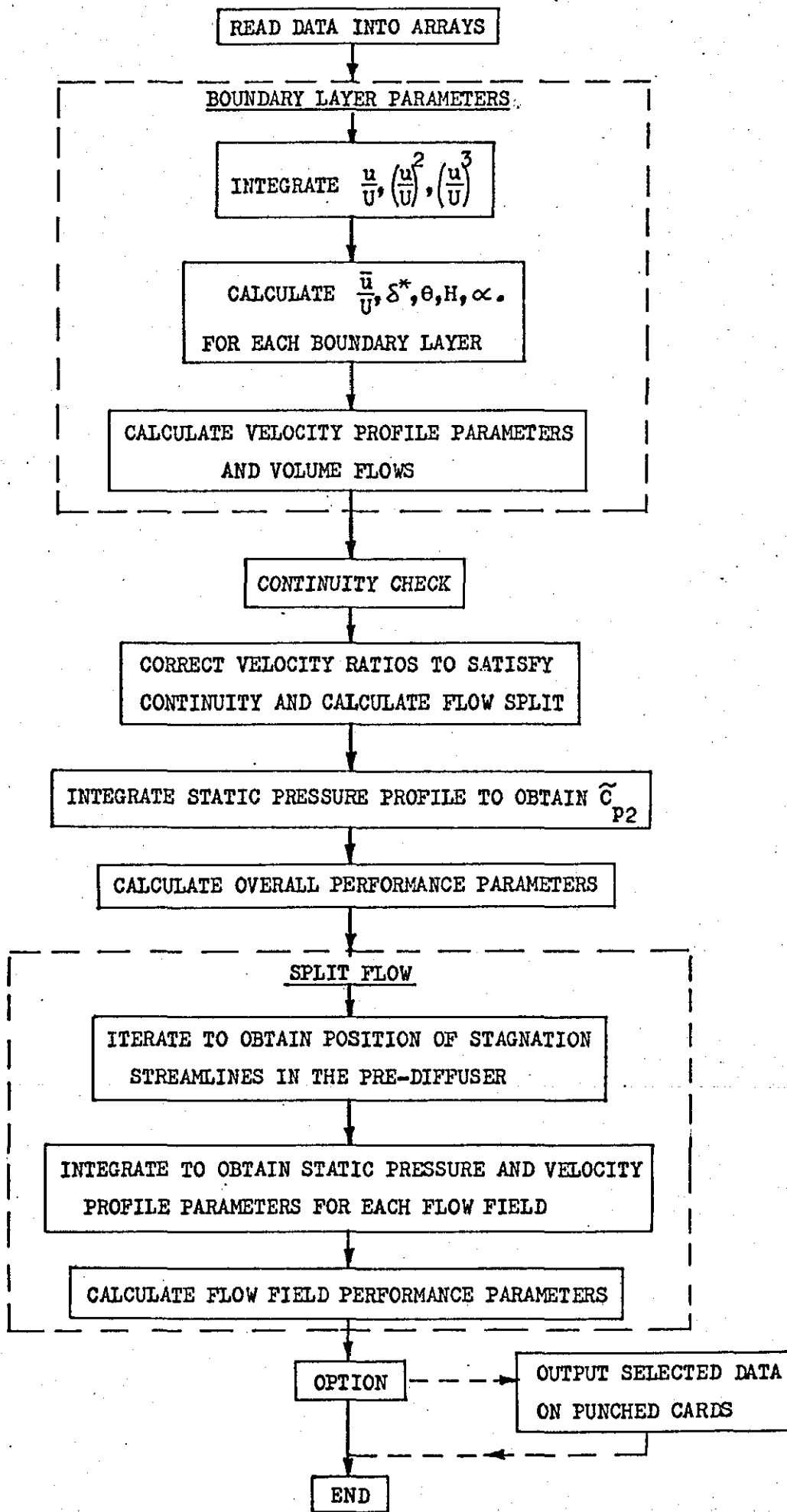


TABLE A4-1 LIST OF PRINCIPAL VARIABLES IN MAIN ANALYSIS PROGRAM

AA ..... area,  $A/\pi$

ANG ..... angle of traverse plane to rig axis (= 0 in this program)

AR ..... area ratio

AREF ..... effective overall area ratio,  $AR_e$

ALPHA, ALFAM, ALFAS ...  $\propto$  (boundary layer, velocity profile, flow field)

ALOSS ..... loss coefficient  $\Delta\tilde{P}/\tilde{q}_1$

ALOS, ALS ... flow field loss coefficient referred to  $\tilde{q}_{1i}$  or  $\tilde{q}_{1o}$

BLOS, BLS ... flow field loss coefficient referred to  $\tilde{q}_1$

CP ..... pressure recovery coeff. referred to  $\bar{q}_1$  or  $\tilde{q}_1$

CPI2, CPI3 .. ideal pressure recovery coeffs.

DR\* ..... step distance,  $\Delta y_i$

DYNHL .....  $\frac{1}{2} \rho U_1^2$  mm. w.g.

ETA\* ..... effectiveness,  $\tilde{\epsilon}$

MTEST ..... number of tests to be analysed

NPTS ..... number of  $u/U$  values for each boundary layer

P2 .....  $(p - p_{w_0})_2$  mm. w.g.

PROB ..... % probability of error in settling length volume flows

Q ..... volume flow,  $(\bar{u}/U) \times (A/\pi)$

QREL .....  $Q/Q_1 \times 100\%$

RQ\* ..... flow split ratio, S

RU ..... ratio of maximum velocities,  $U/U_1$

RW ..... wall radius

S, SUM ..... numerical integral of specified parameter

SK\* ..... velocity profile radial distortion factor, RD

UND ..... value of  $u/U$  for velocity profile

UM, DSTAR, THETA, H ... boundary layer parameters,  $\bar{u}/U$ ,  $S^*$ ,  $\theta$ , H

W ..... indicator (1 = inner wall, -1 = outer wall)

Subscripts (last character(s) of variable names)

1 ..... inlet station

2 ..... pre-diffuser outlet

3 ..... settling length (Stn. 4 in present terminology)

I ..... inner

O ..... outer

S, STAR ..... parameters for each flow field

TOT ..... total for each station (e.g. area, volume flow)

\* Note: The symbols representing these parameters have been changed since the program was first written (Nov. 1971).

Table A4-2 LISTING OF MAIN PERFORMANCE ANALYSIS PROGRAM

( PROGRAM P1, LANGUAGE:FORTRAN IV )

|       |                                                         |     |
|-------|---------------------------------------------------------|-----|
|       | MASTER DIFFUSER PERFORMANCE ANALYSIS MK5                | 001 |
| C**** | CALCS. REVISED ACCORDING TO NEW SYSTEM. 24/11/72.       | 002 |
| C**** | I/P, O/P FORMATS REVISED 19/5/72.                       | 003 |
|       | DIMENSION UND( 80,8),P2(80,4),PV(80,4)                  | 004 |
|       | DIMENSION NPTS(8),DR(8),RW(8),W(8),DEL(8),AA(8),DELR(8) | 005 |
|       | DIMENSION UM(8),DSTAR(8),THETA(8),H(8),ALPHA(8),Q(8)    | 006 |
|       | DIMENSION NPTOT(8),ATOT(8),UMH(8),QTOT(8),ALFAM(8)      | 007 |
|       | DIMENSION CP(8),RU(8),RSTAR(3),QRS(3),ERROR(3)          | 008 |
|       | DIMENSION AS(4),NPS(4),CPS(4),ALFAS(4)                  | 009 |
|       | DIMENSION UMS(4),CPSS(8),RUS(2)                         | 010 |
|       | DIMENSION QREL(8),DISC(8),RTRU(4),FRACT(4)              | 011 |
|       | DIMENSION RAS(8)                                        | 012 |
|       | COMMON /CPODATA/T(5,20),P(30,20)                        | 013 |
|       | COMMON /CPOBF/B(25,20),F(15,20)                         | 014 |
|       | COMMON /CPOHP/HP(11,20)                                 | 015 |
|       | COMMON /MEAN/UM                                         | 016 |
|       | NM=0                                                    | 017 |
|       | READ (1,11) MTEST                                       | 018 |
| 11    | FORMAT (10)                                             | 019 |
|       | DO 1 J=1,2                                              | 020 |
|       | READ (1,6) NPTS(J),DR(J),RW(J),W(J),DEL(J)              | 021 |
|       | READ (1,8) (UND(I,J),I=1,NPTS(J))                       | 022 |
| 1     | CONTINUE                                                | 023 |
|       | J1=1                                                    | 024 |
|       | J2=2                                                    | 025 |
|       | DELR(1)=RW(2)-RW(1)                                     | 026 |
|       | DELR(2)=DELR(1)                                         | 027 |
|       | GO TO 10                                                | 028 |
| 3     | CONTINUE                                                | 029 |
|       | DO 1001 K=1,MTEST                                       | 030 |
|       | READ (1,2) DDR,ARAT,ANG,KRO,KBI,RQA                     | 031 |
| 2     | FORMAT (3F0.0,2I0,F0.0)                                 | 032 |
|       | WRITE .....                                             | 033 |
|       | READ (1,5) QIN,TEMP,BARO                                | 034 |
| 5     | FORMAT (3F0.0)                                          | 035 |
|       | PIN=BARO-1.12*QIN/13.6                                  | 036 |
|       | RHOST=1.222                                             | 037 |
|       | RHOR=PIN+288./760./TEMP                                 | 038 |
|       | RHO=RHOST*RHOR                                          | 039 |
|       | VISC=0.00001455                                         | 040 |
|       | VIN=SQRT(19.62*QIN/RHO)                                 | 041 |
|       | PR=BARO/760.                                            | 042 |
|       | REDH=3.0*0.0254*VIN/VISC                                | 043 |
|       | WRITE .....                                             | 044 |
|       | DO 12 J=3,8                                             | 045 |
|       | READ (1,6) NPTS(J),DR(J),RW(J),W(J),DEL(J)              | 046 |
| 6     | FORMAT (12,4F0.0)                                       | 047 |
|       | READ (1,8) (UND(I,J),I=1,NPTS(J))                       | 048 |
| 8     | FORMAT(10F0.0)                                          | 049 |
| 12    | CONTINUE                                                | 050 |
|       | DO 15 J=1,8,2                                           | 051 |
|       | DELR(J)=RW(J+1)-RW(J)                                   | 052 |
|       | DELR(J+1)=DELR(J)                                       | 053 |
| 15    | CONTINUE                                                | 054 |

Table A4-2 LISTING OF PROGRAM P1 (Cont'd)

|       |                                                             |     |
|-------|-------------------------------------------------------------|-----|
| C**** | INITIATE BOUNDARY LAYER CALCS.                              | 055 |
|       | J1=3                                                        | 056 |
|       | J2=8                                                        | 057 |
| 10    | DO 30 J=J1,J2,2                                             | 058 |
|       | JK=J+1                                                      | 059 |
|       | NPTOT(J)=NPTS(J)+NPTS(JK)                                   | 060 |
|       | NP=NPTS(J)+1                                                | 061 |
|       | DO 50 I=NP,NPTOT(J)                                         | 062 |
|       | L=NPTOT(J)+1-I                                              | 063 |
|       | UND(I,J)=UND(L,JK)                                          | 064 |
| 50    | CONTINUE                                                    | 065 |
|       | DO 51 I=1,NPTOT(J)                                          | 066 |
|       | L=NPTOT(J)+1-I                                              | 067 |
|       | UND(I,JK)=UND(L,J)                                          | 068 |
| 51    | CONTINUE                                                    | 069 |
| 30    | CONTINUE                                                    | 070 |
|       | DO 501 J=J1,J2                                              | 071 |
|       | N=NPTS(J)                                                   | 072 |
|       | DR1=DR(J)                                                   | 073 |
|       | RW1=RW(J)                                                   | 074 |
|       | W1=W(J)                                                     | 075 |
|       | X=FLOAT(N)                                                  | 076 |
|       | RM=RW1+W1*X*DR1                                             | 077 |
| C**** | FORMULATION OF INTEGRALS.                                   | 078 |
|       | CALL INTEGRAL(1,0,N1,RW1,RM,SUM1,UND,80,8,DR1,RW1,W1,0.0,J) | 079 |
|       | CALL INTEGRAL(2,0,N1,RW1,RM,SUM2,UND,80,8,DR1,RW1,W1,0.0,J) | 080 |
|       | CALL INTEGRAL(3,0,N1,RW1,RM,SUM3,UND,80,8,DR1,RW1,W1,0.0,J) | 081 |
| C**** | CALCULATE B=L PARAMETERS.                                   | 082 |
|       | AA(J)=W1*(RM**2.-RW1**2.)                                   | 083 |
| 25    | AA1=AA(J)                                                   | 084 |
|       | UM(J)=2.*SUM1/AA1                                           | 085 |
|       | DSTAR(J)=(AA1/(2.*RW1)+SUM1/RW1)*100./DELR(J)               | 086 |
|       | THETA(J)=(SUM1+SUM2)/RW1*100./DELR(J)                       | 087 |
|       | H(J)=DSTAR(J)/THETA(J)                                      | 088 |
|       | ALPHA(J)=2.*SUM3/(AA1*UM(J)**3.)                            | 089 |
|       | Q(J)=UM(J)*AA1                                              | 090 |
|       | IF (J.EQ.2) GO TO 3                                         | 091 |
| 501   | CONTINUE                                                    | 092 |
|       | WRITE                                                       | 093 |
|       | SKI=(DSTAR(5)-DSTAR(6))/(DSTAR(5)+DSTAR(6))                 | 094 |
|       | SK0=(DSTAR(7)-DSTAR(8))/(DSTAR(7)+DSTAR(8))                 | 095 |
|       | SK2=(DSTAR(3)-DSTAR(4))/(DSTAR(3)+DSTAR(4))                 | 096 |
|       | WRITE                                                       | 097 |
| C**** | CALCULATE MEAN B=L PARAMETERS.                              | 098 |
|       | DO 55 J=1,8,2                                               | 099 |
|       | J1=J+1                                                      | 100 |
|       | ATOT(J)=AA(J)+AA(J1)                                        | 101 |
|       | UMM(J)=(UM(J)*AA(J)+UM(J1)*AA(J1))/ATOT(J)                  | 102 |
|       | QTOT(J)=Q(J)+Q(J1)                                          | 103 |
|       | ALFAM(J)=(ALPHA(J)*Q(J)+ALPHA(J1)*Q(J1))/QTOT(J)            | 104 |
| 55    | CONTINUE                                                    | 105 |
|       | QB1I=Q(1)/QTOT(1)                                           | 106 |
|       | QB1O=Q(2)/QTOT(1)                                           | 107 |
|       | QB2I=Q(3)/QTOT(3)                                           | 108 |
|       | QB2O=Q(4)/QTOT(3)                                           | 109 |



Table A4-2 LISTING OF PROGRAM P1 (Cont'd)

|      |                                                                         |     |
|------|-------------------------------------------------------------------------|-----|
| C*** | CONTINUITY CHECK,                                                       | 110 |
|      | READ (1,40) (RU(J),J=1,8,2),PROBI,PROBO                                 | 111 |
| 40   | FORMAT (6F0.0)                                                          | 112 |
|      | DO 160 J=1,8,2                                                          | 113 |
|      | QREL(J)=QTOT(J)+RU(J)*100./ATOT(1)/UMM(1)                               | 114 |
| 160  | CONTINUE                                                                | 115 |
|      | QLT=QREL(5)+QREL(7)                                                     | 116 |
|      | DISC(1)=QREL(1)=100.                                                    | 117 |
|      | DISC(3)=QREL(3)=100.                                                    | 118 |
|      | DISC(7)=QLT-100.                                                        | 119 |
|      | WRITE . . . . .                                                         | 120 |
| C*** | CORRECT VEL. RATIOS TO SATISFY CONTINUITY.                              | 121 |
|      | RU3=RU(3)                                                               | 122 |
|      | RU5=RU(5)                                                               | 123 |
|      | RU7=RU(7)                                                               | 124 |
|      | QREL3=QREL(3)                                                           | 125 |
|      | QLT1=QLT                                                                | 126 |
|      | RQ1=QREL(7)/QREL(5)                                                     | 127 |
|      | CONST=(PROBI*QREL(5)+PROBO*QREL(7))/DISC(7)                             | 128 |
|      | RU(5)=RU5*(1.=PROBI/CONST)                                              | 129 |
|      | RU(7)=RU7*(1.=PROBO/CONST)                                              | 130 |
|      | RU(3)=RU3*100./QREL(3)                                                  | 131 |
|      | DO 166 J=3,8,2                                                          | 132 |
|      | QREL(J)=QTOT(J)+RU(J)*100./QTOT(1)                                      | 133 |
| 166  | CONTINUE                                                                | 134 |
|      | RQ=QREL(7)/QREL(5)                                                      | 135 |
|      | QLT=QREL(5)+QREL(7)                                                     | 136 |
|      | CU3=RU(3)/RU3*100.=100.                                                 | 137 |
|      | CU5=RU(5)/RU5*100.=100.                                                 | 138 |
|      | CU7=RU(7)/RU7*100.=100.                                                 | 139 |
|      | CQ3=QREL(3)/QREL3*100.=100.                                             | 140 |
|      | CQ5=QLT/QLT1*100.=100.                                                  | 141 |
|      | CRQ=RQ/RQ1*100.=100.                                                    | 142 |
|      | WRITE . . . . .                                                         | 143 |
|      | READ (1,31) NP2,CPW,DYNH1                                               | 144 |
| 31   | FORMAT (12,2F0.0)                                                       | 145 |
|      | READ (1,32) (P2(I,3),I=1,NP2)                                           | 146 |
| 32   | FORMAT (110F0.0)                                                        | 147 |
|      | DO 110 I=1,NP2                                                          | 148 |
|      | PV(I,3)=P2(I,3)*UND(I,3)                                                | 149 |
|      | L=NP2+1=1                                                               | 150 |
|      | PV(I,4)=PV(L,3)                                                         | 151 |
| 110  | CONTINUE                                                                | 152 |
|      | CALL INTEGRAL(1,0,N2,RW(3),RW(4),SUM5,PV,80,4,DR(3),RW(3),W(3),0.0,1,3) | 154 |
|      | QM1=DYNH1*UMM(1)**2.                                                    | 155 |
|      | CP(3)=CPW*2.*SUM5/(ATOT(3)*QM1)/UMM(3)                                  | 156 |
| C*** | CALCULATE OVERALL PERFORMANCE.                                          | 157 |
|      | READ (1,57) CP(1),CP(5),CP(7)                                           | 158 |
| 57   | FORMAT (3F0.0)                                                          | 159 |
| C*** | CONVERT TO NEW SYSTEM DIVIDE BY ALPHA 1 MEAN.                           | 160 |
|      | DO 61 I=1,7,2                                                           | 161 |
| 61   | CP(I)=CP(I)/ALFAM(1)                                                    | 162 |
|      | AR2=ATOT(3)/ATOT(1)                                                     | 163 |
|      | ALOSS2=1.0 -ALFAM(3)/ALFAM(1)/AR2/AR2 =CP(3)                            | 164 |
|      | RUM3I=UMM(5)+RU(5)/UMM(1)                                               | 165 |
|      | RUM3O=UMM(7)+RU(7)/UMM(1)                                               | 166 |
|      | CPM3=(CP(5)+QREL(5)+CP(7)+QREL(7))/QLT                                  | 167 |
|      | TERM2=(ALFAM(5)+QREL(5)+RUM3I**2.+ALFAM(7)+QREL(7)+RUM3O**2.)/QLT       | 169 |
|      | ALOSS3=1.0=TERM2/ALFAM(1)=CPM3                                          | 169 |
|      | CPM2=CP(3)                                                              | 170 |

Table A4-2 LISTING OF PROGRAM P1 (Cont'd)

|      |                                                                    |     |
|------|--------------------------------------------------------------------|-----|
|      | DO 113 J=1,3,2                                                     | 171 |
| C*** | DETERMINE INITIAL RSTAR.                                           | 172 |
|      | QLIM=0.5                                                           | 173 |
|      | CALL SPLITMK2(QREL(5),QLIM,RSTAR(J),RW(J),UND,80,8,RU(J),QTOT(1),D |     |
|      | 1R(J),W(J),0.0,J)                                                  | 175 |
|      | DRS1=(RSTAR(1)=RW(1))/DEL(1)                                       | 176 |
|      | DRS3=(RSTAR(3)=RW(3))/DEL(3)                                       | 177 |
|      | ERROR(J)=QLIM                                                      | 178 |
|      | AS(J)=RSTAR(J)**2=RW(J)**2                                         | 179 |
|      | AS(J+1)=RW(J+1)**2=RSTAR(J)**2                                     | 180 |
| 113  | CONTINUE                                                           | 181 |
| C*** | CALCULATE SPLIT U/UMAX,ALPHA.                                      | 182 |
|      | DO 130 J=1,4,2                                                     | 183 |
|      | CALL INTEGRAL(1,0,NPS(J),RW(J),RSTAR(J),S1,UND,80,8,DR(J),RW(J),W( |     |
|      | 1J),0.0,J)                                                         | 185 |
|      | CALL INTEGRAL(3,0,NPS(J),RW(J),RSTAR(J),S3,UND,80,8,DR(J),RW(J),W( |     |
|      | 1J),0.0,J)                                                         | 187 |
|      | UMS(J)=2.*S1/AS(J)                                                 | 188 |
|      | ALFAS(J)=2.*S3/(AS(J)*UMS(J)**3)                                   | 189 |
|      | UMS(J+1)=(UMM(J)*ATOT(J)-UMS(J)*AS(J))/AS(J+1)                     | 190 |
|      | ALFAS(J+1)=(ALFAM(J)+100.=ALFAS(J)*QREL(5))/QREL(7)                | 191 |
| 130  | CONTINUE                                                           | 192 |
| C*** | CALCULATE CPSTAR, 1&0.                                             | 193 |
|      | CALL INTEGRAL(1,0,NPS(3),RW(3),RSTAR(3),S1,PV,80,4,DR(3),RW(3),W(3 |     |
|      | 1),0.0,3)                                                          | 195 |
|      | CPS(3)=CPW+2.*S1/(AS(3)*QM1)/UMS(3)                                | 196 |
|      | CPS(3)=CPS(3)/ALFAM(1)                                             | 197 |
|      | CPS(4)=(CP(3)+100.=CPS(3)*QREL(5))/QREL(7)                         | 198 |
| C*** | CALCULATE SPLIT PERFORMANCE ETC.                                   | 199 |
|      | RAS(1)=ALFAM(1)/ALFAS(1)                                           | 200 |
|      | RAS(2)=ALFAM(1)/ALFAS(2)                                           | 201 |
|      | RUS(1)=UMM(1)/UMS(1)                                               | 202 |
|      | RUS(2)=UMM(1)/UMS(2)                                               | 203 |
|      | CPSS(3)=CPS(3)*RUS(1)**2*RAS(1)                                    | 204 |
|      | CPSS(4)=CPS(4)*RUS(2)**2*RAS(2)                                    | 205 |
|      | CPSS(5)=CP(5)*RUS(1)**2*RAS(1)                                     | 206 |
|      | CPSS(7)=CP(7)*RUS(2)**2*RAS(2)                                     | 207 |
|      | UUO=UMS(4)/UMS(2)*RU(3)                                            | 208 |
|      | UUI=UMS(3)/UMS(1)*RU(3)                                            | 209 |
|      | ALOSI2= 1.0 =ALFAS(3)*UUI**2/ALFAS(1)=CPSS(3)                      | 210 |
|      | BLOSI2=ALOSI2/RUS(1)**2/RAS(1)                                     | 211 |
|      | BLOSO2=(ALOSI2+100.=BLOSI2*QREL(5))/QREL(7)                        | 212 |
|      | ALQSO2=BLOSO2*RUS(2)**2*RAS(2)                                     | 213 |
|      | UUO3=UMM(7)/UMS(2)*RU(7)                                           | 214 |
|      | UUI3=UMM(5)/UMS(1)*RU(5)                                           | 215 |
|      | ALS13I= 1.0 =ALFAM(5)*UUI3**2/ALFAS(1)=CPSS(5)                     | 216 |
|      | ALS13O= 1.0 =ALFAM(7)*UUO3**2/ALFAS(2)=CPSS(7)                     | 217 |
|      | ALS23I=ALS13I=ALOSI2                                               | 218 |
|      | ALS23O=ALS13O=ALOSO2                                               | 219 |
|      | BLS13I=ALS13I/RUS(1)**2/RAS(1)                                     | 220 |
|      | BLS13O=ALS13O/RUS(2)**2/RAS(2)                                     | 221 |
|      | BLS23I=BLS13I=BLOSI2                                               | 222 |
|      | BLS23O=BLS13O=BLOSO2                                               | 223 |
|      | ALS23I=ALS23I/UUI**2+ALFAS(1)/ALFAS(3)                             | 224 |
|      | ALS23O=ALS23O/UUO**2+ALFAS(2)/ALFAS(4)                             | 225 |
|      | AR3I=ATOT(5)/ATOT(1)                                               | 226 |
|      | AR3O=ATOT(7)/ATOT(1)                                               | 227 |
|      | CPI2=1.0=1.0/AR2/AR2/ALFAM(1)                                      | 228 |
|      | CPI3=1.=(1./(1.+RQ))**3.*(1./AR3I/AR3I+RQ**3./AR3O/AR3O)           | 229 |
|      | AREF=SQRT(1./(1.=CPI3))                                            | 230 |
|      | CPI3=(CPI3=1.0)/ALFAM(1)+1.0                                       | 231 |

Table A4-2 LISTING OF PROGRAM P1 (Cont'd)

|      |                     |     |
|------|---------------------|-----|
|      | AR23=AREF/AR2       | 232 |
|      | ARSI2=AS(3)/AS(1)   | 233 |
|      | ARSO2=AS(4)/AS(2)   | 234 |
|      | ARSI3=ATOT(5)/AS(1) | 235 |
|      | ARSO3=ATOT(7)/AS(2) | 236 |
|      | ARI23=ARSI3/ARSI2   | 237 |
|      | ARO23=ARSO3/ARSO2   | 238 |
|      | ETA2=CPM2/CPI2*100. | 239 |
|      | ETA3=CPM3/CPI3*100. | 240 |
|      | WRITE .....         | 241 |
| 1001 | CONTINUE            | 242 |
| 1000 | STOP                | 243 |
|      | END                 | 244 |

|      |                                                                     |     |
|------|---------------------------------------------------------------------|-----|
|      | SUBROUTINE SPLITMK2(QSP,QLIM,RS,RW,V,NR,NC,RV,Q1,DR,W,ANG,J)        | 245 |
| C*** | THIS SUBROUTINE CALCULATES THE STAGNATION STREAMLINE RADIUS (RS) IN | 246 |
| C*** | THE PRE-DIFFUSER GIVEN THE INNER ANNULUS FLOW (QSP)                 | 247 |
|      | DIMENSION V(NR,NC),UM(8)                                            | 248 |
|      | COMMON /MEAN/UM                                                     | 249 |
|      | RS=SQRT(RV**2+W*QSP*Q1/UM(J)/100.)                                  | 250 |
|      | DO 10 K=1,100                                                       | 251 |
|      | CALL INTEGRAL(1,0,N2,RW,RS,S,V,NR,NC,DR,RW,W,ANG,J)                 | 252 |
|      | QRS=2.*S*RV*100./Q1                                                 | 253 |
|      | DQ=QSP*QRS                                                          | 254 |
|      | WRITE (2,5) N2,RS,DQ                                                | 255 |
| 5    | FORMAT (5X,13,2F10.3)                                               | 256 |
|      | IF (ABS(DQ).LT.QLIM) GO TO 20                                       | 257 |
| 10   | RS=RS+0.005*W*DQ*Q1/RS/RV/V(N2,J)                                   | 258 |
| 20   | RETURN                                                              | 259 |
|      | END                                                                 | 260 |

|    |                                              |     |
|----|----------------------------------------------|-----|
|    | SUBROUTINE FIT3 (X,Y,E1,E2,E3,E,C)           | 261 |
|    | DIMENSION X(10),Y(10),P(4,3),Q(3,2),R(2)     | 262 |
|    | DIMENSION E(3),C(3)                          | 263 |
|    | E(1)=E1                                      | 264 |
|    | E(2)=E2                                      | 265 |
|    | E(3)=E3                                      | 266 |
|    | DO 10 J=1,3                                  | 267 |
|    | DO 5 I=1,3                                   | 268 |
| 5  | P(I,J)=X(J)**E(I)                            | 269 |
| 10 | P(4,J)=Y(J)                                  | 270 |
|    | DO 15 J=1,2                                  | 271 |
|    | J1=J+1                                       | 272 |
|    | DO 15 I=1,3                                  | 273 |
|    | I1=I+1                                       | 274 |
| 15 | Q(I,J)=P(I1,J1)/P(I,J1)-P(I1,1)/P(I,1)       | 275 |
|    | DO 20 I=1,2                                  | 276 |
|    | I1=I+1                                       | 277 |
| 20 | R(I)=Q(I1,2)/Q(I,2)-Q(I1,1)/Q(I,1)           | 278 |
|    | C(3)=R(2)/R(1)                               | 279 |
|    | C(2)=(Q(3,1)-C(3)*Q(2,1))/Q(1,1)             | 280 |
|    | C(1)=(P(4,1)-C(3)*P(3,1)-C(2)*P(2,1))/P(1,1) | 281 |
|    | RETURN                                       | 282 |
|    | END                                          | 283 |

Table A4-2 LISTING OF PROGRAM P1 (Cont'd)

|     |                                                                      |     |
|-----|----------------------------------------------------------------------|-----|
|     | FUNCTION RAD(I,RW,W,DR,R,ANG)                                        | 284 |
|     | R=RW+W*COS(ANG)*(FLOAT(I)=0.5)*DR                                    | 285 |
|     | RAD=R                                                                | 286 |
|     | RETURN                                                               | 287 |
|     | END                                                                  | 288 |
|     | <br>                                                                 |     |
|     | SUBROUTINE INTEGRAL(IPOWER,N1,N2,R1,R2,SUM,V,NR,NC,DR,RW,W,ANG,J)    | 289 |
|     | DIMENSION V(NR,NC),X(60),Y(60),Z(10)                                 | 290 |
|     | DIMENSION E(3)                                                       | 291 |
|     | C**** THIS SUBROUTINE CALCULATES THE INTEGRAL (SUM) OF UND**IPOWER   | 292 |
|     | C**** BETWEEN THE LIMITS R = R1 TO R2. THE INTEGRAL FOR EACH ELEMENT | 293 |
|     | C**** IS OBTAINED ANALYTICALLY USING A CURVE FIT BY "FIT3".          | 294 |
|     | C**** I.E. SUM = INTEGRAL(UND**IPOWER*RADIUS)*DR                     | 295 |
|     | NN1=N1                                                               | 296 |
|     | SUM=0.0                                                              | 297 |
|     | IF (N1.GT.1) GO TO 15                                                | 298 |
|     | SUM=(RW+W*DR*0.5)*DR*0.5*(0.7*V(1,J))**IPOWER                        | 299 |
|     | DO 10 I=1,3                                                          | 300 |
|     | X(I)=RAD(I,RW,W,DR,R,ANG)                                            | 301 |
| 10  | Y(I)=V(I,J)**IPOWER*X(I)                                             | 302 |
|     | R1=X(1)                                                              | 303 |
|     | CALL FIT3 (X,Y,0.0,1.0,2.0,E,Z)                                      | 304 |
|     | X2=X(2)                                                              | 305 |
|     | DRC=W*(X(3)-R2)                                                      | 306 |
|     | IF (DRC.GT.0.0) X2=R2                                                | 307 |
|     | A=Z(3)*X2**3/3.+Z(2)*X2**2/2.+Z(1)*X2                                | 308 |
|     | B=Z(3)*R1**3/3.+Z(2)*R1**2/2.+Z(1)*R1                                | 309 |
|     | SUM=SUM+(A-B)*W                                                      | 310 |
|     | IF (DRC.GT.0.0) GO TO 999                                            | 311 |
|     | IF (N1.LT.2) NN1=2                                                   | 312 |
| 15  | DO 30 I=NN1,100                                                      | 313 |
|     | K1=1                                                                 | 314 |
|     | DO 20 K=(I=1),(I+1)                                                  | 315 |
|     | X(K1)=RAD(K,RW,W,DR,R,ANG)                                           | 316 |
|     | Y(K1)=V(K,J)**IPOWER*X(K1)                                           | 317 |
| 20  | K1=K1+1                                                              | 318 |
|     | CALL FIT3 (X,Y,0.0,1.0,2.0,E,Z)                                      | 319 |
|     | X2=X(3)                                                              | 320 |
|     | DRC=W*(X(3)-R2)                                                      | 321 |
|     | IF (DRC.GT.0.0) X2=R2                                                | 322 |
|     | A=Z(3)*X2**3/3.+Z(2)*X2**2/2.+Z(1)*X2                                | 323 |
|     | B=Z(3)*X(2)**3/3.+Z(2)*X(2)**2/2.+Z(1)*X(2)                          | 324 |
|     | N2=I+1                                                               | 325 |
|     | SUM=SUM+(A-B)*W                                                      | 326 |
|     | IF (DRC.GT.0.0) GO TO 999                                            | 327 |
| 30  | CONTINUE                                                             | 328 |
|     | WRITE (2,40) I                                                       | 329 |
| 40  | FORMAT (10X,'INTEGRAL NO. POINTS I,13/')                             | 330 |
| 999 | SUM=SUM/COS(ANG)                                                     | 331 |
|     | RETURN                                                               | 332 |
|     | END                                                                  | 333 |
|     | FINISH                                                               | 334 |

TABLE A4-3 SAMPLE CALCULATIONS FOR TEST 3-0718/A

| CALCULATION                                                                                                                                                                                                                                                                                                                                                                                                                                                                                                     | REFERENCE                                                                             |
|-----------------------------------------------------------------------------------------------------------------------------------------------------------------------------------------------------------------------------------------------------------------------------------------------------------------------------------------------------------------------------------------------------------------------------------------------------------------------------------------------------------------|---------------------------------------------------------------------------------------|
| <p><u>1. Pre-diffuser Pressure Recovery Coefficient</u></p> $\tilde{c}_{p_2} = c_{p_{wo_2}} + \frac{(\tilde{p} - p_{wo})_2}{\alpha_1 \bar{q}_1}$ <p>where: <math>c_{p_{wo_2}} = 0.4603/\alpha_1 = 0.4603/1.0615 = 0.4336</math></p> <p><math>(\tilde{p} - p_{wo})_2 = 2.67 \text{ mm. w.g.}</math></p> <p>and <math>\bar{q}_1 = 54.8 \times (.8744)^2 = 41.90 \text{ mm. w.g.}</math></p> <p>hence <math>\tilde{c}_{p_2} = 0.4336 + \frac{2.67}{1.0615 \times 41.9} = \underline{\underline{0.4936}}</math></p> | <p>see Table A3-5</p> <p>see Fig. A3-1</p> <p>Line 155</p> <p>Lines 156 &amp; 162</p> |
| <p><u>2. Pre-diffuser Loss Coefficient</u></p> $\tilde{\lambda}_{1-2} = 1 - \frac{\alpha_2}{\alpha_1 AR^2} - \tilde{c}_{p_2}$ <p>where <math>\alpha_2 = 1.5265</math> and <math>AR = 1.780</math></p> <p>hence <math>\tilde{\lambda}_{1-2} = 1 - \frac{1.5265}{1.0615 \times (1.78)^2} - 0.4936 = \underline{\underline{0.0525}}</math></p>                                                                                                                                                                     | <p>Eqn. 1-3-15</p> <p>Line 164</p>                                                    |
| <p><u>3. Pre-diffuser Effectiveness</u></p> $\tilde{\xi}_2 = (\tilde{c}_p/c_{p'})_2 = \tilde{c}_{p_2} / \left(1 - \frac{1}{\alpha_1 AR^2}\right)$ <p>hence <math>\tilde{\xi}_2 = (0.4936/0.7027) \times 100 = \underline{\underline{70.25\%}}</math></p>                                                                                                                                                                                                                                                        | <p>Eqn. 1-3-12</p> <p>Line 239</p>                                                    |
| <p><u>4. Flow Split Ratio</u></p> <p>Using the velocity ratios corrected for errors in observed mass flow (see lines 122 to 134) we have,</p> $S = 2.15 \left(\frac{\bar{u}}{\bar{U}}\right)_{4_0} \left(\frac{U_{4_0}}{U_1}\right) \left(\frac{U_1}{U_{4_i}}\right) \left(\frac{\bar{U}}{\bar{u}}\right)_{4_i}$ <p>hence <math>S = 2.15 \times (.9396 \times .4397) / (.5281 \times .9256) = \underline{\underline{1.817}}</math></p>                                                                          | <p>Equivalent to Line 135</p>                                                         |

TABLE A4-3 SAMPLE CALCULATIONS FOR TEST 3-0718/A (continued)

| CALCULATION                                                                                                                                                                                                                                                                                                                                                                                                                                                                                                                                                                                                                 | REFERENCE                                               |
|-----------------------------------------------------------------------------------------------------------------------------------------------------------------------------------------------------------------------------------------------------------------------------------------------------------------------------------------------------------------------------------------------------------------------------------------------------------------------------------------------------------------------------------------------------------------------------------------------------------------------------|---------------------------------------------------------|
| <p>Also <math>Q_i = \left(\frac{1}{1+S}\right)</math> and <math>Q_o = \left(\frac{S}{1+S}\right)</math><br/>                     hence <math>Q_i = \underline{35.50\%}</math> and <math>Q_o = \underline{64.50\%}</math></p>                                                                                                                                                                                                                                                                                                                                                                                                | <p>See Eqn. 1-3-22</p>                                  |
| <p><u>5. Overall Pressure Recovery</u></p> $\tilde{C}_{p4} = (Q_i C_{p4_i} + Q_o C_{p4_o}) / (Q_i + Q_o)$ <p>hence <math>\tilde{C}_{p4} = (.355 \times .4208 + .645 \times .5977) = \underline{0.5349}</math></p>                                                                                                                                                                                                                                                                                                                                                                                                           | <p>Eqn. 1-3-18<br/>Line 167</p>                         |
| <p><u>6. Overall Loss Coefficient</u></p> $\tilde{\lambda}_{1-4} = 1 - (\text{TERM2})/\alpha_1 - \tilde{C}_{p4}$ <p>where <math>\text{TERM2} = \frac{1}{(Q_i + Q_o)} \left\{ \alpha_{4_i} \left(\frac{\bar{u}_{4_i}}{\bar{u}_1}\right)^2 Q_i + \alpha_{4_o} \left(\frac{\bar{u}_{4_o}}{\bar{u}_1}\right)^2 Q_o \right\}</math></p> $= 1.0298 \left(\frac{.9256 \times .5281}{.8744}\right)^2 \times .355 + 1.0282 \left(\frac{.9396 \times .4397}{.8744}\right)^2 \times .645$ $= .11425 + .14805 = \underline{0.2623}$ <p>hence <math>\tilde{\lambda}_{1-4} = 1 - (0.2623/1.0615) - 0.5349 = \underline{0.2179}</math></p> | <p>See Eqn. 1-3-17<br/>Line 168<br/>Line 169</p>        |
| <p><u>7. Overall Effectiveness</u></p> $\tilde{\eta}_4 = \tilde{C}_{p4} / C_{p4}^*$ <p>where <math>C_{p4}^* = 1 - \frac{1}{\alpha_1} \left(\frac{1}{1+S}\right)^3 \left\{ \frac{1}{AR_i^2} + \frac{S^3}{AR_o^2} \right\}</math></p> $= 1 - \frac{1}{1.0615} \left(\frac{1}{2.817}\right)^3 \left\{ \frac{1}{0.635^2} + \frac{1.817^3}{1.365^2} \right\} = \underline{0.7598}$ <p>hence <math>\tilde{\eta}_4 = (0.5349/0.7598) \times 100 = \underline{70.40\%}</math></p>                                                                                                                                                   | <p>Eqn. 1-3-25<br/>Lines 229 &amp; 231<br/>Line 240</p> |

Table A4-4 MAIN PERFORMANCE ANALYSIS PROGRAM OUTPUT  
LISTING FOR Test 3-0718/A

\*\*\*\*\* TEST RIG GEOMETRY \*\*\*\*\*  
 \*  
 \* N=D DUMP GAP(D/H2) = 0.70 \*  
 \*  
 \* PRE DIFFUSER : AREA RATIO = 1.80 INCLUDED ANGLE=12.0DEG. \*  
 \*  
 \* BLOCKAGE(NOM): THROTTLE TURNS 57; INNER ANNULUS, 60 % \*  
 \*  
 \* APPROX. FLOW SPLIT = 1.70 \*  
 \*  
 \*\*\*\*\*

INLET MAXIMUM VELOCITY = 30.37 M/SEC.  
 INLET REYNOLDS' NUMBER = 159072. (N=D)  
 AMBIENT TEMPERATURE = 299.0 DEG.K.  
 AMBIENT PRESSURE RATIO = 0.996 (P/P=ISA)  
 RIG AIR DENSITY RATIO = 0.954 (D/D=ISA)

INDIVIDUAL BOUNDARY-LAYER PARAMETERS.

|                | $\frac{UBAR}{UMAX}$ | DELTA STAR %H | THETA XH | SHAPE FACTOR | ALPHA  |
|----------------|---------------------|---------------|----------|--------------|--------|
| INLET ( INNER  | 0.8754              | 6.413         | 4.728    | 1.3565       | 1.0601 |
| ( OUTER        | 0.8734              | 6.169         | 4.516    | 1.3661       | 1.0627 |
| OUTLET ( INNER | 0.5999              | 26.435        | 8.755    | 3.0194       | 1.8309 |
| ( OUTER        | 0.7576              | 9.207         | 5.321    | 1.7303       | 1.2130 |
| S/L INNER ( I  | 0.9106              | 1.526         | 1.042    | 1.4647       | 1.0660 |
| ( O            | 0.9283              | 5.414         | 4.448    | 1.2172       | 1.0236 |
| S/L OUTER ( I  | 0.9494              | 1.723         | 1.252    | 1.3759       | 1.0332 |
| ( O            | 0.9350              | 4.170         | 3.349    | 1.2449       | 1.0258 |

PRE-DIFFUSER OUTLET RADIAL DISTORTION FACTOR = 0.48  
 INNER S/L " " " = 0.56  
 OUTER S/L " " " = 0.42

VELOCITY PROFILE PARAMETERS.

|           | INLET  | OUTLET | SETTLING LENGTH |        |
|-----------|--------|--------|-----------------|--------|
|           |        |        | INNER           | OUTER  |
| UBAR/UMAX | 0.8744 | 0.6684 | 0.9256          | 0.9396 |
| ALPHA BAR | 1.0615 | 1.5265 | 1.0298          | 1.0282 |

Table A4-4 PROGRAM P1 OUTPUT FOR Test 3-0718/A (Cont'd)

CONTINUITY CHECK.

|           | INLET  | OUTLET | SETTLING - LENGTH |       |        |
|-----------|--------|--------|-------------------|-------|--------|
|           |        |        | INNER             | OUTER | TOTAL  |
| FLOW %Q1  | 100.00 | 101.51 | 36.98             | 67.18 | 104.16 |
| ERROR %Q1 | 0.00   | 1.51   | ---               | ---   | 4.16   |

CORRECTIONS MADE TO SATISFY CONTINUITY.

|            | U2/U1  | U41/U1 | U40/U1 | Q2/Q1% | Q4/Q1% | S     |
|------------|--------|--------|--------|--------|--------|-------|
| ORIGINAL:  | 0.7460 | 0.5500 | 0.4580 | 101.51 | 104.16 | 1.817 |
| CORRECTED: | 0.7340 | 0.5281 | 0.4397 | 100.00 | 100.00 | 1.817 |
| % CHANGE   | -1.49  | -3.99  | -3.99  | -1.49  | -3.99  | 0.00  |

PROBABILITY OF ERROR IN Q41 = 50. %

PROBABILITY OF ERROR IN Q40 = 50. %

SPLIT FLOW ITERATION RESULTS:

|        | QR13   | DQ-%Q1<br>(ERROR) | YS/DR |
|--------|--------|-------------------|-------|
| INLET  | 35.505 | -0.002            | 0.388 |
| OUTLET | 35.505 | -0.148            | 0.499 |

MEAN EXPANSION RATIOS (AREA RATIOS)

|                    | DIFFUSER<br>(1-2) | S/L<br>(2-4) | OVERALL<br>(1-4) |
|--------------------|-------------------|--------------|------------------|
| SPLIT FLOW (INNER) | 2.236             | 0.771        | 1.723            |
| (OUTER)            | 1.514             | 1.428        | 2.161            |
| EFFECTIVE OVERALL  | 1.780             | 1.113        | 1.980            |



Table A4-4 PROGRAM P1 OUTPUT FOR Test 3-0718/A (Cont'd)

SPLIT FLOW BOUNDARY LAYER PARAMETERS.

(PRE-DIFFUSER)

|                | INLET  |        | OUTLET |        |
|----------------|--------|--------|--------|--------|
|                | INNER  | OUTER  | INNER  | OUTER  |
| UBAR/UMAX-STAR | 0.8424 | 0.8930 | 0.5149 | 0.8008 |
| ALPHA STAR     | 1.0642 | 1.0600 | 1.9914 | 1.2707 |

SPLIT FLOW PERFORMANCE DATA.

|           | PRE-DIFFUSER       |                    | SETTLING LENGTH    |                    |
|-----------|--------------------|--------------------|--------------------|--------------------|
|           | INNER              | OUTER              | INNER              | OUTER              |
| CP-STAR   | 0.5197<br>(0.5584) | 0.4793<br>(0.4601) | 0.4208<br>(0.4522) | 0.5977<br>(0.5738) |
| LAMDA     | 0.0596<br>(0.0641) | 0.0485<br>(0.0466) | 0.2066<br>(0.2220) | 0.2276<br>(0.2185) |
| LAMDA 2-4 | ---                | ---                | 0.1470<br>(0.4184) | 0.1791<br>(0.3303) |

NOTE: THE FIGURES IN PARENTHESES ARE REFERRED TO SPLIT FLOW ENTRY M.W.M DYNAMIC PRESSURE (e.g.  $\alpha_i \frac{1}{2} \rho u_i^2$ )

OVERALL PERFORMANCE DATA.

|                   | DIFFUSER<br>OUTLET-2 | SETTLING LENGTH:-          |        |        |
|-------------------|----------------------|----------------------------|--------|--------|
|                   |                      | MEAN                       | INNER  | OUTER  |
| PRESSURE RECOVERY | 0.4936               | 0.5349                     | 0.4208 | 0.5977 |
| LOSS COEFFICIENT  | 0.0525               | 0.2179 (SEE SPLIT RESULTS) |        |        |

EFFECTIVENESS-2 = 70.25 % EFFECTIVENESS-4 = 70.40 %

Fig. A4-3 FLOW DIAGRAM FOR HEAD RAKE DATA ANALYSIS PROGRAM (P4).

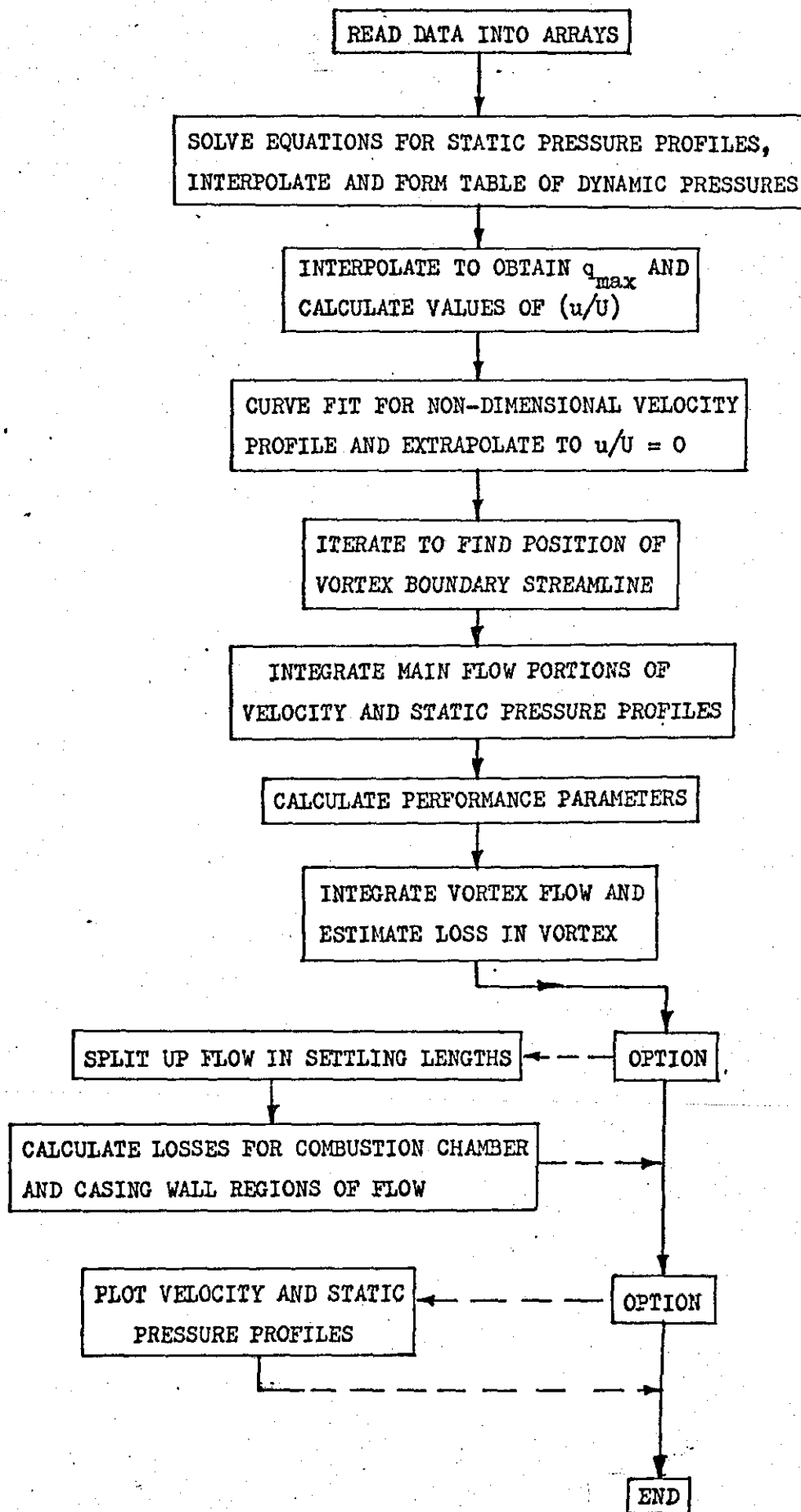


Table A4-5 PROGRAM P4 OUTPUT FOR TEST 3-0718/A.

TEST NO. 3-0718

INNER: QMAX = 29.50 U/U1 = 0.7720

OUTER: QMAX = 41.06 U/U1 = 0.9107

| ----- INNER ANNULUS ----- |                 |        | ----- OUTER ANNULUS ----- |                 |        |
|---------------------------|-----------------|--------|---------------------------|-----------------|--------|
| YH/H3                     | P-PH<br>mm.w.g. | U/UMAX | YH/H3                     | P-PH<br>mm.w.g. | U/UMAX |
| 0.020                     | 0.811           | 0.989  | 0.020                     | 1.137           | 0.990  |
| 0.060                     | 2.307           | 0.956  | 0.060                     | 3.216           | 1.000  |
| 0.100                     | 3.646           | 0.909  | 0.100                     | 5.052           | 0.981  |
| 0.140                     | 4.837           | 0.847  | 0.140                     | 6.663           | 0.934  |
| 0.180                     | 5.892           | 0.796  | 0.180                     | 8.069           | 0.888  |
| 0.220                     | 6.821           | 0.745  | 0.220                     | 9.288           | 0.831  |
| 0.260                     | 7.633           | 0.696  | 0.260                     | 10.337          | 0.763  |
| 0.300                     | 8.337           | 0.646  | 0.300                     | 11.232          | 0.689  |
| 0.340                     | 8.924           | 0.595  | 0.340                     | 11.989          | 0.613  |
| 0.380                     | 9.461           | 0.543  | 0.380                     | 12.623          | 0.532  |
| 0.420                     | 9.999           | 0.492  | 0.420                     | 13.148          | 0.445  |
| 0.460                     | 10.564          | 0.440  | 0.460                     | 13.577          | 0.352  |
| 0.500                     | 10.564          | 0.388  | 0.500                     | 13.923          | 0.253  |
| 0.540                     | 10.808          | 0.335  | 0.540                     | 14.196          | 0.149  |
| 0.580                     | 11.002          | 0.282  | 0.580                     | 14.407          | 0.038  |
| 0.620                     | 11.153          | 0.229  | 0.620                     | 14.568          | 0.000  |
| 0.660                     | 11.263          | 0.176  | 0.660                     | 14.685          | 0.000  |
| 0.700                     | 11.353          | 0.122  | 0.700                     | 14.769          | 0.000  |
| 0.740                     | 11.412          | 0.068  | 0.740                     | 14.825          | 0.000  |
| 0.780                     | 11.452          | 0.014  | 0.780                     | 14.861          | 0.000  |
| 0.820                     | 11.477          | 0.000  | 0.820                     | 14.882          | 0.000  |

B=L PARAMETERS

|       | HEAD   |        | VORTEX |          |
|-------|--------|--------|--------|----------|
|       | U/UMAX | ALPHA  | U/UMAX | FLOW %Q1 |
| INNER | 0.5836 | 1.5404 | 0.0135 | 0.13     |
| OUTER | 0.7204 | 1.1241 | 0.1121 | 4.90     |

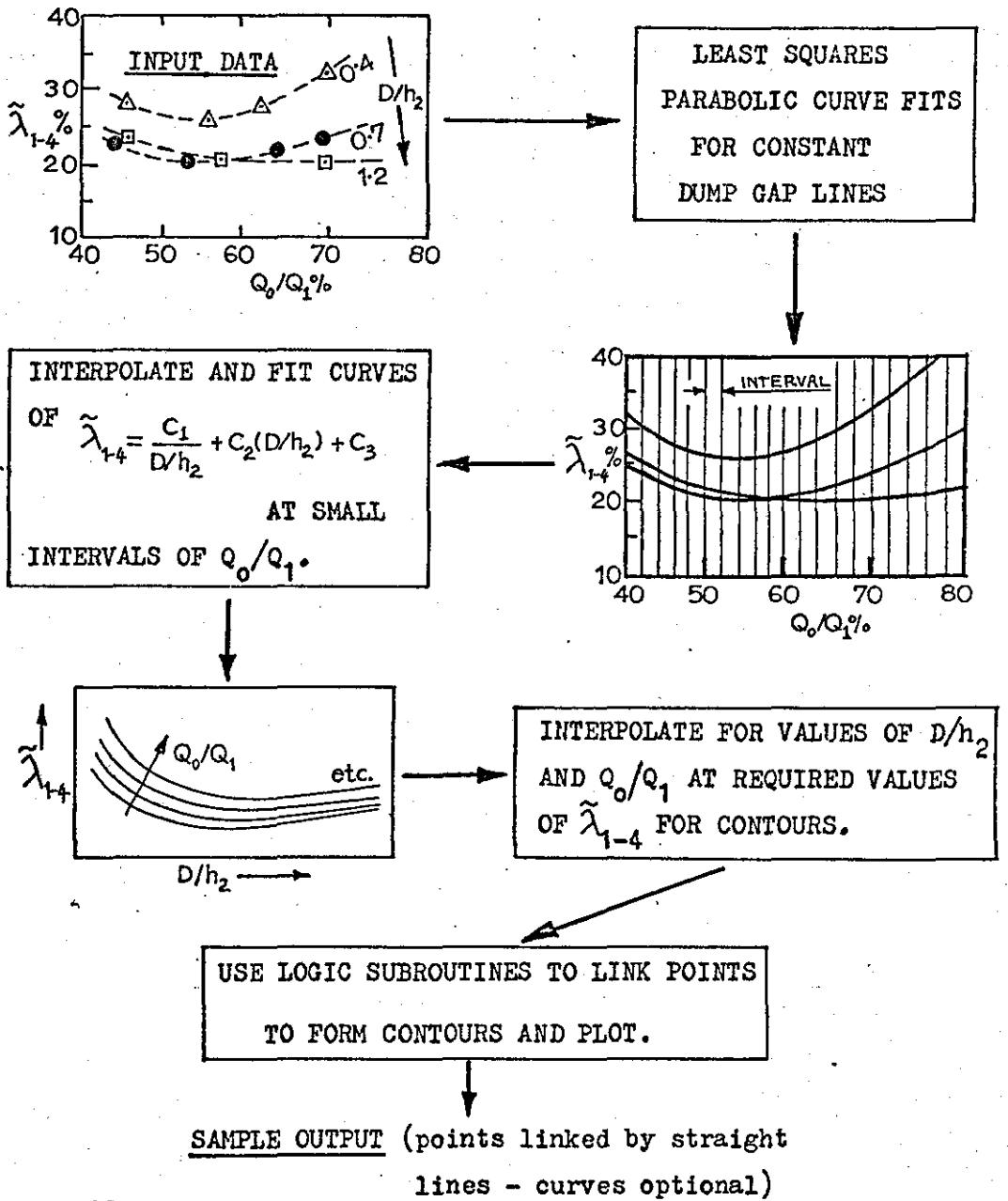
STAGNATION STREAMLINE: YH1/H3 = 0.708 YH0/H3 = 0.423

PERFORMANCE UP TO HEAD

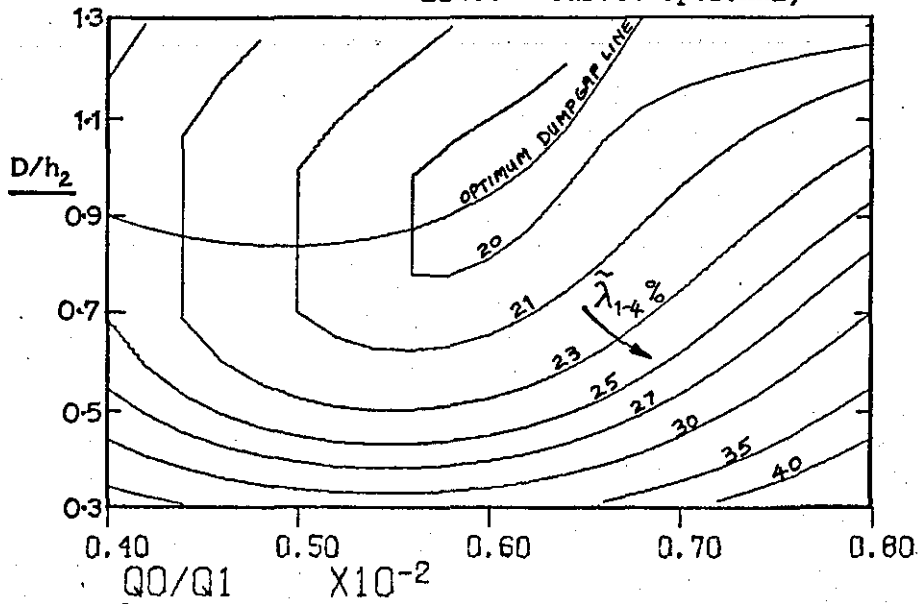
|       | CP3    | HEAD        |             | VORTEX                 |
|-------|--------|-------------|-------------|------------------------|
|       |        | LOSS<br>1-3 | LOSS<br>2-3 | INDUCED<br>LOSS COEFF. |
| INNER | 0.4025 | 0.1428      | 0.0832      | 0.0000                 |
| OUTER | 0.2356 | 0.0882      | 0.0397      | 0.0048                 |
| MEAN  | 0.2951 | 0.1058      | --          | --                     |

Fig. A4-4 METHOD OF ANALYSING PERFORMANCE CONTOUR MAPS (PROGRAM P3)

(Sample data for Overall Loss Coefficient, Diffuser 3)



SAMPLE OUTPUT (points linked by straight lines - curves optional)



APPENDIX 5.

PRE-DIFFUSER OUTLET PROFILES

Fig. A5-1 PRE-DIFFUSER OUTLET VELOCITY PROFILES FOR 'CT' TESTS.

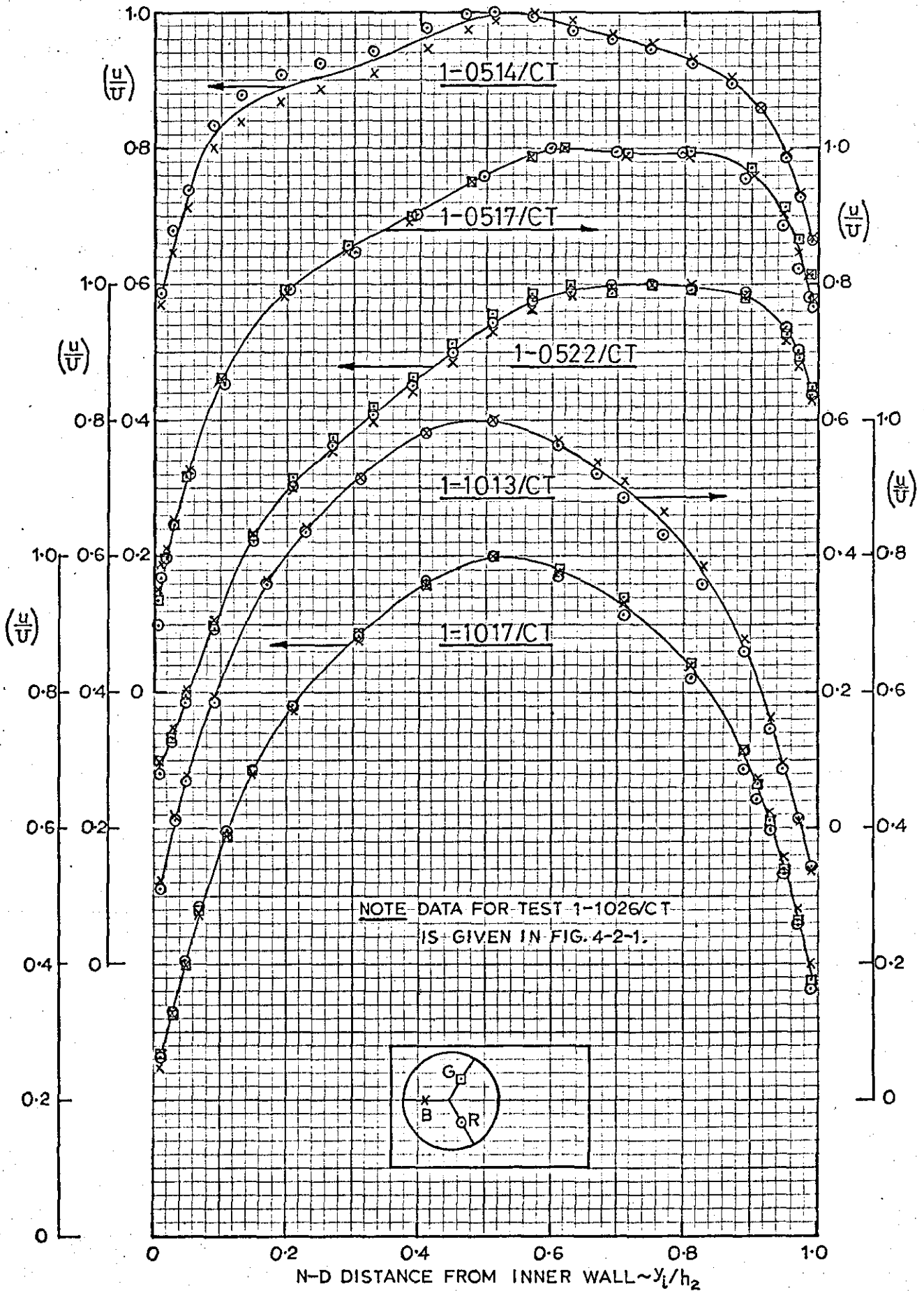


Fig.A5-2 PRE-DIFFUSER OUTLET VELOCITY PROFILES FOR "CT" TESTS.

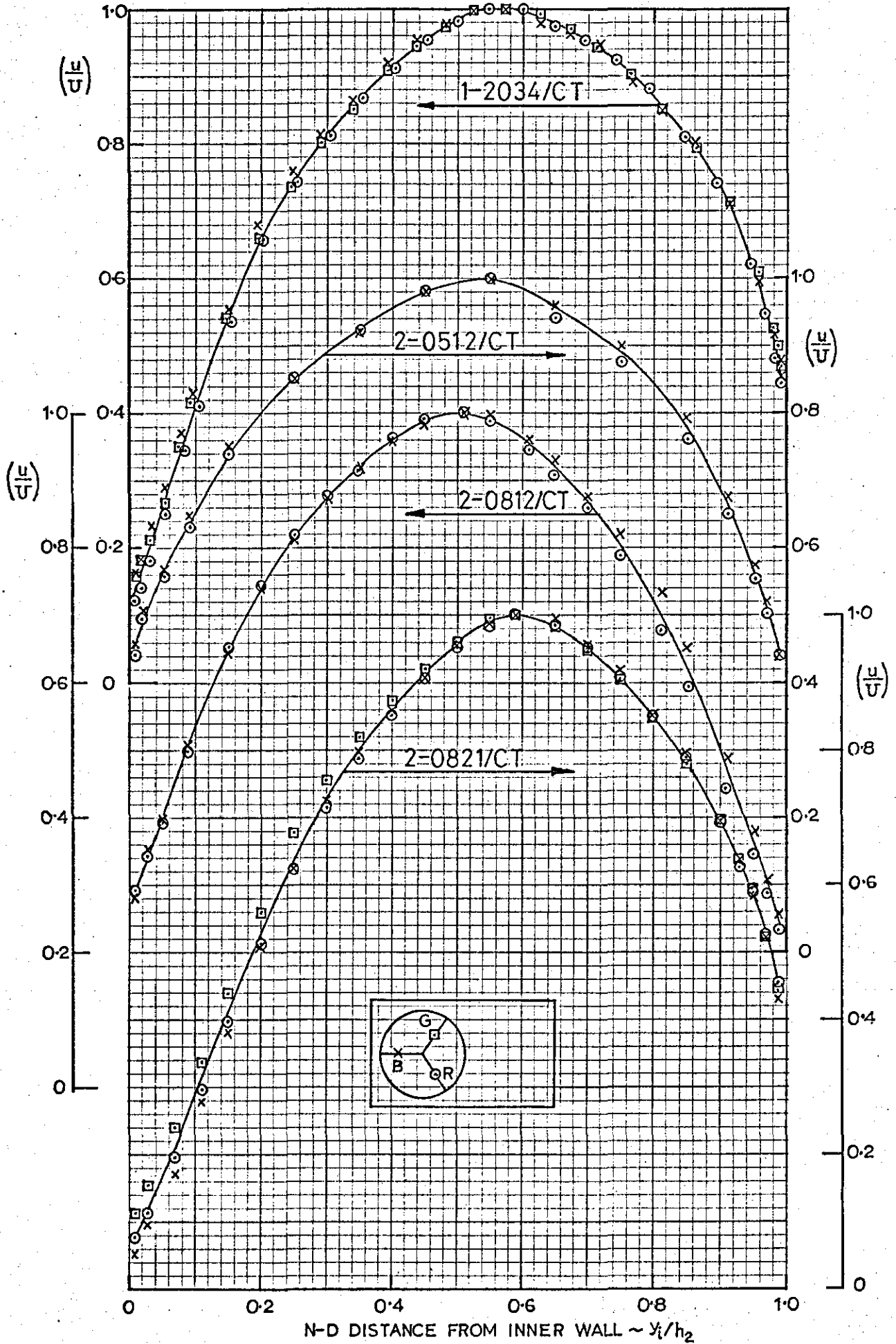


Fig.A5-3 PRE-DIFFUSER OUTLET VELOCITY PROFILES FOR "CT" TESTS.

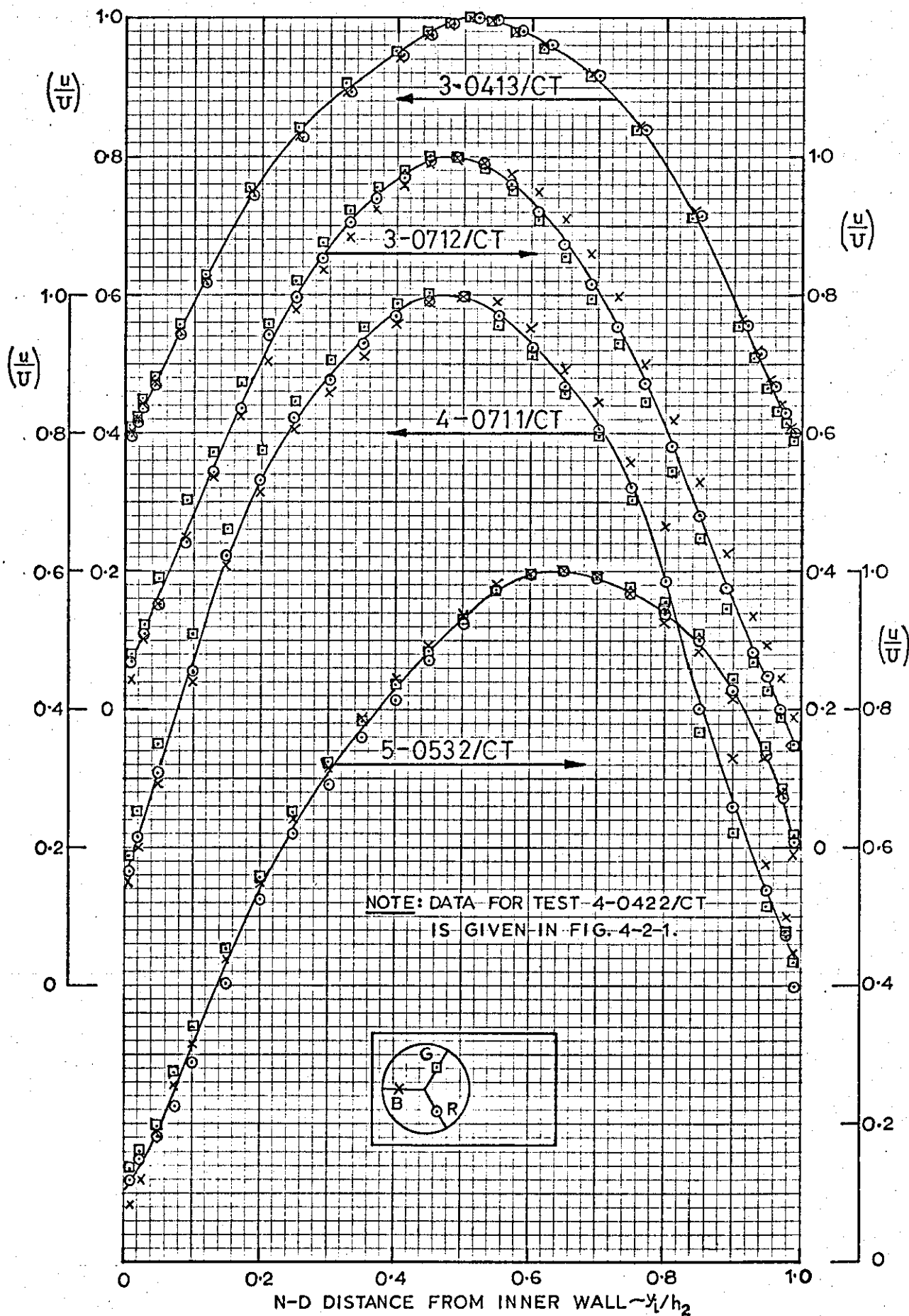


Fig.A5-4

PRE-DIFFUSER OUTLET PROFILES  
FOR TEST SERIES 1-0.5

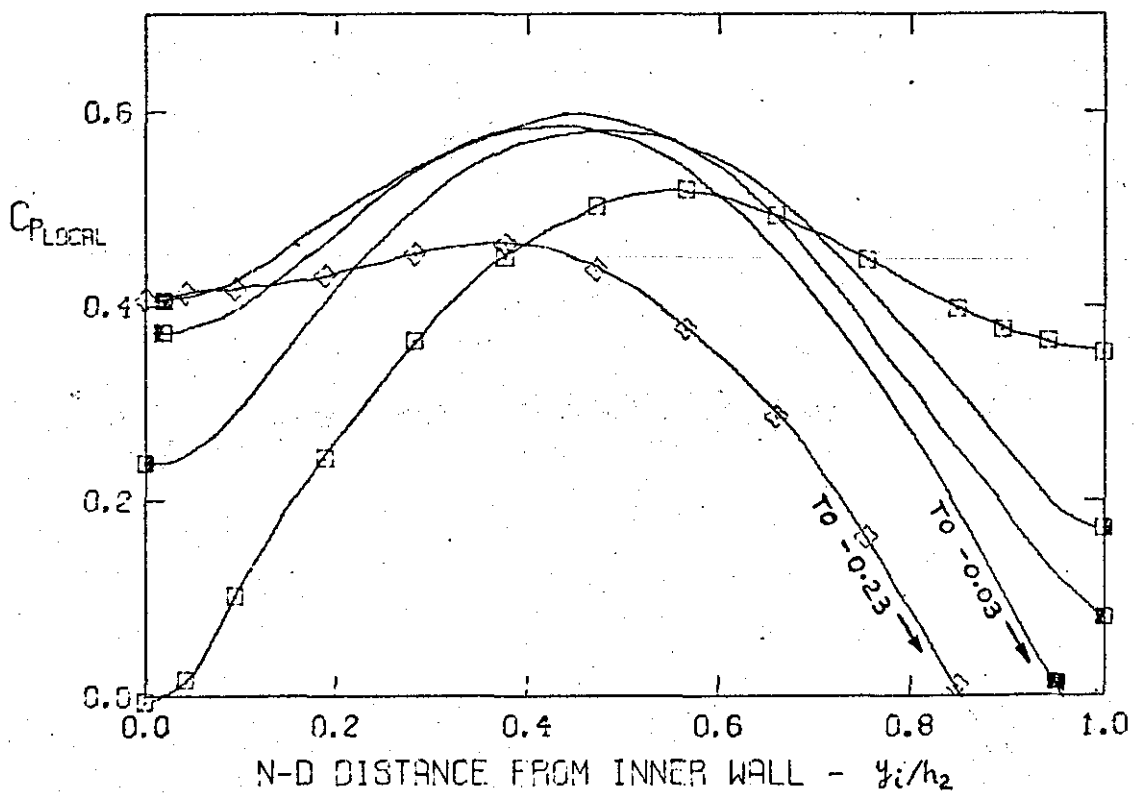
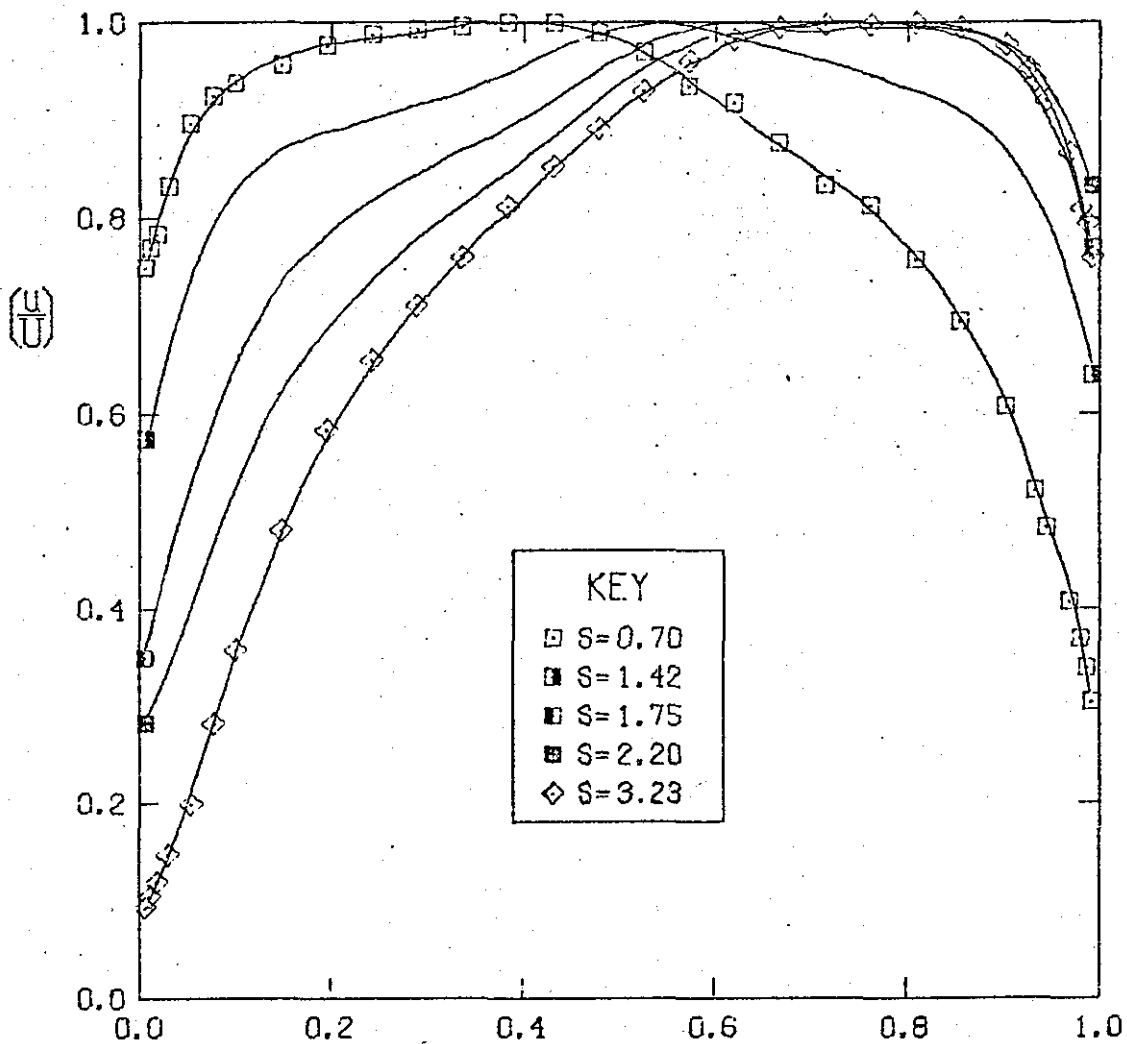




Fig. A5-5

PRE-DIFFUSER OUTLET PROFILES  
FOR TEST SERIES 1-1,0

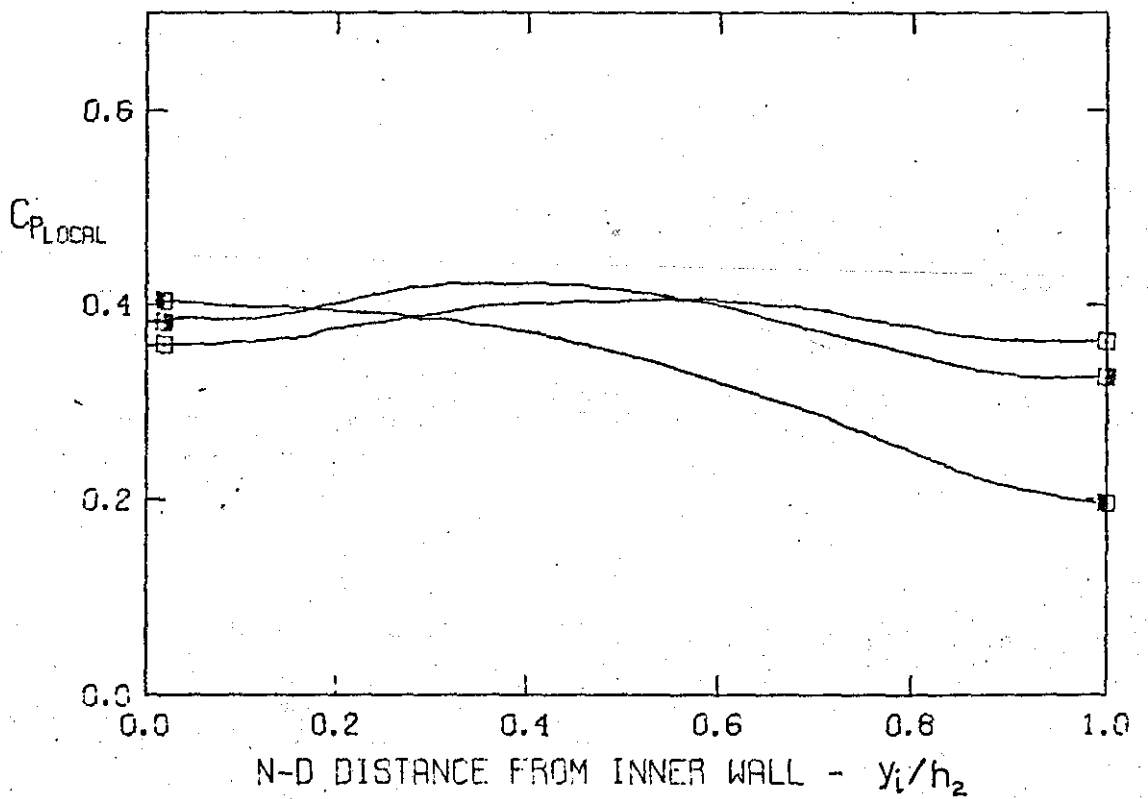
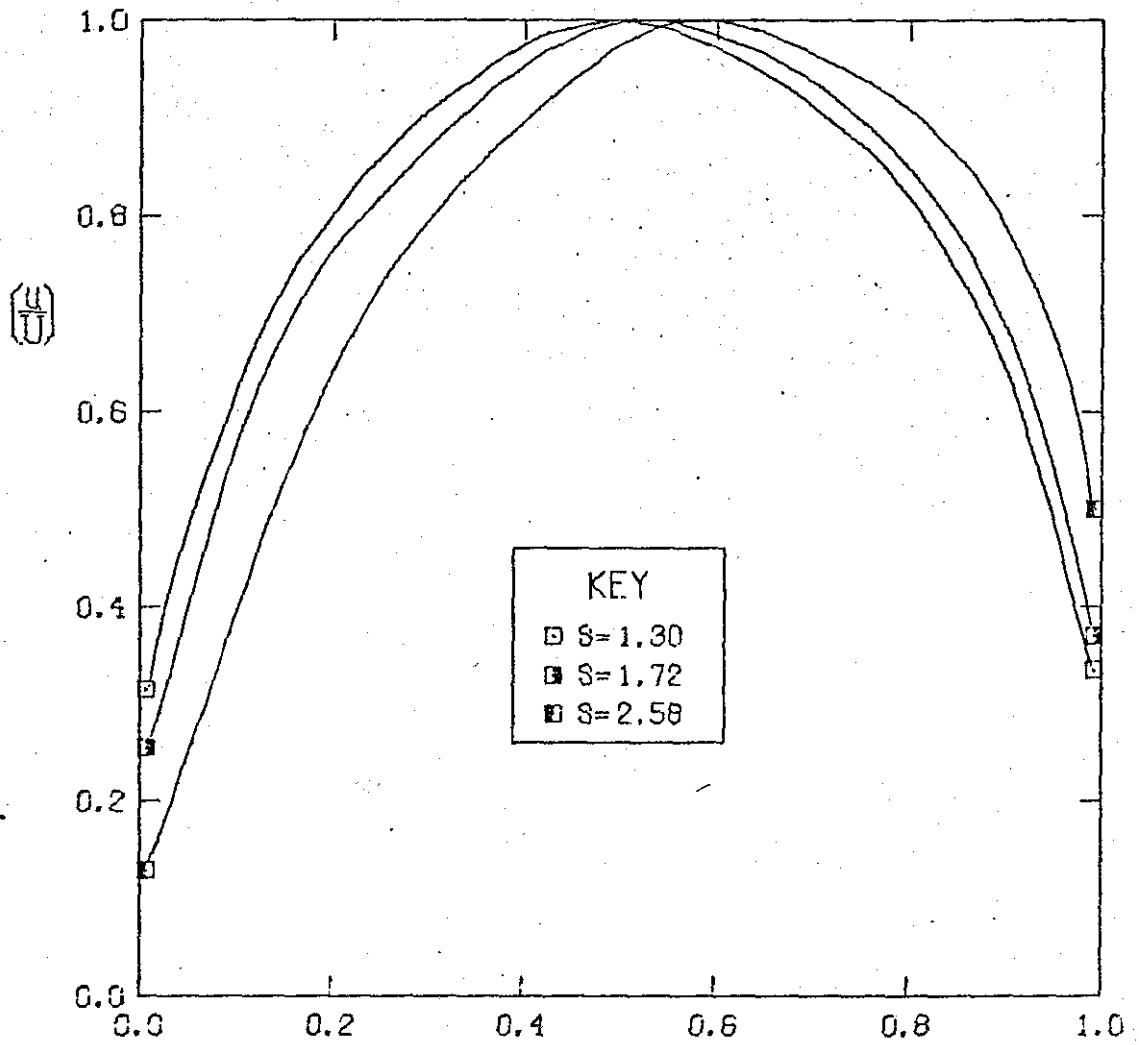


Fig.A5-6

PRE-DIFFUSER OUTLET PROFILES  
FOR TEST SERIES 1-2.0

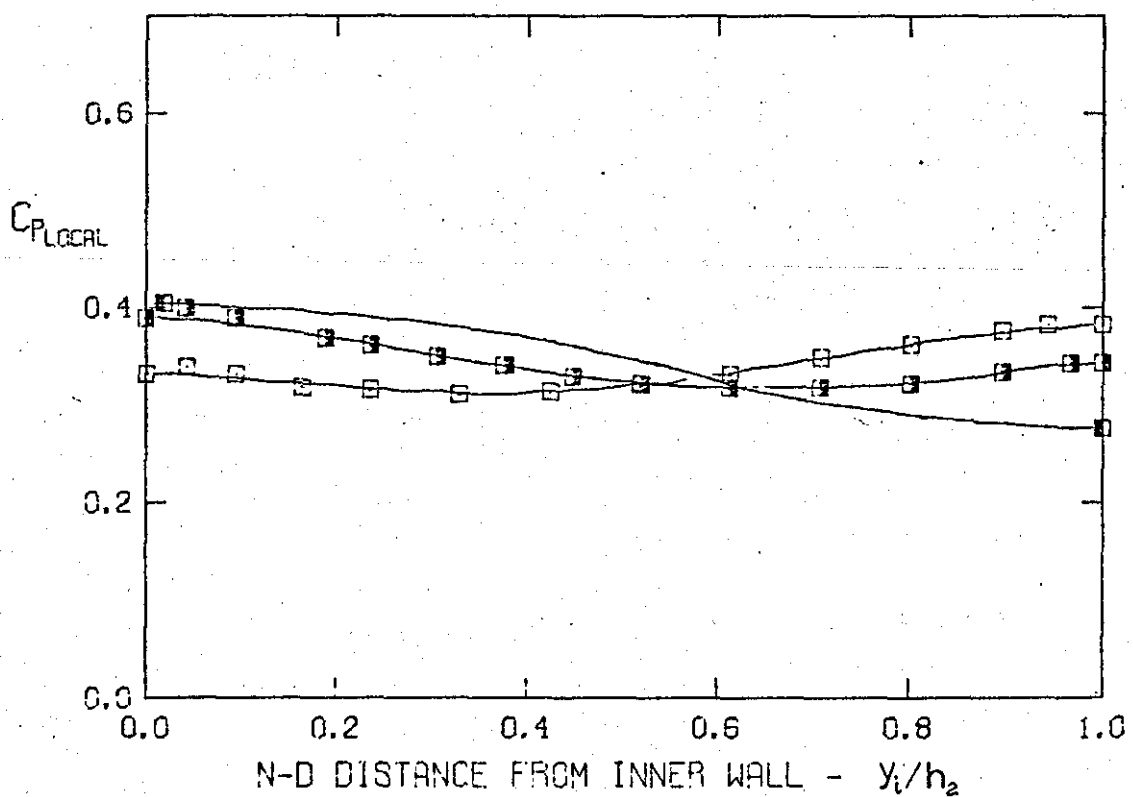
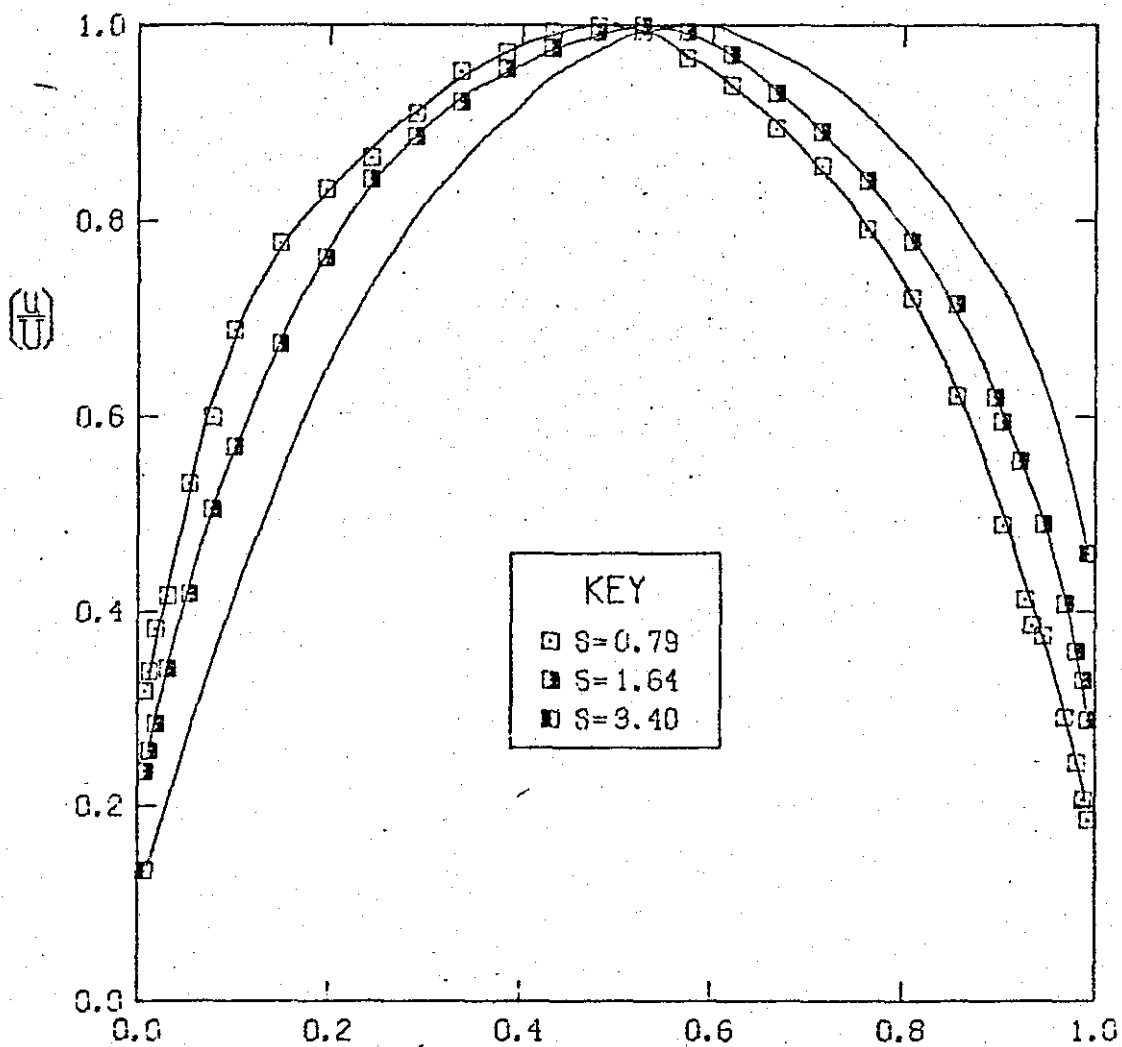


Fig. A5-7

PRE-DIFFUSER OUTLET PROFILES  
FOR TEST SERIES 2-0.5

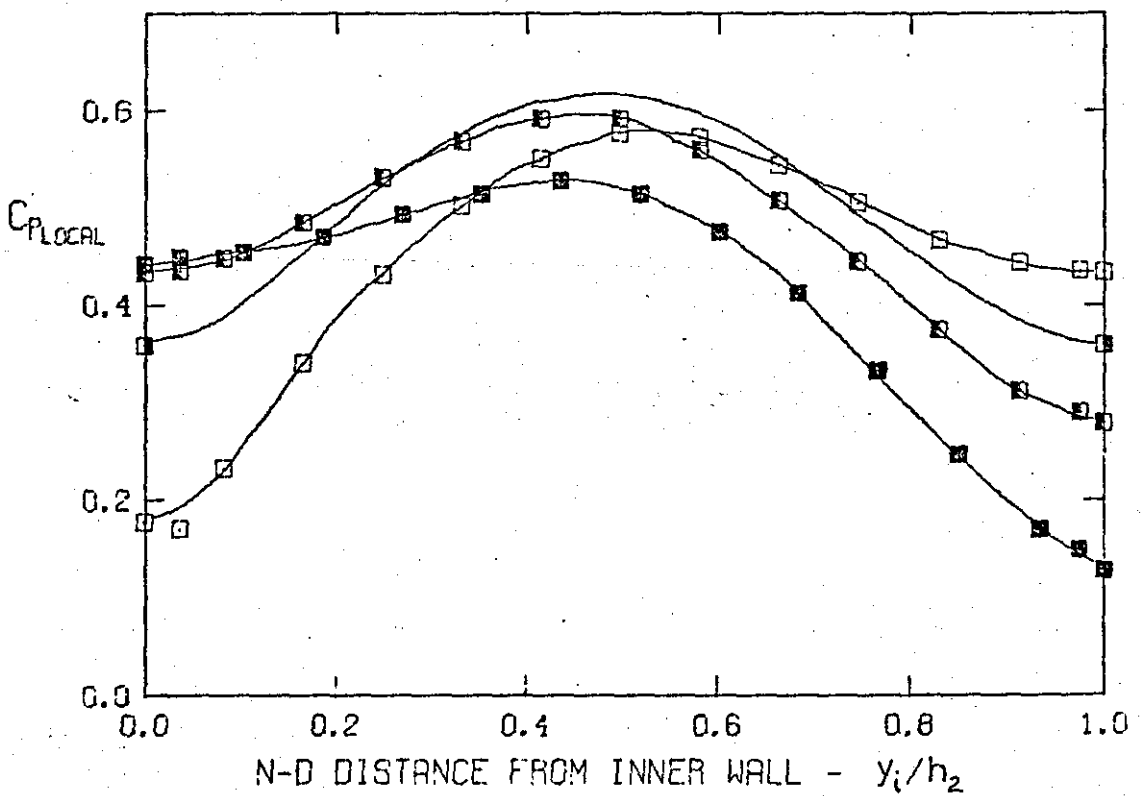
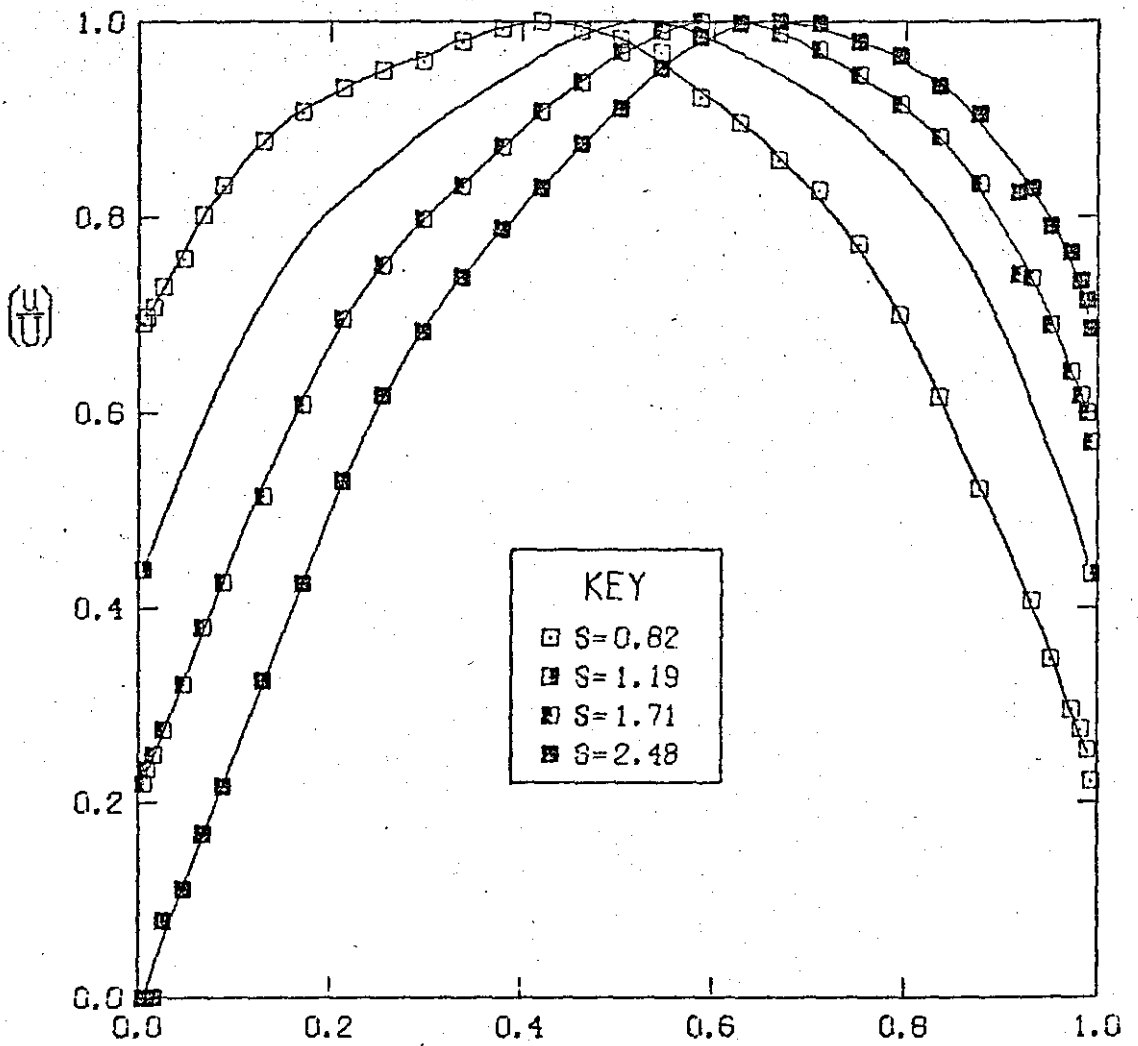


Fig. A5-8

PRE-DIFFUSER OUTLET PROFILES  
FOR TEST SERIES 2-0,8

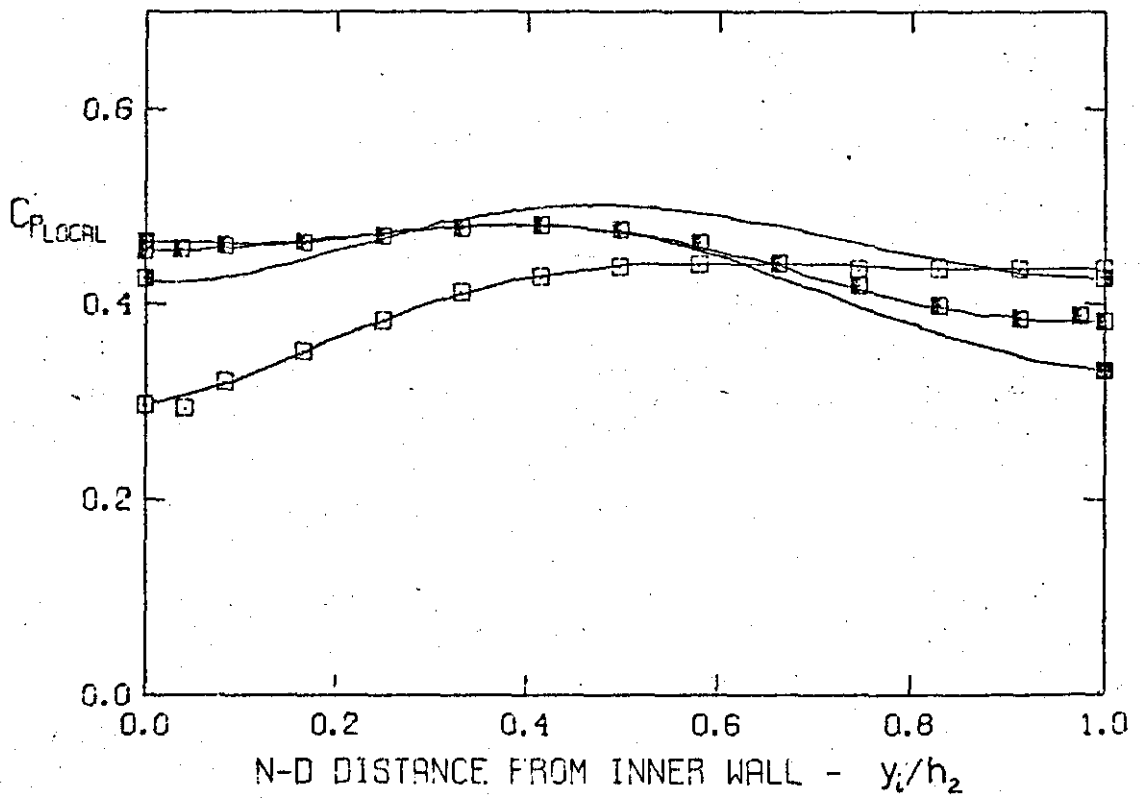
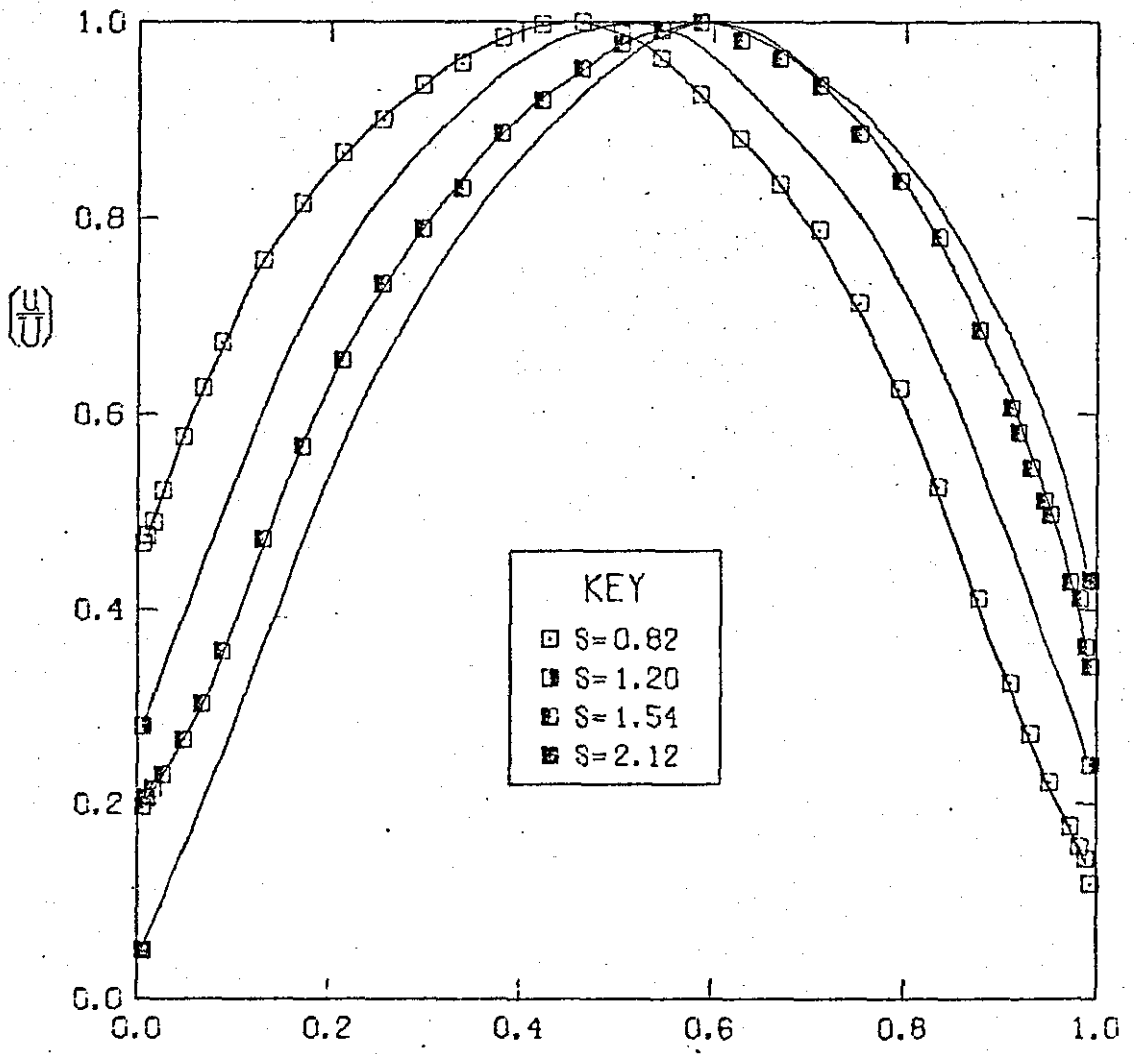


Fig.A5-9

PRE-DIFFUSER OUTLET PROFILES  
FOR TEST SERIES 2-1.5

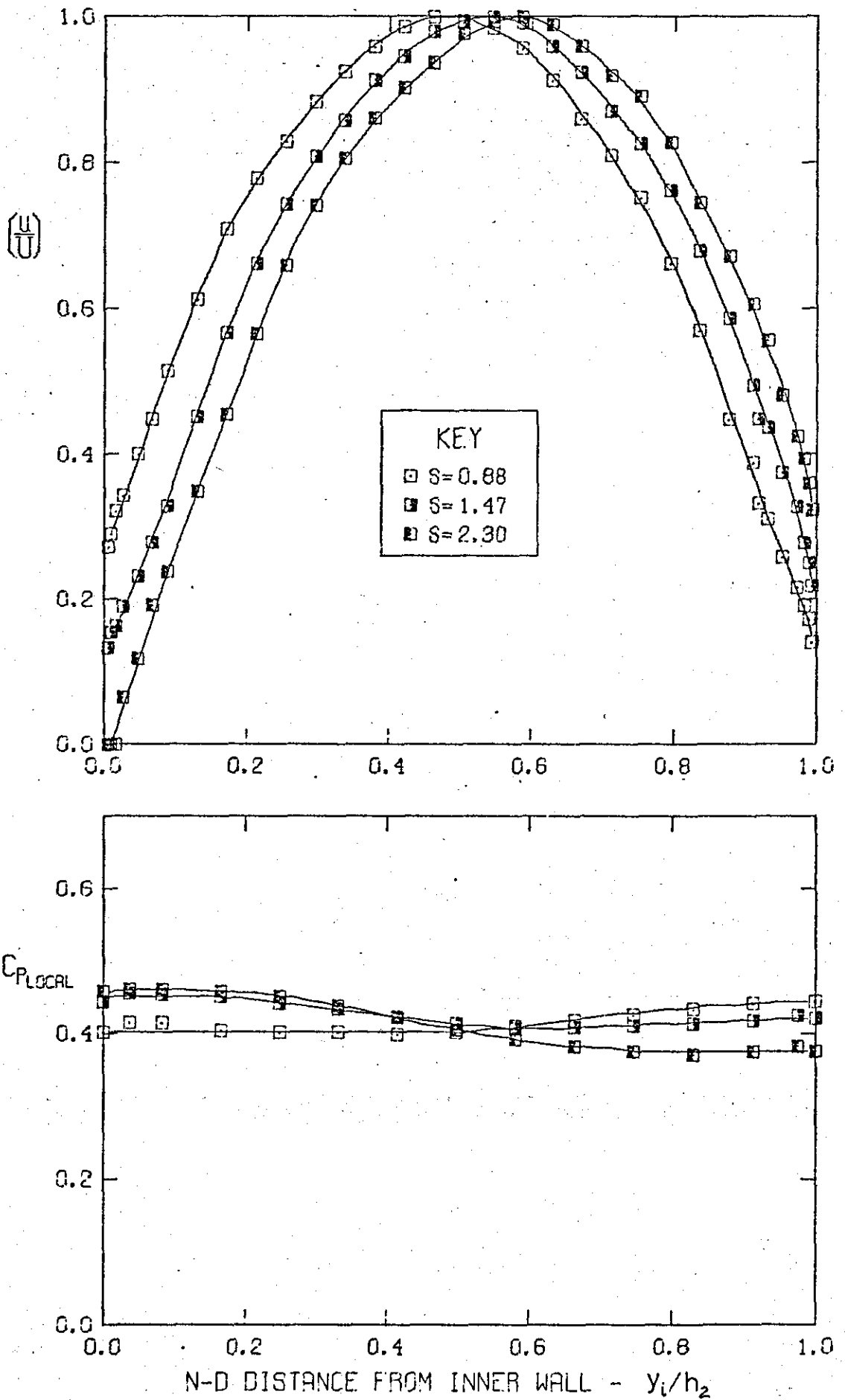


Fig.A5-10

PRE-DIFFUSER OUTLET PROFILES  
FOR TEST SERIES 4-0.4

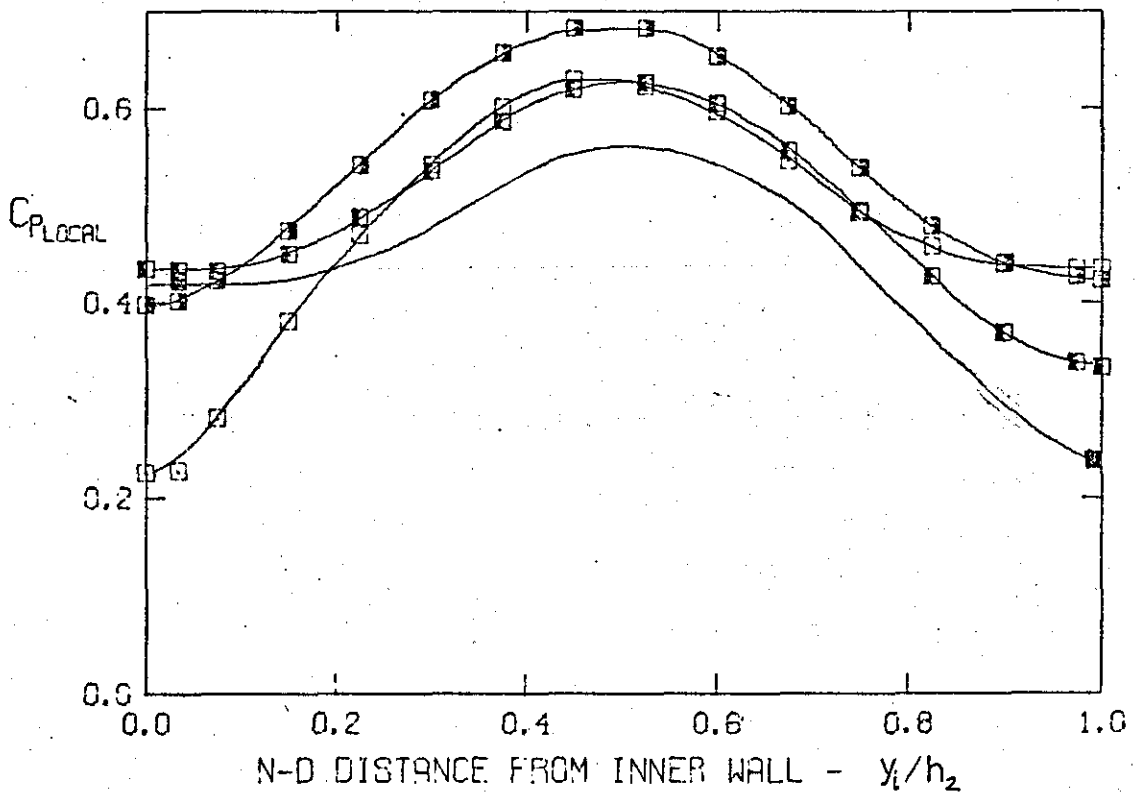
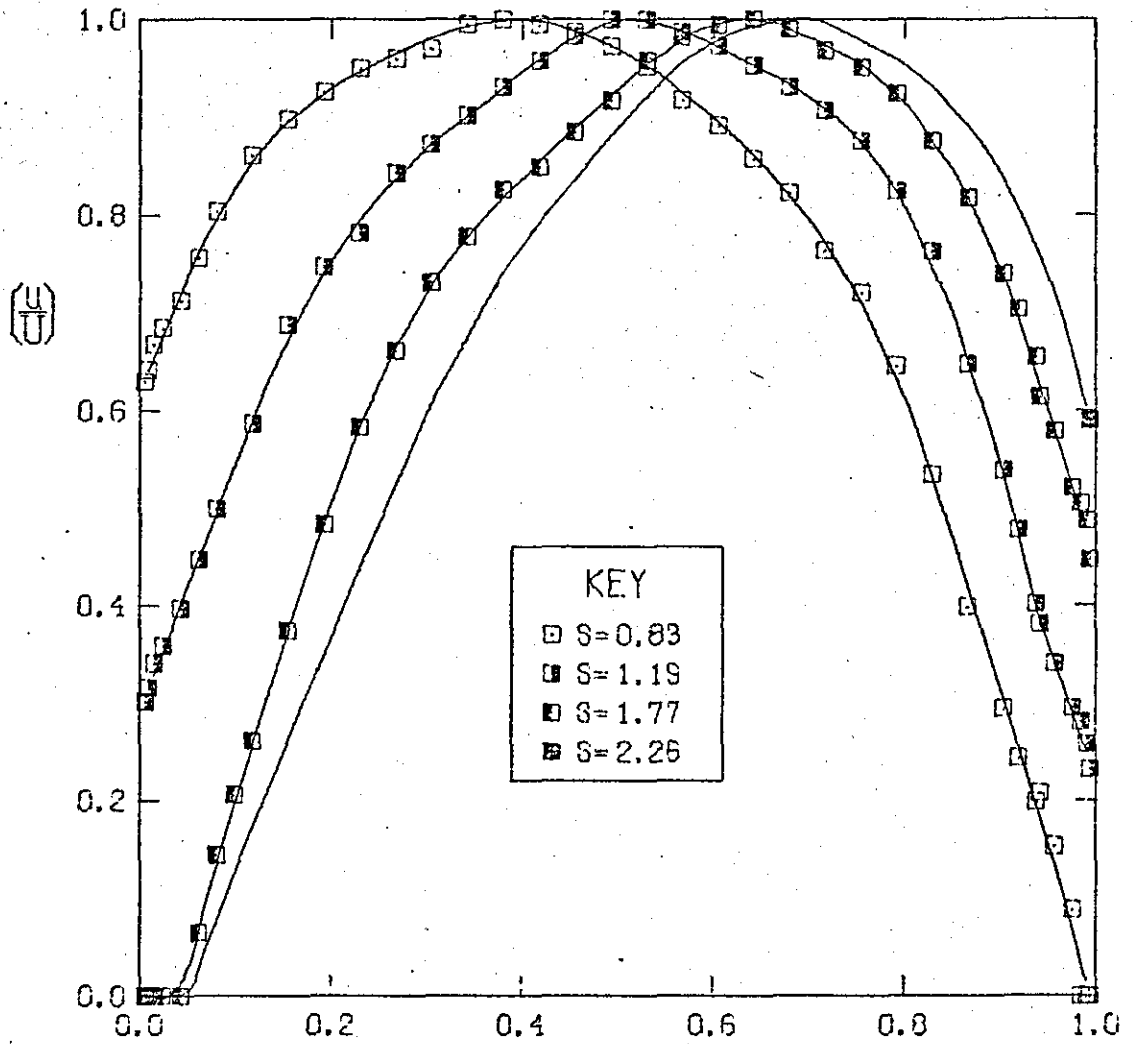


Fig.A5-11

PRE-DIFFUSER OUTLET PROFILES  
FOR TEST SERIES 4-0.7

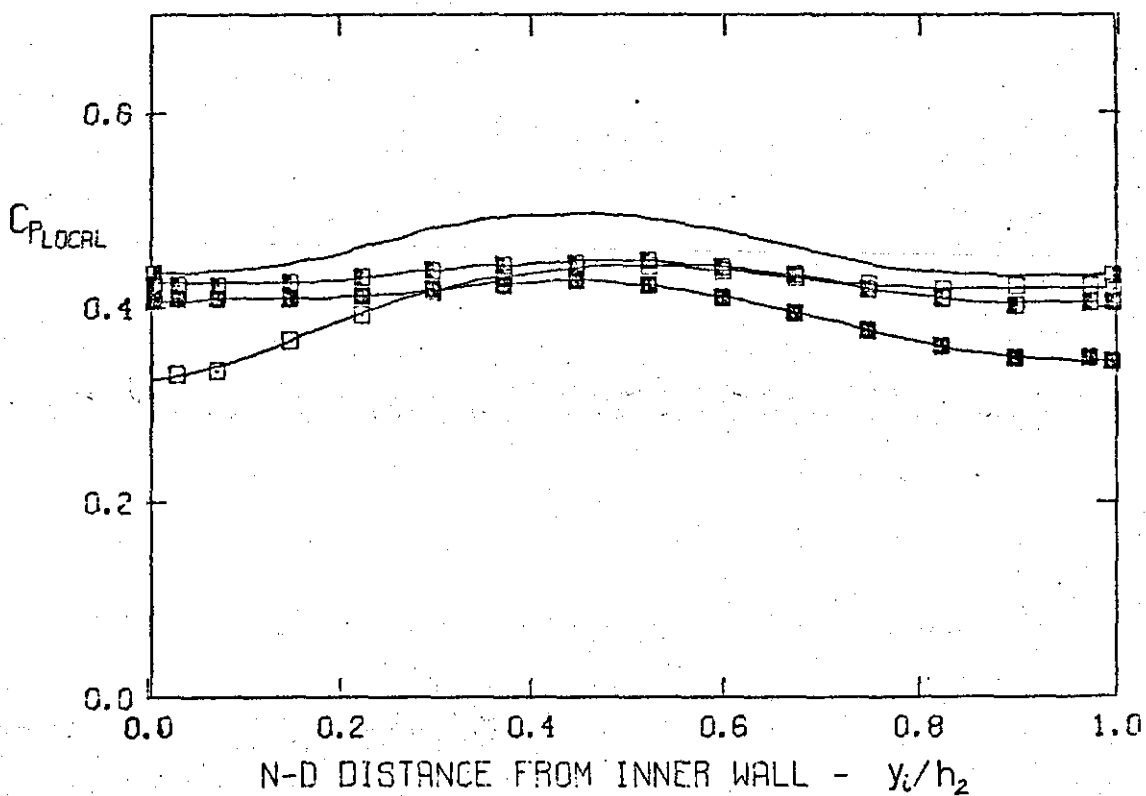
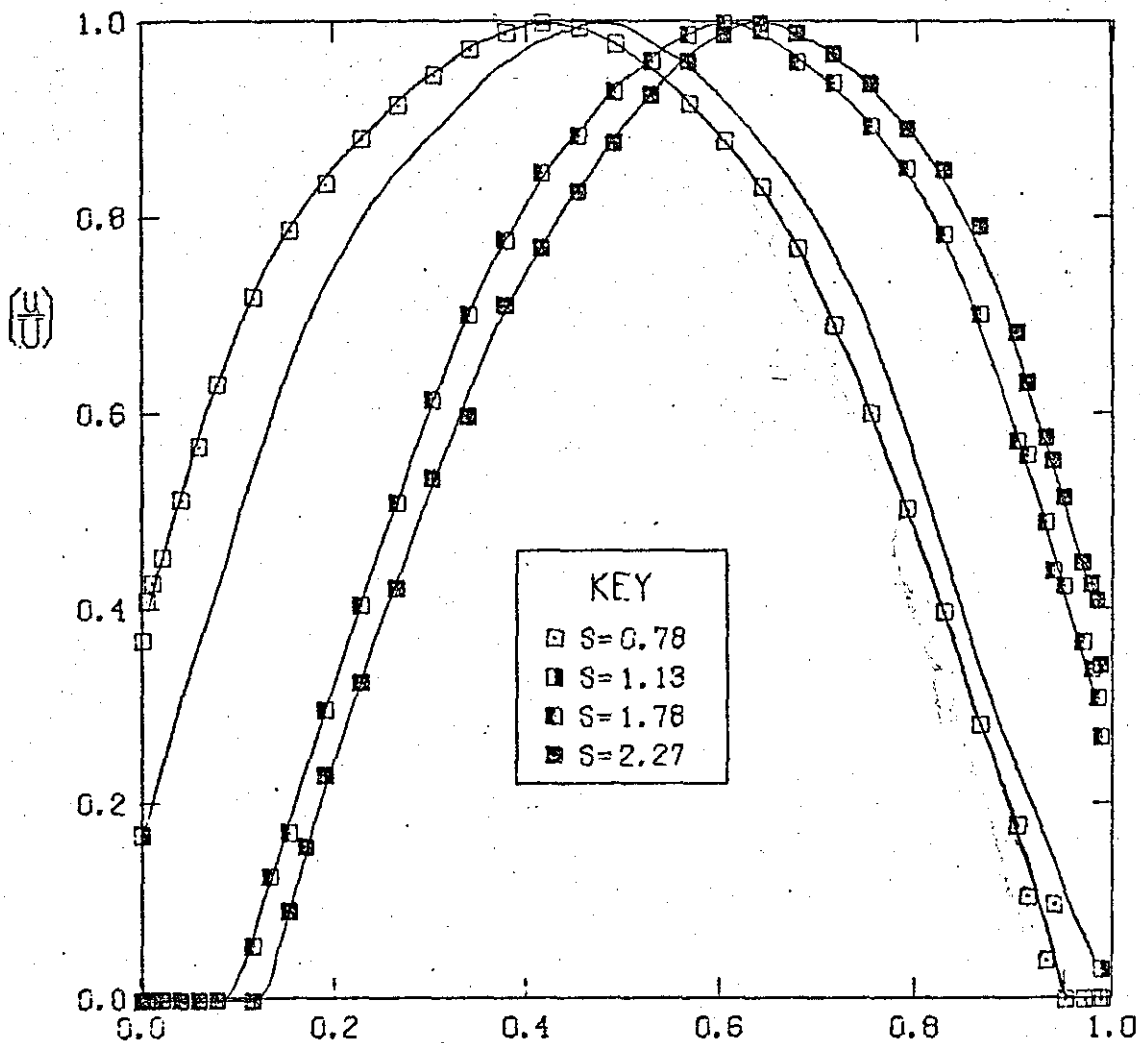


Fig.A5-12

PRE-DIFFUSER OUTLET PROFILES  
FOR TEST SERIES 4-1,2

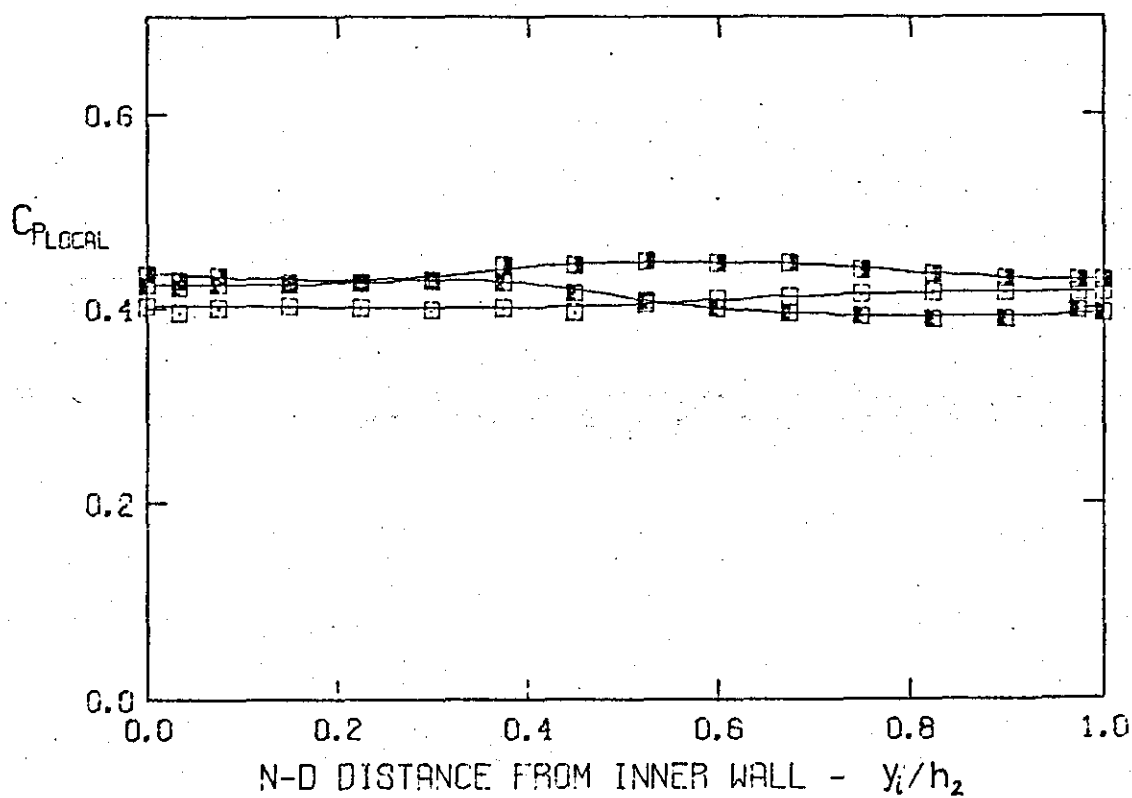
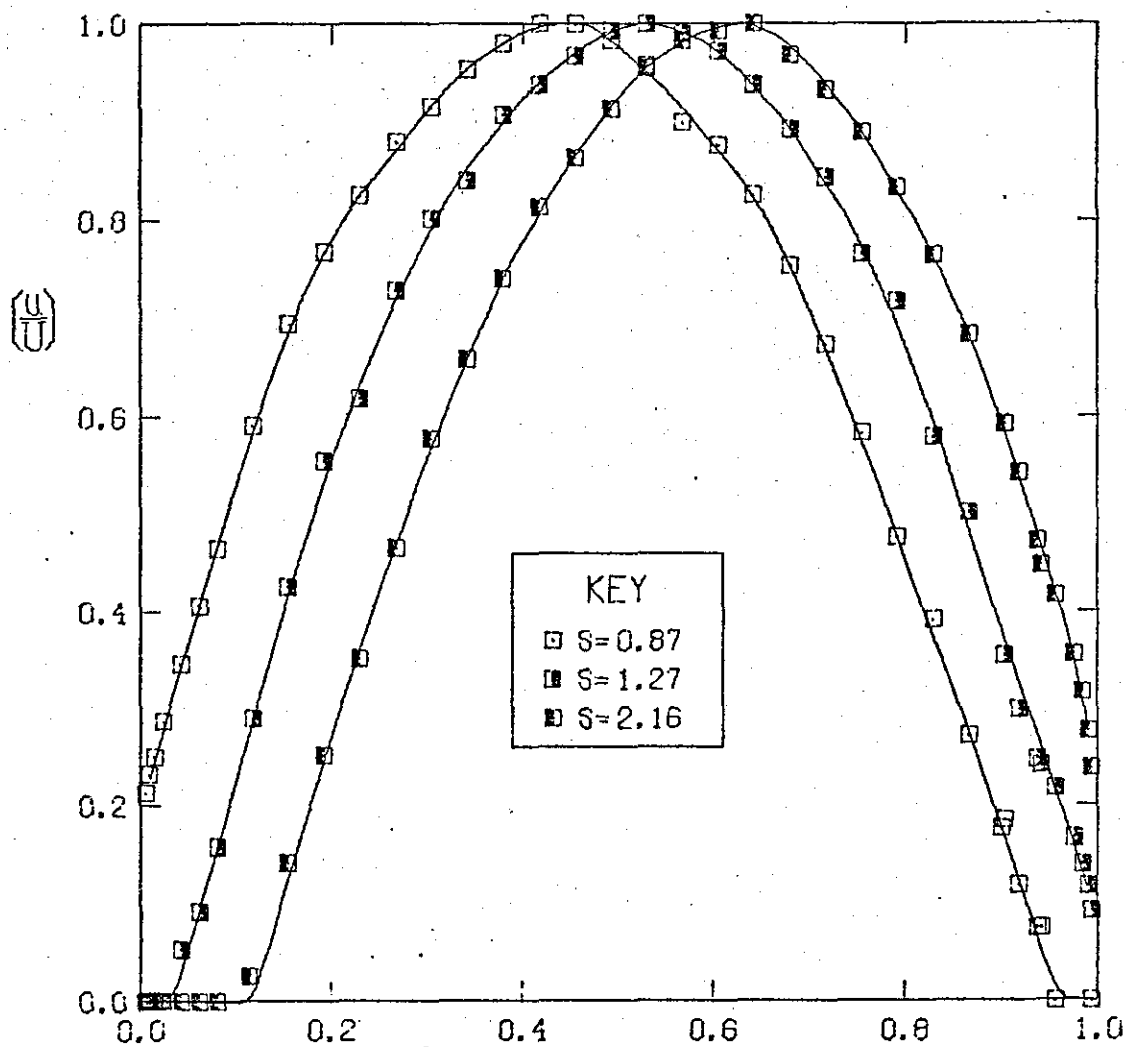




Fig. A5-13

PRE-DIFFUSER OUTLET PROFILES  
FOR TEST SERIES 5-0.5

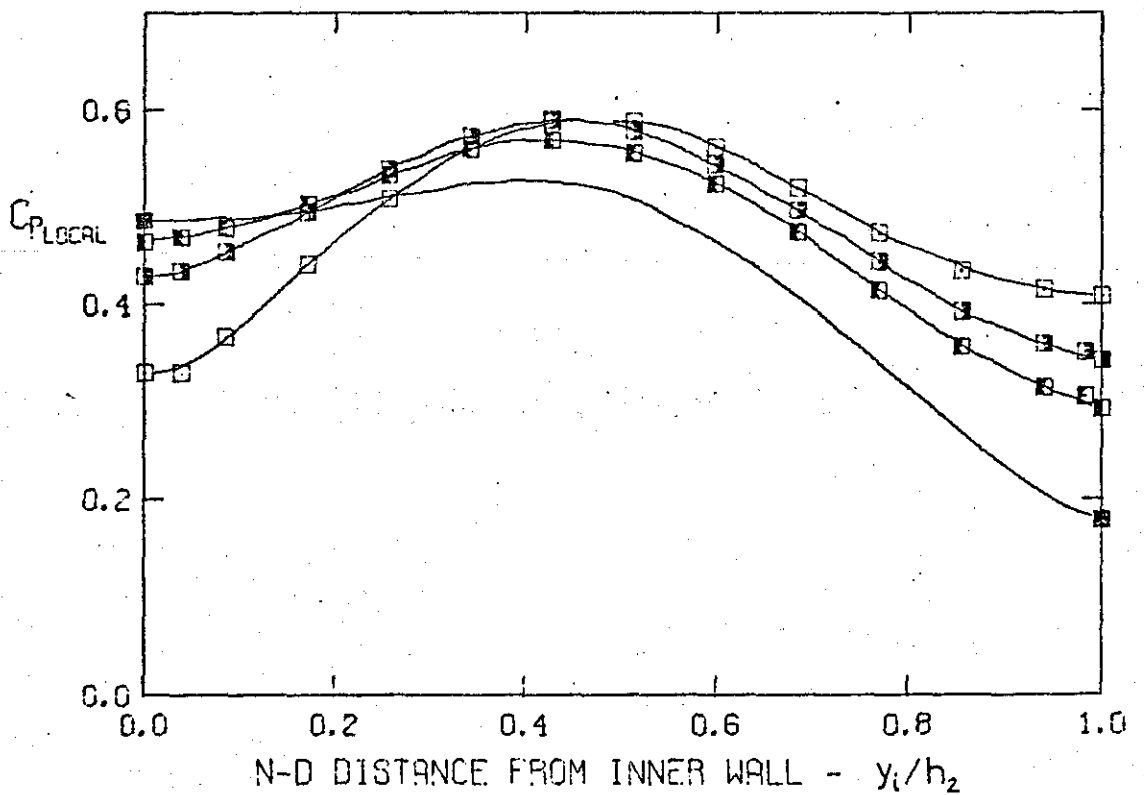
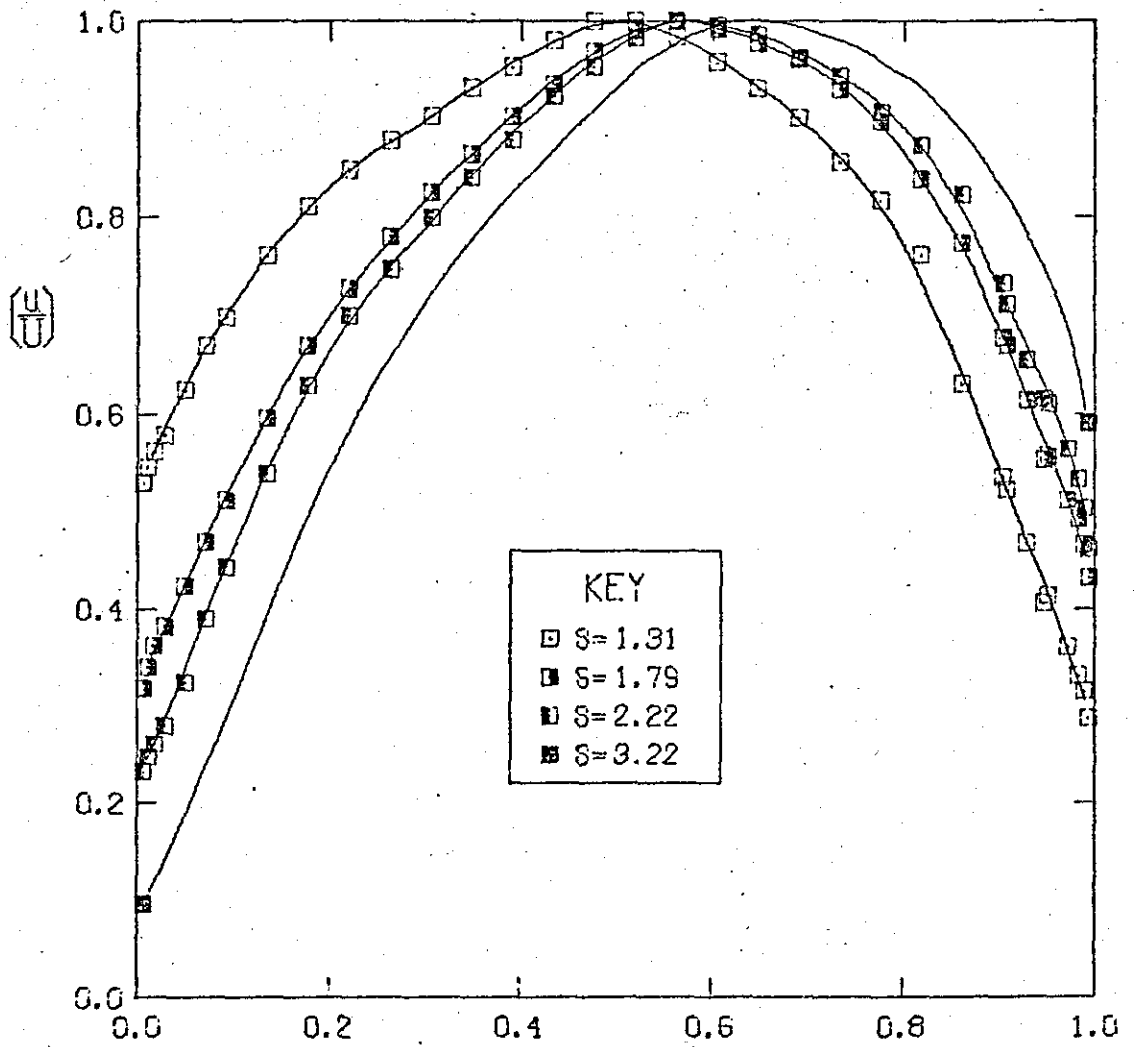


Fig. A5-14

PRE-DIFFUSER OUTLET PROFILES  
FOR TEST SERIES 5-0,8

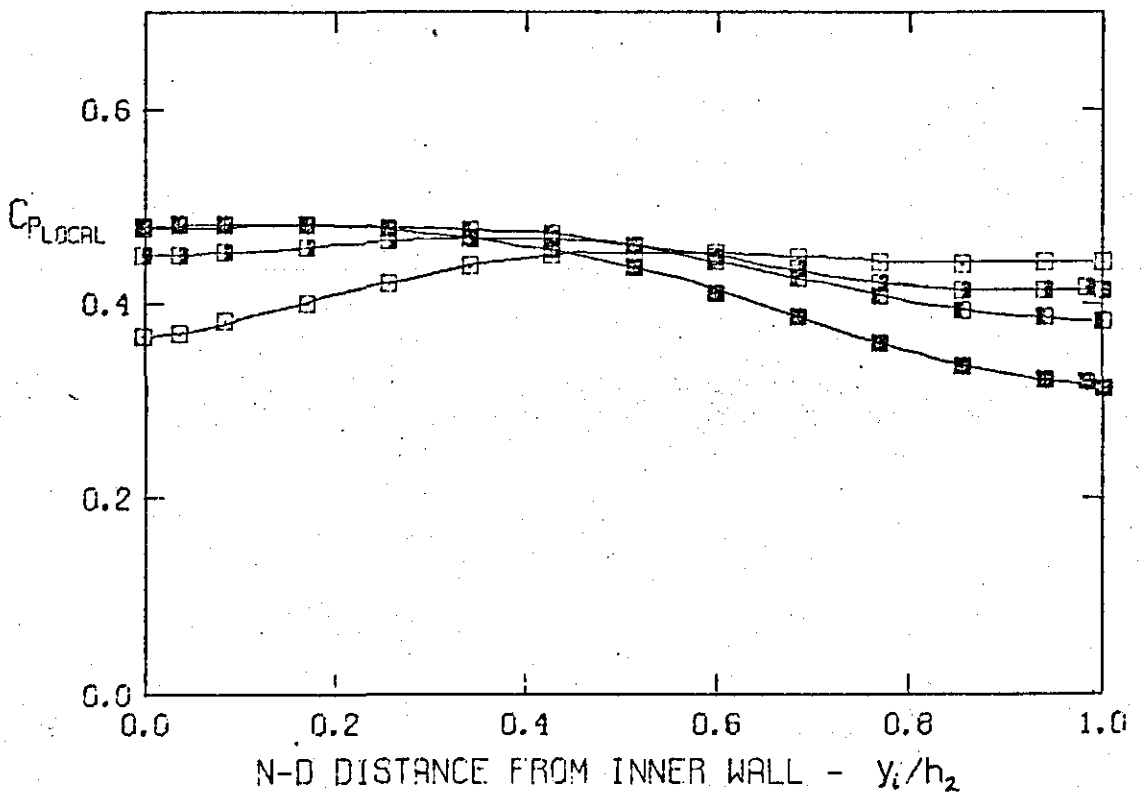
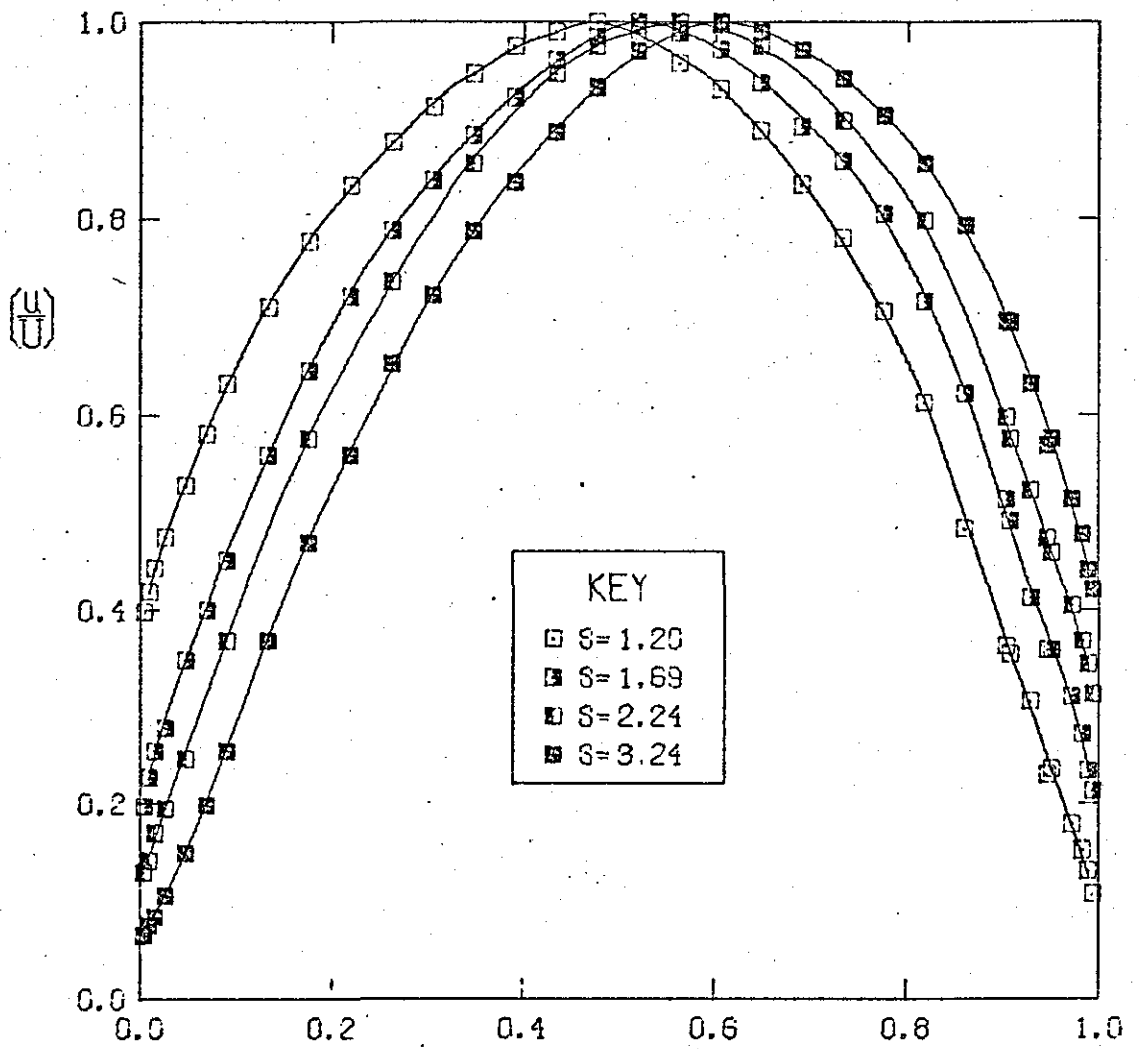


Fig.A5-15

PRE-DIFFUSER OUTLET PROFILES  
FOR TEST SERIES 5-1,5

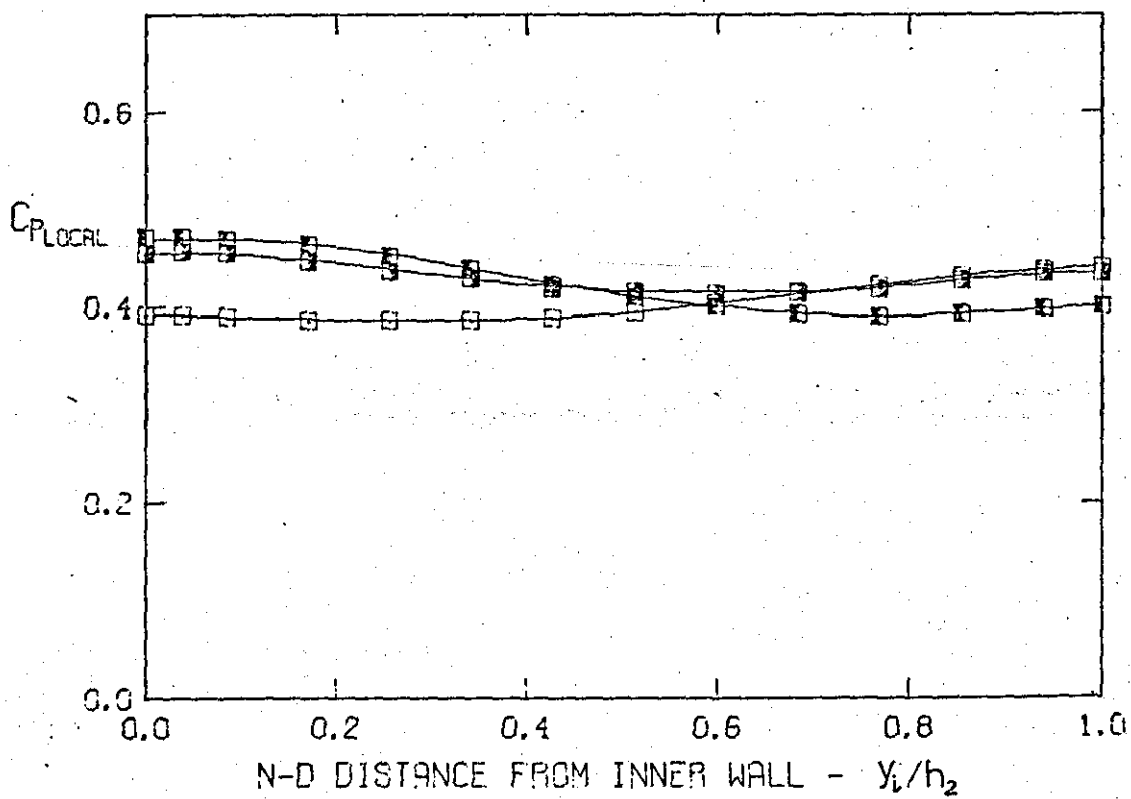
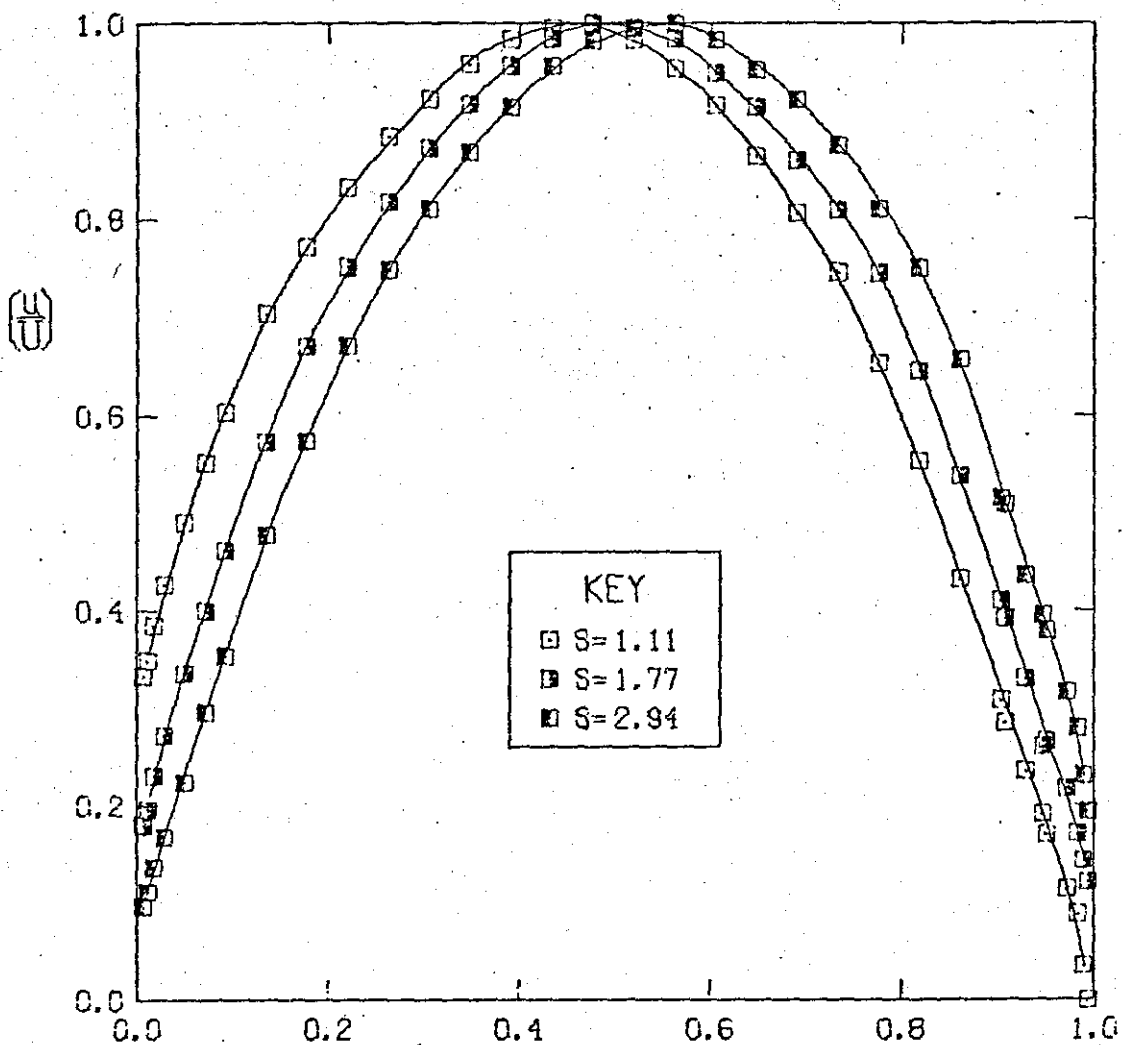


Fig.A6-1.

HEAD STATIC PRESSURE AND VELOCITY PROFILES  
FOR TEST SERIES 2-05.

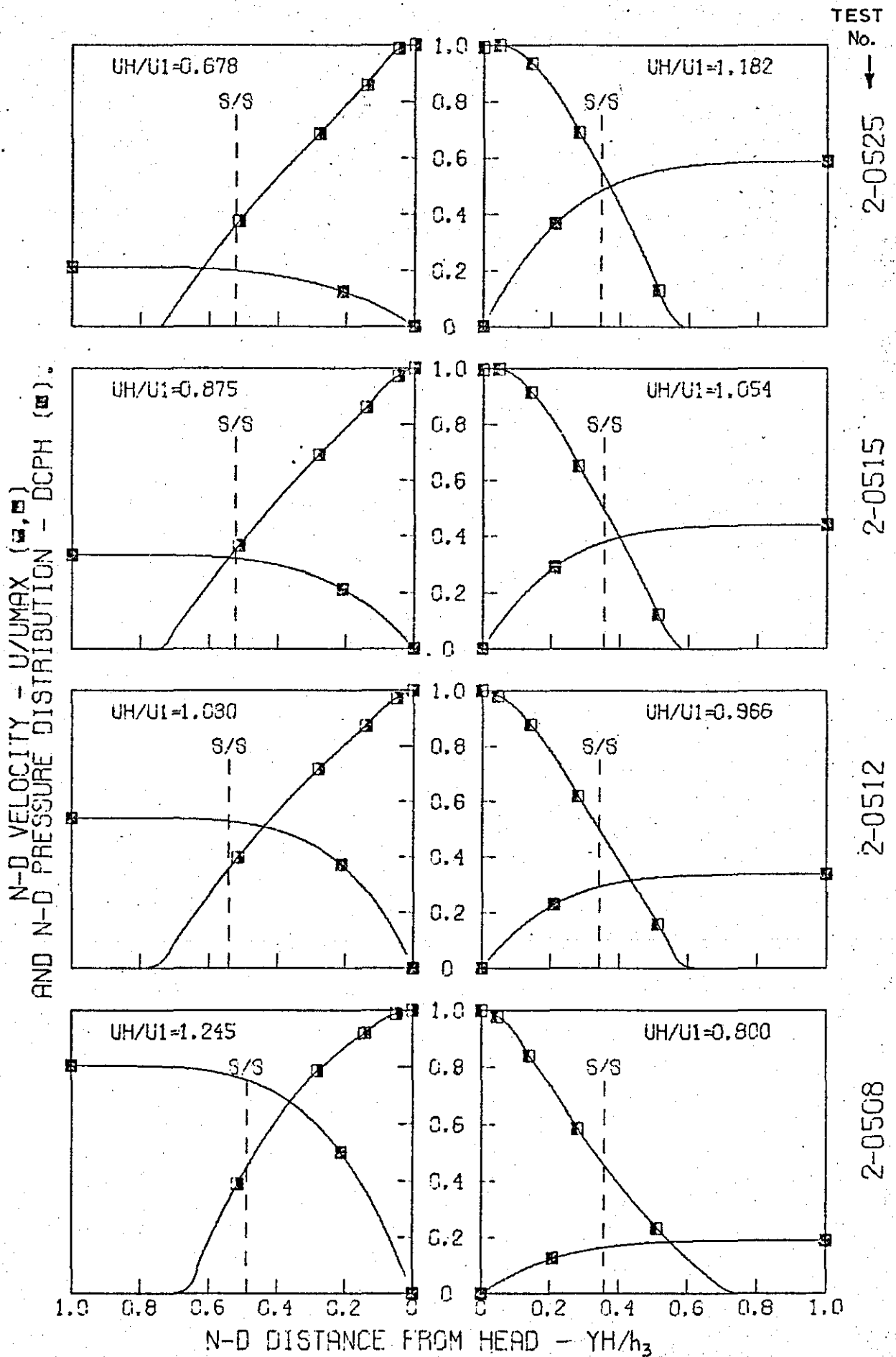
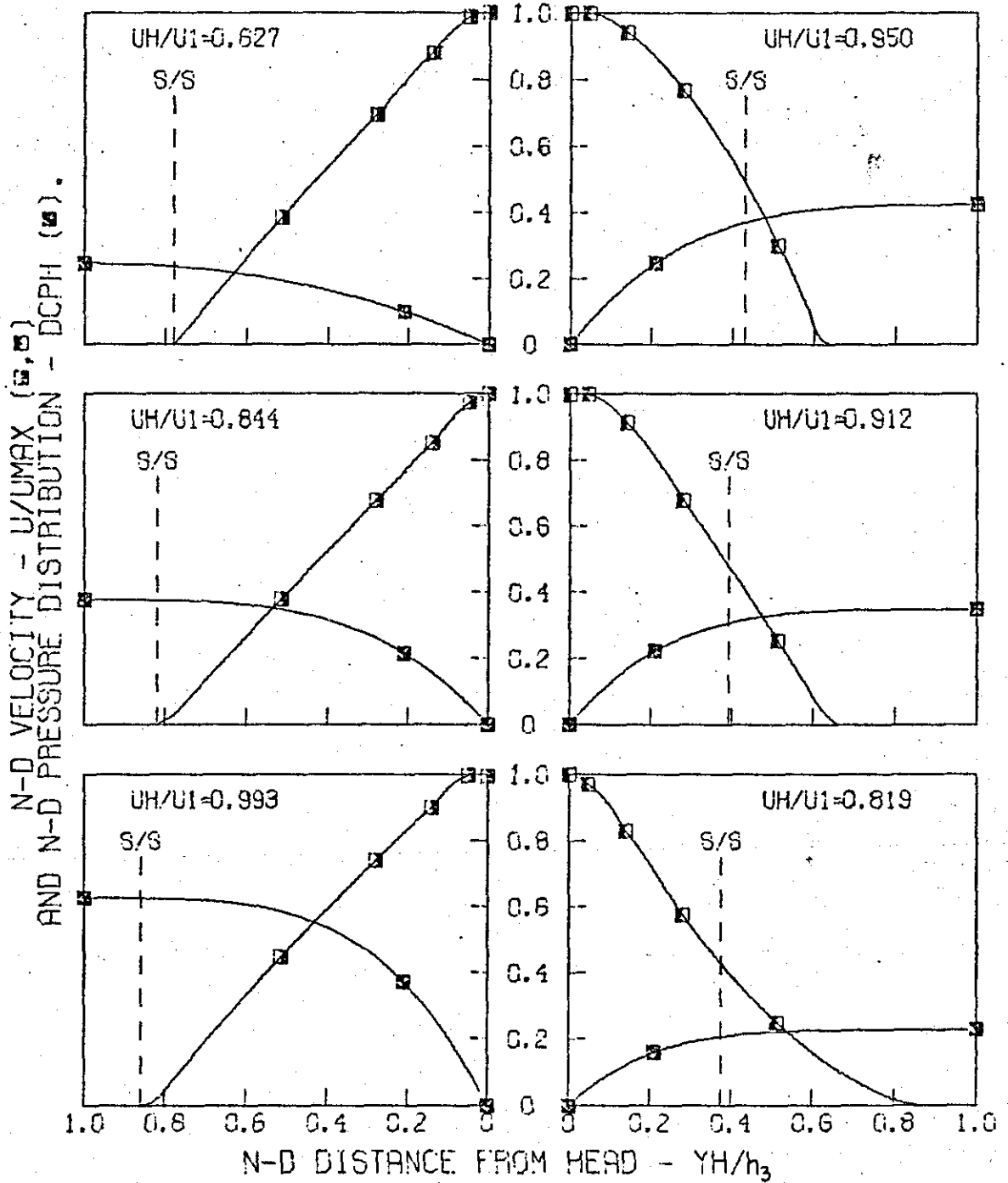


Fig. A6-2.

HEAD STATIC PRESSURE AND VELOCITY PROFILES  
FOR TEST SERIES 2-15.



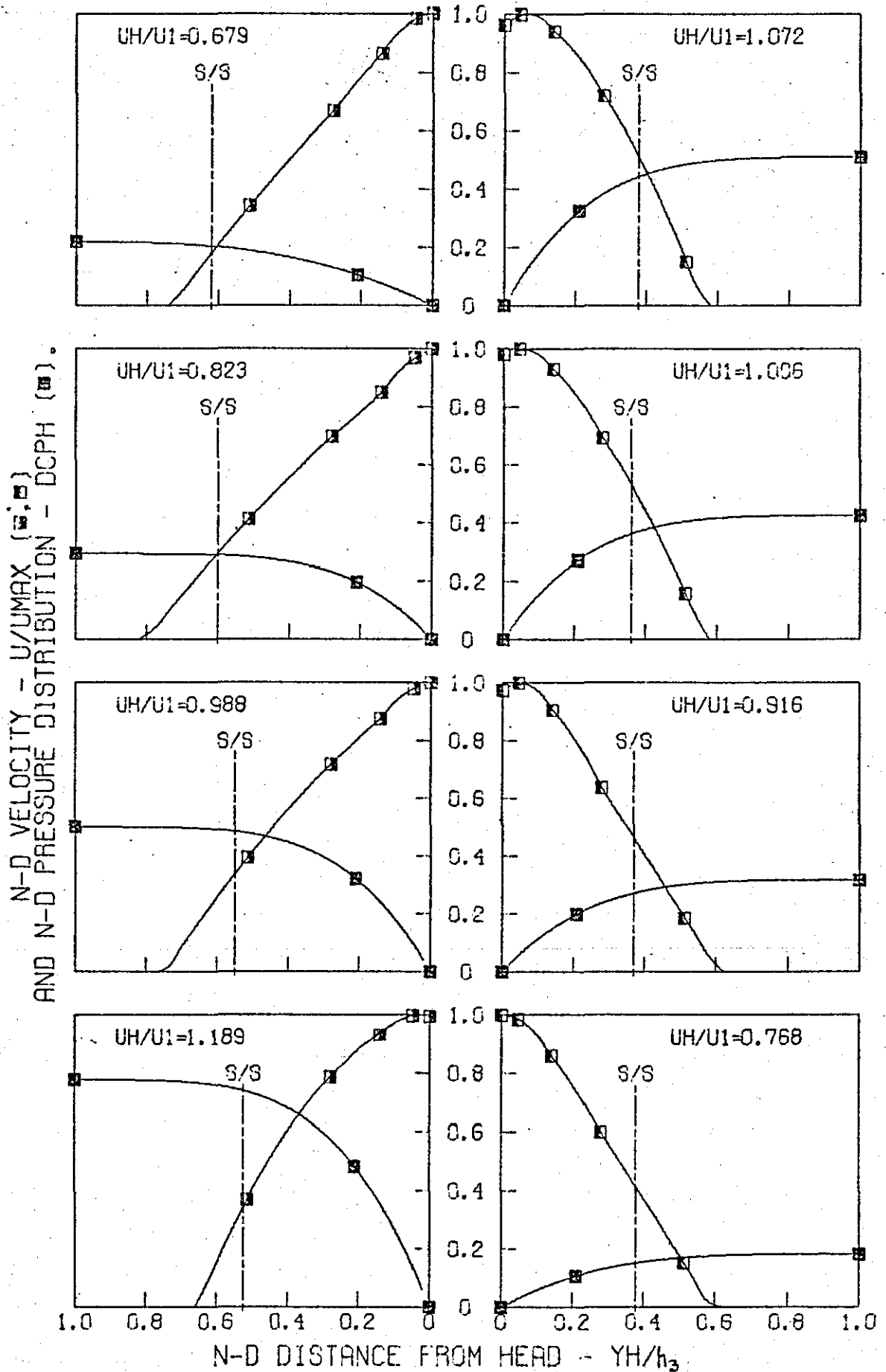
2-1522

2-1515

2-1509

Fig. A6-3.

HEAD STATIC PRESSURE AND VELOCITY PROFILES  
FOR TEST SERIES 3-04.



3-0422

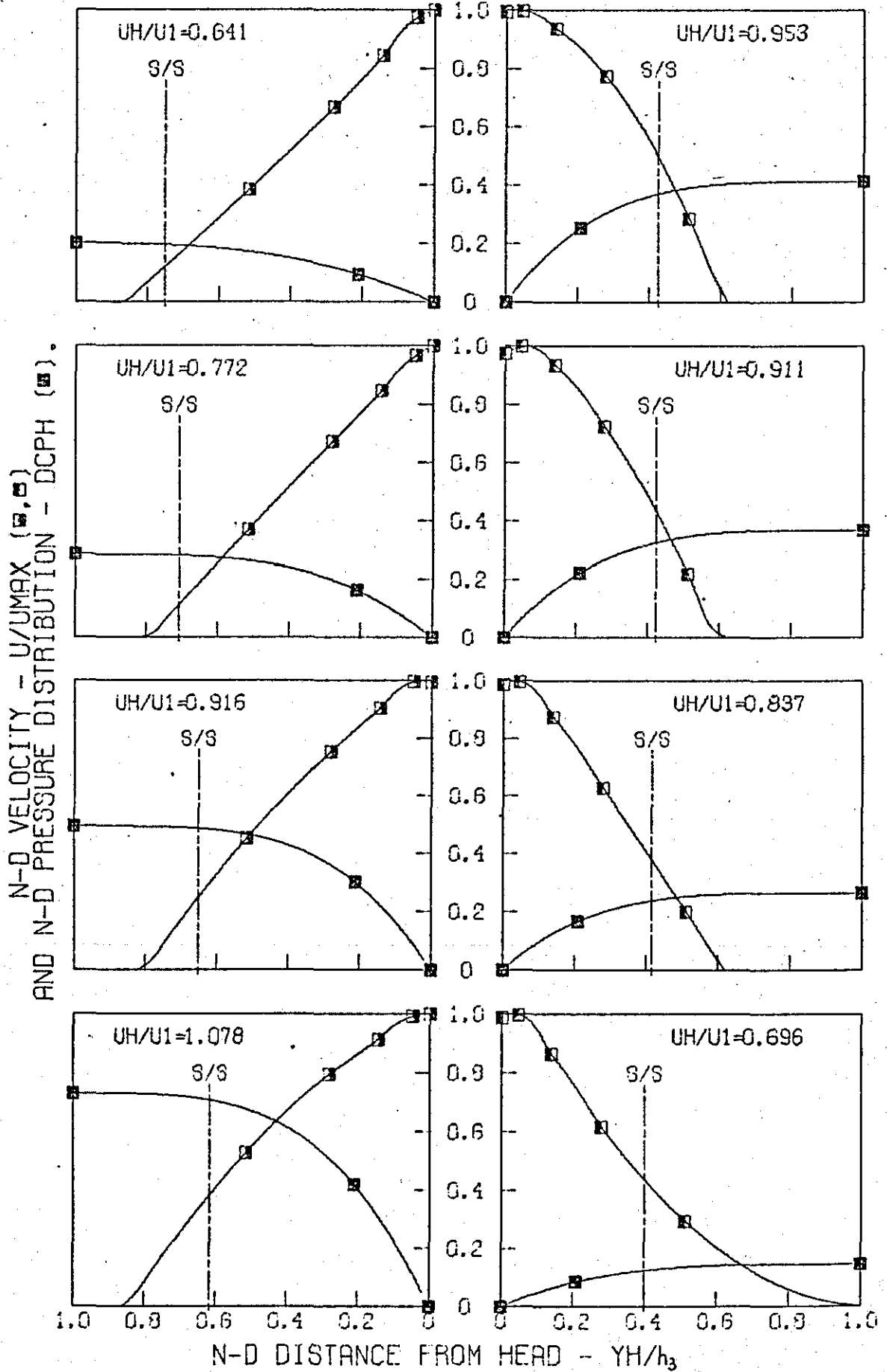
3-0416

3-0412

3-0408

Fig. A 6-4.

HEAD STATIC PRESSURE AND VELOCITY PROFILES  
FOR TEST SERIES 3-07.



3-0722

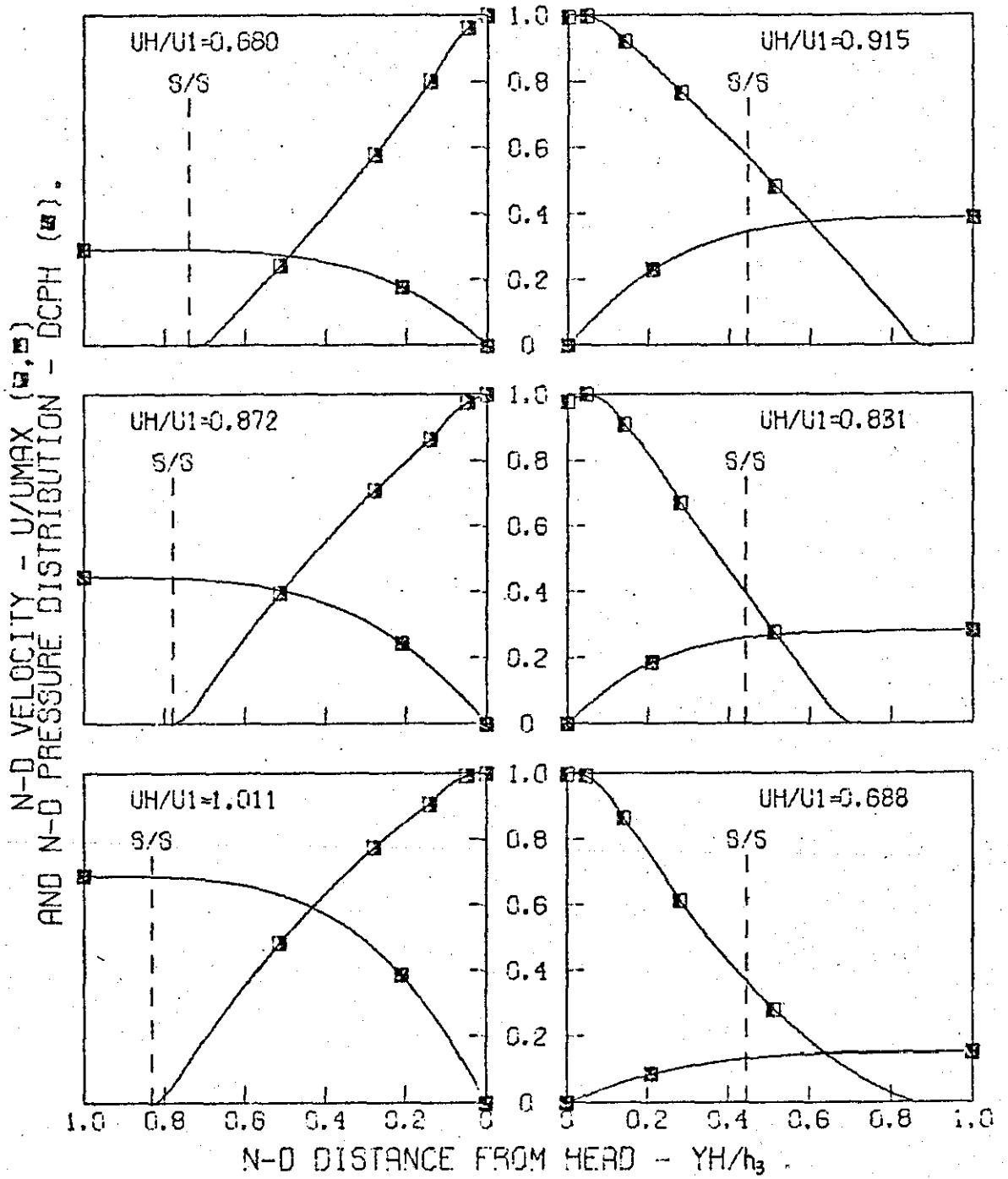
3-0717

3-0712

3-0708

Fig. A6-5.

HEAD STATIC PRESSURE AND VELOCITY PROFILES  
FOR TEST SERIES 3-12.



3-1222

3-1214

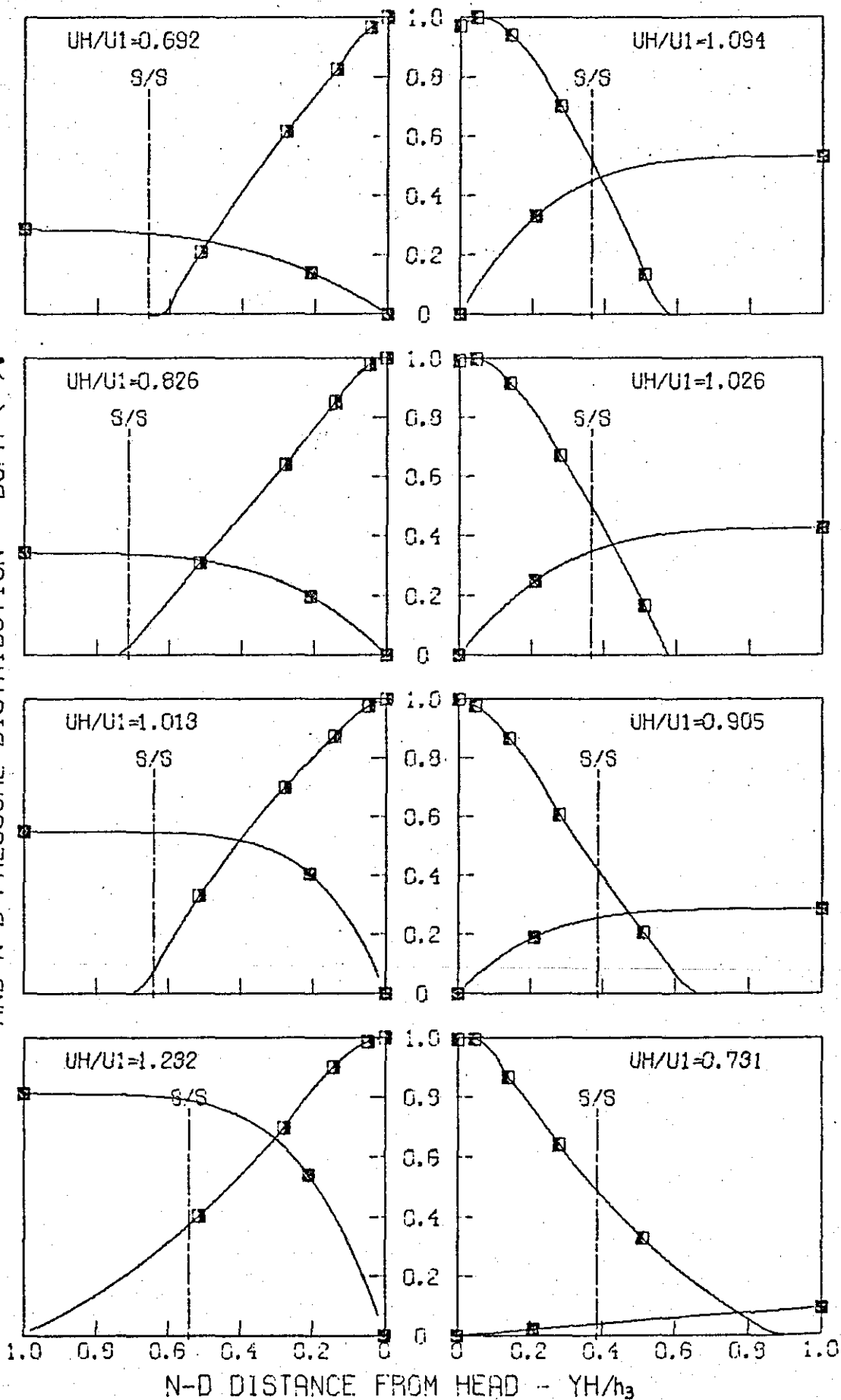
3-1208



Fig. A6-6.

HEAD STATIC PRESSURE AND VELOCITY PROFILES  
FOR TEST SERIES 4-04.

N-D VELOCITY - U/UMAX (□, □)  
AND N-D PRESSURE DISTRIBUTION - DCPH (□).



4-0422

4-0417

4-0412

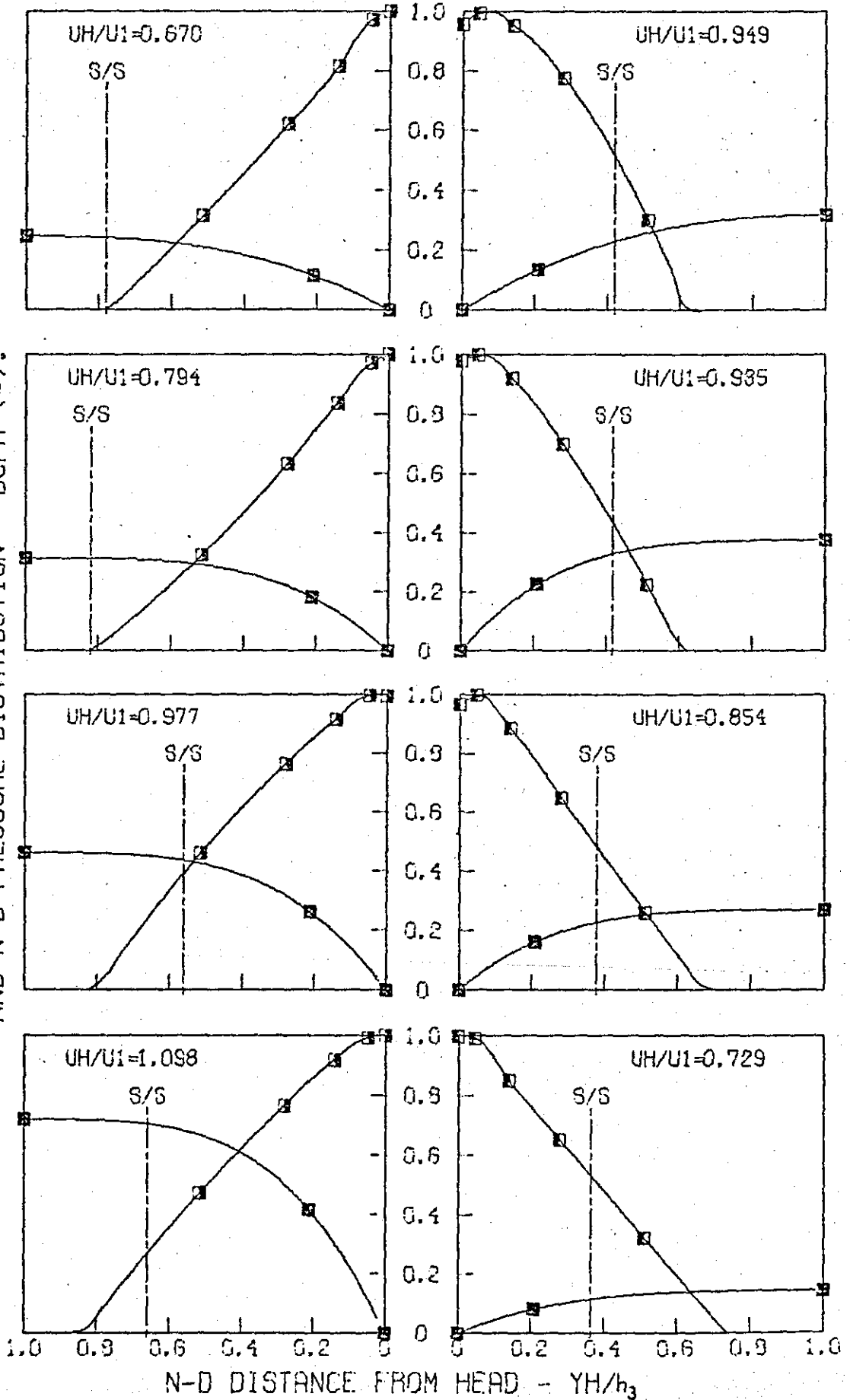
4-0408

Fig.A6-7.

HEAD STATIC PRESSURE AND VELOCITY PROFILES  
FOR TEST SERIES 4-07.

NOTE: DATA FOR TEST SERS. 4-12 IS GIVEN IN FIG. 5-2-1.

N-D VELOCITY - U/UMAX (□, ▣)  
AND N-D PRESSURE DISTRIBUTION - DCPH (■).



4-0722

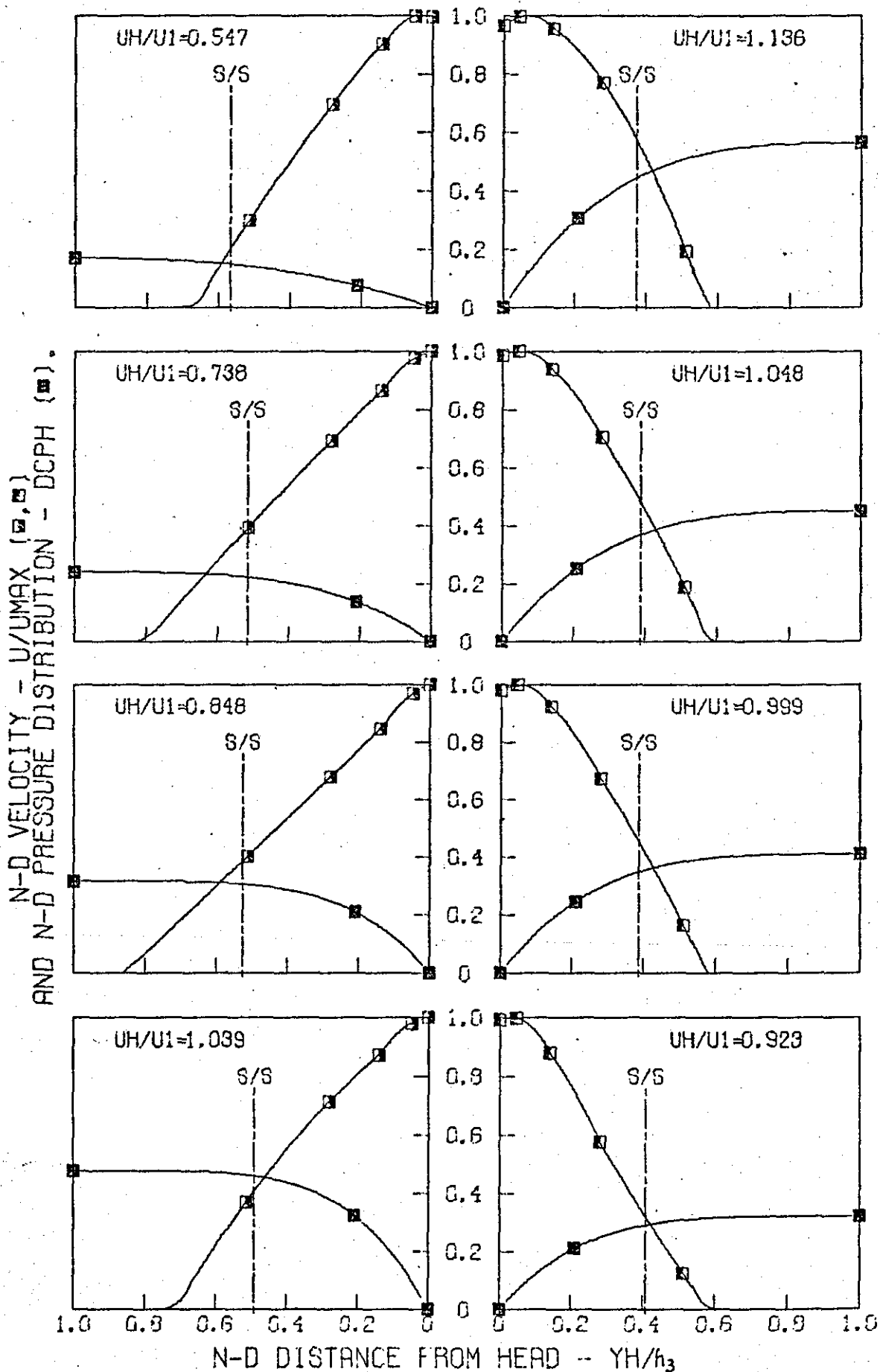
4-0717

4-0712

4-0708

Fig.A6-8.

HEAD STATIC PRESSURE AND VELOCITY PROFILES  
FOR TEST SERIES 5-05.



5-0532

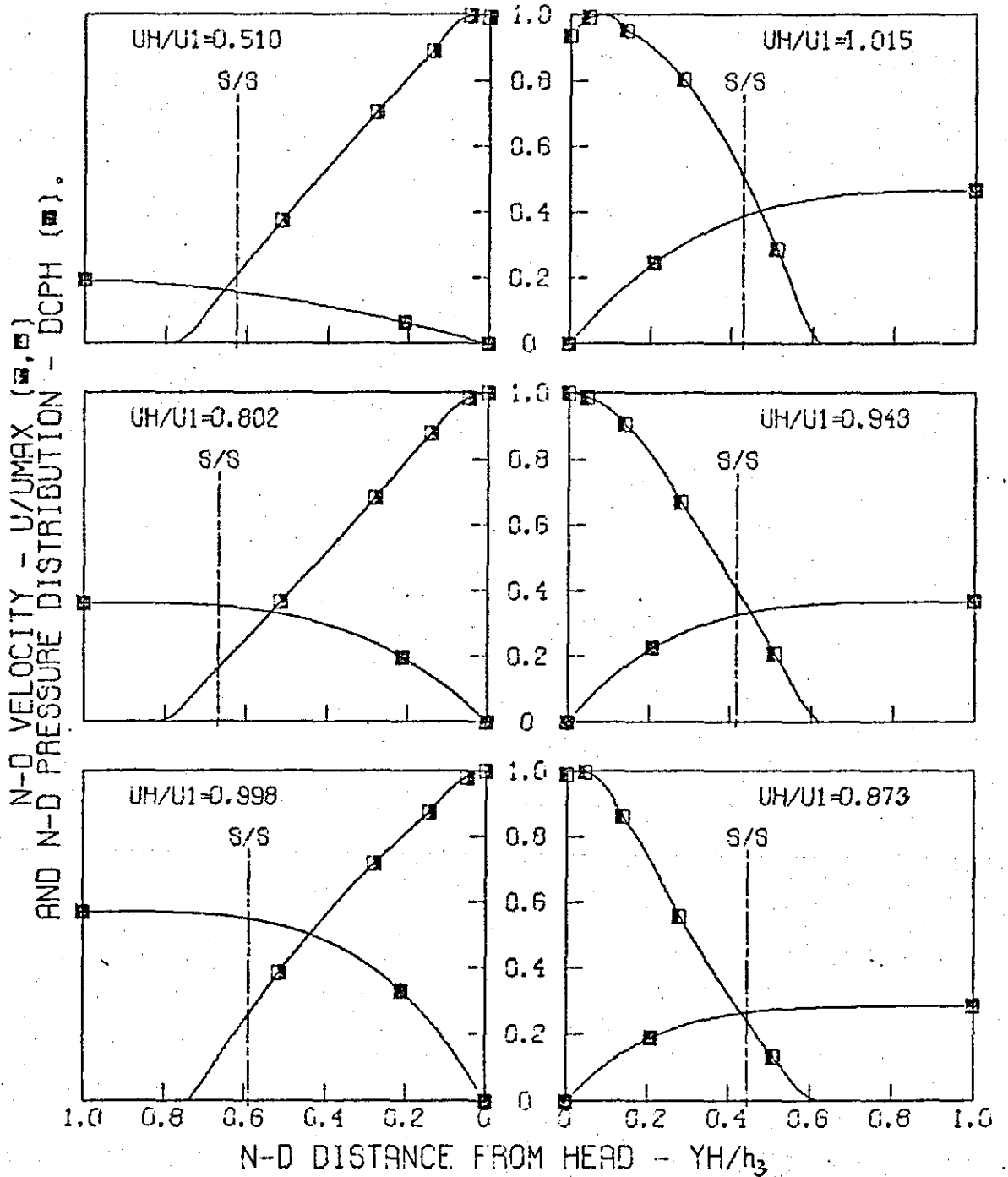
5-0522

5-0517

5-0512

Fig.A6-9.

HEAD STATIC PRESSURE AND VELOCITY PROFILES  
FOR TEST SERIES 5-08.



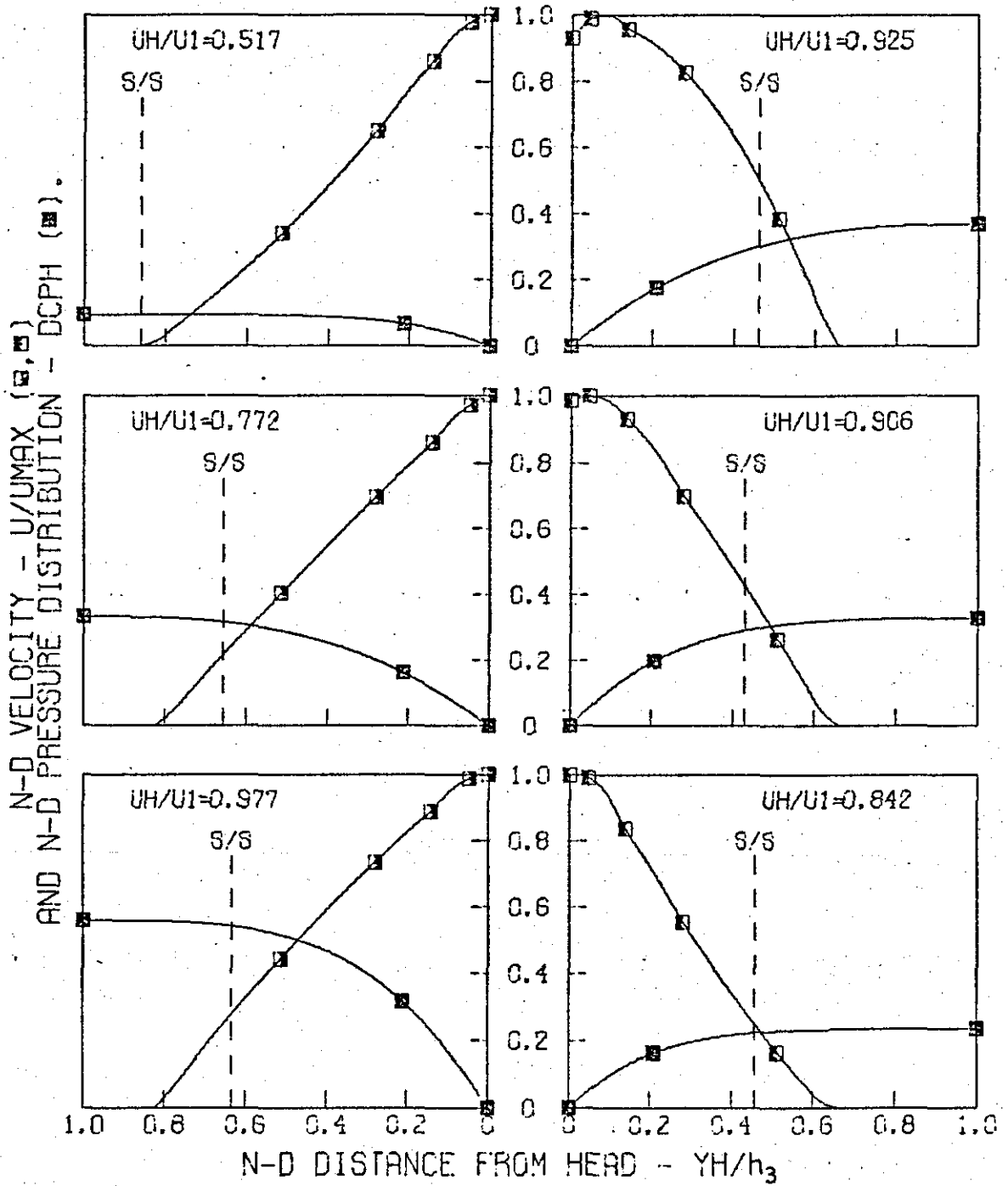
5-0832

5-0817

5-0812

Fig.A6-10.

HEAD STATIC PRESSURE AND VELOCITY PROFILES  
FOR TEST SERIES 5-15.



5-1530

5-1518

5-1511

APPENDIX 7.

Fig.A7-1 SETTLING LENGTH VELOCITY PROFILES  
FOR TEST SERIES 1-0.5

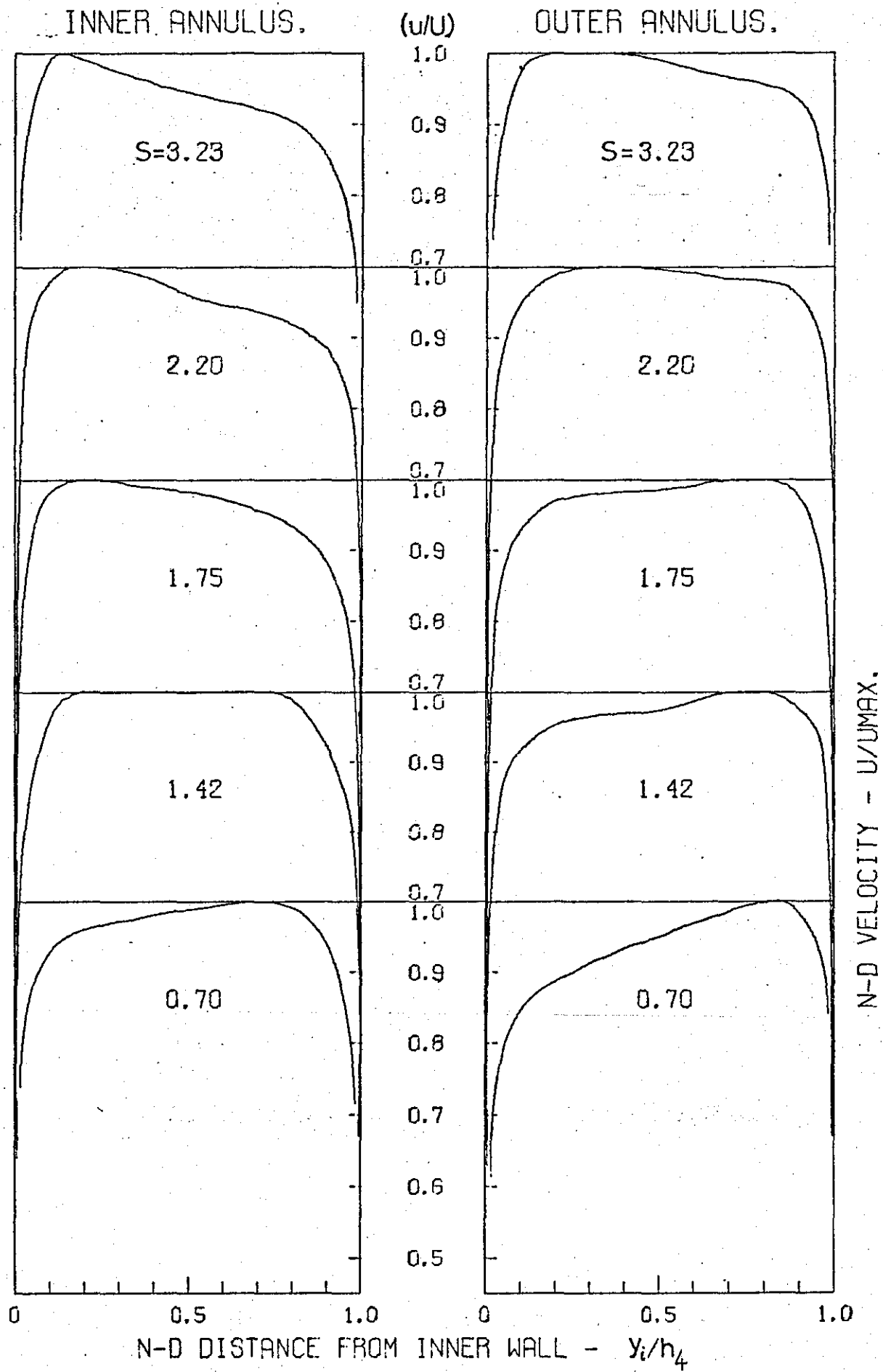


Fig.A7-2 SETTLING LENGTH VELOCITY PROFILES  
FOR TEST SERIES 1-1.0

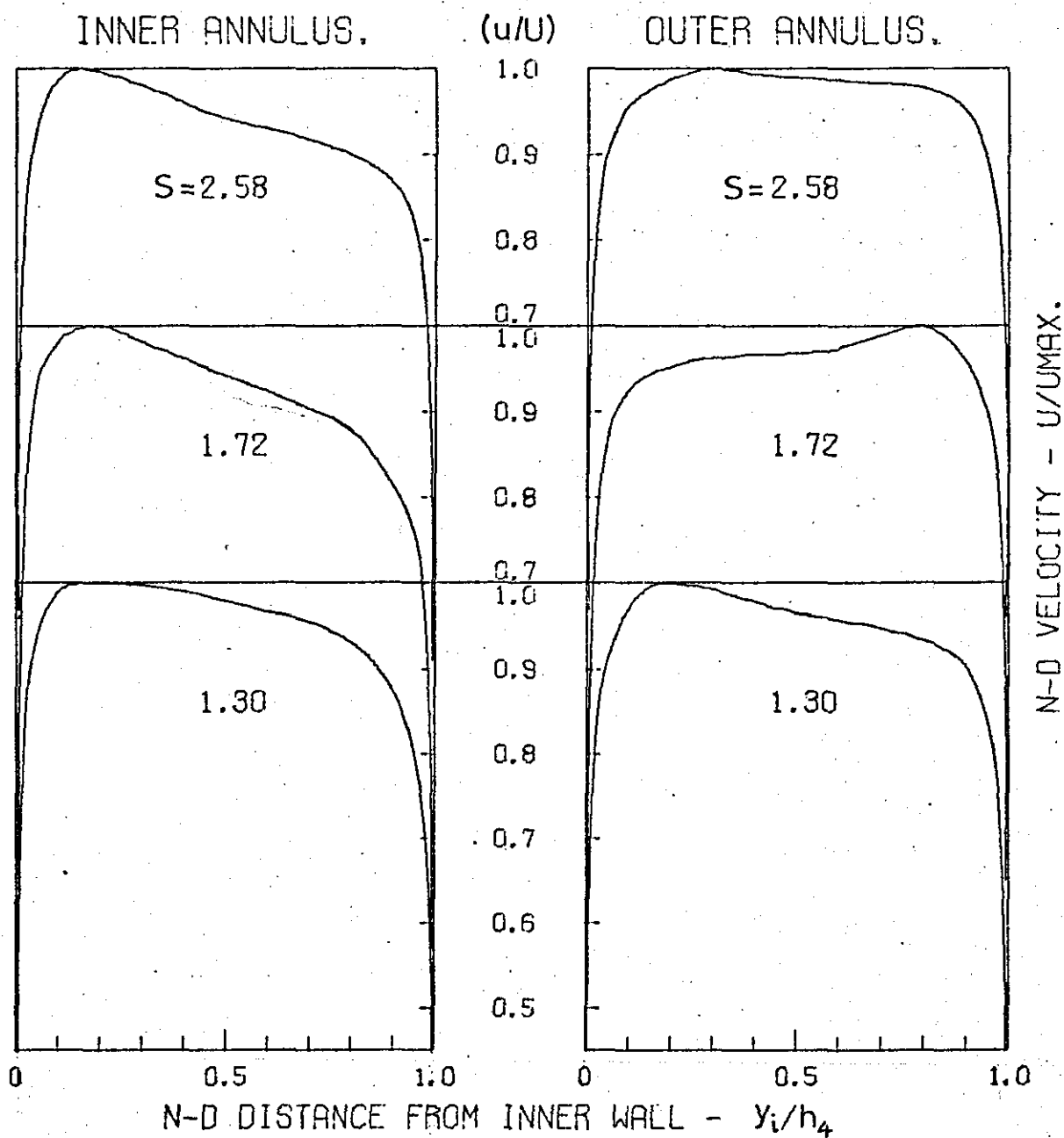


Fig.A7-3 SETTLING LENGTH VELOCITY PROFILES  
FOR TEST SERIES 1-2.0

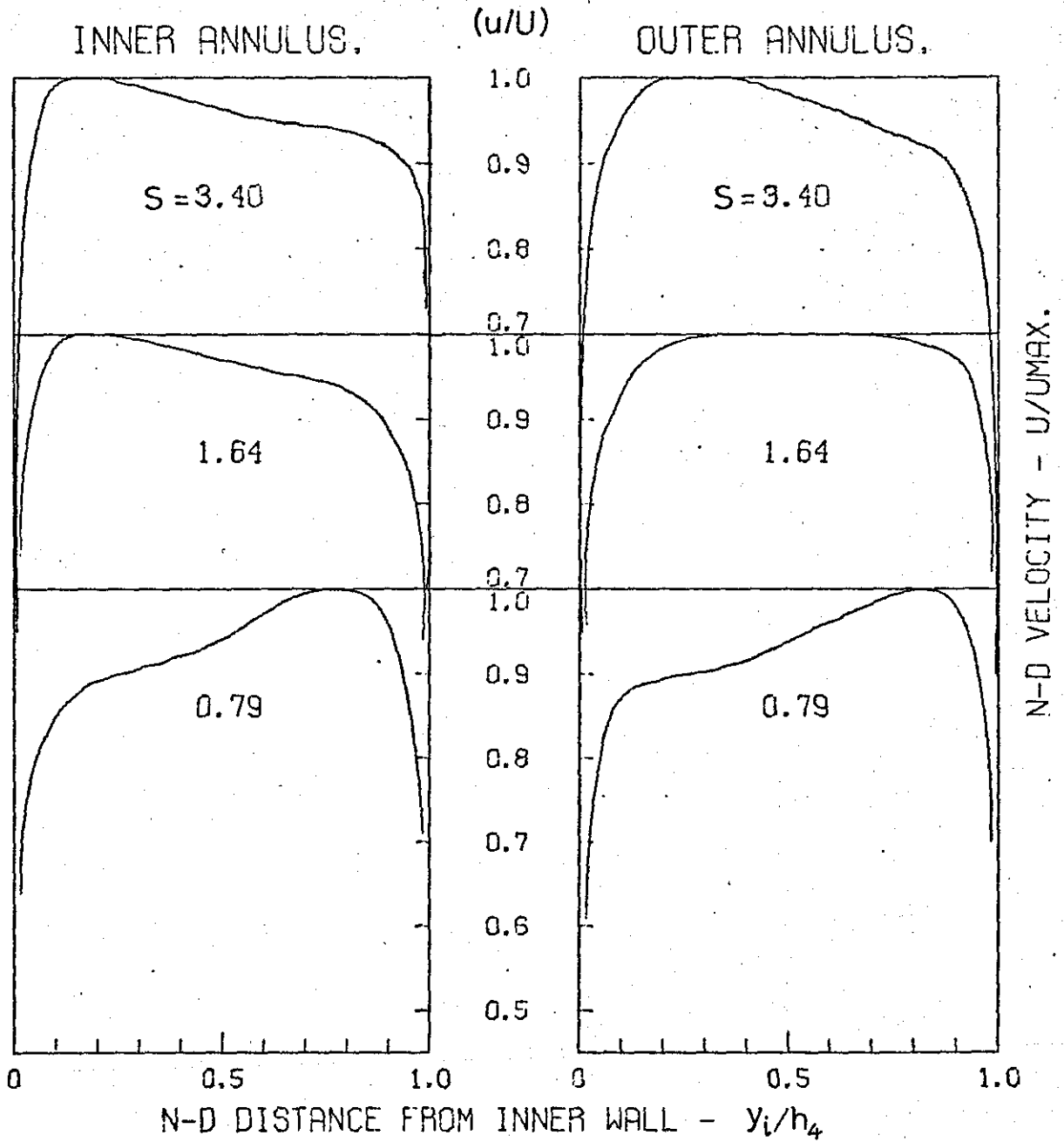




Fig.A7-4 SETTLING LENGTH VELOCITY PROFILES  
FOR TEST SERIES 2-0,5

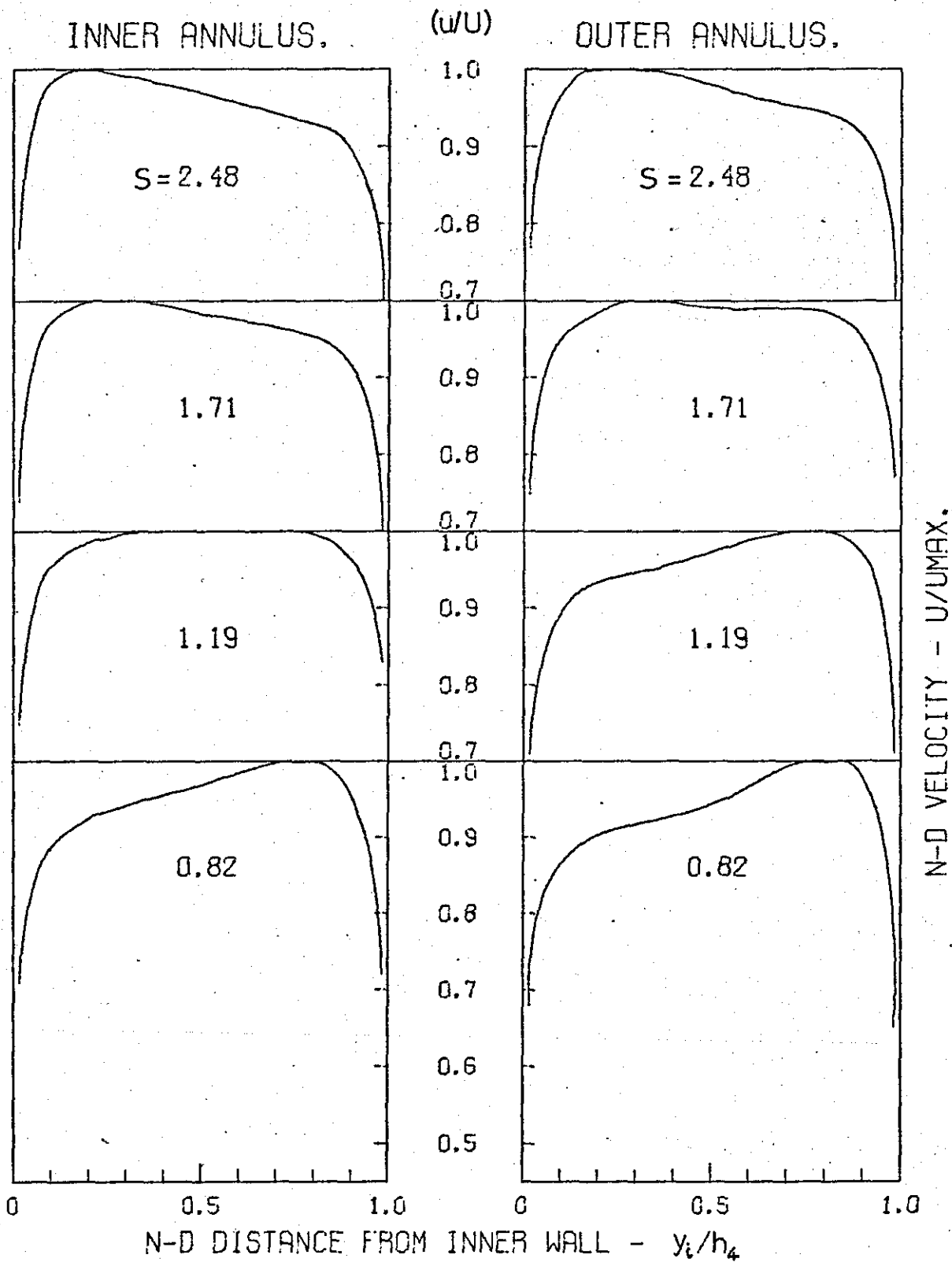


Fig.A7-5 SETTLING LENGTH VELOCITY PROFILES  
FOR TEST SERIES 2-0.8

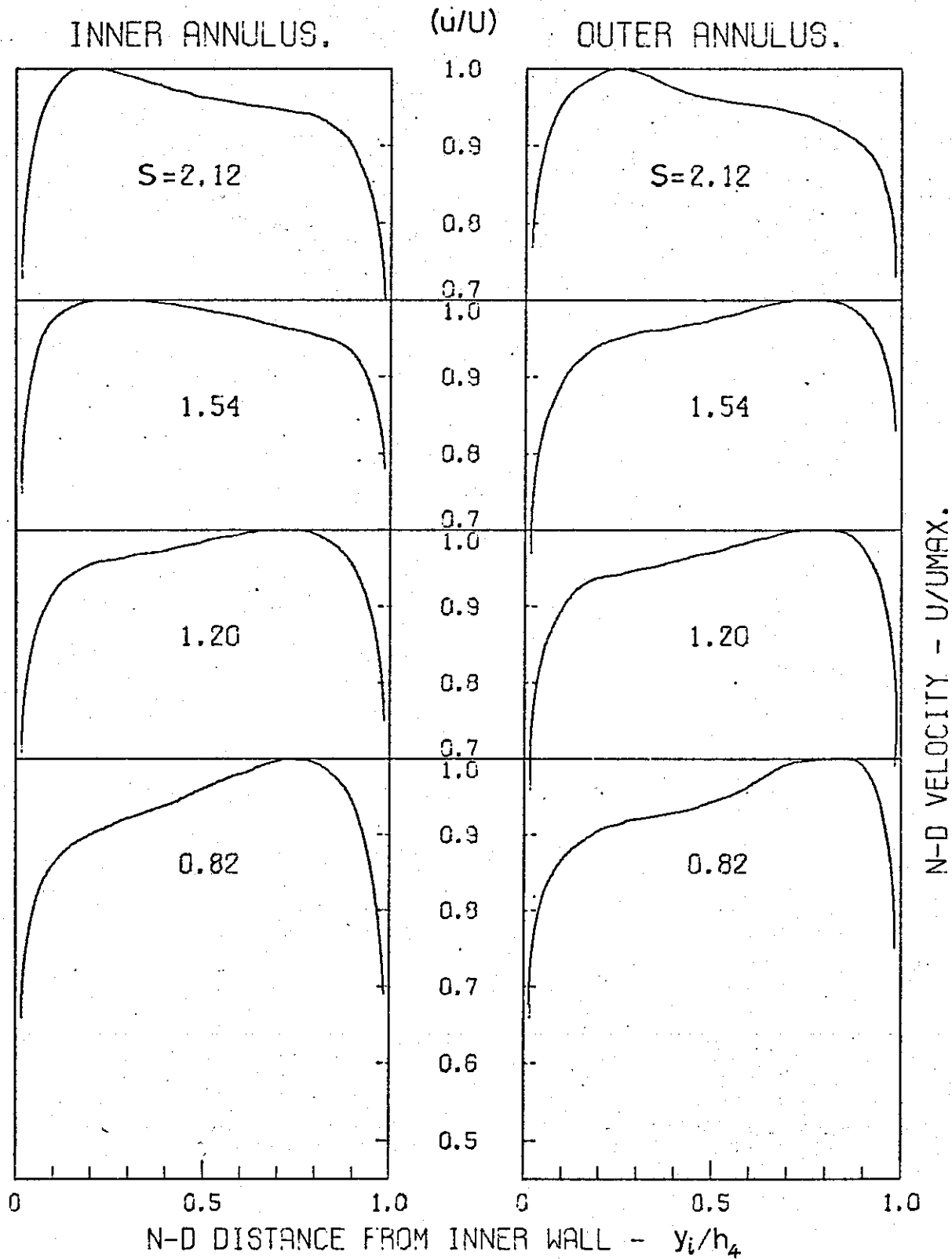
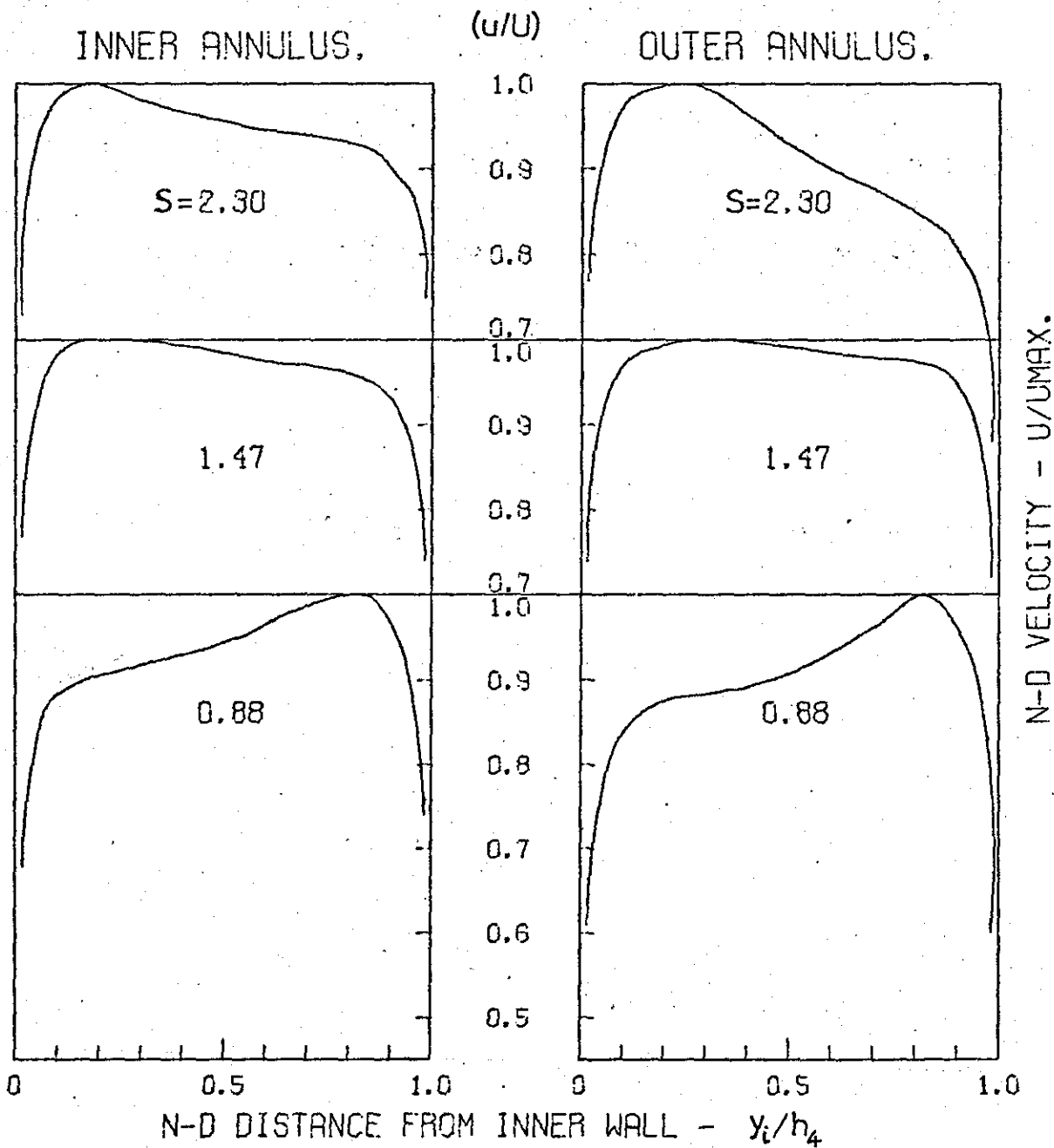


Fig.A7-6 SETTLING LENGTH VELOCITY PROFILES  
FOR TEST SERIES 2-1.5



FigA7-7 SETTLING LENGTH VELOCITY PROFILES  
FOR TEST SERIES 4-0.4

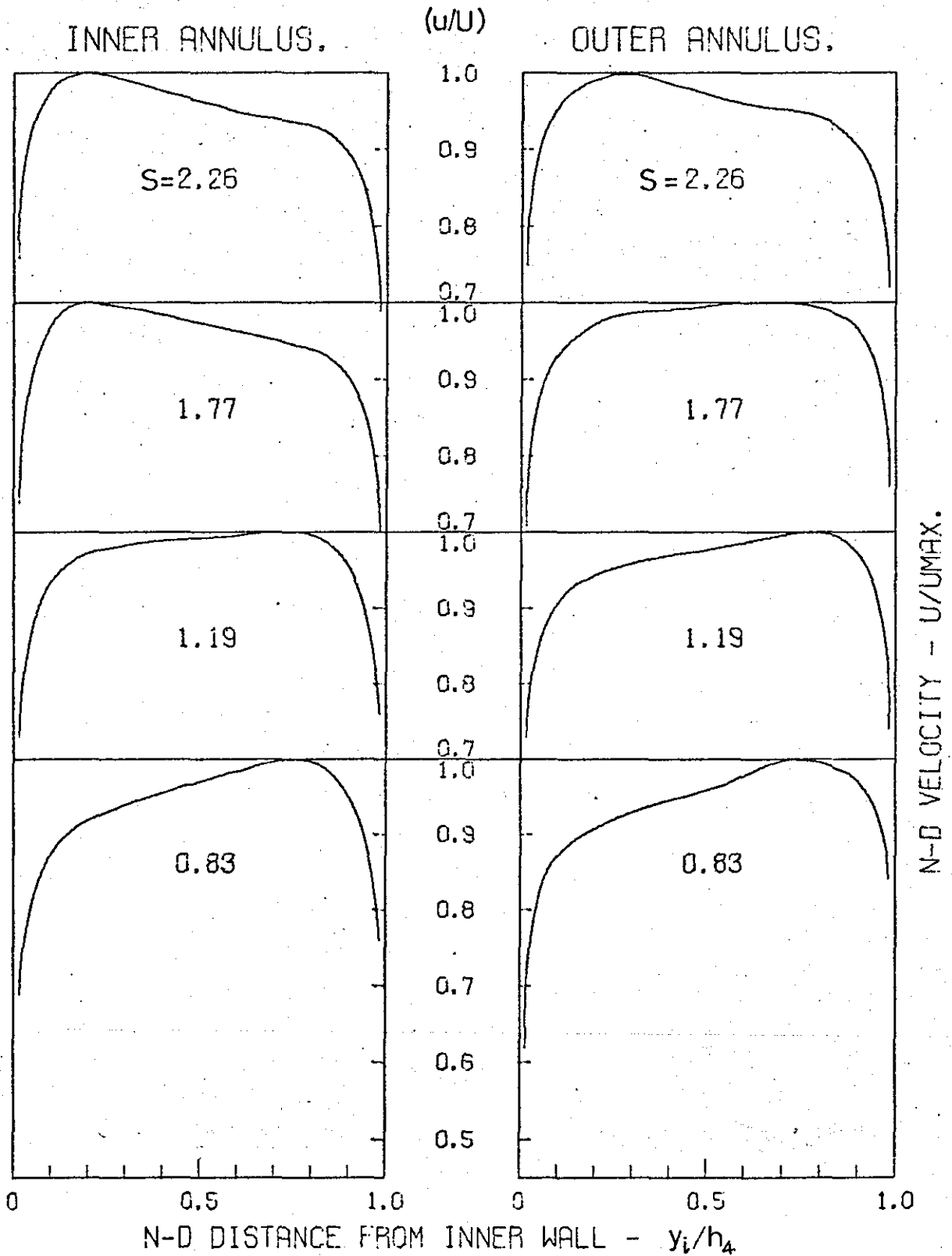


Fig.A7-8 SETTLING LENGTH VELOCITY PROFILES  
FOR TEST SERIES 4-0.7

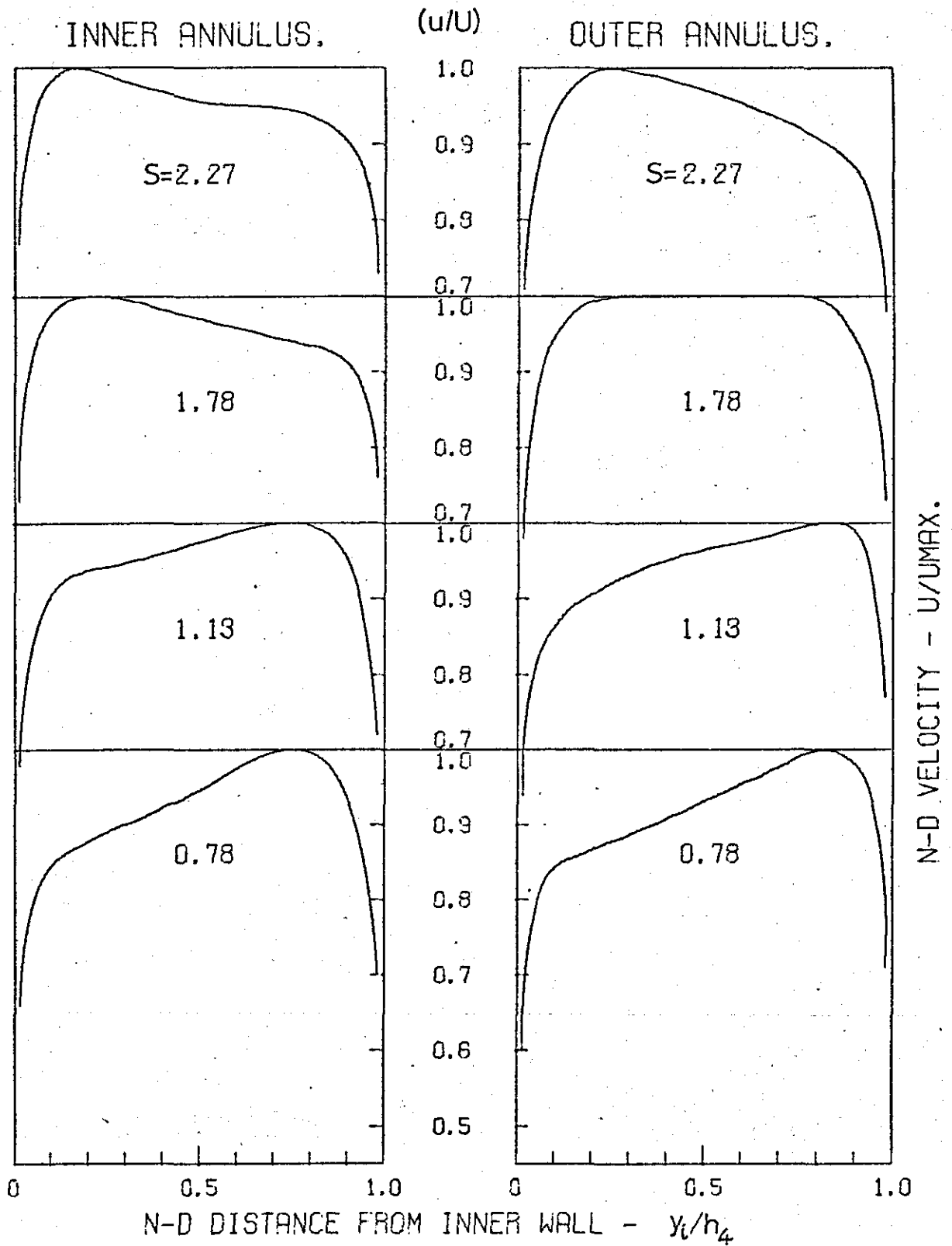


Fig.A7-9 SETTLING LENGTH VELOCITY PROFILES  
FOR TEST SERIES 4-1.2

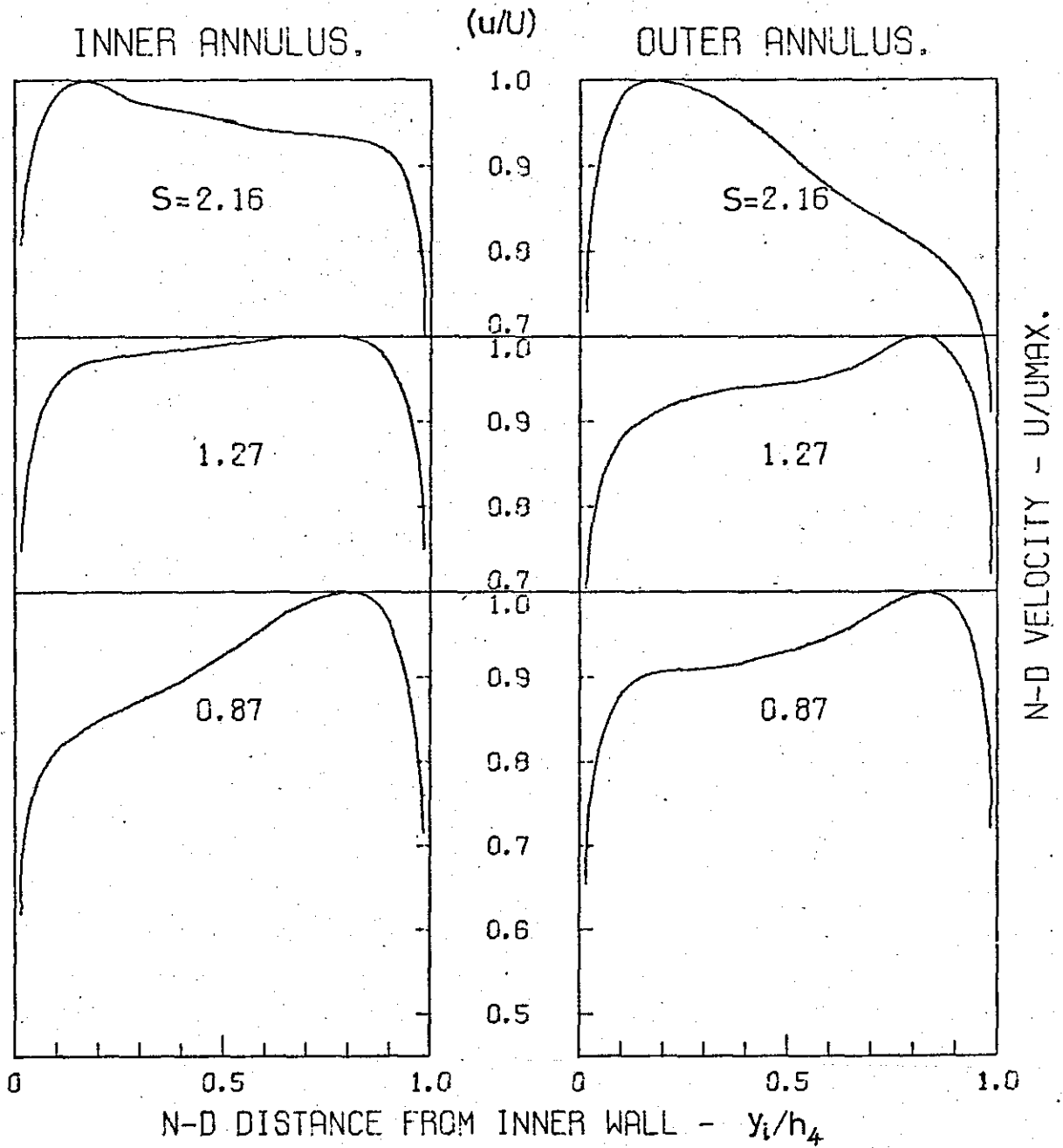


Fig A7-10 SETTLING LENGTH VELOCITY PROFILES  
FOR TEST SERIES 5-0.5

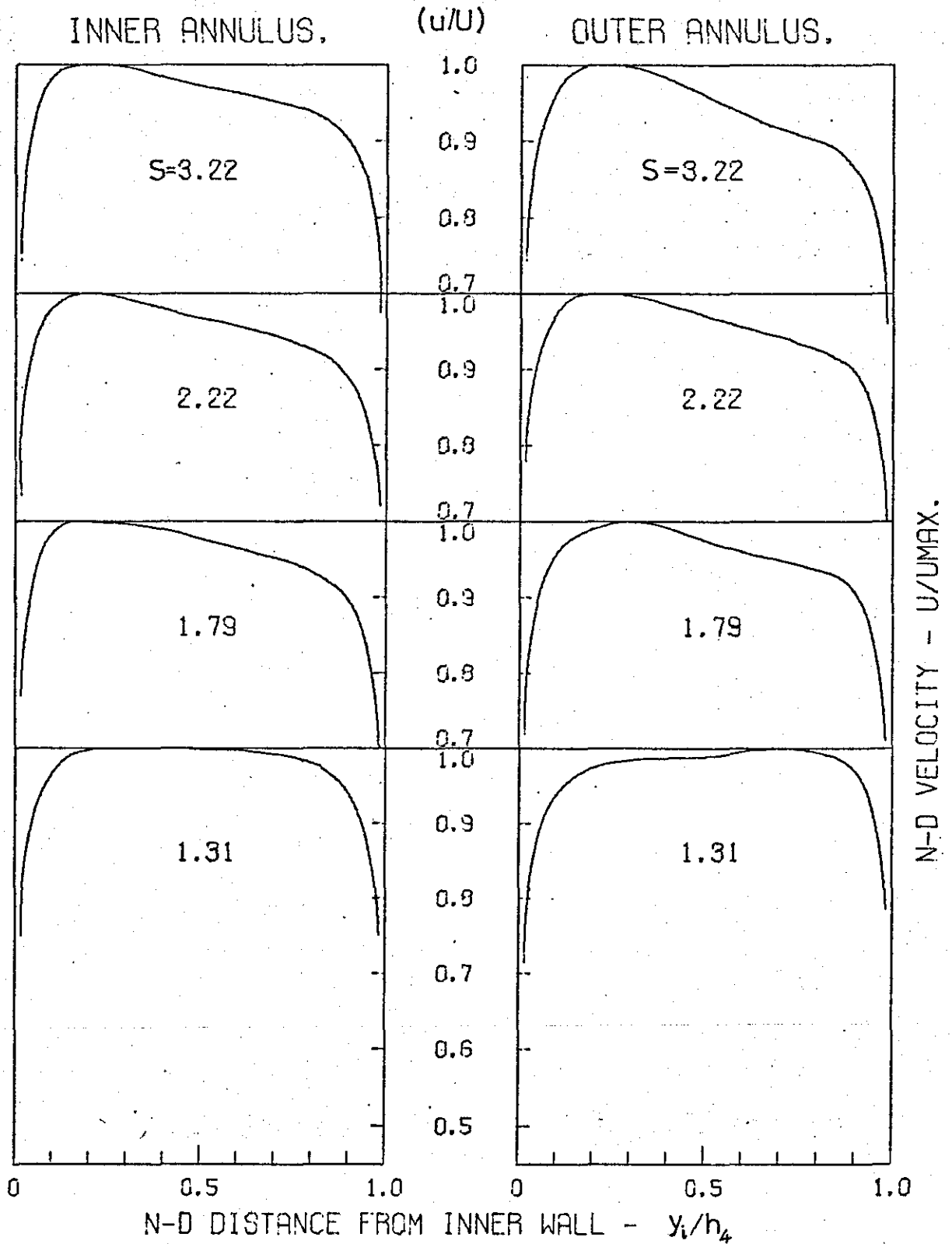


Fig.A7-11 SETTLING LENGTH VELOCITY PROFILES  
FOR TEST SERIES 5-0.8

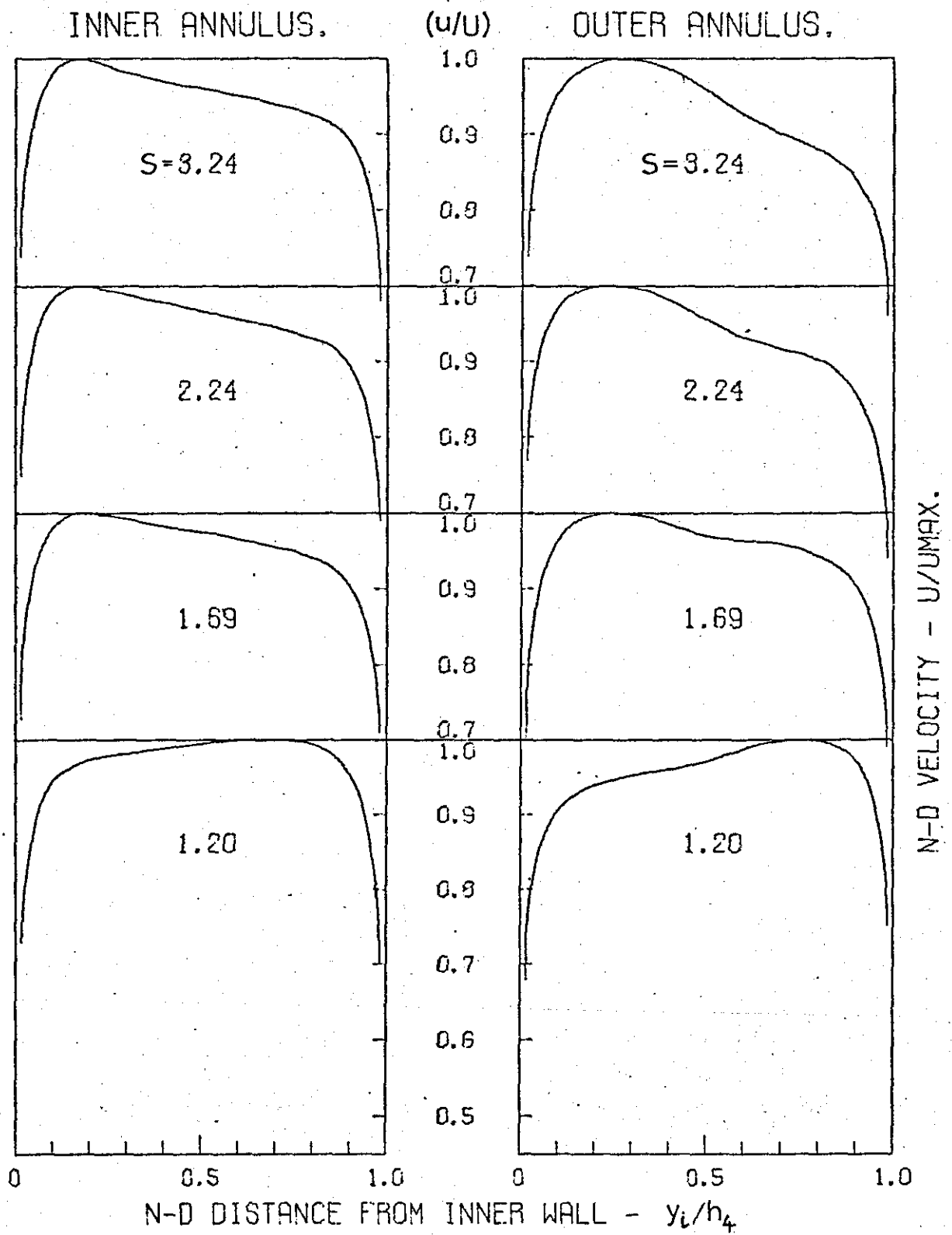
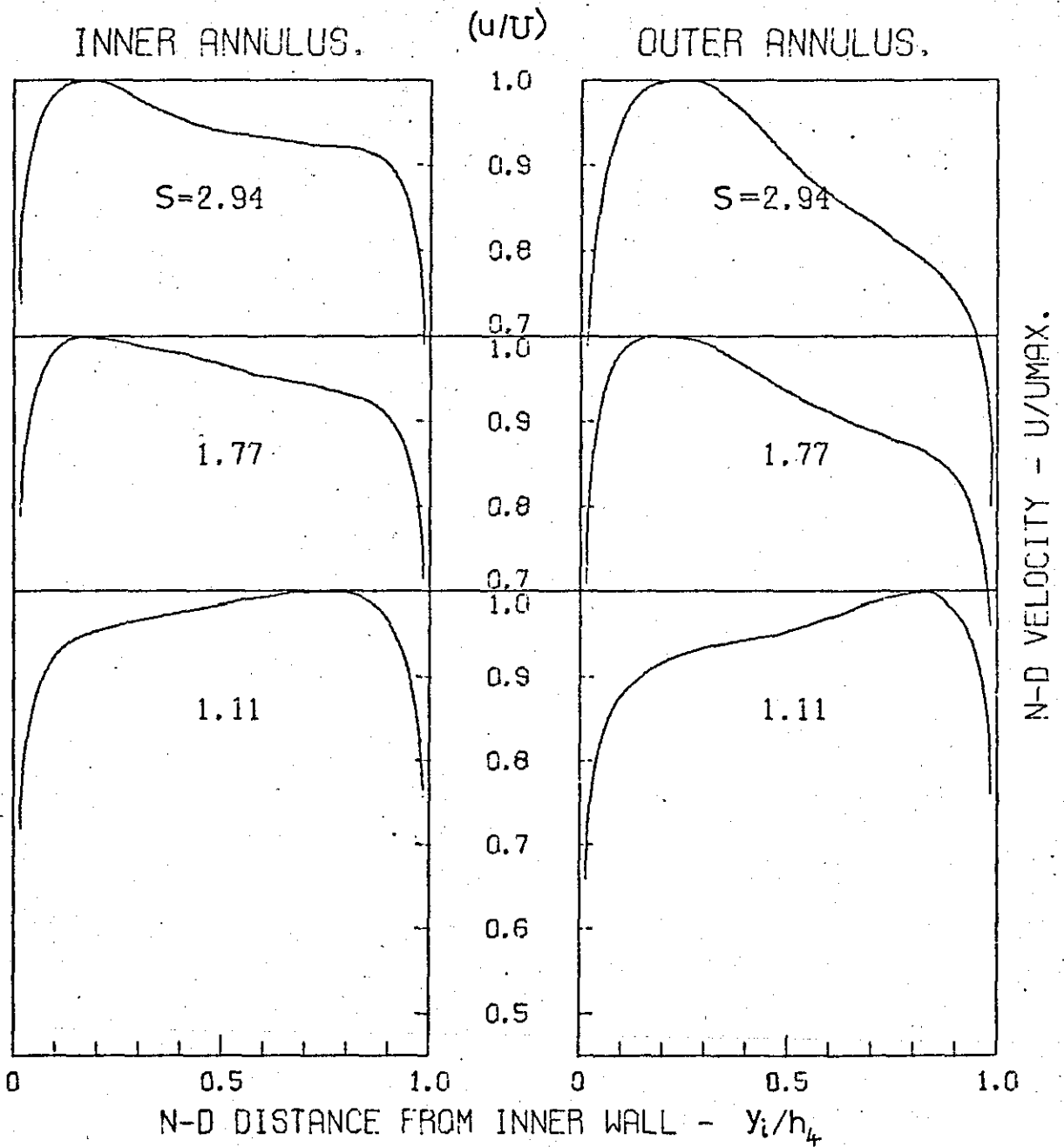




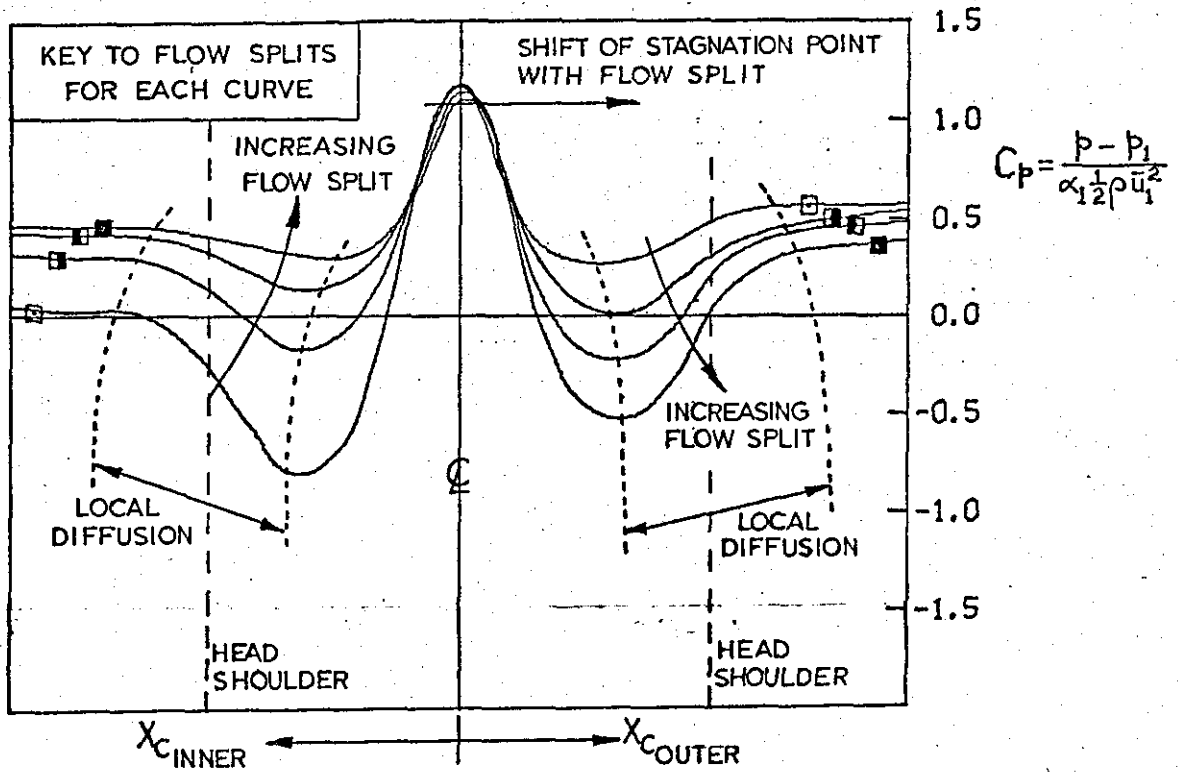
Fig.A7-12 SETTLING LENGTH VELOCITY PROFILES  
FOR TEST SERIES 5-1.5



APPENDIX 8.

COMBUSTION CHAMBER STATIC PRESSURE DISTRIBUTIONS

Fig.A8-1 KEY TO STATIC PRESSURE DISTRIBUTION PLOTS.



SCALE: 1 to 3.142

0 20 40 60 80 100 mm.

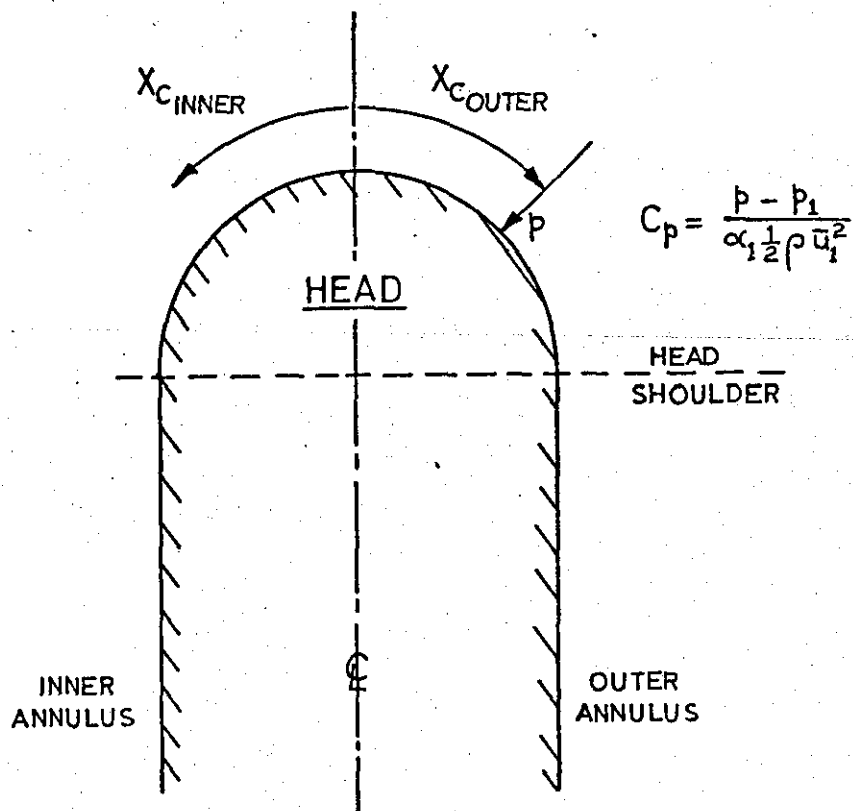


Fig. A8-2

'COMBUSTION CHAMBER' STATIC PRESSURE  
DISTRIBUTIONS FOR DIFFUSER 1

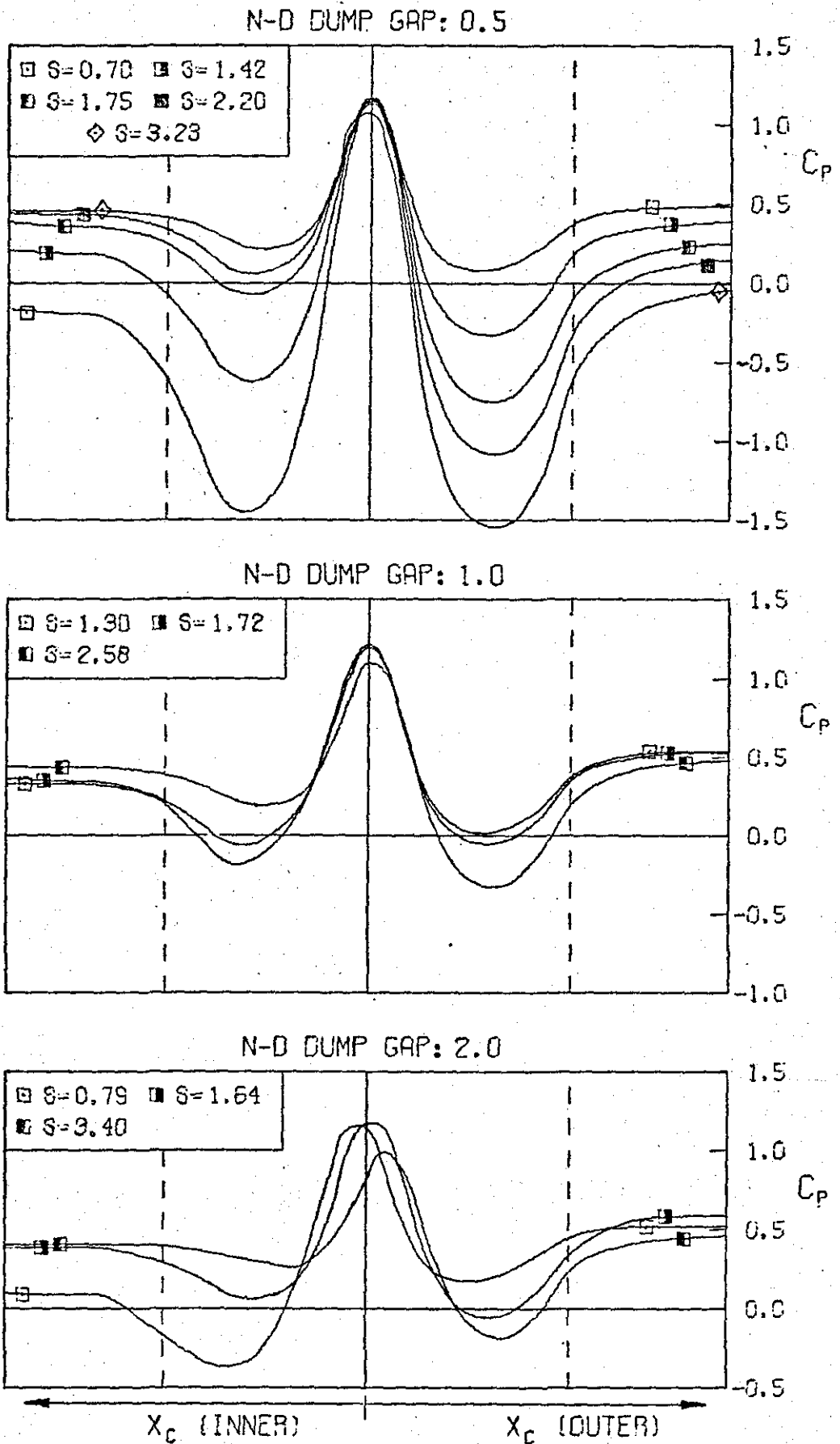
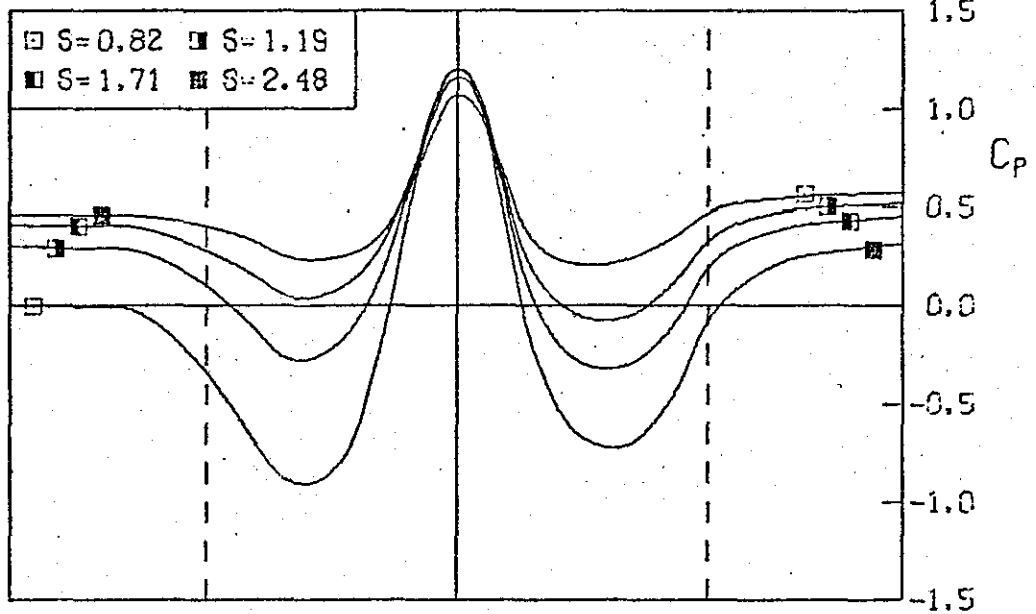


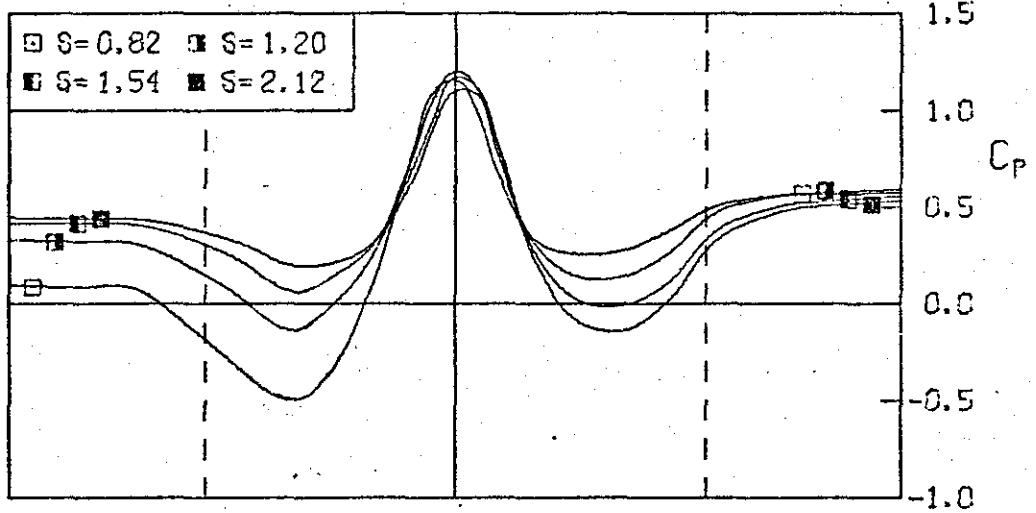
Fig.A8-3

'COMBUSTION CHAMBER' STATIC PRESSURE  
DISTRIBUTIONS FOR DIFFUSER 2

N-D DUMP GAP: 0.5



N-D DUMP GAP: 0.8



N-D DUMP GAP: 1.5

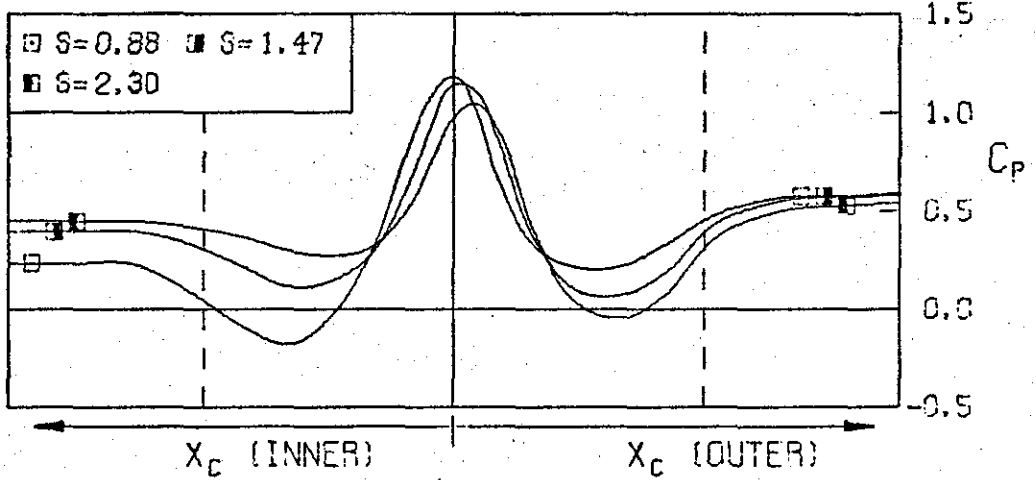
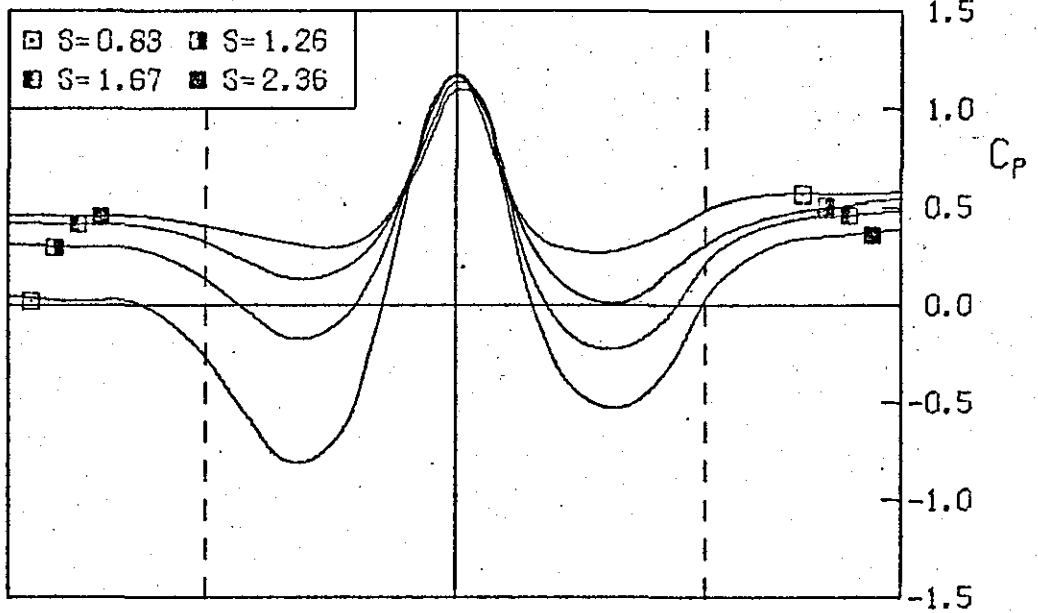


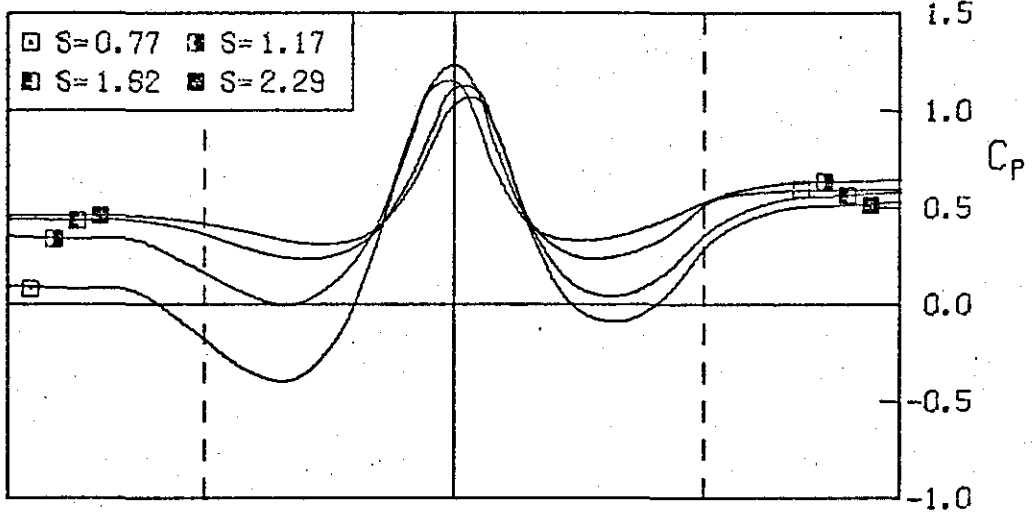
Fig. A8-4

'COMBUSTION CHAMBER' STATIC PRESSURE  
DISTRIBUTIONS FOR DIFFUSER 3

N-D DUMP GAP: 0.4



N-D DUMP GAP: 0.7



N-D DUMP GAP: 1.2

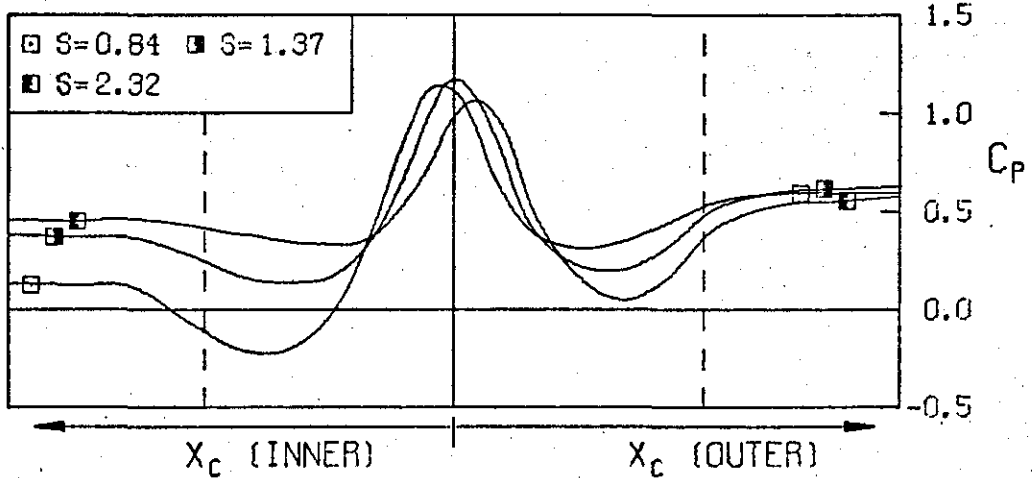
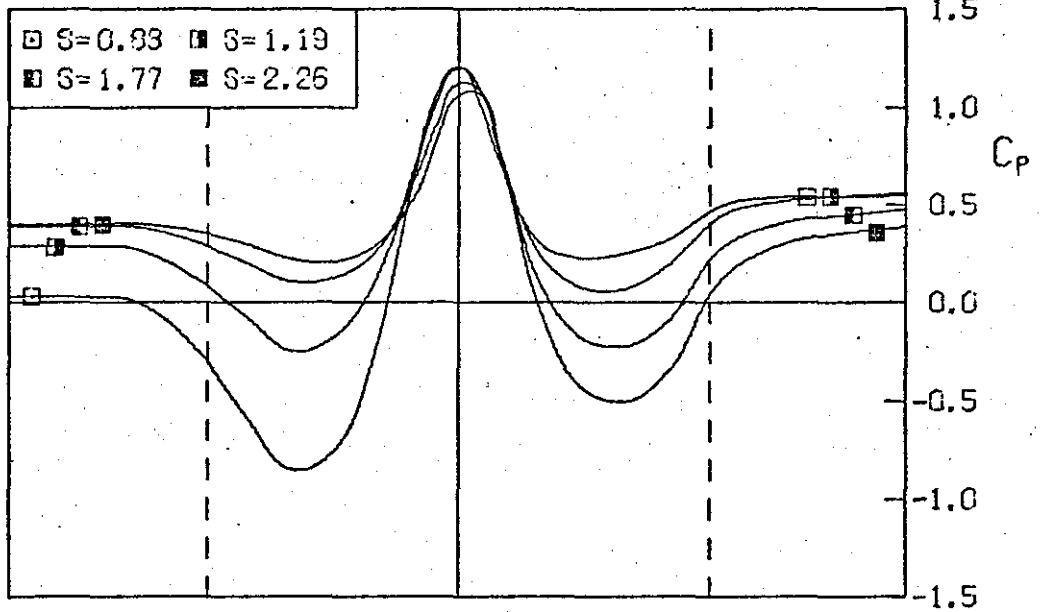


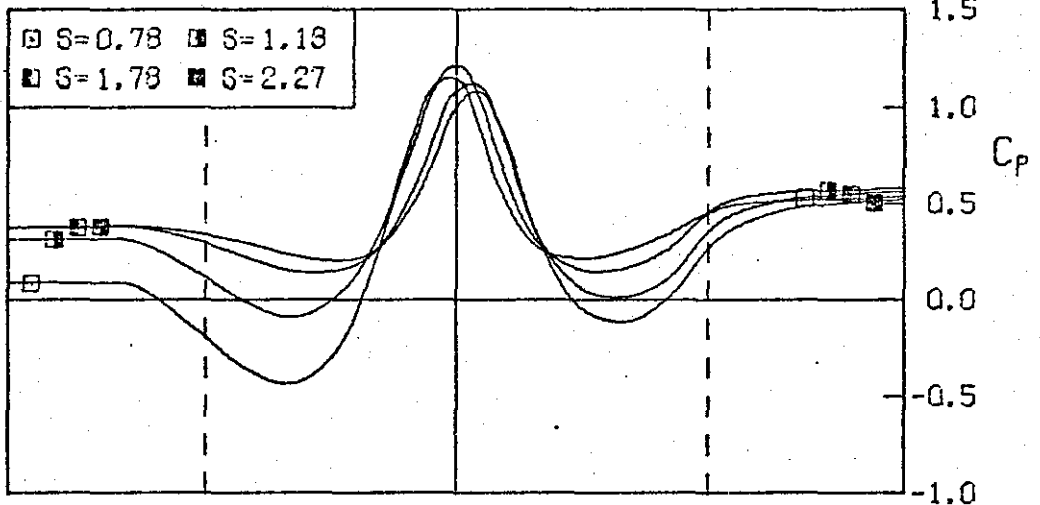
Fig. A8-5

'COMBUSTION CHAMBER' STATIC PRESSURE  
DISTRIBUTIONS FOR DIFFUSER 4

N-D DUMP GAP: 0.4



N-D DUMP GAP: 0.7



N-D DUMP GAP: 1.2

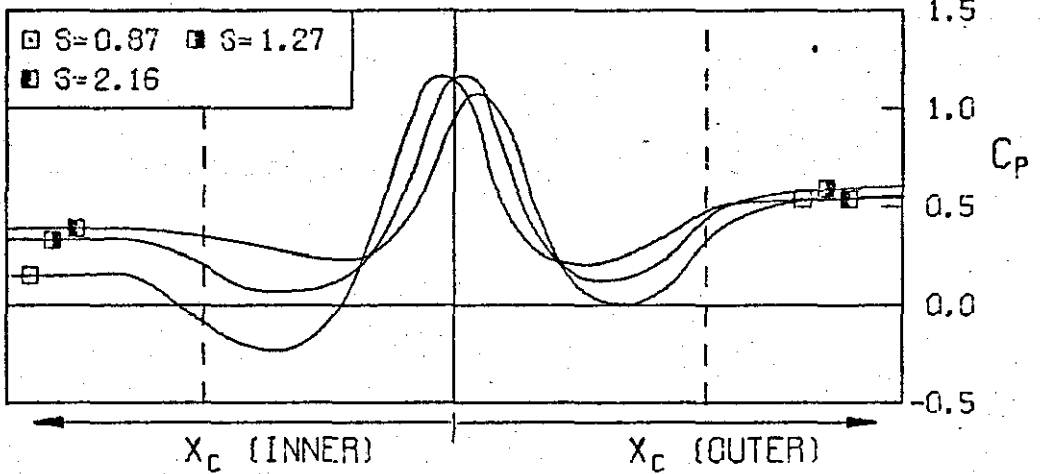


Fig. A8-6

'COMBUSTION CHAMBER' STATIC PRESSURE  
DISTRIBUTIONS FOR DIFFUSER 5

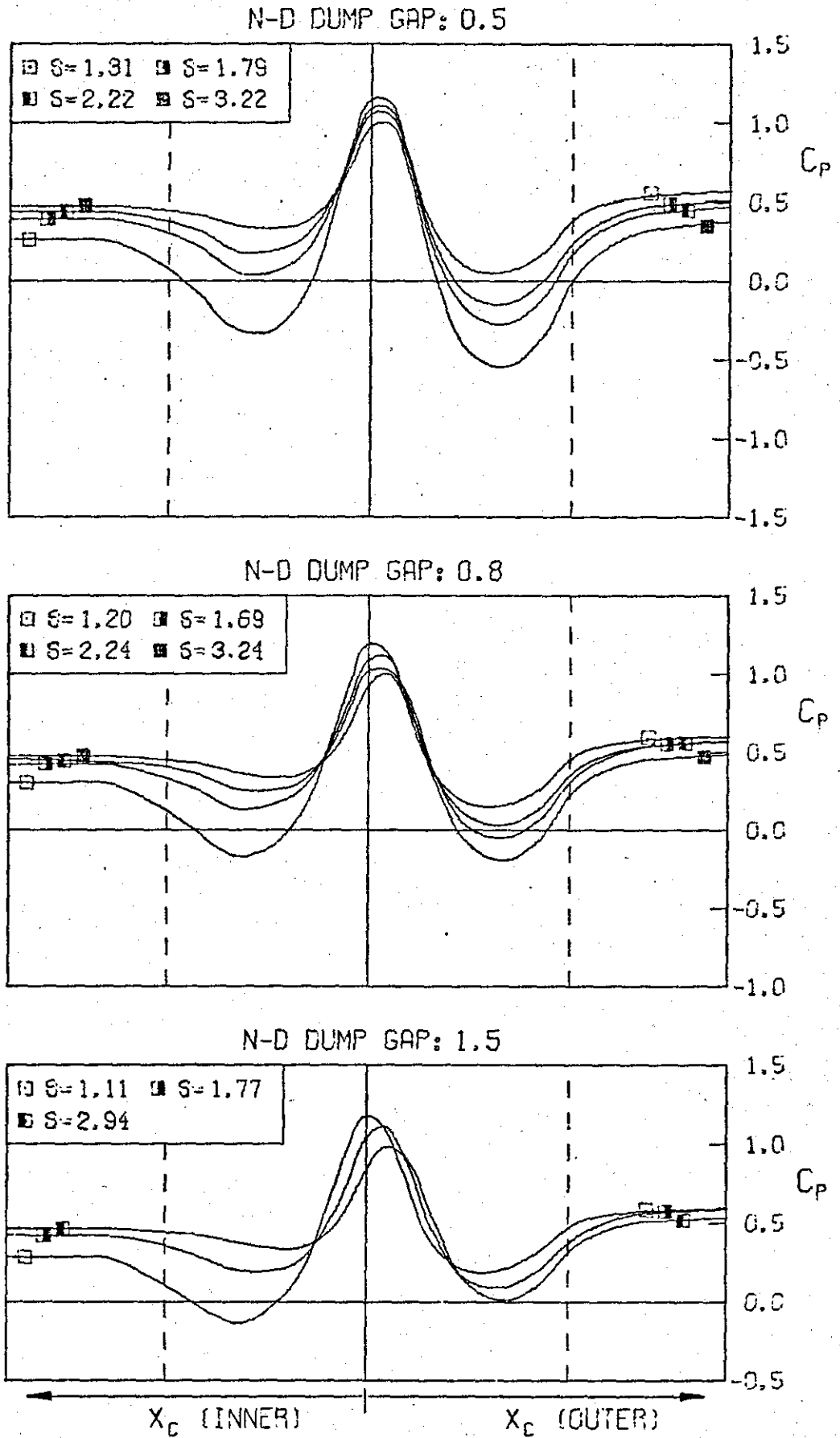


Table A9-1 BOUNDARY LAYER AND VELOCITY PROFILE PARAMETERS.

DIFFUSER 1, AR=1.4, 2φ=12°

| TEST No.  | PRE-DIFFUSER OUTLET    |          |               |                        |          |               |                  |                 |            | SETTLING LENGTHS   |           |                    |           |
|-----------|------------------------|----------|---------------|------------------------|----------|---------------|------------------|-----------------|------------|--------------------|-----------|--------------------|-----------|
|           | INNER B-L              |          |               | OUTER B-L              |          |               | VELOCITY PROFILE |                 |            | INNER              |           | OUTER              |           |
|           | $\delta_{2i}^* \% h_2$ | $H_{2i}$ | $\alpha_{2i}$ | $\delta_{2o}^* \% h_2$ | $H_{2o}$ | $\alpha_{2o}$ | $RD_2$           | $(\bar{U}/U)_2$ | $\alpha_2$ | $(\bar{U}/U)_{4i}$ | $RD_{4i}$ | $(\bar{U}/U)_{4o}$ | $RD_{4o}$ |
| 1-0507/A  | 2.16                   | 1.227    | 1.021         | 11.48                  | 1.604    | 1.152         | -0.68            | 0.853           | 1.098      | 0.946              | 0.18      | 0.919              | 0.71      |
| 1-0514/CT | 6.44                   | 1.280    | 1.041         | 4.05                   | 1.260    | 1.036         | 0.23             | 0.898           | 1.039      | 0.954              | -0.09     | 0.946              | 0.44      |
| 1-0517/CT | 12.12                  | 1.519    | 1.117         | 1.68                   | 1.266    | 1.022         | 0.76             | 0.874           | 1.075      | 0.933              | -0.48     | 0.951              | 0.31      |
| 1-0521/CT | 16.43                  | 1.674    | 1.175         | 1.15                   | 1.255    | 1.021         | 0.87             | 0.841           | 1.126      | 0.926              | -0.54     | 0.956              | -0.03     |
| 1-0532/A  | 21.89                  | 2.101    | 1.351         | 1.34                   | 1.300    | 1.027         | 0.88             | 0.791           | 1.233      | 0.910              | -0.63     | 0.950              | -0.32     |
| 1-1013/CT | 10.50                  | 1.645    | 1.163         | 9.60                   | 1.641    | 1.164         | 0.04             | 0.800           | 1.164      | 0.932              | -0.55     | 0.931              | -0.48     |
| 1-1017/CT | 12.57                  | 1.758    | 1.206         | 8.25                   | 1.574    | 1.138         | 0.21             | 0.797           | 1.173      | 0.896              | -0.66     | 0.938              | 0.39      |
| 1-1025/CT | 17.90                  | 2.096    | 1.362         | 5.60                   | 1.411    | 1.078         | 0.52             | 0.779           | 1.222      | 0.912              | -0.63     | 0.953              | -0.14     |
| 1-2007/A  | 9.38                   | 1.609    | 1.145         | 12.81                  | 1.913    | 1.282         | -0.15            | 0.774           | 1.217      | 0.911              | 0.57      | 0.912              | 0.62      |
| 1-2016/A  | 12.06                  | 1.767    | 1.208         | 10.11                  | 1.690    | 1.188         | 0.09             | 0.781           | 1.198      | 0.932              | -0.52     | 0.957              | 0.16      |
| 1-2033/A  | 16.92                  | 2.089    | 1.346         | 6.86                   | 1.470    | 1.103         | 0.42             | 0.774           | 1.229      | 0.938              | -0.48     | 0.930              | -0.42     |

Table A9-1



Table A9-2 BOUNDARY LAYER AND VELOCITY PROFILE PARAMETERS.

DIFFUSER 2, AR=1.6, 2φ=12°

| TEST No.  | PRE-DIFFUSER OUTLET    |          |               |                        |          |               |                  |                 |            | SETTLING LENGTHS   |           |                    |           |
|-----------|------------------------|----------|---------------|------------------------|----------|---------------|------------------|-----------------|------------|--------------------|-----------|--------------------|-----------|
|           | INNER B-L              |          |               | OUTER B-L              |          |               | VELOCITY PROFILE |                 |            | INNER              |           | OUTER              |           |
|           | $\delta_{2i}^* \% h_2$ | $H_{2i}$ | $\alpha_{2i}$ | $\delta_{2o}^* \% h_2$ | $H_{2o}$ | $\alpha_{2o}$ | $RD_2$           | $(\bar{U})/U_2$ | $\alpha_2$ | $(\bar{U})/U_{4i}$ | $RD_{4i}$ | $(\bar{U})/U_{4o}$ | $RD_{4o}$ |
| 2-0508/A  | 4.42                   | 1.255    | 1.035         | 14.26                  | 1.883    | 1.277         | -0.53            | 0.801           | 1.171      | 0.932              | 0.45      | 0.918              | 0.57      |
| 2-0511/CT | 10.11                  | 1.488    | 1.111         | 8.19                   | 1.516    | 1.120         | 0.10             | 0.819           | 1.115      | 0.964              | 0.14      | 0.936              | 0.45      |
| 2-0517/A  | 16.80                  | 1.858    | 1.262         | 5.17                   | 1.365    | 1.067         | 0.53             | 0.795           | 1.171      | 0.944              | -0.36     | 0.956              | -0.07     |
| 2-0524/A  | 24.68                  | 2.498    | 1.546         | 3.26                   | 1.277    | 1.040         | 0.77             | 0.748           | 1.322      | 0.933              | -0.53     | 0.942              | -0.43     |
| 2-0808/A  | 8.15                   | 1.485    | 1.107         | 17.22                  | 2.312    | 1.496         | -0.36            | 0.735           | 1.307      | 0.918              | 0.47      | 0.922              | 0.65      |
| 2-0812/CT | 12.94                  | 1.781    | 1.229         | 12.84                  | 1.922    | 1.297         | 0.00             | 0.742           | 1.265      | 0.945              | 0.32      | 0.936              | 0.48      |
| 2-0815/A  | 17.92                  | 2.050    | 1.349         | 8.67                   | 1.664    | 1.179         | 0.35             | 0.746           | 1.269      | 0.950              | -0.33     | 0.942              | 0.54      |
| 2-0821/CT | 21.93                  | 2.425    | 1.538         | 7.42                   | 1.531    | 1.126         | 0.49             | 0.725           | 1.329      | 0.931              | -0.48     | 0.931              | -0.45     |
| 2-1508/A  | 12.37                  | 1.791    | 1.233         | 15.31                  | 2.172    | 1.419         | -0.11            | 0.719           | 1.331      | 0.921              | 0.59      | 0.889              | 0.64      |
| 2-1514/A  | 17.48                  | 2.194    | 1.410         | 11.77                  | 1.876    | 1.279         | 0.20             | 0.715           | 1.344      | 0.950              | -0.37     | 0.955              | -0.22     |
| 2-1523/A  | 21.88                  | 2.622    | 1.596         | 9.18                   | 1.676    | 1.189         | 0.41             | 0.706           | 1.395      | 0.930              | -0.53     | 0.893              | -0.69     |

Table A9-3 BOUNDARY LAYER AND VELOCITY PROFILE PARAMETERS.

DIFFUSER 3, AR=1.8, 2φ=12°

| TEST No.  | PRE-DIFFUSER OUTLET |          |               |                     |          |               |                  |                 |            | SETTLING LENGTHS   |           |                    |           |
|-----------|---------------------|----------|---------------|---------------------|----------|---------------|------------------|-----------------|------------|--------------------|-----------|--------------------|-----------|
|           | INNER B-L           |          |               | OUTER B-L           |          |               | VELOCITY PROFILE |                 |            | INNER              |           | OUTER              |           |
|           | $\delta_{2i}^*/h_2$ | $H_{2i}$ | $\alpha_{2i}$ | $\delta_{2o}^*/h_2$ | $H_{2o}$ | $\alpha_{2o}$ | $RD_2$           | $(\bar{U}/U)_2$ | $\alpha_2$ | $(\bar{U}/U)_{4i}$ | $RD_{4i}$ | $(\bar{U}/U)_{4o}$ | $RD_{4o}$ |
| 3-0408/A  | 4.98                | 1.263    | 1.039         | 16.69               | 2.064    | 1.370         | -0.54            | 0.766           | 1.231      | 0.936              | 0.42      | 0.913              | 0.63      |
| 3-0412/CT | 11.92               | 1.576    | 1.147         | 9.96                | 1.662    | 1.182         | 0.09             | 0.784           | 1.165      | 0.959              | -0.09     | 0.940              | 0.47      |
| 3-0416/A  | 21.82               | 2.122    | 1.403         | 5.77                | 1.428    | 1.089         | 0.58             | 0.747           | 1.257      | 0.932              | -0.52     | 0.950              | -0.13     |
| 3-0423/A  | 31.49               | 3.110    | 1.864         | 3.66                | 1.304    | 1.050         | 0.79             | 0.689           | 1.523      | 0.918              | -0.61     | 0.935              | -0.43     |
| 3-0707/A  | 8.95                | 1.581    | 1.151         | 20.65               | 2.723    | 1.687         | -0.40            | 0.687           | 1.462      | 0.912              | 0.55      | 0.926              | 0.61      |
| 3-0711/CT | 14.07               | 1.899    | 1.282         | 16.30               | 2.261    | 1.489         | -0.07            | 0.693           | 1.386      | 0.957              | 0.15      | 0.929              | 0.57      |
| 3-0718/A  | 26.44               | 3.019    | 1.831         | 9.21                | 1.730    | 1.213         | 0.48             | 0.668           | 1.527      | 0.926              | -0.56     | 0.940              | -0.42     |
| 3-0722/A  | 30.76               | 3.383    | 2.053         | 7.09                | 1.569    | 1.142         | 0.62             | 0.659           | 1.593      | 0.923              | -0.59     | 0.908              | -0.56     |
| 3-1208/A  | 12.38               | 1.846    | 1.265         | 20.24               | 2.719    | 1.719         | -0.24            | 0.662           | 1.514      | 0.901              | 0.62      | 0.908              | 0.68      |
| 3-1213/A  | 19.36               | 2.406    | 1.535         | 14.66               | 2.210    | 1.448         | 0.14             | 0.667           | 1.489      | 0.961              | -0.15     | 0.960              | 0.33      |
| 3-1223/A  | 27.78               | 3.239    | 1.944         | 9.85                | 1.775    | 1.237         | 0.48             | 0.650           | 1.594      | 0.922              | -0.66     | 0.876              | -0.73     |

Table A9-4 BOUNDARY LAYER AND VELOCITY PROFILE PARAMETERS.

DIFFUSER 4, AR=1.8, 2φ=18°

| TEST No.  | PRE-DIFFUSER OUTLET    |          |               |                        |          |               |                  |                         |            | SETTLING LENGTHS           |           |                            |           |
|-----------|------------------------|----------|---------------|------------------------|----------|---------------|------------------|-------------------------|------------|----------------------------|-----------|----------------------------|-----------|
|           | INNER B-L              |          |               | OUTER B-L              |          |               | VELOCITY PROFILE |                         |            | INNER                      |           | OUTER                      |           |
|           | $\delta_{2i}^* \% h_2$ | $H_{2i}$ | $\alpha_{2i}$ | $\delta_{2o}^* \% h_2$ | $H_{2o}$ | $\alpha_{2o}$ | $RD_2$           | $(\frac{\bar{U}}{U})_2$ | $\alpha_2$ | $(\frac{\bar{U}}{U})_{4i}$ | $RD_{4i}$ | $(\frac{\bar{U}}{U})_{4o}$ | $RD_{4o}$ |
| 4-0408/A  | 4.62                   | 1.311    | 1.049         | 18.18                  | 2.526    | 1.534         | -0.59            | 0.752                   | 1.324      | 0.929                      | 0.48      | 0.927                      | 0.62      |
| 4-0411/A  | 12.86                  | 1.714    | 1.203         | 11.01                  | 1.915    | 1.264         | 0.08             | 0.764                   | 1.235      | 0.953                      | 0.20      | 0.943                      | 0.44      |
| 4-0417/A  | 24.58                  | 2.794    | 1.628         | 6.12                   | 1.525    | 1.122         | 0.60             | 0.720                   | 1.401      | 0.934                      | -0.44     | 0.955                      | 0.23      |
| 4-0422/CT | 29.63                  | 3.078    | 1.785         | 3.98                   | 1.368    | 1.068         | 0.76             | 0.701                   | 1.494      | 0.929                      | -0.54     | 0.936                      | -0.39     |
| 4-0707/A  | 8.62                   | 1.573    | 1.140         | 22.33                  | 3.375    | 1.963         | -0.44            | 0.671                   | 1.581      | 0.907                      | 0.53      | 0.902                      | 0.69      |
| 4-0711/CT | 13.82                  | 2.002    | 1.314         | 18.38                  | 2.795    | 1.715         | -0.14            | 0.671                   | 1.521      | 0.934                      | 0.40      | 0.926                      | 0.63      |
| 4-0717/A  | 29.87                  | 3.876    | 2.217         | 9.20                   | 1.788    | 1.233         | 0.53             | 0.639                   | 1.710      | 0.938                      | -0.44     | 0.957                      | 0.06      |
| 4-0722/A  | 33.54                  | 4.142    | 2.373         | 7.10                   | 1.639    | 1.167         | 0.65             | 0.632                   | 1.777      | 0.933                      | -0.53     | 0.920                      | -0.42     |
| 4-1208/A  | 12.11                  | 1.908    | 1.279         | 22.26                  | 3.300    | 1.982         | -0.30            | 0.642                   | 1.652      | 0.895                      | 0.66      | 0.914                      | 0.65      |
| 4-1212/A  | 21.24                  | 2.983    | 1.746         | 14.94                  | 2.372    | 1.508         | 0.17             | 0.647                   | 1.619      | 0.956                      | 0.25      | 0.921                      | 0.59      |
| 4-1221/A  | 31.51                  | 4.073    | 2.304         | 9.50                   | 1.830    | 1.258         | 0.54             | 0.622                   | 1.790      | 0.930                      | -0.58     | 0.876                      | -0.73     |

Table A9-5 BOUNDARY LAYER AND VELOCITY PROFILE PARAMETERS.

DIFFUSER 5, AR=1.6, 2φ=11.3°(Canted)

| TEST No.  | PRE-DIFFUSER OUTLET      |          |               |                          |          |               |                  |                 |            | SETTLING LENGTHS   |           |                    |           |
|-----------|--------------------------|----------|---------------|--------------------------|----------|---------------|------------------|-----------------|------------|--------------------|-----------|--------------------|-----------|
|           | INNER B-L                |          |               | OUTER B-L                |          |               | VELOCITY PROFILE |                 |            | INNER              |           | OUTER              |           |
|           | $\delta_{2i}^*/\rho h_2$ | $H_{2i}$ | $\alpha_{2i}$ | $\delta_{2o}^*/\rho h_2$ | $H_{2o}$ | $\alpha_{2o}$ | $RD_2$           | $(\bar{U}/U)_2$ | $\alpha_2$ | $(\bar{U}/U)_{4i}$ | $RD_{4i}$ | $(\bar{U}/U)_{4o}$ | $RD_{4o}$ |
| 5-0513/A  | 8.58                     | 1.384    | 1.076         | 11.43                    | 1.781    | 1.230         | -0.14            | 0.796           | 1.154      | 0.959              | -0.15     | 0.956              | 0.27      |
| 5-0517/A  | 14.48                    | 1.682    | 1.194         | 7.57                     | 1.540    | 1.128         | 0.31             | 0.788           | 1.162      | 0.937              | -0.50     | 0.934              | -0.38     |
| 5-0522/A  | 16.59                    | 1.848    | 1.264         | 6.55                     | 1.467    | 1.101         | 0.43             | 0.781           | 1.186      | 0.931              | -0.52     | 0.934              | -0.52     |
| 5-0532/CT | 22.24                    | 2.255    | 1.447         | 4.20                     | 1.350    | 1.060         | 0.68             | 0.758           | 1.273      | 0.936              | -0.49     | 0.918              | -0.56     |
| 5-0812/A  | 9.77                     | 1.546    | 1.132         | 15.93                    | 2.259    | 1.457         | -0.24            | 0.735           | 1.296      | 0.953              | 0.15      | 0.940              | 0.47      |
| 5-0816/A  | 15.06                    | 1.882    | 1.279         | 12.06                    | 1.923    | 1.291         | 0.11             | 0.732           | 1.285      | 0.937              | -0.45     | 0.936              | -0.40     |
| 5-0822/A  | 17.82                    | 2.126    | 1.383         | 9.50                     | 1.729    | 1.206         | 0.30             | 0.737           | 1.295      | 0.931              | -0.52     | 0.917              | -0.60     |
| 5-0832/A  | 22.46                    | 2.437    | 1.541         | 7.09                     | 1.547    | 1.131         | 0.52             | 0.723           | 1.343      | 0.926              | -0.53     | 0.910              | -0.56     |
| 5-1511/A  | 10.09                    | 1.643    | 1.168         | 17.77                    | 2.507    | 1.571         | -0.28            | 0.712           | 1.378      | 0.949              | 0.35      | 0.927              | 0.60      |
| 5-1517/A  | 14.04                    | 1.946    | 1.304         | 14.52                    | 2.169    | 1.398         | -0.02            | 0.714           | 1.355      | 0.936              | -0.55     | 0.902              | -0.65     |
| 5-1529/A  | 17.69                    | 2.204    | 1.403         | 11.18                    | 1.901    | 1.284         | 0.23             | 0.719           | 1.346      | 0.921              | -0.60     | 0.862              | -0.68     |

Table A10-1 PERFORMANCE PARAMETERS - DIFFUSER 1 (AR=1.4, 2φ=12°)

| TEST No.  | FLOW SPLIT | CONTINUITY CHECK  |                   | OVERALL PERFORMANCE     |                  |                      |                   |                   | PRE-DIFFUSER            |                  |                      |
|-----------|------------|-------------------|-------------------|-------------------------|------------------|----------------------|-------------------|-------------------|-------------------------|------------------|----------------------|
|           | S          | $\Delta Q_2\%Q_1$ | $\Delta Q_4\%Q_1$ | $\tilde{\lambda}_{1-4}$ | $\tilde{C}_{P4}$ | $\tilde{\Sigma}_4\%$ | $\tilde{C}_{P4i}$ | $\tilde{C}_{P4o}$ | $\tilde{\lambda}_{1-2}$ | $\tilde{C}_{P2}$ | $\tilde{\Sigma}_2\%$ |
| 1-0507/A  | 0.705      | 4.77              | 2.93              | 0.390                   | 0.089            | 18.11                | -0.198            | 0.496             | 0.080                   | 0.377            | 74.66                |
| 1-0514/CT | 1.417      | -1.81             | -0.04             | 0.409                   | 0.315            | 42.96                | 0.240             | 0.367             | 0.053                   | 0.433            | 85.76                |
| 1-0517/CT | 1.754      | 1.49              | 0.01              | 0.436                   | 0.313            | 41.26                | 0.372             | 0.279             | 0.037                   | 0.431            | 85.29                |
| 1-0521/CT | 2.109      | -0.15             | 4.12              | 0.478                   | 0.278            | 36.43                | 0.436             | 0.207             | 0.046                   | 0.397            | 78.56                |
| 1-0532/A  | 3.227      | 2.33              | 0.60              | 0.612                   | 0.125            | 16.85                | 0.457             | 0.023             | 0.138                   | 0.252            | 49.83                |
| 1-1013/CT | 1.300      | -0.00             | 2.51              | 0.247                   | 0.458            | 63.96                | 0.318             | 0.566             | 0.038                   | 0.387            | 76.50                |
| 1-1017/CT | 1.719      | 0.07              | -0.70             | 0.261                   | 0.485            | 64.17                | 0.386             | 0.543             | 0.033                   | 0.387            | 76.52                |
| 1-1025/CT | 2.575      | 2.62              | -1.05             | 0.289                   | 0.463            | 60.92                | 0.420             | 0.480             | 0.080                   | 0.315            | 62.39                |
| 1-2007/A  | 0.787      | 2.65              | 1.14              | 0.257                   | 0.274            | 50.09                | 0.080             | 0.521             | 0.066                   | 0.332            | 65.76                |
| 1-2016/A  | 1.642      | 5.32              | 0.47              | 0.231                   | 0.513            | 68.20                | 0.382             | 0.593             | 0.071                   | 0.337            | 66.60                |
| 1-2033/A  | 3.395      | 1.94              | 0.03              | 0.239                   | 0.490            | 66.32                | 0.393             | 0.519             | 0.057                   | 0.335            | 66.33                |

APPENDIX 10 PERFORMANCE PARAMETERS

Table A10-1

Table A10-2 PERFORMANCE PARAMETERS - DIFFUSER 2 (AR=1.6, 2 $\phi$ =12 $^\circ$ )

| TEST No.  | FLOW SPLIT | CONTINUITY CHECK  |                   | OVERALL PERFORMANCE     |                   |                        |                      |                      | PRE-DIFFUSER            |                   |                        |
|-----------|------------|-------------------|-------------------|-------------------------|-------------------|------------------------|----------------------|----------------------|-------------------------|-------------------|------------------------|
|           | S          | $\Delta Q_2\%Q_1$ | $\Delta Q_4\%Q_1$ | $\tilde{\lambda}_{1-4}$ | $\tilde{C}_{P_4}$ | $\tilde{\epsilon}_4\%$ | $\tilde{C}_{P_{4i}}$ | $\tilde{C}_{P_{4o}}$ | $\tilde{\lambda}_{1-2}$ | $\tilde{C}_{P_2}$ | $\tilde{\epsilon}_2\%$ |
| 2-0508/A  | 0.820      | 3.58              | 3.01              | 0.317                   | 0.236             | 41.72                  | -0.023               | 0.552                | 0.089                   | 0.469             | 75.33                  |
| 2-0511/CT | 1.199      | 0.84              | 1.08              | 0.275                   | 0.416             | 59.58                  | 0.278                | 0.531                | 0.065                   | 0.514             | 82.59                  |
| 2-0517/A  | 1.712      | 3.17              | 0.01              | 0.303                   | 0.447             | 59.11                  | 0.398                | 0.475                | 0.074                   | 0.484             | 77.79                  |
| 2-0524/A  | 2.485      | 4.90              | 2.67              | 0.372                   | 0.383             | 50.26                  | 0.451                | 0.355                | 0.103                   | 0.399             | 64.04                  |
| 2-0808/A  | 0.815      | 3.28              | 4.15              | 0.264                   | 0.285             | 50.57                  | 0.049                | 0.575                | 0.096                   | 0.411             | 65.95                  |
| 2-0812/CT | 1.208      | -0.21             | 1.98              | 0.226                   | 0.465             | 66.48                  | 0.311                | 0.594                | 0.053                   | 0.470             | 75.53                  |
| 2-0815/A  | 1.540      | 3.80              | 0.82              | 0.232                   | 0.506             | 67.98                  | 0.397                | 0.577                | 0.064                   | 0.458             | 73.52                  |
| 2-0821/CT | 2.122      | 2.33              | 1.16              | 0.243                   | 0.515             | 67.40                  | 0.435                | 0.553                | 0.067                   | 0.431             | 69.24                  |
| 2-1508/A  | 0.882      | 4.40              | 0.35              | 0.201                   | 0.384             | 64.29                  | 0.214                | 0.577                | 0.086                   | 0.412             | 66.21                  |
| 2-1514/A  | 1.473      | 3.08              | 1.07              | 0.214                   | 0.519             | 70.19                  | 0.390                | 0.606                | 0.071                   | 0.422             | 67.72                  |
| 2-1523/A  | 2.303      | 3.54              | 2.91              | 0.219                   | 0.536             | 70.16                  | 0.433                | 0.580                | 0.070                   | 0.404             | 64.83                  |

Table A10-3 PERFORMANCE PARAMETERS - DIFFUSER 3 (AR=1.8,  $\phi=12^\circ$ )

| TEST No.  | FLOW SPLIT | CONTINUITY CHECK  |                   | OVERALL PERFORMANCE     |                  |                      |                   |                   | PRE-DIFFUSER            |                  |                      |
|-----------|------------|-------------------|-------------------|-------------------------|------------------|----------------------|-------------------|-------------------|-------------------------|------------------|----------------------|
|           | S          | $\Delta Q_2\%Q_1$ | $\Delta Q_4\%Q_1$ | $\tilde{\lambda}_{1-4}$ | $\tilde{C}_{P4}$ | $\tilde{\Sigma}_4\%$ | $\tilde{C}_{P4i}$ | $\tilde{C}_{P4o}$ | $\tilde{\lambda}_{1-2}$ | $\tilde{C}_{P2}$ | $\tilde{\Sigma}_2\%$ |
| 3-0408/A  | 0.828      | 2.97              | 0.94              | 0.283                   | 0.276            | 48.32                | 0.020             | 0.585             | 0.077                   | 0.557            | 79.23                |
| 3-0412/CT | 1.262      | -0.24             | 1.07              | 0.259                   | 0.444            | 62.43                | 0.296             | 0.561             | 0.064                   | 0.590            | 83.90                |
| 3-0416/A  | 1.649      | 2.23              | 0.80              | 0.275                   | 0.471            | 62.55                | 0.404             | 0.512             | 0.059                   | 0.568            | 80.77                |
| 3-0423/A  | 2.357      | 0.09              | 0.79              | 0.321                   | 0.436            | 57.11                | 0.452             | 0.429             | 0.067                   | 0.480            | 68.38                |
| 3-0707/A  | 0.776      | 5.05              | 3.92              | 0.232                   | 0.293            | 54.19                | 0.059             | 0.594             | 0.078                   | 0.487            | 69.33                |
| 3-0711/CT | 1.174      | 0.87              | 1.80              | 0.202                   | 0.483            | 69.69                | 0.316             | 0.626             | 0.045                   | 0.543            | 77.23                |
| 3-0718/A  | 1.817      | 1.51              | 4.16              | 0.218                   | 0.535            | 70.40                | 0.421             | 0.598             | 0.052                   | 0.494            | 70.25                |
| 3-0722/A  | 2.296      | 2.36              | 1.58              | 0.232                   | 0.524            | 68.56                | 0.441             | 0.560             | 0.068                   | 0.458            | 65.25                |
| 3-1208/A  | 0.876      | 4.78              | 3.02              | 0.233                   | 0.326            | 56.77                | 0.114             | 0.581             | 0.083                   | 0.467            | 66.43                |
| 3-1213/A  | 1.368      | 4.22              | 1.46              | 0.206                   | 0.514            | 70.69                | 0.362             | 0.625             | 0.067                   | 0.490            | 69.72                |
| 3-1223/A  | 2.323      | 2.63              | 0.39              | 0.198                   | 0.556            | 72.78                | 0.453             | 0.600             | 0.058                   | 0.468            | 66.60                |

Table A10-4 PERFORMANCE PARAMETERS - DIFFUSER 4 (AR=18,2φ=18°)

| TEST No.  | FLOW SPLIT<br>S | CONTINUITY CHECK  |                   | OVERALL PERFORMANCE     |                  |                      |                   |                   | PRE-DIFFUSER            |                  |                      |
|-----------|-----------------|-------------------|-------------------|-------------------------|------------------|----------------------|-------------------|-------------------|-------------------------|------------------|----------------------|
|           |                 | $\Delta Q_2\%Q_1$ | $\Delta Q_4\%Q_1$ | $\tilde{\lambda}_{1-4}$ | $\tilde{C}_{P4}$ | $\tilde{\Sigma}_4\%$ | $\tilde{C}_{P4i}$ | $\tilde{C}_{P4o}$ | $\tilde{\lambda}_{1-2}$ | $\tilde{C}_{P2}$ | $\tilde{\Sigma}_2\%$ |
| 4-0408/A  | 0.827           | 5.38              | 2.98              | 0.304                   | 0.254            | 44.46                | 0.011             | 0.546             | 0.096                   | 0.510            | 72.63                |
| 4-0411/A  | 1.104           | 3.11              | 1.30              | 0.254                   | 0.436            | 62.48                | 0.279             | 0.567             | 0.057                   | 0.575            | 81.88                |
| 4-0417/A  | 1.768           | 2.11              | 2.76              | 0.288                   | 0.463            | 61.12                | 0.382             | 0.510             | 0.065                   | 0.519            | 73.86                |
| 4-0422/CT | 2.254           | 4.16              | 2.76              | 0.330                   | 0.428            | 55.97                | 0.402             | 0.439             | 0.105                   | 0.451            | 64.21                |
| 4-0707/A  | 0.776           | 6.79              | 3.12              | 0.264                   | 0.260            | 48.12                | 0.054             | 0.527             | 0.114                   | 0.416            | 59.21                |
| 4-0711/CT | 1.133           | 3.48              | 2.36              | 0.230                   | 0.444            | 64.92                | 0.291             | 0.579             | 0.078                   | 0.470            | 66.90                |
| 4-0717/A  | 1.776           | 1.08              | 1.53              | 0.238                   | 0.514            | 67.71                | 0.370             | 0.594             | 0.060                   | 0.432            | 61.47                |
| 4-0722/A  | 2.267           | 3.28              | 0.98              | 0.255                   | 0.502            | 65.76                | 0.375             | 0.559             | 0.076                   | 0.396            | 56.33                |
| 4-1208/A  | 0.865           | 5.94              | 3.68              | 0.256                   | 0.318            | 53.92                | 0.136             | 0.529             | 0.103                   | 0.405            | 57.67                |
| 4-1212/A  | 1.266           | 5.29              | 1.93              | 0.241                   | 0.463            | 65.06                | 0.314             | 0.580             | 0.079                   | 0.440            | 62.63                |
| 4-1221/A  | 2.162           | 2.63              | 0.57              | 0.241                   | 0.514            | 67.25                | 0.373             | 0.579             | 0.063                   | 0.405            | 57.59                |



Table A10-5 PERFORMANCE PARAMETERS - DIFFUSER 5 (AR=16,  $2\phi=11.3^\circ$ , Canted)

| TEST No.  | FLOW SPLIT<br>S | CONTINUITY CHECK  |                   | OVERALL PERFORMANCE     |                  |                   |                   |                   | PRE-DIFFUSER            |                  |                   |
|-----------|-----------------|-------------------|-------------------|-------------------------|------------------|-------------------|-------------------|-------------------|-------------------------|------------------|-------------------|
|           |                 | $\Delta Q_2\%Q_1$ | $\Delta Q_4\%Q_1$ | $\tilde{\lambda}_{1-4}$ | $\tilde{C}_{P4}$ | $\tilde{\xi}_4\%$ | $\tilde{C}_{P4i}$ | $\tilde{C}_{P4o}$ | $\tilde{\lambda}_{1-2}$ | $\tilde{C}_{P2}$ | $\tilde{\xi}_2\%$ |
| 5-0513/A  | 1.310           | 4.22              | 0.23              | 0.270                   | 0.442            | 61.48             | 0.252             | 0.586             | 0.066                   | 0.503            | 80.28             |
| 5-0517/A  | 1.787           | 4.26              | 1.45              | 0.267                   | 0.485            | 63.95             | 0.384             | 0.542             | 0.067                   | 0.500            | 79.76             |
| 5-0522/A  | 2.220           | 4.76              | 2.15              | 0.274                   | 0.484            | 63.37             | 0.432             | 0.508             | 0.078                   | 0.480            | 76.48             |
| 5-0532/CT | 3.206           | 3.71              | 2.17              | 0.309                   | 0.428            | 57.47             | 0.471             | 0.415             | 0.111                   | 0.414            | 66.01             |
| 5-0812/A  | 1.201           | 4.54              | 1.61              | 0.229                   | 0.461            | 66.03             | 0.289             | 0.605             | 0.082                   | 0.434            | 69.27             |
| 5-0816/A  | 1.695           | 3.58              | 1.26              | 0.220                   | 0.528            | 69.99             | 0.411             | 0.598             | 0.074                   | 0.446            | 71.18             |
| 5-0822/A  | 2.241           | 5.16              | 2.11              | 0.219                   | 0.538            | 70.35             | 0.450             | 0.577             | 0.074                   | 0.443            | 70.65             |
| 5-0832/A  | 3.237           | 5.18              | 1.47              | 0.229                   | 0.506            | 68.07             | 0.471             | 0.517             | 0.091                   | 0.409            | 65.17             |
| 5-1511/A  | 1.105           | 5.09              | 1.42              | 0.228                   | 0.440            | 65.04             | 0.270             | 0.594             | 0.087                   | 0.399            | 63.65             |
| 5-1517/A  | 1.767           | 4.07              | 2.31              | 0.212                   | 0.539            | 71.09             | 0.419             | 0.607             | 0.069                   | 0.425            | 67.82             |
| 5-1529/A  | 2.944           | 4.45              | 0.78              | 0.208                   | 0.531            | 70.65             | 0.458             | 0.556             | 0.082                   | 0.416            | 66.29             |

Table A10-5

